4 December 2009 | $10

Science

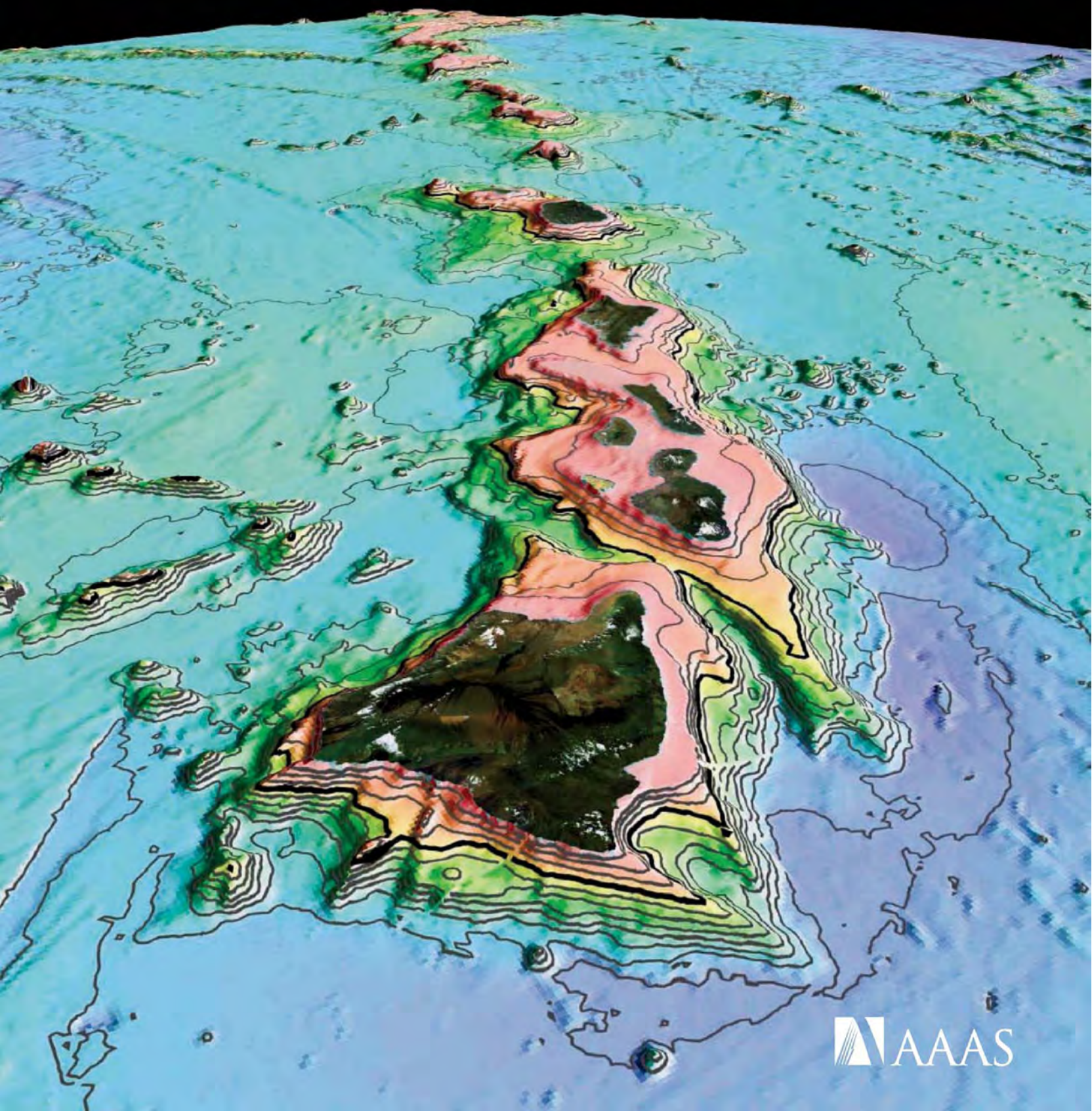

AAAS

You can deliver. We can help.

Invitrogen transfection solutions

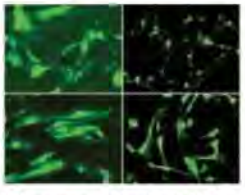

"I have evaluated the Lipofectamine™ LTX and Plus Reagents, and am very happy with the results."

– *Melanie Van Stry*
St. Jude University

Invitrogen can help you deliver your DNA or siRNA into any type of cell, even hard-to-transfect cells such as primary and stem cells. We have the right transfection solution for the right application.

- Lipofectamine™ LTX with PLUS Reagent—plasmid delivery
- Lipofectamine™ RNAiMAX Transfection Reagent—siRNA delivery

Give it a try. Request a free sample from your local Invitrogen sales representative or go to www.invitrogen.com/trytransfection.

Get real results, not artifacts. Use transfection solutions that deliver.

invitrogen™

AAAS, Publisher of *Science*
presents the sponsors and supporters of the

2010 Annual Meeting

Bridging Science and Society

18—22 February • San Diego

AAAS wishes to thank our sponsors and supporters:

Presenting Sponsor

Canada

SUBARU

HELMHOLTZ ASSOCIATION

EUROPEAN RESEARCH
SUCCESS THROUGH COOPERATION
www.ec.europa.eu/research

Johnson & Johnson
PHARMACEUTICAL RESEARCH & DEVELOPMENT, L.L.C.

NSF

THE KAVLI FOUNDATION

In addition generous funding for AAAS Awards is provided by the ***Kavli Foundation*** and ***Affymetrix.***

Be part of a proven equation:

Your Organization + AAAS Annual Meeting = Global Visibility

Call today about the benefits of sponsorships currently available:

Jill C. Perla
AAAS Meetings
Direct Dial: (202) 326-6736
E-mail: jperla@aaas.org

AAAS
ADVANCING SCIENCE, SERVING SOCIETY

GE Healthcare
Life Sciences

Inspired Again

Who better to draw inspiration for the new ÄKTA™ avant system than from customers using the 30,000 ÄKTA systems already in use around the world? Well, you spoke and we listened. The new ÄKTA avant system for process development is faster — enabling quicker insights. It minimizes the chance of error, even while working at higher speeds. And it allows for direct, reliable scalability. At GE Healthcare, our focus is on helping scientists achieve even more, faster. It's a commitment we have in our genes. And all this is backed by the service, support, and investment in the future that being part of GE can bring.

Want to know more? Why not talk with us today. Visit **www.gelifesciences.com/aktaavant**

I **ÄKTA** I Amersham I Biacore I IN Cell Analyzer I Whatman I GE Service I

The New ÄKTA avant

imagination at work

First published September 2009
GE Healthcare Bio-Sciences AB, Björkgatan 30, 751 84 Uppsala, Sweden
GE12-09

EDITORIAL

NEWS OF THE WEEK

NEWS FOCUS

LETTERS

BOOKS *ET AL.*

POLICY FORUM

PERSPECTIVES

page 1334

page 1348

ESSAY

CONTENTS continued >>

COVER

Topography of the Hawaiian Islands and surrounding sea floor, from ship soundings and satellite altimetry displayed using Google Earth. A Report on page 1388 describes images of the deep structure of the Hawaiian hot spot obtained from a large-aperture network of ocean bottom and land seismometers. Global bathymetry overlays for Google Earth are available at http://topex.ucsd.edu/WWW_html/mar_topo.html.

Image: David Sandwell/University of California, San Diego; Paul Wessel/University of Hawaii

DEPARTMENTS

Gene expression and function analysis sample and assay technologies by QIAGEN

Enjoy first-time success

Rely on QIAGEN's manual and automated workflow solutions for:

- **Sample collection and disruption**
- **RNA stabilization and purification**
- **Real-time PCR and RT-PCR and gene expression assays**
- **RNAi and gene silencing**
- **miRNA purification and assays**
- **Methylation analysis in epigenetics research**
- **Protein sample preparation and assays**

Making improvements in life possible — www.qiagen.com

QIAGEN®

GEEPad03095 1WW

Sample & Assay Technologies

REVIEW

BREVIA

RESEARCH ARTICLES

REPORTS

pages 1352, 1369, & 1412

page 1391

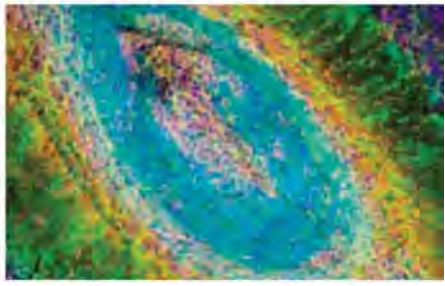

page 1424

CONTENTS continued >>

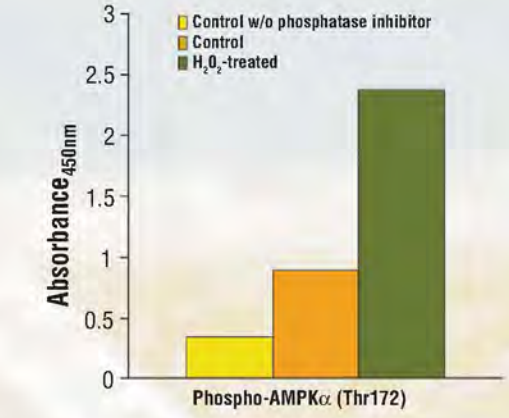

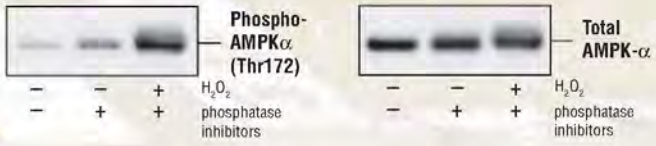

PathScan® Sandwich ELISA Kits & Antibody Pairs

from Cell Signaling Technology®

Above: *Treatment of C2C12 cells with H_2O_2 stimulates phosphorylation of AMPKα at Thr172, detected by the* ***PathScan® Phospho-AMPKα (Thr172) Sandwich ELISA Kit #7959****. The absorbance readings at 450 nm are shown in the top figure, while the corresponding western blots using Phospho-AMPKα (Thr172) (D79.5E) XP™ Rabbit mAb #4188 (left panel) or AMPKα (23A3) Rabbit mAb #2603 (right panel) are shown in the bottom figure.*

Unparalleled product quality, validation and technical support

- Over 140 PathScan® ELISA Kits covering a broad spectrum of signaling pathways
- In-house development, production and validation ensures the highest product quality
- Technical support provided by the same scientists that develop and produce the products
- Matched modification state and total ELISA kits and Antibody Pairs available
- Custom 96- and 384-well formatting available upon request

New PathScan® Chemiluminescent Kits offer the broadest dynamic range and assay sensitivity while requiring half the sample size due to the use of low volume microplates.

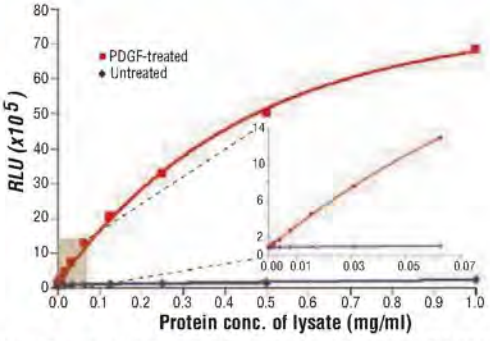

PathScan® Phospho-Akt1 (Ser473) Chemiluminescent Sandwich ELISA Kit #7134

for quality products you can trust...

www.cellsignal.com

Cell Signaling TECHNOLOGY®

Orders (toll-free) 1-877-616-2355 | **Technical support** (toll-free) 1-877-678-8324 support@cellsignal.com | **Inquiries** info@cellsignal.com | **Environmental Commitment** eco.cellsignal.com

SCIENCEONLINE

SCIENCEXPRESS
www.sciencexpress.org

Dendritic Mechanisms Underlying Rapid Synaptic Activation of Fast-Spiking Hippocampal Interneurons
H. Hu et al.

Potassium channel enrichment in the dendrites of hippocampal basket cells defines a mechanism of neural network function.
10.1126/science.1177876

Therapeutic Silencing of MicroRNA-122 in Primates with Chronic Hepatitis C Virus Infection
R. E. Lanford et al.

Targeting a microRNA required for hepatitis C virus infection reduces disease symptoms in chimpanzees.
10.1126/science.1178178
>> Science *Podcast*

Targeted 3′ Processing of Antisense Transcripts Triggers *Arabidopsis FLC* Chromatin Silencing
F. Liu et al.

A backward transcript of the *FLOWERING LOCUS C* gene of *Arabidopsis* is involved in regulation of the sense-strand transcription.
10.1126/science.1180278

Iron Partitioning and Density Changes of Pyrolite in Earth's Lower Mantle
T. Irifune et al.

Increasing the compositional complexity of mantle samples causes an electronic spin transition to occur at lower pressures.
10.1126/science.1181443

SCIENCENOW
www.sciencenow.org
Highlights From Our Daily News Coverage

Coral Reefs Act Like Sunscreen

Skeletons absorb UV light to protect inhabitants.

Do Titan's Lakes Migrate South for the Winter?

Orbital cycles of Saturn's moon could be causing lakes to pull up stakes.

Americans' Eating Habits More Wasteful Than Ever

Nearly 40% of U.S. food ends up in the garbage, study says.

SCIENCESIGNALING
www.sciencesignaling.org
The Signal Transduction Knowledge Environment

EDITORIAL GUIDE: Living by the Numbers
M. B. Yaffe

Articles should be judged on their own merit, not the impact factor of the journal in which they are published.

RESEARCH ARTICLE: Protein Kinase G Controls Brown Fat Cell Differentiation and Mitochondrial Biogenesis
B. Haas et al.

PKG regulates differentiation and thermogenic function in brown adipose tissue.

RESEARCH ARTICLE: RIAM Regulates the Cytoskeletal Distribution and Activation of PLC-γ1 in T cells
N. Patsoukis et al.

RIAM, an adaptor protein that regulates integrin signaling, is found to also function in T cell receptor–proximal signaling.

PROTOCOL: Quantitative Analysis of Protein-Lipid Interactions Using Tryptophan Fluorescence
C. A. Kraft et al.

The intrinsic fluorescence of tryptophan can be used to quantify the interaction between proteins and lipids.

PODCAST
A. Pfeifer and A. M. VanHook

Protein kinase G is required for the differentiation and fat-burning function of brown adipose tissue.

SCIENCECAREERS
www.sciencecareers.org/career_magazine
Free Career Resources for Scientists

Translating Lupus
K. Hede

An encounter with a lupus patient crystallized one scientist's concept of "translational research."

Taken for Granted: NIH's Dr. Ruth
B. L. Benderly

Ruth L. Kirschstein's life of service provides a powerful example for young scientists.

Mind Matters: In Defense of Downtime
I. S. Levine

Working longer does not necessarily mean getting more done.

CTSciNet: The Clinical and Translational Science Network

Experience the leading social career resource for clinical and translational scientists.

SCIENCETRANSLATIONAL MEDICINE
www.sciencetranslationalmedicine.org
Integrating Medicine and Science

EDITORIAL: Peer-to-Peer Sharing Spurs Scientific Innovation
E. A. Zerhouni

Changes in pharmaceutical industry practices can accelerate discoveries.

COMMENTARY: A Call for Sharing—Adapting Pharmaceutical Research to New Realities
B. H. Munos et al.

Collaborations stand to gain from loosening intellectual property restrictions.

RESEARCH ARTICLE: Identification of an Autoantigen Demonstrates a Link Between Interstitial Lung Disease and a Defect in Central Tolerance
A. K. Shum et al.

A defect in immune tolerance may underlie lung damage in autoimmune diseases.

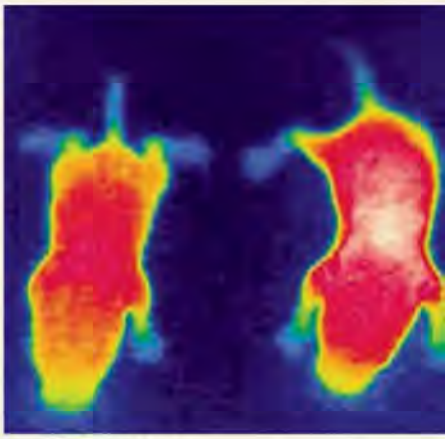

SCIENCESIGNALING
Brown fat and body temperature.

CREDIT: BODO HAAS/INSTITUTE FOR PHARMACOLOGY AND TOXICOLOGY, UNIVERSITY OF BONN

SCIENCEPODCAST
www.sciencemag.org/multimedia/podcast
Free Weekly Show

Download the 4 December *Science* Podcast to hear about a microRNA target for treating hepatitis C, the combined effects of nitrogen and CO_2 on plant diversity, the future of evolution, and more.

ORIGINSBLOG
blogs.sciencemag.org/origins
A History of Beginnings

SCIENCEINSIDER
blogs.sciencemag.org/scienceinsider
Science Policy News and Analysis

SCIENCE (ISSN 0036-8075) is published weekly on Friday, except the last week in December, by the American Association for the Advancement of Science, 1200 New York Avenue, NW, Washington, DC 20005. Periodicals Mail postage (publication No. 484460) paid at Washington, DC, and additional mailing offices. The title SCIENCE is a registered trademark of the AAAS. Domestic individual membership and subscription (51 issues): $146 ($74 allocated to subscription). Domestic institutional subscription (51 issues): $835; Foreign postage extra: Mexico, Caribbean (surface mail) $55; other countries (air assist delivery) $85. First class, airmail, student, and emeritus rates on request. Canadian rates with GST available upon request, GST #1254 88122. Publications Mail Agreement Number 1069624. **Printed in the U.S.A.**

Change of address: Allow 4 weeks, giving old and new addresses and 8-digit account number. **Postmaster:** Send change of address to AAAS, P.O. Box 96178, Washington, DC 20090–6178. **Single-copy sales:** $10.00 current issue, $15.00 back issue prepaid includes surface postage; bulk rates on request. *Science* is indexed in the *Reader's Guide to Periodical Literature* and in several specialized indexes.

AAAS
ADVANCING SCIENCE, SERVING SOCIETY

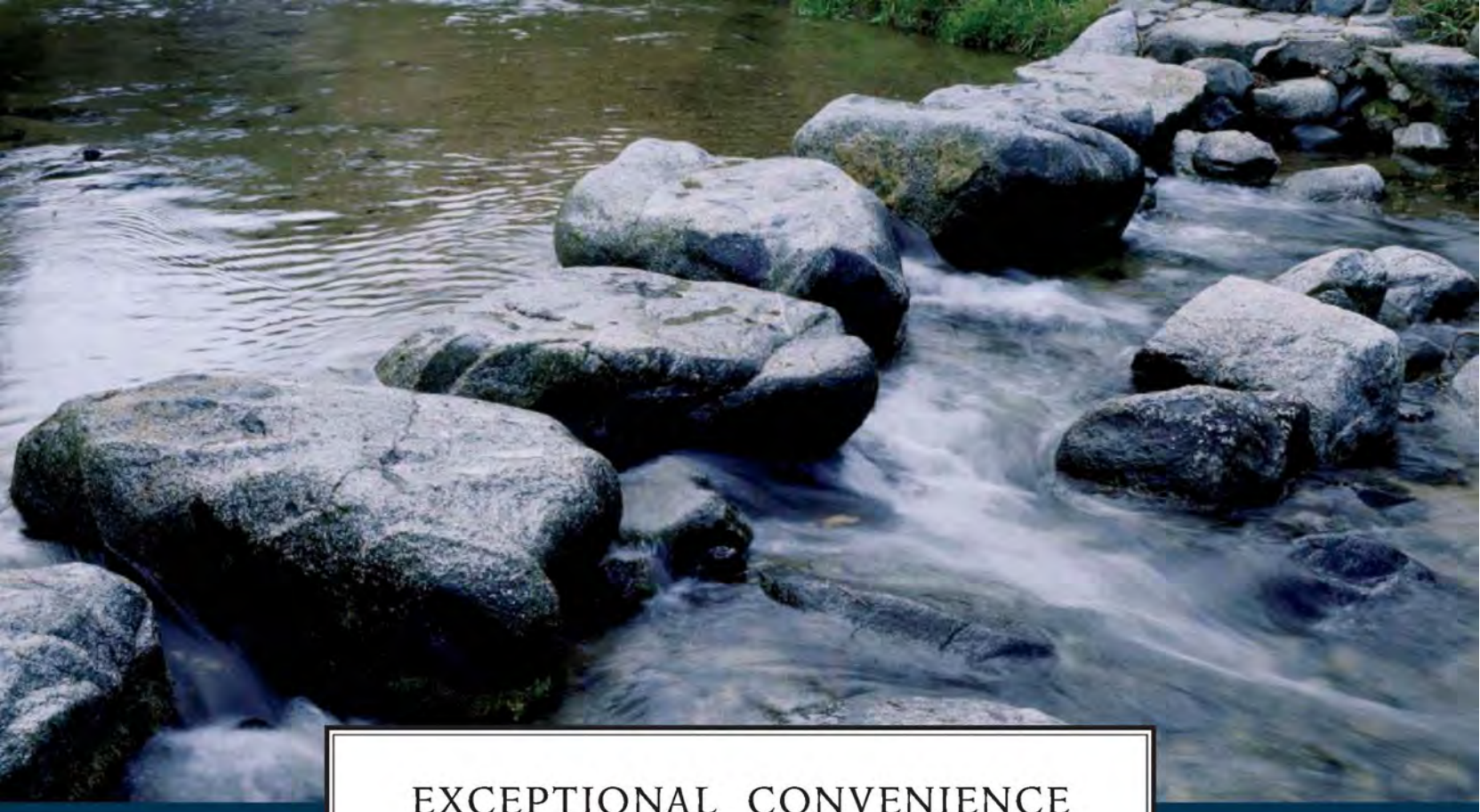

EXCEPTIONAL CONVENIENCE

Restriction Enzymes from New England Biolabs

With 35 years of experience in enzyme technology, New England Biolabs offers unmatched convenience when selecting a restriction enzyme. With over 160 enzymes recommended for use in a single buffer, reactions can be set up quickly and easily. For additional flexibility, try a High Fidelity (HF) enzyme with reduced star activity. Reaction times can be shortened to as little as 5 minutes using one of our Time-Saver qualified enzymes. With over 220 specificities to choose from, NEB enzymes deliver convenience you can count on.

The convenience of NEB Restriction Enzymes*

** As of 3/26/09*

Advantages:

- **Selection** – More specificities than any other supplier
- **Convenience** – Optimal activity for over 160 enzymes in a single buffer NEB 4
- **Quality** – State-of-the-art production and stringent QCs
- **Innovation** – HF enzymes engineered for reduced star activity
- **Performance** – Guaranteed

NEW ENGLAND BioLabs® Inc.
enabling technologies in the life sciences

CLONING & MAPPING	DNA AMPLIFICATION & PCR	RNA ANALYSIS	PROTEIN EXPRESSION & ANALYSIS	GENE EXPRESSION & CELLULAR ANALYSIS

www.neb.com

EDITED BY STELLA HURTLEY

CO_2 and Miocene Climate Change

Atmospheric carbon dioxide is a powerful greenhouse gas believed to be one of the most important determinants of climate. Ice cores provide a detailed and direct record of CO_2 concentrations over the past 800,000 years, but not earlier. **Tripati *et al.*** (p. 1394, published online 8 October) report B/Ca measurements of planktonic foraminifera, from which they can infer atmospheric CO_2 concentrations, for the past 20 million years. The concentration of atmospheric CO_2 was similar to preindustrial values for the past 10 millions years, but between 15 and 20 million years ago, during the warm lower Miocene epoch, CO_2 was more abundant, and major climate transitions toward cooler conditions occurred when CO_2 decreased substantially.

CREDITS (TOP TO BOTTOM): TRIPATI *ET AL.*; MELILLO *ET AL.*

Zeroing in on Zoonoses

Influenza, plague, and Lyme disease are classic examples of zoonoses—diseases that circulate in livestock and wildlife, as well as in humans. When a pathogen transfers among multiple hosts, the dynamics of circulation, transmission, and outbreak are complex. **Lloyd-Smith *et al.*** (p. 1362) review the use of analytical mathematical tools, particularly modeling, in the development of control policies and research agendas. Significant gaps are highlighted in analytical efforts during spillover transmission from animals into humans. Moreover, the tendency has been to focus on pathogens with simpler life cycles and of immediate global urgency, such as influenza, whereas insect-transmitted pathogens with complex, multihost life cycles are less well understood.

Nascent Chains Revealed

Detailed analysis of protein translation and translocation across membranes requires the identification and structural analysis of intermediates involved in these processes (see the Perspective by **Kampmann and Blobel**). **Seidelt *et al.*** (p. 1412, published online 29 October) report the visualization by cryo-electron microscopy of a nascent polypeptide chain in the tunnel of the ribosome at 5.8 angstroms. This resolution allows analysis of the conformation and distinct contacts of the nascent chain within the ribosomal tunnel, which suggests a mechanism by which translational stalling is induced by this peptide. Protein translocation across cellular membranes involves the Sec61 protein, a component of a protein-conducting channel. Whether Sec61 acts as a monomer or as an oligomer during protein translocation has been unclear. **Becker *et al.*** (p. 1369, published online 29 October) describe active yeast and mammalian ribosome-Sec61 structures that show the Sec61 complex interacting with the ribosome and a nascent secretory protein signal sequence. The analysis unambiguously reveals that the active protein-conducting channel is a single Sec61 copy with its central pore serving as conduit for the nascent polypeptide.

ABA Receptor Up Close

Plants face a variety of environmental stresses, including drought, salinity, and cold. In the face of such stresses, the plant hormone abscisic acid (ABA) triggers adaptive physiological responses. **Nishimura *et al.*** (p. 1373, published online 22 October; see the Perspective by **Sussman and Phillips**) have now analyzed the crystal structure of one member of the ABA receptor family, PYR1 (pyrabactin resistance 1). The ABA molecule binds within an internal pocket of PYR1, where it probably induces a conformational change.

Elliptical Galaxy Evolution

Our closest elliptical galaxy, M32, represents a rare class of elliptical galaxies that are too compact for their luminosities. Only a handful of elliptical galaxies with luminosities and sizes comparable to M32 have been found, making it difficult to understand how they evolved. **Chilingarian *et al.*** (p. 1379, published online 1 October) present a sample of 21 compact elliptical galaxies gathered through automated data mining of the Hubble Space Telescope Legacy Archive and other databases by means of virtual observatory tools. The results suggest that tidal stripping of more massive progenitor galaxies produces compact elliptical galaxies.

Earth's Plume Plumbing

Volcanic hot spots, such as the one that continues to build the Hawaiian Islands, are thought to form by one of two mechanisms: Either mantle plumes bring hot, buoyant material to the surface from deep within the Earth's interior, or extensive processing of the upper mantle by plate tectonics causes localized volcanism in stressed or heterogeneous crust. **Wolfe *et al.*** (p. 1388; see the cover; see the news story by **Kerr**) used an extensive array of ocean-bottom and land-based seismometers to reveal the structure of the mantle beneath Hawaii. These high-resolution images reveal a high-temperature plume originating from the lower mantle.

Biofuel Backfire

For compelling economical, geopolitical, and environmental reasons, biofuels are considered an attractive alternative to fossil fuels for meeting future global energy demands. **Melillo *et al.*** (p. 1397, published online 22 October), however, suggest that a few serious drawbacks related to land use need to be considered. Based on a combined biogeochemistry and economic model, indirect land use (for example, clearing forested land for food crops to compensate for increased biofuel crop production on current farmlands) is predicted to generate more soil carbon loss than directly harvesting biofuel crops. Furthermore, increased fertilizer use for biofuels will add large amounts of nitrous oxide—a more effective heat-trapping molecule than carbon dioxide—to the atmosphere. Policy decisions regarding land and crop management thus need to consider the long-term implications of increased biofuel production.

Continued on page 1317

ACROSS THE HALL OR ACROSS THE GLOBE, REFMAN KEEPS EVERYBODY ON THE SAME PAGE.

No matter where you or your colleagues are in the world, so are your references. With Reference Manager,® you can collaborate with others on a network—or even the Web. Simplify your publishing with Reference Manager where you can search Internet databases, organize your references and create instant bibliographies. Plus, with newly added features you can do even more.

- Attach any file to a record and create a single Reference Manager repository
- Cite While You Write™ with a Reference Manager tab on the Word 2007 ribbon
- Use Web Publisher to collaborate with colleagues

Reference Manager 12

Download a free trial
www.refman.com

Simplify your life and keep everybody on the same page today.
800-722-1227 • 760-438-5526 • rs.info@thomson.com

THOMSON REUTERS

Continued from page 1315

Mitigating Nitrogen Enrichment?

Nitrogen enrichment reduces the species diversity of plants in herbaceous communities. By contrast, the effects of increasing CO_2 on plant species richness is poorly documented, and the interaction of both N deposition and CO_2 elevation are unknown. **Reich** (p. 1399; see the Perspective by **Collins**) performed a 10-year open-air field experiment in a North American perennial grassland assemblage. Reductions in plant species richness resulting from N deposition were half as large under elevated CO_2 concentrations as under ambient atmospheric CO_2. Given that both N and CO_2 are projected to increase globally, these results provide a pointer to the types of ecological change that could be expected, at least in relatively simple plant communities.

Metamorphosis Receptor Identified

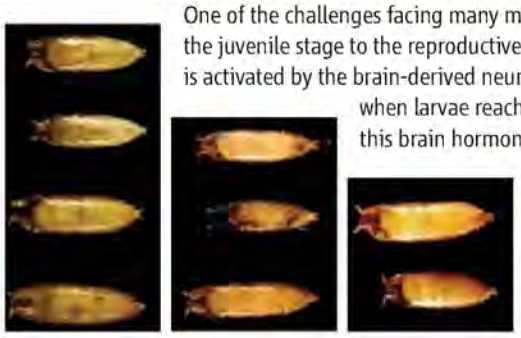

One of the challenges facing many multicellular organisms is when to change from the juvenile stage to the reproductively mature adult. In insects, this metamorphosis is activated by the brain-derived neuropeptide, prothoracicotropic hormone (PTTH), when larvae reach a characteristic weight. Almost a century after this brain hormone was discovered, **Rewitz *et al.*** (p. 1403) have identified the PTTH receptor and its signaling cascade. The PTTH receptor is Torso (a receptor tyrosine kinase that signals through Ras/Raf/Erk), which patterns the embryonic termini during early development in response to the distantly related PTTH factor, Trunk.

For the Love of Science

Which is a better predictor of a student's continued participation in science, facile understanding or personal interest? **Hulleman and Harackiewicz** (p. 1410) designed an experiment to find out what drives high-school students. First-year high-school students were asked either to write about what they had just learned or about how what they had just learned connected to some facet of their personal lives. Connections of personal relevance were stronger than good grades for predicting interest in further science courses and future science careers. This low-cost intervention seemed to have its largest effect on students who began the class with the least amount of confidence in their abilities.

Targeting DNA Gyrase

DNA gyrase, an enzyme that unwinds double-stranded DNA, is essential in bacteria, but missing in humans, and is thus an important antibiotic target. DNA gyrase is inhibited by the well-known fluoroquinolines and aminocoumarins antibiotics, as well as by symocyclinones—bifunctional antibiotics comprising an aminocoumarin and a polyketide group. Surprisingly, symocyclinones, unlike aminocoumarin inhibitors, do not inhibit DNA gyrase GTPase activity, but instead inhibit binding to DNA. Now **Edwards *et al.*** (p. 1415) use biochemical and structural studies to show that the two functional groups of the antibiotic bind in separate pockets on the gyrase. Each group is a relatively weak inhibitor that together potently inhibit DNA binding.

Coordinating Neuronal Assemblies

Theoretical models predict the existence of so-called hub neurons—highly connected cells that strongly influence the synchronization of spiking activity in a large group of neurons. However, experimental evidence for the existence of these neuronal hubs is lacking. **Bonifazi *et al.*** (p. 1419) used high-resolution, two-photon calcium imaging to measure spontaneous calcium fluctuations in hundreds of neurons simultaneously and determined the relative timing of these fluctuations. Examination of functional connectivity maps, based on temporal correlation measurements, revealed a subpopulation of GABAergic hub neurons displaying a remarkably widespread axonal arborization that orchestrated network synchrony in developing hippocampal networks. Spontaneous network synchronizations in developing hippocampus caused giant depolarizing potentials in individual neurons, and manipulating the spike activity in potential hub cells influenced network activity.

CREDITS: REWTIZ *ET AL.*

Celebrating 25 Years of Excellence...

AstraZeneca proudly announces the 25TH Annual Excellence in Chemistry Award Winners

Pictured from left are Peter Bernstein (Committee Co-Chair), Eric Jacobsen, Martin Burke, Christopher Chang, and Marc Chapdelaine (Committee Co-Chair)

2009 Awardees:

Professor Christopher Chang
University of California - Berkeley

Professor Martin Burke
The University of Illinois, Urbana-Champaign

Distinguished Lecturer:

Professor Eric Jacobsen
Harvard University (1993 AstraZeneca Excellence in Chemistry Awardee)

At AstraZeneca, we recognize that advances in medicine rely on innovations in chemistry. To reward outstanding contributions to the art of organic chemistry, the Excellence in Chemistry Award is presented annually to two talented academic researchers who have demonstrated distinct achievements in synthetic, mechanistic, or bioorganic chemistry. The existence of this Awards Symposium, now celebrating its 25th Anniversary, is a testament to AstraZeneca's commitment to support high-level academic research. This support leads to discoveries that further our understanding of diseases and new therapeutic approaches that ultimately benefit patients. In selecting these awardees, our senior scientists consult a world-leading chemist, who also serves as the distinguished lecturer.

With best wishes for continued innovation and excellence in chemical research, AstraZeneca congratulates this year's award winners.

AstraZeneca Excellence in Chemistry Award 2009

www.astrazeneca-us.com

AstraZeneca

Sir David King is director of the Smith School of Enterprise and the Environment, University of Oxford, UK, and the former Chief Scientific Adviser of the UK.

The Climate in Copenhagen

WITH JUST DAYS TO GO BEFORE THE UNITED NATIONS (UN) SUMMIT IN COPENHAGEN THAT IS supposed to define the world's strategy regarding climate change, the news seems unremittingly bad. The rumors speak of deadlock and little or no chance of reaching the crucial agreement that will enable us to avert climate catastrophe. Though this news has apparently taken many people by surprise, it is neither surprising nor necessarily disastrous. The worst possible outcome at Copenhagen would be a weak protocol that solves nothing. The best outcome would be an agreement to delay the final protocol for another year. By the time the parties to the UN's Framework Convention on Climate Change meet in Mexico in December 2010, we could finally be in a position to set up a protocol with the power to solve the worst crisis that humans have ever faced collectively.

Global warming is a global problem, and we need a solution that involves everybody—industrialized and developing countries alike. Anything else means that emissions will simply "leak" from the countries where CO_2 rules apply to those that are not part of the agreement. Kyoto offered a patched solution with its bureaucratic Clean Development Mechanism. British Premier Gordon Brown recently proposed the creation of a fund of some $100 billion per year to allow poorer countries to adapt and mitigate. But these solutions are clumsy and smack of reactive micromanagement.

The answer lies in a protocol that aspires to develop a fully global cap-and-trade scheme that puts a single high price on carbon's head. This would solve all the problems at a stroke. With CO_2 levels in the atmosphere now at 389 parts per million (ppm), rising at 2 ppm each year, the best we probably can aim for is an upper limit of around 450 ppm. To do that, we need to bring annual global emissions down from about 30 gigatons (Gt) of CO_2 today to 18 Gt by midcentury. Taking into account the predicted rise in population, that gives us an allowance of 2 tons of CO_2 per person per year.

Setting this value as a trading limit would allow each nation in the industrialized world to assign a straightforward downward trajectory that takes it from today's level to 2 tons per person per year by 2050. Rapidly developing countries such as China and India, which have relatively low levels of emissions per capita, could temporarily increase their emissions before these too would start to fall toward the magic figure of 2 tons. The world's poorest countries, which have per capita CO_2 emissions below the 2-ton limit and also are the ones that will be hardest hit by climate change, could benefit if included in this process, by selling their excess emission credits. This would produce cash to enable poorer countries to adapt to the ravages of climate change and provide an incentive for them to develop low-carbon technology, solving the problem of leakage. With the promise of carbon trading, no poorer country would choose to take on the high-carbon technologies that the rest of the world is abandoning. Rwanda's President Kagame, speaking for the African Union, recently gave support to this proposal.

To work this idea up to a fully functioning protocol will take time. It will also take leadership. The ponderous pace set by thousands of negotiators will never yield a meaningful protocol without action by visionary leaders prepared to take a long view of the world's future. Britain was the first to declare a unilateral target for reduced emissions, followed by the European Union. Now targets have been declared by Brazil, Japan, China, and, to some extent, India. At Copenhagen, I believe that many other heads of states will be encouraged to follow suit, including President Obama. However, this will just be the first step in the long haul toward Mexico 2010. It will not be easy, but if instead of restricting yet another trade to the developed world, we can apply cap and trade to the whole world, we could provide the basis for managing the problem of climate change once and for all.

– Sir David King

10.1126/science.1185072

Eppendorf Consumables – it's Your sample

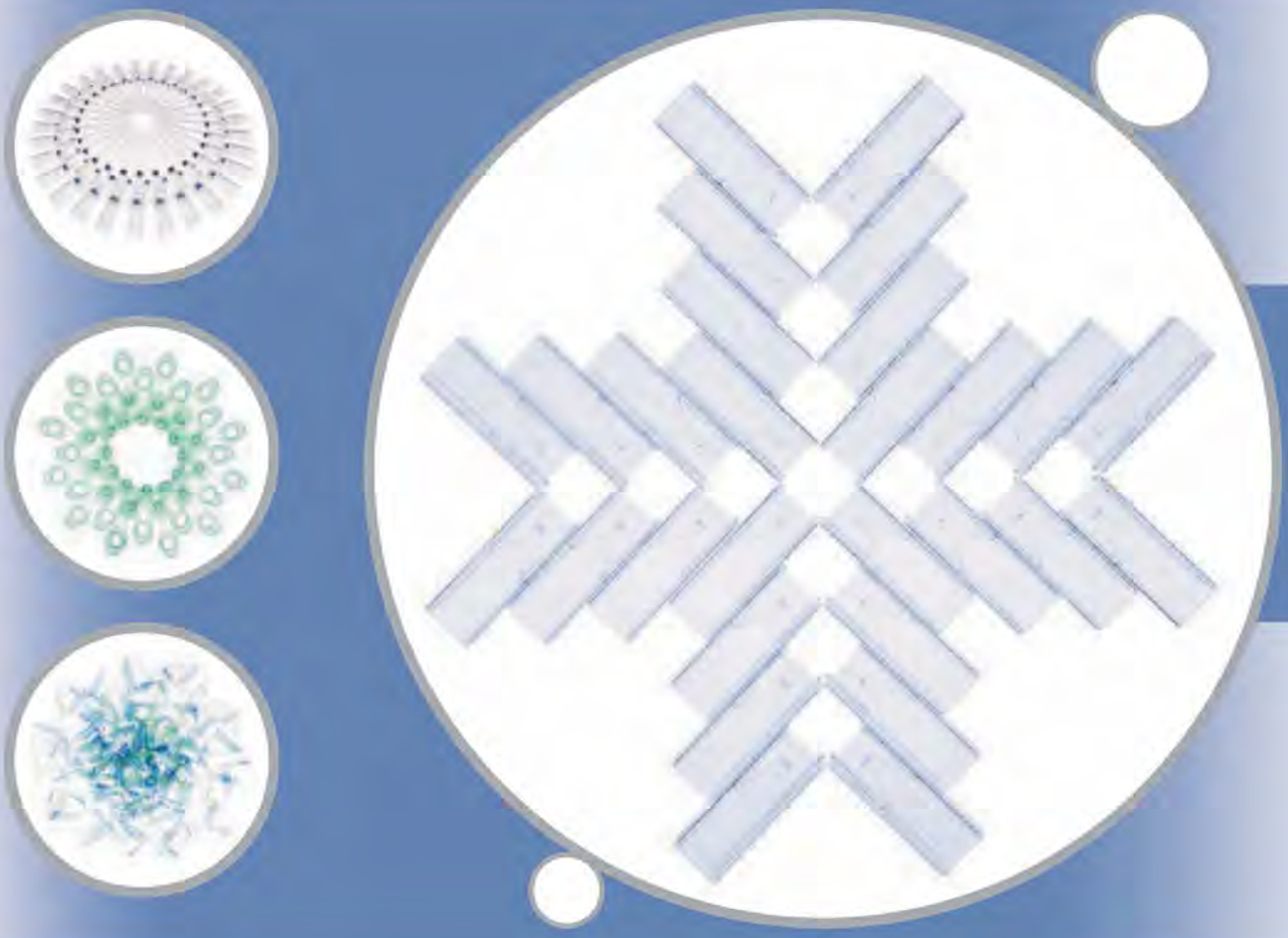

Make the best of it!

Top quality for your sample.

Each of your valuable samples deserves the best treatment. See for yourself how the Eppendorf disposable cuvette, the UVette®, will save time and reduce costs.

Imprecise results or sample contamination can be time consuming and expensive. Therefore, the close environment of each sample should be adapted to its specific quality and purity needs. This can involve a specific purity level or the absence of certain substances, but also stability, reliability, or geometry. The patented* Eppendorf UVette® is designed to cover all the specific needs of your samples for photometric measurements!

Eppendorf disposable UVette®

- UV- and VIS-transparent between 220 nm and 1,600 nm
- Two optical path lengths (2 mm and 10 mm)
- Tapered cuvette base for accurate filling
- Small sample volume ≥ 50 µl
- Certified PCR-clean and protein-free quality available
- Recovery of samples without the risk of degradation or contamination

Learn more about Eppendorf consumables:
www.eppendorf.com/consumables

*Covered by US patent 6,249,345

eppendorf

In touch with life

Your local distributor www.eppendorf.com/worldwide · **Application Support** E-Mail: support@eppendorf.com
Eppendorf AG · Hamburg · Germany · Tel: +49 40 538 01-0 · Eppendorf North America, Inc. · USA · Tel.: +1 800 645 3050

Filamentous bacteria.

IMMUNOLOGY

Microbial Influences

Our guts are colonized by trillions of commensal microbiota, whose influence on our immune systems is just beginning to be appreciated. Altered colonization has been associated with diseases such as allergy and inflammatory bowel disease, suggesting that commensals may play an important role in regulating immune system responses; to what extent, however, is not yet understood.

Gaboriau-Routhiau *et al.* have addressed this issue by comparing germ-free and normally colonized mice. They found that commensal microbiota were critical for maintaining T cell homeostasis in the gut. Germ-free mice exhibited altered gene expression profiles of cytokines and transcription factors that were associated with T helper cell–mediated immune responses. Recolonization with microbiota derived from mouse fecal matter restored normal expression patterns. Surprisingly, this effect was largely restricted to one strain of bacteria: the segmented filamentous bacteria (SFB). Similar findings were obtained by Ivanov *et al.*, who demonstrated the effects of SFB on interleukin 17–producing T helper cell responses. Thus, these results indicate that T cell immunity is regulated by both host- and microbiota-derived factors and that microbes may actively shape T cell populations in the gut. — KLM

Immunity **31**, 677 (2009); *Cell* **139**, 485 (2009).

BIOMEDICINE

How Antioxidants Might Help

Most studies of mammalian aging eventually lead to the mitochondrion, the energy-producing organelle. A prevailing hypothesis has been that damaging byproducts of mitochondrial respiration, called reactive oxygen species (ROS), accumulate as we age and cause mitochondrial dysfunction, which manifests at the organismal level as age-related disorders. Yet this hypothesis is at odds with growing evidence that an increase in the biogenesis of mitochondria can have beneficial anti-aging effects. Illustrating this dilemma are two studies of mice in which genetic manipulations altered mitochondrial function. For mice deficient in the proapoptotic protein Bak, Someya *et al.* found that mitochondria actively contribute to age-related hearing loss by mediating the death of cochlear cells in the ear. The death of these cells was triggered by oxidative stress and could be suppressed by antioxidants. Independently, Wenz *et al.* found that increased muscle expression of peroxisome proliferator–activated receptor-γ coactivator α (PGC-1α), a protein that up-regulates mitochondrial biogenesis, not only prevented age-associated loss of muscle mass, but also had beneficial effects on whole-body metabolism. Why the salutary effects of increased mitochondrial biogenesis are not counteracted by a parallel increase in damaging ROS remains unclear, but could involve increased turnover of the "older" ROS-damaged organelles. — PAK

Proc. Natl. Acad. Sci. U.S.A. **106**, 19432; 10.1073/pnas.0911570106 (2009).

CLIMATE SCIENCE

Holding the Line

Roughly one-third of all the CO_2 emitted by human activity is ultimately absorbed by the ocean, a process that has helped slow down the rate of increase of atmospheric CO_2 concentrations. As the ocean continues to absorb CO_2, however, the rate at which it does so is expected to decrease because of the changes in carbonate chemistry that CO_2 uptake causes. Global warming should then accelerate, a frightening prospect considering how quickly temperatures are rising already. Several studies have shown that the uptake of atmospheric CO_2 by some regions of the ocean has slowed already, but does that mean that the integrated world ocean has become a less effective CO_2 sink? Knorr combines data from ice cores, direct atmospheric measurements, and emission inventories to show that the global fraction of emitted CO_2 that remains in the atmosphere has stayed constant over the past 160 years, at least within the limits of uncertainty of the measurements. Khatiwala *et al.* also fail to detect a significant recent change in the fraction of CO_2 that the ocean is absorbing, in an examination of both ocean and terrestrial CO_2 sinks for the longer period of the past two and a half centuries. That is welcome news, but not reason to be complacent about the future, as sooner or later the capacity of the ocean to absorb CO_2 will be reduced. The real question is why we have not seen evidence of that reduction already. — HJS

Geophys. Res. Lett. **36**, L21710 (2009); *Nature* **462**, 346 (2009).

Continued on page 1323

CREDITS (LEFT, TOP AND BOTTOM): GABORIAU-ROUTHIAU *ET AL.*, *CELL* **139**, 485 (2009); (RIGHT) JUPITERIMAGES

Freedom of Expression

Assays and Panels for Human Targets of Your Choice

Now online: realtimeready.roche.com
Custom assay selection and custom panel configuration on the RealTime ready Configurator.

Function tested custom qPCR assays are now only a few clicks away with the new RealTime ready Configurator. Use this free online assay selection and shopping tool to order single assays or to configure your own custom panels on LightCycler® 480 Multiwell Plates.

- **Analyze your knockdown experiments or microarray results in the context of complex biological pathways or signaling cascades.**
- **Conveniently select assays and configure your custom panel with interactive pathway maps or pre-selected targets.**
- **Simply add cDNA and master mix to run these pre-plated, dried assays on your LightCycler® 480 Instrument.**

Rely on function tested qPCR assays based on proven Universal ProbeLibrary technology.

Visit ***www.realtimeready.roche.com*** to learn more or to start configuring your next assay.

Roche Diagnostics GmbH
Roche Applied Science
Werk Penzberg
82372 Penzberg, Germany

Roche

Continued from page 1321

CHEMISTRY

Photocharged by Graphene

Although the basal plane of graphite is relatively unreactive, the unusually high conductivity and zero band-gap of graphene (an isolated single layer of graphite) portend greater reactivity. Liu *et al.* examined the photoreactivity of benzoyl peroxide with a graphene sheet suspended in toluene. Laser excitation at several visible wavelengths led to the addition of phenyl groups to the graphene surface, and the rate of reaction increased with decreasing irradiation wavelength at the same total power. The reaction did not proceed thermally but could occur at very low laser power. The presence of air only led to unrelated photo-oxidation reactions. The authors argue that the reaction proceeds through a hot-electron mechanism, in which a surface-adsorbed benzoyl peroxide molecule accepts a photoelectron ejected from graphene into its lowest unoccupied orbital, and then decomposes into phenyl radicals. — PDS

J. Am. Chem. Soc. **131**, 10.1021/ja9043906 (2009).

ECOLOGY

Fly-by-Night Sex

Fig trees are totally dependent on species-specific fig wasps that carry pollen between trees. The wasps are weak nocturnal fliers and live for only 2 days at most, and neighboring trees flower asynchronously, so species survival (of both tree and wasp) depends entirely on successful transits.

By physical mapping and genetic fingerprinting, Ahmed *et al.* measured the gene flow in 79 fig trees along 250 km of the Ugab River in Namibia. Fruit was collected from individual trees and paternity was assigned to enable tracking of the insect pollinators; fig wasps were shown to move over distances as large as 160 km. Within this population, gene flow was predominantly unidirectional, suggesting that the insects were borne by the easterly winds. The authors conclude that the long-distance pollination of isolated individuals helps to maintain both the plant and insect populations and enables them to overcome the barrier effects of habitat fragmentation. — LMZ

CREDIT: AHMED *ET AL.*, *PROC. NATL. ACAD. SCI. U.S.A.* **106**, 10.1073/PNAS.0902213106 (2009)

Proc. Natl. Acad. Sci. U.S.A. **106**, 10.1073/pnas.0902213106 (2009).

CELL BIOLOGY

Stress Testing the ER

The antibody-producing cells of our immune system are able to secrete their own weight in antibodies each day. This prodigious feat relies on the endoplasmic reticulum (ER), which is a network of internal membranes in eukaryotic cells and which ensures that secreted proteins are folded and packaged correctly. Misfolded proteins are horrifically sticky and potentially harmful; luckily, the ER detects, via the unfolded protein response (UPR), when it is full up and boosts its handling capacity by, for example, increasing the expression of ER-resident chaperone proteins that untangle protein aggregates.

Schuck *et al.* find that a dramatic expansion of the area and volume of the ER during the UPR helps to alleviate the refolding bottleneck. The UPR drives ER expansion through increased synthesis of membrane lipids, which are incorporated into the peripheral ER. The shape of the ER enlargements, be they sheets or tubules, does not seem critical; rather, it is the increase in volume, which facilitates protein refolding and reduces the chance of aggregation, and the increase in surface area, which promotes membrane-associated degradation processes. — GR

J. Cell Biol. **187**, 525 (2009).

MATERIALS SCIENCE

Exploiting Evaporation

There are many approaches available to pattern soft materials such as colloidal films, but they often require multiple processing steps and allow deposition of only a few particle layers. A method called evaporative lithography overcomes these limitations, and Harris *et al.* now show that the method also enables the creation of patterns from binary mixtures of particles. Evaporative lithography exploits the fact that when aqueous and organic droplets dry, particles within the droplets are deposited in different patterns. Aqueous droplet evaporation leads to the familiar coffee-ring effect, whereas when nonaqueous droplets evaporate, most particles are deposited at the center. Use of a mask modulates the evaporative landscape of a drying droplet or film, resulting in pattern formation. The authors demonstrate generation of diverse patterns by tuning the mask design, mixture composition, and particle size ratio for an aqueous mixture of silica microspheres and sulphonated polystyrene nanoparticles. The method is simple and versatile and may be used to pattern colloidal, polymeric, and biomolecular species. — JFU

Philos. Trans. R. Soc. London Ser. A **367**, 5157 (2009).

www.sciencemag.org

Science

1200 New York Avenue, NW
Washington, DC 20005
Editorial: 202-326-6550, FAX 202-289-7562
News: 202-326-6581, FAX 202-371-9227
Bateman House, 82-88 Hills Road
Cambridge, UK CB2 1LQ
+44 (0) 1223 326500, FAX +44 (0) 1223 326501

SUBSCRIPTION SERVICES For change of address, missing issues, new orders and renewals, and payment questions: 866-434-AAAS (2227) or 202-326-6417, FAX 202-842-1065. Mailing addresses: AAAS, P.O. Box 96178, Washington, DC 20090-6178 or AAAS Member Services, 1200 New York Avenue, NW, Washington, DC 20005

INSTITUTIONAL SITE LICENSES please call 202-326-6755 for any questions or information

REPRINTS: Author Inquiries 800-635-7181
Commercial Inquiries 803-359-4578

PERMISSIONS 202-326-7074, FAX 202-682-0816

MEMBER BENEFITS AAAS/Barnes&Noble.com bookstore www.aaas.org/bn; AAAS Online Store www.apisource.com/aaas/ code MKB6; AAAS Travels: Betchart Expeditions 800-252-4910; Apple Store www.apple.com/eppstore/aaas; Bank of America MasterCard 1-800-833-6262 priority code FAA3YU; Cold Spring Harbor Laboratory Press Publications www.cshlpress.com/affiliates/aaas.htm; GEICO Auto Insurance www.geico.com/landingpage/go51.htm?logo=17624; Hertz 800-654-2200 CDP#343457; Office Depot https://bsd.officedepot.com/portalLogin.do; Seabury & Smith Life Insurance 800-424-9883; Subaru VIP Program 202-326-6417; VIP Moving Services www.vipmayflower.com/domestic/index.html; Other Benefits: AAAS Member Services 202-326-6417 or www.aaasmember.org.

science_editors@aaas.org	(for general editorial queries)
science_letters@aaas.org	(for queries about letters)
science_reviews@aaas.org	(for returning manuscript reviews)
science_bookrevs@aaas.org	(for book review queries)

Published by the American Association for the Advancement of Science (AAAS), *Science* serves its readers as a forum for the presentation and discussion of important issues related to the advancement of science, including the presentation of minority or conflicting points of view, rather than by publishing only material on which a consensus has been reached. Accordingly, all articles published in *Science*—including editorials, news and comment, and book reviews—are signed and reflect the individual views of the authors and not official points of view adopted by AAAS or the institutions with which the authors are affiliated.

AAAS was founded in 1848 and incorporated in 1874. Its mission is to advance science, engineering, and innovation throughout the world for the benefit of all people. The goals of the association are to: enhance communication among scientists, engineers, and the public; promote and defend the integrity of science and its use; strengthen support for the science and technology enterprise; provide a voice for science on societal issues; promote the responsible use of science in public policy; strengthen and diversify the science and technology workforce; foster education in science and technology for everyone; increase public engagement with science and technology; and advance international cooperation in science.

INFORMATION FOR AUTHORS
See pages 807 and 808 of the 6 February 2009 issue or access www.sciencemag.org/about/authors

EDITOR-IN-CHIEF **Bruce Alberts**
EXECUTIVE EDITOR **Monica M. Bradford**
NEWS EDITOR **Colin Norman**
MANAGING EDITOR, RESEARCH JOURNALS **Katrina L. Kelner**
DEPUTY EDITORS **R. Brooks Hanson, Barbara R. Jasny, Andrew M. Sugden**

EDITORIAL SENIOR EDITORS/COMMENTARY Lisa D. Chong, Brad Wible; SENIOR EDITORS Gilbert J. Chin, Pamela J. Hines, Paula A. Kiberstis (Boston), Marc S. Lavine (Toronto), Beverly A. Purnell, L. Bryan Ray, Guy Riddihough, H. Jesse Smith, Phillip D. Szuromi (Tennessee), Valda Vinson, Jake S. Yeston; ASSOCIATE EDITORS Kristen L. Mueller, Jelena Stajic, Nicholas S. Wigginton, Laura M. Zahn; RESEARCH ASSOCIATE Alexis Wynne Mogul; ONLINE EDITOR Stewart Wills; ASSOCIATE ONLINE EDITORS Robert Frederick, Tara S. Marathe; WEB CONTENT DEVELOPER Martyn Green; BOOK REVIEW EDITOR Sherman J. Suter; ASSOCIATE LETTERS EDITOR Jennifer Sills; EDITORIAL MANAGER Cara Tate; SENIOR COPY EDITORS Jeffrey E. Cook, Cynthia Howe, Harry Jach, Barbara P. Ordway, Trista Wagoner; COPY EDITORS Chris Filiatreau, Lauren Kmec; EDITORIAL COORDINATORS Carolyn Kyle, Beverly Shields; PUBLICATIONS ASSISTANTS Ramatoulaye Diop, Joi S. Granger, Jeffrey Hearn, Lisa Johnson, Scott Miller, Jerry Richardson, Jennifer A. Seibert, Brian White, Anita Wynn; EDITORIAL ASSISTANTS Emily Guise, Michael Hicks, Patricia M. Moore, Miriam Weinberg; EXECUTIVE ASSISTANT Sylvia S. Kihara; ADMINISTRATIVE SUPPORT Maryrose Madrid; EDITORIAL FELLOW Melissa R. McCartney

NEWS DEPUTY NEWS EDITORS Robert Coontz, Eliot Marshall, Jeffrey Mervis, Leslie Roberts; CONTRIBUTING EDITORS Elizabeth Culotta, Polly Shulman; NEWS WRITERS Yudhijit Bhattacharjee, Adrian Cho, Jennifer Couzin, David Grimm, Constance Holden, Jocelyn Kaiser, Sam Kean, Richard A. Kerr, Eli Kintisch, Andrew Lawler (New England), Greg Miller, Elizabeth Pennisi, Robert F. Service (Pacific NW), Erik Stokstad; INTERNS Michael Torrice, Jue Wang; CONTRIBUTING CORRESPONDENTS Jon Cohen (San Diego, CA), Daniel Ferber, Ann Gibbons, Robert Koenig, Mitch Leslie, Charles C. Mann, Virginia Morell, Gary Taubes; COPY EDITORS Linda B. Felaco, Melvin Gatling, Melissa Raimondi; ADMINISTRATIVE SUPPORT Scherraine Mack, Fannie Groom; BUREAUS New England: 207-549-7755; San Diego, CA: 760-942-3252, FAX 760-942-4979; Pacific Northwest: 503-963-1940

PRODUCTION DIRECTOR James Landry; SENIOR MANAGER Wendy K. Shank; ASSISTANT MANAGER Rebecca Doshi; SENIOR SPECIALISTS Steve Forrester, Chris Redwood; SPECIALIST Anthony Rosen; PREFLIGHT DIRECTOR David M. Tompkins; MANAGER Marcus Spiegler; SPECIALIST Jason Hillman

ART DIRECTOR Yael Kats; ASSOCIATE ART DIRECTOR Laura Creveling; SENIOR ILLUSTRATORS Chris Bickel, Katharine Sutliff; ILLUSTRATOR Yana Greenman; SENIOR ART ASSOCIATES Holly Bishop, Preston Huey, Nayomi Kevitiyagala; ART ASSOCIATES Jessica Newfield, Matthew Twombly; PHOTO EDITOR Leslie Blizard

SCIENCE INTERNATIONAL

EUROPE (science@science-int.co.uk) EDITORIAL: INTERNATIONAL MANAGING EDITOR Andrew M. Sugden; SENIOR EDITOR/COMMENTARY Julia Fahrenkamp-Uppenbrink; SENIOR EDITORS Caroline Ash, Stella M. Hurtley, Ian S. Osborne, Peter Stern; ASSOCIATE EDITOR Maria Cruz; LOCUM EDITOR Helen Pickersgill; EDITORIAL SUPPORT Deborah Dennison, Rachel Roberts, Alice Whaley; ADMINISTRATIVE SUPPORT John Cannell, Janet Clements, Louise Moore; NEWS: EUROPE NEWS EDITOR John Travis; DEPUTY NEWS EDITOR Daniel Clery; CONTRIBUTING CORRESPONDENTS Michael Balter (Paris), John Bohannon (Vienna), Martin Enserink (Amsterdam and Paris), Gretchen Vogel (Berlin)

LATIN AMERICA CONTRIBUTING CORRESPONDENT Antonio Regalado

ASIA Japan Office: Asca Corporation, Tomoko Furusawa, Rustic Bldg. 7F, 77 Tenjin-cho, Shinjuku-ku, Tokyo 162-0808, Japan; +81 3 6802 4616, FAX +81 3 6802 4615, inquiry@sciencemag.jp; ASIA NEWS EDITOR Richard Stone (Beijing: rstone@aaas.org); CONTRIBUTING CORRESPONDENTS Dennis Normile [Japan: +81 (0) 3 3391 0630, FAX +81 (0) 3 5936 3531; dnormile@gol.com]; Hao Xin [China: +86 (0) 10 6307 4439 or 6307 3676, FAX +86 (0) 10 6307 4358; cindyhao@gmail.com]; Pallava Bagla [South Asia: +91 (0) 11 2271 2896; pbagla@vsnl.com]

EXECUTIVE PUBLISHER **Alan I. Leshner**
PUBLISHER **Beth Rosner**

FULFILLMENT SYSTEMS AND OPERATIONS (membership@aaas.org); DIRECTOR Waylon Butler; SENIOR SYSTEMS ANALYST Nomuna Nyamaa; CUSTOMER SERVICE SUPERVISOR Pat Butler; SPECIALISTS Latoya Casteel, LaVonda Crawford, Vicki Linton, April Marshall; DATA ENTRY SUPERVISOR Cynthia Johnson; SPECIALISTS Shirlene Hall, Tarrika Hill, William Jones

BUSINESS OPERATIONS AND ADMINISTRATION DIRECTOR Deborah Rivera-Wienhold; ASSISTANT DIRECTOR, BUSINESS OPERATIONS Randy Yi; MANAGER, BUSINESS ANALYSIS Eric Knott; MANAGER, BUSINESS OPERATIONS Jessica Tierney; FINANCIAL ANALYSTS Priti Pamnani, Celeste Troxler; RIGHTS AND PERMISSIONS: ADMINISTRATOR Emilie David; ASSOCIATE Elizabeth Sandler; MARKETING DIRECTOR Ian King; MARKETING MANAGERS Allison Pritchard, Alison Chandler, Julianne Wielga; MARKETING ASSOCIATES Aimee Aponte, Mary Ellen Crowley, Adrian Parham, Wendy Wise; MARKETING EXECUTIVE Jennifer Reeves; DIRECTOR, SITE LICENSING Tom Ryan; DIRECTOR, CORPORATE RELATIONS Eileen Bernadette Moran; PUBLISHER RELATIONS, eRESOURCES SPECIALIST Kiki Forsythe; SENIOR PUBLISHER RELATIONS SPECIALIST Catherine Holland; PUBLISHER RELATIONS, EAST COAST Phillip Smith; PUBLISHER RELATIONS, WEST COAST Philip Tsolakidis; FULFILLMENT SUPERVISOR Iquo Edim; FULFILLMENT COORDINATOR Carrie MacDonald; MARKETING MANAGER Christina Schlecht; MARKETING ASSOCIATE Mary Lagnaoui; ELECTRONIC MEDIA: MANAGER Lizabeth Harman; PROJECT MANAGER Trista Snyder; ASSISTANT MANAGER Lisa Stanford; SENIOR PRODUCTION SPECIALISTS Ryan Atkins, Christopher Coleman, Walter Jones; PRODUCTION SPECIALISTS Nichele Johnston, Kimberly Oster DIRECTOR, WEB AND NEW MEDIA Will Collins

ADVERTISING DIRECTOR, WORLDWIDE AD SALES Bill Moran
COMMERCIAL EDITOR Sean Sanders: 202-326-6430
PROJECT DIRECTOR, OUTREACH Brianna Blaser

PRODUCT (science_advertising@aaas.org); MIDWEST/WEST COAST/W. CANADA Rick Bongiovanni: 330-405-7080, FAX 330-405-7081; EAST COAST/E. CANADA Laurie Faraday: 508-747-9395, FAX 617-507-8189; UK/EUROPE/ASIA Roger Goncalves: TEL/FAX +41 43 243 1358; JAPAN ASCA Corporation, Nanako Ide +81 (0) 3 6802 4616, FAX +81 (0) 3 6802 4615; ads@sciencemag.jp; SENIOR TRAFFIC ASSOCIATE Deiandra Simms

WORLDWIDE ASSOCIATE DIRECTOR OF *SCIENCE* CAREERS Tracy Holmes: +44 (0) 1223 326525, FAX +44 (0) 1223 326532

CLASSIFIED (advertise@sciencecareers.org); U.S.: SALES MANAGER Daryl Anderson: 202-326-6543; MIDWEST Tina Burks: 202-326-6577; EAST COAST Alexis Fleming: 202-326-6578; WEST/SOUTH CENTRAL Nicholas Hintibidze: 202-326-6533; SALES COORDINATORS Rohan Edmonson, Shirley Young; SALES Susanne Kharraz, Dan Pennington, Alex Palmer; SALES ASSISTANT Lisa Patterson; JAPAN ASCA Corporation, Jie Chin +81 (0) 3 6802 4616, FAX +81 (0) 3 6802 4615; careerads@sciencemag.jp; ADVERTISING SUPPORT MANAGER Karen Foote: 202-326-6740; ADVERTISING PRODUCTION OPERATIONS MANAGER Deborah Tompkins; SENIOR PRODUCTION SPECIALIST/GRAPHIC DESIGNER Amy Hardcastle; SENIOR PRODUCTION SPECIALIST Robert Buck; SENIOR TRAFFIC ASSOCIATE Christine Hall

PCR Products

Switch to Superior High Fidelity PCR

PrimeSTAR®

Top Five Reasons to Switch to PrimeSTAR®:

- **Higher Accuracy:** A strong exonuclease activity results in an extremely low error rate, with only 15 errors per 480,000 bp on a GC-rich template.
- **Higher Efficiency:** Higher than *Taq* Polymerase.
- **Robust Amplifications:** A single PCR cycling protocol can be used to amplify products of varying sizes.
- **Greater Specificity:** The antibody mediated Hot Start formulation prevents false initiation events during reaction assembly.
- **Excellent with GC-Rich Targets:** Robust performance with GC-rich templates using the GC buffer formulation.

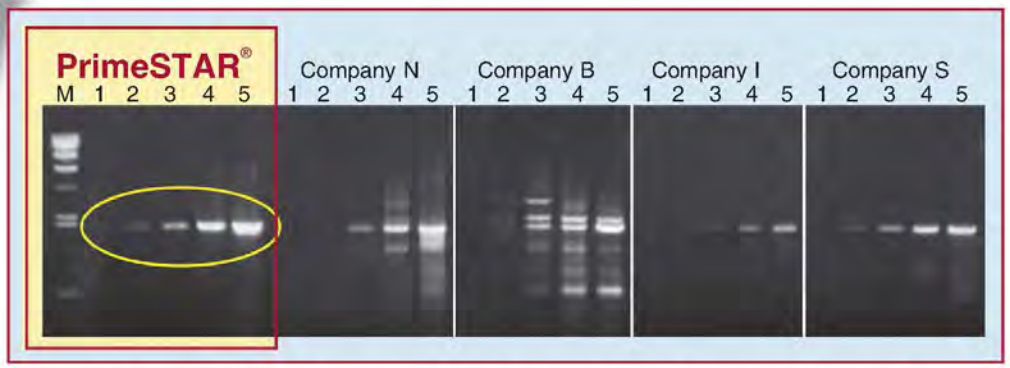

Amplification Efficiency of a 2 kb Human Genomic DNA Fragment (DCLRE1A). Excellent sensitivity and yield are observed when amplifying with PrimeSTAR®. Quantities: Lane1: 0 ng (dH_2O), Lane 2: 100 pg, Lane 3: 1 ng, Lane 4: 10 ng, Lane 5: 100 ng.

TaKaRa

For more information
www.takara-bio.com

Japan:
Takara Bio Inc.
+81 77 543 7247
www.takara-bio.com

USA:
Takara Bio USA
A Division of Clontech Laboratories, Inc
888-251-6618
www.takarabiousa.com

Europe:
Takara Bio Europe S.A.S.
+33 1 3904 6880
www.takara-bio.eu

China:
Takara Biotechnology (Dalian) Co., Ltd.
+86 411 8764 1681
www.takara.com.cn

Korea:
Takara Korea Biomedical Inc.
+82 2 2081 2525
www.takara.co.kr

Give and Ye Shall Receive

Give *Science* with full AAAS benefits. Get our special gift rate and our new shirt!

$99 Professional gift rate
(reg. $146)

$50 Postdoc/Student gift rate
(reg. $99/$75)

Make the holidays happier for a promising young researcher, family member, friend, or student. *Science* is the gift that lasts all year—and includes all the benefits of membership in AAAS.

Get our new "Explain Your Research" shirt—FREE! With its playful graphics, it makes just the right fashion statement at holiday gatherings, and other social events all year long.

You'll enjoy something else as well: the satisfaction of helping to support AAAS and our international, public policy, and educational programs—the ones that advance science and serve society. Happy holidays, indeed!

A $22.50 value—yours FREE when you give *Science!*

AAAS + U = Δ

Detail on back

Order now: visit promo.aaas.org/explain or call 866-434-2227.

Please order at least two weeks before the holiday you're celebrating, so we have time to send your gift recipient a letter announcing your gift. Non-U.S. recipients may receive *Science* Digital edition at the special gift rate. Check online for print edition rates. $74 allocated to *Science* for Professional memberships, $50 for Postdoc/Student memberships. Please allow 4 weeks for receipt of first issue. Prices valid through 1/31/10.

Science
AAAS

Where Did All The Food Go?

After the biggest meal of the year, Americans might reflect on the fate of those moldering Thanksgiving leftovers.

Here's a data point to start with: At least one-third of the United States food supply goes to waste, according to researchers at the National Institutes of Health.

Usually, waste is estimated through consumer interviews or garbage inspections. Physiologist Kevin Hall and mathematician Carson Chow of the National Institute of Diabetes and Digestive and Kidney Diseases tried another approach: modeling metabolism. They estimated how much American adults eat per capita (2300 calories) from their average weight (80 kg), then compared the figure with the food available for U.S. consumers, as reported to the Food and Agriculture Organization of the United Nations.

The difference between calories produced and consumed, they say, is food wasted. That was about 900 calories a day in 1974, rising to 1400 by 2003—up to 40% of the food supply and far more than the U.S. Department of Agriculture's estimate of just over 25%. "We called it the missing mass of American food," Chow says.

The researchers, reporting in November in *PLoS ONE*, hope to expand their analysis to other countries, including Japan, which has the reputation of being more frugal.

Treasure Map

More than peace hinges on Israeli-Palestinian border talks; the fate of the Holy Land's archaeological heritage is at stake, too. Now negotiators at least know where that heritage lies. About 7000 archaeological sites, some kept secret for decades by the Israeli military, are revealed in an online map at http://digitallibrary.usc.edu/wbarc.

The data, covering many West Bank sites that critics say Israelis excavated in violation of international law, were released in response to a lawsuit by Israeli archaeologists (*Science*, 18 April 2008, p. 302). "The scale of work conducted in the West Bank during the occupation"—15% of the sites on the map—"is now transparent," says David Ilan, director of the Nelson Glueck School of Biblical Archaeology in Jerusalem. Sites particularly important to Israel include Battir, "sort of a Custer's Last Stand place, where a great rebellion against Rome was crushed," says Lynn Dodd, an archaeologist at the University of Southern California in Los Angeles. "This map will probably make people focus on the fact that [such] sites may pass out of [Israel's] control" unless Israel negotiates for them.

The map is designed to inform peace talks, but many archaeologists are keen to use it. "Because it includes a range of other data, like occupation periods, site type, and finds, the map is also an excellent research tool," says Ran Boytner, an archaeologist at the University of California, Los Angeles.

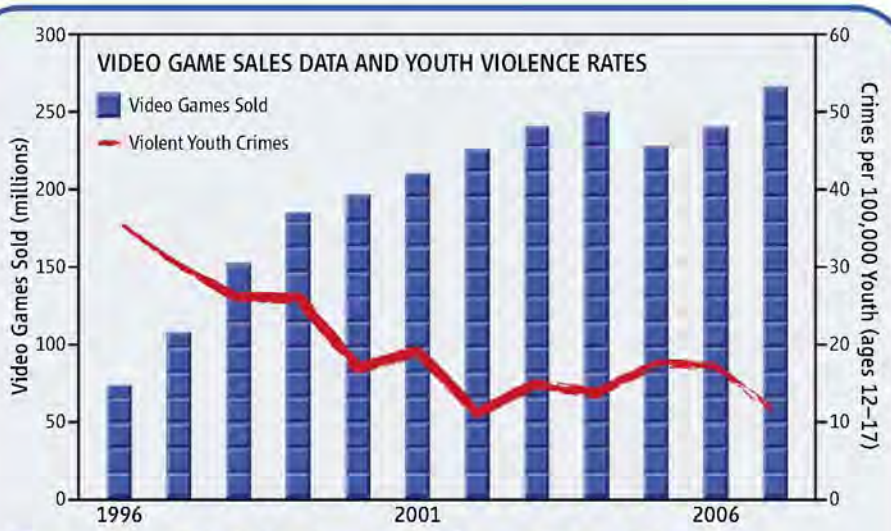

Doom Didn't Make Me Do It

Oceans of studies—laboratory, longitudinal, and brain-imaging—haven't settled the question of whether violent TV programs and video games cause people to be violent. Now Christopher Ferguson, a psychologist at Texas A&M International University in Laredo, has weighed in with a graph showing that as video game sales have soared, youth violence has declined. Ferguson contends that lab-based experiments on "aggression" bear little relationship to actual violence. Psychologist L. Rowell Huesmann of the University of Michigan, Ann Arbor, says the graph is a "red herring" and that early viewing of violence has repeatedly been shown to influence later behavior.

Infant Fossil

A living baby coelacanth was captured on video, probably for the first time anywhere, by Japanese researchers off Indonesia in early October. Known as "living fossils," coelacanths plied the Devonian waters 365 million years ago. With their lobe-shaped, limblike fins, they are seen as close evolutionary kin to four-limbed land animals. Scientists thought that they had gone extinct with the dinosaurs until a coelacanth was netted off South Africa in 1938. In the past decade, several have been spotted off Indonesia and the east coast of Africa.

This baby was found swimming in deep water off Sulawesi Island by researchers from Aquamarine Fukushima, a sea museum in Iwaki, northeast of Tokyo. It was about 31.5 centimeters long, as scaled by laser beams flashed from a remotely operated vehicle. It will grow to about 150 centimeters, judging by the six adults the team has spotted over the past 4 years.

SOURCES: THE NPD GROUP INC./RETAIL TRACKING SERVICE; CHILDSTATS.GOV; CREDITS (TOP TO BOTTOM): AQUAMARINE FUKUSHIMA; COURTESY OF USC DIGITIAL LIBRARY

Indications of a deep plume under Hawaii
1330

The future of evolution
1334

AGRICULTURAL RESEARCH

International Centers and Donors Warily Eye Sweeping Changes

The Consultative Group on International Agricultural Research (CGIAR) is facing what could be the biggest shakeup in its 38-year history as members meeting in Washington, D.C., on 7 and 8 December vote on far-reaching reforms. The delegates—representing donors, countries, international foundations, and development organizations—will likely vote to convert CGIAR from a voluntary association into a legal entity with power over a trust fund so it can enforce systemwide priorities. But the success of the venture hinges on deciding how to set and evaluate the research agenda without simply adding a layer of bureaucracy to the system.

"There is still a lot of work to do on these changes," says Elizabeth Woods, an agricultural economist with the Queensland government in Brisbane, Australia, who chairs the board of the International Rice Research Institute (IRRI) in Los Baños, Philippines.

Dealing with the CGIAR centers "was getting more and more complicated" for donors, says Jonathan Wadsworth, an adviser at the United Kingdom's Department for International Development, one of the major supporters. Although a CGIAR science council set priorities, centers could ignore them, Wadsworth says. So donors increasingly funded specific projects. Such tied funding grew from about 30% of total CGIAR funding a decade ago to about 70% now. And no one is happy. Wadsworth says donors evaluate programs and sometimes meddle in center management, tasks for which they are ill-suited. Center scientists have been spending more time accounting for hundreds of small projects. "We are torn in 64 different directions by different donors and their agendas," says Carlos Seré, director of the International Livestock Research Institute in Nairobi. And with core funding shrinking, center directors find it hard to plan for the long term. "It is extraordinarily difficult to accumulate the amounts needed for infrastructure investment," says Woods.

Several formal studies led to an action plan, says CGIAR Director Ren Wang. If approved, CGIAR will become a legal entity with two parts: a consortium representing the centers and a fund to bring the donors together. The intent "is to agree on roles for the funders and roles for the doers," says Shey Tata, CGIAR's lead financial officer. The consortium will be governed by a board, likely comprising scientists and development experts, and the fund will be run by donors. The consortium and the fund will together decide on a so-called strategy and results framework, which will set research objectives through a number of megaprograms expected to involve multiple centers. Two of the seven megaprograms are "genomics and global food crop improvements" and "agriculture, nutrition, and health."

Getting old. Shrinking core funding has crimped facility investment at the International Rice Research Institute in the Philippines.

The restructuring could create efficiencies. "Instead of 15 centers negotiating with 65 donors, it will boil down to much higher-level but reduced interactions between one big consortium and one pooled source of funds," Wadsworth says. Wang says donors have indicated that they will rely on standardized program evaluations by the consortium, reducing reporting requirements for numerous small research projects. Sharing procurement, human resources, and other services could save up to $130 million a year, Wang says.

Center directors and board members generally support reform. "Anything that makes [CGIAR] nimbler, more efficient, and able to respond with the best science to the serious food security problems facing the world would be welcome," says Robert Zeigler, director general of IRRI. And donors are embracing the idea. The United Kingdom intends to at least double contributions to CGIAR to £40 million annually by 2014, depending on the progress of reforms, Wadsworth says. Wang says Australia, the Netherlands, the United States, and Switzerland have all pledged to increase funding significantly. He says the target is an annual income of $1 billion by 2013, roughly double the 2008 figure.

The sticking point is the strategy and results framework and its megaprograms. "The process went ahead too hastily without [sufficient] consultation with researchers," says Ryotaro Suzuki, director of international research at Japan's Ministry of Agriculture. Wang agrees that the megaprograms are more thematic than specific. At the same time, the framework envisions precisely measuring results from each project, such as percentage increases in productivity and the number of people lifted out of poverty. "We can't be accountable for things beyond our control," says Seré. He is also concerned that the programs focus on cereals and slight the vegetable crops and livestock that generate income for small holders and food for local communities. These areas "are much less addressed by public investment," he says. Woods worries that the cost of another administrative layer, at least during a multiyear transition period, could swallow a lot of the rising contributions.

But the upside could be greater impacts, says William Dar, director general of the International Crops Research Institute for the Semi-Arid Tropics in Patancheru, India. If, after 5 years, there is more long-term support for agricultural research with the majority in unrestricted core funding, "I will give a very positive verdict on this reform process," he says. **–DENNIS NORMILE**

CREDIT: IRRI

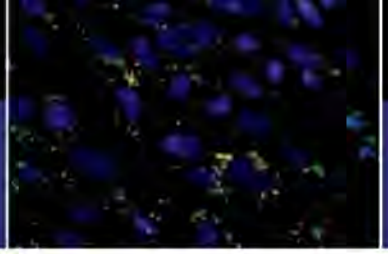

Expanded roles for prionlike proteins?

1337

Pollock fishery in trouble

1340

SCIENCE AND SOCIETY

Stolen E-mails Turn Up Heat on Climate Change Rhetoric

The theft and unauthorized release last month of 1000 private e-mail messages from the servers of the Climatic Research Unit (CRU) at the University of East Anglia in the United Kingdom has provided a glimpse into the fractious world of climate science. The public airing of frank conversations among powerful scientists about sensitive topics such as possible holes in their data and the use of contrarian papers in major reports comes at a pivotal time for climate science, just days before a meeting of world leaders in Copenhagen.

The messages—whether hacked or released by a disgruntled insider—have raised thorny questions about the proper behavior of researchers who feel under siege for their science. How willing should they be to share their raw data with their staunchest critics? "It's very difficult to admit that your data are not as strong as you wish it were, especially if you know that will be used against you," says Nicholas Steneck, an expert on research integrity at the University of Michigan, Ann Arbor. And yet the "circle the wagons" mentality conveyed in numerous messages could inflict lasting "damage to the public credibility of climate research," warns climate scientist Judith Curry of the Georgia Institute of Technology in Atlanta.

In limbo. CRU's Jones has stepped down as director while a review is under way.

But openness just leads to twisted interpretations, says NASA climate researcher Gavin Schmidt. "You can't have a spelling mistake in a paper without it being evidence on the floor of the Senate that the system is corrupt," says Schmidt.

Four e-mail exchanges have received most of the media attention. The first regards a research finding considered by most scientists as a canonical fact: that the globe warmed by roughly 0.7°C in the 20th century. That fact derives in large part from global temperature data recorded by stations on land and sea, as analyzed independently by groups at East Anglia, NASA, and the U.S. National Oceanic and Atmospheric Administration.

Referring to requests for climate data from critics, CRU Director Phil Jones wrote in 2005 that "I think I'll delete the file rather than send to anyone." In May 2009, Jones told Michael Mann of Pennsylvania State University, University Park, to "delete any emails" to a colleague about their work on the Intergovernmental Panel on Climate Change (IPCC) report and to ask a third colleague to do the same. (Mann says he conveyed the message but deleted no messages himself.) Through a spokesperson, Jones declined an interview request. But in a statement he said that "no record" has been deleted amid a bombardment of "Freedom of Information requests." CRU acknowledged in August that it deleted old data on digital tapes to make space for a move.

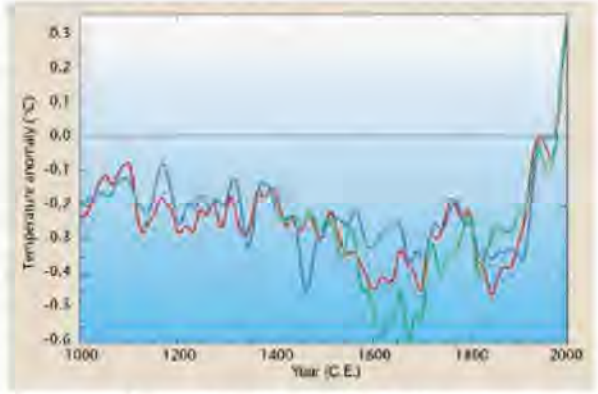

Ever upward? One pilfered e-mail described how climate scientists decided to graft measured temperatures after 1960 onto earlier data from proxies to "hide" a decline in the proxy data.

A second message relates to a chapter in the 2007 IPCC report that Jones edited. In 2004, he suggested that two recent papers on temperature trends didn't deserve to be published in a peer-reviewed journal. "I can't see either of these papers being in the next IPCC report," he wrote Mann. "Kevin [Trenberth] and I will keep them out somehow - even if we have to redefine what the peer-review literature is." But Trenberth, of the National Center for Atmospheric Research in Boulder, Colorado, says the papers were indeed considered. Thomas Karl, director of the National Climatic Data Center in Asheville, North Carolina, an official reviewer for the chapter, says the IPCC's peer-review procedures "were sacrosanct." Both papers wound up being cited.

A third message is viewed by critics as an acknowledgement that global warming has ceased. "The fact is that we can't account for the lack of warming at the moment and it is a travesty that we can't," wrote Trenberth in October. Contrarians have noted the lack of record new highs in global temperature since 1998 (*Science*, 2 October, p. 28). But Trenberth was actually bemoaning something else. "The observing system we have is inadequate for tracking energy flow through the climate system," he observed, affecting the forecasting of year-to-year climate changes.

A fourth message, about assembling a diagram for a 1999 World Meteorological Organization report, has been misinterpreted, says Trenberth (see graphic). Scientists believe proxy data such as tree rings are valuable for reconstructing past climates, but certain tree-ring data became unreliable midway through the century. So scientists used proxy data for all but the final 40 years of the millennium before switching to instrumental data in 1961. "Reasonable people," writes Stephen McIntyre, a retired industry consultant and prominent blogger, might conclude that the decision not to show the divergence of the two data sets was "simply a trick" to avoid giving fuel to skeptics.

Whatever their meaning, the messages have emboldened opponents. Some are calling for congressional hearings and, possibly, lawsuits. Penn State says that it is "looking into" the matter, and the University of East Anglia has announced an investigation into the theft and contents of the e-mails.

Scientists know they will need every bit of credibility to defend their findings from future attacks. But Curry suggests that it would be better to bring the skeptics into the fold than to keep them out. That way, she says, the critics will "quickly run out of steam and become irrelevant."

–ELI KINTISCH

SOURCE: UNIVERSITY OF EAST ANGLIA

MANTLE DYNAMICS

Sea-Floor Study Gives Plumes From the Deep Mantle a Boost

Earth's interior is like a pot of boiling water—very viscous, very slowly churning water. The great debate about how Earth's interior operates to shed internal heat and shape the surface began with disagreements over whether two layers in the pot—the upper and lower mantle—always remain separate, like oil and water.

That debate ended when seismologists imaged Earth's cold, brittle surface scum, the tectonic plates, and saw some of them diving all the way into the lower mantle. For the past decade, geoscientists have been focusing on the opposite question: whether plumes of hot, buoyant rock from the lower mantle are rising to the surface to fuel volcanic hot spots.

On page 1388, eight researchers weigh in with the most detailed seismic imaging yet beneath the world's most iconic hot spot, the island of Hawaii. "I do think it's a strong case" for a deep plume, says lead author Cecily Wolfe of the University of Hawaii, Manoa. Most in the often-contentious field of seismic imaging don't go quite so far. But the quality of the data and the apparent Hawaiian plume's resemblance to theorists' expectations has won some cautious support for the work. "They're doing their best. It looks promising," says seismologist Barbara Romanowicz of the University of California, Berkeley. But the question of deep plumes "is still a little open," she says.

To gather information about the mantle beneath Hawaii, researchers had to cast a wide net. Seismologists image mantle features by compiling records of seismic waves that have passed from an earthquake source through the feature of interest and on to a seismometer. Warmer-than-average rock slows a wave down; colder rock speeds it up. Seismic tomographers imaging the mantle combine wave travel times in much the way radiologists combine x-rays to create computed tomography scans of the human body. In one tomographic study, seismologists imaging the whole mantle reported seeing a couple of dozen deep plumes scattered around the globe (*Science*, 22 September 2006, p. 1726).

Geoscientists have long recognized that a single hot spot of persistent volcanic activity created the Hawaiian island chain as the Pacific plate moved over the hot spot. But tomographers trying to see how deep-seated the hot spot's source is face a special challenge: Because of the remoteness of large earthquakes around the Pacific's Ring of Fire, seismometers on the Hawaiian Islands receive few seismic waves that would have passed through any deep plume. So researchers in the Hawaiian Plume-Lithosphere Undersea Melt Experiment (PLUME) stepped away from their subject. Deploying 10 conventional seismometers on the Hawaiian Islands and ocean-bottom seismometers at another 73 sites in waters as much as 5500 meters deep, the team created a seismic "eye" centered on the island of Hawaii and 1000 kilometers across. The network could pick up both seismic shear waves (S waves) that had passed through the upper mantle beneath Hawaii and—vital to imaging any deep plume—SKS waves that had passed upward from Earth's core.

The PLUME images, the authors write, "suggest that the Hawaiian hotspot is the result of an upwelling, high-temperature plume from the lower mantle." They show a hotter-than-average column of rock extending downward at least 1500 kilometers, topped by a "pancake" of hot rock where a plume would spread outward after hitting the cold, rigid tectonic plate. There's also a parabola-shaped feature of high-wave-speed material where computer models of plume behavior show a curtain of cold, descending rock. The plume's inferred temperature of 300°C above its surroundings at 900 kilometers' depth fits expectations. And, perhaps most telling, the apparent plume tilts downward toward the southeast—the way computer models show the churning mantle "blowing" a plume, like smoke rising from a chimney.

Reaction to the PLUME imaging is varied. "The tomography is pretty good," says marine geophysicist and regional tomographer Donald Forsyth of Brown University. "It's not an absolute slam dunk, [but] I'm fairly convinced there's an anomaly [in seismic velocities] going down on the order of 1500 kilometers, though it's hard to say if it's continuous."

Tomographer Jeannot Trampert of the University of Utrecht, the Netherlands, is more skeptical. The signature of a deep plume "is so weak it's hard to say" if it's real, he says. He suspects that the apparent plume may be just an echo of some nearby deep-mantle feature that lies just outside the tunnel view of PLUME.

The obvious candidate for a plume imposter is the edge of the nearby Pacific "large low-shear-wave-velocity province," more familiarly called a superpile. To test that possibility, Wolfe and colleagues reconstructed their deep-plume signal under the assumption that it was created entirely by the superpile in the nearby lowermost mantle. If the superpile were entirely responsible, the resulting image should resemble the edge of a superpile. "To me, it doesn't look like the proposed superpile," says Wolfe. "It looks like a doughnut."

The superpile could still be the source, the researchers write, but a deep plume "remains a more straightforward solution." Trampert remains unconvinced. "They do not address it in a satisfactory way," he says. Everyone does agree that the PLUME observations remain to be fully mined for information on any plume, and that global data might be profitably merged with the regional data. But just where or when the slam-dunk evidence might emerge is anyone's guess.

–RICHARD A. KERR

Lotta hot spot. The island of Hawaii—150 kilometers across and rising 10,203 meters from the sea floor—has been built from volcanic outpourings (dark flows) that may have risen from more than 1500 kilometers down.

CREDIT: COURTESY OF THE HAWAII SYNERGY PROJECT OF THE HAWAII INSTITUTE OF GEOPHYSICS AND PLANETOLOGY, UNIVERSITY OF HAWAII, MANOA

SCIENCE POLICY

European Union Selects Unknown For Top Science Post

The two women tapped to head the European Union's efforts on science and climate over the next 5 years have a lot in common. Both were elected to parliament in their mid-20s—one in Denmark and the other in Ireland—but left politics later on. Both wrote for national newspapers and had stints in television broadcasting. Both are described as strong-willed and smart.

The difference is that one is virtually unknown to scientists and science policymakers, and the other is almost an international celebrity. Danish energy and climate minister Connie Hedegaard, nominated last week to become the first European commissioner for climate action, was picked as one of the world's 100 most influential people by *Time* magazine in April and this month will host the Copenhagen climate talks. In contrast, Máire Geoghegan-Quinn, the proposed new commissioner for research and innovation, has spent the past 9 years examining the E.U.'s finances as the Irish representative of the less-than-glamorous Court of Auditors in Luxembourg.

Brussels-bound. Nominated to lead Europe's research and climate programs are Máire Geoghegan-Quinn (*top*) and Connie Hedegaard.

The nominations, announced on 27 November by European Commission President José Manuel Barroso, are the outcome of delicate backroom talks in which E.U. member states jockey for posts in Brussels. The entire slate of 27 proposed commissioners—one from each country—is subject to hearings and a vote by the European Parliament, scheduled for 26 January.

Before being nominated as the boss of E.U. science, Geoghegan-Quinn, 59, held various posts in the Irish government, including minister of state for European affairs between 1987 and 1991. She left politics in 1997 and joined the Court of Auditors 3 years later. Several European science leaders *Science* contacted said they could not comment on her nomination simply because they had never heard of her.

Frank Gannon, director-general of the Science Foundation Ireland and a former head of the European Molecular Biology Organization, does know, and admires, Geoghegan-Quinn—he once lived across the road from her in Galway. She's an "intelligent and straightforward person," he says. "I think she will bring a lot of qualities to the job." Gannon points out that Janez Potočnik, the Slovenian economist who currently holds the post, was new to science as well in 2004 and "was an excellent commissioner."

Despite her lack of science-policy experience, Geoghegan-Quinn may have a head start on important decisions regarding Framework Programme 8 (FP8), the next of Europe's gargantuan research funding programs, which is slated to start in 2014. The Court of Auditors, Geoghegan-Quinn's former outpost, said in a highly critical report in October that FP6, which ran from 2002 through 2006, failed to meet some of its key objectives; for instance, large international networks funded to foster innovation and collaboration often fell apart after funding dried up, the report said. (A spokesperson for the court says Geoghegan-Quinn had no personal involvement in the report.) Geoghegan-Quinn would also help decide whether to increase the budget of the European Research Council (ERC), the new funding agency through which some 15% of FP7's €50 billion is spent. The ERC rewards individual investigators, rather than networks, and uses excellence as a criterion instead of political and economical considerations.

Potočnik will stay on as a commissioner but move to the environment post, now arguably diluted by the creation of a separate post for climate. Hedegaard, 49, who will fill that post, has earned the respect of climate advocates for her efforts to make Denmark's economy greener and for her "great personal commitment" to the Copenhagen summit, says Joris den Blanken, Greenpeace's E.U. climate and energy policy director at its Brussels office. **–MARTIN ENSERINK**

CREDITS: EUROPEAN COMMISSION

*Science*Insider

From the *Science* Policy Blog

President Barack Obama will attend the **Copenhagen climate meeting** and probably announce a U.S. commitment, contingent on congressional agreement, to a 17% cut in greenhouse gas emissions relative to 2005 by 2020. http://bit.ly/55ZEgd

The Presidential Commission for the Study of **Bioethical Issues** will be chaired by Amy Gutmann, a political scientist and the president of the University of Pennsylvania. Bioethicists expect the new commission to be more policy-oriented and pragmatic than its predecessor, which focused on philosophical and moral issues in biomedical research. http://bit.ly/8TWHCu

In one of the first signs that **HIV prevention** efforts have begun to make a dent on a global scale, new infections appear to have dropped by 17% over the past 8 years, according to a new report by the Joint United Nations Programme on HIV/AIDS and the World Health Organization. http://bit.ly/5Bu0me

India and the United States signed a deal on 24 November that includes a full suite of technical cooperation agreements, including shared work on food, wind power, extreme weather, and nuclear energy. http://bit.ly/5f1a1T

The neurologist and biomechanics expert in charge of the **National Football League**'s committee on mild traumatic brain injury resigned last week. The league appears to be changing its attitude toward growing evidence that head injuries suffered on the field can lead to personality changes, dementia, and other problems later in life. http://bit.ly/8TK2fM

The world's largest atom smasher, the **Large Hadron Collider**, has set a new record for accelerating subatomic particles to high energy. On 30 November, protons whizzed around the 27-kilometer-long accelerator at an energy of 1.18 tera–electron volts—20% higher than the previous standard. http://bit.ly/5pBvJ0

For more science policy news, visit **blogs.sciencemag.org/scienceinsider**.

STEM EDUCATION

Web Site Matches U.S. Scientists With Teachers Looking for Help

Kate Lievens and Jack Hidary live in very different worlds. But the elementary school teacher and the neuroscientist-turned–serial entrepreneur have something in common: a new, interactive Web site designed to match scientists and classroom teachers from across the United States in projects aimed at improving learning.

The site (nationallabday.org) is one element in a White House initiative to encourage private-private partnerships in STEM (science, technology, engineering, and mathematics) education. Hidary has agreed to run the site, and Lievens is one of the first teachers to participate.

The initiative, dubbed Educate to Innovate, doesn't involve any new federal dollars. But it got a boost last week from President Barack Obama, who praised the private sector's promised investment of $260 million in a variety of projects, some new but many with a long track record, ranging from after-school robotics competitions to educational video games, and from science-themed television shows to better professional development for teachers. "The success we seek [in improving STEM education] is not going to be attained by government alone," the president told scientists, educators, business leaders, and philanthropists at a 23 November rally in a federal office building next door to the White House. "[I] encourage folks to think of new and creative ways of engaging young people in science and engineering."

Hidary says the idea for the Web site was hatched less than 3 months ago in a meeting with officials from the White House Office of Science and Technology Policy (OSTP). "A number of us were involved in TechNet Day," says Hidary, referring to an effort to promote the role of information technology in society. His background seemed perfect for launching what Hidary describes as "eHarmony for science": He began his career as a neuroimaging fellow at the National Institutes of Health in the early 1990s before making it big in financial information services. In 1995, he started his first Internet company, EarthWeb/Dice, and a decade later he sold a second company, Vista Research, to McGraw-Hill and turned to community philanthropy. "He is a passionate and extremely hard-working advocate," notes Rick Weiss, senior policy analyst and director of strategic communications at OSTP.

Within weeks, Hidary had won promises from the American Chemical Society, the National Science Teachers Association (NSTA), and other professional groups to enlist their members. He's raised more than $1 million from various organizations and has borrowed Jan Cuny, a program officer from the National Science Foundation's computing directorate, to manage the project's Washington, D.C., office.

Helping hands. Ariel Gragnolati works with seventh-graders as part of a program that brings scientists into San Francisco schools.

National Lab Day (NLD) is a misnomer for the project, admits Hidary. "It's actually a yearlong series of activities," he explains. "We're not interested in another boutique program. We want something that will really galvanize people on a national scale." Obama said he expects the partnerships formed through the Web site to "reach 10 million young people with hands-on learning" by next spring, when organizers hope the president will keynote a second event to celebrate its success.

Lievens, a veteran teacher at Earl Hanson Elementary School in Rock Island, Illinois, signed up the first day the site went live. A former physical education teacher who became a reading specialist, Lievens took an environmental sciences course this summer at a nearby college that rekindled her latent interest in science. She joined NSTA and began thinking about how to work the Mississippi River, only a few blocks from the school, into her science classes.

What about having her fifth- and sixth-graders test the quality of the water from that mighty river, which they drink every day? "The kids really get fired up when they can connect what they are learning to their everyday lives," says Lievens. She also thought it would be fun. "Anytime you can make it a little messy, they're more likely to remember the lesson."

Lievens imagined her students taking water samples and examining them under a microscope, visiting the local water-treatment plant, and maybe even learning a little hydrology and environmental chemistry. But with no formal training in science, she knew that she'd need assistance. Last week, it arrived in the form of an NSTA e-mail alert describing the new Web site. "I'm eager to see who responds," she says.

Rebecca Smith knows more than a little about what it takes to pull off a successful STEM partnership program. A biochemist at the University of California, San Francisco, she's co-director of the Science and Health Education Partnership (SEP), which since 1987 has been matching area scientists with San Francisco schoolteachers (biochemistry.ucsf.edu/programs/sep). This year they expect to deploy 80 such teams, representing more than 200 scientists.

Smith, whose program can tap an embarrassment of riches from academia and industry, applauds NLD for trying to reach areas that lack such a large talent pool. She also offers Hidary some pointers: Take the time to make good matches, don't expect too much, monitor the partnerships closely, and stick with it. But the most important ingredient, she says, may be mutual respect and trust.

Hidary acknowledges the good work of SEP and many other programs and hopes that NLD can build on their successes. "We already know that project-based, hands-on learning works," he says. "The challenge now is to scale up. And the only way to do that is through massive partnerships."

–JEFFREY MERVIS

CREDIT: CARROLL TOM

INDIA

Stem Cell Center to Rise in Biology Hub

BANGALORE—India's fledgling stem cell R&D effort is set to receive a major boost. Construction began here last month on the Institute for Stem Cell Biology and Regenerative Medicine (inStem), a $50 million center to be built alongside an existing biology powerhouse—the National Centre for Biological Sciences (NCBS)—and a planned $12 million technology center that will seek to commercialize the biocluster's findings. "We hope that this intertwined environment can be transformative," says NCBS Director K. VijayRaghavan, who will serve as inStem's first director.

Initial plans include launching an international collaboration using stem cells to probe the molecular mechanisms of cardiovascular diseases. inStem will also link up with the Centre for Stem Cell Research at Christian Medical College in Vellore, which specializes in translational and clinical research. "inStem should help both in human resources and capacity building on one hand and accelerate progress in therapeutic possibilities on the other," says D. Balasubramaniam, who led a government task force that recommended setting up inStem.

Team inStem. The new institute's dean, Jyotsna Dhawan (*right*), and lab manager Wendie Dockstader, who moved to Bangalore from Iowa.

inStem's team includes two deans—Jyotsna Dhawan of NCBS and S. Ramaswamy of the University of Iowa, Iowa City, who is returning to his home country after 18 years in the United States. "Bioscience research in India is in an exponential growth phase," says Ramaswamy. "The excitement of being able to … shape this growth was irresistible." inStem expects to ramp up to 40 researchers after its new facility, shared with NCBS, opens in June 2011. **–N. N. SACHITANAND**

N. N. Sachitanand is a writer in Bangalore.

ScienceNOW.org

From *Science*'s Online Daily News Site

Coral Reefs Act Like Sunscreen

Living on a coral reef is a bit like living in a tanning bed. As the sun's rays shine through the water and reflect off the reef, they strike corals, their symbiotic photosynthetic algae, and other inhabitants from above and below. So what keeps these creatures from being fried? A new study suggests that coral acts as a sunscreen, absorbing UV light and limiting the harm it inflicts on the reef's denizens.
http://bit.ly/uvcoral

Milky Way Grew by Swallowing Other Galaxies

The motto "E Pluribus Unum" ("out of many, one") could be applied to the Milky Way. Astronomers have obtained new evidence that our home galaxy contains pieces of many former galaxies. The findings strengthen the idea that large galaxies don't emerge whole from single, gigantic clouds of dust and gas. Rather, they grow by swallowing their neighbors.
http://bit.ly/galaxygulp

Americans' Eating Habits Grow More Wasteful

After their biggest meal of the year, Americans might reflect on the fate of those moldering Thanksgiving leftovers. Nearly 40% of the food supply in the United States goes to waste, according to a new study, and the problem has been getting worse.
http://bit.ly/wasteful

Why Suffocating Is Scary

Breathe too much carbon dioxide (CO_2), and you'll suffocate. That's why people begin to panic if they breathe air enriched with the gas. One reason this happens, according to a new study in mice, is because breathing CO_2 triggers chemical sensors in a crucial part of the brain's fear circuitry. The findings could point the way to new treatments for anxiety disorders.
http://bit.ly/co2suffocation

Titan Lakes Migrate South for the Winter

Imagine if all of the water in the Great Lakes evaporated, moved to the Southern Hemisphere, and rained down to form new lakes in Argentina. Then thousands of years later, the process repeated and the water returned north. That's what researchers say could be happening on Titan, Saturn's largest moon. Understanding the process could shed light on how long-term climate cycles operate on other worlds.
http://bit.ly/titanlakes

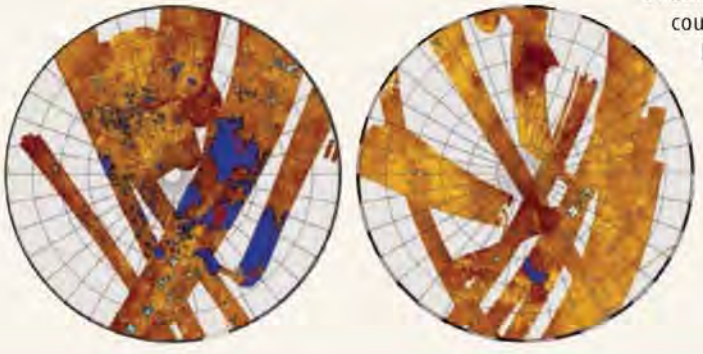

Wet, dry. Cassini's passes over Titan have revealed many lakes (blue) in the north but few in the south.

CREDITS (TOP TO BOTTOM): COURTESY OF J. DHAWAN; NASA/JPL/SPACE SCIENCE INSTITUTE

On the Origin of Tomorrow

IN THE FINAL WORDS OF THE FINAL sentence of *On the Origin of Species*, Charles Darwin gave a nod to the future. "There is grandeur in this view of life, with its several powers, having been originally breathed into a few forms or into one; and that, whilst this planet has gone cycling on according to the fixed law of gravity, from so simple a beginning endless forms most beautiful and most wonderful have been, and are being, evolved."

Darwin recognized that as long as the ingredients for the evolutionary process still exist, life has the potential to change. He didn't believe it was possible to forecast evolution's course, but he did expect humans would have a big effect. In his day, they had already demonstrated their power with the triumphs of domestication, such as breeding dogs from wolves. Darwin recognized that we humans can also wipe out entire species. He knew the dodo's fate, and in 1874 he signed a petition to save the last surviving Aldabra giant tortoises on the Seychelles Islands in the Indian Ocean.

Darwin also expected that our own species would change. As Western powers colonized other parts of the world, he predicted that some populations would become extinct. But Darwin also felt a cautious optimism. "Looking to future generations," he wrote in *The Descent of Man*, "there is no cause to fear that the social instincts will grow weaker, and we may expect that virtuous habits will grow stronger." And unlike other species, humans could bring about this change consciously, through cultural evolution.

As the world celebrates the 150th anniversary of the publication of *On the Origin of Species* this year, scientists continue to think deeply about what comes next. But the complexity of evolution still makes forecasting hard. "As Yogi Berra once said, 'Prediction is very difficult. Especially about the future,' " says Stephen Stearns, an evolutionary biologist at Yale University.

Yet evolutionary biologists also feel a new sense of urgency about understanding what lies ahead. Since Darwin's day, humans have gained an unprecedented influence over our own evolution. At the same time, our actions, be it causing climate change, modifying the genomes of other organisms, or introducing invasive species, are creating new sources of natural selection on the flora and fauna around us. "The decisions we and our children make are going to have much more influence over the shape of evolution in the foreseeable future than physical events," says Andrew Knoll, a paleontologist at Harvard University.

Shaping our genome

If there's one thing that's certain, it's that humans, like other living things, will continue to evolve. "Evolution is unstoppable," says Lawrence Moran of the University of Toronto in Canada. But that doesn't mean that humans are marching on a path toward becoming giant-brained, telepathic creatures out of *Star Trek*. All it means is that the human genome will continue to change from generation to generation.

A background mutation rate guarantees this process. Each baby's DNA carries about 130 new mutations. Most of them have no effect on our well-being. People can pass these neutral mutations down to their offspring without harm, and over time, a small fraction of them will end up spreading across entire populations, or even the entire species, thanks to random luck.

Natural selection can cause mutations that help individuals survive and reproduce to spread much faster than neutral ones. Exactly which mutations natural selection will favor, however, depends on the environment in which we live. And over the past 10,000 years, we humans have dramatically changed that environment. We have fostered new diseases to which humans have adapted, for example. But in other cases, civilization has shielded us from the environment, weakening the power of natural selection.

One of the best known examples of human-driven evolution is malaria. Early farmers cleared forests and created fields where malaria-carrying mosquitoes could lay eggs in pools of water. As malaria spread, natural selection favored those humans with defenses against the disease. One such defense comes from a variant of a hemoglobin gene that makes it hard for parasites to reproduce in blood cells. One copy of the gene reduces your chance of contracting malaria. Two copies cause sickle cell anemia.

On the other hand, civilization has also blunted some of natural selection's power over humans, particularly in the 150 years since Darwin published *On the Origin of Species*. Back then, for example, some children had the misfortune to be born with defective copies of a gene for an enzyme that breaks down amino acids in the food they ate. This disorder, known as phenylketonuria, generally led to severe brain damage. Few people with severe phenylketonuria were able to pass on their genes. But today, now that scientists know what causes the disease, people with phenylketonuria can enjoy fairly normal lives simply by being careful about the foods that they eat, and they pass their genes on to their children. Other medical advances, from eyeglasses to antibiotics, may also allow some potentially detrimental genes to become more common than in the past.

Yet medical advances and other changes to human life have not stopped natural selection, nor will they in the future. HIV, for example, first evolved into a human pathogen in the early 1900s and today takes a devastating toll in many parts of the world. Genes that provide some resistance to the virus may be favored by natural selection in places where HIV is particularly common.

Even in affluent parts of the world like the United States, natural selection has not stopped. Subtle differences in people's health influence how many children they have and thus can gradually change entire populations.

THE YEAR OF DARWIN

This essay is the last in a monthly series. For more on evolutionary origins online, see the Origins blog at **blogs.sciencemag.org/origins.** For more on the Origin of Tomorrow, listen to a podcast by author Carl Zimmer at **www.sciencemag.org/multimedia/podcast.**

CREDITS (TOP TO BOTTOM): K. SUTLIFF/*SCIENCE* (JUPITERIMAGES.COM); WIKIPEDIA/GEORGE RICHMOND, FROM ORIGINS, RICHARD LEAKEY AND ROBERT LEWIN

Lost species. Darwin worried that the Aldabra giant tortoise (*left*) would become extinct like the dodo (*below*).

In a report published online 26 October in the *Proceedings of the National Academy of Sciences*, Stearns and his colleagues documented natural selection in 2238 U.S. women. The women were subjects in the Framingham Heart Study, which has tracked the health of thousands of people in Framingham, Massachusetts, since 1948. The scientists searched for traits that were correlated with having a higher number of children. Then they checked to see whether those traits tended to be passed down from mother to child—in other words, whether they were genetically based.

The scientists discovered that a handful of traits are indeed being favored by natural selection. Women with a genetic tendency for low cholesterol, for example, had more children on average than women with high cholesterol. A greater body weight was also linked with greater reproductive success, as was shorter height, lower blood pressure, an older age at menopause, and having one's first child at an earlier age.

Stearns and his colleagues now know which traits are selected in the women of Framingham, but they have yet to determine exactly what advantage each trait confers—a situation that evolutionary biologists often face when documenting natural selection. Nevertheless, based on the strength of the natural selection they have measured, the scientists predict that after 10 generations, the women of Framingham will give birth, on average, a few months younger than today, have 3.6% lower cholesterol, and will be 1.3% shorter.

Of course, even this prediction is subject to change. Women with higher cholesterol may eventually be able to enjoy higher fertility rates thanks to cholesterol-lowering drugs, says Stearns, wiping out the differences in reproductive rates. "Selection is always operating," says Stearns, "but the traits on which it operates shift with ecology and culture."

Along with natural selection, it's also conceivable that one day genetic engineering will change human DNA directly. In September, scientists at the Oregon National Primate Research Center reported that they could replace the DNA in the mitochondria of a monkey embryo with mitochondrial DNA from another monkey. In July, scientists at the Center for Regenerative Medicine in Barcelona, Spain, reported that they had repaired human stem cells carrying genes for an inherited blood disorder. Both studies hint that eventually scientists will be able to alter the genes of future generations.

But even if a child was born with engineered genes in our lifetime, that milestone wouldn't mean much for the evolution of our species. Those engineered genes would be swamped by the billions of mutations that emerge naturally in the babies born every year. Yet although engineered genes aren't likely to provide enough reproductive advantage to spread on their own, they may still become common. John Hawks, an anthropologist at the University of Wisconsin, Madison, speculates that if genetic engineering becomes cheap enough and provides an attractive trait—such as staying thin—economics could spread a gene even if natural selection can't. "I think people would buy it," says Hawks.

Human-powered evolution

Genetically engineered humans may still be science fiction, but genetically engineered animals, plants, and microbes are all here already. In 2008, farmers planted 125 million hectares of genetically modified crops. Many of these crops carry genes from other species. Corn, cotton, and other plants have been engineered to carry a gene produced by bacteria, for example, so that they can make an enzyme that can kill insects. With big countries such as China and India dramatically ramping up their use of genetically modified crops, this evolutionary trend will likely continue.

In the near future, scientists may start to engineer life in a more profound way, manufacturing new species from scratch. The idea would be to design a microbe on a computer, combining genes with different functions into genetic networks. Scientists could then synthesize the new genome from raw DNA and insert it into an empty microbial

> "The decisions we and our children make are going to have much more influence over the shape of evolution in the foreseeable future than physical events."
>
> —Andrew Knoll, Harvard University

Engineering genomes. Humans are finding many ways to radically manipulate DNA, from genetically modified cotton (*left*) to bacteria with "transplanted" genomes (*center*) to monkeys born from DNA transferred to empty eggs.

Alien invaders. Human-introduced species such as kudzu and cane toads (*inset*) can drive evolution in new directions.

cell that would come to life. J. Craig Venter and his colleagues at the J. Craig Venter Institute in Rockville, Maryland, have taken a series of key steps toward that goal, such as performing a "genome transplant" on a microbe.

If Venter succeeds, his artificial life would be a triumph of human ingenuity, but it would probably be a minor blip on the biosphere's radar. Synthetic biologists want to make microbes to serve our own ends, such as making fuel and medicines. Burdened with genes for these functions, the microbes will likely be ill equipped to compete in the wild against species that have adapted for millions of years. For the foreseeable future, synthetic microbes will probably survive only in the refuge of a laboratory or a fermentation tank. "I will venture a prediction," says Adam Wilkins, a biologist at the University of Cambridge in the United Kingdom. "This kind of biotech engineering might succeed in creating some rather weird and wonderful organisms. But the net effect on evolution will be nil—that is, outside the laboratory."

But humans, Wilkins is quick to point out, don't need synthetic biology to have a big effect on the evolution of life. Chainsaws, fishing lines, and smokestacks do just fine. Many fisheries, for example, have established rules for keeping fish only above a certain size. As a result, natural selection has favored fish that become sexually mature at smaller sizes. On land, hunters have had a similar effect by going after big game. Bighorn sheep, for example, now grow horns 25% smaller than they did 30 years ago.

Humans have also triggered bursts of evolutionary change by introducing species to new habitats. In Australia, for example, cane toads brought in from South America in 1935 have became a continent-wide pest. They're devouring some small native species, and their poisonous skin is killing off some of their predators. Scientists have discovered that the toads are evolving in their new home: Toads at the leading edge of the invasion are growing longer legs and moving faster than their ancestors, speeding up the invasion. The native species are responding as well. Australian snakes are evolving resistance to the cane toad poison.

Stephen Palumbi, a biologist at Stanford University in Palo Alto, California, expects that human-induced natural selection will become much stronger in the future. "In the last century, we were having a big impact, but it wasn't everywhere," says Palumbi. "But global climate change is an 'everywhere' impact, and that's different."

Plants and animals are already responding to the warming climate by shifting their ranges to find the most comfortable temperatures. But moving won't be a solution for many species, which will face barriers such as deserts or cities. They will have to adapt to survive—a process scientists have already detected in some species, such as red squirrels in Canada, which have evolved to breed earlier in the spring.

Extra carbon dioxide is creating a second worldwide evolutionary pressure as it dissolves into the ocean. There it is turning into carbonic acid and lowering the pH. Continued acidification will make it more difficult for corals and other marine animals to build skeletons and shells from calcium carbonate. Organisms will need to adapt to survive in these new conditions.

Taking a toll. Increased carbon dioxide from burning fossil fuels is lowering the pH of the oceans, destroying corals.

"We know that things can evolve quickly, but can they evolve fast enough?" asks Palumbi. He and many other scientists suspect that for many species the answer is no. Unless we can ease up on the biosphere, they warn that the biggest feature of evolution in the near future will be extinctions.

Knoll points out some disturbing parallels between today's crisis and a pulse of mass extinctions that occurred 252 million years ago, wiping out an estimated 96% of species in the oceans and 70% of species on land. A rapid increase in carbon dioxide in the atmosphere led, among other things, to ocean acidification. For animals that depended on calcium carbonate, "you had about a 90% chance of going extinct," says Knoll. "Corals, sponges, brachiopods, they all kicked the can."

Knoll doesn't expect human-driven mass extinctions to be as bad as that ancient one. But they could still be unimaginably huge. "If we lose half the species on the planet, our grandchildren are not going to see them restored," says Knoll. "It will take millions of years."

A drop in biodiversity may bring with it a collapse of many ecosystems. Coupled with a rapid increase in global temperatures, ocean acidification, and other changes, we may be pushing the environment into a state we've never experienced as a civilization. Such a stress could put our species under intense natural selection as well.

Taking the long view

One way or another, life will survive this current crisis. But where is life headed in the very distant future? To find out, planetary scientist King-Fai Li of the California Institute of Technology in Pasadena and his colleagues built a model of Earth and the sun and watched it evolve for billions of years. In their simulation, the sun gets brighter, as it has since it first formed. The extra energy speeds up the rate at which carbon dioxide is drawn out of Earth's atmosphere, cooling it off. But after about 2 billion years, this cooling mechanism breaks down, and Earth heats up, ending up like its lifeless neighbor, Venus.

But Li's model does not include a clever species like our own, which can use its brain to influence the planet. Would it be possible to extend the life span of Earth's biosphere? "I am not going to rule out any talented civilizations that will be able to do that," says Li.

–CARL ZIMMER

Carl Zimmer is the author of *The Tangled Bank: An Introduction to Evolution* (Roberts and Co., 2009).

NEURODEGENERATION

Could They All Be Prion Diseases?

Recent studies renew interest in the idea that many neurodegenerative diseases may involve prionlike mechanisms

Suspicious activity. Peptide aggregates (yellow) similar to those involved in Huntington's disease display prionlike behavior.

CREDIT: C. E. O'BRIEN, J. E. LACKNER, AND R. R. KOPITO

The idea that proteins can be agents of disease was once heretical, but two Nobel Prizes later all but the most die-hard skeptics have been convinced that misfolded proteins called prions are the cause of several neurodegenerative disorders in humans and other animals. In disorders such as scrapie, mad cow disease, and Creutzfeldt-Jakob disease, misfolded molecules of a naturally occurring protein act like bad role models, encouraging normally folded proteins to misfold and clump together. As aggregates of misfolded proteins spread through the brain, nerve cells stop working properly and eventually die.

A recent flurry of papers has revived interest in the idea that such mechanisms may play a role in an even wider range of neurodegenerative disorders, including two of the most dreaded scourges of old age: Alzheimer's and Parkinson's diseases. Such diseases almost certainly aren't contagious like true prion diseases are, at least in ordinary circumstances, but they may propagate through the nervous system in much the same way. The idea is actually decades old and seems to have originated with Daniel Carleton Gajdusek, who won a share of the 1976 Nobel Prize in physiology or medicine for his work on kuru, a prion disease he claimed was transmitted by ritualistic cannibalism among the Fore people of New Guinea. But until very recently, there was little experimental evidence for prionlike mechanisms in other neurodegenerative disorders, says Lary Walker, a neuroscientist at Emory University in Atlanta. "It's an old idea with new legs," Walker said in his introduction to a recent online seminar on this topic hosted by the Alzheimer Research Forum (Alzforum).

Evidence from recent animal studies suggests that many of the misfolded proteins thought to play a central role in a wide range of neurodegenerative disorders can, like prions, "seed" the misfolding and aggregation of their normally folded kin. In some cases, these pathological protein clusters appear to propagate from cell to cell. Such a mechanism could help explain several puzzles—such as why some neurodegenerative disorders tend to spread from one part of the nervous system to another in a characteristic pattern, and why some researchers have found pathological protein deposits in fetal stem cells transplanted into the brains of Parkinson's patients (*Science*, 11 April 2008, p. 167).

"Twenty, 30 years ago, when people were proposing these links, we didn't know that networks degenerate [in characteristic patterns], and we didn't have fetal transplants," says Marc Diamond, a neurologist at Washington University School of Medicine in St. Louis, Missouri. The prion concept helps integrate much of what's known about neurodegenerative diseases, Diamond says. "The reason it's catching on is that it makes a lot of sense." Like a growing number of researchers, Diamond thinks the prion concept may not only help researchers gain a better understanding of neurodegenerative diseases but also point to treatment strategies they might not have considered otherwise.

Killer proteins

The high prevalence of kuru in the Fore people is one of the great medical mystery stories of all time. The disease spread in a manner that suggested infection, yet it caused no fever or other inflammatory response. Gajdusek won the Nobel for his work suggesting that kuru was transmitted by cannibalism practiced as part of funeral rites among the Fore. But the infectious agent remained a puzzle. In laboratory experiments with infected brain tissue, the infectious agent survived heat, chemicals, and ultraviolet light that destroy the infectivity of viruses and bacteria.

In the early 1980s, Stanley Prusiner of the University of California (UC), San Francisco, proposed that proteins could be the infectious agent. It was a radical notion: All infectious agents known at the time contained DNA or RNA, the genetic blueprints for replication. But Prusiner proposed that infectious proteins, or prions, spread disease not by replicating themselves but by encouraging other proteins to undergo a conformational change. He won the 1997 Nobel Prize (some thought prematurely) for work supporting the prion hypothesis (*Science*, 10 October 1997, p. 214).

Prusiner's theory explained the kuru puzzle, but both Gajdusek and Prusiner were interested in applying the idea to a variety of other disorders. After all, autopsy studies commonly found suspicious clumps of protein in the brains of people who died of Alzheimer's, Parkinson's, and other neurodegenerative diseases. As early as the 1960s, Gajdusek tried injecting extracts of brain tissue from Alzheimer's patients into monkeys and chimps. But these efforts, and later attempts by other researchers, yielded inconsistent results.

Disease can develop decades after exposure to prions in humans, and researchers had to wait years to see whether experiments in primates had any effect, says Walker. Enter the transgenic mouse: In a study published in 2000 in *The Journal of Neuroscience*, Walker and colleagues injected extracts from the brains of Alzheimer's patients into genetically engineered mice susceptible to the disease (normal mice are not susceptible). They injected one side of the brain in each animal. Within a few months, the mice developed widespread plaques made up of β-amyloid peptide, a hallmark of Alzheimer's disease, on the injected side of the brain. That indicated that

Acting Like a Prion Isn't Always Bad

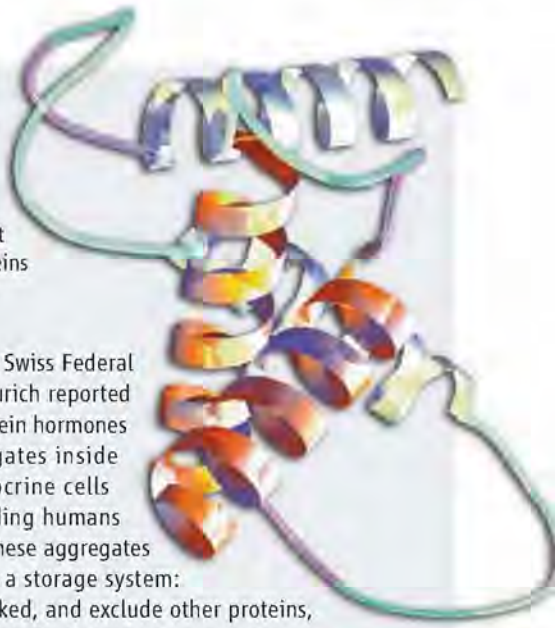

Bad influence. Aggregation of prion proteins (*right*) can destroy the nervous system, but similar behavior in other proteins may have more positive roles.

In mad cow disease and related disorders, misfolded proteins called prions cause normal proteins to misfold and clump together, spreading havoc through the nervous system. Virtually any protein can misbehave like this when the conditions are right, and some researchers now suspect that prionlike mechanisms of protein misfolding and propagation may underlie a wide range of neurodegenerative disorders (see main text). But if this type of behavior in proteins is so dangerous, why hasn't evolution selected against it? One possibility is that it hasn't had to: Many of these diseases strike late in life, after the reproductive years are over.

It's also possible that this type of protein folding isn't always bad, says Adriano Aguzzi, a prion researcher at the University Hospital of Zurich in Switzerland. "Having a protein that can exist in an on-and-off state where the on state is infectious is a wonderful way of transmitting information," Aguzzi says. "Nature would be very stupid if it didn't utilize this system in order to solve specific problems during evolution."

Indeed, recent studies suggest that proteins that behave like prions play important roles in a wide variety of normal biological functions in organisms ranging from bacteria to humans. In some bacteria, prionlike proteins create a fibrous matrix that helps cells adhere to surfaces and stick together to form colonies. In some fungi that live in wet environments, such proteins form a film that reduces the surface tension at the water's surface, enabling spores or fruiting bodies to form. In insects they help strengthen eggshells and may lend strength to spiders' silk.

In 2006, researchers led by biochemist Jeffrey Kelly of The Scripps Research Institute in San Diego, California, reported in *PLoS Biology* that in bovine cells a protein called PMel17 forms self-propagating aggregates that play a role in the synthesis of melanin, a pigment in the skin and eyes that protects against ultraviolet rays. More recently, researchers led by structural biologist Roland Riek of the Swiss Federal Institute of Technology in Zurich reported that several peptide and protein hormones pack into prionlike aggregates inside secretory granules in endocrine cells from several species, including humans (*Science*, 17 July, p. 328). These aggregates have several advantages as a storage system: They are stable, densely packed, and exclude other proteins, helping to keep the granules' contents pure.

Even in the nervous system, prionlike proteins may have beneficial roles. In 2003, neuroscientist Eric Kandel of Columbia University and colleagues reported in *Cell* that a protein with prionlike properties plays a role in long-term memory in the sea slug *Aplysia californica*. At October's meeting of the Society for Neuroscience in Chicago, Illinois, Kandel described new work extending these findings to mice and bolstering his group's argument that self-propagating aggregates of these proteins may be involved in "tagging" specific synapses for strengthening when a long-term memory is created.

"Prions and prionlike phenomena are much more common than we realized," Aguzzi says. "These things that are cropping up now are the tip of the iceberg."

–G.M.

something in the brain extracts can seed plaque formation, although whether the seed is β-amyloid peptide itself remained unclear.

More recent work led by Walker and Mathias Jucker at the University of Tübingen in Germany bolsters the case that β-amyloid is the culprit. In one experiment, the researchers found that brain extracts treated with antibodies to remove β-amyloid did not seed aggregation of β-amyloid when injected into mice (*Science*, 22 September 2006, p. 1781). And in the 4 August issue of the *Proceedings of the National Academy of Sciences* (*PNAS*), they reported that stainless steel wires coated with brain extract and then heated to kill microbes still caused β-amyloid deposits to form when implanted into the brains of mice. After 6 months, deposits had spread to neighboring brain regions. To Walker and others, such findings suggest that β-amyloid can induce deposits to form and spread through the brain—much as prions do. Walker says his group is working to create synthetic β-amyloid for a more definitive experiment: If a synthetic peptide can seed plaques, that should rule out the possibility that a microbe or some other factor in the brain extracts is to blame.

Other researchers have been finding similar hints of prionlike behavior in other proteins associated with neurodegenerative disorders. Diamond and colleagues have found that aggregates of misfolded tau, a protein that forms pathological tangles in the brains of people with Alzheimer's disease and frontotemporal dementia, can be taken up by cultured mouse cells. Then, once inside the cells, the misfolded tau appears to encourage normally folded tau to misfold and aggregate, they reported 8 May in *The Journal of Biological Chemistry*. In July, European researchers reported similar findings in vivo: Injecting brain extracts containing misfolded tau into the brains of mice triggered tau misfolding and aggregation that spread from the injection site to nearby brain regions, they reported in *Nature Cell Biology*.

Early clues. Studies by Daniel Carleton Gajdusek (*left*) with the Fore people led to early clues about prion diseases.

Another suspect protein, α-synuclein, the main component of the "Lewy bodies" found in the brains of people with Parkinson's disease and certain types of dementia, also appears to propagate from cell to cell. In the 4 August issue of *PNAS*, researchers led by Eliezer Masliah of UC San Diego and Seung-Jae Lee of Konkuk University in Seoul reported that rogue aggregates of α-synuclein can pass from cell to cell and spur the formation of Lewy body–like aggregates in cultured human neurons. Experiments with

CREDITS (TOP TO BOTTOM): JEAN-PAUL JOUBERT/PHOTO RESEARCHERS INC.; NIH/NINDS

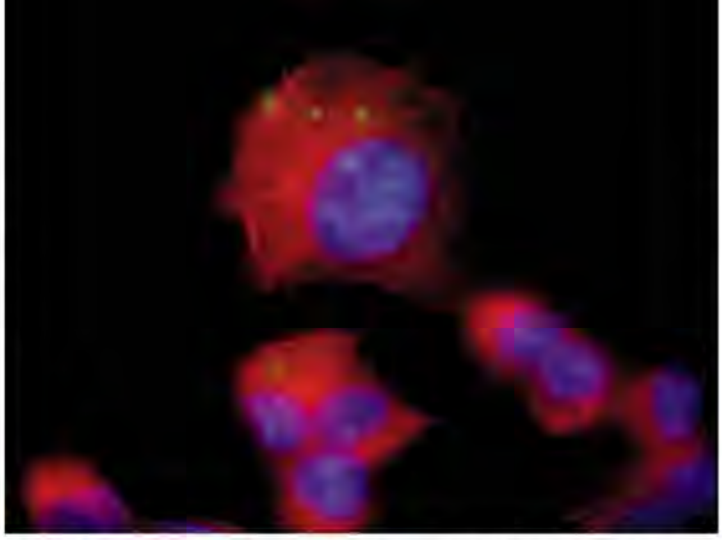

Tangled up. Aggregates of tau protein (green specks) can transfer from one cultured cell to another.

cultured rat and mouse cells, reported in the same paper, suggested that α-synuclein triggers cell death in neurons and neural stem cells. "Cells that take it up form new aggregates, and they get sick and eventually die," Masliah says.

If α-synuclein spreads from neuron to neuron in the intact human brain, that might explain findings from two research groups that reported last year that fetal cells transplanted into the brains of Parkinson's patients contained deposits of α-synuclein—something that's unheard of in such young cells, the oldest of which had survived for 16 years before the patient died. (A third team found no pathology in transplanted cells.) The findings surprised many researchers who had assumed that deposits build up inside cells over many decades and don't jump from cell to cell. Cell-to-cell transmission of α-synuclein wouldn't necessarily doom stem cell therapies for Parkinson's disease, but it may present yet another obstacle, Masliah says. "We'd like to engineer those fetal cells to be resistant to the aggregates," he says. One possibility, he suggests, would be to engineer them to overexpress enzymes that can break down aggregates.

Is it contagious?

The list goes on. Misfolded huntingtin protein, the culprit in Huntington's disease, can find its way from the extracellular fluid to the inside of cultured cells and trigger aggregation, according to a report by Stanford University cell biologist Ron Kopito and colleagues in the February issue of *Nature Cell Biology*. And at the Alzforum seminar, Neil Cashman of the University of British Columbia, Vancouver, in Canada described unpublished findings from his group that hint at prionlike behavior in SOD1, a protein thought to be central to neurodegeneration in amyotrophic lateral sclerosis. "We're getting a lot of hints from a lot of diseases," Kopito says. "Together, it adds up to an emerging picture that deserves some pretty close attention."

These recent studies "expand the prion concept to other proteins … [and] show that under certain conditions the process of protein aggregation can be transmissible" from cell to cell, says Claudio Soto, a molecular biologist who studies neurodegenerative disease at the University of Texas Medical School at Houston. "What remains to be seen is whether or not this occurs in real life," Soto says.

So far there's virtually no evidence that proteins other than prions can transmit disease from one individual to another, notes Adriano Aguzzi, a prion researcher at the University Hospital of Zurich in Switzerland. One exception, Aguzzi says, may be amyloid A amyloidosis, a protein misfolding disorder that affects the spleen, liver, and other organs. Japanese researchers reported in *PNAS* in 2008 that misfolded amyloid A can be transmitted from one captive cheetah to another via feces. (The disease is a major cause of illness and death in these endangered cats.) A 2007 paper in *PNAS* suggested that foie gras prepared from duck or goose liver can transmit amyloidosis when fed to mice.

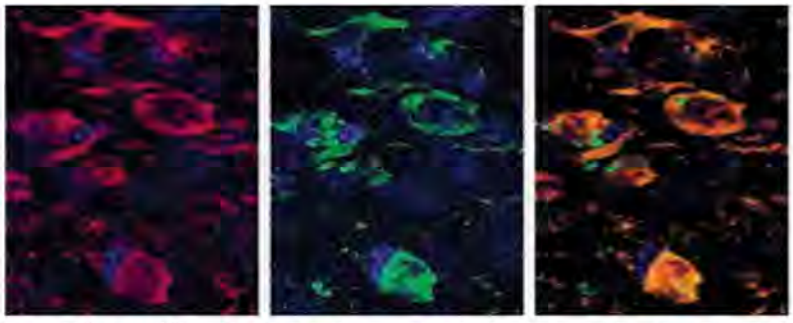

A spreading problem. Aggregates of α-synuclein (red, *left*; orange in merged panel on *right*) can pass between mouse neural stem cells (green, *middle*).

Most researchers say it's unlikely that diseases like Alzheimer's and Parkinson's are contagious in the usual sense of the word. "I think what's special about prion diseases is that prions are indestructible," says Walker. "There's practically nothing you can do to get rid of them within the realm of what we consider normal sterilization." Most protein aggregates are more fragile, which may limit their ability to jump from one person (or animal) to another. All the same, Walker says the issue merits closer study. His experiments with the stainless steel wires, he notes, suggest at least a theoretical possibility that surgical instruments could transmit the disease.

Window of opportunity

Even if most neurodegenerative diseases don't spread from individual to individual like true prion diseases do, the possibility that they may spread from cell to cell in an analogous way opens up new options for treating them, say some researchers. If aggregates of tau jump from cell to cell to spread disease instead of building up slowly inside cells, for example, that presents an opportunity to cut them off with antibodies or other molecules that can't get inside cells, says Diamond. His group has been designing antibodies that specifically target misfolded forms of tau. Cashman's group has been taking a similar approach for SOD1. Both presented promising preliminary results from animal experiments at the Alzforum seminar.

Another approach is to use small molecules designed to latch on to specific parts of a protein and prevent it from misfolding, says Jeffrey Kelly, a biochemist at The Scripps Research Institute in San Diego, California. In July, FoldRx Pharmaceuticals, a company Kelly cofounded, announced encouraging results from a phase II/III clinical trial of a compound that prevents protein misfolding and aggregation in people with a rare but fatal disease called transthyretin amyloid polyneuropathy. The disease affects the peripheral nerves, causing loss of function in the hands and feet, before spreading to the autonomic nervous system, which regulates digestion and other essential functions. Untreated, the disease causes drastic weight loss, but patients who took the drug for 18 months reversed course and started gaining weight, Kelly says. That suggests that the drug slows the disease's impact on the autonomic nervous system, Kelly says. "We're pretty excited about this, and I think it will energize efforts on other amyloid diseases that focus on preventing this process."

–GREG MILLER

CREDITS (TOP TO BOTTOM): BESS FROST AND MARC DIAMOND; PAULA DESPLATS, ELIEZER MASLIAH, AND SEUNG-JAE LEE

FISHERY MANAGEMENT

Can Science Keep Alaska's Bering Sea Pollock Fishery Healthy?

The pollock fishery in the chill waters of the eastern Bering Sea is said to be the best managed in the world. But a surprising decline in numbers has scientists worried

Plentiful pollock? The Bering Sea fishery is America's largest.

CREDIT: NATALIE FOBES/CORBIS

Every January along the continental shelf in the eastern Bering Sea, a great mass of spawning, olive-green fish surge through the nutrient-rich waters. These are walleye pollock (*Theragra chalcogramma*), social fish that tip the scales at 700 grams when mature. The pollock spawn in waters north of the Aleutian Islands, where the bounty serves as food for marine mammals, seabirds, fish—and humans: The eastern Bering Sea pollock fishery is the largest and most lucrative in North America. Each year it brings in $1 billion and supplies millions of meals in the form of fish sticks, fast-food fish fillets, imitation crabmeat, and roe.

The fishery is remarkable not only for its size but also, to date, for its sustainability: It's certified as sustainable by the London-based Marine Stewardship Council, and catch limits are recommended by scientists who judge the state of the fishery with surveys and state-of-the-art models; there's even a major ecosystem study funded by the U.S. National Science Foundation (NSF).

This year's data are sparking concern, however. Previous predictions of a sizable uptick in pollock numbers weren't borne out by recent surveys. Instead, there are dramatically fewer pollock than scientists had estimated just a year ago. The stock is at its lowest level since 1980, and Greenpeace has put the fishery on its red list of unsustainable harvests.

Last week in Seattle, Washington, responding to the lower numbers, scientists advising the North Pacific Fishery Management Council (NPFMC) recommended that the catch, rather than being raised from this year's low as expected, stay low again in 2010. Given the uncertainty, some argue that the harvest should be cut even further. The council itself will vote on the recommendation next week. "This time last year we said the stock was going up," says marine biologist Lowell Fritz of the Alaska Fisheries Science Center (AFSC) in Seattle, who argued for a lower quota. "But it didn't. And that is cause for concern."

Fritz and others say that the revised estimates and dwindling numbers raise questions about how well-managed the fishery really is, and whether the researchers' reams of data and calculations can produce what all parties want: a long-term sustainable fishery in a healthy ecosystem. "It's tricky," says Douglas DeMaster, science and research director of AFSC, who's based in Juneau. "How far can we knock down a single species before impacting the ecosystem? We don't know yet." But even though the fishery is at a low point, "it is not overfished," he says. "And we're working hard to make sure it never is."

The big haul

Pollock are found across the North Pacific from Puget Sound to the Sea of Japan. But they are especially abundant in the waters of the Bering Sea's continental shelf. Once regarded as commercially worthless, pollock gained value after Japanese trawlers developed a process for reducing its white meat into a protein paste called surimi. And after the North Atlantic cod fishery collapsed in the 1990s, pollock fishing surged. The Bering Sea pollock fishery is now the world's largest single-species fishery, averaging more than 1 million metric tons annually. But pollock are not immune to overfishing: Other formerly abundant pollock fisheries in the region, including an exceptionally rich one called the Donut Hole (see graph, p. 1341), were heavily fished in the 1980s and 1990s and have never recovered.

In the eastern Bering Sea, fishing boats hauled up an average of 1.33 million metric tons of pollock each year between 2001 and 2007. In 2007, however, surveys showed that pollock numbers were down. So scientists recommended—and fishers abided by—a reduced quota of 1 million metric tons in 2008. NPFMC reduced the 2009 catch by another 18% to 815,000 metric tons.

But the scientists' models predicted better news ahead, and last fall they estimated that in 2010 the stock could sustain a catch close to previous levels. To assess the health of the pollock population, AFSC researchers gather data about the sex, size, weight, and condition of the fish from scientist-observers aboard the fishing vessels and take abundance data from annual bottom-trawl and acoustic midwater-trawl surveys. The scientists track the fish in age classes. Pollock reproduce prolifically, live nearly 11 years, and are mostly fished beginning at age 4, as many fishing vessels selectively target areas preferred by older, larger, and more valuable fish.

So when the next season opens in January 2010, fish that hatched in 2006 will be included in the catch. And it is this 2006 class that has surprised and disappointed scientists. As 1-year-olds and 2-year-olds, this age group appeared particularly plentiful. "It looked like an above-average class," says James Ianelli, an AFSC fisheries biologist in Seattle who heads the modeling team and is lead author of the pollock assessment report released on 17 November. But this year's bottom-trawl survey found fewer fish, and the midwater acoustic trawl was even worse, down 30% from last year's estimate. "There were fewer 3-year-olds than our model predicted," says Ianelli, and older fish were largely absent.

Why were 3-year-old pollock relatively scarce? "It could be they had poor survival rates as 1-year-olds, or maybe they are staying more toward the bottom. We've also had 4 years of record-cold bottom temperatures," which could affect the fish's distribution, says Ianelli.

Whatever the reason, the discrepancy between the previous and the most recent surveys, coupled with the continuing decline, has set off alarm bells. "It surprised people because we [scientists] almost always get the trend right," says Fritz. "But we really missed this one; we were off by 30%. And that makes me think we're in new territory."

In November 2008, scientists had estimated that the population could sustain a catch of 1.23 million metric tons in 2010. But last week the 15 members of the NPFMC Bering Sea Groundfish Plan Team, after much debate, voted instead for a catch of 813,000 metric tons. The vote was split, with seven scientists recommending a further cut to 738,000 metric tons.

Driving the system

Despite the lower number, Ianelli and DeMaster say the fishery remains healthy. There's enough of a buffer built into the model to assure that the spawning stock never drops below 20% of its estimated unfished numbers, says DeMaster. "It's a conservative approach," he says, meant to ensure that enough young fish will be produced every year to replace those caught. This year's stock is at 27%.

To better understand the pollock's cycles, and what factors in the ecosystem affect them, scientists are busy incorporating more data about the ecosystem—on ocean temperature, zooplankton production, pollock predators, and climate—into their models. "We're in the third year of our Bering Sea Project," says marine biologist Mike Sigler at AFSC in Juneau, referring to a 6-year, $52 million NSF and North Pacific Research Board–funded study of the eastern Bering Sea's ecosystem. "It's already helping us understand these changes in pollock."

Researchers have found that many poor age-class years seem to be tied to less sea ice and warmer ocean waters. "That's the pattern for the [pollock] classes from 2001 to 2005," says Sigler. However, the drop in the 2006 class remains puzzling, because there was plenty of sea ice and colder water that year. Sigler hopes to have an explanation by 2012, when the project ends.

Regardless of the cause, the spawning mass has declined, and AFSC's harvest rules have in turn limited the catch, says fisheries scientist Steven Martell of the University of British Columbia, Vancouver, in Canada. "There's been a 45% reduction in catches over the last 4 years," he says. But if those reductions aren't sufficient and the stock doesn't recover as projected in the next few years, he warns that the fishery "will certainly be in trouble" and could be closed.

Others think that the catch should be reduced even further now. "The pollock fishery is the most valuable fishery in the U.S.," says Jeremy Jackson, a marine ecologist at the Scripps Institution of Oceanography in San Diego, California. "More is known about it than any other fishery in the world. Yet despite all the wonderful data and fancy models, they've failed to protect the pollock or the Bering Sea ecosystem. We need to call 'Time out!'"

Jackson says that although including ecosystem effects in pollock management is worthwhile, the researchers also need to look at "the effects of pollock fishing on the ecosystem." He notes that pollock is a staple for northern fur seals and endangered Steller sea lions, both of which are struggling (*Science*, 4 April 2008, p. 44).

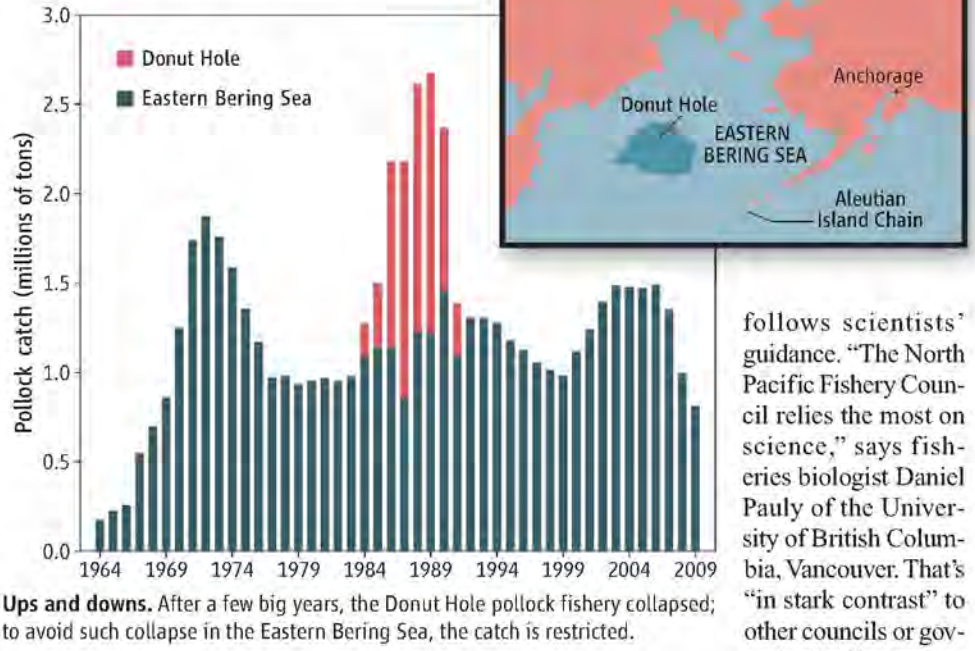

Ups and downs. After a few big years, the Donut Hole pollock fishery collapsed; to avoid such collapse in the Eastern Bering Sea, the catch is restricted.

Critics say worries about the fishery stem from a fundamental issue: It's managed primarily to get the maximum sustainable yield from a single species. "It can't make a legitimate claim to [being] an ecosystem-based fishery, as long as it maintains this single-species focus," says Timothy Ragen, director of the Marine Mammal Commission in Bethesda, Maryland.

Jackson and others say that when faced with questionable data, as scientists were this year, it would be better to reduce the quota even further. Fritz says he tried to persuade the Plan Team to do that but failed. "Can we recognize the danger signals and react appropriately and in time, if the fishery is really in trouble?" he asks.

But the fishery is required by law to also consider the socioeconomic effects of its decisions. The pollock fishery is one of Alaska's largest employers, and former Alaska Senator Ted Stevens once brought the entire U.S. government to a halt to protest (and eventually overturn) restrictions upon it. "There's a lot of policy in this process," says DeMaster. "It's not entirely science."

Still, many say that the pollock fishery continues to be one of the best-managed in the world, largely because the Fishery Council, unlike some other big fisheries, follows scientists' guidance. "The North Pacific Fishery Council relies the most on science," says fisheries biologist Daniel Pauly of the University of British Columbia, Vancouver. That's "in stark contrast" to other councils or governing bodies such as the European Commission, he says, where fisheries sometimes ignore scientific advice and adopt high quotas, "and the stocks [such as bluefin tuna] suffer accordingly."

So when fishing-fleet representatives and others gather in Anchorage next week at the Fishery Council's meeting to set next year's quotas, the scientists' recommendations likely will be adopted. "We know the scientists are concerned," says Donna Parker of the Seattle-based fishing firm, Arctic Storm Management Group . "They treat our fishery like a cultivated field, and we expect they will manage it well into the future."

–VIRGINIA MORELL

SOURCE: J. IANELLI ET AL./ALASKA FISHERIES SCIENCE CENTER/NATIONAL MARINE FISHERIES SERVICE

PARTICLE PHYSICS

Seeking a Shortcut to the High-Energy Frontier

An accelerator that smashes exotic particles called muons promises more bang from a smaller accelerator—if physicists can actually build it

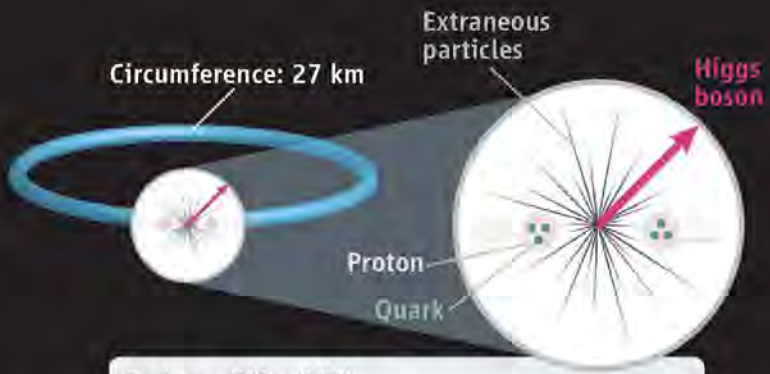

Proton collider (LHC)
Pros: Taking laps, protons reach very high energy **Cons:** Because they have internal parts, protons make messy, inefficient collisions

BATAVIA, ILLINOIS—When you fall behind, you need a comeback plan, and physicists here at the Fermi National Accelerator Laboratory (Fermilab) think they have a dandy. They're losing their title as keepers of the world's highest-energy particle smasher, but they have an idea for a wild new one that might vault them back to the energy frontier. They're hoping the U.S. Department of Energy (DOE) will give them enough money to find out whether their idea is a dream machine—or a technological nightmare.

For 24 years, Fermilab's Tevatron collider has held the energy record for particle collisions, firing protons into antiprotons at a maximum of 2 tera–electron volts (TeV). But researchers at the European particle physics lab, CERN, near Geneva, Switzerland, are finally revving up the 27-kilometer-long, $5.5 billion Large Hadron Collider (LHC), which aims to blast protons into other protons at 14 TeV. With the Tevatron facing obsolescence, Fermilab physicists hope to build a beast called a muon collider.

The new machine, the topic of a workshop here last month, would smash muons, which are heavier cousins of electrons, into antimuons. In principle, it could reach energies as high as rivals already in the planning stages—the 30-kilometer-long straight-shot International Linear Collider (ILC) that would fire electrons into positrons and a higher-energy electron-positron collider called the Compact Linear Collider (CLIC) being developed at CERN. But a muon collider would be much smaller. As cost scales with size, it could also be cheaper than the other machines.

That's *if* a muon collider can be built. Unlike electrons or protons, muons are radioactive. So the facility would have to generate the particles, accelerate them, and smash them together in the fraction of a second before they decay. Physicists would also have to protect their equipment from the intense radiation emanating from the muons and limit the amount flowing out of the lab.

Interest in the exotic machine has grown because the more conventional plans hatched by U.S. physicists have stalled. Three years ago, they were hoping to host the ILC, with construction to start as early as 2012. But DOE officials blanched when researchers estimated that it would cost at least $7 billion (*Science*, 9 February 2007, p. 746). DOE officials now think the price of the ILC could top $20 billion, including inflation and contingency, and have said the project cannot be realized until the mid-2020s.

That delay has created an opening for supporters of the muon collider, and they seem to have DOE's ear. At an advisory panel meeting in October, William Brinkman, head of DOE's Office of Science, told *Science*: "I'd like to see Fermilab do something with a muon accelerator. That would be something novel, rather than spending time beating our brains out building the next biggest accelerator."

But is a muon collider a machine impossible? "The problems range from hard to very hard to ultrahard," says Fermilab Director Pier Oddone. Researchers have requested $16 million per year over 5 years just to determine if a muon collider can be built, he says. Even that may be asking too much, says Daniel Schulte, an accelerator physicist at CERN. "That's—oh God, how do I put this?—an ambitious goal."

The best of both worlds

Particle colliders generally come in two types: those that smash protons or antiprotons and those that smash electrons and positrons. A muon collider might combine the advantages of proton and electron machines.

For revving particle beams to the highest energies, nothing beats a proton accelerator. At 14 TeV, the LHC will blast out massive new particles or even open new dimensions of space, or so researchers hope. However, as with any proton collider, the LHC will reveal those things in a messy way.

Protons contain other particles called quarks and gluons. So when one proton tears through another, debris flies every which way. "It's like two cans of Campbell's soup," says Vladimir Shiltsev, an accelerator physicist at Fermilab. "You collide them and soup splashes everywhere. But God knows what actually happened." Within the mess, typically only one gluon scores a direct hit on another, so only ⅙ to ⅒ of the protons' energy goes to make new particles.

In contrast, electrons and positrons have no internal parts. So they make clean collisions in which all the energy can go into making new particles. That's why physicists say that the logical successor to the LHC is an electron-positron collider. The ILC would generate collisions at 0.5 TeV, which might be enough to map the terrain the LHC will open. If not, the 40-kilometer-long CLIC would make 3-TeV collisions by using a lower-energy beam to drive a higher-energy one.

There is a catch, however. Because every action has a reaction, charged particles radiate when their paths are forced to curve. Responding readily to a sideways shove, lightweight electrons and positrons give off copious x-rays that sap their energy and prevent them from reaching TeV-level energies in a circular accelerator, or "synchrotron." So both the ILC and CLIC would use two huge linear accelerators facing each other. That's an inefficient arrangement, as the electrons and positrons collide only once instead of repeatedly, as happens in a circular machine.

Muons share the better features of protons and electrons. Like protons, they are heavy, weighing 207 times as much as electrons. So they radiate little energy as their paths bend and could reach high energy in a relatively small synchrotron. Like electrons, however, muons have no parts, so their clean collisions permit all the energy to go into new particles. "Basically, we can do very efficient acceleration and reach a

CREDIT: J. NEWFIELD/*SCIENCE*

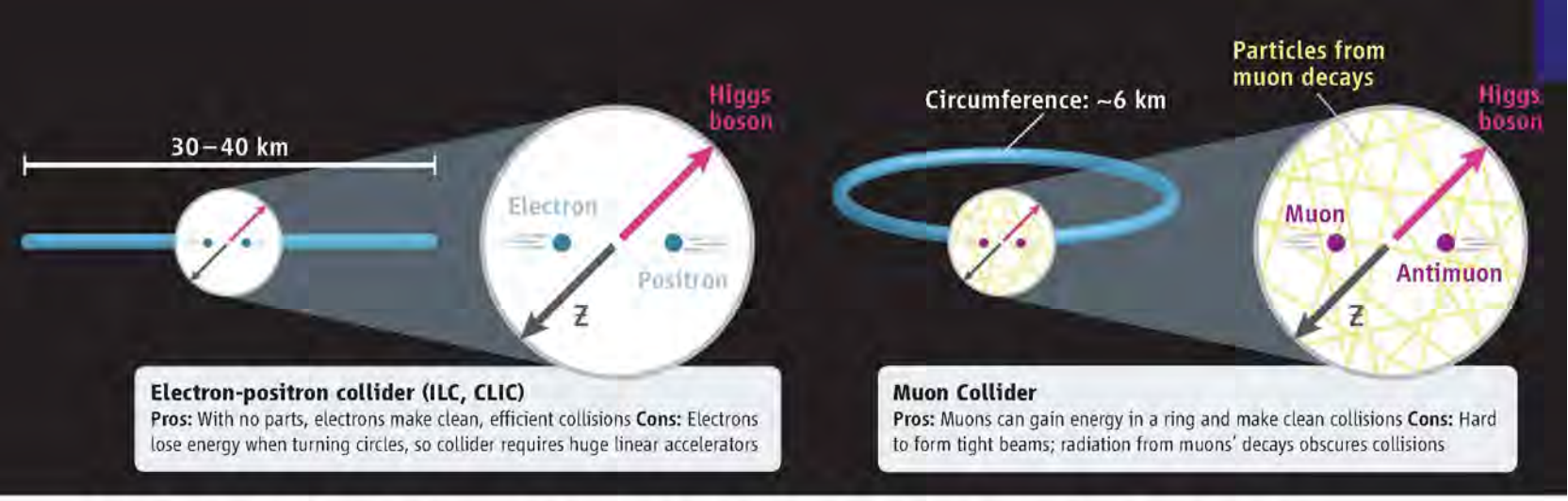

Hot stuff. A muon collider would share the strengths of proton and electron accelerators, but the muons' radioactivity poses a major challenge.

higher energy with a much smaller machine than any electron collider or proton collider," Shiltsev says. A muon collider would fit comfortably on Fermilab's 2750-hectare campus, he says.

The machine might also fit into Fermilab's other plans. Sometime in the next decade, lab officials hope to build a proton source, known as Project X, to generate neutrinos and study their interactions and pursue other subjects on the "intensity frontier" (*Science*, 31 August 2007, p. 1155). A muon collider would also need a proton source like Project X.

Challenges galore

A muon collider poses daunting challenges, however. Physicists must generate the muons and antimuons by blasting protons into a metal target. They must gather the particles into bunches and "cool" them so that they nestle together. The bunches of muons and bunches of antimuons must then pass through a series of accelerators and into a final synchrotron, where they would circulate in opposite directions and collide.

"The problems range from hard to very hard to ultrahard."

—FERMILAB DIRECTOR PIER ODDONE

All of this must happen before the muons decay. If a muon zings along at 1.5 TeV, the time dilation of special relativity stretches its lifetime to 30 milliseconds—up from 2 microseconds when it's still. That's time enough for 500 circuits in the final ring, says Michael Zisman of Lawrence Berkeley National Laboratory in California, if everything goes smoothly.

Accelerator physicists' biggest challenge will be cooling the muons. Cooling reduces the relative motion of particles within a bunch, and because electrons radiate so easily, physicists can cool them by simply sending them around a synchrotron for a while. As the electrons in a bunch radiate, the bunch contracts like a balloon shoved into a refrigerator. Muons radiate very little, so that approach won't work for them.

Instead, physicists are considering a scheme called ionization cooling. In it, the muons would run alternately through liquid hydrogen, to slow their motion in all directions, and through chambers filled with radio waves, to speed them up in just one direction. An incredibly high magnetic field—50 tesla, or 1 million times Earth's field—is needed to keep the muons from flying away. "The techniques we need are beyond state-of-the-art," says Fermilab's Stephen Geer. Researchers in the United Kingdom are currently trying to demonstrate the technique in small-scale bench tests.

Radiation will also cause headaches for accelerator designers. Muons decay into electrons and neutrinos, and the electrons would convey enough power to overheat the superconducting magnets that would guide the muons around the ring. So researchers are considering novel designs with slots to let the radiation out.

The radiation would also generate particle "backgrounds" that might overwhelm the desired signals from the collisions. Simulations suggest that 100,000 neutrons and 10 million photons would flood each square centimeter of a particle detector during each bunch crossing, Fermilab's Marcel Demarteau said at the workshop. All that extraneous particle pollution might render the muon collider irrelevant as a follow-up to the LHC, says Barry Barish, a physicist at the California Institute of Technology in Pasadena, who leads the ILC design team: "The whole point of going to electron-positron collisions is to get an environment that's clean enough to do all the things you can't do at the LHC," he says.

Perhaps most problematically, the muon collider will send radiation beyond the lab's boundary. Neutrinos hardly interact with matter, so those from the muon decays would pierce Earth in all horizontal directions and emerge from its curved surface tens of kilometers away. There they would be numerous enough to knock loose other particles and create interacting radiation. Scientists say they can keep such radiation at safe and legal levels by building the collider 200 meters underground and limiting the muons in the beam. Convincing the public, however, may be more difficult.

Which collider, when?

Such obstacles led physicists to write off a muon collider in the 1990s. But recent advances have prompted a reconsideration. For example, physicists once lacked a suitable source of muons, but researchers have recently demonstrated a mercury target that can provide enough of them, says Fermilab's Nikolai Mokhov.

All agree that before any decision can be made on the next collider, the LHC has to reveal at what energy new particles will emerge, which will take 3 or 4 years. If the answer is in the neighborhood of 0.5 TeV, then the ILC would be the way to go, says Fermilab's Oddone. If the range is higher, then the options would be a muon collider or CLIC. "If we need a higher-energy machine, we want to have put the muon collider into contention" by that time, Oddone says.

But even that goal strikes some as optimistic. Jean-Pierre Delahaye, an accelerator physicist at CERN, says researchers plan to publish a report next year that shows that CLIC is feasible. That is 24 years after they came up with the idea. "I would bet a bottle of champagne—a case—that [a feasibility study] will take at least as long for a muon collider," he says. If so, 5 years won't be nearly long enough to tell whether the idea of a muon collider is too good to be true.

—ADRIAN CHO

Screening science
1348

Nickel-based electrodes mimic hydrogenases
1355

LETTERS | BOOKS | POLICY FORUM | EDUCATION FORUM | PERSPECTIVES

LETTERS

edited by Jennifer Sills

Biofuels: Social Benefits

IN THEIR POLICY FORUM "BENEFICIAL BIOFUELS—THE FOOD, energy, and environment trilemma" (17 July, p. 270), D. Tilman *et al.* argue that the search for beneficial biofuels should focus on feedstocks that (i) do not compete with food crops, (ii) do not lead to land-clearing, and (iii) offer real greenhouse-gas reductions. We suggest a fourth criterion: the maximization of social benefits.

Indonesia's oil palm industry provides employment for 4.5 million people (*1*). Many smallholder producers also derive significant economic benefits (*2*, *3*). However, the negative impacts of oil palm development are also widely reported and include poor wages and labor standards, impacts on health and local culture, "land grabbing," and the loss of environmental goods and services (*4*, *5*). Although the cultivation of biofuel feedstocks may represent an opportunity for rural development (*6*, *7*), the social impacts need to be carefully assessed.

Oil palm fruit. The social impacts of the oil palm industry must be assessed.

Four of the five biomass sources outlined by Tilman *et al.* may be of less merit upon inclusion of this criterion. Cultivation on degraded or abandoned lands may indeed minimize competition with food production. However, if such lands support the subsistence of rural communities, biofuel development will likely result in social costs, especially given that the rights of these communities are often poorly protected (*8*, *9*). Furthermore, the potential use of crop and forestry residues or municipal and industrial wastes in developed nations to produce next-generation biofuels may undermine demand for feedstocks from tropical developing countries that currently supply international markets.

Coherent biofuels policies must also address the social context of agricultural production if biofuels are to make a sustainable contribution toward reducing climate change and safeguarding food security. Tilman *et al.*'s selection criteria are valuable but should include the potential opportunities and risks to rural communities afforded by biofuel feedstock cultivation.

LUCY RIST,* JANICE SER HUAY LEE, LIAN PIN KOH

Institute for Terrestrial Ecosystems, Eidgenössische Technische Hochschule (ETH) Zürich, Zürich 8092, Switzerland.

*To whom correspondence should be addressed. E-mail: lucy.rist@env.ethz.ch

References

1. H. J. Sargeant, "Vegetation fires in Sumatra, Indonesia. Oil palm agriculture in the wetlands of Sumatra: Destruction or development?" (European Union and Ministry of Forestry, Jakarta, Indonesia, 2001).
2. Z. Zen, C. Barlow, R. Gondowarsito, *Oil Palm Industry Econ. J.* **6**, 18 (2006).
3. W. R. Susila, *J. Litbang Pertanian* **23**, 107 (2004).
4. M. Colchester, W. Aik Pang, W. M. Chuo, T. Jalong, "Land is life: Land rights and oil palm development in Sarawak" (Forest Peoples Programme and Perkumpulan Sawit Watch, Indonesia, 2007).
5. M. Colchester *et al.*, "Promised land: Palm oil and land acquisition in Indonesia: Implications for local communities and indigenous peoples" [Forest Peoples Programme, Sawit Watch, Association for Community- and Ecology-Based Law Reform (HuMA), and World Agroforestry Centre (ICRAF), Indonesia, 2006].
6. J. Pickett *et al.*, "Sustainable biofuels: Prospects and challenges" (The Royal Society, London, 2008).
7. Editorial, *Nature* **449**, 637 (2007).
8. D. Rajagopal, paper presented at the International Conference "Linkages between energy and water management for agriculture in developing countries," Hyderabad, India, 29 to 30 January 2007, sponsored by the International Water Management Institute (IWMI) and Food and Agriculture Organization of the United Nations (FAO).
9. African Press Agency, "Thousands of Tanzanian peasants to be displaced for biofuel farm," African Press Agency, 12 August 2007; http://pacbiofuel.blogspot.com/2007/08/pbn-thousands-of-tanzanian-peasants-to.html.

Biofuels: By-Products

IN THE POLICY FORUM "BENEFICIAL BIOFUELS—the food, energy, and environment trilemma" (17 July, p. 270), D. Tilman *et al.* emphasized the importance of a life-cycle assessment that includes the impact of biofuels production on future food supplies, greenhouse gas emissions, and environmental consequences of clearing virgin land and potential reduction in biodiversity. We agree that these potential impacts are crucial and add a fourth component: environmental and health impacts of the co-products or by-products that arise during generation of biofuels from feedstocks.

For example, maize-based ethanol production results in the production of dried distillers' grain plus solubles or wet distillers' grains, which are sold primarily as livestock and poultry feed (*1*). Unfortunately, any mycotoxins in the original maize become up to three times as concentrated in these co-products (*2*–*4*). Hence, including the co-products in livestock and poultry diets can cause adverse health effects in animals, resulting in potential economic losses to livestock and poultry industries (*1*). Although the next-generation feedstocks proposed by Tilman *et al.* do not include maize grain, similar environmental and health risks of by-products and co-products and their potential uses should be considered in any life-cycle assessment used to drive national biofuels policy.

Converting municipal and industrial waste to liquid fuels, as proposed by Tilman *et al.*, would provide a potentially sustainable pathway for this waste to replace current treatment and disposal approaches. This use of an industrial waste stream has the potential to eliminate a costly expense for industries and turn it into a new profit center. One example is paper sludge, a waste material that currently goes

CREDIT: WIKIMEDIA COMMONS

Plant hormone receptor identified, at last
1356

Life science prize essay
1360

into landfills at a cost of $60 to $100 per dry ton (*5*). However, production of biofuels from waste materials may release chemicals such as dioxins and heavy metals that could result in unintended environmental and public health exposures. Industrial market research should explore whether suitable sustainable pathways exist for co-products that will simultaneously generate revenue streams and reduce the potential for adverse exposures.

THOMAS M. BIKSEY[1,2] AND FELICIA WU[2]*

[1]WSP Environment and Energy, Pittsburgh, PA 15220, USA. [2]Department of Environmental and Occupational Health, University of Pittsburgh, Pittsburgh, PA 15219, USA.

*To whom correspondence should be addressed. E-mail: few8@pitt.edu

References

1. F. Wu, G. P. Munkvold, *J. Agric. Food Chem.* **56**, 3900 (2008).
2. G. A. Bennett, J. L. Richard, *Food Technol.* **50**, 235 (1996).
3. G. S. Murthy *et al.*, *Cereal Chem.* **82**, 302 (2005).
4. A. W. Schaafsma *et al.*, *J. Sci. Food Agric.* **89**, 1574 (2009).
5. D. Burden, "Cellulosic ethanol profile" [Agricultural Marketing Resource Center (AgMRC), Iowa State University, August 2009].

Biofuels: Algae

IN THE POLICY FORUM "BENEFICIAL BIOFUELS—the food, energy, and environment trilemma" (17 July, p. 270), D. Tilman *et al.* concisely summarize the Gordian knot entangling the food and environmental implications of biofuel development. However, they overlook algae as a solution. Others have concluded that microalgae are the only source of renewable biodiesel that can meet global demand for transport fuels (*1*, *2*).

Tilman *et al.* argue cogently that "biofuels done right" must derive from feedstocks with low greenhouse gas emissions and little or no competition with food production. Algae are likely to win on both counts. For example, had the 67 million acres of soybeans cultivated in 2007 gone entirely to biodiesel, they would have displaced 6% of the United States' on-road petroleum diesel use; the same acreage used for algal culture would yield more than 100% of the petroleum diesel usage, even assuming modest algal productivity (*3*).

Microalgae are typically at least an order of magnitude more productive than even the fastest growing terrestrial feedstock crops, require no soil, and can be grown in eutrophied water (fresh or saline), which is unsuitable for agriculture or human consumption. Thus, algal production does not compete for scarce arable land and can remove nutrients and contaminants from waterways. Although rigorous life-cycle analyses are not yet available, the prospects for carbon-neutral or negative production of algal fuels on commercial scales appear bright (*3*).

J. EMMETT DUFFY,[1]* ELIZABETH A. CANUEL,[1] WALTER ADEY,[2] JOHN P. SWADDLE[3]

[1]Virginia Institute of Marine Science, The College of William and Mary, Gloucester Point, VA 23062, USA. [2]National Museum of Natural History, Smithsonian Institution, Washington, DC 20013–7012, USA. [3]Environmental Science and Policy Program, The College of William and Mary, Williamsburg, VA 23187, USA.

*To whom correspondence should be addressed. E-mail: jeduffy@vims.edu

References

1. Y. Chisti, *Biotechnol. Adv.* **25**, 294 (2007).
2. Y. Chisti, *Trends Biotechnol.* **26**, 126 (2008).
3. U.S. Department of Energy Biomass Program, "National algal biofuels technology roadmap" (draft report, 2009); https://e-center.doe.gov/iips/faopor.nsf/UNID/79E3ABCACC9AC14A852575CA00799D99/sfile/AlgalBiofuels_Roadmap_7.pdf.

Biofuels: Forests and Carbon

IN THE POLICY FORUM "BENEFICIAL BIOFUELS—the food, energy, and environment trilemma" (17 July, p. 270), D. Tilman *et al.* neglected to mention the role of forests and carbon capture and storage. Trees offer promise as an energy crop in areas where they grow well on degraded lands. A new and permanent reservoir of carbon is created as planted forest develops toward a steady state where mature trees mix with young saplings. Furthermore, forests offer a great variety of ecosystem services such as biodiversity promotion, nutrient retention, and flood protection. Timber crops can be harvested at any time during the year, and the durable wood serves as an interim energy storage—two assets for energy transport logistics. The carbon budget of wood is competitive against other materials in end uses such as construction (*1*).

Opportunities to use side-products from wood-processing industries in electricity production should be fully explored. Biopower in any case deserves attention. Greenhouse gas benefits are better achieved making electricity than fuels (*2*–*4*).

PEKKA E. KAUPPI* AND LAURA SAIKKU

Faculty of Biosciences, University of Helsinki, Helsinki, Finland.

*To whom correspondence should be addressed. E-mail: pekka.kauppi@helsinki.fi

References

1. L. Gustavsson *et al.*, *Mitigation Adapt. Strategies Global Change* **11**, 667 (2006).
2. J. E. Campbell, D. B. Lobell, C. B. Field, *Science* **324**, 1055 (2009); published online 7 May 2009 (10.1126/science.1168885).
3. S. Soimakallio *et al.*, *Energy Pol.* **37**, 80 (2009).
4. J. Ohlrogge *et al.*, *Science* **324**, 1019 (2009).

Biofuels: Beware Crop Residues

IN THE POLICY FORUM "BENEFICIAL BIOFUELS—the food, energy, and environment trilemma" (17 July, p. 270), D. Tilman *et al.* propose using crop residues and harvesting biomass from double crops and mixed cropping systems. We point out the potential risks of doing so.

Retention of crop residues on soils, including the biomass produced from cover crops, is essential to numerous ecosystem services such as carbon sequestration, conservation of soil and water, and high use-efficiency of inputs for increasing and sustaining agronomic productivity. The agrarian stagnation and perpetual food deficit in sub-Saharan Africa is attributed to severe soil degradation (*1*, *2*), caused by extractive farming practices that involve continuous removal of crop residues for use as traditional biofuels and cattle feed. This has created a negative nutrient budget. Soils are a source of greenhouse gases (CO_2, CH_4, and N_2O) when prone to accelerated erosion and when under management that creates negative carbon and nutrient budgets. Crop residues and other biosolids are essential to maintain activity and species diversity of soil biota (micro-

Letters to the Editor

Letters (~300 words) discuss material published in *Science* in the previous 3 months or issues of general interest. They can be submitted through the Web (www.submit2science.org) or by regular mail (1200 New York Ave., NW, Washington, DC 20005, USA). Letters are not acknowledged upon receipt, nor are authors generally consulted before publication. Whether published in full or in part, letters are subject to editing for clarity and space.

and macroorganisms) and to improve soil structure and tilth (*3*–*5*). Indiscriminate removal of crop residues and harvesting of biomass from cropland soils is supported neither by science nor by conventional wisdom.

RATTAN LAL[1]* AND DAVID PIMENTEL[2]

[1]School of Natural Resources, The Ohio State University, Columbus, OH 43210, USA. [2]College of Agriculture and Life Sciences, Cornell University, Ithaca, NY 14853, USA.

*To whom correspondence should be addressed. E-mail: lal.1@osu.edu

References

1. P. A. Sanchez, *Science* **295**, 2019 (2002).
2. J. Henoa, C. Baanante, "Agricultural production and soil nutrient mining in Africa: Implications for resource conservation and policy development" [International Fertilizer Development Center (IFDC), Muscle Shoals, AL, 2006]; www.africafertilizersummit.org/Background_Papers/03%20Henao%20and%20Baanante--Agricultural%20Production.pdf.
3. R. Lal, D. Pimentel, *Soil Tillage Res.* **93**, 237 (2007).
4. R. Lal, *CSA News* **52**, 12 (2007).
5. H. Blanco-Canqui, R. Lal, *Geoderma* **145**, 335 (2008).

Biofuels: Steer Clear of Degraded Land

WE DISAGREE WITH D. TILMAN *ET AL.* ("Beneficial biofuels—the food, energy, and environment trilemma" Policy Forum, 17 July, p. 270) that perennial plants should be grown on degraded lands that can no longer be used for agriculture. If land is fertile enough to grow plants that offer substantial yields for biofuels, it should be suitable for agriculture as well. Even if not used today, this land could be kept as a productive reserve and used later to combat the foreseeable problems in feeding the world in the future (*1*). If the land is not fertile enough for that purpose, the perennial energy plants will probably be dependent on anthropogenic inputs such as fertilizers and, in some regions, irrigation. These are the factors disrupting the energy balance; nitrogen fertilization is the basis for N_2O emissions with the potential to overcompensate all greenhouse gains (*2*). Economically, such plantations would not be viable without intensive farming practices, raising doubts regarding the expected benefits for biodiversity and wildlife.

Given that currently only about 10% of the global primary energy demand is covered by renewable resources and that humans already appropriate large percentages of the potentially available biomass (20 to 40% globally, 50% in some industrialized countries, up to 90% in intensively farmed regions) (*3*), we are skeptical about the potential of biofuels. We join Tilman *et al.* in urgently requesting additional research, but we cannot support their demand that "a robust biofuels industry should be enabled" now. We'd better look before we leap.

JOACHIM H. SPANGENBERG[1,2]*
AND JOSEF SETTELE[2]

[1]Sustainable Europe Research Institute Germany, 51103 Cologne, Germany. [2]Department of Community Ecology, UFZ–Helmholtz Centre for Environmental Research, 06120 Halle, Germany.

*To whom correspondence should be addressed. E-mail: Joachim.Spangenberg@gmx.de

--References

1. J. M. Alston, J. M. Beddow, P. G. Pardey, *Science* **325**, 1209 (2009).
2. P. J. Crutzen, *Atmos. Chem. Phys.* **8**, 389 (2008).
3. H. Haberl *et al.*, *Agr. Ecosyst. Env.* **102**, 213 (2004).

Response

THE LETTERS ABOUT OUR COMMENTARY RAISE issues with which, for the most part, we agree. They amplify our assertion that each biofuel should be evaluated on its net benefit to society based on a full life-cycle analysis that includes, among other factors, its effects on net energy supply, the global food system, greenhouse-gas emissions, soil carbon and soil fertility, water and air quality, and biodiversity. We agree with Rist *et al.* that the social context and international equity issues associated with food and biofuel merit inclusion in such analyses. We support the suggestion by Biksey and Wu that health and environmental impacts of biofuels and their co-products should be included. Other biomass sources, such as algae (Duffy *et al.*) and other technologies, such as biomass combined with carbon capture and storage (Kauppi and Saikku), merit evaluation and consideration. We agree with Lal and Pimentel that biomass should be grown so as to maintain or increase soil fertility. Contrary to Spangenberg and Settele, we believe that appropriate perennials can give reasonable yields and increase soil carbon stores when grown with low inputs on degraded soils (*1*). In a world that is increasingly rich and energy-hungry, solutions are more likely to be wise tradeoffs than miracles. Because substantial components of the global transportation system have no viable substitutes for liquid fuels, it is important and timely, as we asserted, to support the emergence of an industry that produces biofuels that offer significant net benefits relative to petroleum. At the same time, we need comprehensive, science-based policies that protect wild lands and make managed lands—including but not limited to land used for biofuels—part of the solution to reducing atmospheric carbon.

DAVID TILMAN,[1]* ROBERT SOCOLOW,[2]
JONATHAN A. FOLEY,[3] JASON HILL,[3] ERIC LARSON,[2]
LEE LYND,[4] STEPHEN PACALA,[2] JOHN REILLY,[5]
TIM SEARCHINGER,[6] CHRIS SOMERVILLE,[7]
ROBERT WILLIAMS[2]

[1]Department of Ecology, Evolution, and Behavior, University of Minnesota, St. Paul, MN 55108, USA. [2]Princeton Environmental Institute, Princeton University, Princeton, NJ 08544, USA. [3]Institute on the Environment, University of Minnesota, St. Paul, MN 55108, USA. [4]Thayer School of Engineering, Dartmouth College, Hanover, NH 03755, USA. [5]Center for Energy and Environmental Policy Research, Massachusetts Institute of Technology, Cambridge, MA 02142, USA. [6]Woodrow Wilson School, Princeton University, Princeton, NJ 08544, USA. [7]Energy Biosciences Institute, University of California Berkeley, Berkeley, CA 94720, USA.

*To whom correspondence should be addressed. E-mail: tilman@umn.edu

Reference

1. D. Tilman, J. Hill, C. Lehman, *Science* **314**, 1598 (2006).

CORRECTIONS AND CLARIFICATIONS

Research Article: "An Argonaute transports siRNAs from the cytoplasm to the nucleus" by S. Guang *et al.* (25 July 2008, p. 537). The rightmost four images in the top panel of Fig. 2A and the top image of Fig. 3A were inadvertently mislabeled and duplicated. Investigators who were not involved in the original experiments have repeated these experiments, which yielded results similar to those originally reported. Our conclusions remain unaltered. The corrected figures are shown below (left).

Reports: "Gender disparity in liver cancer due to sex differences in MyD88-dependent IL-6 production" by W. E. Naugler *et al.* (6 July 2007, p. 121). The originally published Fig. 3B inadvertently duplicated Fig. 3E. The corrected 3B, along with originally published 3E, is provided below (right).

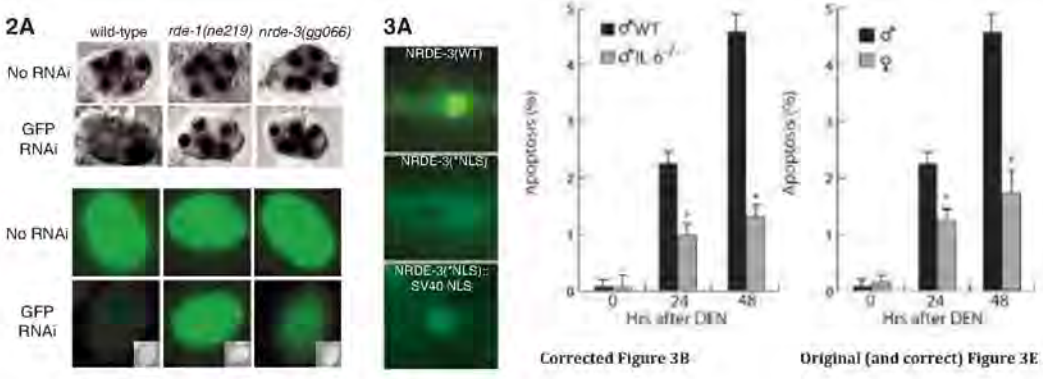

Corrected Figure 3B

Original (and correct) Figure 3E

HISTORY OF SCIENCE

Researchers Writing for the Public

Melinda Baldwin

Who speaks for science? Who is responsible for informing the public about the latest conclusions in biology, physics, or medical research? Today, the answer is almost certainly "not scientists." Only a handful of our scientific luminaries venture into the world of popular writing—Stephen Hawking's *A Brief History of Time* (*1*) is an obvious example—and most scientists will never pick up a pen to write an article intended for anyone other than their scientific peers. Science reporting in newspapers and on television is generally left in the hands of journalists, although not without frequent laments over the way scientific findings tend to grow—or be misinterpreted entirely—in the retelling.

Peter Bowler's *Science for All* tells the story of an entirely different relationship between the scientific community and popular science writing. A great deal has been written about popular science in the Victorian era, when famous men of science such as T. H. Huxley or John Tyndall could make a healthy income from popular writing and lecturing. Most scholars have assumed that scientists abandoned direct communication with the public in the early 20th century, once science firmly established itself as a respectable, stable profession. But Bowler (a historian of science at Queen's University, Belfast) seeks to challenge this notion. On the contrary, he argues, the first generation of professionalized scientists in Britain frequently participated in writing for a popular audience.

Bowler's book provides an impressively thorough survey of the different types of popular science writing, from bestsellers like physicist Arthur S. Eddington's *The Nature of the Physical World* (*2*) to the *Encyclopedia Britannica* to science magazines like *Discovery* and the sensationalistic *Popular Science Siftings*. Particularly interesting is Bowler's account of publishers' educational series, a now-defunct genre that provided British publishers with strong profits in the early decades of the 20th century. Series such as the "Cambridge Manuals of Science and Literature" from Cambridge University Press or the "Home University Library" from Williams and Norgate were designed to reach buyers who sought to supplement their education by reading books on the latest developments in knowledge—a brand of educational self-improvement for which British social conditions created a unique demand.

So why has this mass of early-20th-century popular writing gone unnoticed? Why have historians assumed that after 1900, professional scientists were discouraged from writing for a broad lay audience? Bowler admits that a few scientists, such as Julian Huxley (T. H. Huxley's grandson) and the Aberdeen zoologist J. Arthur Thomson, achieved popular success at the expense of their scientific credibility: Huxley had difficulty being elected as a fellow of the Royal Society because he had resigned his university post to make his career as a writer, and Thomson never achieved the coveted FRS.

But Bowler suggests that such cases have been overemphasized and convincingly makes the point that so long as a scientist continued to produce high-quality research (which Huxley and Thomson did not), popular writings did not affect his scientific credibility. The eminent geneticist J. B. S. Haldane, for example, wrote prolifically for newspapers and magazines, including the controversial Communist newspaper *Daily Worker*, without abandoning his research or complicating his election as a fellow of the Royal Society. Similarly, Eddington could write about relativity for a popular audience and James Jeans could turn his popular lectures into the bestselling *The Mysterious Universe* (*3*) without risking their standing in the eyes of their scientific colleagues. Furthermore, Bowler demonstrates that less-distinguished junior professors often turned to popular writing to supplement paltry academic incomes and that doing so was not seen as compromising to one's future scientific career.

The book's readability is somewhat hampered by Bowler's structural choices. The book is divided into three parts, of which the second and third contain the true heart of Bowler's argument: the account of the varied genres of popular science publishing and his discussion of the backgrounds of the scientists who wrote for the popular press. Bowler begins the book by discussing different visions of science that his scientist-popularizers sought to promote through their writings. In his introduction, he admits that this material "is not the primary focus of [his] study" and that much historical schol-

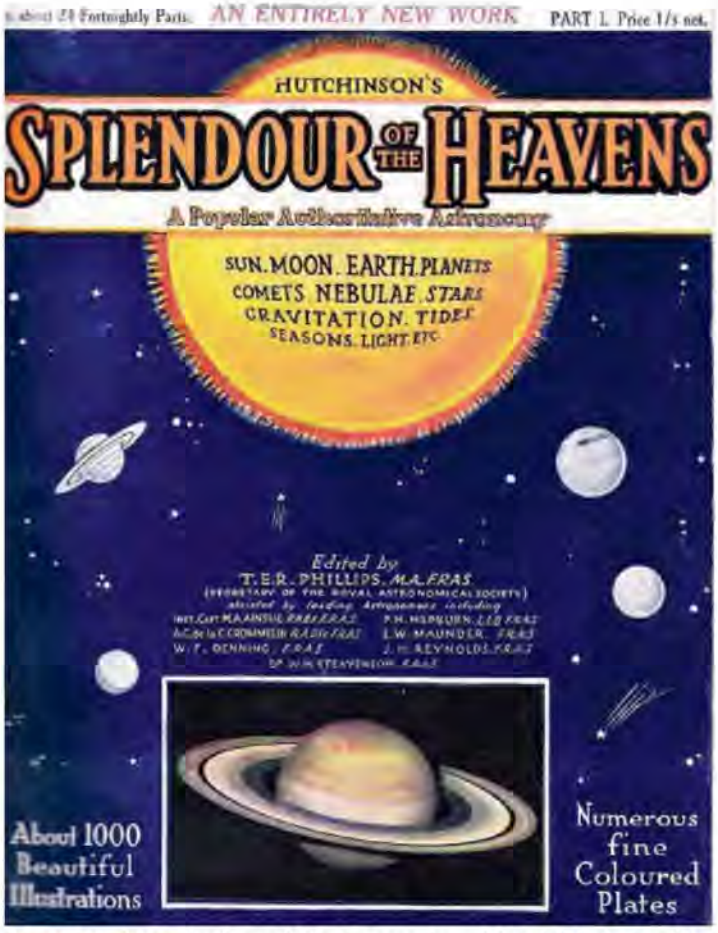

24-part series. *Splendour of the Heavens*, issued fortnightly by Hutchinson's in 1923–24, was filled with contributions from fellows of the Royal Astronomical Society.

Science for All
The Popularization of Science in Early Twentieth-Century Britain

by Peter J. Bowler

University of Chicago Press, Chicago, 2009. 351 pp. $45, £31. ISBN 9780226068633.

The reviewer is at the History of Science Program, Princeton University, 129 Dickinson Hall, Princeton, NJ 08544, USA. E-mail: mcbaldwi@princeton.edu

CREDIT: COURTESY PETER J. BOWLER/FROM *SCIENCE FOR ALL*

arship has already been done on the various motives behind popular science writing. The result, unfortunately, is that the three chapters on "Topics and themes in popular science" feel dry and dutiful, like a comprehensive but unenthusiastic literature review designed to assure Bowler's fellow historians that he is familiar with the existing scholarship on the topic.

The author's desire to get the less-interesting chapters out of the way early is understandable. But when the rest of the book is so rich, it seems a shame to begin with the least original content. Readers who find themselves bogged down in the early chapters might abandon the book entirely and miss out on Bowler's fascinating account of the varied genres of popular science and the stories of the men (and the handful of women) responsible for creating this material.

Structural difficulties aside, *Science for All* is carefully researched, lucidly argued, and extremely interesting. Not only a valuable contribution to historical scholarship, the book challenges readers to consider whether the division between research and popular science writing is in fact an integral part of professionalized science—and whether this division must necessarily endure in the future.

References

1. S. W. Hawking, *A Brief History of Time: From the Big Bang to Black Holes* (Bantam, London, 1988).
2. A. S. Eddington, *The Nature of the Physical World* (Cambridge Univ. Press, Cambridge, 1928).
3. J. Jean, *The Mysterious Universe* (Cambridge Univ. Press, Cambridge, 1930).

10.1126/science.1183425

FILM

Science Goes Hollywood

Cat Bohannon,* Anthony DeCostanzo,* Tim Requarth,* Abba Dawesar, Annegret Falkner, Stuart Firestein,† Cynthia Jung, Anna North, Rachel Riederer, Kim Tingley, Greg Wayne

Under gently glittering chandeliers and taxidermy mounts of animal heads, a young, hip crowd of scientists and film buffs stood around sipping cocktails and conversing about learned matters. The Bell House, a performance space near New York City's Gowanus Canal, is a common zone for such activities. What was unusual about this particular October evening was that the crowd specifically gathered to be inspired by science. They participated in a "Sketchy Science" drawing contest, competing for t-shirts and bar tabs for the best spontaneous depiction of the future of science. They then sat down together and watched a string of "Quirky Science Shorts"—short films that in some way made an art of representing science. Waiting for them at their seats were small slips of paper, on which they were asked to vote for their favorite film. Their choices would help determine which filmmaker received a cash award.

Is this the way that science finally becomes cool? Alongside events such as the World Science Fair and the TED conference, New York's Imagine Science Film Festival (now in its second year) attracts bright young people under the auspices of merging science and art. The festival's panel reviewed over 300 submissions to select four feature films and 46 shorts from nine countries for the two-week event. Screenings, panel discussions, and question-and-answer sessions were held in universities, art house cinemas, and bars scattered about Manhattan, Brooklyn, and Queens. In mid-October, we set off in scientist-artist pairs to see whether the festival really did bridge the gap between science and art.

The festival included a sweeping range of genres. The offerings included a handful of traditional documentaries and biopics—for instance, a feature film loosely based on Eric Kandel's autobiography *In Search of Memory*. The majority, however, were more experimental: a five-minute animation about the secret lives of magnetic fields, a quirky mini-documentary of a boy's determination to save redheads from extinction, the story of a photon named Dave. These diverse works had been selected for how creatively they negotiated the boundaries between entertainment and information. The hope, of course, is that scientists will not be the only audience for something like the Imagine Science Film Festival. By making science entertaining, perhaps filmmakers can provide the general public greater access to scientific ideas.

Alexis Gambis—the festival's founder and artistic director (who recently received a Ph.D. in molecular biology and genetics)—wanted to ensure that the films were not only entertaining but also accurate in their representations of science. Not surprisingly, the most successful films were those that involved close collaboration between scientists and filmmakers. Harry Kloor and Dan St. Pierre's animated feature *Quantum Quest*, which follows a photon from the Sun to the Cassini spacecraft, is one such film. The photon, Dave, finds himself on a mission to deliver an important artifact to Cassini in an effort to protect it from the evil forces of anti-matter, "the Void." Although the plot and characters feel familiar, Dave's story provides a creative device that links together a series of remarkable images acquired from actual NASA missions. (These whiz-bang images suggest it was no accident that public support for NASA surged after the release of the Hubble photographs.) The free screening was followed by a discussion with Kloor and retired NASA astronaut Daniel Barry. Many of the festival sessions included such postscreening conversations, which offered audiences access to some top researchers. With few tickets running more than $10 (and many of them flat-out free), New Yorkers were given the opportunity to lift the veil between themselves and the lab by asking scientists questions.

Leonardo.

CREDIT: *LEONARDO*/COURTESY IMAGINE SCIENCE FILM FESTIVAL

Part teaching tool, part entertainment, *Quantum Quest* is neither contentious nor deeply philosophical, but it does use actual scientific data. Although, in comparison with other films at the festival, it runs short on specific findings, that is balanced by its commendable effort to make science fiction a little more accountable.

It's a little more difficult to say how Kanji Nakajima's *The Clone Returns Home* represents any current science. The festival's most overtly sci-fi feature film tells the story of an astronaut named Kohei who, after he dies in space, is

*These authors led the review. †To whom correspondence should be addressed: Department of Biological Sciences, Columbia University, New York, NY 10027, USA. E-mail: sjf24@columbia.edu

cloned—as a full-grown adult, with all his memories intact. The "cloning" process, which involves a machine that builds skin on top of muscle on top of bone, is rather far-fetched. The film, however, is less about the realities of human cloning than about the question of what it would mean to "copy" a person who has died. When he awakes, the copy of Kohei experiences psychological distress. He is tormented by an apparition of his former self, much as he was tormented, as a boy, by the death of his twin brother.

The Clone Returns Home.

CREDIT: *THE CLONE RETURNS HOME*/COURTESY IMAGINE SCIENCE FILM FESTIVAL

The film fell short of an accurate depiction of any current advances in cloning technology. Shockingly, at least for a film festival that claims to accurately represent science, the film even advances a profoundly anti-materialist message: that an exact physical copy of a human being may still be inauthentic or damaged in some way. According to the film, such copies lack a spiritual property that's intrinsic only to the original being. Does this anti-materialism make the film anti-science? Its inclusion in the festival does raise the point that purely imaginative films can still stimulate discussion about real science—for example, the implications of cloning a dead pet or developing specialized clones for organ replacement.

Nick Rutter and Helen Cooper's *Ginger*, a standout short in the festival, successfully conveyed serious scientific information while maintaining a playful storyline. Their simple film revolves around a young English boy who wants to understand why he has red hair, a condition that seems to infiltrate almost all aspects of his life. He begins to wonder whether redheaded people are going extinct, and this pondering soon leads him to the strange subtleties of genetics. Is the red-hair gene disappearing from the genome? Will it survive? Although not a scientist, the young man nonetheless searches for an answer as a scientist might. He seeks out and interviews molecular biologists and geneticists. These researchers don't skimp on the technical facts, but the film never loses its levity. This blend of curiosity with technical detail was a wonderful reflection of how engaging science can be. Here, the process of science isn't an arcane intellectual practice, but a type of problem-solving that we all can use when we want an answer. That point illustrates what is perhaps one of the larger issues at stake for the film festival: not how science and art differ but rather what they share in common.

Competition for the festival's three prizes was fierce. The jury comprised Gambis, science writer Carl Zimmer, and comic book writer Chris Claremont. The Audience Award went to *Leonardo*, by Jim Capobianco (who wrote the screenplay for *Ratatouille*). This 9.5-minute animated film approaches innovation and creativity through da Vinci's dream of flight. Claire Bardet won the Scientist Award for *MEPE*, her 2007 video that features a strange private detective and the evolutionary patterns of the gene in mammals.

The *Nature* Scientific Merit Award (for the most scientifically accurate film) went to *Magnetic Movie*, directed by the self-described "semiconductor duo," Ruth Jarman and Joe Gerhardt. The power of their short movie hinged on a single fact: that "magnetic fields are, by their nature, invisible." During a residency at the Space Sciences Laboratory in Berkeley, the artists overlaid ordinary lab scenes with animations of magnetic fields inspired by the lab's work on solar flares. The animations rendered the magnetic fields immediately tangible; they become turbulent ribbons of a massive unseen force swarming in a silent room. Static crackling, as if from a distant radio, accompanied the emerging fluxes of twists and loops. Rather than attempt to explicate electromagnetism, the film allowed the audience to simply experience it. In a sense, the animations provided a brief moment of artificial mastery: an approximation of the intuition a physicist might have when walking into a room and seeing chunks of metal. In other words, viewers got to feel, for a moment, like scientists.

The traditional means for putting an audience "in the shoes" of a scientist is the documentary biopic. Petra Seeger's *In Search of Memory* follows Nobel Laureate Eric Kandel's trip in a well-explored trope in Holocaust narratives: victims return to the site of trauma and reencounter the landscape of their memories of the war. The film escapes predictability by using the trip to frame the larger story of Kandel's research and advances in memory science. Even as his wife struggles to remember where, exactly, a secret tunnel near a French abbey was located, the film cuts to Kandel explaining how memories like these are encoded and persist. Through this cross-cutting structure, we learn both about Kandel and the basic principles of his research.

In one of the film's most striking moments, Kandel's postdoc Harshad Vishwasrao watches a computer screen in the dark as fluorescent packages of RNA float down a neuron from the nucleus toward the synapse. These, he explains, trigger "budding" that will eventually grow new presynaptic terminals and thereby strengthen the connection between the cells—that is, the strength of a particular element of a memory. The image is inherently beautiful: specks of green moving down a pale stem, and the subsequent growth like a phosphorescent vine twining around itself. As the image projects through Vishwasrao's glasses, we realize we are seeing an unusual reflection of ourselves: we are this flesh, we are these brains, and we are not "housed" by them. As Kandel says, "we are our memories."

Imagine Science Film Festival

Alexis Gambis, artistic director

New York.
15–25 October 2009.
www.imaginesciencefilms.com.

When the festival wound down and audiences scattered into cabs and local bars, it was hard to say how the general public was affected by what had taken place. Many members of the crowds were scientists or in some way already connected to the sciences. That said, the festival is still a young event. As it gains recognition in coming years, the diversity of the audience should grow. For its part, the Imagine Science Foundation will soon host a workshop for scientists and filmmakers wishing to collaborate on original projects. With any luck, we'll see some of those projects at next year's festival.

References and Notes

1. *Science* and AAAS were presenting sponsors of the festival.

10.1126/science.1184536

ENVIRONMENT

The End of Deforestation in the Brazilian Amazon

Government commitments and market transitions lay the foundation for an effort to save the forest and reduce carbon emission.

Daniel Nepstad,[1,2‡] Britaldo S. Soares-Filho,[3‡] Frank Merry,[1,2*] André Lima,[2] Paulo Moutinho,[1,2] John Carter,[4] Maria Bowman,[1,2†] Andrea Cattaneo,[1] Hermann Rodrigues,[3] Stephan Schwartzman,[5] David G. McGrath,[1,2,6‡] Claudia M. Stickler,[1,2,7] Ruben Lubowski,[5] Pedro Piris-Cabezas,[5,8] Sergio Rivero,[6] Ane Alencar,[2,7] Oriana Almeida,[2,6] Osvaldo Stella[2]

Brazil has two major opportunities to end the clearing of its Amazon forest and to reduce global greenhouse gas emissions substantially. The first is its formal announcement within United Nations climate treaty negotiations in 2008 of an Amazon deforestation reduction target, which prompted Norway to commit $1 billion if it sustains progress toward this target (*1*). The second is a widespread marketplace transition within the beef and soy industries, the main drivers of deforestation, to exclude Amazon deforesters from their supply chains (*2*) [supplementary online material (SOM), section (§) 4]. According to our analysis, these recent developments finally make feasible the end of deforestation in the Brazilian Amazon, which could result in a 2 to 5% reduction in global carbon emissions. The $7 to $18 billion beyond Brazil's current budget outlays that may be needed to stop the clearing [a range intermediate to previous cost estimates (*3*, *4*)] could be provided by the REDD (Reducing Emissions from Deforestation and Forest Degradation) mechanism for compensating deforestation reduction that is under negotiation within the UN climate treaty (*5*), or by payments for tropical forest carbon credits under a U.S. cap-and-trade system (*6*).

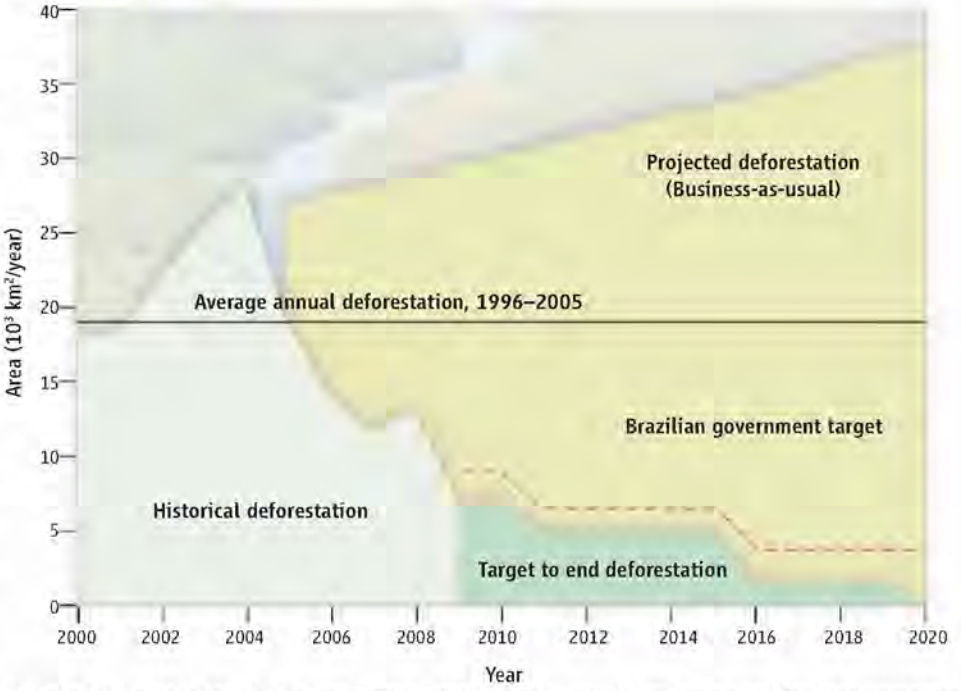

Historical deforestation in the Brazilian Amazon and future deforestation under three scenarios. The first scenario simulates deforestation from 2005 into the future under business-as-usual conditions that assume economic trends and governance levels through 2003 (*14*). The intermediate curve is the current deforestation reduction target of the Brazilian government (*8*), and the lower curve, which ends deforestation in 2020, is the scenario analyzed here (SOM, § 2).

Deforestation History

Brazil has been the world leader in tropical deforestation, clearing an average of 19,500 km²/year from 1996 to 2005. This forest conversion to pasture and farmland released 0.7 to 1.4 $GtCO_2e$ (billion tons of CO_2 equivalents) per year to the atmosphere (*7*) (SOM, § 1). In 2008, the Brazilian government committed to reducing deforestation to 20% of the historical (1996–2005) rate by 2020 (*8*) (SOM, § 2), motivated by plummeting rates of forest clearing. From July 2005 to July 2009, deforestation declined to 36% of its historical levels (see figure, above). To help achieve this reduction, Brazil expanded the network of Amazon protected areas from 1.26 to 1.82 million km²; the network now contains 51% of the region's remaining forest area (*9*) (table S4). Federal campaigns to publicize and cancel credit for illegal land holdings, to pressure buyers of Amazon products, and to imprison illegal operators may have contributed to the decline, as did a retraction of the region's cattle and soy industries (SOM, § 3, and fig. S1).

Steps to End Deforestation

For Brazil to build upon its success and end deforestation, even if the profitability of Amazon cattle ranching and soy farming soar in the coming years, it must support low-deforestation livelihoods for forest peoples and smallholder farmers, expand the law-abiding "responsible" fraction of the cattle and soy sectors, improve law enforcement, and effectively manage protected areas.

Indigenous groups and traditional forest communities, totaling 420,000 people, have defended their perimeters from incursions by deforesters (*9*, *10*), but have never received compensation for this enforcement service. There are also 400,000 smallholder farms (up to 100 ha) (*11*) established in forested or marginal lands that could shift to low-deforestation production systems.

Cattle ranching, associated with four-fifths of Amazon deforestation, must stabilize and intensify on a diminishing area of pastureland, ceding space to a modest expansion of relatively lucrative soy production (SOM, § 3). Support within the cattle and soy sectors for declining deforestation could be strengthened by identifying, rewarding, and expanding

[1]Woods Hole Research Center, Falmouth, MA 02540, USA. [2]Instituto de Pesquisa Ambiental da Amazonia, Brasília-DF 71.503-505, Brazil. [3]Universidade Federal de Minas Gerais, Belo Horizonte, MG 31270-901, Brazil. [4]Aliança da Terra, Goiânia, GO 74.670-600, Brazil. [5]Environmental Defense Fund, Washington, DC 20009, USA. [6]University of Florida, Gainesville, FL 32611–7315, USA. [7]Universidad Rey Juan Carlos, Tulipán s/n, 28933, Móstoles, Spain. [8]Universidade Federal do Pará, 66.075-110, Belém, Pará, Brazil.

*Present address: Gordon and Betty Moore Foundation, Palo Alto, CA 94304, USA.
†Present address: University of California, Berkeley, Berkeley, CA 94720, USA.
‡Authors for correspondence. E-mail: dnepstad@whrc.org and britaldo@csr.ufmg.br

the pool of "responsible" producers striving to comply with the law and to practice good land stewardship. Legal compliance could be facilitated through approval and implementation of land-use zoning plans, which lower the legal forest reserve requirement on private properties in farming and ranching regions (*12*). This requirement was abruptly raised from 50 to 80% of each property in 1996 without effective mechanisms for facilitating compliance (*2*) (SOM, § 6). The substantial flow of federal farm credit could be redirected toward the intensification of cattle production and support for forest-based economies (SOM, § 7). Market exclusion of deforesters (*2*) could be strengthened through government measures that penalize companies and banks that indiscriminately do business with Amazon farmers and cattle ranchers.

Some farmers and ranchers will need compensation for the opportunity costs incurred in maintaining private forests. Five landholder compensation qualification criteria could be used, including forest cover beyond 50% of the property (SOM, § 6).

What Will It Cost and Who Will Pay?

We estimated the potential cost of a 10-year program for ending deforestation (see figure, page1350). Using spatially explicit economic models and programmatic estimates, we assess budgetary costs of ending deforestation assuming that the benefits of reduced deforestation outweigh the opportunity costs to society. These benefits include reduced forest fire, air pollution, flooding, biodiversity loss, soil erosion, and, perhaps, rainfall inhibition (*3*, *13*). They are difficult to quantify and are largely untreated in most economic models (*4*), even though they lower the net costs of reducing deforestation.

Annual investments in community forest-based economic activities, health, education, and cultural preservation for the region's indigenous and traditional forest peoples and smallholder farmers would total $3.6 to $7.2 billion from 2010 to 2020 (see table, below and SOM, § 5). The total opportunity cost potentially incurred by landholders is estimated at $14 billion (table S3 and fig. S9), or $26 billion if a minimum forest cover of 60% is imposed for each Amazon state to avoid rainfall inhibition (*13*) (SOM § 8). However, our estimate includes only those private forests that would qualify for compensation, which represent only 10 to 15% of potential opportunity costs (see table, below, and SOM, § 6).

Combining these costs with additional investments in law enforcement and protected area management gives a total budget of $7 to $18 billion (see table, below, and SOM, § 9). Already initiated by the Norway commitment, this investment could reduce carbon emissions from 2010 to 2020 by ~6 $GtCO_2e$ below the historical baseline and by 12 $GtCO_2e$ below projected emissions (see figure, page 1350) (*14*), culminating in annual emissions reductions that are 2 to 5% of global emissions rates in 2000–2006 (SOM, § 2). Under a REDD system, as designed in the American Clean Energy Security Act passed by the U.S. House of Representatives, reductions under Brazil's deforestation target could generate revenues valued from $37 billion to $111 billion between 2013 and 2020 (*6*) (SOM, § 10), providing a margin for expanding the program to end deforestation.

Ending deforestation in the Brazilian Amazon in 2020 with less than 20% of the forest cleared (table S4) would be an extraordinary and extremely difficult achievement, perhaps unique in the history of frontier expansion. The likelihood of success, however, is greatly enhanced by state-level programs that link zoning and property registries with statewide deforestation reduction targets (SOM § 11). The Governors' Climate and Forests Task Force is working to connect these Amazon state programs with international emissions offset programs under development for California and other U.S. states (*15*). State-level programs must also eventually link up with the federal "Amazon Fund," where the Norwegian commitment resides (*1*). Most tropical nations will require time to develop Brazil's institutional capacity, civil society organization, and legal framework (*16*). Ending deforestation in the Brazilian Amazon and reducing it elsewhere in the tropics is a cost-effective approach to climate change mitigation with multiple benefits (*13*, *16*).

Estimated costs of a program to end deforestation in the Brazilian Amazon

Region or state	Forest peoples' fund (10^6 U.S. $)		Enforcement and landholder compensation (10^6 U.S. $)		Protected area management (10^6 U.S. $)		Total cost (10^6 U.S. $)	
	Low	High	Low	High	Low	High	Low	High
Brazilian Amazon	3,606	7,213	1,459	6,502	1,456	4,368	6,521	18,082
Acre	252	503	106	147	54	163	412	813
Amapá	68	135	13	12	56	168	136	315
Amazonas	565	1,129	229	116	546	1,639	1,340	2,884
Maranhão	189	377	13	248	10	31	212	656
Mato Grosso	335	669	693	4,135	80	240	1,107	5,044
Pará	1,357	2,715	280	639	488	1,464	2,125	4,818
Rondônia	580	1,159	94	1,127	79	238	752	2,524
Roraima	116	231	27	19	90	271	233	522
Tocantins	147	293	4	60	51	154	202	507

Ending deforestation in the Brazilian Amazon by 2020. These estimates for costs incurred from 2010 to 2020 assume that current budgetary outlays from the Brazilian government continue. (SOM § 9)

References and Notes

1. J. Tollefson, *Nature* **460**, 936 (2009).
2. D. C. Nepstad *et al.*, *Conserv. Biol.* **20**, 1595 (2006).
3. D. C. Nepstad *et al.*, *The Costs and Benefits of Reducing Carbon Emissions from Deforestation and Forest Degradation in the Brazilian Amazon* (Woods Hole Research Center, Falmouth, MA, 2007); http://whrc.org/policy/BaliReports/index.htm.
4. G. E. Kindermann *et al.*, *Proc. Natl. Acad. Sci. U.S.A.* **105**, 10302 (2008).
5. R. E. Gullison *et al.*, *Science* **316**, 985 (2007).
6. P. Piris-Cabezas, R. Lubowski, *The Brazilian National Plan on Climate Change: Potential Impacts in a U.S. Cap-and-Trade System* (Environmental Defense Fund, Washington, DC, 2009); www.edf.org/documents/10563_Brazilian_national_plan_on_climate_change.pdf.
7. R. A. Houghton, in *Tropical Deforestation and Climate Change*, P. Moutinho, S. Schwartzman, Eds. [Amazon Institute for Environmental Research (IPAM), Belém, Pará, Brazil, 2005] pp. 13–21.
8. Government of Brazil, Presidential decree 6.263, 21 November 2007, *National Climate Change Plan* (Government of Brazil, Brasília, 2008); www.mma.gov.br/estruturas/smcq_climaticas/_arquivos/plano_nacional_mudanca_clima.pdf.
9. B. S. Soares-Filho *et al.*, *Reducing Carbon Emissions from Deforestation: The Role of ARPA's Protected Areas in the Brazilian Amazon* (IPAM, Belém, Pará, Brazil, 2008).
10. D. Nepstad *et al.*, *Conserv. Biol.* **20**, 65 (2006).
11. Instituto Brasileiro de Geografia e Estatística (IBGE), *Censo agropecuário de 2006*; www.ibge.gov.br.
12. A. Lima, *Zoneamento ecologico-economico: A luz dos direitos socioambientais* (Jurus Editora, Curitiba, Brazil, 2005).
13. C. M. Stickler *et al.*, *Glob. Change Biol.* **15**, 2803 (2009).
14. B. S. Soares-Filho *et al.*, *Nature* **440**, 520 (2006).
15. Governors' Climate and Forests Task Force, www.climatechange.ca.gov/forestry_task_force/index.html.
16. A. Angelsen *et al.*, *Reducing Emissions from Deforestation and Forest Degradation (REDD): An Options Assessment Report* (Meridian Institute, Washington, DC, 2009); www.redd-oar.org/ (accessed 14 September 2009).

17. Supported by the National Science Foundation, the National Aeronautics and Space Administration (LBA-ECO), the Gordon and Betty Moore Foundation, the David and Lucille Packard Foundation, the Electric Power Research Institute, Linden Conservation Trust, the Blue Moon Foundation, and the Global Opportunities Fund, government of the United Kingdom. K. Schwalbe assisted with editing and graphics; P. Moreira, Foster Brown, and three anonymous reviewers provided comments on an earlier draft.

Supporting Online Material

www.sciencemag.org/cgi/content/full/325/5945/1350/DC1

10.1126/science.1182108

BIOCHEMISTRY

Nascent Proteins Caught in the Act

Cryo–electron microscopy structures visualize two types of nascent polypeptide chains that affect either protein translocation across membranes or regulation of bacterial gene expression.

Martin Kampmann and Günter Blobel

X-ray crystallographic snapshots of ribosomes, associated translation factors, and transfer RNA (tRNA) have allowed dynamic aspects of protein translation to be reconstructed. What is still missing is a detailed structural understanding of events coupled to translation. Two landmark papers in this issue (*1*, *2*) use cryo–electron microscopy (cryoEM) to obtain information at subnanometer resolution, enabling the direct visualization of nascent polypeptide chains in the ribosomal tunnel. The two different nascent chains of ribosome-nascent chain complexes (RNCs) instruct two distinct downstream pathways.

In the first paper, Becker *et al.* (page 1369) (*1*) show how an amino-terminal signal peptide that has emerged from the ribosomal tunnel engages the protein-conducting channel; the latter was isolated from the endoplasmic reticulum (ER) using detergent. When embedded in the ER, this protein-conducting channel serves as a conduit for translocation of secretory proteins or for the insertion of integral membrane proteins into the ER.

To transport a protein across the ER membrane while the protein is being translated by the ribosome (see the first figure), the signal peptide of the nascent chain first engages the signal recognition particle (SRP) in the cytoplasm; the RNC-SRP complex is then targeted to the SRP receptor in the ER; concomitant with guanosine triphosphate (GTP) hydrolysis and SRP release, the signal peptide is handed over to the protein-conducting channel and thereby initiates cotranslational translocation of the nascent secretory protein across the membrane. In the case of nascent membrane proteins, the protein-conducting channel can be opened laterally to displace a hydrophobic transmembrane segment to the lipid bilayer.

Intermediates of this dynamic process have previously been visualized by cryo-EM. An RNC-SRP complex (*3*) showed that SRP binding overlaps with all four known binding sites for the protein-conducting channel on the large ribosomal subunit. Snapshots of the RNC-SRP–SRP receptor complex (*4*) have shown that at least two of these binding sites are cleared in preparation for binding to the protein-conducting channel.

The protein-conducting channel consists of three integral membrane proteins: Sec 61α, β, and γ in the mammalian Sec61 complex and SecY, E, and G in the homologous bacterial SecY complex. Previous snapshots of RNC bound to the protein-conducting channel (*5*–*7*) showed low resolution of the protein-conducting channel, such that an x-ray structure of an archaebacterial SecY complex (*8*) could not be fitted unambiguously into the EM map. The x-ray structure suggested that a single Sec61 trimer could form a channel, but the cryo-EM maps suggested that as many as four Sec trimers may be attached to one ribosome (*5*–*7*).

Because of a dramatic improvement in resolution into the subnanometer range, Becker *et al.* can now show that the RNC-bound protein-conducting channel consists of one Sec61 trimer, in agreement with the proposals based on the x-ray structure (*8*). Moreover, using homology modeling of the SecY complex, Becker *et al.* were able to assign two loops of the Sec61 complex that interact with ribosomal RNA and protein components near the tunnel exit. They could also trace the tRNA-bound nascent chain from the peptidyl-transferase center through the entire tunnel to the pore in the protein-conducting channel (*1*).

Obviously, snapshots at even higher resolution could reveal even more detailed information of the dynamic processes summarized in the first figure. For example, the electrophysiological observations on protein-conducting channels in the ER membrane, revealed by puromycin treatment (*9*), and in the bacterial plasma membrane, opened by synthetic signal peptide (*10*), need to be explained at atomic resolution. So far, cryo-EM studies of the protein-conducting channel were carried out using detergent-solubilized material. In its native lipid environment, it may display more physiological conformational responses.

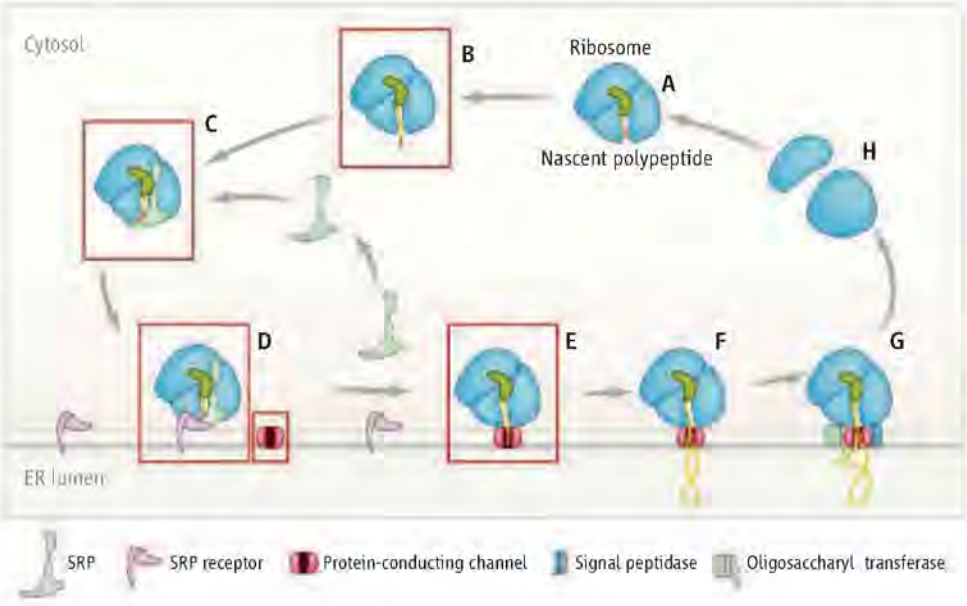

Cotranslational translocation. Snapshots of intermediates provided by cryo-EM and x-ray crystallography are indicated by red boxes. (**A**) A ribosome translates a protein containing an amino-terminal signal peptide. (**B**) Once the signal peptide has emerged from the exit tunnel of the ribosome (*1*), it is recognized by the SRP (**C**) (*3*) and targeted to the ER membrane, where the SRP receptor repositions the SRP (**D**) (*4*) to prepare the RNC for interaction with the protein-conducting channel (*8*). SRP and its receptor dissociate after GTP hydrolysis, and (**E**) the signal peptide is inserted into the protein-conducting channel (*1*). A cryo-EM snapshot of this RNC with detergent-solubilized protein-conducting channel is presented by Becker *et al.*, who assembled this complex by omitting steps C and D. (**F**) The protein is translocated across the ER membrane and (**G**) further processed by signal peptidase and oligosaccharyl transferase complexes that are likely to associate with the protein-conducting channel to form the translocon. (**H**) Once translation is terminated, the ribosomal subunits are released from the ER.

CREDIT: ADAPTED BY P. HUEY/*SCIENCE*

Howard Hughes Medical Institute and The Rockefeller University, New York, NY 10065, USA. E-mail: martin.kampmann@rockefeller.edu; blobel@rockefeller.edu

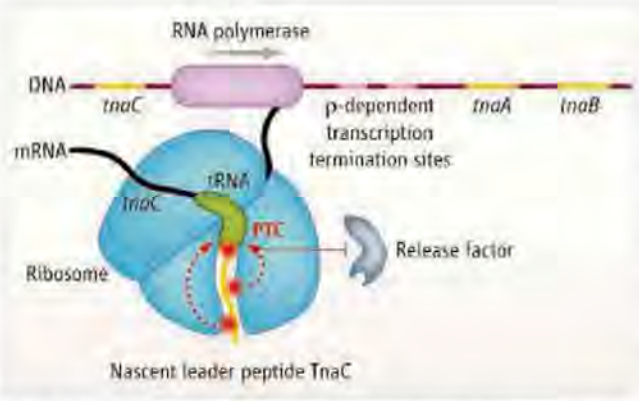

Regulation of the bacterial tryptophanase operon. At low tryptophan concentrations, ribosomes are released from the mRNA after translating the TnaC leader peptide. This allows rho helicase to terminate transcription at sites upstream from the *tnaA* and *tnaB* genes, which encode tryptophanase and tryptophan permease. In the presence of high tryptophan concentrations, the interaction of the nascent leader peptide with the tunnel stalls translation by preventing the action of release factors in the peptidyl transferase center. The ribosome remains bound to the mRNA, thus preventing termination of transcription by rho helicase and allowing complete transcription of the tryptophanase operon. Seidelt *et al.* now report a cryo-EM structure of a ribosome stalled during the translation of TnaC. The structure shows specific interactions between the nascent chain and the tunnel, and the authors propose relay pathways to the peptidyl transferase center.

The large surface of the large ribosomal subunit apposed to the ER membrane may provide additional binding sites for enzymes such as signal peptidase and oligosaccharyl transferase, which work cotranslationally in concert with the protein-conducting channel to form the "translocon." In fact, one of the previously characterized ribosome-binding proteins, ribophorin, is part of the oligosaccharyl transferase complex. The interaction of these and other integral membrane proteins of the translocon with the protein-conducting channel and the apposed large ribosomal subunit surface must not interfere with lateral opening of the channel, so that transmembrane segments of nascent integral membrane proteins can exit into the lipid bilayer.

In the second paper, Seidelt *et al.* (page 1412) (*2*) assembled an RNC containing the "leader" peptide (*11*) of the tryptophanase operon, a cluster of genes in bacteria that are transcribed as one messenger RNA (mRNA). In the presence of high concentrations of tryptophan, the leader peptide of the tryptophanase operon causes stalling of translation and thereby allows complete transcription of the operon (*12*) (see the second figure). This is an example of regulation of translation-coupled transcription in bacteria by the nascent peptide. The 6 Å resolution of this complex allowed the nascent chain to be traced in the tunnel and its interactions with surrounding nucleotides and ribosomal proteins to be delineated (*2*). Seidelt *et al.* suggest how the conformational changes induced by these interactions are relayed to the peptidyl transferase center, where the authors observed distinct conformations of individual bases that are incompatible with the termination of translation by release factors (*2*).

The tunnel in the large ribosomal subunit is clearly not just a passive conduit for the nascent chain, but rather a compartment in a dynamic molecular dialogue with the nascent chain. This interplay might not only affect the structure and function of the ribosome and associated factors, but also the conformation and folding of the nascent chain. Once emerged from the ribosome, nascent chains containing a single peptide can engage the SRP, the protein-conducting channel and other downstream factors in translation-coupled translocation.

References and Notes

1. T. Becker *et al.*, *Science* **326**, 1369 (2009); published online 29 October 2009 (10.1126/science.1178535).
2. B. Seidelt *et al.*, *Science* **326**, 1412 (2009); published online 29 October 2009 (10.1126/science.1177662).
3. M. Halic *et al.*, *Nature* **427**, 808 (2004).
4. M. Halic *et al.*, *Science* **312**, 745 (2006).
5. R. Beckmann *et al.*, *Cell* **107**, 361 (2001).
6. K. Mitra *et al.*, *Nature* **438**, 318 (2005).
7. J. F. Menetret *et al.*, *J. Mol. Biol.* **348**, 445 (2005).
8. B. Van den Berg *et al.*, *Nature* **427**, 36 (2004).
9. S. M. Simon, G. Blobel, *Cell* **65**, 371 (1991).
10. S. M. Simon, G. Blobel, *Cell* **69**, 677 (1992).
11. The synonymous use in the literature of the terms "leader" peptide and "signal" peptide should be discouraged, as a signal peptide is exclusively involved in targeting the nascent chain for membrane translocation, whereas a leader peptide regulates translation-coupled transcription in bacteria.
12. F. Gong, C. Yanofsky, *Science* **297**, 1864 (2002).

10.1126/science.1183690

ECOLOGY

Biodiversity Under Global Change

A long-term experiment into plant community responses to elevated carbon dioxide and nitrogen yields surprising results.

Scott L. Collins

Many common plant species, such as prairie grasses, have evolved traits for the efficient capture and use of two key resources that limit terrestrial productivity: nitrogen (N) and carbon dioxide (CO_2). Over the past 60 years, human activity has vastly increased the availability of these resources. Atmospheric CO_2 concentration has increased by 40%, and N availability has more than doubled. These changes are likely to have important consequences for species interactions, community structure, and ecosystem functioning. On page 1399 of this issue, Reich investigates one important consequence, biodiversity loss, based on a long-term elevated CO_2 and nitrogen fertilization experiment (*1*).

The individual consequences of either elevated CO_2 or N on ecosystem structure and function have been studied intensively. Numerous experimental and empirical studies have shown that higher N availability increases aboveground net primary production and decreases species diversity (*2*, *3*). Higher aboveground net primary production intensifies competition for aboveground resources, such as light. As production increases, light availability beneath the canopy falls, leading to a loss of understory species and a decline in diversity (*4*). Elevated CO_2 can also increase aboveground net primary production (*5*). Yet, we know little about the impact of increased CO_2 on species diversity (*6*), and next to nothing about the interactive effects of N and CO_2 on plant community structure.

Reich now presents the results of 10 years of experimental addition of CO_2 and N on plant community structure in synthetic grassland communities at the Cedar Creek LTER (Long Term Ecological Research) site in Minnesota. Like the somewhat sim-

Department of Biology, University of New Mexico, Albuquerque, NM 87131, USA. E-mail: scollins@sevilleta.unm.edu

The BioCON experiment at the Cedar Creek LTER site in Minnesota.

ilar experiment in annual serpentine grassland at Jasper Ridge, California (*5*, *6*), the Biodiversity, CO_2, and Nitrogen (BioCON) experiment at Cedar Creek (see the figure) is one of the few long-running field experiments investigating the interactive effects of increased CO_2 and N on ecosystem structure and function. In the current study, Reich focuses on the interactive effects of CO_2 and N on plant species diversity. The results are noteworthy, important, and surprising.

Given that both N and CO_2 increase production independently and synergistically in this system (*7*) and that higher aboveground net primary production generally decreases diversity, one might predict the combined effects of N and CO_2 on diversity to be additive or even synergistic. Indeed, Zavaleta *et al.* (*6*) found that effects of multiple global change factors on diversity were additive in California grassland. Instead, Reich found that although elevated CO_2 reduced diversity by 2% and N addition reduced diversity by 16%, in combination, N and CO_2 reduced diversity by only 8%. Elevated CO_2 has been shown to counteract N effects on aboveground net primary production (*5*), but this is the first study to show that elevated CO_2 can reduce biodiversity loss.

What are the mechanisms behind this surprising response? Essentially, N and CO_2 differentially affect key processes that drive the productivity-diversity relationship. First, CO_2 increases aboveground net primary production, which increases N uptake by the vegetation, and at elevated N supply reduces plant-available N in the soil. Second, N fertilization leads to dominance by nitrophile plants, and this change in species composition in higher-N plots results in no net decrease in light penetration through the canopy. Moreover, CO_2 and N fertilization have opposing effects on the C:N ratio in plant tissues. Increasing both resources reduces progressive N limitation (*8*), a phenomenon that limits aboveground net primary production under elevated CO_2 alone. Finally, CO_2 and N have opposing effects on soil water content. Plants grown in elevated CO_2 experience reduced water stress, whereas elevated N in this case leads to higher root biomass, higher water uptake by plants, and therefore lower soil water content. Thus, together CO_2 and N have opposing rather than synergistic or additive effects on community structure.

The BioCON design has limitations. The synthetic communities contain 16 species, with four species each from four functional groups (C_4 grasses, C_3 grasses, legumes, and nonlegume forbs). This design is often used to determine how species diversity affects ecosystem functioning. It is less effective for studying biodiversity loss as a result of changing ecosystem structure. The amelioration of species loss in combination, relative to N addition alone, is a counterintuitive and somewhat encouraging outcome, but its generality must be challenged with additional experiments in other plant communities and with other limiting resources.

Conservation of biodiversity remains a high priority for ecological research. Biodiversity has many benefits, including increased community stability, increased resistance to invasive species, and higher resistance to diseases (*9*). Individually, many global change drivers negatively impact biodiversity. However, when such drivers have opposite effects on mechanisms controlling community structure, multiple global change drivers in some cases may actually increase community stability.

The BioCON experiment is a rare gem in long-term ecological research, and the results generated thus far have been highly informative when addressing aggregate properties, such as the impact of species diversity and resource availability on ecosystem processes. More work on different plant communities is needed, however, before we can comfortably extrapolate the results to other communities and other global change drivers. There is thus an urgent need for more multifactor experiments to better understand how ecosystems will respond as human activities continue to alter global biogeochemical cycles.

References

1. P. B. Reich, *Science* **326**, 1399 (2009)
2. C. J. Stevens, N. B. Dise, J. O. Mountford, D. J. Gowing, *Science* **303**, 1876 (2004).
3. K. N. Suding *et al.*, *Proc. Natl. Acad. Sci. U.S.A.* **102**, 4387 (2005).
4. Y. Hautier, P. A. Niklaus, A. Hector, *Science* **324**, 636 (2009).
5. M. R. Shaw *et al.*, *Science* **298**, 1987 (2002).
6. E. S. Zavaleta *et al.*, *Proc. Natl. Acad. Sci. U.S.A.* **100**, 7650 (2003).
7. P. B. Reich *et al.*, *Nature* **410**, 809 (2001).
8. P. B. Reich, B. A. Hungate, Y. Luo, *Annu. Rev. Ecol. Evol. Syst.* **37**, 611 (2006).
9. D. Tilman, *Ecology* **80**, 1455 (1999).

10.1126/science.1183271

CREDIT: CEDAR CREEK ECOSYSTEMS SCIENCE RESERVE

CHEMISTRY

Nailing Down Nickel for Electrocatalysis

A nickel compound bound to carbon nanotubes catalyzes a key reaction for hydrogen fuel cells and electrolyzers, the interconversion of protons and hydrogen in water.

Michael Hambourger[1] and Thomas A. Moore[2]

Electrocatalysis is central to the further development of proton-exchange membrane (PEM) electrolyzers and fuel cells (*1*), which can operate as compact units for powering homes or vehicles. A single device could both store energy by generating hydrogen during times of electrical surplus and release energy by oxidizing the hydrogen fuel at times of excess demand (see the figure). Today, this goal is best achieved with expensive, noble metal catalysts. However, reversible catalysts based on abundant materials are essential for such devices to have a substantial impact on sustainable energy systems. On page 1384 of this issue, Le Goff *et al.* (*2*) report a hydrogen electrode based on nickel, an abundant element, in which the catalyst is immobilized on a carbon nanotube support. This catalyst effects the reversible interconversion between hydrogen ions (H^+) and hydrogen (H_2) under aqueous conditions, and provides an important initial step toward a practical, non-noble metal hydrogen electrode.

Although the necessity of developing renewable energy sources is clear (*3*), the diffuse nature of the major resources, solar and wind, and the asynchronicity between their availability and demand, requires better methods of concentrating and storing energy (*4*, *5*). For example, peak solar radiation delivers at best only about 1 horsepower (750 W) available for work per square meter of sun-exposed surface (current technologies provide much less). Inexpensive devices that could concentrate and store renewable energy, and operate in reverse to release energy on demand, would be ideal for off-grid applications, such as in villages throughout the developing world. Within the developed world, reversible energy storage offers the possibility of reducing global power demands by salvaging electrical energy that is otherwise wasted at times of low demand.

Photosynthetic organisms solved the problems of solar energy concentration and storage by accumulating energy-rich molecules (fuels) during the day and "burning" them isothermally in fuel cells (mitochondria) upon demand, day and night. Renewable energy storage is equally applicable in human-engineered systems. Batteries or the combination of fuels and fuel cells are among the promising candidates for the storage of electrical energy (*6*). However, large storage capacities are more readily envisioned via fuel cells, in which fuel storage is separate from the energy-converting electrochemical processes. Moreover, the high energy densities of fuels (especially hydrogen) and the ease of resupply make them particularly attractive for transportation.

The nickel complex reported by Le Goff *et al.* is closely related to those previously investigated by DuBois and colleagues (*7*–*9*). In these compounds, soft diphosphine ligands stabilize low oxidation states of nickel and provide an environment favorable for catalytic turnover. The introduction of basic residues in close proximity to the central nickel atom helps to control proton motion during the catalytic cycle. In the work of Le Goff *et al.*, surface immobilization of the catalyst allows operation under aqueous conditions, which is crucial for deploying such catalysts in PEM electrolyzers and fuel cells. In contrast, previous work with related catalysts relied on organic solvents and exogenous acid or base. Le Goff *et al.* tested the catalyst under conditions comparable to those encountered in PEM devices and demonstrated sustained performance for both the production (>100,000 turnovers, or cycles of the reaction) and oxidation (>35,000 turnovers) of hydrogen.

This nickel compound is reminiscent of the active sites of hydrogenase enzymes, which catalyze the reversible interconversion between H^+ and H_2 at high rates using common metals (*10*). As such, the nickel-

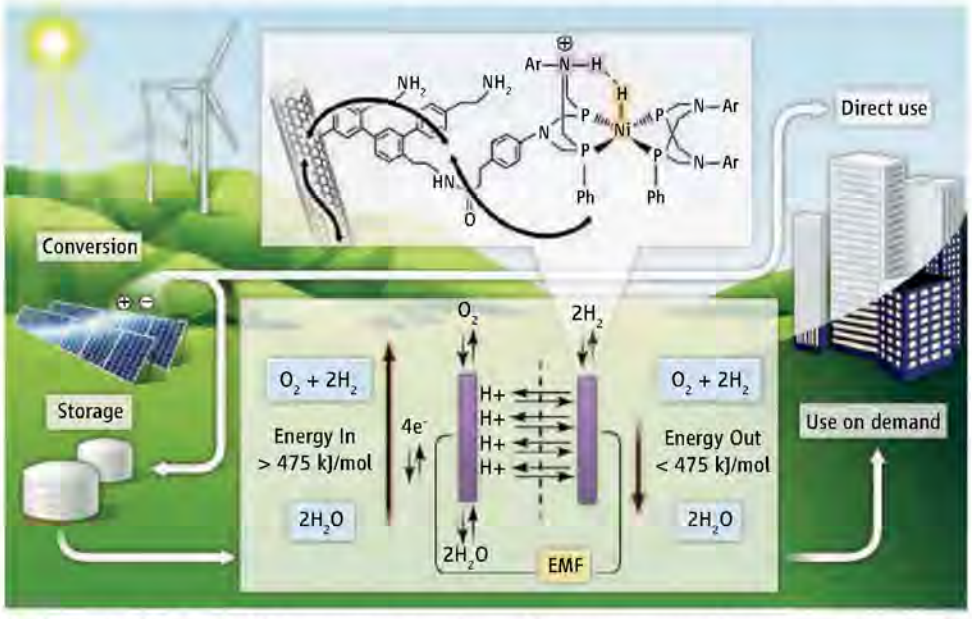

A schematic of a sustainable energy economy. Renewable energy sources, left, are converted to electricity and transported to end-users, right. Electrolyzers and fuel cells based on hydrogen provide one route for energy storage, which is critical for widespread implementation. The efficiency of the energy storage and release cycle depicted in the lower inset depends on the rario of the energy input and output; EMF is electromotive force. Inefficiencies largely result from the overpotential required to drive the reaction at a desired rate. Good catalysts minimize the overpotential, thereby optimizing the efficiency. The nickel-based catalyst reported by Le Goff *et al.* (upper inset: Ar, aryl, and Ph, phenyl) is a step toward developing a practical hydrogen electrode based on Earth-abundant materials. The basic site (purple) assists in proton abstraction or donation coupled to the redox chemistry occurring at the nickel site (orange), during either the oxidation or the production of hydrogen. The dark arrows illustrate electron transfer pathways.

CREDIT: Y. GREENMAN/SCIENCE

[1]A. R. Smith Department of Chemistry, Appalachian State University, Boone, NC 28608, USA. [2]Center for Bioenergy and Photosynthesis, and Department of Chemistry and Biochemistry, Arizona State University, Tempe, AZ 85287–1604, USA. E-mail: tmoore@asu.edu; hambourgerms@appstate.edu

bisdiphosphine catalyst is a fine example of a functional hydrogenase mimic (*11*). However, the catalyst is stable under aerobic conditions, unlike most natural hydrogenases, which are inhibited by oxygen, many irreversibly (*1*, *12*).

Despite the present advance, challenges remain. The catalyst reported by Le Goff *et al.* has turnover rates approximately one-tenth as high as those of related complexes previously reported (*8*), possibly because of the bulky functional groups used for immobilization. The current densities are two orders of magnitude lower than those achieved with a commercial platinum electrode. Nonetheless, given the ability to tune the catalytic activity of this family of nickel complexes (*7*), further optimization of the compound could result in a viable, non-noble metal catalyst for the hydrogen electrode of PEM electrolyzers and fuel cells. Similar advances in the development of a reversible, efficient oxygen electrode could close a solar-to-fuel-to-work loop by allowing the inexpensive interconversion between renewable electricity and fuels. Such a system could be transformative, minimizing the environmental impacts of an energy-intensive first-world economy, while promoting third-world development by enabling lights, refrigeration, and telecommunications essential for education, health, and empowering populations to control their own destinies.

References

1. R. H. Jones, G. J. Thomas, Eds., *Materials for the Hydrogen Economy* (CRC Press, Boca Raton, FL, 2008).
2. A. Le Goff *et al.*, *Science* **326**, 1384 (2009).
3. J. Rockström *et al.*, *Nature* **461**, 472 (2009).
4. N. S. Lewis, D. G. Nocera, *Proc. Natl. Acad. Sci. U.S.A.* **103**, 15729 (2006).
5. M. Hambourger *et al.*, *Chem. Soc. Rev.* **38**, 25 (2009).
6. A. Manthiram, A. V. Murugan, A. Sarkar, T. Muraliganth, *Energy Environ. Sci.* **1**, 621 (2008).
7. A. D. Wilson *et al.*, *J. Am. Chem. Soc.* **128**, 358 (2006).
8. A. D. Wilson *et al.*, *Proc. Natl. Acad. Sci. U.S.A.* **104**, 6951 (2007).
9. M. R. DuBois, D. L. DuBois, *Acc. Chem. Res.*; published online 31 July 2009 (10.10201/ar900110c).
10. J. C. Fontecilla-Camps, A. Volbeda, C. Cavazza, Y. Nicolet, *Chem. Rev.* **107**, 4273 (2007).
11. S. Canaguier, V. Artero, M. Fontecave, *Dalton Trans.* **2008**, 315 (2008).
12. W. Lubitz, E. J. Reijerse, J. Messinger, *Energy Environ. Sci.* **1**, 15 (2008).

10.1126/science.1183836

PLANT SCIENCE

How Plant Cells Go to Sleep for a Long, Long Time

Crystal structures reveal the conformational change elicited when the plant hormone abscisic acid binds to its receptor.

Michael R. Sussman and George N. Phillips Jr.

Seeds are plant spores—desiccated, dormant cells in which metabolism and growth have been drastically slowed, so that the organism can wait out adverse conditions. This is especially important for plants, which cannot run away from environmental threats. Instead of motility, they use dormancy to outlast adversarial conditions caused by pathogens or severe weather. Indeed, some seeds remain viable for hundreds of years. On page 1373 of this issue, Nishimura *et al.* (*1*) and four other groups (*2*–*5*) report the initial biochemical mechanisms that allow the complex cellular machinery of this multicellular eukaryote to live for so long in a dormant state.

Since its discovery five decades ago, the plant hormone abscisic acid has been known to control dormancy. For example, after fertilization, when the zygote (fertilized egg cell) has divided and formed the embryo, the concentration of abscisic acid rises, triggering the desiccation and dormancy process. Conversely, after seeds absorb water, they only break dormancy and germinate when the abscisic acid concentration falls. Genetic analyses in the flowering plant *Arabidopsis thaliana*, maize, and other model plants have revealed some key players in the abscisic acid response, including a transcription factor encoded by the *viviparous* gene (*vp1*). Mutant maize embryos lacking this gene ignore the abscisic acid signal to become desiccated and dormant, and instead germinate right on the cob inside the ear (*6*) (see the figure). Another key gene, *abscisic acid–insensitive 1* (*ABI1*), encodes a protein phosphatase, whose activation is required to transduce the cellular response to abscisic acid.

CREDIT: D.R. MCCARTY AND K. KOCH

Can't get to sleep. The *vp1* gene integrates abscisic acid hormone signaling with a regulatory network for plant seed development. Seeds from a mutant maize line lacking the VP1 transcription factor do not perceive the abscisic acid signal to become dormant. Hence, the embryos do not desiccate and "go to sleep," and instead start germinating right on the cob, coincident with the biosynthesis of anthocyanin pigment in endosperm. [Photo is reproduced from (*6*) with permission from the American Society of Plant Biologists.]

Over the past decade, mainly through genetic studies of *Arabidopsis* and rice, the receptor proteins for each of the five traditional plant hormones (auxin, gibberellin, cytokinin, ethylene, and abscisic acid) have gradually become known, but the abscisic acid receptor has been the most difficult to identify, despite several disappointing, false claims. The situation improved with the publication of two recent studies (*7*, *8*) indicating that receptors for this hormone are a group of small soluble proteins referred to as Pyrabactin Resistance 1 (PYR1), or PYR-like (PYL), encoded by a dozen or so genes. When abscisic acid enters a plant cell, the receptor forms a binary complex with it that can then immediately bind to, and inhibit, the ABI class of protein phosphatases. The PYR1/PYL receptors are members of a family called Pathogenesis-Related proteins (PR-10), characterized by steroidogenic acute regulatory lipid transfer (START) sequence motifs. Although recent biochemical and genetic data showed that this family of proteins was most likely a receptor (*7*, *8*), the weakest part of the evidence was the abscisic acid binding analysis and the lack

Biotechnology Center and the Department of Biochemistry, University of Wisconsin-Madison, Madison, WI 53706, USA. E-mail: msussman@wisc.edu

of details on how this binding could result in inhibition of the phosphatase. By determining the crystal structures of members of the receptor family, with and without bound abscisic acid and phosphatase, high-definition structural images of the initial steps in abscisic acid action are now available.

Collectively, the five studies (*1*–*5*) provide crystal structures of abscisic acid bound to its receptor, and four studies (*2*–*5*) go on to show the precise structural basis of the inhibition of the phosphatase active site. Dynamic measurements of nuclear magnetic resonance chemical shifts in solution corroborate the conclusions based on the crystal structures, in which the following scenario occurs: Abscisic acid binds to a pocket completely within a PYR-PYL homodimer, which then undergoes a conformational change resulting in a gate closing over this pocket, and a latch forming on the gate. This results in the tight binding of the hormone, which simultaneously exposes surfaces on the PYL protein that interact with the phosphatase and weaken the PYR-PYL dimer interface. The separation of PYR-PYL into monomers and interaction of these newly formed surfaces with the phosphatase active site function like a tightly bound competitive inhibitor. Removal of abscisic acid reverses the process, and the phosphatase is returned to its active state. This model is further substantiated by a large number of mutational studies, both in vitro with purified recombinant proteins and in transgenic plants and plant extracts.

So, is this model valid, and is there more to discover? Although it is clear that the details of abscisic acid binding to PYL proteins and the changes that result in binding to, and inhibition of, the phosphatase are nicely worked out, many questions remain. It is not clear whether all of the PYR and PYL proteins bind to abscisic acid, and why there are so many receptors. Are these hormone receptors widely expressed among plants? Whether these proteins have different tissue specificities or unique functionalizations, such as having differing affinities for abscisic acid or the phosphatase targets, needs to be determined. Further, what are all of the immediate substrates and/or binding partners for the phosphatase in plant cells? Data indicate that the phosphatase interacts with one or more protein kinases early in the abscisic acid signaling cascade. This creates the possibility that the time course and number of changes in the phosphorylation status of downstream proteins could be very complex because both sides of the amplification mechanism—adding and removing phosphates (by kinases and phosphatases, respectively)—might be involved at almost the same time. It is fascinating that whereas more than a thousand protein kinases genes are encoded within the plant genome, there are many fewer phosphatase genes. Furthermore, up to now, naturally occurring hormones seem to act directly on kinases, and it is the kinases that have been heralded as the central players of regulatory action and specificity, as shown mainly from work done in animals. It appears that abscisic acid is an example of a naturally occurring hormone having a protein phosphatase as part of its receptor action, rather than acting directly through a kinase. It will be interesting to note whether other eukaryotes are using similar mechanisms.

It is heartening that despite a poor start in the receptor characterization field, the START proteins turn out to be the key to abscisic acid action. The structural studies help explain how plants outsmart their adversaries and outlast poor environmental conditions, by going to sleep.

References

1. N. Nishimura *et al.*, *Science* **326**, 1373 (2009); published online 22 October 2009 (10.1126/science.1181829).
2. K. Melcher *et al.*, *Nature* 10.1038/nature08613 (2009).
3. K.-i. Miyazono *et al.*, *Nature* 10.1038/nature08583 (2009).
4. P. Yin *et al.*, *Nat. Struct. Mol. Biol.* 10.1038/nsmb1730 (2009).
5. J. Santiago *et al.*, *Nature* 10.1038/nature08591 (2009).
6. D. R. McCarty, C. B. Carson, P. S. Stinard, D. S. Robertson, *Plant Cell* **1**, 523 (1989).
7. S.-Y. Park *et al.*, *Science* **324**, 1068 (2009).
8. Y. Ma *et al.*, *Science* **324**, 1064 (2009).

10.1126/science.1184135

PHYSICS

Quantum Nonlocality: How Does Nature Do It?

Measurements of correlations between spatially separated systems provide insights into the conceptual foundations of quantum physics.

Nicolas Gisin

From early childhood we know that to interact with an object, we have either to go to it or to throw something at it. Yet, contrary to all our daily experience, there are spatially separated quantum systems that exhibit nonlocal correlations. Exploring how nature performs its trick of quantum nonlocality (*1*) has led to new experiments that provide a deeper understanding of the tension between quantum physics and relativity and to proposals for disruptive technologies.

Consider two spatially separated quantum systems, one controlled by Alice, the other by Bob. They may perform some measurements on their respective systems and collect the results. After amassing probability distributions associated with their experiments, comparison of results can then tell them about any correlation between the experiments. It is establishing the structure of the correlations that distinguishes local from nonlocal. However, correlations are everywhere. For example, consider two cups of the same color, either both red or both green, one in Alice's and one in Bob's hands. If they look at the color of their cups, Alice's and Bob's results are correlated. In this classic example, the correlation is obvious. Alice and Bob had only partial information: They knew that both had the same color, but not which color. The quantum situation is profoundly different. Quantum theory claims that a pure state provides a complete description of the two systems. It was the development of this idea that led Einstein, Podolsky, and Rosen (*2*) to believe that quantum theory was incomplete, in the same sense that it could not provide the "which color" answer.

What can correlations tell you about nonlocality? In 1964, John Bell introduced a logical formulation, the now-famous Bell's inequality, which provided a refutable test for correlations being local or nonlocal. If the inequality was satisfied, then the correlations must be local. A violation of Bell's inequality not only tells us something about quantum physics, but more impressively, tells us that some spatially separated systems exhibit non-

Group of Applied Physics, University of Geneva, 1211 Geneva 4, Switzerland. E-mail: nicolas.gisin@unige.ch

Under test. Tests of Bell inequality exploiting Earth's 24-hour rotation, setting stringent lower bounds on any hypothetical faster-than-light influence that could have explained the observed nonlocal correlations.

local correlations. This must be true for any future theory that is put forward as a complete quantum theory. Consequently, it is nature herself that is nonlocal.

There remains much uneasiness with nonlocality (*3*, *4*). A part of that comes from a confusion between nonlocal correlations and nonlocal signaling, whereby the possibility to signal at arbitrarily fast speeds is a clear contradiction to relativity. However, it is important to state that the nonlocal correlations of quantum physics are nonsignaling. That is, they do not communicate information. This should remove some of the uneasiness. Furthermore, in a nonsignaling world, correlations can be nonlocal only if the measurement results were not predetermined. Indeed, if the results were predetermined (and accessible with future theories and technologies), then one could exploit nonlocal correlations to signal. This fact has recently been used to produce bit strings with proven randomness (*5*). This is fascinating because it places quantum nonlocality no longer at the center of a debate full of prejudice, but as a resource for future quantum technologies.

The pioneering experiment by Clauser and Aspect probing the Bell test (*6*) suffered from a few loopholes, but these have since been separately closed (*7*, *8*). Still, correlations cry out for explanations, as emphasized by Bell. When confronted with nonlocal correlations, one feels that the two systems somehow influence each other (e.g., Einstein's famous spooky action at a distance). This is also the way textbooks describe the process: A first measurement triggers a collapse of the entire state function, hence modifying the state at the distant side. In recent years these intuitions have been taken seriously, leading to new experimental tests. If there is an influence from Alice to Bob, it must propagate faster than light, as existing experiments have already demonstrated violation of Bell's inequality between spacelike separated regions (*9*). But a faster-than-light speed can only be defined with respect to a hypothetical universal privileged reference frame. The basic idea is that if correlations are due to some "hidden influence" that propagates at finite speed, then, if the two measurements are sufficiently well synchronized, the influence doesn't arrive on time and one shouldn't observe nonlocal correlations. There remains the problem, however, that one doesn't know a priori the privileged frame in which one should synchronize the measurements. This difficulty was recently circumvented by taking advantage of Earth's 24-hour rotation, thus setting stringent lower bounds on the speed of these hypothetical influences (see the figure) (*10*). Hence, nonlocal correlations happen without one system influencing the other. In another set of experiments the two observers, Alice and Bob, were set in motion in opposite directions in such a way that in their own inertial reference frame each of them felt that they had performed their measurement first and could thus not be influenced by their partner (*11*, *12*). Hence, quantum correlations happen without any time-ordering.

All of today's experimental evidence points to the conclusion that nature is nonlocal. This has implications both for our worldview and for future technologies. Quantum key distribution (QKD) is the most advanced application of quantum information science. Today's commercial QKD systems rely on sound principles, but their implementation has to be thoroughly tested to check for unwanted side channels that an adversary could exploit. For example, the photons emitted by Alice could, in addition to carrying a quantum bit encoded in its polarization state, also carry redundant information unwittingly encoded in the timing of the photons, or in their spectra. This is possible because today's QKD systems do not rely on nonlocal correlations. If they did, the mere fact that the correlations between the data collected by Alice and Bob violate Bell's inequality would suffice to guarantee the absence of any side channel. This was the intuition of Ekert in 1991 (*13*) but was proven only recently (*14*, *15*). The consequence (*16*) is that it will be possible to buy cryptography systems from one's adversary as the observation of nonlocal correlations will guarantee the proper functioning of the system.

In modern quantum physics, entanglement is fundamental; furthermore, space is irrelevant—at least in quantum information science, space plays no central role and time is a mere discrete clock parameter. In relativity, space-time is fundamental and there is no place for nonlocal correlations. To put the tension in other words: No story in space-time can tell us how nonlocal correlations happen; hence, nonlocal quantum correlations seem to emerge, somehow, from outside space-time.

References and Notes

1. Talk delivered at the first John Steward Bell prize award ceremony; http://hosting.epresence.tv/IOS/1/watch/45.aspx.
2. A. Einstein *et al.*, *Phys. Rev.* **47**, 777 (1935).
3. Some conclude that it must be realism that is faulty. But I don't see in which sense this could save locality? Moreover, realism is often confused with determinism, an uninteresting terminology issue.
4. N. Gisin, http://arxiv.org/abs/0901.4255v2 (2009).
5. S. Pironio *et al.*, http://arxiv.org/abs/0911.3427 (2009).
6. S. J. Freedman, J. F. Clauser, *Phys. Rev. Lett.* **28**, 938 (1972).
7. A. Aspect *et al.*, *Phys. Rev. Lett.* **49**, 91 (1982).
8. D. N. Matsukevich *et al.*, *Phys. Rev. Lett.* **100**, 150404 (2008).
9. D. Salart *et al.*, *Phys. Rev. Lett.* **100**, 220404 (2008).
10. D. Salart *et al.*, *Nature* **454**, 861 (2008).
11. N. Gisin *et al.*, *Ann. Phys.* **9**, 831 (2000).
12. A. Stefanov, H. Zbinden, N. Gisin, *Phys. Rev. Lett.* **88**, 120404 (2002).
13. A. K. Ekert, *Phys. Rev. Lett.* **67**, 661 (1991).
14. J. Barrett *et al.*, *Phys. Rev. Lett.* **95**, 010503 (2005).
15. S. Pironio *et al.*, *N. J. Phys.* **11**, 045021 (2009).
16. A. K. Ekert, *Phys. World* (September 2009), pp. 28–32.

10.1126/science.1182103

RETROSPECTIVE

Paul C. Zamecnik (1912–2009)

A biochemist's determination and brilliance unlocked the mystery of protein synthesis and created a new field of drug development.

Kurt J. Isselbacher

Paul Zamecnik's scientific curiosity was tweaked when the fat lady died. As a young medical resident in Cleveland, Ohio, a morbidly obese woman under his care died within a week of hospitalization. At autopsy, he was struck by the excessive amount of fat in her tissue but only minimal protein, and began to wonder how proteins were actually synthesized. It was 1936, and Zamecnik's effort to answer that question proved to occupy his thinking and research for much of his scientific career.

After working on toxic shock syndrome during World War II at Harvard's Collis P. Huntington Memorial Hospital for Cancer Research, Zamecnik established a laboratory at the Massachusetts General Hospital (MGH), focusing on the mechanisms of protein synthesis. Fortunately, in the late 1940s, the carbon-14 (^{14}C) isotope was available as a tracer, and he enlisted Robert Loftfield to synthesize ^{14}C-labeled amino acids. Zamecnik promptly showed that ^{14}C–amino acids were incorporated into proteins in rat liver, but realized that to dissect the intermediary events, a cell-free system was needed. He achieved that with colleague Nancy Bucher, who was working on hepatic cholesterol biosynthesis. With this system in hand in 1956, his laboratory had a succession of major achievements. Together with Mahlon Hoagland and Mary Stephenson, he showed that adenosine 5′-triphosphate was required for protein synthesis, and that ribosomes were the site of protein assembly. Zamecnik further discovered that a soluble small molecular RNA—later called transfer RNA (tRNA)—was essential.

tRNA proved to be the adaptor molecule proposed by Francis Crick as to how DNA might be translated into an amino acid sequence. James Watson remarked at the time that if a cell-free system could be developed in the model bacterium *Escherichia coli*, the field could take off. Again, the Zamecnik group accomplished this in short order, and it attracted the prompt attention of scientists including Marshall Nirenberg, Heinrich Matthaei, Har Gorbind Khorana, and Robert Holley. Deciphering the genetic code quickly followed. Years later, Zamecnik, in somewhat lamenting tones, told me, "Our cell-free bacterial protein synthesizing system opened a floodgate of exciting research. We felt as if we were left standing on Mt. St. Michel while the incoming tide roared past us."

In 1978, while working on the structure of Rous sarcoma virus (RSV), Zamecnik showed that a short chain of nucleotides—a synthetic antisense chain—could bind to the complementary sequence of messenger RNA (mRNA). He successfully used antisense oligonucleotides to block the replication, transcription, and translation of RSV in chicken fibroblasts. Thus, a new concept for drug development was born and later, Zamecnik and co-workers used antisense inhibition to interfere with the growth of influenza virus, HIV, malaria parasites, and *Mycobacterium tuberculosis* in vitro. The recently discovered mechanisms by which small interfering RNA and microRNA control gene expression depend on the hybridization of single-strand oligomers of ~22 nucleotides with target mRNAs. In fact, in 1987, Zamecnik published the first evidence for the existence of microRNAs and suggested presciently that they might function as metabolic regulators.

Paul C. Zamecnik was born in 1912 and grew up in Cleveland. He received a bachelor's degree from Dartmouth College in 1933 and medical degree from Harvard Medical School in 1936. He applied for a surgical internship at MGH but was put on a waiting list. After a year back in Cleveland at Lakeside Hospital, he became an intern at the Collis P. Huntington Hospital of Harvard University where he cared for cancer patients. However, he found clinical medicine wanting and felt there was nothing one could really do for patients. He was told that if he was interested in protein synthesis he should work with Max Bergmann at the Rockefeller Institute for Medical Research. After being told by Bergmann that "I want a chemist, not a medical man," Zamecnik obtained a fellowship to work with Kaj Linderstrøm-Lang at the Carlsberg Laboratory in Denmark. However, the Nazi invasion of Denmark cut his stay short and on returning home, Bergmann accepted him in his lab.

Bergmann believed that protein synthesis was the reverse of proteolysis, but Zamecnik had his doubts. In the mid-1940s, Fritz Lipmann came to the MGH from Denmark and at lunch with him one day, Zamecnik said, "You don't really think these Bergmann enzymes have anything to do with protein synthesis, do you?" Lipmann thought there was a whole new pathway in which amino acids were energized. That led to Zamecnik's quest to find out whether Bergmann or Lipmann was correct. It was obviously Lipmann.

In 1956, Zamecnik became the Collis P. Huntington Professor of Oncologic Medicine at Harvard Medical School and continued research at MGH until reaching mandatory retirement in 1979. He moved his lab to the Worcester Foundation for Medical Research in Massachusetts and in 1997 returned to MGH as a senior scientist affiliated with its Cancer Center. He continued to be remarkably productive, showing that the insertion of oligonucleotides by transhybridization could correct the cystic fibrosis gene mutation, and using antisense oligonucleotides to inhibit *M. tuberculosis* cell wall synthesis. He was at work on these and other projects until 4 weeks before his death on 27 October.

Zamecnik received many prestigious awards including the National Medal of Science in 1991 and the Albert Lasker Award for Special Achievement in Medical Science in 1996. In making the presentation, Joseph Goldstein, Chair of the Lasker Jury, noted that "Zamecnik's identification of transfer RNA is a landmark in the history of science. In this one experiment biochemistry and genetics became fused into the new science of molecular biology and the door was opened for creating the genetic code."

Paul Zamecnik was admired by his peers and colleagues for his integrity, generosity, originality, and wisdom. He was reserved and modest and viewed his accomplishments with a quiet and dignified humility.

10.1126/science.1184725

Massachusetts General Hospital Center for Cancer Research, Harvard Medical School, Charlestown, MA 02129, USA. E-mail: kisselbacher@partners.org

CREDIT: ZAMECNIK ARCHIVE

GE PRIZE ESSAY

The Molecular Basis of Size Differences

Regulation of morphogen signaling controls tissue size.

Michael A. Crickmore

GE Healthcare and *Science* are pleased to present the prize-winning essay by Michael A. Crickmore, a regional winner from North America, who is the Grand Prize winner of the GE & *Science* Prize for Young Life Scientists.

Size differences account for a great deal of the diversity found in the animal kingdom, but we still have much to learn about how sizes are programmed. Generally, the cells of different animals are comparable in size, and all animals begin as a single cell. This leaves the number of cells accumulated as the main determinant of animal size. We can reasonably expect the genes controlling cell number to be conserved among animals. So it seems that size-determining genes must be deployed in the elephant in such a way that it amasses several hundred thousand times more cells than the mouse. Which are these genes and how do they control size? I asked this question in a more experimentally tractable context: How do body parts of a single animal become different sizes? Fingers, toes, and ribs are sets of structures whose members are similar in form but differ in size. Although we know that Hox transcription factors specify the identity of individual fingers, toes, and ribs, little is known about how their individual sizes are programmed.

Fortunately, a similar situation exists in an experimental model system, the fruit fly, *Drosophila melanogaster*. *Drosophila* has two true wings that develop from imaginal discs of 50,000 cells and two smaller balancing organs called halteres that form from imaginal discs of 10,000 cells. We know that all differences between these appendages are specified by the expression of the Hox gene *Ultrabithoax* (*Ubx*) in the haltere and its absence from the wing (*1*). Thus I was able to ask how the expression of this single gene limits the size of the haltere.

My first insight came from removing *Ubx* function from random clusters of haltere cells (*2*). As expected, the resulting *Ubx* mosaic halteres are larger than wild-type halteres. Surprisingly, however, the overgrowth is not restricted to the *Ubx* mutant tissue but spreads to the wild-type tissue as well. This means that *Ubx* does not control haltere size cell-autonomously by, for example, acting directly on cell cycle or apoptotic checkpoints. Rather, I hypothesized that, because of their fundamental and non-autonomous role in the control of tissue growth and patterning, alterations in morphogen signaling might underlie changes in organ size. Indeed, transcription of *decapentaplegic* (*dpp*), a growth-promoting morphogen of the BMP family, is reduced in the haltere in comparison with the wing (*2*). Furthermore, the pattern of Dpp pathway activation is altered between the haltere and the wing, not just quantitatively but also qualitatively (see the figure). In the wing, Dpp travels far from its source to form a broad activity gradient. In the haltere, I found Dpp signaling to be largely restricted to the cells in which it is produced (*2*). Because receptor binding impedes morphogen mobility, I examined the expression pattern of the Dpp receptor *thickveins* (*tkv*) and found it to be strongly up-regulated in the haltere compared with the wing. I was able to show that the Dpp mobility restriction in the haltere is due in large part to transcriptional up-regulation of *tkv*. The alterations in transcription of *dpp* and *tkv* account for much of the reduced size of the haltere relative to the wing (*2*).

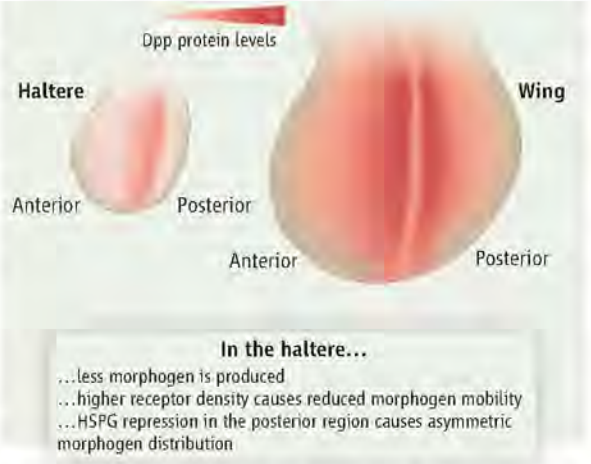

Morphogen distribution in the haltere and wing-size regulation. Ubx reduces the size of the haltere imaginal disc relative to that of the wing by decreasing the production and mobility of growth-promoting morphogens (for example, Dpp). *Ubx* impedes morphogen mobility in the haltere by up-regulating the receptor throughout the haltere and repressing an HSPG in the posterior half of the haltere. Reduced morphogen availability causes a reduction in haltere size relative to the wing.

The mechanism by which *Ubx* orchestrates these changes in the haltere is a telling example of selector gene function. *Ubx* converts one *tkv* repressor into a repressor of a second *tkv* repressor, thereby upregulating *tkv* levels in all haltere cells. The resulting elevated receptor density traps secreted Dpp at or near its site of production, leading to high Dpp signaling in the cells that transcribe *dpp*. This triggers a negative autoregulatory loop through which Dpp signaling represses *dpp* transcription, leading to a global reduction in the amount of Dpp in the tissue (*2*). This demonstrates how a fairly subtle modification of a regulatory network, effected by a selector gene, can set off a chain of events that has powerful ramifications for morphogen signaling and organ size.

Hox modulation of components of morphogen signaling pathways seems likely to define a general principle of size regulation (*3*). For example, the Wnt and Hedgehog morphogen pathways are also altered in the haltere relative to the wing (*4*, *5*). The mobilities of BMPs, Wnts, Hedgehogs, and other morphogens are promoted by heparan sulfate proteoglycans (HSPGs) (*6*). In the haltere, I found that *Ubx* works with the posterior transcription factor *engrailed* to selectively repress the HSPG *dally* in the posterior compartment. As a consequence, morphogen mobility is severely impaired in the posterior side of the tissue, causing the posterior of the haltere to be smaller than the anterior (*5*) (see the figure).

As is clear from the examples above, it is critical that the production levels of size-regulating genes such as *dpp*, *tkv*, and *dally* be precisely controlled. In the haltere, the same is true of the regulator of the size regulators: Heterozygous *Ubx* mutant

Laboratory of Neurogenetics and Behavior, Rockefeller University, New York, NY, 10065, USA. E-mail: mcrickmore@rockefeller.edu

CREDIT: ADAPTED BY P. HUEY/SCIENCE

flies have enlarged halteres (*1*), and flies with extra copies of the *Ubx* locus have shrunken halteres (*7*). While studying how Ubx levels are controlled in wild-type halteres, I found that when Ubx protein levels rise, subsets of overlapping transcriptional input into the *Ubx* promoter become silenced (*8*). This silencing likely buffers against inappropriately high cellular Ubx concentrations and may stabilize Ubx levels against the unpredictability of genetic variation. I found that when *Ubx* enhancer-reporting lab strains are outcrossed to various wild-collected *D. melanogaster* strains, dramatic enhancer silencing is seen in a large fraction of the resulting progeny (*8*). Despite (or perhaps because of) the silencing of subsets of *Ubx* enhancers, Ubx protein levels remain normal in the outcrossed progeny, and their halteres develop perfectly. Only through the use of the sensitive transcriptional reporter lines available in the *Ubx* locus is the chaos beneath this calm surface revealed. It may be that if we look close enough, we will find similar systems operating to generate stereotyped expression levels of many concentration-dependent transcription factors.

In conclusion, my thesis work has shown that alterations in morphogen signaling landscapes underlie differences in tissue sizes. Transcription factors manipulate the extent and intensity of morphogen signaling through the control of morphogen production and mobility. At least some size-controlling genes autoregulate their production levels to ensure reliable size outcomes in the face of natural genetic variation. These findings help explain how size differences are generated and how the genes that orchestrate size changes are themselves regulated. But is the regulation of morphogen signaling capable of explaining size differences as great as those between elephants and mice? Or are the growth effectors downstream of morphogen signaling also differentially tuned to create specific sizes for specific contexts? And how exactly do changes in patterns of morphogen activity translate into changes in size? Sizeable questions, all.

References

1. E. B. Lewis, *Nature* **276**, 565 (1978).
2. M. A. Crickmore, R. S. Mann, *Science* **313**, 63 (2006).
3. M. A. Crickmore, R. S. Mann, *Bioessays* **30**, 843 (2008).
4. S. D. Weatherbee, G. Halder, J. Kim, A. Hudson, S. Carroll, *Genes Dev.* **12**, 1474 (1998).
5. M. A. Crickmore, R. S. Mann, *Development* **134**, 327 (2007).
6. X. Lin, *Development* **131**, 6009 (2004).
7. S. M. Smolik-Utlaut, *Genetics* **124**, 357 (1990).
8. M. A. Crickmore, V. Ranade, R. S. Mann, *PLoS Genet.* **5**, e1000633 (2009).

10.1126/science.1184444

2009 Grand Prize Winner

Michael A. Crickmore, the author of the prize-winning essay, was born in Flint, MI, but as a child he moved with his mother and brother to suburban Los Angeles and finally to Philadelphia. He became serious about science only after college while working as a technician in Ken Irvine's lab at Rutgers University. Inspired by the ideas of Dragana Rogulja, an Irvine lab graduate student studying size control, Dr. Crickmore did his graduate work on size in Richard Mann's lab at Columbia University. But his long-term interests lie in understanding how the brain works, something he is now trying to address as a postdoctoctoral fellow in Leslie Vosshall's lab at The Rockefeller University in New York City, where he lives with his wife Dragana and their little boy Cy.

Regional Winners

Europe: **Michaela Gack** for her essay "Regulation of RIG-I-Mediated Antiviral Innate Immunity." Dr. Gack was born in Coburg, Germany. She studied molecular medicine at the Friedrich-Alexander University (FAU) Erlangen-Nuremberg, Germany, and in September 2005 joined the newly established exchange program between the graduate training program of the FAU Erlangen-Nuremberg and Harvard Medical School (HMS) in Boston. Dr. Gack completed a Ph.D. project in the laboratory of Jae Jung at the New England Primate Center of HMS. Her postdoctoral studies were conducted at the University of Southern California, Los Angeles. Since April 2009, she has been an Independent Instructor at the Department of Microbiology and Molecular Genetics of HMS, where she continues to investigate innate immune responses against viral infections and viral immune evasion mechanisms.

Japan: **Masahiro Kitano** for his essay "Imaging of Rab5 Activity Identifies Essential Regulators for Phagosome Maturation." Dr. Kitano was born in 1980 and grew up in Bieicho, Japan, a town famous for beautiful scenic hills. He attended Kyoto University, where he received a bachelor's degree in pharmaceutical science in 2003 and a master's degree in physical and organic chemistry in 2005. A strong interest in molecular imaging led him to join Michiyuki Matsuda's laboratory at Osaka University, where he developed a biosensor to identify regulators of the phagosome maturation process. Dr. Kitano completed his Ph.D. in September 2008 and is currently studying the dynamics of immune cells *in vivo* as a Special Postdoctoral Researcher in the laboratory of Takaharu Okada at the RIKEN Yokahama Institute.

All Other Countries: **Tommy Kaplan** for his essay "From DNA Sequence to Chromatin Dynamics: Computational Analysis of Transcriptional Regulation." Dr. Kaplan received his B.Sc. in Computer Science and Cognitive Studies from The Hebrew University of Jerusalem, Israel. His Ph.D. research, in computational biology, focused on various aspects of transcriptional regulation, under the supervision of Nir Friedman and Hanah Margalit at The Hebrew University, and in close collaboration with Ollie Rando at Harvard/University of Massachusetts. Since 2002, Dr. Kaplan has been involved in teaching the combined B.Sc./M.Sc. program in Computer Science and Life Sciences at The Hebrew University. Currently, he is a postdoctoral fellow in Mike Eisen's lab at the University of California, Berkeley, where he develops computational models to understand the evolution and control of gene expression during the early developmental stages of fruit fly embryos. In his spare time, Dr. Kaplan enjoys mountain biking, reading, and hiking in Northern California with his wife and two sons.

For the full text of essays by the regional winners and for information about applying for next year's awards, see *Science* Online at www.sciencemag.org/feature/data/prizes/ge/index.dtl.

Epidemic Dynamics at the Human-Animal Interface

James O. Lloyd-Smith,[1,2]† Dylan George,[2,3]* Kim M. Pepin,[4]* Virginia E. Pitzer,[2,4]* Juliet R. C. Pulliam,[2]* Andrew P. Dobson,[5] Peter J. Hudson,[2,4] Bryan T. Grenfell[2,4,5]

Few infectious diseases are entirely human-specific: Most human pathogens also circulate in animals or else originated in nonhuman hosts. Influenza, plague, and trypanosomiasis are classic examples of zoonotic infections that transmit from animals to humans. The multihost ecology of zoonoses leads to complex dynamics, and analytical tools, such as mathematical modeling, are vital to the development of effective control policies and research agendas. Much attention has focused on modeling pathogens with simpler life cycles and immediate global urgency, such as influenza and severe acute respiratory syndrome. Meanwhile, vector-transmitted, chronic, and protozoan infections have been neglected, as have crucial processes such as cross-species transmission. Progress in understanding and combating zoonoses requires a new generation of models that addresses a broader set of pathogen life histories and integrates across host species and scientific disciplines.

A recent survey of all recognized human pathogens revealed that over half are zoonotic (*1*, *2*), and nearly all of the most important human pathogens are either zoonotic or originated as zoonoses before adapting to humans (*3*). The three most devastating pandemics in human history, the Black Death, Spanish influenza, and HIV/AIDS, were caused by zoonoses (*4*), as were 60 to 76% of recent emerging infectious disease events (*2*, *5*). Underlying these patterns are specific public health challenges arising from the complex multihost ecology of zoonotic infections (*6*, *7*), as well as accelerating environmental and anthropogenic changes that are altering the rates and nature of contact between human and animal populations (*8*–*10*). Following a series of recent outbreaks [e.g., avian and swine influenza, West Nile virus, and severe acute respiratory syndrome (SARS)], a rising sense of urgency has stimulated a broad increase in research on zoonoses, ranging from dissection of the molecular determinants of host specificity (*11*) to viral prospecting in African rain forests (*12*). Such endeavors have produced important insights into underlying patterns and basic mechanisms of disease, but integrating this new knowledge across scales and applying the results to public health policy are difficult given the nonlinear and cross-species interactions inherent to zoonotic infections (*13*). These complexities can be addressed by harnessing the integrative power and mechanistic insights attainable from analysis of population dynamic models of zoonotic transmission. Here, we review the role of dynamical modeling in the study of zoonoses through an analysis of the current status of the field. Our specific goals are to detect gaps in present knowledge and to identify the priorities for future research that will unify, focus, and propel the interdisciplinary push to combat zoonoses.

A Taxonomy for Zoonotic Dynamics

Wolfe *et al.* (*3*) proposed a useful classification scheme for pathogens, delineating five stages spanning the range from those exclusively infecting animals (stage I) to those exclusively infecting humans (stage V). The zoonotic component of this scheme (stages II to IV) can be divided into the constituent phases of transmission and associated epidemiological mechanisms (Fig. 1A). Stage II pathogens are those, like West Nile virus or *Brucella abortus*, that can transmit from animals to humans to cause "primary" infections but do not exhibit human-to-human ("secondary") transmission. Stage III pathogens, such as monkeypox virus and *Leishmania infantum*, spill over into human populations from animal reservoirs and can cause limited cycles of human-to-human transmission that stutter to extinction. Stage IV pathogens originate and persist in animal reservoirs but can cause self-sustaining chains of transmission in human populations; examples include *Yersinia pestis* (plague) and pandemic influenza.

Our approach diverges from Wolfe *et al.* by basing the distinction among stages II to IV on the basic reproductive number, R_0, from the perspective of the human hosts. This quantity, defined as the expected number of secondary cases produced by a typical infectious individual in a wholly susceptible population, is a central concept in epidemiological theory (*14*, *15*). R_0 enables us to distinguish stages II to IV on dynamical grounds because it quantitatively demarcates pathogens capable of sustained transmission among humans (those with $R_0 > 1$) from those doomed to stutter to local extinction ($R_0 < 1$) or those with no human-to-human transmission ($R_0 = 0$).

The dynamics of all zoonoses involve multiple phases, including transmission in the animal reservoir, spillover transmission into humans, and possibly stuttering or sustained transmission among humans. Cross-species spillover transmission is the defining characteristic of a zoonosis, and examination of the factors influencing the force of infection from animals to humans reveals three distinct components (Fig. 1B): the prevalence of infection in the animal reservoir, the rate at which humans come into contact with these animals, and the probability that humans become infected when contact occurs. These components are each influenced by diverse properties of natural, agricultural, and human systems, with important differences driven by the pathogen's mode of transmission. Important quantitative or qualitative differences may also arise between zoonoses that use wildlife rather than domesticated animals as reservoirs, owing to differences in frequency, duration, and nature of cross-species contacts and in opportunities for human intervention.

Dynamical Models for Zoonoses

Mathematical models of the population dynamics of infectious diseases (*14*, *15*) use a well-established (and ever-growing) body of theory to construct simplified representations of epidemiological systems. Crucially, dynamical models explicitly represent the key population groups and central processes of epidemic spread. Infectious diseases differ from chronic conditions such as cancer or heart disease, because the risk of infection depends not only on personal risk factors but also upon the state of other individuals in the population. This leads to nonlinear interactions among subgroups in a population that can result in complex and sometimes counterintuitive epidemic behavior. In the fundamental susceptible-infected-recovered (SIR) model, groups of individuals within the host population are classified as "susceptible" to infection, "infected" and able to transmit the pathogen, or "recovered" and immune to reinfection (Fig. 2A). Transmission of infection to new cases is driven by contacts between susceptible and infectious individuals. Although crude, this model reproduces the classical epidemic curve (Fig. 2B) and has been remarkably successful in elucidating fundamental principles, including the "tipping point" threshold for epidemics to take off if is greater than 1, and the potential to achieve "herd immunity" through vaccination programs.

Because of the emphasis on mechanism, dynamical models can address questions outside the scope of statistical and geospatial analyses (Fig. 2C). By adjusting parameter values or reformulat-

[1]Department of Ecology and Evolutionary Biology, University of California at Los Angeles, Los Angeles, CA 90095, USA. [2]Fogarty International Center, National Institutes of Health, Bethesda, MD 20892, USA. [3]Department of Biology, Colorado State University, Fort Collins, CO 80523, USA. [4]Center for Infectious Disease Dynamics, Pennsylvania State University, University Park, PA 16802, USA. [5]Department of Ecology and Evolutionary Biology, and Woodrow Wilson School, Princeton University, Princeton, NJ 08544, USA

*These authors (listed alphabetically) contributed equally to this work.

†To whom correspondence should be addressed. E-mail: jlloydsmith@ucla.edu

ing mechanisms, modelers can perform "what if" experiments to study problems that are ethically or logistically unfeasible to study in the real world, for example, by exploring the efficacy of different control measures or extrapolating population-level consequences of clinical or laboratory findings. Such cross-scale synthesis also enables researchers to extract key characteristics of epidemics, such as changes in the value of the "effective" reproductive number (R_e) as control measures are imposed or the supply of susceptible hosts is depleted. Models can also evaluate the potential influence of unknown information, helping to set priorities for data collection and to define the uncertainty associated with model outcomes. Finally, dynamical models can be used to predict future trends of disease spread, although such projections must be accompanied by a comprehensive uncertainty analysis.

Population dynamic modeling has made major contributions to our understanding of zoonotic infections. During the bovine spongiform encephalopathy (BSE) epidemic in Britain, models were used to extract and synthesize basic knowledge from clinical and epidemiological data, while also extrapolating trends from unfolding evidence about the mysterious pathogen (*16*, *17*). Models of rabies transmission have provided biological insight, guided vaccination policy, and predicted spatial spread (*18*–*20*). Following the emergence of SARS coronavirus (SARS-CoV), models were applied to measure the virus's transmissibility and to refine plans for epidemic containment via infection control and case isolation (*21*, *22*). Modeling studies predicted that quarantine would be a relatively inefficient means of controlling SARS (*23*, *24*), and this was confirmed in later analyses of outbreak data (*25*).

Comparative analyses have characterized epidemiological phenomena, such as host heterogeneity, across suites of zoonotic pathogens and have coupled the findings to models to study dy-

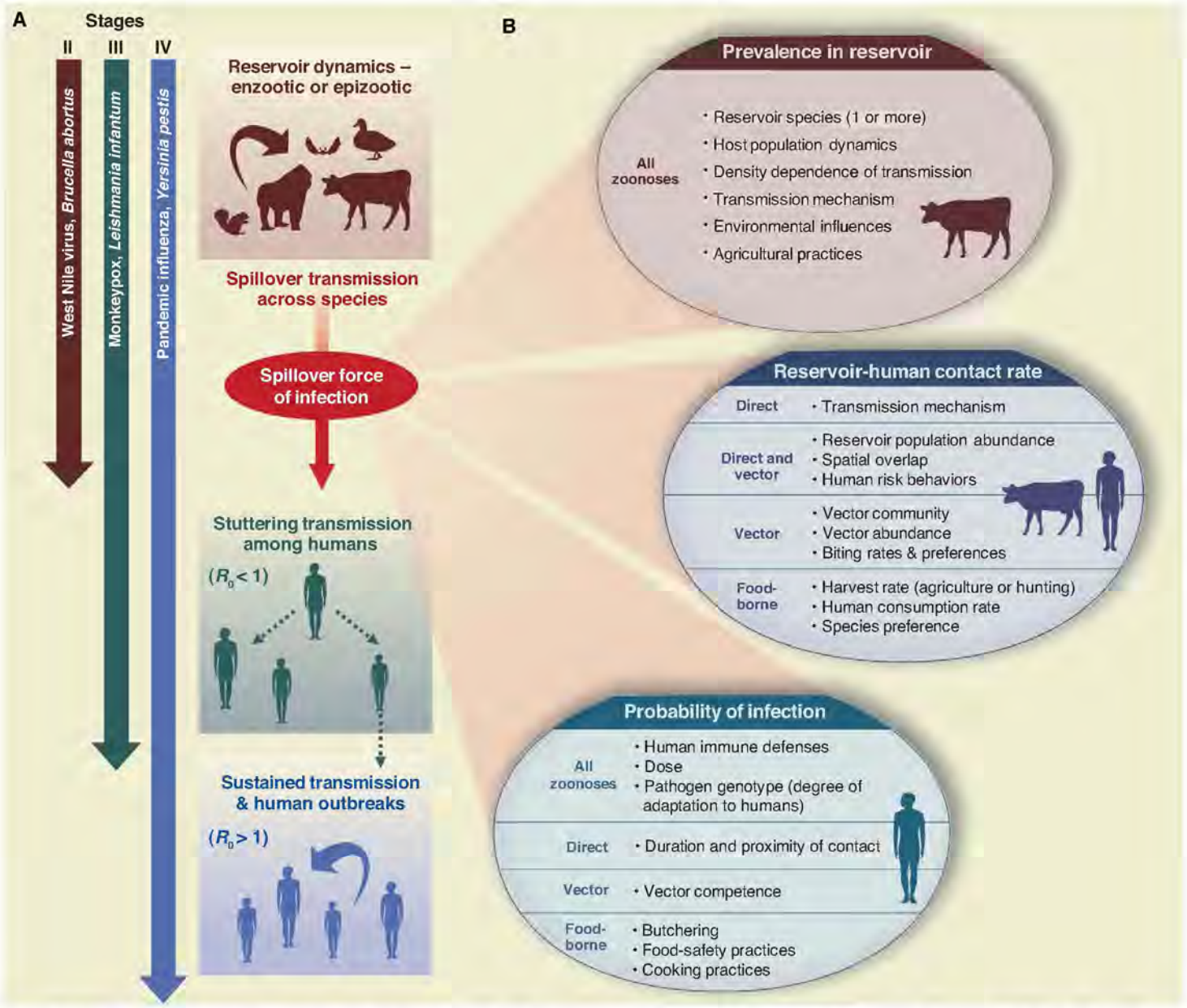

Fig. 1. (**A**) Schematic diagram of zoonotic transmission dynamics. Zoonoses can involve as many as four dynamical phases, including enzootic or epizootic circulation in the animal reservoir, spillover transmission from animals to humans, and sometimes self-limiting stuttering chains of human-to-human transmission or sustained transmission leading to outbreaks. Adapting Wolfe *et al.* (*6*), we classify zoonotic pathogens into three stages (II, III, and IV) according to their transmissibility among humans. (**B**) The spillover force of infection is determined by the product of three major components. The force of infection is defined as the per capita rate of infection of susceptible humans. Beneath each major component is a list of contributing factors drawn from many disciplines; these factors may pertain to all zoonoses or to particular transmission modes, as indicated.

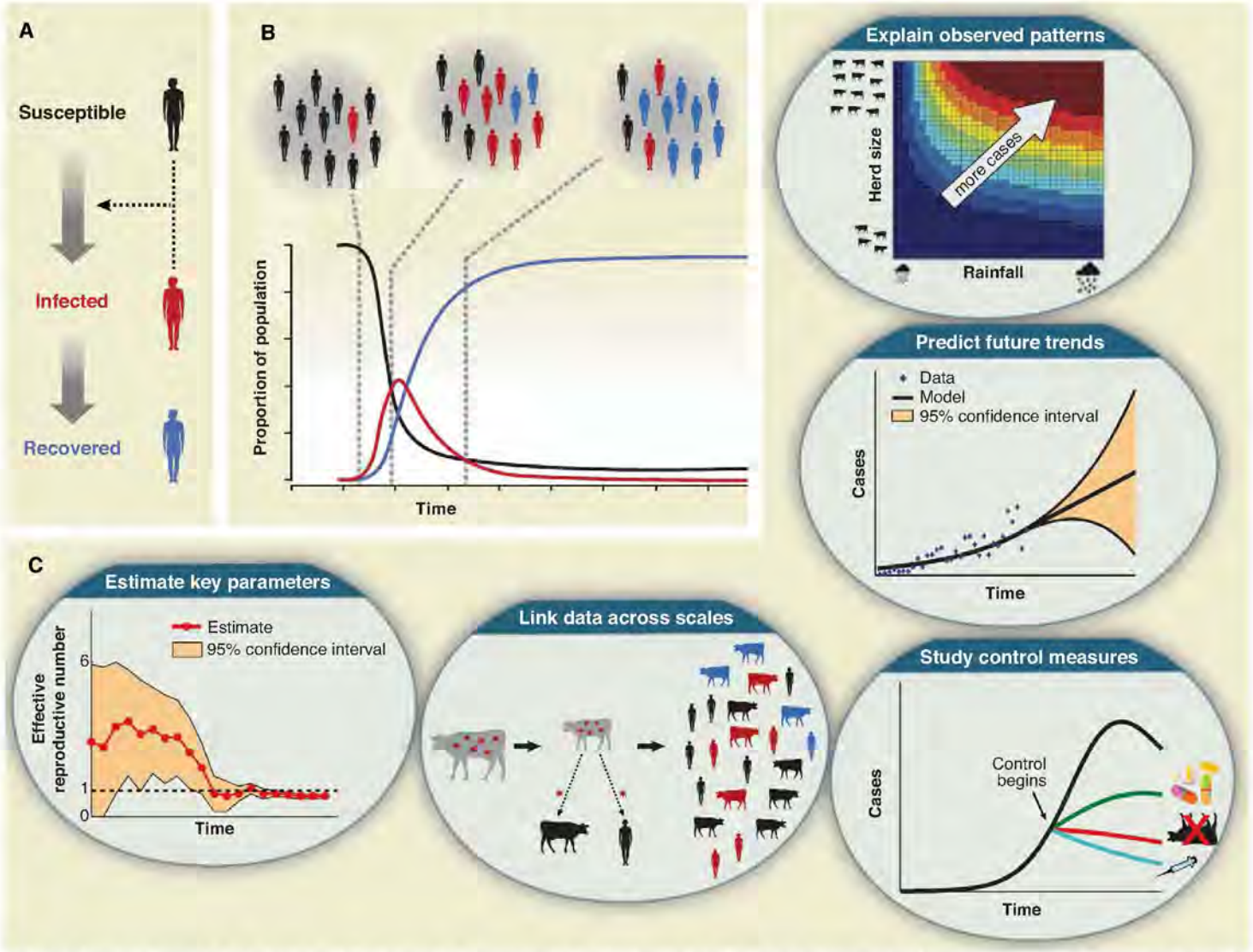

Fig. 2. Dynamical models for epidemics. (**A**) Schematic diagram of the basic SIR model, showing progression of hosts from susceptible to infected to recovered states. The dotted arrows represent transmission of infection to new cases resulting from contacts between susceptible and infected individuals. (**B**) The simple epidemic curve (red) predicted by the SIR model for a closed population (i.e., without renewal by immigration or birth of new hosts) and $R_0 > 1$. The curves for the declining proportion of hosts that are susceptible to infection is black and for the rising proportion that are recovered and immune is blue. (**C**) Dynamical models provide unique insights and allow researchers to ask questions that cannot be addressed by other methods. For example, these models enable estimation of epidemiological parameters linked to key mechanisms, integration of data spanning multiple spatial scales, comparison of alternative control strategies, prediction of future trends, and explanation of observed patterns based on mechanistic hypotheses.

namical consequences (*26*, *27*). For instance, analysis of detailed outbreak data shows that highly infectious "superspreaders" exist for all pathogens (although to varying degrees), and modeling shows that their existence makes outbreaks rarer but more explosive (*26*). Theoretical studies have illuminated central mechanisms relevant to zoonotic dynamics: Analysis of the population dynamics of multihost pathogens revealed the influence of host species diversity on reservoir dynamics and spillover risk (*28*), while a hybrid transmission-evolution model showed the potential for stage III zoonoses to adapt to humans before their stuttering chains of transmission die out (*29*). Zoonotic dynamics have clear parallels with invasion biology (as spillover, stuttering chains, and outbreaks correspond roughly to the invasion phases of introduction, establishment, and population expansion), raising the possibility of fruitful cross-fertilization between theoretical frameworks for these fields (*30*).

In contrast to the complete lack of application of models during the last influenza pandemic in 1968, dynamical models now play a key role in preparing for and responding to pandemic influenza strains [e.g., (*31*)]. For example, school closure has been identified as an important control measure during the early phase of pandemic spread (*32*) and was implemented in cities across the United States that were affected by the novel H1N1 influenza ("swine flu") in Spring 2009. Models of both influenza and SARS have exposed the futility of imposing travel restrictions once a pathogen is already spreading within a region [e.g., (*24*, *33*)], and such restrictions were largely avoided, following the recognition that the 2009 H1N1 influenza strain was already widespread when it was discovered. Meanwhile, established methods for the estimation of R_0 have helped to speed determination of this crucial parameter for the pandemic strain (*34*).

Surveying the Field: Skews and Gaps

Where has modeling research concentrated across the gamut of zoonotic pathogens and epidemiological challenges? Where are the major gaps in our knowledge, and how can dynamical models be used to integrate empirical findings, guide health policy, and drive innovative research?

We systematically surveyed 442 modeling studies addressing 85 species of zoonotic pathogens, and found surprising gaps and tremendous skews in coverage (for details, see supporting online material). Viral diseases have dominated zoonotic modeling, led by pandemic influenza, SARS, and rabies, which together account for almost half of all zoonotic models (Table 1 and fig. S1). Bacterial and protozoan pathogens have

received much less attention relative to their importance. Vector-borne and food-borne zoonoses also have been neglected by dynamical modelers compared with infections transmitted by direct contact. Consequently, many zoonotic diseases of great public health concern, such as leptospirosis and yellow fever, have rarely been modeled (Table 1), and so we lack a formal framework to understand the transmission dynamics of these diseases or to respond to sudden changes in their epidemiology.

The current literature often fails to account for the multihost ecology of zoonotic pathogens. The great majority of modeling studies consider just a single phase of the zoonotic process, typically focusing on dynamics in the reservoir or outbreaks in the human population (fig. S2). Models incorporating spillover transmission—the defining process of zoonotic dynamics—are dismayingly rare. For directly transmitted zoonoses, we found only six dynamical studies that include a mechanistic model of animal-to-human spillover. For vector-borne and food-borne infections, this number is higher but still a clear minority. Rather than integrating across host species and dynamical phases to address questions aimed at the zoonotic nature of these pathogens, too often we find zoonoses being treated "piece-wise" as a concatenation of single-host processes (or worse, some phases are ignored completely).

A similar gap is evident in the modeling of stuttering chains of transmission (fig. S2), wherein zoonotic pathogens transmit inefficiently among humans so any minor outbreaks triggered by spillover events inevitably die out. Despite their limited epidemic potential, such pathogens present epidemiologists with considerable challenges that are often best addressed by using mathematical models. For instance, monkeypox virus has long been known to spread inefficiently among humans, but its transmissibility appears to be rising as population immunity drops because fewer people have been vaccinated against smallpox (*35*, *36*). Surveillance data for stage III zoonoses, such as monkeypox, Nipah virus, or H5N1 avian influenza, can be analyzed to estimate human-to-human transmissibility and to define signatures of possible viral adaptation to humans (*37*). Given that pathogens in this class are the best-identified threats for future pandemics in the human population, study of their dynamics should be prioritized for attention.

Several patterns stand out among the existing models (fig. S3). They have been primarily applied to studying the efficacy of control measures, with the secondary aims of estimating epidemiological parameters of interest and explaining observed patterns in field data. Prediction of future trends is a major focus for models of pandemic influenza and BSE, but this aim is rarely applied to other pathogens. Equally notable are the questions missing from these studies. The dynamics of pathogen populations within individual hosts have rarely been included in models of zoonotic transmission dynamics, with the notable exception of food-borne pathogens, where the association between pathogen titers in livestock (before and during processing into meat) and infection risk to humans has been studied. Evolutionary issues are similarly neglected, despite the pressing concerns surrounding adaptation to humans and pandemic emergence for several pathogens. It is particularly striking that of the 62 models of SARS dynamics we found, none deals with pathogen evolution, despite the accumulating evidence that the virus was adapting rapidly as it circulated among humans (*38*). This gap remains because of the paucity of data linking pathogen genotypes to phenotypes (in particular, transmissibility) at the population scale. This is an important and tractable topic for empirical and theoretical research, especially given the increasing availability of genetic sequence data (*39*). Interactions among pathogen species have also been largely neglected, even though empirical data show that coinfections are relatively common and that different pathogens can facilitate or hamper each other's spread through direct or immune-mediated interactions (*40*). Finally, there has been little research that integrates transmission dynamics of zoonoses with economic considerations, despite the clear relevance of this synthesis to control policy (e.g., *32*).

Data and the Link to Reality

A crucial component of a robust and applicable science of zoonotic dynamics is the use of data to estimate parameters and to validate model output, and another is the thoughtful treatment of data-limited situations based on rigorous sensitivity analysis. Although most studies use some data to parameterize or validate models, their use is highly variable (fig. S3B). At the simplest, many authors borrow data-derived parameter values from earlier studies or fit model projections to epidemic curves. More advanced studies use dynamical reasoning to arrive at new methods of gleaning insights from available data (e.g., *41*). For studies aimed at projecting epidemic trends, the gold standard is to validate model output by comparing it with independently gathered data that has not been used for the construction of the model. Notable examples include the "post-diction" of global spread of the 1968 influenza pandemic, based on air traffic data (*42*), and the validation of BSE

Table 1. Modeling effort for selected zoonotic pathogens, organized by pathogen stage (see Fig. 1A) and number of published dynamical models. Abbreviations: EV, encephalitis virus; HF, hemorrhagic fever; BSE, bovine spongiform encephalopathy.

Pathogen stage	Number of modeling studies				
	0	1 to 5	6 to 10	11 to 20	>20
II (Spillover only)	*Babesia microti* *Bartonella henselae* *Chlamydophila psittaci* *Coxiella burnetii* *Francisella tularensis* Hendra virus *Rickettsia prowazekii* *Rickettsia typhi* *Streptococcus suis* Venezuelan equine EV	*Bacillus anthracis* *Campylobacter jejuni* Japanese EV *Leptospira interrogans* Puumala virus *Salmonella typhimurium* Tick-borne EV	*Brucella abortus* Louping ill virus *Toxoplasma gondii* *Trypanosoma brucei rhodesiense* West Nile virus	*Borrelia burgdorferi* Sin Nombre virus *Trypanosoma cruzi*	BSE Rabies virus
III (Spillover + stuttering chains)	Andes virus Lassa virus Machupo virus Nipah virus	*Leishmania chagasi* Crimean-Congo HF virus Monkeypox virus *Yersinia enterocolitica*	*Leishmania infantum*	*E. coli* O157:H7	Influenza A (avian) *Mycobacterium bovis*
IV (Spillover + possible outbreaks)	Barmah forest virus Dengue virus (sylvatic) *Leishmania donovani* Marburg virus Mayaro virus	Chikungunya virus Ebola virus Ross River virus Yellow fever virus		*Yersinia pestis*	Influenza A (pandemic) SARS-CoV

models developed for England, by using independent data from Northern Ireland (*43*). Models can also interact powerfully with population-level experiments to confirm mechanisms underlying observed patterns (*44*).

Broad patterns of data usage are, of course, determined by the availability of relevant data sets. The free availability of epidemic curves led to two-thirds of SARS modeling studies' incorporating population-level data, and early analyses of SARS disease progression enabled widespread use of data-driven parameters (*45*). For influenza, the well-known clinical course of infection has enabled widespread use of data in parameterizing models, but model-fitting to epidemic curves has been less common. Studies focusing on zoonoses in their animal reservoirs (e.g., rabies and bovine tuberculosis) have relied largely on individual-level parameters, owing to the relative rarity of collated population data for animal diseases. In contrast, however, all the BSE models were fit to population data, which reflects the intensive and cumulative study of the British epidemic and later application of these methods to BSE data from other countries.

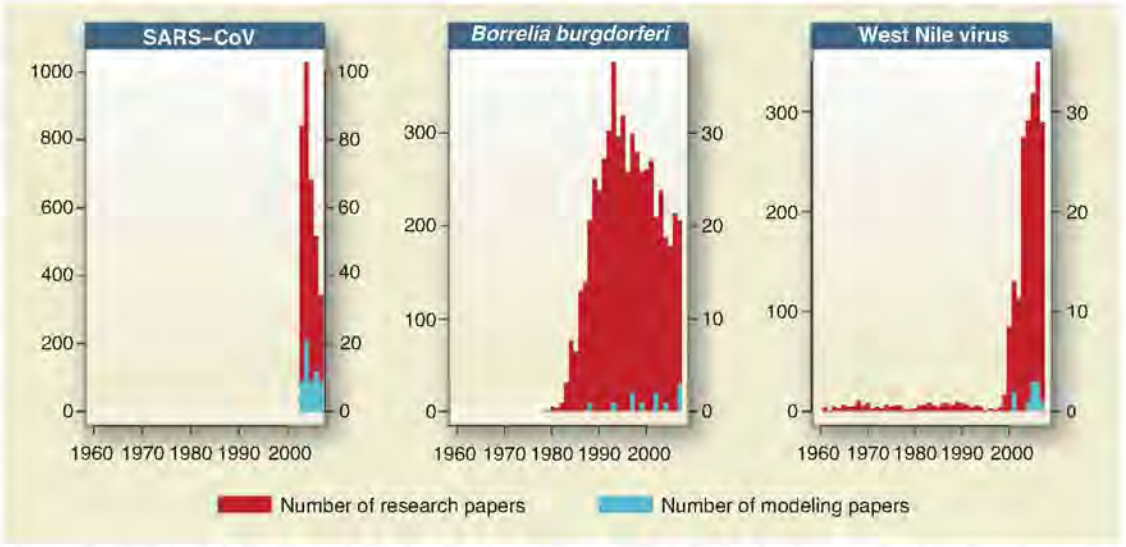

Fig. 3. Temporal profiles of total research effort (red) and modeling effort (blue) for recently emerged zoonoses. Figure panels have different *y*-axis scaling, but in each instance, the scaling for number of modeling studies (right axis) is 1/10th that for the total number of research papers (left axis).

Data-free modeling tends to be more common for pathogens that have fewer models overall; this likely reflects either the complete unavailability of data or the lack of opportunity to borrow data-informed parameter values from other studies. However, a broad and vibrant literature has applied statistical methods to analyze the epidemiological and spatial patterns of zoonotic infections [e.g., (*46, 47*)], and opportunities to link these findings with dynamical models too often go unrealized.

Looking beyond the use of data, the best modeling studies are those that engage substantively, and realistically, with current thinking in biology or public health. However, detail and model complexity are not equivalent to realism, and a simple model can yield more insight than a massive simulation that is not fully understood. Detailed simulation models are necessary to address some important questions, but model complexity should be increased cautiously and with an awareness of the associated costs of reduced transparency, a multiplicity of often unknown parameters, and the resulting need for intensive investigation of how model assumptions may influence conclusions [e.g., (*31*)]. A hierarchical approach, comparing the behavior of models with different degrees of detail, can aid the design and interpretation of complex models.

Response Dynamics and the Determinants of Effort

Given the prevailing focus of zoonotic models on designing and assessing control measures, as well as the unique potential of models to estimate important characteristics of epidemics, it is instructive to consider the timeliness with which modelers respond to emerging threats. For zoonotic pathogens that either were newly discovered or have made sizable range shifts in recent decades, we constructed temporal profiles of the scientific literature to characterize the dynamics of the modeling community's response (Fig. 3 and fig. S4). The poster child for rapid response is SARS, for which several modeling analyses were completed within months of the pathogen's and epidemic's discovery and were influential in designing outbreak control measures. For *Borrelia burgdorferi*, the causative agent of Lyme disease, a 10-year delay from discovery to the first model has been followed by intermittent modeling efforts, perhaps reflecting the difficulty of constructing mechanistic models for a vector-borne pathogen with a multihost sylvatic cycle that is still being characterized, coupled with a vector having a complex life-history incorporating multiyear time delays. West Nile virus exemplifies a different pattern, in which low-level scientific interest suddenly surges following incursions into new geographic territory (wealthy nations in particular), and sporadic modeling efforts follow a few years later.

A sense of urgency and global risk motivates the community to produce and publish dynamical models quickly. Regrettably, for those zoonoses largely restricted to developing countries, such as trypanosomiasis (sleeping sickness), leishmaniasis, and leptospirosis, neglect still applies (Table 1 and fig. S1) despite their substantial public health impacts. A further, essential factor is the existence of good clinical and epidemiological data to construct and validate models. Here we stress that data must be made publicly available, preferably in real time as occurred for SARS, to maximize both the research opportunity and the resulting public good of scientifically derived policy. The early availability of genetic sequence data for the current H1N1 influenza pandemic has been exemplary in this regard, but unfortunately the corresponding epidemiological data have been less systematically accessible.

Finally, a key determinant of modeling effort is pathogen life history—in particular the extent to which a pathogen matches the assumptions of the basic SIR family of epidemic models. For infections that are acute, symptomatic, and directly transmitted, models can be constructed (and often parameterized) by using "off-the-shelf" techniques, greatly speeding the analysis of newly identified disease threats and enabling extension of the models to address more sophisticated questions. Hence, an important priority for ongoing research is to expand the class of pathogens for which there are readily available modeling templates and applied examples of their connection to data sets, beyond those that conform easily to the standard SIR model.

The Way Forward: Crossing Species, Crossing Disciplines

Significant shortfalls in dynamical studies of particular diseases, as well as entire classes of zoonotic pathogens (notably protozoan and vector-borne infections), can be clearly discerned in the literature (Table 1 and fig. S1). In contrast, some zoonoses, such as influenza, SARS, and BSE, have acted as crucibles for development of new methods for understanding epidemiological complexities, particularly where well-resolved data are available. Unfortunately, even these models have been restricted in scope, and there is a need for new models that integrate across phases of zoonotic dynamics and that incorporate evolutionary, economic, and within-host considerations.

An especially worrying gap is modeling of spillover transmission from animals to humans. The force of infection across species boundaries can be broken into its constituent factors (Fig. 1B), including universal components such as the

role of human susceptibility, risk behaviors, and infection prevalence in the reservoir, as well as particular details related to transmission routes and pathogen-specific biology. Spillover risk also can be influenced by dynamical phenomena: One innovative study posits that epizootic peaks of hantavirus in rodent reservoirs, with accompanying spikes in numbers of newly infected rodents excreting large quantities of virus, lead to high concentrations of virus in the environment and hence an increased risk of human infection (*48*). Further research will reveal whether such hypotheses may hold true generally across zoonotic systems.

It is initially surprising that most of the best models of spillover have been developed for the more complex vector-borne and food-borne zoonoses, but this arises because the process of transmission can often be observed directly in such systems. Studies of vector-borne infections have used quantitative frameworks to integrate data on host competency, vector feeding preferences, and environmental conditions to be able to estimate spillover risk from different ecological pathways, although without explicitly incorporating dynamics (*49*). The food safety literature has treated the risk of pathogens crossing from animal hosts to human exposures in vivid mechanistic detail (*50*), setting a high standard to be matched by disease ecologists. For directly transmitted zoonoses, it is straightforward to construct a basic model with cross-species transmission (*20*), but it is very challenging to delve into underlying mechanisms and estimate key parameters, particularly the cross-species contact rate and the resulting probability of infection, which typically arise from multiple and largely unobserved ecological, behavioral, and physiological factors. Research in this area is clearly limited by available data from multiple host species, but the plummeting cost of genetic sequencing brings exciting opportunities for mapping cross-species transmission (*51*).

A second major gap lies in analysis of stuttering chains of inefficient human-to-human transmission following spillover. Data from these settings are dominated by stochastic effects and heterogeneities among hosts and environments, and analysis is complicated by the fundamental problem of distinguishing between primary and secondary cases. The central challenges in the study of stage III zoonoses include quantifying the rate of human-to-human transmission against a background of spillover and monitoring for changes in pathogen transmissibility that may represent steps toward emergence of new stage IV pathogens (*29*).

The study of zoonotic dynamics offers a unique window into fundamental questions of pathogen ecology and evolution and provides vital insights into public health issues. We need models to reveal the points of vulnerability where intervention against zoonoses will be most effective and to highlight the gaps in data collection. We need to know when particular zoonotic phases, e.g., reservoir transmission, spillover from animals to humans, stuttering transmission, or incipient outbreaks among humans, can be targeted to optimize epidemiological outcomes while reducing cost. How should health policy be adapted to account for environmental change or regional differences in ecology and sociology? How might zoonotic pathogens evolve in response to anthropogenic forces or control strategies? Dynamical models, rooted in data, provide an essential framework for addressing these critical questions.

References and Notes

1. M. E. J. Woolhouse, S. Gowtage-Sequeria, *Emerg. Infect. Dis.* **11**, 1842 (2005).
2. L. H. Taylor, S. M. Latham, M. E. J. Woolhouse, *Philos. Trans. R. Soc. London B Biol. Sci.* **356**, 983 (2001).
3. N. D. Wolfe, C. P. Dunavan, J. Diamond, *Nature* **447**, 279 (2007).
4. D. M. Morens, G. K. Folkers, A. S. Fauci, *Lancet Infect. Dis.* **8**, 710 (2008).
5. K. E. Jones *et al.*, *Nature* **451**, 990 (2008).
6. S. R. Palmer, E. J. L. Soulsby, D. I. H. Simpson, *Zoonoses: Biology, Clinical Practice, and Public Health Control* (Oxford Univ. Press, New York, 1998).
7. J. E. Childs, *Curr. Top. Microbiol. Immunol.* **315**, 389 (2007).
8. R. A. Weiss, A. J. McMichael, *Nat. Med.* **10**, S70 (2004).
9. M. S. Smolinksy, M. A. Hamburg, J. Lederburg, Eds., *Microbial Threats to Health: Emergence, Detection, and Response* (Institute of Medicine, National Academies Press, Washington, DC, 2003).
10. R. Hassan, R. Scholes, N. Ash, Eds., *Ecosystems and Human Well-Being: Current State and Trends: Findings of the Conditions and Trends Working Group Millennium Ecosystem Assessment*, vol. 1 (Island Press, Washington, DC, 2005).
11. T. Kuiken *et al.*, *Science* **312**, 394 (2006).
12. N. D. Wolfe, P. Daszak, A. M. Kilpatrick, D. S. Burke, *Emerg. Infect. Dis.* **11**, 1822 (2005).
13. P. Daszak *et al.*, *Curr. Top. Microbiol. Immunol.* **315**, 463 (2007).
14. R. M. Anderson, R. M. May, *Infectious Diseases of Humans: Dynamics and Control* (Oxford Univ. Press, Oxford, 1991).
15. M. J. Keeling, P. Rohani, *Modeling Infectious Diseases in Humans and Animals* (Princeton Univ. Press, Princeton, NJ, 2008).
16. R. M. Anderson *et al.*, *Nature* **382**, 779 (1996).
17. N. M. Ferguson, C. A. Donnelly, M. E. J. Woolhouse, R. M. Anderson, *Philos. Trans. R. Soc. London B Biol. Sci.* **352**, 803 (1997).
18. C. A. Russell, D. L. Smith, J. E. Childs, L. A. Real, *PLoS Biol.* **3**, e88 (2005).
19. K. Hampson *et al.*, *PLoS Biol.* **7**, e1000053 (2009).
20. D. L. Smith, B. Lucey, L. A. Waller, J. E. Childs, L. A. Real, *Proc. Natl. Acad. Sci. U.S.A.* **99**, 3668 (2002).
21. S. Riley *et al.*, *Science* **300**, 1961 (2003).
22. M. Lipsitch *et al.*, *Science* **300**, 1966 (2003).
23. J. O. Lloyd-Smith, A. P. Galvani, W. M. Getz, *Proc. R. Soc. London B. Biol. Sci.* **270**, 1979 (2003).
24. A. B. Gumel *et al.*, *Proc. R. Soc. London B. Biol. Sci.* **271**, 2223 (2004).
25. Y. H. Hsieh *et al.*, *J. Theor. Biol.* **244**, 729 (2007).
26. J. O. Lloyd-Smith, S. J. Schreiber, P. E. Kopp, W. M. Getz, *Nature* **438**, 355 (2005).
27. M. E. J. Woolhouse *et al.*, *Proc. Natl. Acad. Sci. U.S.A.* **94**, 338 (1997).
28. A. Dobson, *Am. Nat.* **164**, S64 (2004).
29. R. Antia, R. R. Regoes, J. C. Koella, C. T. Bergstrom, *Nature* **426**, 658 (2003).
30. J. E. Childs, J. A. Richt, J. S. Mackenzie, *Curr. Top. Microbiol. Immunol.* **315**, 1 (2007).
31. M. E. Halloran *et al.*, *Proc. Natl. Acad. Sci. U.S.A.* **105**, 4639 (2008).
32. S. Cauchemez *et al.*, *Lancet Infect. Dis.* **9**, 473 (2009).
33. B. S. Cooper, R. J. Pitman, W. J. Edmunds, N. J. Gay, *PLoS Med.* **3**, e212 (2006).
34. C. Fraser *et al.*, *Science* **324**, 1557 (2009).
35. A. W. Rimoin *et al.*, *Emerg. Infect. Dis.* **13**, 934 (2007).
36. P. E. M. Fine, Z. Jezek, B. Grab, H. Dixon, *Int. J. Epidemiol.* **17**, 643 (1988).
37. N. M. Ferguson, C. Fraser, C. A. Donnelly, A. C. Ghani, R. M. Anderson, *Science* **304**, 968 (2004).
38. T. Sheahan *et al.*, *J. Virol.* **82**, 2274 (2008).
39. B. T. Grenfell *et al.*, *Science* **303**, 327 (2004).
40. A. L. Graham, I. M. Cattadori, J. O. Lloyd-Smith, M. J. Ferrari, O. N. Bjornstad, *Trends Parasitol.* **23**, 284 (2007).
41. J. Wallinga, P. Teunis, *Am. J. Epidemiol.* **160**, 509 (2004).
42. L. A. Rvachev, I. M. Longini Jr., *Math. Biosci.* **75**, 3 (1985).
43. N. M. Ferguson, A. C. Ghani, C. A. Donnelly, G. O. Denny, R. M. Anderson, *Proc. R. Soc. London B. Biol. Sci.* **265**, 545 (1998).
44. M. K. Laurenson, R. A. Norman, L. Gilbert, H. W. Reid, P. J. Hudson, *J. Anim. Ecol.* **72**, 177 (2003).
45. C. A. Donnelly *et al.*, *Lancet* **361**, 1761 (2003).
46. R. J. King, D. H. Campbell-Lendrum, C. R. Davies, *Emerg. Infect. Dis.* **10**, 598 (2004).
47. R. S. Ostfeld, C. D. Canham, K. Oggenfuss, R. J. Winchcombe, F. Keesing, *PLoS Biol.* **4**, e145 (2006).
48. F. Sauvage, M. Langlais, D. Pontier, *Epidemiol. Infect.* **135**, 46 (2007).
49. A. M. Kilpatrick, P. Daszak, M. J. Jones, P. P. Marra, L. D. Kramer, *Proc. R. Soc. London B. Biol. Sci.* **273**, 2327 (2006).
50. D. Jordan, S. A. McEwen, A. M. Lammerding, W. B. McNab, J. B. Wilson, *Prev. Vet. Med.* **41**, 55 (1999).
51. H. D. Song *et al.*, *Proc. Natl. Acad. Sci. U.S.A.* **102**, 2430 (2005).

52. This work was supported by the Research and Policy for Infectious Disease Dynamics (RAPIDD) program of the Science and Technology Directorate, U.S. Department of Homeland Security, and the Fogarty International Center, NIH. We are grateful to O. Bjornstad, E. McKenzie, M. Poss, A. Read, and L. Simonsen for valuable comments and to B. Gee for assistance with figure preparation. J.L.-S. is grateful for the support of the De Logi Chair in Biological Sciences.

Supporting Online Material

www.sciencemag.org/cgi/content/full/326/5958/1362/DC1
Materials and Methods
SOM Text
Figs. S1 to S4
Tables S1 to S3
References

10.1126/science.1177345

Harnessing Carbon Payments to Protect Biodiversity

Oscar Venter,[1]* William F. Laurance,[2,3] Takuya Iwamura,[1] Kerrie A. Wilson,[1] Richard A. Fuller,[1] Hugh P. Possingham[1]

The rapid destruction of tropical forests produces ~20% of anthropogenic carbon emissions and poses one of the greatest perils to global biodiversity (*1*). A highly anticipated carbon-payment mechanism termed REDD (reduced emissions from deforestation and degradation) is increasing incentives to protect threatened forests (*2*). REDD funding could soon dwarf all other spending for tropical conservation (*3*).

Although designed to limit harmful climate change, REDD could provide additional benefits, such as the conservation of biodiversity. Yet without specific provisions for biodiversity, REDD is likely to protect forests that are most cost-effective for reducing carbon emissions (*3*). Here, we critically assess how well such forests protect biodiversity.

We modeled business-as-usual deforestation for the decade from 2006 to 2015 for 68 developing countries (http://unfccc.int) that suffered net forest loss between 1990 and 2005 (table S1). We used a decision-theory framework (*4*) to optimally schedule the allocation of REDD funds to protect forests from deforestation. Our modeling incorporated data on forest extent and carbon content, current protected areas, business-as-usual deforestation rates, deforestation ceilings, and agricultural opportunity costs (table S1) (*5*). Two funding scenarios were explored, effecting 20 and 40% reductions in business-as-usual deforestation rates. We quantified the return on investment for biodiversity from protecting forests by using the species-area relationship with data on the number of country-endemic, forest-dwelling mammal, bird, and amphibian species in each country (table S2) (*5*).

Our analyses suggest deforestation in developing countries could release 9.0 billion tons of carbon into the atmosphere over 10 years. If expected deforestation could be reduced by 20%, funding for cost-effective REDD would be expended in just eight countries (Fig. 1A and table S3). Funds would go almost entirely to South America, primarily Brazil (74%), where agricultural opportunity costs are relatively low. No funds would be allotted to Asia, which has sizeable revenues from oil palm, rubber, rice, and maize that increase the opportunity costs of REDD (table S1). This funding pattern appears robust to model and parameter uncertainty (*5*), although countries such as Indonesia could conceivably receive increased funding if we accounted for emissions from peat degradation (*6*). Reducing deforestation by 40% distributes funds across 20 countries, but most are still concentrated in South America (fig. S1A and table S3).

Importantly, if REDD focuses solely on cost-effectively reducing carbon emissions, its benefits for biodiversity are low, protecting only slightly more vertebrate species than if funds were allocated at random among forest-losing countries (Fig. 1A and fig. S1A). However, if the same REDD funds were targeted to protect biodiversity, almost four times the number of species would be protected (Fig. 1B and fig. S1B). In this case spending would tend to shift toward Southeast Asian and Indian Ocean nations. This is because species extinctions are most effectively minimized by protecting biodiversity "hot spots"—areas with high species richness and endemism and relatively little remaining forest (*7*)—such as the Philippines, Madagascar, and Indonesia.

There is a trade-off between protecting biodiversity and reducing emissions, but that trade-off is highly nonlinear (fig. S2). This means that, through careful targeting of REDD funds, allocation solutions can be found that come close to maximizing both objectives simultaneously. We discover that the biodiversity benefits of REDD can be doubled while incurring just a 4 to 8% reduction in carbon benefits, depending on the amount of REDD funds expended (fig. S2). Our compromise scheme is broadly similar to that which maximizes emissions reductions but diverts some funding to nations that are jointly valuable for carbon and biodiversity (Fig. 1C and fig. S1C).

Our approach sharply increased the biodiversity benefits of REDD by explicitly incorporating biodiversity values into carbon payments (*5*). A timely opportunity exists to include such provisions within REDD schemes being negotiated under the United Nations Framework Convention on Climate Change. Additionally, private conservation groups could promote biodiversity by using some of their budgets to subsidize REDD programs in high-biodiversity countries, making them more cost-competitive for REDD funding. Lastly, some purchasers of REDD carbon credits, such as certain corporations or nations, might pay a premium to save imperiled ecosystems or areas with high-profile species.

Modest adjustments in REDD strategies could dramatically improve their capacity to conserve imperiled biodiversity. Without such a targeted approach, the biodiversity benefits of REDD will be far more limited than is otherwise possible.

References and Notes

1. W. F. Laurance, *Bioscience* **58**, 286 (2008).
2. R. E. Gullison *et al.*, *Science* **316**, 985 (2007); published online 10 May 2007 (10.1126/science.1136163).
3. L. Miles, V. Kapos, *Science* **320**, 1454 (2008).
4. K. A. Wilson, M. F. McBride, M. Bode, H. P. Possingham, *Nature* **440**, 337 (2006).
5. Materials and methods are available as supporting material on *Science* Online.
6. O. Venter *et al.*, *Conserv. Lett.* **2**, 123 (2009).
7. N. Myers, R. A. Mittermeier, C. G. Mittermeier, G. A. B. da Fonseca, J. Kent, *Nature* **403**, 853 (2000).
8. We thank T. Gardner and two anonymous referees for comments and the Endeavor Research Fellowship, National Science and Engineering Research Council of Canada, Australian Research Council, and Commonwealth Environmental Research Facility for support.

Supporting Online Material

www.sciencemag.org/cgi/content/full/326/5958/1368/DC1
Materials and Methods
Figs. S1 and S2
Tables S1 to S4
References

7 August 2009; accepted 25 September 2009
10.1126/science.1180289

[1]The Ecology Centre, University of Queensland, Brisbane, Queensland 4072, Australia. [2]School of Marine and Tropical Biology, James Cook University, Cairns, Queensland 4870, Australia. [3]Smithsonian Tropical Research Institute, Apartado 0843-03092, Balboa, Ancón, Republic of Panama.

*To whom correspondence should be addressed. E-mail: oventer@uq.edu.au

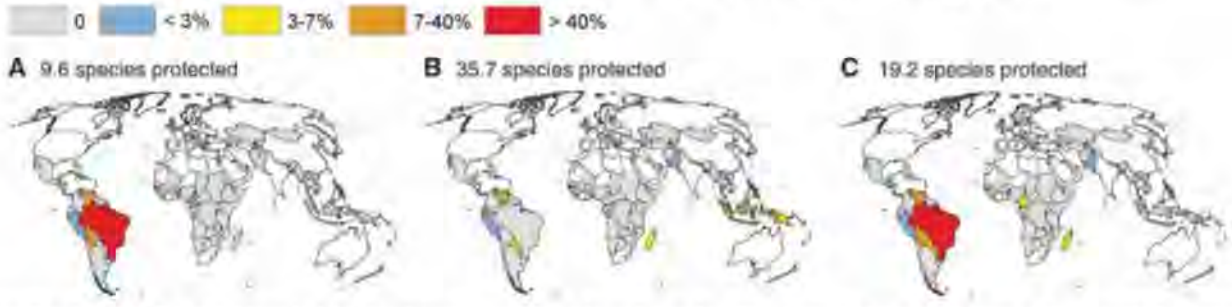

Fig. 1. Proportions of REDD funds allocated to forest-losing countries to (**A**) minimize carbon emissions, (**B**) minimize loss of forest vertebrates, and (**C**) minimize carbon emissions while simultaneously doubling benefits to biodiversity. These three scenarios would reduce deforestation by up to 20%. Shown above each map is the expected number of averted forest mammal, bird, and amphibian extinctions (a random allocation of funds protects 8.4 species on average). Countries in white are not losing net forest cover and so are excluded from the analysis.

Structure of Monomeric Yeast and Mammalian Sec61 Complexes Interacting with the Translating Ribosome

Thomas Becker,[1] Shashi Bhushan,[1] Alexander Jarasch,[1] Jean-Paul Armache,[1] Soledad Funes,[1,2] Fabrice Jossinet,[3] James Gumbart,[4] Thorsten Mielke,[5,6] Otto Berninghausen,[1] Klaus Schulten,[4] Eric Westhof,[3] Reid Gilmore,[7] Elisabet C. Mandon,[7]* Roland Beckmann[1]*

The trimeric Sec61/SecY complex is a protein-conducting channel (PCC) for secretory and membrane proteins. Although Sec complexes can form oligomers, it has been suggested that a single copy may serve as an active PCC. We determined subnanometer-resolution cryo–electron microscopy structures of eukaryotic ribosome-Sec61 complexes. In combination with biochemical data, we found that in both idle and active states, the Sec complex is not oligomeric and interacts mainly via two cytoplasmic loops with the universal ribosomal adaptor site. In the active state, the ribosomal tunnel and a central pore of the monomeric PCC were occupied by the nascent chain, contacting loop 6 of the Sec complex. This provides a structural basis for the activity of a solitary Sec complex in cotranslational protein translocation.

The protein-conducting channel (PCC) of the canonical secretory pathway is formed in all cells by the Sec61/SecY complex. It engages in the post- and cotranslational translocation of secretory proteins across and the insertion of integral membrane proteins into the membrane of the endoplasmic reticulum in eukaryotes and the plasma membrane of bacteria (*1*, *2*).

In the cotranslational translocation mode, the ribosome with an emerging signal sequence is targeted to the membrane by the signal recognition particle (SRP) and its receptor (*3*). Here, the Sec complex acts as a receptor for the ribosome via its cytosolic loops (*4*). The alignment of the ribosomal tunnel with a central pore of the PCC allows direct movement of the nascent chain from the ribosomal tunnel exit across or into the membrane (*5*, *6*).

The PCC-forming heterotrimeric Sec complex consists of one large subunit (Sec61α in Mammalia, Sec61p/Ssh1p in yeast, SecY in bacteria) and two small subunits (Sec61β, γ in eukaryotes and SecE, G in bacteria). Conflicting models have been presented as to how many of these heterotrimers are necessary to build an active PCC, and there has been some disagreement about the actual path of the polypeptide chain. The *Escherichia coli* SecYEG complex forms back-to-back dimers in two-dimensional (2D) crystals (*7*), and low-resolution single-particle electron microscopy (EM) data revealed a pentagonal ringlike morphology of the PCC interpreted as oligomers (*5*, *6*, *8*–*12*). The monomeric crystal structure of an archaeal SecYEβ complex (*13*), in combination with chemical cross-linking data (*14*), led to the interpretation that a single copy of the Sec complex is sufficient to serve as an active PCC, even when assembled into a dimer for posttranslational translocation (*15*) or a tetramer for cotranslational translocation (*8*). Recent low-resolution cryo-EM data of inactive ribosome-Sec complexes were interpreted to represent single copies of Sec complexes (*16*, *17*), and crystal structures of the bacterial SecY-SecA complex also show a single copy (*18*). However, because all these structures are either of low resolution or lack translocating peptides, two main questions remain: (i) What conformational and (ii) what oligomeric states can be adopted by the PCC in the different modes of activity, such as signal sequence recognition and vertical and lateral gating?

Cryo-EM and 3D reconstruction. For structure determination by cryo-EM, we used digitonin-solubilized purified Ssh1 complex (Sec sixty-one homolog 1 from the yeast *Saccharomyces cerevisiae*) containing Ssh1p, Sbh2p, and Sss1p (*19*). This complex is active in the cotranslational translocation mode only (i.e., when ribosome-bound) (*20*, *21*).

We reconstituted the Ssh1 complex with in vitro programmed 80*S* ribosomes carrying a nascent polypeptide chain [ribosome–nascent chain complexes (RNCs)] (*6*, *22*). The peptide includes the first 120 amino acids of the type II membrane protein dipeptidyl aminopeptidase B (DP120), together with its signal-anchor sequence, long enough to allow a loop insertion into the PCC (*23*). As in the case of the Sec61 complex (*6*), we observed specific and stable binding of the Ssh1 complex to RNCs.

Cryo-EM analysis revealed heterogeneity of the sample, and a thorough sorting regimen applied to the data set (fig. S1) (*24*) resulted in a number of structures at subnanometer resolution, three of which were analyzed further: (i) the programmed (active) 80*S*-Ssh1 complex, (ii) the nonprogrammed (idle) 80*S*-Ssh1 complex without a peptidyl-tRNA, and (iii) the programmed 80*S*

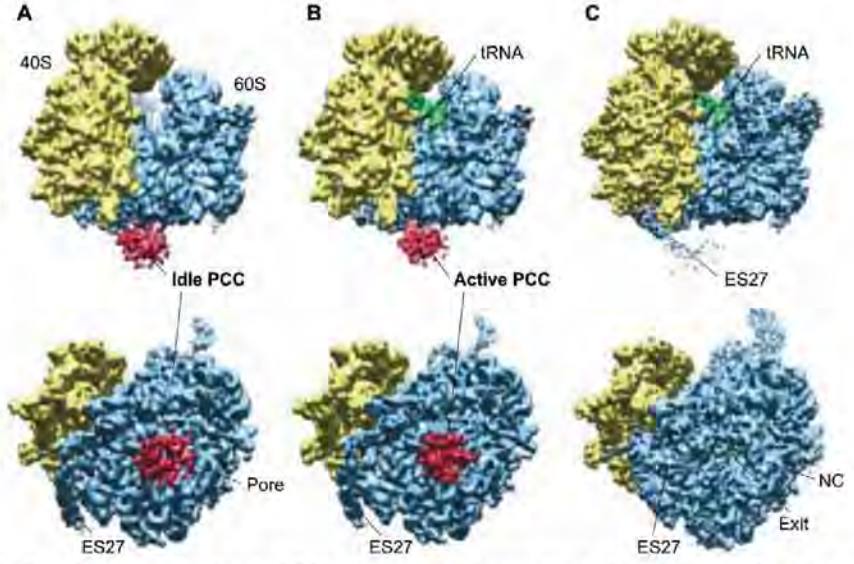

Fig. 1. Cryo-EM reconstructions of 80*S* ribosome-Ssh1 complexes. Cryo-EM reconstructions of the idle (**A**) and active (**B**) 80*S*-Ssh1 complex at 9 Å resolution. (**C**) Map of the 80*S* ribosome with ES27 in the exit conformation at 8 Å. Color code: 40*S* subunit, yellow; 60*S* subunit, blue; P-site tRNA/nascent polypeptide chain, green; Ssh1 complexes (PCC), red. NC, nascent chain.

[1]Gene Center Munich and Center for Integrated Protein Science, Department of Chemistry and Biochemistry, Ludwig-Maximilians-Universität München, Feodor-Lynen-Strasse 25, 81377 Munich, Germany. [2]Departamento de Bioquímica, Instituto de Fisiología Celular, Circuito Exterior s/n, Ciudad Universitaria, Universidad Nacional Autónoma de México, Mexico, Distrito Federal, 04510, Mexico. [3]Institut de Biologie Moléculaire et Cellulaire du CNRS, Architecture et Réactivité de l'ARN, Université de Strasbourg, 15 rue René Descartes, F-67084 Strasbourg, France. [4]Department of Physics, Beckman Institute, University of Illinois at Urbana-Champaign, Urbana, IL 61801, USA. [5]Ultrastrukturnetzwerk, Max Planck Institute for Molecular Genetics, Ihnestrasse 63-73, D-14195 Berlin, Germany. [6]Institut für Medizinische Physik und Biophysik, Charite–Universitätsmedizin Berlin, Ziegelstrasse 5-9, 10117-Berlin, Germany. [7]Department of Biochemistry and Molecular Pharmacology, University of Massachusetts Medical School, 364 Plantation Street, Worcester, MA 01605, USA.

*To whom correspondence should be addressed. E-mail: elisabet.mandon@umassmed.edu (E.M.); beckmann@lmb.uni-muenchen.de (R.B.)

ribosome with ES27 in exit conformation without Ssh1 complex (Fig. 1 and fig. S2). The 3D reconstruction of all programmed ribosomes resulted in a 6.1 Å map of the yeast 80*S* ribosome (fig. S2).

As expected, the Ssh1 complex was bound at the exit site of the ribosome, similar to the Sec61 complex (*6*). However, because of apparent flexibility of the ribosome-PCC connection, the PCC density was not as well resolved as the ribosome. Two notable features of the PCC density were observed: (i) The size of the density appeared to be smaller than previously observed, and (ii) a central pore was visible in the idle complex.

Visualization of the nascent chain and ribosomal model of the tunnel exit site. When cutting through the densities, the idle complex without a tRNA revealed an empty ribosomal tunnel leading directly to the central pore in the PCC density (Fig. 2A). In contrast, the pore in the active PCC was occupied by additional density. Here, even applying different contour or filtering parameters did not lead to the appearance of a porelike feature (Fig. 2B). Notably, the active complexes revealed additional density in the ribosomal tunnel, representing the nascent polypeptide chain (Fig. 2, B and C). For the RNC with ES27 in the exit-site conformation, the nascent-chain density could be traced from the CCA end of the tRNA almost continuously to the tunnel exit (Fig. 2, C and F). For further analysis, we generated a molecular model of the tunnel exit region based on the yeast RNC map at ~6 Å resolution (*24*). It includes models for the proteins rpL4, rpL17, rpL19, rpL25, rpL26, rpL31, rpL35, and rpL39, as well as the ribosomal RNA (rRNA) helices H5 to H7, H24, H50, and the extension ES24 of H59 (Fig. 2, D and E).

Oligomeric state and molecular model of the ribosome-bound yeast Ssh1 complex. We employed a double-tag approach (*25*) to analyze the oligomeric state of the Ssh1 complex in the cell: We engineered a yeast strain to express, in similar amounts, two differently tagged forms of Ssh1p (T7-Ssh1p and AU1-Ssh1p), both of which are functional (*4*, *24*). We used antibodies against one of the tags for nondenaturing immunoprecipitation of digitonin-solubilized Ssh1 complex in the presence of RNCs. We then used the second antibody to probe whether the second tag could be coprecipitated, which is indicative of hetero-oligomer formation. Pull-down by the first antibody did not yield any detectable amounts of the second tag, independent of the order of antibody usage (Fig. 3A). Therefore, the stably ribosome-bound Ssh1 complex is likely to exist mainly as a single copy. However, we cannot exclude the possibility that the Ssh1 complex may assemble into a transient or detergent-sensitive oligomer in the membrane.

Using this result, we analyzed the cryo-EM densities of the idle and active Ssh1 complexes to dock homology models based on the crystal structure of the archaeal SecYEβ complex (*13*). Tetramers, trimers, or dimers (*12*, *26*) could not be accommodated in the observed density (fig. S3). Only a single copy of the Ssh1 complex fit (Fig. 3B), which is in agreement with our pull-down experiment, biochemical data (*27*–*29*), and low-resolution cryo-EM data of inactive complexes (*16*, *17*). The final models required minor adjustments, mainly of cytoplasmic loops L6 and L8, as well as the C-terminal tail (*24*). Though the model accounts for the majority of the observed density, a remaining belt-shaped density that surrounds the fitted molecule (Fig. 3, B and C, and fig. S3B) most likely corresponds to the detergent micelle. Taken together, the yeast PCC consists of a single Sec61 (Ssh1) complex when bound to a nontranslating or signal-sequence–carrying ribosome. The overall conformation is

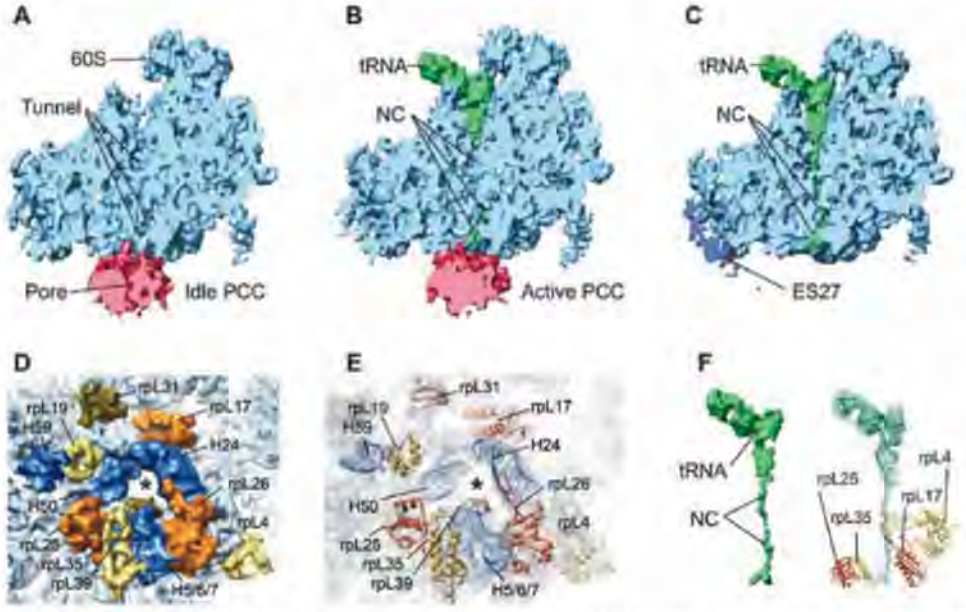

Fig. 2. Visualization of the PCC pore, nascent polypeptide chain, and molecular model. Cut density for the 60*S* subunit and the idle (**A**) and active (**B**) Ssh1 complex is shown as in Fig. 1A. (**C**) Same as in (A), except ES27 in the exit position (dark blue) and P-site tRNA are shown. (**D**) Bottom view of the 6.1 Å RNC map as in Fig. 1. Density for rRNA and ribosomal proteins is highlighted. The asterisk indicates tunnel exit. (**E**) Same as in (D), showing molecular models. (**F**) (Left) Isolated density for the P-site tRNA and the nascent DP120 chain (NC) as in (C). (Right) Molecular model for the yeast P-site tRNAAsp and the nascent DP120 peptide with ribosomal proteins (E).

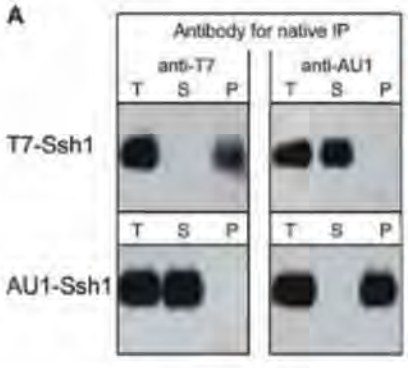

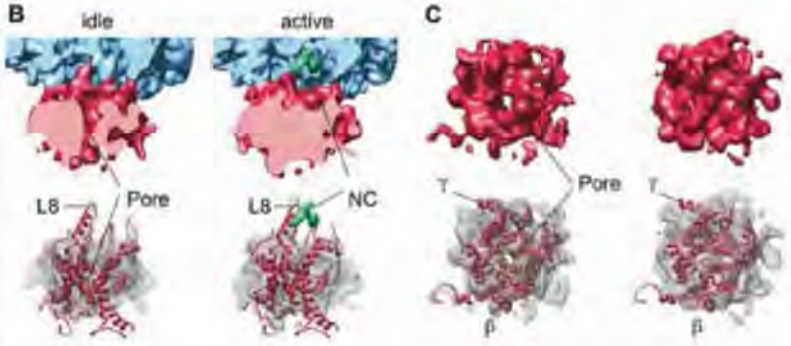

Fig. 3. A monomeric ribosome-bound Ssh1 complex. (**A**) Native immunoprecipitation (IP) of epitope tagged Ssh1 complexes. Microsomes from yeast cells expressing T7 and AU1-tagged Ssh1p were repopulated with RNCs, solubilized, and subjected to native immunoprecipitation with anti-T7 or anti-AU1 antibodies. Total extract (T), supernatant (S), and immunoprecipitate (P) fractions were analyzed by immunoblot with the use of an anti-T7–goat or an anti-AU1–rabbit antibody to detect T7-Ssh1p and AU1-Ssh1p. (**B**) (Top) Close-up side views on idle (left) and active (right) PCC (as in Fig. 2, A and B). (Bottom) Homology models of a monomeric Ssh1 complex (red) fitted into the densities of idle and active Ssh1 complexes (transparent mesh). The cytosolic loop L8 of Ssh1p (red), Sbh1p (β, dark red), and Sss1p (γ, magenta) is indicated. The nascent chain (NC) is shown in green. (**C**) Same as (B), but with top views shown.

very similar between the idle and active PCC, suggesting that major structural transitions may not be required for the PCC to switch between these states. The presence of density in the central pore of the PCC bound to the active ribosome suggests that the pore of a single Sec complex is used by the nascent polypeptide chain.

Interaction of the PCC with the ribosome and the nascent chain. In both states, we perceived four main connections that are similar to those observed for the yeast ribosome-Sec61 complex (table S1) (*6*). The main connections (C2 and C4) correspond to the L8 and L6 cytoplasmic loops of the PCC; similar to inactive ribosome-Sec complexes (*16*, *17*), the connections use the universal ribosomal adaptor site (*22*) including mainly the rpL25/rpL35 proteins and rRNA helices H7 and H50 (Fig. 4, A and B). We tested the contribution of the two loops of Ssh1p to the ribosome interaction by performing ribosome-binding assays. Mutational analysis by charge inversion of conserved, positively charged residues such as R411 (*30*) in the L8 loop showed that this loop is necessary for ribosome binding (Fig. 4, C and D). In contrast to findings for SecYEG (*16*), a mutation in loop L6 of the conserved R278 did not result in a loss of ribosome binding, indicating that it may not directly participate in establishing the high-affinity interaction with the ribosome. Similarly in the yeast Sec61 complex, point mutations in L8 lead to severe defects in ribosome binding, whereas mutations of the basic residues in L6 do not substantially reduce ribosome binding affinity (*4*). Two additional connections were (i) C1, established between rRNA helix H59 and, probably, the N terminus of Ssh1p, and (ii) C3, involving rpL26 and rRNA helix H24 and, probably, the C terminus of Ssh1p, including TM10.

The nascent chain was in very close proximity to (and probably contacting) the L6 loop of the Ssh1 complex (Fig. 4B). Thus, loop L6 may

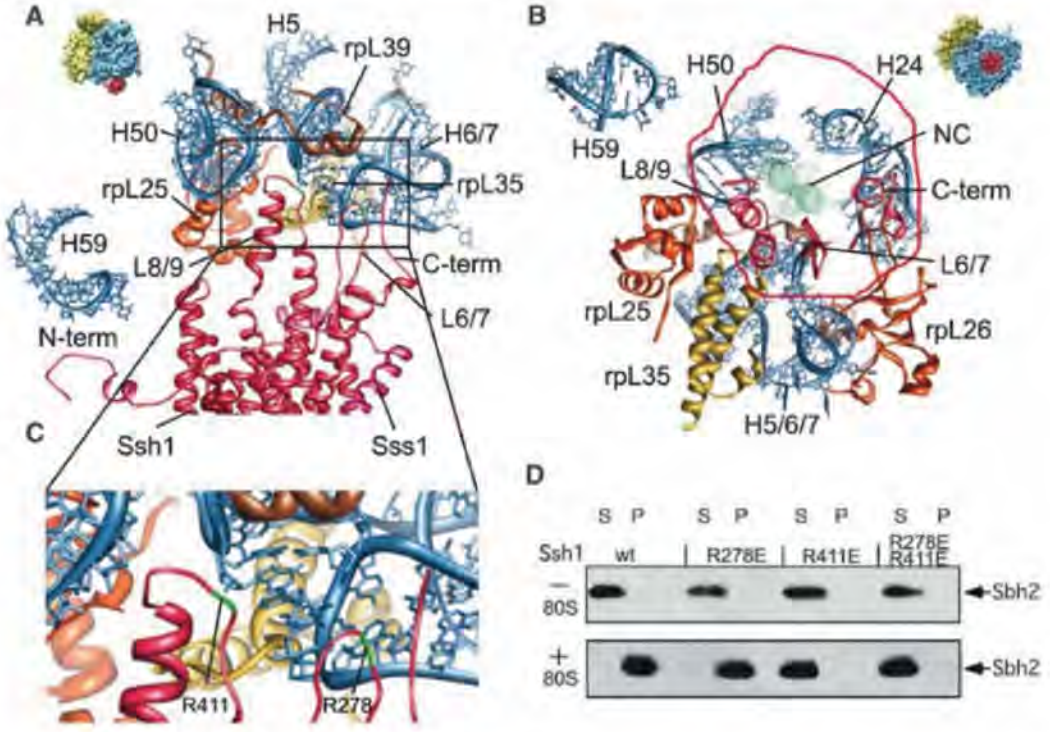

Fig. 4. Interaction of the PCC with the ribosome and the nascent chain. (**A** to **C**) Molecular models for rRNA and ribosomal proteins are shown as in Fig. 2E (and for the Ssh1 complex as in Fig. 3). Views focus on the cytosolic half of the Ssh1 model (A) and the cytosolic loops L6, L8, and the C terminus (B). (C) Close-up on interactions of cytosolic loops L6 and L8. The positions of the conserved R278 and R411 are indicated (green). (**D**) Purified Ssh1 complexes from wild-type and L6 and L8 mutants were incubated in the presence or absence of yeast ribosomes before centrifugation yielding supernatant (S) and pellet (P) fractions. After SDS–polyacrylamide gel electrophoresis, Sbh2p was detected with the use of anti-FLAG antibodies.

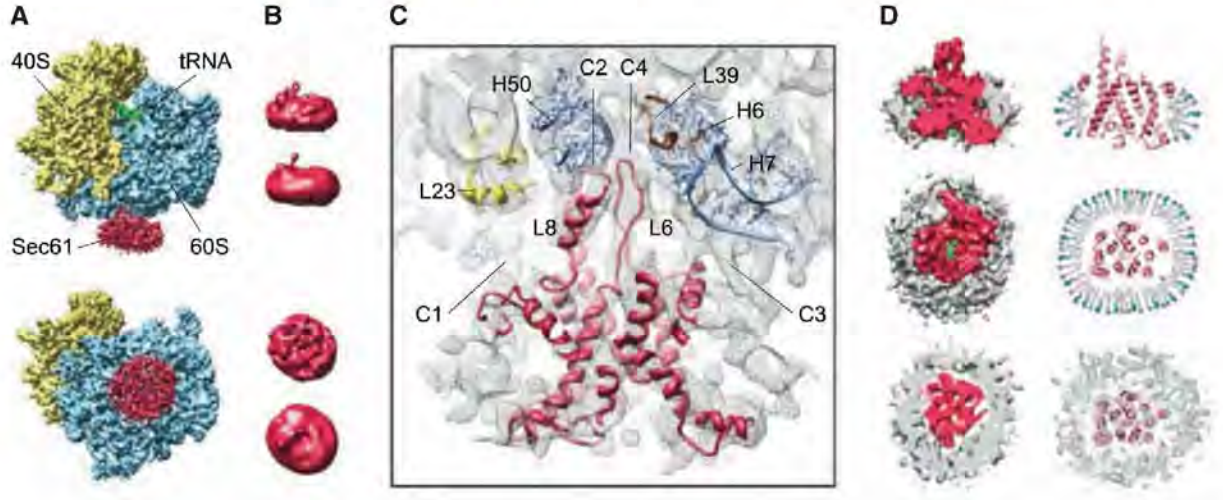

Fig. 5. The RNC-bound mammalian Sec61 complex is a monomer surrounded by a micelle. (**A**) Cryo-EM reconstruction of the 80*S* RNC-Sec61 complex at 6.5 Å resolution. (Top) Side view; (bottom) bottom view. (**B**) Isolated density for the Sec61 complex low-pass filtered at 12 Å (top) and 22 Å (bottom). (**C**) Side view of the ribosome-bound Sec61 complex. The Sec61 model is shown in red; models for ribosomal proteins and rRNA are as shown in Fig. 2D. The monomeric Sec61 complex was fitted into the central portion of the density surrounded by a rim of extra density representing a mixed detergent/lipid micelle. Connections C1 to C4 are indicated. (**D**) (Top left) Side view of the cut densities for the Sec61 complex (red), the surrounding mixed micelle (gray), and the nascent DP120 polypeptide chain and/or the signal-anchor sequence (green). (Right) Schematic drawing of the mixed micelle of phospholipids (gray) and detergent molecules (blue) surrounding the PCC (red ribbons). (Middle) Isolated densities and schematic drawing as shown in the upper section in a top view (left) or sliced within the plane of the membrane (right). (Bottom) Sliced top views, represented as in the middle section (left) or as red ribbons for the Sec61 model and transparent mesh for the electron density (right).

function in sensing or guiding the emerging peptide to the pore of the PCC, consistent with its observed role in translocation (*4*, *31*).

The mammalian Sec61 complex bound to an active ribosome. We determined the structure of the mammalian Sec61 complex from *Canis familiaris* bound to an active DP120 signal anchor containing 80*S* ribosome (*Triticum aestivum*) (*6*, *22*) at 6.5 Å resolution (Fig. 5A). It is considerably larger than that observed for the yeast Ssh1 complex and, when filtered to lower resolution, is very similar to the previously observed densities of mammalian Sec61 (Fig. 5B) (*8*, *17*).

Closer inspection, however, revealed distinct structural features such as central rodlike densities surrounded by two belts of weaker and stronger density, respectively. We calculated a homology model of the Sec61 complex and fitted the helices into the central, rodlike densities requiring only minor adjustments with the use of molecular dynamics flexible fitting (MDFF) (Fig. 5C and fig. S4) (*32*). We observed the same four major connections to the ribosome (Fig. 5C) (*6*), with the two central connections representing the cytoplasmic loops L6 and L8 of the Sec61 complex reaching into the ribosomal tunnel exit via the universal adaptor site (fig. S5 and table S2), similar to the inactive complex (*17*). Compared with the Ssh1 complex, the loops were somewhat rotated without changing the overall position of the Sec complex (fig. S5). Thus, the binding mode appears to be well conserved and is basically the same in inactive and active complexes.

The weak proximal and strong distal beltlike density surrounding the central Sec61 complex did not show any rodlike features and apparently represents a mixed detergent/lipid micelle, as suggested before at lower resolution (*17*). As expected in a micelle, we observed a characteristic density distribution (*33*) of regions containing acyl chains or polar head groups of phospholipids (Fig. 5D and fig. S4). Substantial amounts of the phospholipids phosphatidylcholine and phosphatidylethanolamine copurified with Sec61 in our preparation (fig. S6), confirming the presence of a mixed micelle. It appears likely that previous reconstructions also represent single copies of the Sec61 or the SecYEG complex in micelles of varying sizes when considering the appearance of the micelle-surrounded, single-copy Sec61 complex filtered to lower resolution.

The identification of just one copy of the Sec61 complex indicates that, also in higher eukaryotes, a single complex is stably recruited to the ribosome in the presence of a signal sequence and is probably sufficient to function as the active PCC. This finding is difficult to reconcile with previous interpretations of Sec complex dimers or even larger oligomers bound to the ribosome.

Conformation of the Sec61 complex and interaction with the nascent chain. We compared the conformation of the ribosome-bound Sec61 complex (Fig. 6A) with available crystal structures (*13*, *18*, *34*) to address two questions: (i) How does the Sec61 complex, in particular the proposed lateral gate, behave in the presence of a signal anchor, and (ii) how is the translocating peptide accommodated in the PCC? The ribosome-bound conformation is most similar to the SecYEβ structure of *Methanocaldococcus jannaschii* (Fig. 6B and fig. S7) (*13*). The region of the proposed lateral gate around helices 2b and 7 of Sec61α was well resolved and indicated only a small movement of helix 2b of clearly less than 5 Å when compared to the SecYEβ structure (Fig. 6B). In contrast, the opening movement observed in the SecYEG-SecA crystal structure (*18*) and in the Fab-bound SecYE (*34*) shifted the entire helix more than 5 Å (fig. S7).

We observed density representing the nascent polypeptide in the ribosomal exit tunnel and also in the central aqueous pore of the Sec61 complex (Fig. 6, C and D). This density was well defined in the last section of the ribosomal tunnel in which it is contacting the Sec61 L6 loop, but then it becomes disordered. In the cytoplasmic ves-

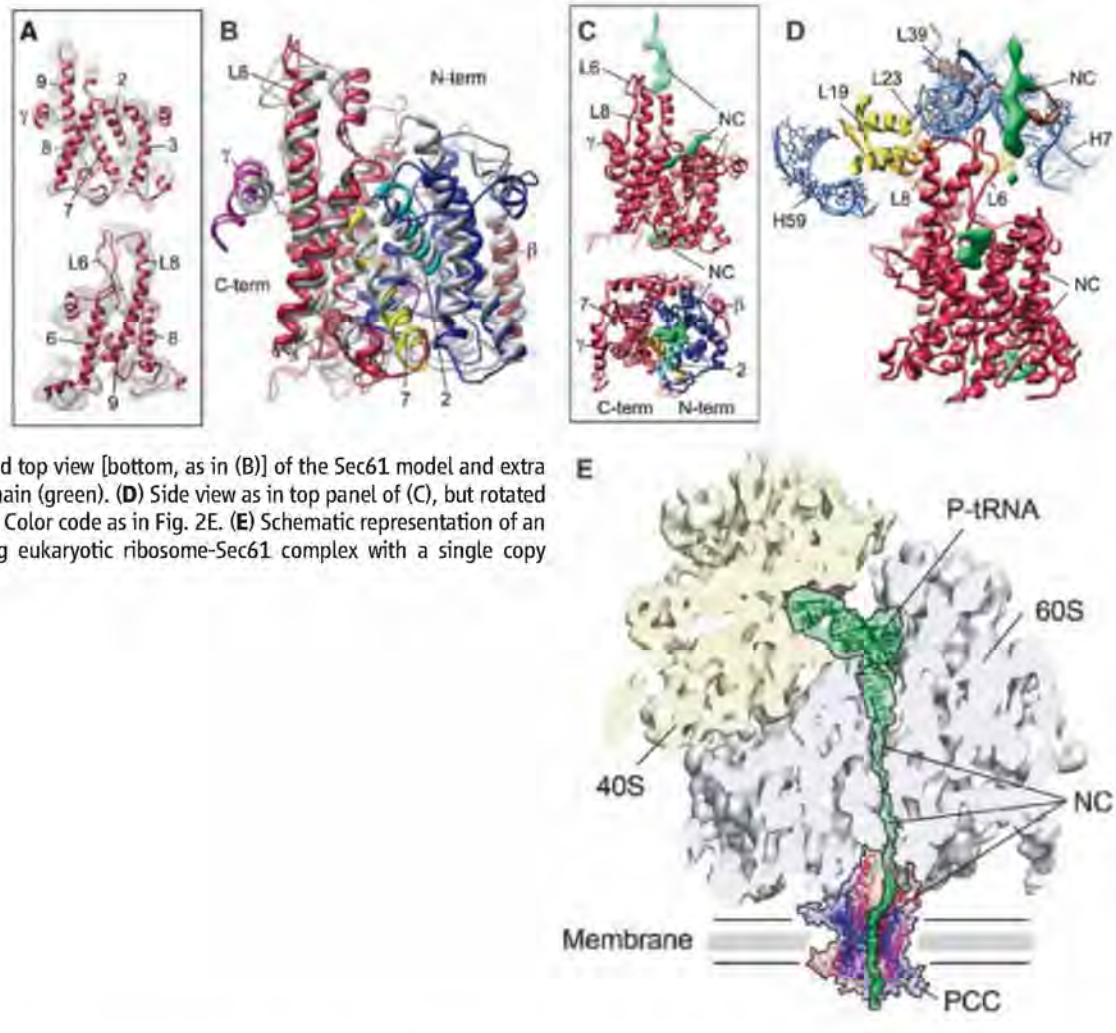

Fig. 6. Conformation and nascent polypeptide chain interactions of the RNC-bound mammalian Sec61 complex. (**A**) Fit of the Sec61 model (red ribbons) into the density (gray transparent mesh). Side views on the lateral gate (top) and cytosolic loops L6 and L8 (bottom). (**B**) Crystal structure of the *M. jannaschii* SecYEβ complex (gray) (*13*) superimposed on an Sec61 model. The C- and N-terminal halves are shown in red and dark blue, transmembrane (TM) helix 7 in yellow, and TM helix 2 in light blue. β (dark red) and γ subunits (SecE, magenta) are indicated. (**C**) Side view [top, as in (A)] and top view [bottom, as in (B)] of the Sec61 model and extra density for the nascent polypeptide chain (green). (**D**) Side view as in top panel of (C), but rotated to focus on the nascent chain (green). Color code as in Fig. 2E. (**E**) Schematic representation of an actively translating and translocating eukaryotic ribosome-Sec61 complex with a single copy acting as PCC.

tibule of the Sec61 complex, we observed a rodlike density contacting the lateral gate helices 2b and 7; in the lumenal vestibule, we found weak and fragmented density. It has been shown previously that in detergent solution the Sec61 complex can productively engage in polypeptide insertion (*6*, *35*, *36*). Hence, for the gating event preceding insertion, we expect that the signal-anchor sequence in our complex is in contact with the PCC. Thus, the rodlike density in the cytoplasmic vestibule (Fig. 6) may resemble the signal-anchor sequence, the position of which would be consistent with previous cross-link data (*37*).

Consequently, the question arises as to what functional state we observe in our complex. One possibility is that the PCC is in the pre-open state, described for the SecYEG-SecA complex (*18*), in which the lateral gate is partially open but the plug is still occluding the central pore. This appears unlikely because the overall conformation, in particular the lateral gate region, is very different (fig. S7C). It appears more likely that we have captured a post-insertion state with a closed or nearly closed lateral gate region. Consistent with this finding, cross-links between helices 2b and 7 revealed a closed lateral gate after insertion of the nascent peptide chain into the SecYEG complex (*38*).

On the basis of our experimental data, several conclusions concerning cotranslational protein translocation can be drawn (Fig. 6E): (i) Only a single copy of the Sec61 complex is recruited to the nontranslating and also the translating ribosome. (ii) In both the yeast Ssh1 complex and the mammalian Sec61 complex, we observed a nascent polypeptide and/or the signal-anchor sequence accommodated within this single-copy PCC, thus strongly indicating that its central pore serves as the conduit for the nascent polypeptide chain. (iii) The lateral gate of the PCC can be in a closed or nearly closed conformation after insertion of the translocating peptide. (iv) The mode of PCC binding to ribosomes appears to be conserved between species and is maintained in the presence or absence of a signal sequence. (v) The main binding site for the PCC is the universal adaptor site at the ribosomal tunnel exit that is contacted mainly by the cytoplasmic loop L8 of the Sec61 complex, whereas loop L6 is also contacting the emerging nascent polypeptide. The observed mode of Sec61 binding fits well with our previous findings that the universal adaptor site also serves to bind SRP (*22*)—mutually exclusive with the PCC—but is then cleared upon SRP receptor interaction to enable PCC binding (*39*).

References and Notes

1. E. C. Mandon, S. F. Trueman, R. Gilmore, *Curr. Opin. Cell Biol.* **21**, 501 (2009).
2. T. A. Rapoport, *Nature* **450**, 663 (2007).
3. M. Halic, R. Beckmann, *Curr. Opin. Struct. Biol.* **15**, 116 (2005).
4. Z. Cheng, Y. Jiang, E. C. Mandon, R. Gilmore, *J. Cell Biol.* **168**, 67 (2005).
5. R. Beckmann *et al.*, *Science* **278**, 2123 (1997).
6. R. Beckmann *et al.*, *Cell* **107**, 361 (2001).
7. C. Breyton, W. Haase, T. A. Rapoport, W. Kühlbrandt, I. Collinson, *Nature* **418**, 662 (2002).
8. J. F. Menetret *et al.*, *J. Mol. Biol.* **348**, 445 (2005).
9. D. Hanein *et al.*, *Cell* **87**, 721 (1996).
10. J.-F. Ménétret *et al.*, *Mol. Cell* **6**, 1219 (2000).
11. D. G. Morgan, J. F. Menetret, A. Neuhof, T. A. Rapoport, C. W. Akey, *J. Mol. Biol.* **324**, 871 (2002).
12. K. Mitra *et al.*, *Nature* **438**, 318 (2005).
13. B. van den Berg *et al.*, *Nature* **427**, 36 (2004).
14. K. S. Cannon, E. Or, W. M. Clemons Jr., Y. Shibata, T. A. Rapoport, *J. Cell Biol.* **169**, 219 (2005).
15. A. R. Osborne, T. A. Rapoport, *Cell* **129**, 97 (2007).
16. J.-F. Menetret *et al.*, *Mol. Cell* **28**, 1083 (2007).
17. J.-F. Menetret *et al.*, *Structure* **16**, 1126 (2008).
18. J. Zimmer, Y. Nam, T. A. Rapoport, *Nature* **455**, 936 (2008).
19. K. Finke *et al.*, *EMBO J.* **15**, 1482 (1996).
20. A. Prinz, E. Hartmann, K. U. Kalies, *Biol. Chem.* **381**, 1025 (2000).
21. S. Wittke, M. Dünnwald, M. Albertsen, N. Johnsson, *Mol. Biol. Cell* **13**, 2223 (2002).
22. M. Halic *et al.*, *Nature* **427**, 808 (2004).
23. D. T. Ng, J. D. Brown, P. Walter, *J. Cell Biol.* **134**, 269 (1996).
24. Materials and methods are available as supporting material on *Science* Online.
25. D. Karaoglu, D. J. Kelleher, R. Gilmore, *Biochemistry* **40**, 12193 (2001).
26. A. R. Osborne, T. A. Rapoport, B. van den Berg, *Annu. Rev. Cell Dev. Biol.* **21**, 529 (2005).
27. T. L. Yahr, W. T. Wickner, *EMBO J.* **19**, 4393 (2000).
28. F. Duong, *EMBO J.* **22**, 4375 (2003).
29. K. U. Kalies, V. Stokes, E. Hartmann, *Biochim. Biophys. Acta* **1783**, 2375 (2008).
30. Single-letter abbreviations for the amino acid residues are as follows: A, Ala; C, Cys; D, Asp; E, Glu; F, Phe; G, Gly; H, His; I, Ile; K, Lys; L, Leu; M, Met; N, Asn; P, Pro; Q, Gln; R, Arg; S, Ser; T, Thr; V, Val; W, Trp; and Y, Tyr.
31. D. Raden, W. Song, R. Gilmore, *J. Cell Biol.* **150**, 53 (2000).
32. L. G. Trabuco, E. Villa, K. Mitra, J. Frank, K. Schulten, *Structure* **16**, 673 (2008).
33. M. le Maire, P. Champeil, J. V. Moller, *Biochim. Biophys. Acta* **1508**, 86 (2000).
34. T. Tsukazaki *et al.*, *Nature* **455**, 988 (2008).
35. B. Jungnickel, T. A. Rapoport, *Cell* **82**, 261 (1995).
36. W. Mothes, B. Jungnickel, J. Brunner, T. Rapoport, *J. Cell Biol.* **142**, 355 (1998).
37. K. Plath, B. M. Wilkinson, C. J. Stirling, T. A. Rapoport, *Mol. Biol. Cell* **15**, 1 (2003).
38. D. J. du Plessis, G. Berrelkamp, N. Nouwen, A. J. Driessen, *J. Biol. Chem.* **284**, 15805 (2009).
39. M. Halic *et al.*, *Science* **312**, 745 (2006).

40. We thank B. Dobberstein (Zentrum für Molekulare Biologie der Universität Heidelberg, Heidelberg, Germany) for microsomal membranes, B. Brügger (Biochemie-Zentrum der Universität Heidelberg, Heidelberg, Germany) for lipid analysis, and J. Frauenfeld and E. van der Sluis for critical discussions. This research was supported by Deutsche Forschungsgemeinschaft grants SFB594, SFB646 (to R.B. and T.B.), and SFB 740 (to T.M.); Knut and Alice Wallenberg Foundation, Stockholm, Sweden (to S.B.); NIH grants P41-RR05969, R01-GM067887 (to K.S.), and GM35687 (to R.G.); NSF grant PHY0822613 (to K.S.); and the European Union and Senatsverwaltung für Wissenschaft, Forschung und Kultur Berlin (UltraStructureNetwork, Anwenderzentrum). Computer time for MDFF was provided through an NSF Large Resources Allocation Committee grant (MCA93S028). Coordinates of the atomic models and cryo-EM maps have been deposited in the PDB [with accession numbers 2ww9 (active Ssh), 2wwa (inactive Ssh), and 2wwb (mammalian translocon)] and in the 3D-EM database [EMD-1651 (yeast) and EMD-1652 (Mammalia)], respectively.

Supporting Online Material

www.sciencemag.org/cgi/content/full/1178535/DC1
Materials and Methods
Figs. S1 to S7
Tables S1 and S2
References

1 July 2009; accepted 21 October 2009
Published online 29 October 2009;
10.1126/science.1178535
Include this information when citing this paper.

Structural Mechanism of Abscisic Acid Binding and Signaling by Dimeric PYR1

Noriyuki Nishimura,[1]* Kenichi Hitomi,[2,3]* Andrew S. Arvai,[2]* Robert P. Rambo,[3]* Chiharu Hitomi,[2] Sean R. Cutler,[4] Julian I. Schroeder,[1] Elizabeth D. Getzoff[2]†

The phytohormone abscisic acid (ABA) acts in seed dormancy, plant development, drought tolerance, and adaptive responses to environmental stresses. Structural mechanisms mediating ABA receptor recognition and signaling remain unknown but are essential for understanding and manipulating abiotic stress resistance. Here, we report structures of pyrabactin resistance 1 (PYR1), a prototypical PYR/PYR1-like (PYL)/regulatory component of ABA receptor (RCAR) protein that functions in early ABA signaling. The crystallographic structure reveals an α/β helix–grip fold and homodimeric assembly, verified in vivo by coimmunoprecipitation. ABA binding within a large internal cavity switches structural motifs distinguishing ABA-free "open-lid" from ABA-bound "closed-lid" conformations. Small-angle x-ray scattering suggests that ABA signals by converting PYR1 to a more compact, symmetric closed-lid dimer. Site-directed PYR1 mutants designed to disrupt hormone binding lose ABA-triggered interactions with type 2C protein phosphatase partners in planta.

The phytohormone abscisic acid (ABA) plays key regulatory roles in physiological pathways for plant growth and development and enables adaptation to abiotic stresses. In the half century since ABA's discovery (*1*, *2*), much has been learned about its downstream signaling network (*3*, *4*), yet protein recognition mechanisms for this hormone have remained enigmatic. Recently, a cluster of homologous genes that activate ABA signaling was identified in *Arabidopsis thaliana* by groups using different methods: (i) yeast two-hybrid screen-

ing, (ii) chemical genetics, and (iii) coimmunoprecipitation analyses (*5*, *6*). In the presence of ABA, the gene products, designated pyrabactin resistance 1 (PYR1) and PYR1-like (PYL), or regulatory components of ABA receptor (RCAR) down-regulate their binding partners, cluster A type 2C protein phosphatase (PP2C) family members (*7*, *8*). These phosphatases, including ABI1, ABI2, PP2CA, HAB1, and HAB2, are negative regulators of early ABA signaling (*9*–*18*). In addition, OST1/SnRK2.6/SnRK2E SNF1-related protein kinases 2 (SnRK2s) are important mediators of ABA signal transduction (*19*–*22*). PYR/PYL/RCAR family members exhibit functional redundancy in ABA perception, and variations in ABA regulation of their binding to PP2C family members (*5*, *6*). Contrasting hypotheses suggest that ABA either binds to PYR/PYL/RCAR proteins directly or forms a molecular "glue" between these proteins and PP2Cs (*5*, *6*, *23*), similar to auxin's role in joining transport inhibitor response 1 (TIR1)–related and AUX/IAA signaling proteins (*24*). Distinct but overlapping functions of different PYR/PYL/RCAR proteins complicate genetic analysis and mechanistic testing in plants but may enhance flexible regulation of ABA signaling to maximize environmental adaptability of plants.

Plant hormone receptors have evolved from diverse protein families (*25*) and operate by distinct protein-hormone and protein-protein binding interactions. Understanding the mechanism of action of ABA receptor(s) has been controversial and challenging, partly attributable to the absence of a structure for an ABA-bound protein complex. Recent structural studies of hormone-bound auxin and gibberellin receptors identified binding sites, characterized protein assemblies,

[1]Division of Biological Sciences, Cell and Developmental Biology Section, University of California at San Diego, La Jolla, CA 92093, USA. [2]Department of Molecular Biology and The Skaggs Institute for Chemical Biology, The Scripps Research Institute, La Jolla, CA 92037, USA. [3]Life Sciences Division, Lawrence Berkeley National Laboratory, Berkeley, CA 94720, USA. [4]Department of Botany and Plant Sciences, Center for Plant Cell Biology, University of California at Riverside, Riverside, CA 92521, USA.

*These authors contributed equally to this work.
†To whom correspondence should be addressed. E-mail: edg@scripps.edu

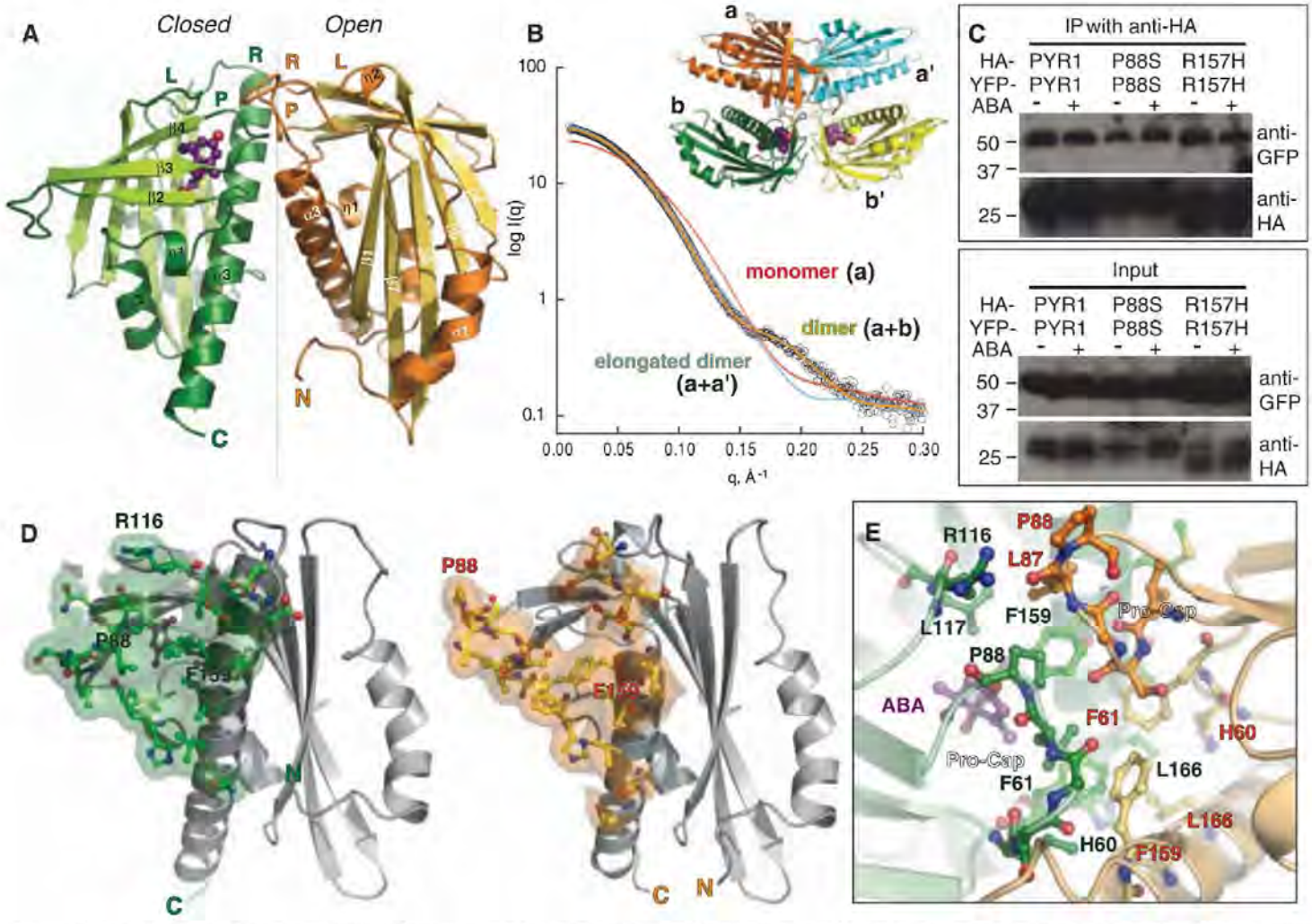

Fig. 1. Dimeric structure of ABA sensor PYR1. (**A**) Crystallographic asymmetric dimer shown as ribbons (labeled β strands and helices) with ABA (purple ball-and-stick model with red oxygen atoms) bound beneath the closed lid of one subunit (left), in a large cavity between the β sheet and long C-terminal α helix. Labeled Pro-Cap (P), Leu-Lock (L), and Recoil (R) structural motifs undergo ABA-induced conformational changes. Vertical line (center) indicates pseudo twofold axis relating the subunits. (**B**) Theoretical SAXS curve (orange line) for asymmetric crystallographic dimer (a+b in inset) matches experimental SAXS data for PYR1 without ABA (open circles), whereas curves calculated assuming a monomer (red) or elongated a+a′ dimer (blue) from crystal lattice (see inset) do not. Curves show the scattering intensity I(q) as a function of the scattering angle 2θ and x-ray wavelength λ, where $q = (4\pi\sin\theta/\lambda)$. (**C**) Coimmunoprecipitation from extracts of plant leaves expressing YFP-tagged PYR1 and HA-tagged PYR1 without (–) and with (+) exogenously applied ABA confirm dimeric PYR1 assembly. After coimmunoprecipitation with an anti-HA matrix, immunoprecipitated (top) and input (bottom) samples were detected with anti–green fluorescent protein (GFP) and anti-HA antibodies. PYR1 wild-type and mutants P88S and R157H are homodimeric in planta, as shown by anti-GFP antibody labeling of YFP-tagged PYR1 coimmunoprecipitated with HA-tagged PYR1. (**D**) Residues and buried surface area contributed to dimer interface by closed-lid (left) and open-lid (right) subunit conformations in asymmetric dimer (*37*). (**E**) PYR1 dimer interface viewed looking down from top in (A) at the interacting lids: open (orange) and closed (green) over ABA (purple). Dimer contacts include the interacting Pro-Cap structural motifs (foreground), plus a side chain–to–main chain hydrogen bond from Arg^{116} in the ABA-bound subunit (top left) to Leu^{87} in the ABA-free subunit.

and enabled major advances in understanding hormone signaling in plants (*24*, *26*, *27*). Here, we report the ABA recognition mechanism by the PYR1 dimer assembly, as revealed by ABA-bound and unbound crystallographic structures and small-angle x-ray scattering (SAXS) in solution, coupled with analysis of structure-based, site-directed mutants by coimmunoprecipitation analyses in vivo. Our results show that ABA binds directly to PYR1 within a large internal, water-filled cavity, rather than acting as a molecular glue at an interface with PP2Cs. The PYR1 structure reveals how both (+)-ABA and (−)-ABA enantiomers can show biological activity. We define the unusual asymmetric homodimeric assembly of PYR1 that allows hormone access and sequestration, discover structural motifs (Pro-Cap, Leu-Lock, and Recoil) that mediate "open-" and "closed-lid" conformations, and deduce a probable mechanism for ABA signal transduction via hormone-induced conformational changes that promote binding of PP2C partners.

PYR1 architecture and dimeric assembly. To understand ABA binding and signaling, we crystallized and determined structures (*28*) of *A. thaliana* PYR1 with the phytohormone (+)-*cis*,*trans* abscisic acid [(S-ABA) fig. S1]. Extensive screening produced crystals in space group P2, but only with ABA. Crystallization trials without hormone were unsuccessful, suggesting conformational flexibility. Initial crystals were obtained with enantiomorphic (+/−)-ABA at pH 5.8, the approximate isoelectric point for both protein and hormone. Diffraction quality crystals were reproducible with (+)-ABA alone, at pH values ranging from 5.4 to 6.8, but were always ABA-dependent. Molecular replacement was accomplished with a probe structure from the pathogenesis-related protein Bet vI (Pfam: PF00407) (*29*) family.

The PYR1 structure, determined to 1.7 Å resolution (Fig. 1A, table S1, and movie S1) is a seven-stranded anti-parallel β sheet wrapped around a long C-terminal α helix. This α/β helix–grip fold is shared by plant pollen allergen Bet vI and mammalian steroidogenic acute regulatory lipid transfer (START) proteins (*30*–*32*). The variable N terminus (fig. S2) forms PYR1 helix α1 arching back over the β sheet (Fig. 1A). β1 is hydrogen bonded with β7, but is covalently linked by helices across the β sheet to β2. In contrast, intervening β strands exhibit nearest-neighbor (+1) connectivity. β7 is connected via a projecting loop to C-terminal α3.

In the crystallographic asymmetric unit, PYR1 assembles into a homodimer of one ABA-bound (Fig. 1A, left) and one ABA-free subunit (Fig. 1A, right), related by an ~170° rotation around a pseudo twofold axis. Roughly perpendicular interactions of α3 helices align the β sheets in parallel (Fig. 1A). To determine whether PYR1 (monomer Mr = 20 kD) forms this dimer in solution, we used multiangle laser light scattering (MALS) and SAXS (*33*, *34*). MALS allowed simultaneous measurements of absolute molecular weight and hydrodynamic radius. In the absence of ABA, PYR1 forms a homodimer in solution (Mr = 40.8 ± 0.4 to 40.9 ± 0.3 kD) under varying pH (5.4 to 7.6) and salt conditions (20 mM NaCl and 20 to 100 mM KCl), including those approximating physiological intracellular levels (100 mM K^+, pH 7.6). Thus, ABA is not required for PYR1-PYR1 homodimer formation. SAXS measurements showed that the PYR1 dimer in solution matched the dimer assembly in the crystallographic asymmetric unit, rather than alternative monomeric, dimeric, or tetrameric packing assemblies within the crystal lattice (Fig. 1B and fig. S3). The maximum intramolecular distance (D_{max} = 68 Å) determined from the SAXS-derived pair-distance distribution function also matched that measured from the crystallographic structure (69.8 Å).

To determine whether PYR1 is homodimeric in planta, we performed *Agrobacterium*-mediated infiltration of *Nicotiana benthamiana* leaves with both yellow fluorescent protein (YFP)– and hemagglutinin (HA)–tagged PYR1, followed by coimmunoprecipitation analyses. PYR1 constitutively formed a dimer in vivo, both in the presence and absence of exogenously applied ABA (Fig. 1C). Thus, the dimer observed in the crystallographic asymmetric unit is evidently a biological unit for PYR1.

In this asymmetric dimer, the interface lies between the crossed α3 helices (Fig. 1A). The roughly triangular surfaces shielded in each subunit are similar but not identical (Fig. 1D). The core of the dimer interface is centered on the asymmetric hydrophobic packing interactions of Phe^{61} and Phe^{159} from both subunits (Fig. 1, D and E), but the dimer packing specificity may depend on interactions (Fig. 1E) of clustered structural motifs that undergo ABA-induced conformational changes (Fig. 1A).

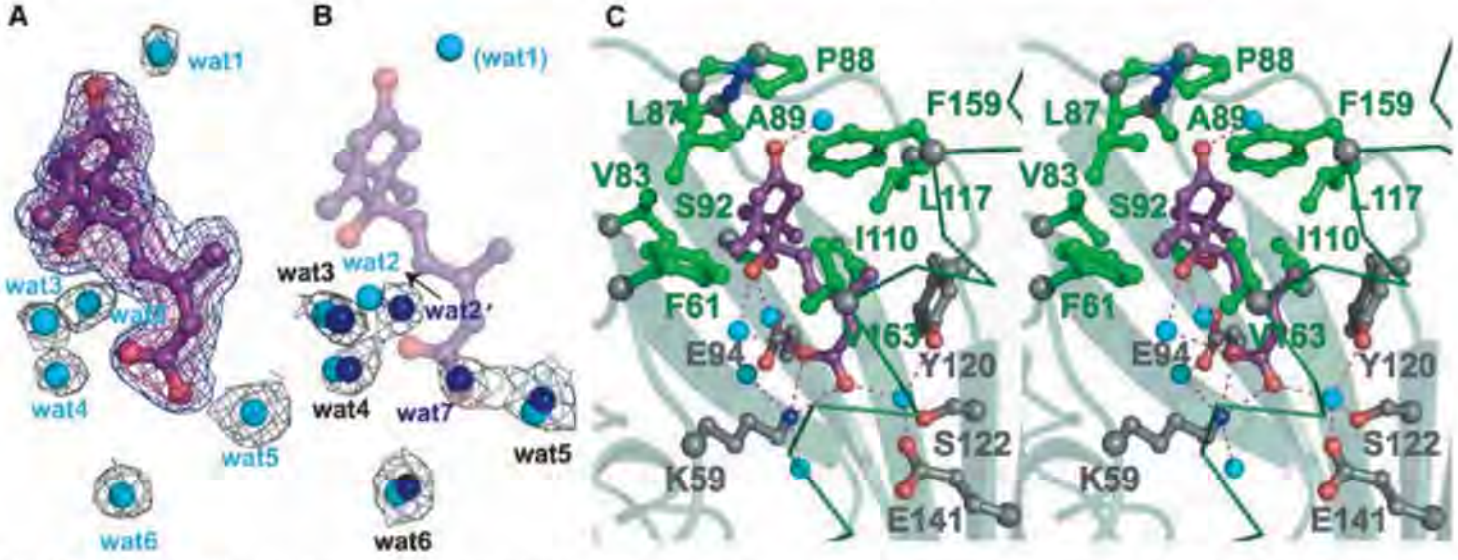

Fig. 2. Water-filled ABA-binding cavity. (**A**) ABA (purple ball-and-stick model, with red oxygen atoms) and adjacent, ordered water molecules (light blue spheres) inside the PYR1 cavity, shown with electron density (mesh). Omit Fo-Fc density for ABA contoured at 3σ (dark blue) and 4σ (magenta); 2Fo-Fc electron density for water molecules contoured at 1σ (black). All maps were calculated after "shaking" coordinates to reduce phase bias. (**B**) Ordered water molecules (dark blue spheres) within the ABA-free subunit cavity, shown with associated 2Fo-Fc electron density, as in (A). ABA (purple) and water molecules (light blue) from the ABA-bound PYR1 subunit [shown in (A)] are superimposed showing conserved water positions. ABA displaces one water molecule (wat7) with the carboxylate, shifts a second (wat2′ to wat2, as shown by arrow), and introduces or stabilizes a third (wat1), which interacts with the ABA carbonyl to stabilize lid closure. (**C**) Stereo view of PYR1 residues contributing to the ABA binding site. Hydrophobic side chains (green ball-and-stick model) surround the ABA ring, whereas hydrogen-bonded (red dashed lines) internal water molecules (light blue spheres) link ABA oxygen atoms (red) to PYR1 hydrophilic side chains (gray ball-and-stick model with red oxygen and blue nitrogen atoms) projecting into the binding cavity. Larger gray spheres show Cα atoms. Lys^{59}, Phe^{61}, Arg^{79}, Val^{83}, Leu^{87}, Pro^{88}, Ala^{89}, Ser^{92}, Glu^{94}, Ile^{110}, Leu^{117}, Tyr^{120}, Ser^{122}, Glu^{141}, Phe^{159}, Val^{163}, and Asn^{167} contribute to forming this large internal cavity.

Abscisic acid binding site inside PYR1. Naturally occurring phytohormone (+)-*cis*,*trans*-ABA, (2Z,4E)-5-[(1S)-1-hydroxy-2,6,6-trimethyl-4-oxocyclohex-2-en-1-yl]-3-methylpenta-2,4-dienoic acid (fig. S1), binds within a large interior cavity of PYR1 between the twisted β sheet and long α3 helix (Fig. 1A). The electron density shows (+)-ABA bound in only one subunit of each PYR1 dimer (Fig. 2, A and B). Hence, the crystal structure resolves both ABA-bound and unbound forms of PYR1. ABA is tethered at both ends by hydrogen bonds to the protein (Fig. 2C). The planar, conjugated, 3-methylpenta-2-*cis*,4-*trans*-dienoic acid tail of ABA extends ~10 Å into a large protein cavity, where the terminal carboxylate is anchored by the inward-pointing Lys^{59} side chain. At the cavity entrance, the ABA carbonyl group links two protein loops via hydrogen bonds with main-chain nitrogen atoms of Ala^{89} and, through a water molecule, Arg^{116}. The adjacent Pro^{88} ring caps the ABA carbonyl to form a lid of the ABA-binding cavity (Fig. 2C); Leu^{87} from the ABA-free subunit reaches across the PYR1 dimer to block the remaining cavity access (Fig. 1E). Thus, PYR1 dimer formation contributes to ABA sequestration.

To biologically test the observed protein-hormone interactions, we made site-directed mutants of PYR1 (fig. S4) designed to weaken ABA binding. To examine their consequences on ABA signaling, these PYR1 mutants were transiently expressed in tobacco leaves, and we analyzed them for function by coimmunoprecipitation assays that detect ABA-triggered interactions between PYR1 and the ABI1 protein phosphatase (Fig. 3). The $Lys^{59} \rightarrow Gln^{59}$ (K59Q) PYR1 mutation, designed to neutralize the counter-ion to the ABA carboxylate (Figs. 2C and 3A), disrupted exogenous ABA-induced PYR1 binding to ABI1 (Fig. 3B). Thirteen of 14 ABA sensor family members conserve Lys^{59}, whereas PYL13 has Gln (fig. S2). Invariant Arg^{116}, which contributes to both ABA binding and the dimer interface (Fig. 1E), was mutated to Gly. The $Arg^{116} \rightarrow Gly^{116}$ (R116G) PYR1 mutation also abolished ABA-induced PYR1 binding to ABI1 (Fig. 3B). These mutational results support the biological relevance of the ABA-binding cavity and dimer interface characterized by our crystal structures.

In PYR1, the ABA ring is surrounded by hydrophobic side chains and sequestered from solution (Fig. 2C). This hydrophobic enclosure can accommodate (+)- or (–)-ABA (fig. S1), as shown by our initial 1.8 Å resolution structure determined with mixed enantiomorphic (+/–)-ABA (fig. S5). Within the PYR1 cavity, (–)-ABA maintains the tethering hydrogen bonds and tail position of (+)-ABA. To accommodate the changed chirality, the (–)-ABA ring is flipped ~180° from the (+)-ABA ring (fig. S5), swapping the ring pucker and axial methyl substituent to the opposite side of the cavity. The ring-flipped binding of (–)-ABA provides a structural basis for its varying bioactivity (*35*) in different PYR/PYL/RCAR proteins (*6*). The ABA hydroxyl group, located on the central chiral carbon (figs. S1 and S3), has no protein hydrogen-bonding partner. Instead, two water molecules bridge the ABA hydroxyl and proximal carboxylate with hydrogen bonds (Fig. 2). Another water molecule links the distal ABA carboxylate oxygen to invariant Tyr^{120}, Ser^{122}, and Glu^{141} (Fig. 2C). This complex water-bridged hydrogen-bonding network also interconnects ABA through Glu^{94} to Ser^{92} and Arg^{79} and through Glu^{141} to Asn^{167}. Chemically induced *Arabidopsis* mutants identified by ABA signaling deficiencies (*6*) include PYR1 mutants with inward-facing Glu^{94} and Glu^{141} mutated to Lys (Fig. 3A). The ABA tail is sandwiched between Ile^{110} and Val^{163} (Fig. 2C), and the large internal PYR1 cavity extends beyond this tail. Thus, most structural elements of PYR1 (fig. S2) contribute to ABA-binding cavity formation: helix α3, strands β3 to β7, and loops preceding β2 and joining β3 to β4 and β5 to β6 (Fig. 1A). This architectural design creates the ABA-binding cavity, hydrogen-bonding network, and conserved ordered waters in the absence of ABA, as seen in the ABA-free subunit of the PYR1 dimer (Fig. 2B).

ABA-induced subunit conformational changes. Superposition of ABA-bound and free subunits of the PYR1 dimer (Fig. 4A) revealed substantial conformational differences in three loop motifs. Upon ABA binding, proline cap ("Pro-Cap," Val^{83}-Asn^{90}) and leucine lock ("Leu-Lock," Glu^{114}-Thr^{118}) motifs fold over ABA to close the lid on the cavity (Fig. 4B), and the "Recoil" motif (Met^{147}-Phe^{159}) coils into helix α3, allowing lid closure (Fig. 4). Between open- and closed-lid conformations, Pro^{88} cis-to-trans isomerization switches the direction in which flanking Leu^{87} and Ala^{89} side chains project (Fig. 4B). A hinge motion of the entire Pro-Cap, pivoting at Ile^{84} and Asn^{90}, directs Leu^{87}, Pro^{88}, and Ala^{89} to close over ABA (Fig. 4B). The closed and open Pro-Caps of the two PYR1 subunits directly interact, contributing substantially to the asymmetric dimer interface (Fig. 1, D and E). This interaction suggests why substitution of Pro^{88} with smaller Ser in the $Pro^{88} \rightarrow Ser^{88}$ (P88S) mutant (Fig. 3A) reduces ABA-induced PYR1 interactions with PP2Cs (*6*).

Similar to the Pro-Cap, the Leu-Lock motif between Glu^{114} and Thr^{118} also undergoes a hinge motion, allowing Leu^{117} to swing inward to lock against the ABA ring (Fig. 4B). When Leu^{117} is locked in, the Arg^{116} side chain projects outward across the dimer interface (Fig. 1, D and E), and the His^{115} ring flips to block solvent access to the methyl substituents of ABA ring carbon C6′ (fig. S1). In the Recoil motif, Arg^{157} interacts with Asp^{155}, capping the N-terminal end of helix α3 in the ABA-free conformation, whereas this helix is N-terminally extended in the ABA-binding form, and Arg^{157} interacts with Glu^{153} or Asp^{161} (Fig. 4B). The $Ser^{152} \rightarrow Leu^{152}$ (S152L) mutant of PYR1 (Fig. 3B), like the P88S mutant, reduces ABA-induced PYR1 interactions with PP2C (*6*). Some PYR/PYL homologs have Cys at the Arg^{157} position of PYR1 (fig. S2), presumably contributing to structural modulation differently, perhaps by disulfide bond formation with nearby Cys^{30}. Conformational changes in the Pro-Cap, Leu-Lock, and Recoil motifs appear concerted (Fig. 4B):

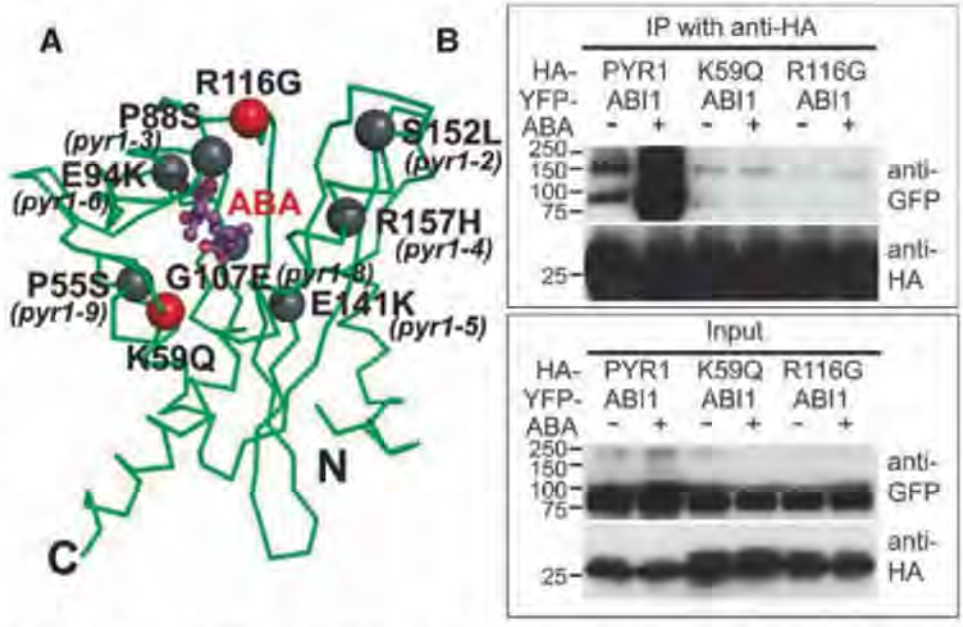

Fig. 3. Disruption of PYR1-ABI1 interactions by single-site PYR1 mutations. **(A)** PYR1 mutants designed from the structure (red) and identified after chemical mutagenesis and screening (gray) (*6*) are mapped to the PYR1 subunit structure (green Cα trace). **(B)** Coimmunoprecipitation from extracts of plant leaves expressing YFP-tagged ABI1 phosphatase with HA-tagged wild-type and mutant PYR1 proteins in planta, both in the absence (–) and presence (+) of exogenously applied ABA. After coimmunoprecipitation by an anti-HA matrix, immunoprecipitated (top) and input (bottom) samples were detected with anti-GFP and anti-HA antibodies (labeled at right). Structure-based PYR1 mutants designed to disrupt ABA binding (K59Q and R116G) folded properly (fig. S5) but lost ABA-induced interactions with ABI1 phosphatase.

Pivoting of invariant Phe[159] of α3 to pack against ABA probably triggers the Recoil motif to coil back into helix α3, thus allowing lid closure by the Pro-Cap and Leu-Lock motifs (movie S2). Hence, direct interactions of ABA with Phe[159], Leu[117], and Leu[87] (Fig. 4B) coordinate interactions of the Recoil, Leu-Lock, and Pro-Cap motifs to complete ABA enclosure.

ABA-induced conformational changes in dimer assembly. ABA-induced conformational changes, monitored by SAXS, render the PYR1 dimer more compact, flatter, and less irregular (Fig. 5). The crystallographic asymmetric dimer, containing one ABA-bound and one ABA-free subunit, produces an excellent fit to PYR1 SAXS curves (Fig. 1B), particularly for data collected in the absence of ABA (χ^2 = 1.2). When excess ABA was added (~four ABA molecules per protein subunit) to the PYR1 dimer in solution, the Guinier radius of gyration decreased (23.71 ± 0.04 to 22.72 ± 0.07 Å), and the pair-distance distribution function describing intramolecular distances became narrower and shifted to shorter distances (Fig. 5A), although the maximum intramolecular distance (D_{max} = 68 Å) remained constant. SAXS data collected in the presence of ABA were not fit as well (χ^2 = 3.3 to 3.4) by the crystallographic dimer or a dimer modeled with two ABA-bound subunits.

Ab initio bead models, derived from solution SAXS experiments for PYR1 in the absence of ABA, are asymmetric and match the crystallographically determined dimer (Fig. 5, B to E). In contrast, ab initio models from SAXS experiments for PYR1 with excess ABA are flatter and more compact (Fig. 5, B and C), consistent with a structural model consisting of two ABA-bound PYR1 subunits related by exact twofold symmetry (Fig. 5, D and F). These shapes depict a flattened biconcave disk resembling a red blood cell (Fig. 5, B and F). The twofold symmetry axis and perpendicular direction traversing both subunits of the dimer form ~60 Å disk diameters, whereas the cross-strand width of the β sheet roughly aligns with the ~30 Å disk thickness. In contrast, the ab initio shapes and crystallographic model representing the PYR1 dimer in the absence of ABA depict a more irregular biconcave disk (Fig. 5, B to E), resulting from asymmetric interactions between open- and closed-lid subunit conformations (Fig. 1E and movie S2) and their ~10° deviation from twofold (180°) symmetry (Fig. 5D).

Implications for ABA perception and signaling. The crystal structure, solution SAXS assemblies, and coimmunoprecipitation in vivo provide key insights into molecular and structural mechanisms mediating hormone recognition and signaling by the ABA sensor PYR1. ABA binding inside an occluded protein cavity shows PYR1 to be a direct ABA receptor and signal transduction partner, like the gibberellin receptor GID1 (*26*, *27*), rather than one of two hormone-linked co-receptors, like auxin-linked TIR1 and AUX/IAA (*24*).

The PYR1 dimer crystal structure is unexpectedly asymmetric, revealing structures of both unbound, open-lid and ABA-bound, closed-lid subunit conformations (Fig. 1A). SAXS analyses of PYR1 without ABA confirm an asymmetric dimer in solution (Fig. 1B). At the crystallographic asymmetric dimer interface, the open and closed Pro-Caps pack tightly with each other (Fig. 1E). This arrangement provides open access for ABA and possible allosteric interchange of open- and closed-lid subunits upon hormone binding (movies S1 and S2). Coimmunoprecipitation assays confirm homodimeric PYR1-PYR1 assembly in vivo, both with and without exogenous ABA (Fig. 1C). In solution, SAXS analyses indicate that saturating ABA converts PYR1 into a flatter, more compact dimer, reflecting an orientation change between subunits (Fig. 5). Together, our data support ABA-induced conformational changes producing a twofold symmetric closed-lid dimer. Consistent with these results, two-dimensional nuclear magnetic resonance spectra show a single PYR1 conformer

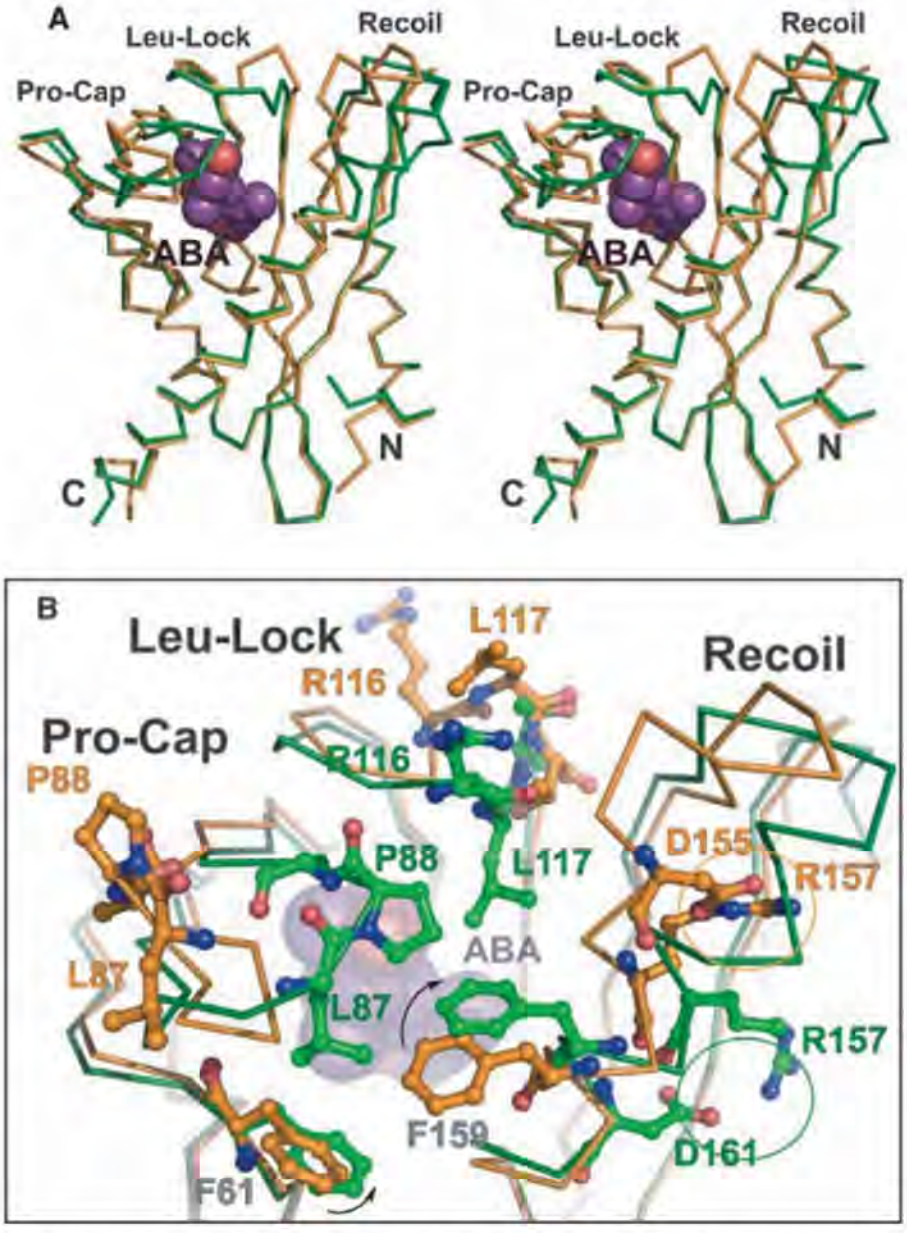

Fig. 4. ABA-induced subunit conformational changes. (**A**) Stereo image showing superposition of ABA-free (orange) and ABA-bound (green) PYR1 Cα traces. ABA-induced helix coiling by the Recoil motif (top right) is coupled to lid closure over ABA (purple with red oxygen atoms) by the Pro-Cap and Leu-Lock structural motifs (top left). (**B**) Enlarged view of ABA-triggered conformational changes in these three structural motifs that close the lid over bound ABA, colored as in (A). ABA (beneath center) triggers rotation of Phe[159] (arrow) to coil the Recoil motif into helix α3 (diagonal at right), switching the Arg[157] charge-charge interaction (circled) to a new partner within (rather than outside) this helix. Pro[88] isomerization from cis (orange, far left) to trans (green, center) converts the open-lid Pro-Cap to the closed-lid conformation, clamping Leu[87], Pro[88], and Ala[89] over ABA. Leu[117] (orange, top center) locks down (green, center) against ABA, closing the Leu-Lock and flipping the preceding Arg[116] side chain (orange, top center) toward the opposing subunit (forward and slightly to the right in this view) across the dimer interface (see also Fig. 1E).

with saturating ABA, but also show multiple conformers without ABA (*6*).

ABA-induced conformational differences in PYR1 subunit structure (Fig. 4) and dimer assembly (Fig. 5) point to a structural mechanism for PYR/PYL/RCAR protein-mediated ABA signal transduction to downstream proteins. The molecular surface of the PYR1 dimer exposes several likely interfaces for ABA-dependent assembly of signalosome complexes with PP2Cs (*5*, *6*, *36*) or other potential partners (Fig. 6). Major ABA-induced subunit conformational changes cluster (Fig. 4) around the interacting lids at the "top" of the asymmetric PYR1 dimer (Figs. 1, A and E, and 6A). Therefore, ABA-induced binding of PP2Cs may occur at interfaces overlapping the closed lids of PYR1. PP2C binding would then favor PYR1 lid closure and decrease the ABA off rate, thus explaining observations that ABA binds more tightly to RCAR1 and PYL5 in the presence of PP2Cs (*5*, *23*). Surfaces of the PYR1 dimer altered by ABA-induced subunit reorientation (Fig. 5D) also provide promising interfaces for signaling to protein partners (Fig. 6).

The phytohormone ABA mediates resistance to abiotic stresses, including drought, salinity, and cold (*3*, *4*). The characterized PYR1 motifs and dimer conformations are key to understanding and future chemical manipulation of phytohormone-induced abiotic stress–resistance responses. The crystallographic structure shows that PYR1 is a direct ABA receptor and sensor, signaling hormone binding within an internal cavity through conformational changes affecting

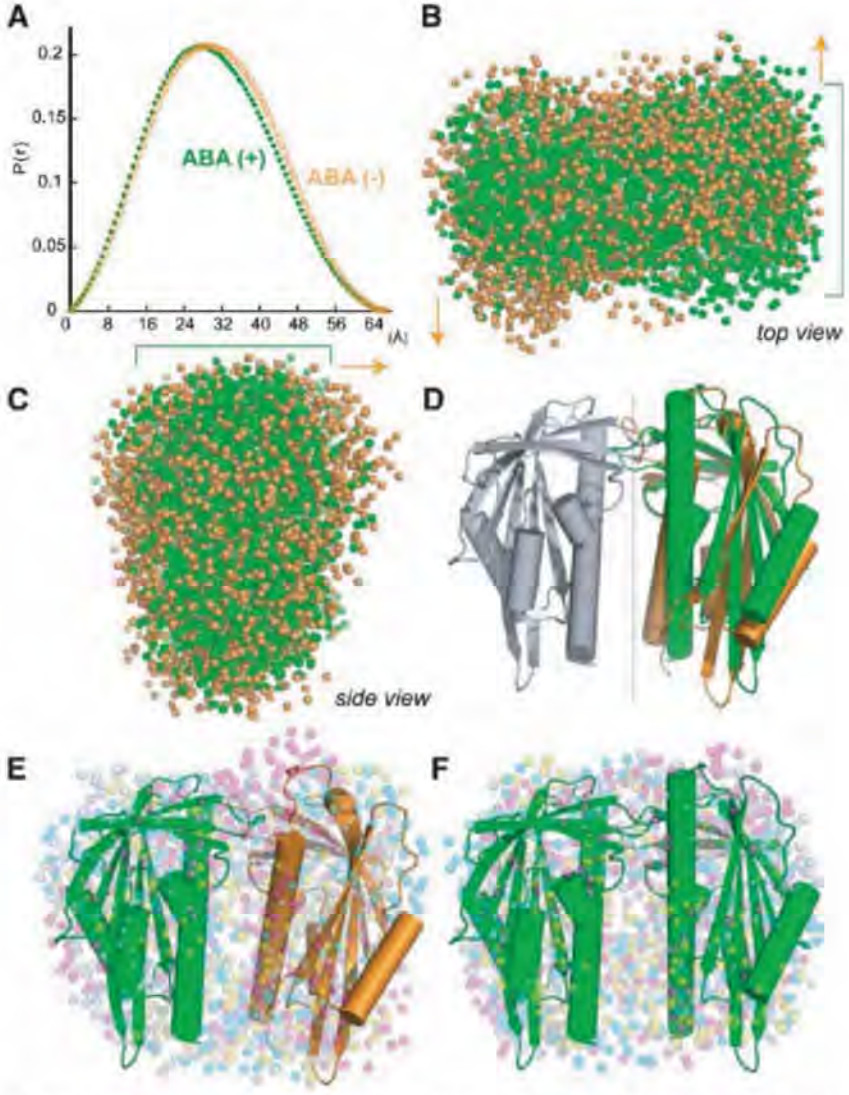

Fig. 5. ABA-induced changes in dimer assembly analyzed by SAXS. (**A**) The pair-distance distribution function describing intramolecular distances in the PYR1 dimer in the absence of ABA (orange) becomes narrower and shifts to shorter distances in the presence of saturating ABA (green). (**B** and **C**) Two sets of eight independent ab initio bead models for the PYR1 dimer, representing SAXS experimental data in the absence (orange) or presence (green) of saturating ABA. Green brackets mark flatter PYR1 disk in the presence of saturating ABA. Orange arrows indicate greater thickness and asymmetry of PYR1 dimer in absence of ABA. ABA-induced changes in subunit orientation make the PYR1 dimer disk flatter and more compact, as seen from top (B) and side (C) relative to orientation in (D). (**D**) Cartoons (depicting α helices as cylinders and β strands as arrows) of the asymmetric crystallographic dimer and a symmetric closed-lid dimer model, aligned by superposition of their common subunit (gray). The ~10° difference in orientation between the second subunits of each dimer (right), highlights the differences between the pseudo twofold axis (~170°) relating subunits (gray and orange) of the asymmetric crystallographic dimer and the exact twofold axis (vertical line) relating subunits (gray and green) of the symmetric dimer model. (**E** and **F**) Independently determined bead models (four sets of colored dots) representing SAXS results in the absence (E) and presence (F) of ABA, each aligned with the corresponding PYR1 structural model (D). The PYR1 dimer assembly shapes determined by SAXS show excellent fits to the crystallographic asymmetric dimer (E) and symmetric dimer model (F). The biconcave, red blood cell shape of the PYR1 dimer is seen by decreased bead density in the center of the PYR1 disks, as well as in the cross section (B), particularly with saturating ABA.

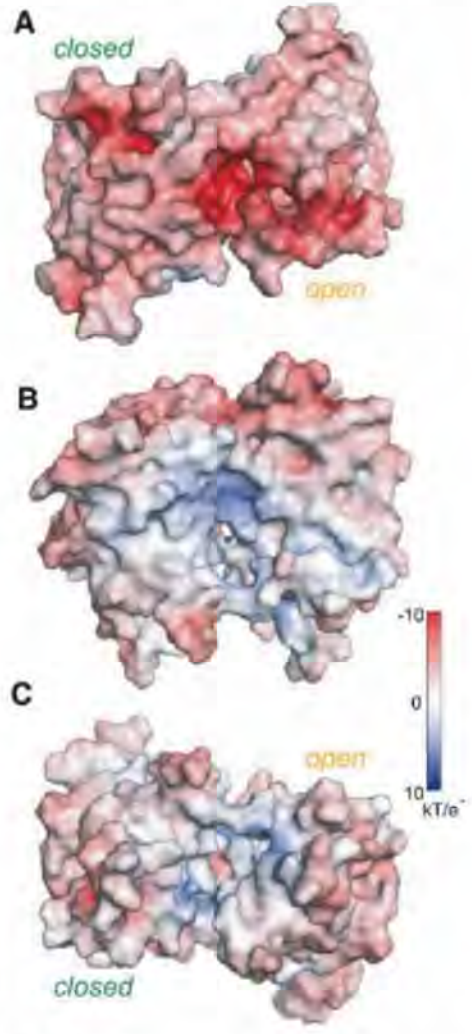

Fig. 6. PYR1 molecular surface color-coded by electrostatic potential. ABA-induced changes in subunit orientation produce conformational changes in the disk-shaped PYR1 dimer at the (**A**) interacting lids (top), (**B**) concave sides, aligned as in Fig. 5, D and E, and (**C**) the cleft (bottom) between C-terminal helices. Conformational changes of charged residues in the Leu-Lock (Glu^{114} and Arg^{116}) and Recoil (Glu^{149}, Glu^{153}, Asp^{154}, Asp^{155}, and Arg^{157}) motifs of each subunit reduce electrostatic surface potential upon lid closure (A).

the dimer interface and assembly. Furthermore, the mechanistic basis of ABA binding reported here provides a framework for future design of alternate ligands for the large ABA-binding cavity to enable chemical activation of abiotic stress resistance in plants.

References and Notes

1. K. Ohkuma, J. L. Lyon, F. T. Addicott, O. E. Smith, *Science* **142**, 1592 (1963).
2. C. F. Eagles, P. F. Wareing, *Nature* **199**, 874 (1963).
3. R. R. Finkelstein, S. S. Gampala, C. D. Rock, *Plant Cell* **14**, S15 (2002).
4. K. Yamaguchi-Shinozaki, K. Shinozaki, *Annu. Rev. Plant Biol.* **57**, 781 (2006).
5. Y. Ma *et al.*, *Science* **324**, 1064 (2009); published online 30 April 2009 (10.1126/science.1172408).
6. S.-Y. Park *et al.*, *Science* **324**, 1068 (2009); published online 30 April 2009 (10.1126/science.1173041).
7. J. Leung *et al.*, *Science* **264**, 1448 (1994).
8. K. Meyer, M. P. Leube, E. Grill, *Science* **264**, 1452 (1994).
9. F. Gosti *et al.*, *Plant Cell* **11**, 1897 (1999).
10. S. Merlot, F. Gosti, D. Guerrier, A. Vavasseur, J. Giraudat, *Plant J.* **25**, 295 (2001).
11. A. Saez *et al.*, *Plant J.* **37**, 354 (2004).
12. N. Leonhardt *et al.*, *Plant Cell* **16**, 596 (2004).
13. G. J. Allen, K. Kuchitsu, S. P. Chu, Y. Murata, J. I. Schroeder, *Plant Cell* **11**, 1785 (1999).
14. Y. Murata, Z. M. Pei, I. C. Mori, J. Schroeder, *Plant Cell* **13**, 2513 (2001).
15. T. Yoshida *et al.*, *Plant Physiol.* **140**, 115 (2006).
16. J. M. Kuhn, A. Boisson-Dernier, M. B. Dizon, M. H. Maktabi, J. I. Schroeder, *Plant Physiol.* **140**, 127 (2006).
17. N. Nishimura *et al.*, *Plant J.* **50**, 935 (2007).
18. S. Rubio *et al.*, *Plant Physiol.* **150**, 1345 (2009).
19. A. C. Mustilli, S. Merlot, A. Vavasseur, F. Fenzi, J. Giraudat, *Plant Cell* **14**, 3089 (2002).
20. R. Yoshida *et al.*, *Plant Cell Physiol.* **43**, 1473 (2002).
21. H. Fujii, P. E. Verslues, J. K. Zhu, *Plant Cell* **19**, 485 (2007).
22. H. Fujii, J. K. Zhu, *Proc. Natl. Acad. Sci. U.S.A.* **106**, 8380 (2009).
23. J. Santiago *et al.*, *Plant J.* **60**, 575 (2009).
24. X. Tan *et al.*, *Nature* **446**, 640 (2007).
25. A. Santner, M. Estelle, *Nature* **459**, 1071 (2009).
26. K. Murase, Y. Hirano, T. P. Sun, T. Hakoshima, *Nature* **456**, 459 (2008).
27. A. Shimada *et al.*, *Nature* **456**, 520 (2008).
28. Materials and methods are available as supporting material on *Science* Online.
29. R. D. Finn *et al.*, *Nucleic Acids Res.* **36**, D281 (2008).
30. L. M. Iyer, E. V. Koonin, L. Aravind, *Proteins* **43**, 134 (2001).
31. M. Gajhede *et al.*, *Nat. Struct. Biol.* **3**, 1040 (1996).
32. Y. Tsujishita, J. H. Hurley, *Nat. Struct. Biol.* **7**, 408 (2000).
33. C. D. Putnam, M. Hammel, G. L. Hura, J. A. Tainer, *Q. Rev. Biophys.* **40**, 191 (2007).
34. G. L. Hura *et al.*, *Nat. Methods* **6**, 606 (2009).
35. E. Sondheimer, E. C. Galson, Y. P. Chang, D. C. Walton, *Science* **174**, 829 (1971).
36. N. Nishimura *et al.*, *Plant J.* published online 26 October 2009 (10.1111/j.1365-313X.2009.04054.x).
37. Single-letter abbreviations for the amino acid residues are as follows: A, Ala; C, Cys; D, Asp; E, Glu; F, Phe; G, Gly; H, His; I, Ile; K, Lys; L, Leu; M, Met; N, Asn; P, Pro; Q, Gln; R, Arg; S, Ser; T, Thr; V, Val; W, Trp; and Y, Tyr.

38. We thank G. Bhabha, J. Christie, M. Hammel, G. L. Hura, D. G. Mendoza-Cozatl, M. E. Pique, D. S. Shin, and J. A. Tainer for discussions, plus the Structurally Integrated BiologY for Life Sciences beamline staff and *Arabidopsis* Biological Resource Center. This research was supported by NIH grants GM060396, ES010337 (J.I.S.), and GM37684 (E.D.G.); NSF grants MCB-0918220 (J.I.S.) and IOS0820508 (S.R.C.); U.S. Department of Energy grants DE-FG02-03ER15449 (J.I.S.) plus DE-AC02-05CH11231 and LBNL-LDRI (R.P.R.); and The Skaggs Institute for Chemical Biology (K.H.). J.I.S. and E.D.G. conceived of the project; E.D.G., J.I.S., K.H., N.N., A.S.A., and R.P.R. designed research; N.N., K.H., A.S.A., R.P.R., and C.H. performed experiments; S.R.C. provided reagents and results before publication; K.H., N.N., A.S.A., R.P.R., J.I.S., and E.D.G. analyzed data; and E.D.G., J.I.S., K.H., and N.N. wrote the paper. Crystallographic coordinates and structure factors are deposited in the Protein Data Bank with accession code 3K3K.

Supporting Online Material

www.sciencemag.org/cgi/content/full/1181829/DC1
Materials and Methods
Figs. S1 to S5
Table S1
References
Movies S1 and S2

11 September 2009; accepted 9 October 2009
Published online 22 October 2009;
10.1126/science.1181829
Include this information when citing this paper.

REPORTS

A Population of Compact Elliptical Galaxies Detected with the Virtual Observatory

Igor Chilingarian,[1,2,3]* Véronique Cayatte,[4] Yves Revaz,[5] Serguei Dodonov,[6] Daniel Durand,[7] Florence Durret,[8,9] Alberto Micol,[10] Eric Slezak[11]

Compact elliptical galaxies are characterized by small sizes and high stellar densities. They are thought to form through tidal stripping of massive progenitors. However, only a handful of them were known, preventing us from understanding the role played by this mechanism in galaxy evolution. We present a population of 21 compact elliptical galaxies gathered with the Virtual Observatory. Follow-up spectroscopy and data mining, using high-resolution images and large databases, show that all the galaxies exhibit old metal-rich stellar populations different from those of dwarf elliptical galaxies of similar masses but similar to those of more massive early-type galaxies, supporting the tidal stripping scenario. Their internal properties are reproduced by numerical simulations, which result in compact, dynamically hot remnants resembling the galaxies in our sample.

Present-day clusters of galaxies host rich populations of dwarf elliptical (dE) and lenticular (dS0) galaxies (*1*) having regular morphology and lacking ongoing star formation and interstellar medium (ISM). These galaxies are thought to form by internal processes, such as supernova feedback to the star formation (*2*), or external agents [ram pressure stripping by hot intergalactic gas (*3*) and/or gravitational harassment (*4*)] acting on gas-rich progenitors. Tidal stripping had not been considered an important mechanism governing galaxy formation until the recent discovery of ultracompact dwarf galaxies (UCDs) (*5*, *6*), that is, very compact stellar systems several times more massive than known globular clusters. However, UCDs [$L \sim 10^7\ L_\odot$ (luminosity of the Sun)] are about two orders of magnitude less luminous than bright dEs and, therefore, can be studied in only a handful of nearby galaxy clusters.

Compact elliptical (cE), or M32-like galaxies, which are also thought to form through tidal stripping (*7*), have luminosities [$\sim 10^9\ L_\odot$ (*8*–*11*)] similar to those of dEs, whereas their half-light radii ($R_e \sim 0.25$ kpc) are several times smaller, resulting in much higher mean surface brightness ($\langle\mu\rangle_e$) values compared with dEs. These two criteria are easy to formalize and apply to members of nearby galaxy clusters at known distances, hence having a known spatial scale. Ground-based optical telescopes cannot resolve objects the size of 0.25 kpc beyond 50 Mpc. To find them in clusters out to 200 Mpc, thus increasing by a factor of 60 the volume of the nearby universe where cEs remain spatially resolved, it is necessary to use the Hubble Space Telescope (HST).

We created a workflow, that is, an automatic data retrieval and analysis system to search for cE galaxies in large data collections provided by the

[1]Observatoire de Paris-Meudon, Laboratoire d'Etude du Rayonnement et de la Matiére en Astrophysique, UMR 8112, 61 Avenue de l'Observatoire, 75014 Paris, France. [2]Sternberg Astronomical Institute, Moscow State University, 13 Universitetsky Prospect, Moscow, 119296, Russia. [3]Observatoire de Paris, VO Paris Data Centre, 61 Avenue de l'Observatoire, 75014 Paris, France. [4]Observatoire de Paris-Meudon, Laboratoire Univers et Théories, UMR 8102, 5 Place Jules Janssen, 92195 Meudon, France. [5]Ecole Polytechnique Fédérale de Lausanne, Laboratory of Astrophysics, 51 Chemin des Maillettes, 1290 Sauverny, Switzerland. [6]Special Astrophysical Observatory, Nizhnij Arkhyz, Zelenchukskij Region, Karachai-Cirkassian Republic, 369167, Russia. [7]National Research Council Canada, Herzberg Institute of Astrophysics, 5071 West Saanich Road, Victoria, BC, V9E 2E7 Canada. [8]CNRS, UMR 7095, Institut d'Astrophysique de Paris, 98 bis, Boulevard Arago, 75014 Paris, France. [9]Université Pierre et Marie Curie Université Paris 06, UMR 7095, Institut d'Astrophysique de Paris, 98 bis, Boulevard Arago, 75014 Paris, France. [10]European Southern Observatory, Karl-Schwarzschild-Strasse 2, 85748 Garching bei München, Germany. [11]University of Nice Sophia Antipolis, CNRS, Observatoire de la Côte d'Azur, BP 4229, 06304 Nice Cedex 4, France.

*To whom correspondence should be addressed. E-mail: igor.chilingarian@obspm.fr

Virtual Observatory [VO (*12*)]. It comprised the following steps: (i) Identify nearby galaxy clusters at redshifts $z < 0.055$ using the VizieR Service (*13*) at the Centre de Données Astronomiques de Strasbourg. Without this condition, our potential candidate cE galaxies would have been too faint for spectroscopic follow-up. (ii) Once the sources were identified, gather more precise measurements using other VO services, including the NASA/IPAC (National Aeronautics and Space Administration/Infrared Processing and Analysis Center) Extragalactic Database (NED) (*14*). (iii) Use the International Virtual Observatory Alliance (IVOA) Simple Image Access Protocol to find and fetch the HST images of selected galaxy clusters from the Hubble Legacy Archive (HLA) (*15*). (iv) For each image, run the SExtractor source identification software (*16*) to obtain half-light radii, total luminosities, and approximate light profiles for all galaxies in each frame. (v) Apply color corrections to homogenize the results for all photometric bands and use the surface brightness–half-light radius criteria to find cE candidates. (vi) Finally, query NED, VizieR, and a database of Sloan Digital Sky Survey Data Release 7 (SDSS DR7) (*17*) to find additional information for candidate objects, such as published redshifts and integrated photometry.

Having applied the workflow to the entire HST Wide-Field Planetary Camera-2 (WFPC2) data collection in the HLA, we ended up with archival images of 63 clusters with 55 candidate cE and tidally stripped elliptical galaxies in 26 of them.

Our workflow, which uses only imaging data, may confuse cE galaxies with (i) foreground or cluster compact star-forming galaxies; (ii) background giant early-type galaxies hosting bright active nuclei (AGN); or (iii) background post-starburst galaxies. Star-forming galaxies can be discriminated automatically through their blue colors if multiband data are available, or by eye, examining their clumpy morphology. The two other cases may arise when the distance to the background object is two to three times the distance to the cluster, that is, <500 Mpc ($z < 0.12$) in our study. The probability of having a post-starburst galaxy at this redshift is very low (*18*), and AGNs can be ruled out by checking x-ray point source catalogs.

We immediately confirmed the nature of 14 cE galaxies (see Fig. 1). For six of them, where archival SDSS DR7 spectra were available, we derived their physical properties: internal kinematics and stellar populations. For the other eight candidate galaxies, we obtained redshifts from the literature through the NED and VizieR services.

To increase the sample of confirmed cE galaxies, we observed three of the galaxy clusters—Abell 160, Abell 189, and Abell 397—hosting seven candidate galaxies altogether having $2.3 \times 10^8 < L_B < 1.1 \times 10^9\ L_\odot$. This was done with the multislit unit of the SCORPIO (Spectral Camera with Optical Reducer for Photometric and Interferometric Observations) spectrograph (*19*) at the Russian 6-m "Big Telescope Alt-azimuthal" (BTA) in August 2008 [see Supporting Online Material (SOM)]. The spectra were fit with high-resolution stellar population models using the NBursts full spectral fitting technique (*20*) (SOM), obtaining precise radial velocities, internal velocity dispersions, luminosity-weighted stellar ages, and metallicities. All seven candidate objects were confirmed to be cluster members having global internal velocity dispersions between 50 and 100 km s^{-1} and old stellar populations. One of them exhibits a possible tidal feature (Fig. 2).

None of the 21 cE galaxies in our sample (summarized in tables S1 and S2) exhibits a young stellar population. The luminosity-weighted metallicities are between $Z_\odot$ (metallicity of the Sun)/2.5 ([Fe/H] = −0.4 dex) and the solar value for all galaxies except for ACO 189 J012325.96+014236.2, where it is as low as $Z_\odot/5$. Three galaxies are offset by >0.3 dex from the luminosity-metallicity relation for early-type galaxies (Fig. 1, bottom); three others reside 0.2 to 0.3 dex above it. The internal velocity dispersions are close to the values expected for the Faber-Jackson (*21*) relation and systematically above those of dEs. All these properties support the scenario in which cE galaxies are created through tidal stripping of intermediate-luminosity disc galaxies.

Tidal stripping of an early-type disc galaxy should primarily affect its extended disc. Its centrally concentrated bulge should be able to survive even severe tidal interactions. After dynamical relaxation, a tidally stripped remnant may slightly expand, decreasing its stellar velocity dispersion. For ISM-deficient galaxies, such as early-type systems in clusters, tidal stripping will not change the overall age and metallicity of their stars, but the total stellar mass will be considerably reduced. Because there is a relation between mean metallicities and stellar masses of galaxies (*22*, *23*), this process will create objects with uncommon stellar populations, that is, systems that are too metal-rich for their observed stellar masses, corresponding to what we see in galaxies populating the central region of the Abell 496 cluster (*24*) and in UCDs (*25*).

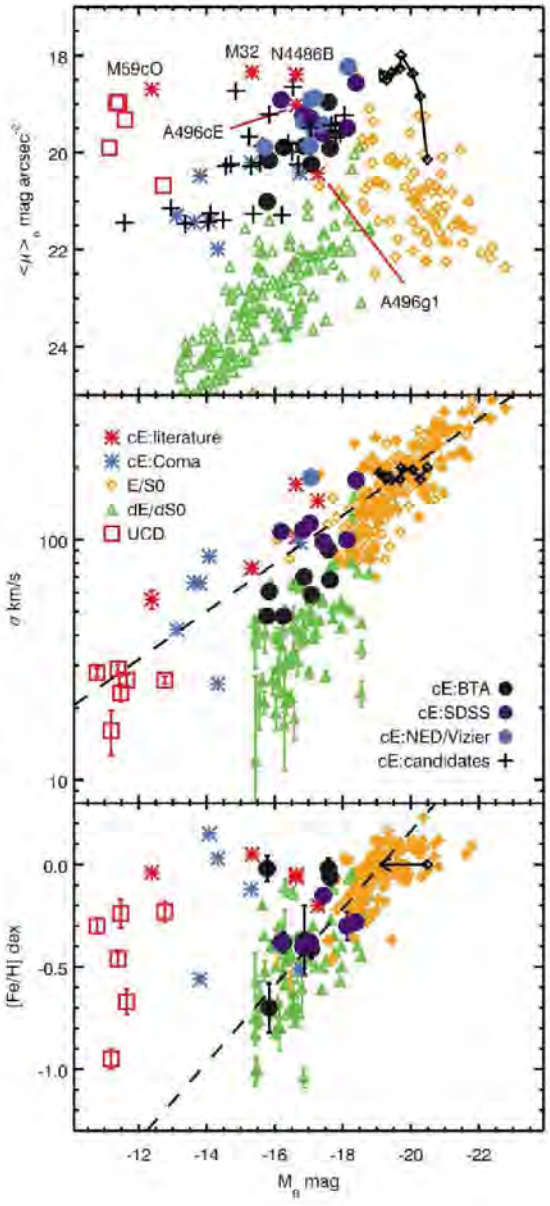

Fig. 1. Structure, dynamics, and stellar populations of early-type galaxies. Mean surface brightness within a half-light radius $\langle\mu\rangle_e$ (top), global stellar velocity dispersion σ (middle) and metallicity [Fe/H] (bottom) of galaxies are displayed as a function of the *B*-band absolute magnitudes. The confirmed tidally stripped galaxies are displayed with filled circles of black, violet, and blue colors for BTA spectroscopy, SDSS spectroscopy, and literature redshifts from NED or VizieR, respectively. Crosses denote the candidate cE galaxies without spectroscopic confirmation. Red asterisks are for known compact elliptical galaxies, and blue asterisks are for recently discovered compact stellar systems in the Coma cluster (*11*). The dashed lines in the middle and bottom panels show the Faber-Jackson (*21*) and luminosity-metallicity (*25*) relations. Literature data [dE/dS0 galaxies (*24*, *29*, *30*); intermediate-luminosity and giant early-type galaxies (*31*); and UCDs (*25*)] are complemented with the data for 140 early-type galaxies in the Coma cluster from the SDSS DR7 spectra obtained with the NBursts technique (SOM). All metallicity measurements shown in the bottom panel, except those of Coma compact stellar systems, are homogeneous because they were obtained using the same data analysis technique. Black path displays the evolution of a simulated barred early-type spiral tidally stripped by the cluster potential on a quasicircular orbit (SOM) followed for 2 billion years.

The stellar metallicity can also be increased by star formation induced by external sources, for example, by mergers or encounters with gas-rich galaxies where tidal compression may dramatically increase the star formation efficiency (*26*). However, in this case, the mean age of the stellar population would decrease because newly formed stars have much lower mass-to-light ratios in the optical than older populations do, contributing significantly to the total light, even with low mass fractions. All the galaxies in our sample exhibit old populations, hence ruling out this scenario.

Tidal effects must be stronger in the vicinities of massive galaxies, in particular around cluster dominant galaxies (cD). To study the efficiency of tidal stripping, we simulated the interaction of a disc galaxy with a galaxy cluster potential using the gadget-2 code (*27*) (see SOM for further

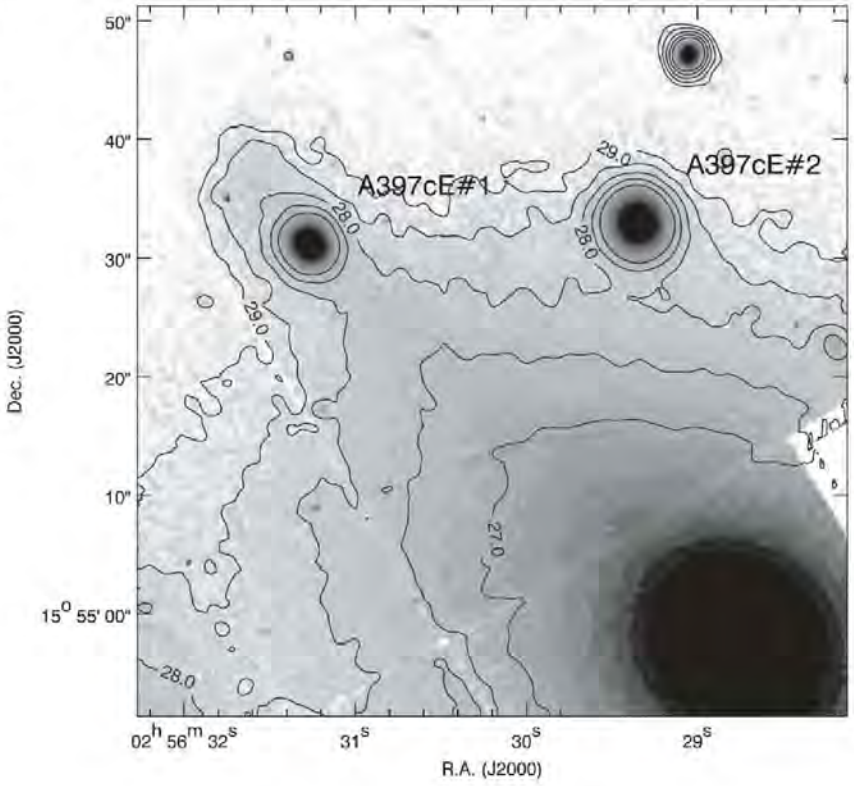

Fig. 2. Fragment of a WFPC2 HST image of the central region of Abell 397 obtained from the HLA with two candidate cE galaxies; north is up, east is left. The overplotted isophotes correspond to surface brightness levels from 29.0 to 27.0 mag arc sec^{-2} in the F814W band, with 0.5 mag arc sec^{-2} interval. A397cE#1 exhibits a prominent extended low surface brightness feature toward the northeast, probably originating from its tidal interaction with the cluster dominant galaxy UGC 2413 in the lower right corner.

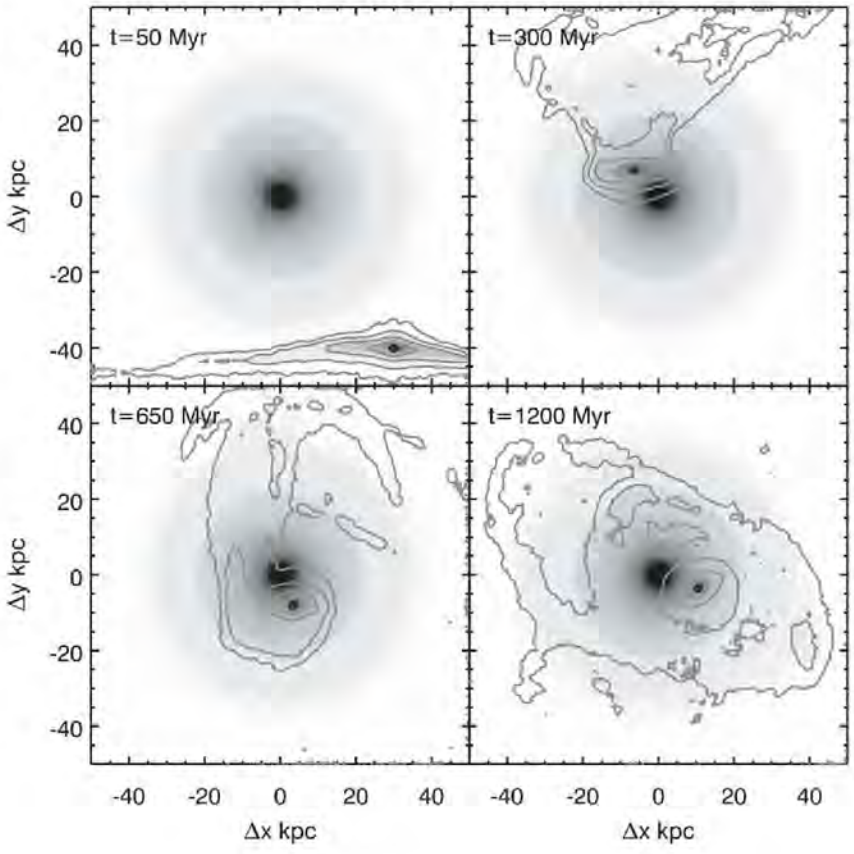

Fig. 3. Numerical simulations of the tidal stripping of an intermediate-luminosity barred disc galaxy. The panels display four snapshots of an *N*-body simulation of the tidal disruption of a barred disc galaxy, initially on a quasicircular orbit, by the cluster cD galaxy shown in the center. The disc galaxy plane is perpendicular to the initial orbital plane. Each panel is 100 by 100 kpc in size; the density scale is logarithmic. The density contours (every 2 mag arc sec^{-2}) are displayed for the stars that initially belonged to the disc galaxy. The simulations demonstrate how the outer disc of a galaxy gets stripped, leaving a compact remnant and stripped material in arcs and tails.

details). We explored the tidal stripping effects at a spatial resolution (~100 pc) several times as high as that of typical simulations of galaxy clusters, checking 32 different orbital configurations. We converted the stellar density maps produced by our simulations into surface brightness and processed them using the SExtractor software in the same way as we did for the search of cE galaxies in HST images.

Our simulations demonstrate the efficiency of tidal stripping in reducing the stellar mass of a disc galaxy. Even in cases of quasicircular orbital configurations, the large-scale stellar disc was heavily stripped, decreasing the galaxy stellar mass by a factor of 2 (Fig. 3) on a time-scale of 600 to 700 million years. We compared the evolution of total magnitude, surface brightness, and internal velocity dispersion of a stripped galaxy to observations (Fig. 1, top and middle). Interactions on radial orbits resulted in heavier mass loss of up to 90%, although a remnant became quickly accreted by a cD galaxy. Presumably, by scaling down the systems in mass, that is, by replacing a giant disc with a low-luminosity or dwarf S0, it should be possible to reproduce the formation of UCD and transitional cE/UCD (*28*, *11*) galaxies.

In our study, we used Virtual Observatory data mining to reclassify cE galaxies from "unique" to "common in certain environmental conditions," that is, more frequent than was previously thought. We confirmed the nature of 21 galaxies selected by the VO workflow with follow-up observations and archival data. We also reproduced their properties with numerical simulations. We can confirm that tidal stripping of the stellar component plays an important role in the morphological transformation of galaxies in dense environments, producing remnants spanning a luminosity range of four orders of magnitude.

References and Notes

1. H. C. Ferguson, B. Binggeli, *Astron. Astrophys. Rev.* **6**, 67 (1994).
2. A. Dekel, J. Silk, *Astrophys. J.* **303**, 39 (1986).
3. J. E. Gunn, J. R. I. Gott, *Astrophys. J.* **176**, 1 (1972).
4. B. Moore, N. Katz, G. Lake, A. Dressler, A. Oemler, *Nature* **379**, 613 (1996).
5. S. Mieske, M. Hilker, L. Infante, *Astron. Astrophys.* **383**, 823 (2002).
6. M. J. Drinkwater *et al.*, *Nature* **423**, 519 (2003).
7. K. Bekki, W. J. Couch, M. J. Drinkwater, M. D. Gregg, *Astrophys. J.* **557**, L39 (2001).
8. A. W. Graham, *Astrophys. J.* **568**, L13 (2002).
9. S. Mieske *et al.*, *Astron. Astrophys.* **430**, L25 (2005).
10. I. Chilingarian *et al.*, *Astron. Astrophys.* **466**, L21 (2007).
11. J. Price *et al.*, *Mon. Not. R. Astron. Soc.* **397**, 1816 (2009).
12. The Virtual Observatory is a realization of an e-Science concept in astronomy with an emphasis on data mining, where data archives and software tools interoperate using a set of peer-reviewed standards and technologies developed by the IVOA (www.ivoa.net). It forms a virtual environment aimed at facilitating astronomical research and increasing scientific output of data by providing transparent access to catalogs, databases, archives, data visualization, and processing and analysis tools.
13. VizieR Catalogue Service; http://vizier.u-strasbg.fr
14. NASA/IPAC Extragalactic Database; http://nedwww.ipac.caltech.edu
15. Hubble Legacy Archive; http://hla.stsci.edu
16. E. Bertin, S. Arnouts, *Astron. Astrophys. Suppl. Ser.* **117**, 393 (1996).
17. K. N. Abazajian *et al.*, *Astrophys. J. Suppl. Ser.* **182**, 543 (2009).
18. T. Goto *et al.*, *Publ. Astron. Soc. Jpn.* **55**, 771 (2003).
19. V. L. Afanasiev, A. V. Moiseev, *Astron. Lett.* **31**, 194 (2005).
20. I. Chilingarian, P. Prugniel, O. Sil'chenko, M. Koleva, *Stellar Populations as Building Blocks of Galaxies*, A. Vazdekis, R. R. Peletier, Eds. (Cambridge Univ. Press, Cambridge, UK, 2007), vol. 241 of *IAU Symposium*, pp. 175–176.
21. S. M. Faber, R. E. Jackson, *Astrophys. J.* **204**, 668 (1976).
22. A. Gallazzi, S. Charlot, J. Brinchmann, S. D. M. White, C. A. Tremonti, *Mon. Not. R. Astron. Soc.* **362**, 41 (2005).
23. A. Renzini, *Annu. Rev. Astron. Astrophys.* **44**, 141 (2006).
24. I. V. Chilingarian *et al.*, *Astron. Astrophys.* **486**, 85 (2008).
25. I. V. Chilingarian, V. Cayatte, G. Bergond, *Mon. Not. R. Astron. Soc.* **390**, 906 (2008).
26. E. Emsellem, G. van de Ven, *Astrophys. J.* **674**, 653 (2008).
27. V. Springel, *Mon. Not. R. Astron. Soc.* **364**, 1105 (2005).
28. I. V. Chilingarian, G. A. Mamon, *Mon. Not. R. Astron. Soc.* **385**, L83 (2008).
29. B. Binggeli, H. Jerjen, *Astron. Astrophys.* **333**, 17 (1998).
30. I. V. Chilingarian, *Mon. Not. R. Astron. Soc.* **394**, 1229 (2009).
31. R. Bender, D. Burstein, S. M. Faber, *Astrophys. J.* **399**, 462 (1992).

32. This study is based on observations made with the NASA/European Space Agency (ESA) Hubble Space Telescope and obtained from the Hubble Legacy Archive, which is a collaboration between the Space Telescope Science Institute (NASA), the Space Telescope European Coordinating Facility (ESA), and the Canadian Astronomy Data Centre (National Research Council Canada/Canadian Space Agency); observations collected with the 6-m telescope of the Special Astrophysical Observatory of the Russian Academy of Sciences operated under the financial support of the Science Department of Russia (registration number 01-43). The simulations were run on the Callisto cluster at the École Polytechnique Fédérale de Lausanne and on the Regor cluster of the Geneva Observatory. This research made use of SAOImage DS9, developed by Smithsonian Astrophysical Observatory; Aladin, developed by the Centre de Données Astronomiques de Strasbourg (CDS), "exploresdss" script by G. Mamon; the VizieR Catalogue access tool (CDS); and the NASA/IPAC Extragalactic Database (NED) operated by the Jet Propulsion Laboratory, California Institute of Technology, under contract with NASA. Funding for the SDSS and SDSS-II has been provided by the Alfred P. Sloan Foundation, the participating institutions, the National Science Foundation, the U.S. Department of Energy, NASA, the Japanese Monbukagakusho, the Max Planck Society, and the Higher Education Funding Council for England. The SDSS Web site is www.sdss.org. The simulation data analysis and galaxy maps were done using the parallelized Python pNbody package (http://obswww.unige.ch/~revaz/pNbody). This work was supported by the Swiss National Science Foundation. I.C. acknowledges additional support from the Russian Foundation for Basic Research, grant 07-02-00229-a. Special thanks to F. Combes and G. Mamon for useful discussions and suggestions and to R. Trilling, who kindly agreed to edit the manuscript. The content of the workflow and its explicit description are available on the Web pages of the VO Paris Data Centre (http://vo-web.obspm.fr) and the European Virtual Observatory EURO-VO.

Supporting Online Material

www.sciencemag.org/cgi/content/full/1175930/DC1
SOM Text
Figs. S1 to S3
Tables S1 and S2
References

6 May 2009; accepted 24 September 2009
Published online 1 October 2009;
10.1126/science.1175930
Include this information when citing this paper.

On the Elusive Twelfth Vibrational State of Beryllium Dimer

Konrad Patkowski,[1]* Vladimír Špirko,[2] Krzysztof Szalewicz[1]

The beryllium dimer has puzzled chemists for roughly 80 years on account of its unexpectedly strong bonding interaction between two nominally closed-shell atoms. Recent spectroscopic measurements characterized the molecule's ground electronic state with sufficient resolution to distinguish 11 vibrational levels; the possibility that a twelfth level lay just below the dissociation threshold remained unresolved. Here we present a potential function, based on ab initio calculations at the full configuration interaction level, that definitively supports the presence of this twelfth vibrational state. "Morphed" versions of this potential, fitted to experimental data, closely reproduce the observed spectra to within 0.1 cm^{-1}, bolstering the strength of the assignment.

Merritt *et al.* (*1*) recently reported a spectroscopic study of the beryllium dimer, an unusual diatomic system that is bound by about 2.5 kcal/mol and has an equilibrium interatomic separation of 2.44 Å. This bond is within the range of van der Waals interactions, but is substantially stronger and shorter than those between other similarly sized closed-shell atoms. Spectroscopic measurements for Be_2 are difficult to perform, and the experiment (*1*) resulted in a markedly altered prediction of the well depth for the ground electronic state: from $D_e = 790 \pm 30\ cm^{-1}$ (*2*, *3*) to $929.7 \pm 2.0\ cm^{-1}$ (*1*). The study also increased the number of identified vibrational levels from 5 to 11. The authors suspected that one more level could exist, but their empirical fit to the measured data predicted only 11 levels, with the vibrational quantum number v ranging from 0 to 10. The existence of a twelfth level, bound by a fraction of a wavenumber,

[1]Department of Physics and Astronomy, University of Delaware, Newark, DE 19716, USA. [2]Department of Molecular Modeling, Institute of Organic Chemistry and Biochemistry, Flemingovo nám. 2, 166 10 Prague 6, Czech Republic.

*To whom correspondence should be addressed. E-mail: patkowsk@udel.edu

would provide information about the shape of the potential at large interatomic separations R and could be relevant to experiments on ultracold trapped atoms (*4*). We show here that the $v = 11$ state can be positively identified from ab initio calculations.

Because Be_2 is a fairly small system (only eight electrons), it has been one of the benchmarks for computational ab initio methods, with more than 100 studies published [see (*5*, *6*) for lists of references]. The calculations are nonetheless difficult due to the *sp* near-degeneracy of the atomic orbitals of beryllium (*6*). This near-degeneracy, which is the reason that Be_2 is more strongly bound than He_2 or Ne_2, results in poor performance of standard electron correlation methods based on single-determinant reference functions. Recent calculations using methods beyond a single-determinant reference consistently gave a well depth significantly deeper than the earlier experimental prediction (*2*, *3*). In particular, the most extensive calculations gave a depth of 938 ± 15 cm^{-1} (*6*), several standard deviations beyond the experimental result up to that point. Thus, the measurement of Merritt *et al.* (*1*) reconciled experiment with theory and provided another example of the predictive power of modern ab initio methods.

Our group has been working for some time on extending the single-point calculations of (*6*) to other interatomic separations. As in (*6*), the interaction energies were constructed here from contributions at several levels of theory up to the frozen-core full configuration interaction method. The effects beyond the frozen-core approximation and relativistic effects were also included. All the calculations used the largest basis sets that exist for Be or that can be currently applied at a given level of theory within reasonable computer resource constraints, and were extrapolated to complete basis set limits. An analysis of the patterns of convergence with the level of theory and size of the basis sets provided estimated uncertainties $\sigma(R)$ of the results. The ab initio interaction energies computed for 20 interatomic separations were fitted by an analytic function of a form often used for van der Waals interactions of atoms:

$$V_{vdW}(R) = (A + BR + C/R + DR^2 + ER^3) \times e^{-\alpha R + \beta R^2} - \sum_{n=3}^{8} f_{2n}(bR)\frac{C_{2n}}{R^{2n}} \quad (1)$$

where $f_n(bR)$ are the Tang-Toennies damping functions (*7*),

$$f_n(bR) = 1 - e^{-bR}\sum_{m=0}^{n}(bR)^m/m! \quad (2)$$

C_n are the asymptotic coefficients (*8*) that were kept constant during the fitting process, and the parameters α, β, b, A, B, C, D, and E were obtained in a nonlinear least-squares fitting procedure with the ab initio results weighted according to their uncertainties $\sigma(R)$. The unweighted root-mean square error (rmse) of the fit is 0.78 cm^{-1}. The values of the fit parameters are given in table S1.

The fit was used to compute rovibrational levels of Be_2, and the results are presented in Table 1. Our purely ab initio potential function V_{vdW} recovers the measured vibrational energies (column "Exp.") with rmse of only 3.4 cm^{-1}, a substantial improvement over the previous best ab initio predictions (*9*–*12*), and furthermore predicts the existence of the $v = 11$ state 0.52 cm^{-1} below the dissociation limit. Merritt *et al.* found a spectral feature quite close to this position [marked by an arrow in Fig. 1 of (*1*)], which they attributed to the onset of the continuum, but which could correspond to the twelfth state. We have also computed the transition intensities for the stimulated emission pumping spectrum recorded in (*1*) (fig. S1) and found that the transition to $v = 11$ should be strong enough to observe.

Our ab initio potential predicts a well 9 cm^{-1} deeper than the empirical potential of Merritt *et al.* To rule out the possibility that this discrepancy might account for the emergence of the $v = 11$ level in the calculation, we generated two additional analytic potentials V_+ and V_-. These potentials share the functional form and the asymptotic

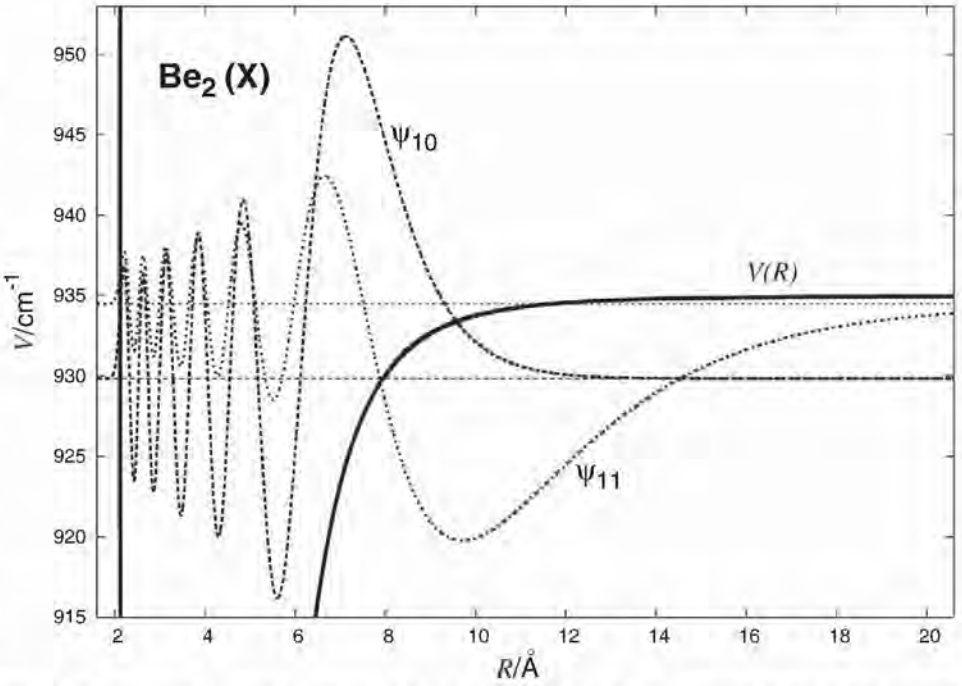

Fig. 1. The calculated wave functions of the $v = 10$ and $v = 11$ vibrational states of the ground electronic state of Be_2. The dashed horizontal lines are the positions of the two states.

Table 1. Comparison of spectra predicted by empirical, ab initio, and morphed potentials with experiment. The energy unit is cm^{-1} and the equilibrium distances R_e are given in Å. The Δ columns present the difference between the values in the preceding column and the experimental values [Exp., from (*1*)]. Emp. refers to the empirical potential in (*1*), V_{vdW} to the ab initio potential, $\tilde{V}^{(2)}_{vdW}$ to the two-parameter morphed potential of Eq. 3 (with $a = 0.99390732$ and $b = 1.00215597$), and $\tilde{V}^{RPC(3)}_{vdW}$ and $\tilde{V}^{RPC(5)}_{vdW}$ to the potential morphed according to three- and five-parameter RPC algorithms, respectively.

v	Exp.	Emp.	Δ	V_{vdW}	Δ	$\tilde{V}^{(2)}_{vdW}$	Δ	$\tilde{V}^{RPC(3)}_{vdW}$	Δ	$\tilde{V}^{RPC(5)}_{vdW}$	Δ
1	222.6	222.7	0.1	222.3	−0.3	221.9	−0.7	221.9	−0.7	222.6	0.0
2	397.1	397.8	0.7	397.6	0.5	396.4	−0.7	396.4	−0.7	397.0	−0.1
3	518.1	518.2	0.1	520.3	2.2	518.2	0.1	518.2	0.1	518.2	0.1
4	594.8	595.4	0.6	597.9	3.1	595.1	0.3	595.1	0.3	594.8	0.0
5	651.5	652.4	0.9	655.1	3.6	652.0	0.5	651.9	0.4	651.5	0.0
6	698.8	699.4	0.6	702.6	3.8	699.2	0.4	699.1	0.3	698.7	−0.1
7	737.7	738.2	0.5	741.7	4.0	738.0	0.3	737.9	0.2	737.6	−0.1
8	768.2	768.8	0.6	772.4	4.2	768.3	0.1	768.2	0.0	768.2	0.0
9	789.9	790.7	0.8	794.3	4.4	789.7	−0.2	789.7	−0.2	790.0	0.1
10	802.6	803.4	0.8	807.1	4.5	802.0	−0.6	802.1	−0.5	802.5	−0.1
11*				811.9	(0.52)	806.4	(0.41)	806.6	(0.44)	807.1	(0.42)
rmse			0.6		3.4		0.4		0.4		< 0.1
D_e		929.7		938.7		933.0		933.2		934.6	
R_e		2.454		2.443		2.438		2.432		2.438	

*The number in parentheses is the separation between the $v = 11$ state and the onset of the continuum. The empirical potential does not support the $v = 11$ bound state.

constants with V_{vdW}, but are fitted to reproduce the values of $E_{int} + \sigma$ and $E_{int} - \sigma$, respectively, instead of the ab initio interaction energies E_{int}. Both V_+ and V_- support the $v = 11$ state, which lies at respective frequencies 0.38 and 0.70 cm^{-1} below the onset of the continuum. Because the minimum depth of V_+ is 922.1 cm^{-1} (i.e., 8 cm^{-1} shallower than the empirical potential), the well depth is clearly not a determining factor in the appearance of the $v = 11$ state.

The ab initio potential reproduces measured transitions with errors about six times larger than the empirical potential of (*1*). To find out if a closer recovery of the transitions does not lead to disappearance of the $v = 11$ level, we developed a semi-empirical, "morphed" form of V_{vdW}. In the morphing process, the ab initio potential is fine-tuned by introducing a small number (up to five in this work) of adjustable parameters with values fitted to experimental data. The simplest form of morphing is a variation of the energy and length scales in the potential

$$\tilde{V}^{(2)}_{vdW}(R) = aV_{vdW}(bR) \qquad (3)$$

via two fitted scaling factors *a*,*b*. The second approach (*8*), an extended version (*13*, *14*) of the reduced potential curve (RPC) method proposed by Jenč and Plíva (*15*), can be viewed as a more general form of scaling. The experimental data points used in the morphing procedure were the vibrational energies and rotational transitions. The fit and the RPC morphing parameters are given in tables S1 and S2.

The predictions of our three morphed potentials are compared with experimental values in Table 1. All show better agreement with measured data than the empirical potential obtained by Merritt *et al.* (*1*). Moreover, there is an order of magnitude improvement relative to the predictions of our ab initio potential, which was distorted to an only minor extent by the morphing (shown by the values of D_e and R_e). All morphed potentials predict the existence of the $v = 11$ level at a position 0.41 to 0.44 cm^{-1} below the dissociation limit, in good agreement with the purely ab initio value. The $v = 11$ vibrational state is not only bound, but supports two excited rotational states.

The failure of the fit of Merritt *et al.* (*1*) to predict the $v = 11$ state can be attributed mainly to its poor asymptotic behavior. Our ab initio calculations were performed for R up to 8 Å, and we used nearly exact van der Waals constants in our fit. Thus, the long-R portion of our fit is very accurate. Merritt *et al.* used a purely exponential form of the fit, which has an unphysical decay at large R. Indeed, the discrepancies of this fit relative to V_{vdW} are up to 2.4 cm^{-1} in the 5 to 8 Å range where the interaction potential ranges between −87 and −5 cm^{-1}. This region is critical for the high-v states, as shown in Fig. 1. The vibrational wave function of the $v = 11$ state has a maximum magnitude around 10 Å. Because this wave function is mainly sensitive to the region of the potential well approximated by the asymptotic $-C_6/R^6$ term, one can use the semi-classical near-dissociation theory of Le Roy and Bernstein (*16*) to determine the number of bound levels. If the experimental dissociation energies of the $v = 9$ and $v = 10$ states are used as input, this theory predicts that there exists one more bound vibrational state above these two. It is gratifying to see that the simple qualitative picture of the near-dissociation theory agrees with our quantitative ab initio description of vibrational levels in the beryllium dimer.

References and Notes

1. J. M. Merritt, V. E. Bondybey, M. C. Heaven, *Science* **324**, 1548 (2009).
2. V. E. Bondybey, *Chem. Phys. Lett.* **109**, 436 (1984).
3. V. E. Bondybey, *Science* **227**, 125 (1985).
4. P. Blythe, B. Roth, U. Frohlich, H. Wenz, S. Schiller, *Phys. Rev. Lett.* **95**, 183002 (2005).
5. I. Røeggen, J. Almlöf, *Int. J. Quantum Chem.* **60**, 453 (1996).
6. K. Patkowski, R. Podeszwa, K. Szalewicz, *J. Phys. Chem. A* **111**, 12822 (2007).
7. K. T. Tang, J. P. Toennies, *J. Chem. Phys.* **80**, 3726 (1984).
8. Materials and methods are available as supporting material on *Science* Online.
9. J. M. L. Martin, *Chem. Phys. Lett.* **303**, 399 (1999).
10. R. J. Gdanitz, *Chem. Phys. Lett.* **312**, 578 (1999).
11. I. Røeggen, L. Veseth, *Int. J. Quantum Chem.* **101**, 201 (2005).
12. V. Špirko, *J. Mol. Spectrosc.* **235**, 268 (2006).
13. O. Bludský, M. Jureček, V. Špirko, B. A. Brandt, F. Jenč, *J. Mol. Spectrosc.* **169**, 555 (1995).
14. V. Špirko, *Collect. Czech. Chem. Commun.* **70**, 731 (2005).
15. F. Jenč, J. Pliva, *Collect. Czech. Chem. Commun.* **19**, 1449 (1962).
16. R. J. Le Roy, R. B. Bernstein, *Chem. Phys. Lett.* **5**, 42 (1970).

17. This work was supported by the NSF grant CHE-0848589, by the Academy of Sciences of the Czech Republic grant IAA400550511 (project Z40550506), and by the Czech Ministry of Education, Youth and Sports grants LC512 and MSM6198959216.

Supporting Online Material

www.sciencemag.org/cgi/content/full/326/5958/1382/DC1
SOM Text
Fig. S1
Tables S1 and S2
References

24 August 2009; accepted 14 October 2009
10.1126/science.1181017

From Hydrogenases to Noble Metal–Free Catalytic Nanomaterials for H_2 Production and Uptake

Alan Le Goff,[1] Vincent Artero,[2]* Bruno Jousselme,[1] Phong Dinh Tran,[2] Nicolas Guillet,[3] Romain Métayé,[1] Aziz Fihri,[2] Serge Palacin,[1]* Marc Fontecave[2,4]

Interconversion of water and hydrogen in unitized regenerative fuel cells is a promising energy storage framework for smoothing out the temporal fluctuations of solar and wind power. However, replacement of presently available platinum catalysts by lower-cost and more abundant materials is a requisite for this technology to become economically viable. Here, we show that the covalent attachment of a nickel bisdiphosphine–based mimic of the active site of hydrogenase enzymes onto multiwalled carbon nanotubes results in a high–surface area cathode material with high catalytic activity under the strongly acidic conditions required in proton exchange membrane technology. Hydrogen evolves from aqueous sulfuric acid solution with very low overvoltages (20 millivolts), and the catalyst exhibits exceptional stability (more than 100,000 turnovers). The same catalyst is also very efficient for hydrogen oxidation in this environment, exhibiting current densities similar to those observed for hydrogenase-based materials.

One dilemma inherent in the widespread use of solar cells and windmills for power generation is that temporal fluctuations in worldwide energy demand do not strictly correlate with the availability of sunlight and wind. An efficient, reversible means of storing excess energy is necessary, and unitized regenerative fuel cells are an attractive option for that purpose. The devices operate by storing energy in hydrogen generated via electrolysis of water and then releasing it as necessary through the reverse reaction. The devices are compact and have low internal resistance. However, they currently rely on platinum for catalysis, which is too scarce and thus too expensive for widespread adoption (*1*). A competitive alternative may be found in microorganisms that metabolize hydrogen using hydrogenase enzymes (*2*, *3*). These metalloproteins bidirectionally catalyze interconversion between H_2 and a pair of protons and electrons (the same

[1]Commissariat à l'Énergie Atomique (CEA), Institut Rayonnement Matière de Saclay, Service de Physique et Chimie des Surfaces et Interfaces, Chemistry of Surfaces and Interfaces group, F-91191 Gif sur Yvette Cedex, France. [2]Laboratoire de Chimie et Biologie des Métaux, Université Joseph Fourier, CNRS UMR 5249, CEA Institut de Recherche en Technologies et Sciences pour le Vivant, 17 rue des Martyrs, F-38054 Grenoble cedex 9, France. [3]Institut Laboratoire d'Innovation pour les Technologies des Energies Nouvelles et les Nanomatériaux (LITEN), CEA LITEN/Département des Technologies de l'Hydrogène, Laboratoire des composants pour Pile à combustible, Electrolyse et Modélisation, 17 rue des Martyrs, F-38054 Grenoble cedex 9, France. [4]Collège de France, 11 place Marcellin-Berthelot, F-75005 Paris, France.

*To whom correspondence should be addressed. E-mail: vincent.artero@cea.fr (V.A.); serge.palacin@cea.fr (S.P.)

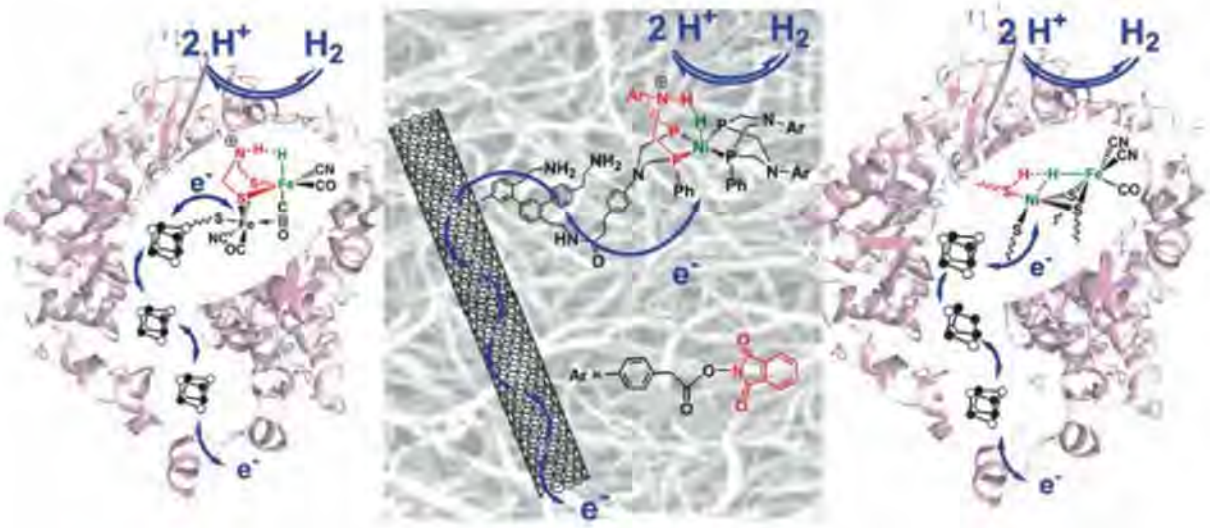

Fig. 1. Architectures of FeFe (**Left**) and NiFe (**Right**) hydrogenases in the reduced active state and schematic representation of the structure of the bio-inspired H_2-evolving nickel catalyst grafted on a carbon nanotube (**Middle**). The structure of the activated phtalimide ester moieties introduced in para position of the nitrogen-bound phenyl residues of the diphosphine ligands in $\mathbf{2}(BF_4)_2$ is also indicated. Blue arrows trace the electron transport chain toward the active site, either through iron-sulfur clusters in the enzymes or through the conductive CNT. The ligands acting as proton relays in heterolytic hydrogen evolution reaction are depicted in red, and the metal centers stabilizing hydride ions are depicted in green. In this simplified representation, the number of phenylene residues shown is arbitrary, and we do not exclude attachment of the nickel complex to two or more surface amine groups.

reaction taking place at electrodes in fuel cells and electrolyzers) as efficiently as platinum nanoparticles do and with remarkably high reaction rates (1500 to 9000 s^{-1} at pH 7 and 37°C in water) (*4*). In addition, when adsorbed on an electrode they operate without the need for any additional applied voltage beyond the equilibrium potential for the H_2O/H_2 couple (*5*–*7*). Unfortunately, hydrogenases suffer from considerable oxygen sensitivity. In addition, their production in the active form can hardly be scaled up to satisfy technological demand.

Because catalysis in hydrogenases requires only iron and nickel metal centers, the active sites (Fig. 1) are strong sources of inspiration for the design of synthetic catalysts that are more sustainable than platinum (*6*, *8*–*13*). In addition, bio-inspired synthetic catalysts are easy to prepare and can often be handled in air, which is key for the integration in a technological device. One of the most successful achievements of the biomimetic approach involves a family of bisdiphosphine nickel complexes (*11*, *14*) that combine very well a nickel center in an electron-rich environment (as found in NiFe hydrogenases) with proton relays provided by a pendant base mimicking the putative azapropanedithiolato cofactor of FeFe hydrogenases (*15*). The presence of basic residues at the vicinity of the catalytic metal center indeed facilitates the formation of H_2 from a coordinated hydride ion and a proton from the ammonium group (Fig. 1). It is thus tempting to address the issue of whether such biomimetic molecular systems can be exploited for the development of efficient and robust electrode materials.

To this end, we have explored the prospect of assembling an electrode by binding these biomimetic nickel complexes to carbon nanotubes (CNTs). Among the advantages of CNTs for this purpose are their high surface areas (facilitating high catalyst loading), their high stability and electrical conductivity (*16*, *17*), and the availability of versatile and straightforward methods

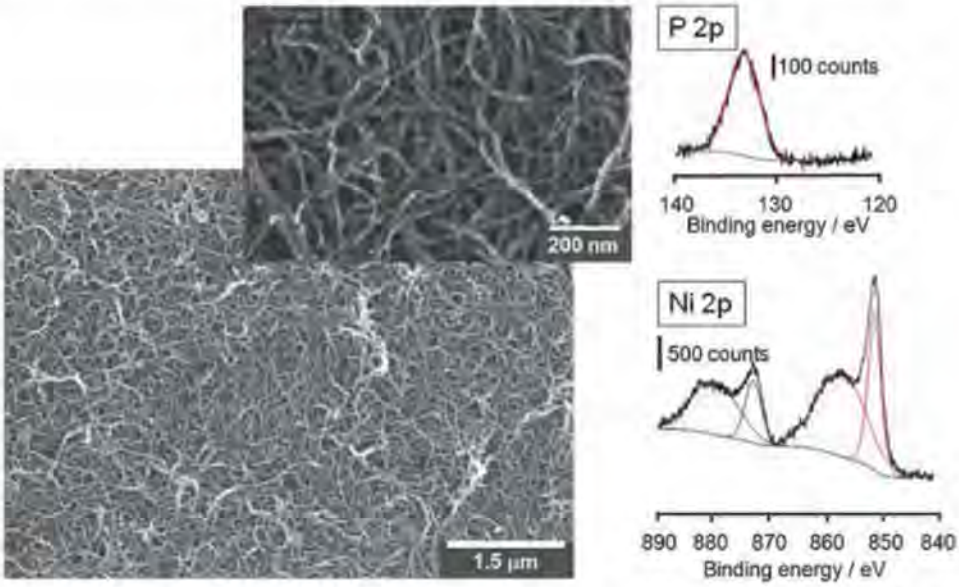

Fig. 2. Scanning electron micrographs of a ITO/MWCNT electrode and decomposed x-ray photoelectron spectra of a Ni-functionalized ITO/MWCNT electrode at (**Top**) P 2p and (**Bottom**) Ni 2p energy levels (red, $2p_{3/2}$; blue, $2p_{1/2}$).

for grafting molecular complexes onto their surfaces (*18*–*20*). For example, electro-reduction of functionalized aryldiazonium salts has been recently used to modify CNT-based electrodes by means of hydrogenases that yield highly active electrocatalytic materials, although these electrodes are useable only under inert atmosphere (*21*).

Cyclic voltammetry (CV) showed that electrodes prepared by depositing a thin film of multiwall CNTs (MWCNTs) (*22*) onto an indium tin oxide (ITO) substrate (fig. S1) by means of a soluble membrane technique reported by Wu *et al.* (*23*) display a quasi-reversible response for ferrocene oxidation in CH_3CN with a peak-to-peak separation (ΔE) of 90 mV (*24*). The high electrode surface area was shown by means of scanning electron microscopy (SEM) (Fig. 2), which revealed bundles of MWCNTs with extensive branching. Covalent attachment of 4-(2-aminoethyl)phenyl groups at the surface of these electrodes was optimally achieved via the electro-reduction of the corresponding protonated diazonium tetrafluoroborate salt $\mathbf{1}(BF_4)_2$ (*25*), cycling between 0.8 and 0.0 V versus normal hydrogen electrode (NHE) at 20 mV s^{-1}. The first scan indicated an irreversible cathodic process ($E_p^c = 0.22$ V versus NHE) corresponding to the grafting of a polyphenylene layer on the MWCNTs electrode (fig. S2). On the two successive scans, a deviation of the reduction peak toward more negative potentials was observed, which is indicative of continuous growth of a conductive polyphenylene layer (Fig. 1). Three-scan CV affords the most homogeneous coverage and the maximum number of

available amine sites (*26*). X-ray photoelectron spectroscopy (XPS) analysis confirmed the presence of both amine and ammonium groups with respective peaks at 399.9 and 401.6 eV corresponding to the energies of the 1 s orbital on the N atom (fig. S3).

Activated phtalimide ester moieties (Fig. 1) have been introduced in para position of the nitrogen-bound phenyl residues of the 1,3,5,7-tetraphenyl-1,5-diaza-3,7-diphosphacyclooctane ligand initially reported by Wilson *et al.* (*14*). The resulting hydrogenase-inspired nickel catalyst **2**$(BF_4)_2$ is air- and moisture-stable, thus straightforward to anchor to the amino-functionalized MWCNT-electrode material via the formation of stable covalent amide linkages. The cyclic voltammogram of **2**$(BF_4)_2$ displays two quasi-reversible cathodic processes at –0.34V (ΔE = 170 mV) and –0.53V versus NHE (ΔE = 100 mV) in CH_3CN (fig. S4 and table S1) (*27*). Addition of a triflate (OTf) salt of protonated dimethylformamide (DMF) [[DMFH]OTf/DMF 1:1 mol/mol, pK_a = 6.1 in CH_3CN (where K_a is the acid dissociation constant), $E°([DMFH]^+/H_2)$ = –0.08 V versus NHE] as an acid source triggers the appearance of an electrocatalytic wave at $E_{1/2}$ = –0.30 V versus NHE assigned to hydrogen evolution (fig. S5). This electrocatalytic behavior is similar to that of the parent complex containing the unfunctionalized 1,3,5,7-tetraphenyl-1,5-diaza-3,7-diphosphacyclooctane ligand (*11*) with respect to redox potential as well as catalytic current enhancement, expressed as the i_c/i_p ratio [where i_c is the catalytic current and i_p is the peak current associated with the $Ni^{II/I}$ couple]. This ratio varies linearly with acid concentration and reaches a plateau at i_c/i_p = 5 and [$DMFH^+$] = 5 mM (fig. S6). The parent complex behaved similarly but plateaued at [$DMFH^+$] = 300 mM and i_c/i_p = 50 (*11*). This difference might arise from the presence of the four bulky anchor groups in **2**$(BF_4)_2$, which slow down the conformational changes required during the catalytic cycle so as to position the proton relays in the vicinity of the metal active site.

Compound **2**$(BF_4)_2$ was successfully anchored to the amino-functionalized electrode in room-temperature CH_3CN through the formation, in the presence of Et_3N, of amide linkages between the ligand of **2**$(BF_4)_2$ and the grafted amine residues. A schematic representation of the resulting functionalized CNTs film is displayed in Fig. 1. The material was characterized by means of CV in CH_3CN and XPS. The cyclic voltammogram (black trace in Fig. 3A) displays a cathodic process at –0.59 V versus NHE (ΔE = 120 mV) assigned to the reduction of the grafted Ni^{II} complex. This signal probably corresponds to a combination of the two monoelectronic waves formerly observed in solution. We posit that these features merge because the first electron transfer step has been slowed, and the corresponding potential shifted to a more negative value, upon complex grafting as a result of an increased reorganization energy of the nickel coordination sphere (*28*). Surface catalyst concentration as high as 1.5 (±0.5) × 10^{-9} mol cm^{-2} could be estimated from the integration of this wave. For comparison, rough ITO electrodes directly functionalized with **2**$(BF_4)_2$ through the reduction of the diazonium salt **1**$(BF_4)_2$ by using the same two-step procedure exhibit surface nickel concentrations in the range of 4.5 (±1.5) × 10^{-11} mol cm^{-2}. The high specific surface provided by the film of MWCNTs thus raises catalyst concentration by almost two orders of magnitude. This difference was reflected in the much larger current response observed in the CV of the Ni-functionalized ITO/MWCNT electrode as compared with a Ni-functionalized ITO electrode (fig. S7).

XPS analysis (Fig. 2 and fig. S8) confirms the presence of the intact nickel complex at the surface of the electrode. Analysis of the Ni $2p_{3/2}$ region shows one sharp peak centered at 856.0 eV, which is a signature of the Ni^{II} ion, whereas the P 2p peak centered at 132.2 eV confirms the presence of metal-bound phosphorous atoms.

Protonation of the grafted nickel complex occurs upon addition of [DMFH]OTf/DMF (1:1 mol/mol) and results in the observation of an irreversible reductive process (E_p^c = –0.31 V versus NHE) 280 mV more positive than that exhibited by grafted **2**$(BF_4)_2$ (Fig. 3A). The electrocatalytic nature of this wave is evidenced by the linear increase of the normalized peak current (i_c/i_p) with increased acid concentration (fig. S9). The electrocatalytic properties of the nickel complex are thus retained in the grafted material, and the electroconductive properties of the MWCNTs induce

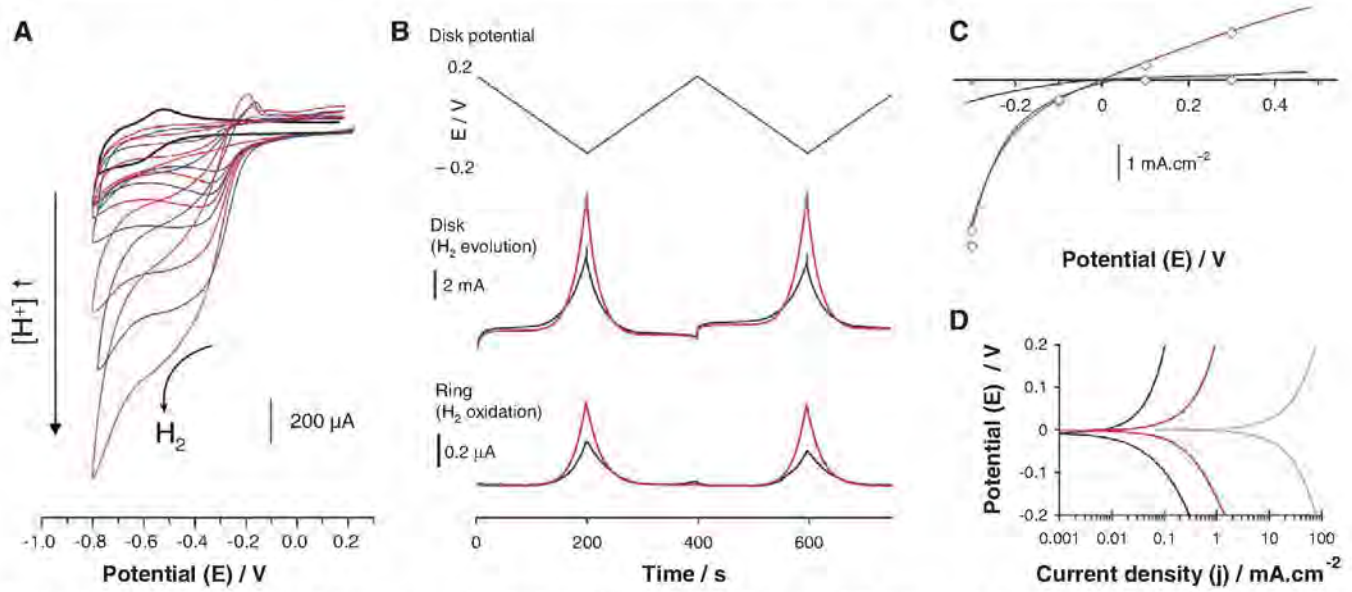

Fig. 3. (**A**) Electrocatalytic behavior of a nickel functionalized ITO/MWCNT electrode (1 cm^2) in CH_3CN with 0.2 M Bu_4NPF_6 electrolyte at various concentrations of the acid 1:1 mol/mol [DMFH]OTf/DMF (0.29, 0.60, 0.90, 1.17, 1.75, 2.34, 3.51, 5.85, and 11.7 mM) (50 mV s^{-1} scan rate). The cyclic voltammogram recorded in the absence of acid is shown in black. (**B**) Rotating ring-disk electrode measurements (5 mV s^{-1}) of hydrogen evolution from a 0.5 M H_2SO_4 aqueous solution on MWCNTs (black) and Ni-functionalized MWCNTs (red) coated with Nafion on a glassy carbon electrode. (Top) Disk potential. (Middle) Disk current density. (Bottom) Pt-ring current (the Pt-ring was held at 0.6 V). (**C**) Evolution of current density as a function of potential for both hydrogen production and uptake from a 0.5 M H_2SO_4 aqueous solution, recorded at a MEA consisting of a GDL assembled with a Nafion membrane (2 mV s^{-1}). Black, unfunctionalized GDL; blue, Ni-functionalized GDL/MWCNT under an atmosphere of N_2; red, Ni-functionalized GDL/MWCNT under an atmosphere of H_2 (10^5 Pa). The *x* axis is positioned at 0 current density. Dots represent stabilized values of current at electrodes set for 10 min at various potentials. (**D**) Logarithmic plots of current density as a function of the potential for both hydrogen production and uptake. The black and red traces correspond to the measurements shown in (C) with the same colors; the gray trace is a measurement on a commercial MEA containing highly dispersed platinum (0.5 mg_{Pt} cm^{-2}). Similar logarithmic plots are obtained when Ni-functionalized MWCNTs are deposited on a glassy carbon disk electrode. Potentials are quoted versus NHE.

a remarkably low overvoltage (200 mV) for hydrogen evolution. For comparison, pristine MWCNTs mediate hydrogen evolution from the same medium at –0.7 V versus NHE (fig. S10), corresponding to a much larger overvoltage (600 mV).

The material's stability and associated ability to catalyze sustained production of H_2 was investigated by means of controlled-potential coulometry experiments in nonaqueous media. The electrolysis of a CH_3CN solution of [DMFH]OTf/DMF (1:1 mol/mol, 0.1 mol.L^{-1}) was performed at a potential of –0.5 V versus NHE in an electrochemical cell coupled to a U-tube for volumetric analysis and a gas chromatograph equipped with a catharometer for hydrogen detection. Under these conditions, H_2 is produced with a sustained current density (J) of 2 mA cm^{-2}. XPS analysis performed after a 1-hour electrolysis experiment confirmed the presence of a molecular nickel-phosphine complex. A >94% faradaic yield can be estimated from the charge (3 C) passed through the electrode (0.5 cm^2) and the amount of hydrogen (15 mmol) produced within 1 hour. Using the surface concentration of the catalyst estimated earlier [$1.5 (\pm 0.5) \times 10^{-9}$ mol.cm^{-2}] affords a turnover number of 20,000 (±30%) achieved within 1 hour. For comparison, previously reported stable molecular catalytic materials based on cobalt porphyrins (*29*) or organometallic rhodium complexes (*30*), incorporated in a Nafion membrane or polypyrrole film, show overvoltages greater than 400 mV or turnover frequencies limited to a few tenths per hour.

Practical applications of such molecular electrode materials require the use of aqueous electrolytes. Catalytic hydrogen production from diluted (pH of 0 to 1) sulfuric acid solutions was demonstrated in two ways. First, we dropcoated an ink made of Ni-functionalized MWCNTs (50 μg) dispersed in a 5 weight percent solution [Nafion dispersion type D520 (DuPont, Wilmington, Delaware)] onto a glassy carbon-disc electrode. After drying, rotating electrode measurements (Fig. 3B) confirmed that H_2 can be produced on the disc electrode and simultaneously detected at a concentric platinum ring held at 0.6 V versus NHE. Analysis of the voltammograms revealed that electrocatalytic hydrogen evolution occurred with an overvoltage of 20 mV, less than a sixth of that observed on pristine MWCNTs (128 mV). Second, we assayed our material in a half-cell configuration, reproducing the experimental conditions found in state-of-the-art proton exchange membrane (PEM) electrolyzers but with the platinum-based active layer replaced by Ni-functionalized MWCNTs. A membrane-electrode assembly (MEA) prepared for that purpose consisted of a Nafion membrane hot-pressed with a gas diffusion layer (GDL), on which the MWCNTs were deposited and further functionalized with $\mathbf{2}(BF_4)_2$. This MEA displayed an electrocatalytic activity for hydrogen evolution much higher than that of unfunctionalized GDL or pristine MWCNTs deposited on GDL under similar conditions (Fig. 3C). A current density of about 4 mA cm^{-2} was measured at 300 mV overvoltage. The stabilized current values measured at a MEA after holding for 10 min at various potentials matched those of the initial voltammogram. This evidence of catalyst stability precludes the formation of nickel-based particles as the catalytically active species. In any case, from the Pourbaix diagram, either nickel oxide/hydroxide compounds or elemental nickel would be unstable under the assay conditions. This MEA was held at –300 mV versus NHE in 0.5 M H_2SO_4 for 10 hours. The current density keeps constant throughout the experiment, with more than 100,000 (±30%) turnovers achieved (fig. S12). Hydrogen evolution was monitored by using gas chromatography during the first 30 min and was found to occur with a quantitative faradaic yield.

The unexpectedly low overvoltage observed here for hydrogen production prompted us to explore this material as a catalyst for the reverse reaction, catalytic hydrogen oxidation. The same membrane-electrode assembly was assayed under the same conditions as described above, except that a hydrogen atmosphere was used instead of nitrogen. In the corresponding voltammogram (Fig. 3C), the cathodic response—hydrogen production—is almost unchanged. However, the anodic wave indicates hydrogen oxidation with a current density of about 2 mA cm^{-2} at 500 mV overvoltage, similar to that found for hydrogenase-modified carbon material such as carbon felt (*31*) or MWCNT electrodes (*21*). The catalytic current, recorded at a lower overvoltage (300 mV), is stable during a 10-hour electrolysis experiment, corresponding to 35,000 (±30%) turnovers (fig. S12). The shape of the voltammogram for positive potentials indicates a kinetic limitation due to the diffusion of hydrogen at the grafted active sites. The same effect has been observed for immobilized hydrogenases (*5*). A logarithmic plot of the current density as a function of potential (Fig. 3D) highlights the transition between H_2 oxidation and production. The point of 0 current density nearly overlaps the standard potential of the H^+/H_2 couple under the experimental conditions, thus confirming the low overvoltage of our Ni-functionalized MEA for H^+/H_2 interconversion. Figure 3D also compares our MEA with a commercial MEA containing highly dispersed platinum (0.5 mg Pt cm^{-2}), which exhibits a current density about two orders of magnitude higher than that of the Ni/MWCNT system. This performance discrepancy is nonetheless balanced by the fact that the latter catalyst loading is limited to 0.06 mg cm^{-2} of an earth-abundant metal. Our results show that the biomimetic nanomaterial reported here offers promising turnover rates under conditions compatible with widespread PEM technology on the basis of commercial proton exchange membranes in acidic electrolytes.

References and Notes

1. R. Bashyam, P. Zelenay, *Nature* **443**, 63 (2006).
2. A. Volbeda *et al.*, *Nature* **373**, 580 (1995).
3. J. W. Peters, W. N. Lanzilotta, B. J. Lemon, L. C. Seefeldt, *Science* **282**, 1853 (1998).
4. V. Artero, M. Fontecave, *Coord. Chem. Rev.* **249**, 1518 (2005).
5. K. A. Vincent, A. Parkin, F. A. Armstrong, *Chem. Rev.* **107**, 4366 (2007).
6. S. Canaguier, V. Artero, M. Fontecave, *Dalton Trans.* 315 (2008).
7. J. C. Fontecilla-Camps, A. Volbeda, C. Cavazza, Y. Nicolet, *Chem. Rev.* **107**, 5411 (2007).
8. C. Tard *et al.*, *Nature* **433**, 610 (2005).
9. S. Ogo *et al.*, *Science* **316**, 585 (2007).
10. C. Mealli, T. B. Rauchfuss, *Angew. Chem. Int. Ed.* **46**, 8942 (2007).
11. A. D. Wilson *et al.*, *Proc. Natl. Acad. Sci. U.S.A.* **104**, 6951 (2007).
12. Z. L. Li, Y. Ohki, K. Tatsumi, *J. Am. Chem. Soc.* **127**, 8950 (2005).
13. M. L. Singleton, N. Bhuvanesh, J. H. Reibenspies, M. Y. Darensbourg, *Angew. Chem. Int. Ed.* **47**, 9492 (2008).
14. A. D. Wilson *et al.*, *J. Am. Chem. Soc.* **128**, 358 (2006).
15. The exact nature of this basic site at the active site of FeFe hydrogenases has been subject to debate, but recent spectroscopic data are in favor of a nitrogen atom (*32*).
16. D. Tasis, N. Tagmatarchis, A. Bianco, M. Prato, *Chem. Rev.* **106**, 1105 (2006).
17. V. Sgobba, D. M. Guldi, *Chem. Soc. Rev.* **38**, 165 (2009).
18. B. Jousselme *et al.*, *J. Electroanal. Chem.* **621**, 277 (2008).
19. J. Pinson, F. Podvorica, *Chem. Soc. Rev.* **34**, 429 (2005).
20. J. L. Bahr *et al.*, *J. Am. Chem. Soc.* **123**, 6536 (2001).
21. M. A. Alonso-Lomillo *et al.*, *Nano Lett.* **7**, 1603 (2007).
22. We chose MWCNTs for their metallic electron conductivity. In addition, they do not require noble metal catalysts for growth and can be easily obtained in high purity.
23. Z. C. Wu *et al.*, *Science* **305**, 1273 (2004).
24. Materials and methods are available as supporting material on *Science* Online.
25. S. Griveau, D. Mercier, C. Vautrin-Ul, A. Chaussé, *Electrochem. Commun.* **9**, 2768 (2007).
26. Alternatively, electrografting can be achieved at a fixed potential of 0.16 V versus NHE with a total charge of 15 mC passed through a 1 cm^2 electrode.
27. Bulk electrolysis of $\mathbf{2}(BF_4)_2$ carried out at –0.75 V versus NHE in CH_3CN confirmed an overall two-electron reduction process, with 1.83 electrons per complex passing through the cell within 3 hours.
28. To support this assignment, we performed a control experiment that entailed grafting a ferrocene derivative, possessing the same activated ester function, instead of the nickel complex. The yield of the second step in the functionalization procedure is probably the same for both complexes. In that case, the typical monoelectronic quasi-reversible process is observed in CH_3CN at 420 mV versus NHE. Integration area of the anodic peak is about half of that obtained with the nickel complex.
29. T. Abe *et al.*, *Polym. Adv. Technol.* **9**, 559 (1998).
30. S. Cosnier, A. Deronzier, N. Vlachopoulos, *J. Chem. Soc. Chem. Commun.* 1259 (1989).
31. M. Hambourger *et al.*, *J. Am. Chem. Soc.* **130**, 2015 (2008).
32. A. Silakov, B. Wenk, E. Reijerse, W. Lubitz, *Phys. Chem. Chem. Phys.* **11**, 6592 (2009).

33. This work was supported by the CEA (Nanosciences program, grant Grafthydro), the CNRS ("Materials" program, grant 961 "projets exploratoires: Interface Science des Matériaux/Vivant") and the Agence Nationale de la Recherche (PAN-H 2008, EnzHyd). The authors thank E. Mayousse and P.-A. Jacques for experimental contribution and V. Derycke for assistance in the SEM characterizations. The authors have filed a European patent application (EP-08 290 988.8) for the grafting procedure of catalysts presented here.

Supporting Online Material

www.sciencemag.org/cgi/content/full/326/5958/1384/DC1
Materials and Methods
Figs. S1 to S12
Table S1
References

28 July 2009; accepted 13 October 2009
10.1126/science.1179773

Mantle Shear-Wave Velocity Structure Beneath the Hawaiian Hot Spot

Cecily J. Wolfe,[1]* Sean C. Solomon,[2] Gabi Laske,[3] John A. Collins,[4] Robert S. Detrick,[4] John A. Orcutt,[3] David Bercovici,[5] Erik H. Hauri[2]

Defining the mantle structure that lies beneath hot spots is important for revealing their depth of origin. Three-dimensional images of shear-wave velocity beneath the Hawaiian Islands, obtained from a network of sea-floor and land seismometers, show an upper-mantle low-velocity anomaly that is elongated in the direction of the island chain and surrounded by a parabola-shaped high-velocity anomaly. Low velocities continue downward to the mantle transition zone between 410 and 660 kilometers depth, a result that is in agreement with prior observations of transition-zone thinning. The inclusion of *SKS* observations extends the resolution downward to a depth of 1500 kilometers and reveals a several-hundred-kilometer-wide region of low velocities beneath and southeast of Hawaii. These images suggest that the Hawaiian hot spot is the result of an upwelling high-temperature plume from the lower mantle.

Hawaii is the archetypal hot spot and has been suggested to be the surface expression of a mantle plume: a localized upwelling of hot buoyant material from Earth's deep mantle (*1*, *2*), although such an origin has been debated. The Hawaiian-Emperor chain of islands and seamounts spans thousands of kilometers; records age-progressive volcanism for >75 million years (*3*); and exhibits a broad ~1000-km-wide region of elevated topography, known as the Hawaiian Swell (Fig. 1A), that surrounds the locus of current volcanism. Estimated to transport a larger buoyancy flux than any other active plume (*4*, *5*), the Hawaiian hot spot has been the focus of numerous geochemical and geodynamical studies [for example, (*4*–*10*)] that attempted to resolve its origin. One of the most straightforward indications of whether a hot spot is the result of a plume is the presence of a narrow, vertically continuous zone of low seismic velocities in the underlying mantle, indicative of higher-than-normal temperatures, anomalous mantle composition, or melt (*11*, *12*).

Global seismic tomography suggests that low seismic velocities may extend from the upper to the lower mantle beneath the Hawaiian hot spot (*13*–*15*), but there remains doubt about how well, and to what depth, narrow plumes may be resolved by such methods (*16*, *17*). Moreover, global models of mantle structure are limited in their resolution near Hawaii by the sparseness of wave paths, given the lack of seismic stations on the ocean floor and the great distances between the islands and most circum-Pacific earthquake sources. Previous investigations of mantle structure near Hawaii using island stations (*18*–*20*) or sea-floor deployments of instruments (*21*, *22*) have been limited in geographic coverage and numbers of instruments. Such experiments have not yielded the high-resolution regional tomographic models needed to settle the debate over even such a basic question as whether the upper mantle beneath the Hawaiian Islands is marked by low seismic velocities and higher-than-normal temperatures, as suggested by some studies (*13*–*15*, *19*), or not, as implied by others [for example, (*23*)].

Here we report results from the Hawaiian Plume-Lithosphere Undersea Melt Experiment (PLUME), which was designed to determine at high resolution the mantle seismic velocity structure beneath the Hawaiian hot spot, to assess the hypothesis that the hot spot is the product of an upwelling plume, and to determine how mantle flow may interact with the overlying lithosphere to generate the Hawaiian Swell. The experiment featured a dense, large-aperture seismic network consisting of two year-long deployments of three dozen broadband ocean-bottom seismometers (OBSs) and the concurrent deployment of 10 portable broadband seismometers on the Hawaiian Islands (Fig. 1A), with all instruments operating continuously to record teleseismic and local earthquakes. During the experiment period, 2146 *S*-wave relative arrival times (direct *S* and *SKS* phases) were collected from 97 earthquakes (*24*) (fig. S1) and corrected for estimated variations in station elevation and crustal thickness. Corrected mean station delay patterns reflect upper-mantle heterogeneity and indicate relatively low velocities beneath and to the west of the Hawaiian Islands and high velocities east of Hawaii and at distant stations around the margins of the swell (Fig. 1B).

The arrival times were inverted for *S*-wave velocity heterogeneity, damped earthquake relocations, and origin time terms using finite-frequency (*13*, *25*) methods. Because of the large station spacing, crossing wave paths were lacking, and vertical resolution was limited in the uppermost mantle. One strategy to mitigate the effect of smearing strong, shallow heterogeneity deeper into a model is to include station terms to partially absorb the effect of shallow structure, but this approach comes at the expense of decreased resolution at shallow depths, and tests indicate that station terms may not successfully absorb structure at depths of 100 to 200 km if such variations are extremely strong. We therefore performed inversions both with (Fig. 2 and fig. S6) and without (Fig. 2 and figs. S7 and S8) station terms. In both cases, a low-velocity anomaly was well resolved in the upper mantle beneath Hawaii and was elongated in a southeast-northwest direction parallel to the Hawaiian Islands. As expected, the

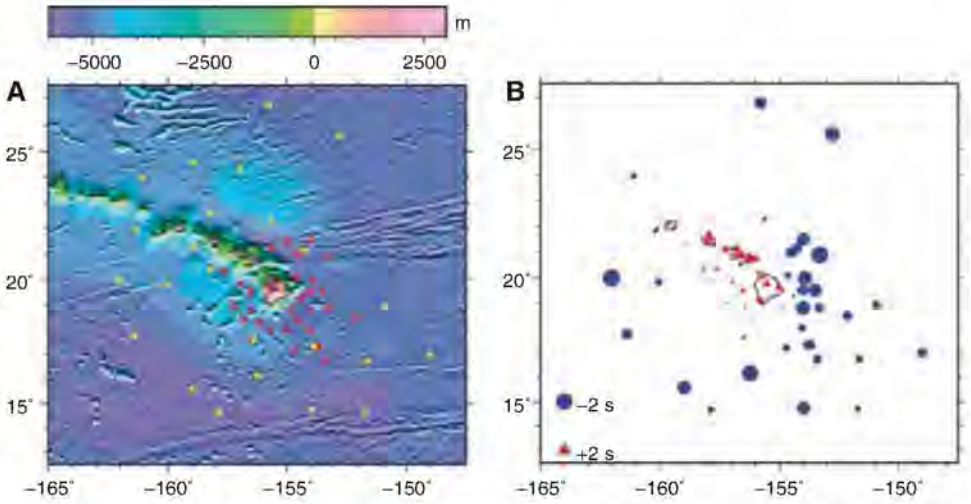

Fig. 1. **(A)** Locations of seismometers used in *S*-wave tomography. Land stations are indicated by blue triangles and OBSs are indicated by red (first deployment; 2005 to 2006) or yellow (second deployment; 2006 to 2007) circles. Only stations that successfully recorded two horizontal components are shown. Bathymetry is taken from (*30*). **(B)** Corrected mean station delays, adjusted to vertical incidence. Early arrivals are shown by blue circles and late arrivals by red triangles, with symbol size scaled linearly to the magnitude of the delay (see scale at lower left).

[1]Hawaii Institute of Geophysics and Planetology, University of Hawaii at Manoa, Honolulu, HI 96822, USA. [2]Department of Terrestrial Magnetism, Carnegie Institution of Washington, Washington, DC 20015, USA. [3]Cecil H. and Ida M. Green Institute of Geophysics and Planetary Physics, Scripps Institution of Oceanography, San Diego, CA 92093, USA. [4]Woods Hole Oceanographic Institution, Woods Hole, MA 02543, USA. [5]Department of Geology and Geophysics, Yale University, New Haven, CT 06520, USA.

*To whom correspondence should be addressed. E-mail: cecily@soest.hawaii.edu

amplitude of upper-mantle heterogeneity was larger in inversions without station terms. A parabola-shaped region of higher-than-average seismic velocity along the edge of the Hawaiian Swell was also observed to extend downward to 300 km depth, although patterns outside its boundaries were constrained only to the southeast, where station coverage extends beyond its edge. Low velocities beneath Hawaii continue into the transition zone, and inversions resolved a broad region of low velocities in the lower mantle from 700 to 1500 km depth southeast of Hawaii (Fig. 3).

The vertical extent of upper mantle structure is not well constrained by our *S*-wave data alone, as illustrated by a two-step inversion (fig. S9). In the first step, we inverted for a model in which all structure was "squeezed" between 50 and 250 km depth. In the second step, we corrected the observations for the effects of the squeezed model and inverted for an additional residual model. The two-step model continued to recover a low-velocity anomaly in the transition zone, and the model deeper than 500 km remained virtually unchanged, but much of the heterogeneity at 300 km depth can be squeezed to shallower depths. Given the tradeoffs between the amplitude and the depth interval of heterogeneity, however, lateral variations at 100 to 200 km depth in this two-step model were extremely large at ±8%. Although reconciliation with surface-wave observations is needed to provide firm limits on the lateral variation in upper-mantle seismic velocities and help resolve these ambiguities, prior surface-wave observations (*21*) and analysis of PLUME data to date indicate mantle *S*-wave velocity heterogeneity of no more than ±4% in the depth interval from 60 to 140 km and are thus inconsistent with the large variations recovered in the two-step model.

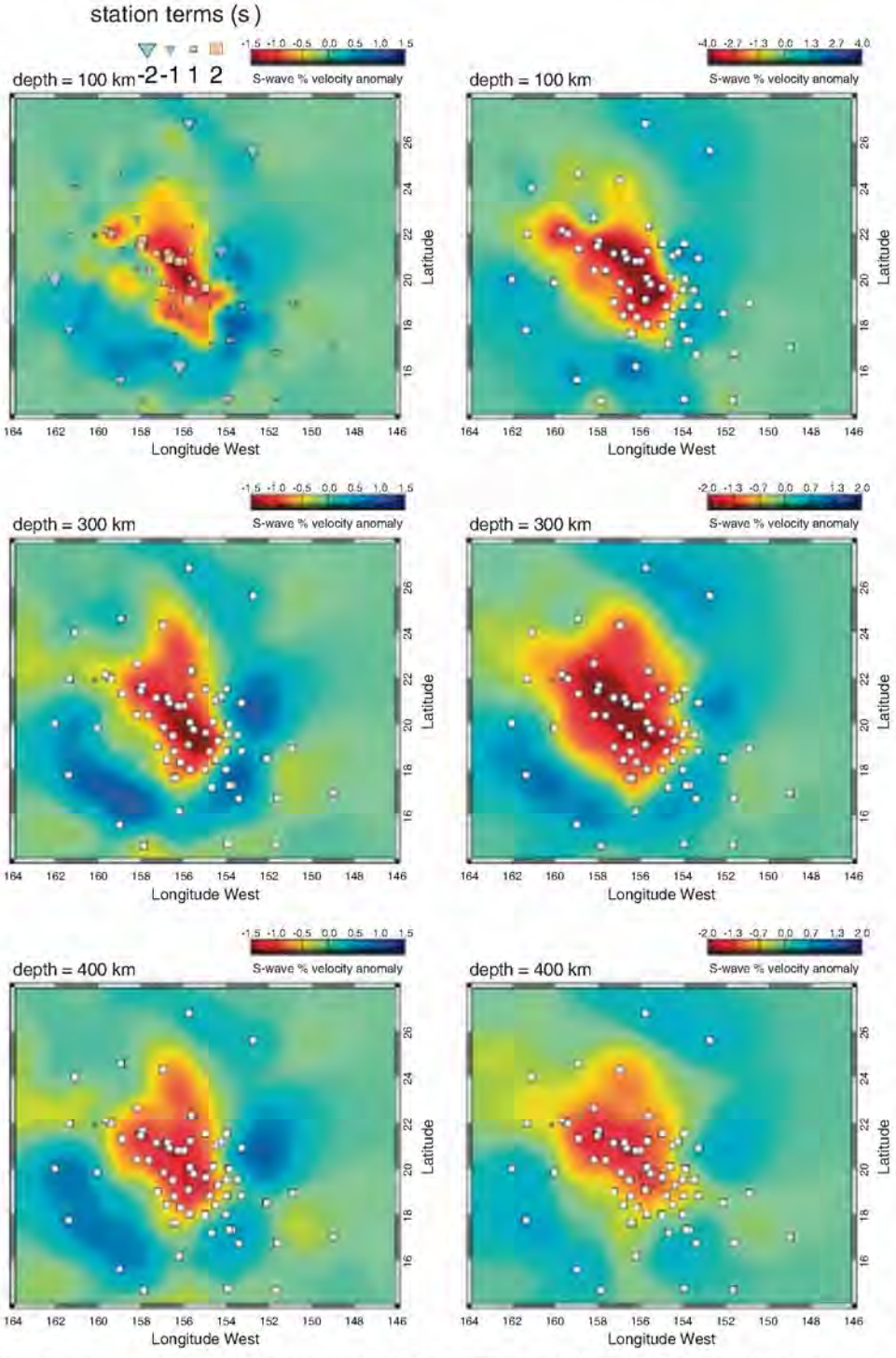

Fig. 2. Upper-mantle velocity heterogeneity at (**top**) 100, (**middle**) 300, and (**bottom**) 400 km depth. The scale of heterogeneity is indicated in the upper right corner of each panel. The left column displays solutions from an inversion with station terms; the right column shows the results of an inversion without station terms.

SKS waves have steeper arrival angles than direct *S* waves do and thus provide wave paths that sample the lower mantle beneath Hawaii (fig. S2). To test how the subset of *SKS* data contributes to the resolution of lower-mantle structure, we performed inversions in which *SKS* phases were excluded (figs. S11 and S12). Direct *S* waves from the first deployment dominantly constrained the low-velocity anomaly in the upper mantle beneath and around the main Hawaiian Islands, but these inversions had less structure in the mantle transition zone (410 to 660 km depth) and negligible lower mantle structure (fig. S11). Including direct *S*-wave data from the second OBS deployment extended the spatial region of the model and improved resolution of the low-velocity anomaly in the upper mantle and transition zone (fig. S12), but lower-mantle heterogeneity remained small. These tests indicate that low velocities in the lower mantle beneath Hawaii are not artifacts of vertical smearing of strong upper-mantle heterogeneity, but instead are driven by the resolving power of *SKS* arrival times. The existence and southeastern position of the lower-mantle anomaly constrained by *SKS* data were affected, however, by the solution for shallower upper-mantle structure (*24*). Heterogeneity deeper than 1500 km is not required by our data alone, but the eventual incorporation of PLUME data into global models may extend the resolution to greater depths. Montelli *et al.* (*13*, *14*) imaged a broad region of low velocities beneath Hawaii that extended downward to 1900 km depth in their global *S*-wave model and to the core/mantle boundary in their *P*-wave model. Our low-velocity anomaly is narrower than the ~10°-wide anomaly displayed by Montelli *et al.* (*13*, *14*), which is probably an indication of the improved horizontal resolution provided by the PLUME data. Resolution tests conducted with a wide variety of cylindrical and checkerboard structures (figs. S16 to S28) demonstrate that the PLUME data set resolves both upper- and lower-mantle structure at the level of our interpretations. One possible biasing effect on our solutions in the lower mantle, however, may come from undetermined structure near the core/mantle boundary

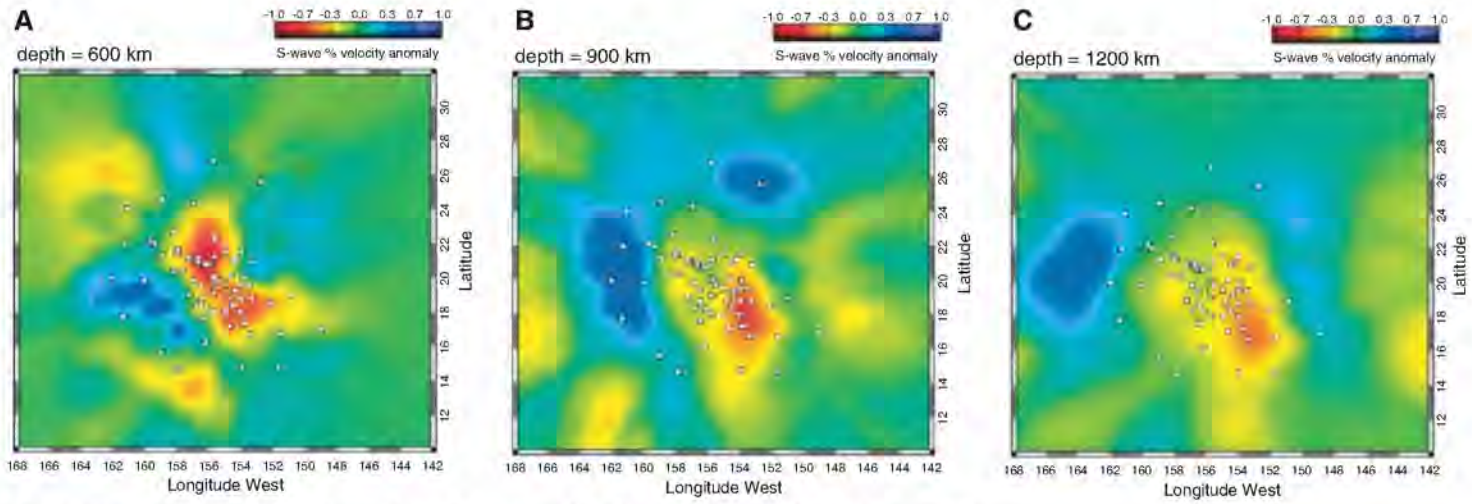

Fig. 3. Velocity heterogeneity (without station terms) at **(A)** 600, **(B)** 900, and **(C)** 1200 km depth.

(*24*), where steep lateral velocity gradients have been observed at the edges of the Pacific large low-shear-velocity province (*26*).

Our results improve the fidelity of *S*-wave mantle imaging around Hawaii as compared with previous efforts and suggest that the upper mantle beneath the islands is characterized by low seismic velocities and, by inference, anomalously high temperatures. The peak-to-peak 3% velocity variations that we imaged at 300 km depth in inversions with station terms corresponds to a temperature variation across the model of 250°C, and the 1.5% contrast near 900 km depth corresponds to a temperature variation of 300°C (*24*). These values are consistent with prior petrologic and geodynamic inferences of a high-temperature plume beneath the Hawaiian hot spot (*4*–*6*, *10*, *27*).

In terms of plume dynamics, the broad, low-velocity anomaly at shallow mantle depths (<200 km) beneath the islands (Figs. 1 and 2) is in agreement with the prediction from geodynamic models of a "pancake" of high-temperature material as the plume impacts and spreads laterally beneath the rigid lithosphere. Some geodynamic models (*6*, *10*) also predict a parabola-shaped curtain of cold downwelling material that isolates plume flow from the surrounding mantle, which is consistent with the parabola-shaped volume of high upper-mantle velocities imaged in our models. Delay patterns display asymmetry around the island of Hawaii (Fig. 1), with greater delays in the western offshore region between Hawaii and Maui (where bathymetry is correspondingly shallower) and earlier arrivals to the east (where the sea floor is deeper). These coupled characteristics of seismic velocity and sea-floor topography probably reflect three-dimensional complexities in uppermost mantle flow and melting (*10*) and provide constraints for improving geodynamic models to resolve finer details of how shallow mantle flow generates uplift and magmatism.

At greater depths, velocity heterogeneity (±1%) within the mantle transition zone is consistent with prior observations of transition-zone thinning along the island chain (*20*, *22*), interpreted as reflecting higher-than-normal temperatures. Although a thermal boundary layer near the base of the transition zone has been suggested as a candidate source region for some plumes, our images display low velocities continuing into the lower mantle, suggesting that the source region for the Hawaiian plume is at still greater depth in the lower mantle. The southeastern location of the center of low velocities is consistent with geodynamic arguments that plume conduits may be tilted by advection within a large-scale mantle flow field (*28*), and the large horizontal aperture of the anomaly is in agreement with predictions that a plume may be wider in the lower mantle because of greater viscosity than in the upper mantle (*29*).

Because Hawaiian lavas are chemically distinct (*7*–*9*) from mid-ocean ridge basalts, both temperature and compositional variations may also contribute to seismic heterogeneity, and the geodynamic characteristics of thermochemical plumes can deviate from the classic features of thermal plumes (*12*). Nonetheless, many aspects of the *S*-wave images derived from the PLUME observations conform to the expected signatures of the mantle plume model.

References and Notes

1. J. T. Wilson, *Can. J. Phys.* **42**, 893 (1963).
2. W. J. Morgan, *Nature* **230**, 42 (1971).
3. R. A. Duncan, R. A. Keller, *Geochem. Geophys. Geosyst.* **5**, Q08L03 (2004).
4. G. F. Davies, *J. Geophys. Res.* **93**, 10467 (1988).
5. N. H. Sleep, *J. Geophys. Res.* **95**, 6715 (1990).
6. N. M. Ribe, U. R. Christensen, *J. Geophys. Res.* **99**, 669 (1994).
7. E. H. Hauri, *Nature* **382**, 415 (1996).
8. A. V. Sobolev, A. W. Hofmann, S. V. Sobolev, I. K. Nikogosian, *Nature* **434**, 590 (2005).
9. M. D. Kurz, W. J. Jenkins, S. R. Hart, D. Clague, *Earth Planet. Sci. Lett.* **66**, 388 (1983).
10. W. B. Moore, G. Schubert, P. Tackley, *Science* **279**, 1008 (1998).
11. V. Courtillot, A. Davaille, J. Besse, J. Stock, *Earth Planet. Sci. Lett.* **205**, 295 (2003).
12. G. Ito, P. E. van Keken, in *Mantle Dynamics*, D. Bercovici, Ed., *Treatise on Geophysics* (Elsevier, New York, 2007), vol. 7, pp. 371–435.
13. R. Montelli *et al.*, *Science* **303**, 338 (2004).
14. R. Montelli, G. Nolet, F. A. Dahlen, G. Masters, *Geochem. Geophys. Geosyst.* **7**, Q11007 (2006).
15. C. Li, R. D. van der Hilst, E. R. Engdahl, S. Burdick, *Geochem. Geophys. Geosyst.* **9**, Q05018 (2008).
16. R. D. van der Hilst, M. V. de Hoop, *Geophys. J. Int.* **163**, 956 (2005).
17. L. Boschi, T. W. Becker, G. Soldati, A. M. Dziewonski, *Geophys. Res. Lett.* **33**, L06302 (2006).
18. X. Li *et al.*, *Nature* **405**, 938 (2000).
19. C. J. Wolfe, S. C. Solomon, P. G. Silver, R. M. Russo, J. C. VanDecar, *Earth Planet. Sci. Lett.* **198**, 129 (2002).
20. Y. Shen, C. J. Wolfe, S. C. Solomon, *Earth Planet. Sci. Lett.* **214**, 143 (2003).
21. G. Laske, J. Phipps Morgan, J. A. Orcutt, in *Plates, Plumes and Planetary Processes*, G. R. Foulger, D. M. Jurdy, Eds. (Special Paper 430, Geological Society of America, Boulder, CO, 2007), pp. 209–233.
22. J. A. Collins, F. L. Vernon, J. A. Orcutt, R. A. Stephen, *Geophys. Res. Lett.* **29**, 1522 (2002).
23. R. Katzman, L. Zhao, T. H. Jordan, *J. Geophys. Res.* **103**, 17933 (1998).
24. Materials and methods are available as supporting material on *Science* Online.
25. F. A. Dahlen, S.-H. Hung, G. Nolet, *Geophys. J. Int.* **141**, 157 (2000).
26. E. J. Garnero, T. Lay, A. McNamara, *Geol. Soc. Am. Spec. Paper* **430**, 79 (2007).
27. C. Herzberg *et al.*, *Geochem. Geophys. Geosyst.* **8**, Q02006 (2007).
28. M. A. Richards, R. W. Griffiths, *Geophys. J. Int.* **94**, 367 (1988).
29. P. E. van Keken, C. W. Gable, *J. Geophys. Res.* **100**, 7137 (1995).
30. W. H. F. Smith, D. T. Sandwell, *Science* **277**, 1956 (1997).

31. We are grateful to NSF for its support of this project. We thank G. Ito and M. Ballmer for helpful discussions, G. Nolet for input regarding methodology, and S. Grand for a copy of his global model. We also acknowledge the crews of the research vessels *Melville*, *Ka'imikai-O-Kanaloa*, and *Kilo Moana*; the *Jason* remotely operated vehicle team; the Ocean Bottom Seismograph Instrument Pool; the Carnegie Institution's portable seismology laboratory; and the hosts of temporary stations on the Hawaiian Islands. We thank L. Boschi and three anonymous reviewers for comments on earlier versions of this paper.

Supporting Online Material

www.sciencemag.org/cgi/content/full/326/5958/1388/DC1
Materials and Methods
SOM Text
Figs. S1 to S33
References

4 August 2009; accepted 8 October 2009
10.1126/science.1180165

Tracking the Variable North Atlantic Sink for Atmospheric CO_2

Andrew J. Watson,[1]* Ute Schuster,[1] Dorothee C. E. Bakker,[1] Nicholas R. Bates,[2] Antoine Corbière,[3] Melchor González-Dávila,[4] Tobias Friedrich,[5] Judith Hauck,[1]† Christoph Heinze,[6] Truls Johannessen,[6] Arne Körtzinger,[5] Nicolas Metzl,[3] Jon Olafsson,[7] Are Olsen,[6,8] Andreas Oschlies,[5] X. Antonio Padin,[9] Benjamin Pfeil,[6] J. Magdalena Santana-Casiano,[4] Tobias Steinhoff,[5] Maciej Telszewski,[1] Aida F. Rios,[9] Douglas W. R. Wallace,[5] Rik Wanninkhof[10]

The oceans are a major sink for atmospheric carbon dioxide (CO_2). Historically, observations have been too sparse to allow accurate tracking of changes in rates of CO_2 uptake over ocean basins, so little is known about how these vary. Here, we show observations indicating substantial variability in the CO_2 uptake by the North Atlantic on time scales of a few years. Further, we use measurements from a coordinated network of instrumented commercial ships to define the annual flux into the North Atlantic, for the year 2005, to a precision of about 10%. This approach offers the prospect of accurately monitoring the changing ocean CO_2 sink for those ocean basins that are well covered by shipping routes.

The natural sinks for atmospheric carbon dioxide have been of great importance in slowing the rate of anthropogenic climate change. Currently, humans emit ~8.5 Pg C $year^{-1}$ from fossil fuel and cement production, with another ~1.5 Pg C $year^{-1}$ produced by land use change (*1*). However, the net increase of the atmospheric concentration is only about half what it would be if all this CO_2 remained in the atmosphere. The remainder is taken up by land vegetation and the ocean in roughly equal measure, as evidenced by simultaneous observations of atmospheric oxygen and CO_2 (*2*). The ocean uptake of anthropogenically produced CO_2 is reducing the pH of surface waters, an acidification that is expected to have appreciable effects on the marine biota over this century (*3*).

Both ocean and land uptake is variable in space and time. Estimates of the magnitude and causes of temporal variations averaged over large areas have come from atmospheric observations in inverse models (*4*–*6*) and from ocean carbon models (*7*, *8*). The atmospheric inversions suggest that ocean regions such as the North Atlantic and Pacific, as well as continental land regions, exhibit variations in their annual fluxes that are a substantial fraction of their means. Ocean carbon cycle models usually suggest much smaller yearly and decadal changes (*7*), so it is not clear how much the ocean sinks actually vary. Neither is it clear whether the overall ocean sink is increasing or decreasing: Most models suggest that it should increase with time as atmospheric CO_2 continues to grow, but recent studies have suggested a "saturation" of the sink in the Southern Ocean (*5*). For the North Atlantic, observations suggest a decrease dating from ~1990 (*9*), especially between 1995–1996 and 2002–2005 (*10*). It has been suggested that such variation is linked to the dominant climate mode over the region, the North Atlantic Oscillation (NAO) (*8*, *10*), but the heterogeneous pattern of CO_2 in the surface ocean has made it difficult to unambiguously identify the nature of this connection. Ocean models forced with atmospheric variation are able to reproduce some of the observational trends, although usually at lower amplitude, and suggest complex patterns of variability within the basins (*8*).

Although the actual air-sea flux of CO_2 is difficult to measure directly, observations of sea-surface fugacity of CO_2 (fCO_2) can be used to infer it. In recent years, volunteer observing ships (VOS) plying regular routes have been instrumented to make such measurements, and there has been a rapid increase in the quantity of data available (*10*–*14*). Figure 1 presents annual flux estimates for the longest-running VOS, for the period 2002 to 2007, between northwestern Europe and the Caribbean [for details of flux calculations, see (*10*), modified as we describe in (*15*)]. A substantial variation in the annual fluxes is seen, more than a factor of two over this time period. The observations show decadal rather than interannual variability, with the flux rising and falling over several years. The variation is presumably climatically forced (*8*, *16*), although a relationship with the NAO is not immediately obvious.

The North Atlantic and Pacific are well covered by shipping, and networks of VOS in these oceans might form the backbone of an observing system to continuously monitor the air-sea exchange of carbon dioxide. In 2005, a trial of such a network in the North Atlantic was initiated under CarboOcean, a European Union–funded project, and here we use a year of observations to map the air-sea flux of the region and to evaluate the performance of the network. Figure 2A shows the location of the observations in 2005 on which our evaluation is based. These include VOS routes established specifically for the project (e.g., 1 and 4) and other routes and time series stations of longer establishment.

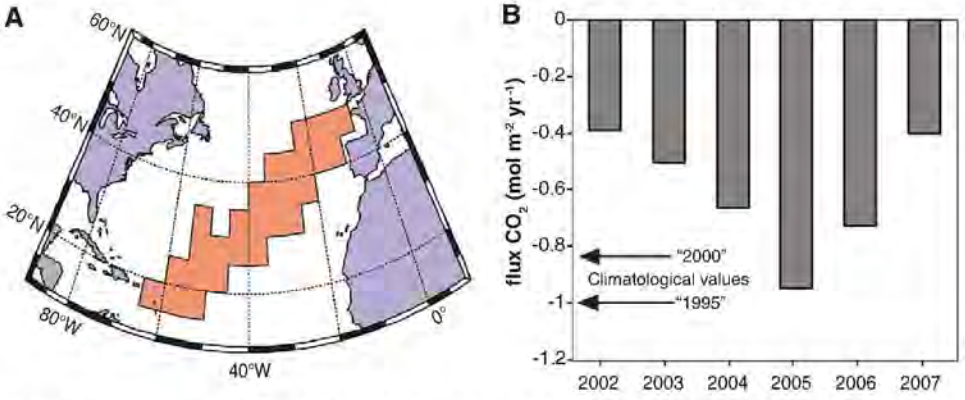

Fig. 1. Annual sea-air fluxes of CO_2 calculated from data on a shipping route between the United Kingdom and the Caribbean. Details of the data collection and the methods of calculating averages and fluxes are given in (*10*), modified as we describe in (*15*). (**A**) Mosaic of 5° by 5° tiles in which data coverage of the UK-Caribbean route is sufficient to calculate annual fluxes over the years 2002 to 2007. (**B**) Annual average fluxes for the enclosed area. The fluxes are negative (e.g., from air to sea), not only for the region as a whole but for every individual tile within it. Fluxes calculated using "climatological" values of air-sea fCO_2 gradient in this region, referenced to 2000 (*14*) or 1995 (*23*), are also indicated. Although these may be indicative of fluxes at these earlier times, they are not strictly applicable to any given year.

[1]School of Environmental Sciences, University of East Anglia, Norwich NR4 7TJ, UK. [2]Bermuda Biological Station for Research, Ferry Reach, GE01, Bermuda. [3]Laboratoire d'Océanographie et du Climat: Expérimentation et Approches Numériques Institut Pierre Simon Laplace, CNRS, Université Pierre et Marie Curie, Case 100, 4 Pl Jussieu, 75252 Paris, France. [4]Universidad de Las Palmas de Gran Canaria, Faculty of Marine Science, Department of Chemistry, Las Palmas, Gran Canaria, Spain. [5]Leibniz Institut für Meereswissenschaften, D-24105 Kiel, Germany. [6]University of Bergen, Geophysical Institute and Bjerknes Centre for Climate Research, Allégaten 55, N5007, Bergen, Norway. [7]Marine Research Institute and University of Iceland, Reykjavik, Iceland. [8]Department of Chemistry, University of Gothenburg, 41296, Göteborg, Sweden. [9]Consejo Superior de Investigaciones Científicas, Instituto de Investigaciones Marinas, Eduardo Cabello 6, Vigo 36208, Spain. [10]National Oceanic and Atmospheric Administration, Atlantic Oceanographic and Meteorological Laboratory, Miami, FL 33149, USA.

*To whom correspondence should be addressed. E-mail: a.watson@uea.ac.uk

†Present address: Alfred Wegener Institute for Polar and Marine Research, Postfach 12 01 61, 27515 Bremerhaven, Germany.

In total, about 125,000 measurements taken in 2005 have gone into this study. Figure 2B shows the locations of observations divided into 2-month periods, to indicate temporal coverage through 2005 (*15*).

To estimate basinwide fluxes, we constructed maps of sea-surface fCO_2 across the region and through time, by the method of developing relationships between the observed fCO_2 and independent variables, for which data products were available covering the entire domain. The variables chosen were sea surface temperature (SST) and mixed layer depth (MLD) (*15*). To obtain a data set of matched parameters from which to begin mappings, these fields were averaged or interpolated onto a 1° by 1° by once-per-day grid, and matched with fCO_2 measurements binned to the same grid, wherever they existed. Observations taken over shelf or shelf-break waters (water depth < 1000 m) were excluded. The rationale for the choice of SST and MLD is that fCO_2 is strongly influenced by temperature change and mixing with subsurface waters, which should be well captured by these variables. Satellite-derived chlorophyll was also initially included (as a proxy for biological activity), but it was found to be of limited utility in predicting fCO_2 and was finally dropped from the analysis. Two different mapping techniques were tested, one based on conventional multivariate linear regressions (MLR) applied after dividing the domain into subregions, and the other based on a self-organizing map (*17*) covering the entire spatial domain and year with a single map (*15*).

Fluxes were calculated from the mappings using the gas exchange equation $F = K\alpha\Delta fCO_2$. Here, $\Delta fCO_2 = fCO_{2surface} - fCO_{2atm}$ is the difference between sea-surface and atmospheric fCO_2, K is the gas transfer velocity (parameterized as a function of wind speed and temperature), and α is the solubility of CO_2 in the surface seawater. This approach has historically suffered from a lack of agreement between parameterizations of K derived from in situ measurements and those calibrated for agreement with the global bomb-derived ^{14}C budget. However, recent reanalysis of the ^{14}C budget has largely resolved these discrepancies (*18*, *19*), leading to increased confidence in estimates of CO_2 fluxes by this method. Parameterization of K used National Centers for Environmental Prediction/National

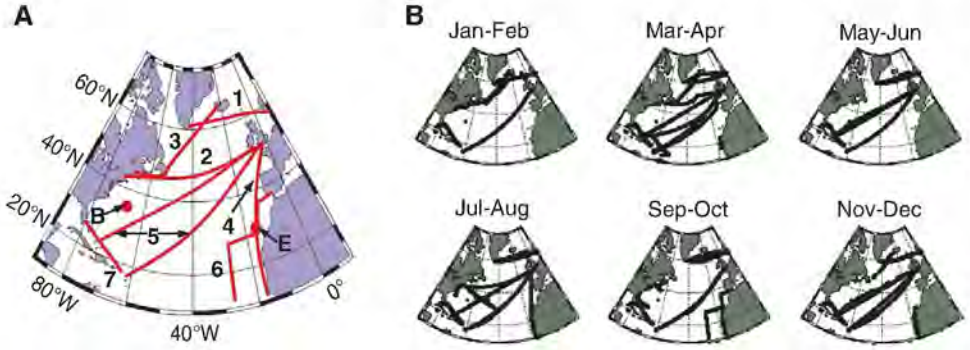

Fig. 2. (**A**) Location of regular VOS routes supplying data to the Carbo-Ocean network in 2005. Also shown are the locations of time series stations (B, Bermuda Atlantic time series station; E, European station for time series in the ocean, Canary Islands). (**B**) Post-plot of data binned into 2-month intervals through the year 2005.

Table 1. Integrated net ocean-to-atmosphere flux (10° to 65°N) across the North Atlantic in 2005. Values in the table are normalized to an area of 3.1 by 10^{13} m^2 for comparison (*15*). Pco_2, partial pressure of CO_2.

Method of interpolation	Value (Pg C $year^{-1}$)	Area average (mol m^{-2} $year^{-1}$)
MLR in 10° latitude bands	−0.274	−0.737
MLR in 20° latitude bands	−0.251	−0.675
MLR in 30° latitude bands	−0.246	−0.661
Self-organizing mapping	−0.238	−0.640
Mean	−0.252	−0.677
Standard deviation	0.015 (6.1%)	0.040
Using 1995 climatological ΔPco_2 values*	−0.340	−0.914
Using 2000 climatological ΔPco_2 values*	−0.300	−0.806

*Estimates made using climatological maps of ocean-atmosphere CO_2 gradient, which are based on analysis of observations spanning many decades, adjusted to 1995 or 2000 using assumptions described by Takahashi *et al.* (*14*, *23*). These flux estimates used identical gas transfer velocities (e.g., calculated using 2005 winds and temperatures) to the upper rows, so that the differences are due to the different ΔfCO_2 fields only. For methodological reasons (*14*), the 1995 climatological value may have overestimated the magnitude of the flux into regions north of 45°N. Both climatological estimates are based on compilations of data collected over decades and are therefore not precise estimates for a given year.

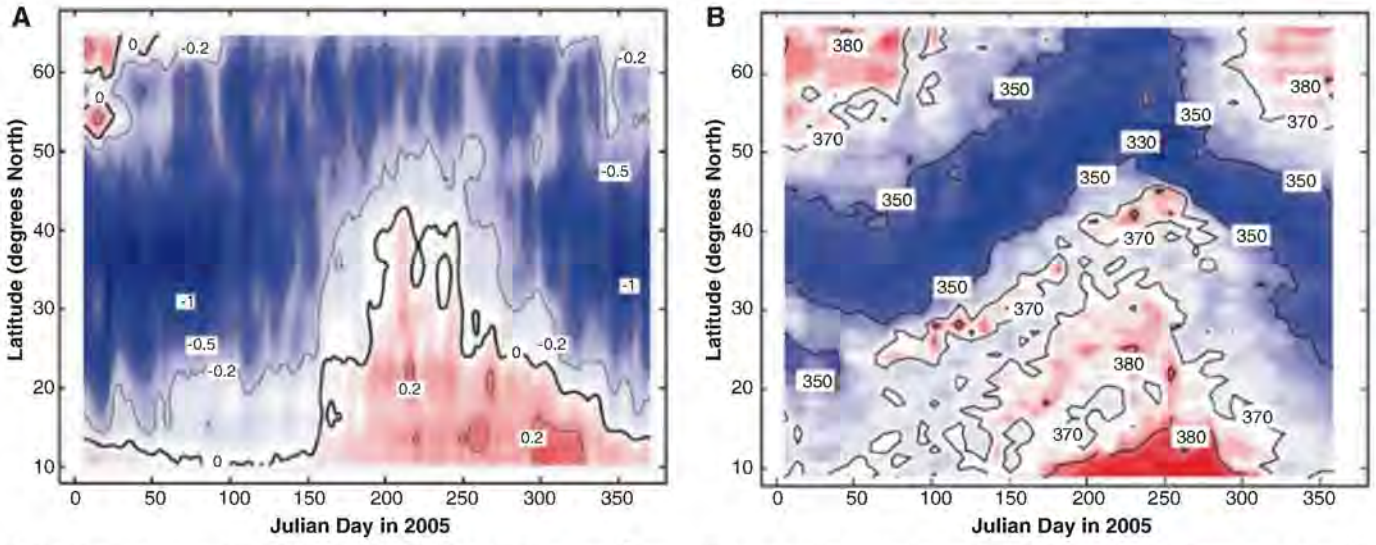

Fig. 3. Contours of ocean-atmosphere flux of CO_2 [(**A**), in Tmol $year^{-1}$ per degree of latitude] and surface ocean fCO_2 [(**B**), in μatm] in the North Atlantic in 2005, as a function of latitude and time. Fluxes are positive from sea to air. The color scheme shades regions of strong positive fluxes and high fCO_2 red, strong negative fluxes and low fCO_2 blue, and near-neutral regions white. The zero flux contour is shown thicker than the others.

Center for Atmospheric Research (NCEP/NCAR) 6-hour winds and surface temperatures (*20*) and the wind-speed relationship of Nightingale *et al.* (*21*). The use of winds with 6-hour time resolution captures the great majority of the short-term variation in gas flux (*15*, *22*).

Table 1 shows values of the flux integrated across the North Atlantic throughout the year 2005, for several different methods of mapping. The stability of the calculation gives us some confidence that the overall flux is well constrained by the observations, so is relatively insensitive to the details of the mapping technique. Shown for comparison are flux estimates using climatological values of fCO_2 referenced to 1995 (*23*) and to 2000 (*14*), but for the same area and using the identical 2005 gas transfer velocities as the observations, so that differences compared to the observations are entirely due to the ΔfCO_2 distribution. For the region as a whole, these both show substantially higher sink strengths. Within the restricted area of the time series in Fig. 1, the climatological values are similar to those of 2005 but considerably larger than other years. Taken together, therefore, these comparisons suggest a decline in sink strength from the 1990s to the present decade, but one which is nonuniform with location.

We used two methods to more formally estimate uncertainties: (i) application of geostatistical techniques, proceeding from semivariograms of the residual fCO_2 fields (*24*) and (ii) application of our methods to fCO_2 fields generated by an eddy-resolving biogeochemical ocean model of the North Atlantic (*25*). These two techniques have very different underlying assumptions. The second method, in particular, explicitly tests for bias introduced by the mapping techniques. Although the uncertainty on the flux at any given point is in general large (*26*), it decreases with integration over larger domains. Both our methods of estimating uncertainty indicate that, integrated over the North Atlantic from 10°N to 65°N, the 1-σ error on the annual mean fCO_2 is ~10% of ΔfCO_2, with somewhat smaller errors propagating through to the derived flux (*15*). The broad agreement between two uncertainty analyses having very different underlying assumptions gives us additional confidence in these estimates.

Year-to-year differences are dominated by variability in ΔfCO_2 (*10*). Hence, annual flux estimates from different years may also be compared with a precision of ~10%. The absolute values, however, have larger uncertainty because of the systematic error arising from the parameterization of gas transfer. Recent estimates for the global gas transfer rate appropriate to CO_2 span a range from 14.6 to 17.1 cm hour^{-1} (*18*, *19*, *27*) and suggest that there remains a ~20% uncertainty here. We therefore quote a flux of 0.25 ± 0.05 Pg C for the 10°N to 65°N region for 2005, where the uncertainty is approximately 1 σ. Our errors compare favorably with previous attempts to observationally constrain surface-atmosphere fluxes over continents or oceans. For example, the recent North American net "natural" sink, calculated from land use analyses, is believed to be 0.49 Pg C year^{-1}, with 95% confidence limits (~2 σ) of 50%, where, however, the estimate is the average over 5- to 10-year periods (*28*), so that interannual variability cannot be addressed. Estimates made by a dense network of atmospheric observations to provide a "top-down" constraint place this sink in the range of 0.4 to 1.0 Pg C year^{-1} (*29*). The VOS network is thus capable of defining the North Atlantic sink to substantially better precision, and somewhat better absolute accuracy, than is currently possible on the land surface.

Figure 3 shows both fCO_2 and air-sea flux integrated across the North Atlantic, as a function of latitude and time through the year (*15*). The figures show a major sink area in winter due to low fCO_2, extending from 20° to 50°N, which migrates northward through the subpolar gyre during the year. In 2005, it reached a maximum flux into the ocean in March and April, and then weakened through the summer. This CO_2 sink is maintained year-round by the cooling, northward transport of surface waters and is accentuated by the unfolding spring and summer phytoplankton bloom. Also prominent is the subtropical gyre annual cycle driven by temperature increase and strongest in the west. In 2005, the subtropical gyre was a net sink during the winter months but developed into a source as the summer progressed.

These broad features are repeated each year and are seen in climatological estimates of the flux (*14*, *23*), but, it now seems clear, they have substantial interannual and decadal variability around the climatology. Recent work using data before 2005 from some of the Atlantic VOS lines indicates that in 2002 to 2004, the net flux into some areas was only ~50% of mid-1990s values (*10*, *13*). Repeating the flux calculation, but replacing the 2005 ΔfCO_2 observations with climatological air-sea CO_2 gradients referenced to 2000 (*14*) or 1995 (*23*), yields annual sinks of respectively 0.30 or 0.34 Pg C (Table 1). Although the climatological values cannot be unambiguously related to the actual situation in any given year, this suggests that ΔfCO_2 was on the order of 20% or more lower in 2005 than 5 to 10 years earlier.

Our work demonstrates that an observing network based on commercial VOS is able to constrain the atmosphere-ocean flux of CO_2 into the North Atlantic with good precision. VOS networks are very cost-efficient because the ships are already in place. VOS also operates in the North Pacific and South Atlantic, and a similar approach should in principle be applicable in these oceans, too. An increasing number of moorings in the equatorial Pacific and Atlantic are also now equipped with instrumentation to observe surface fCO_2, so that a greatly improved precision of in situ observation of at least the Northern Hemisphere oceans is now possible. Such an observing system will greatly aid in understanding the ocean sink for atmospheric carbon dioxide and the progress of ocean acidification. It will also provide a valuable "top-down" constraint on the land sinks, which are more heterogeneous and thus more difficult to observe directly.

References and Notes

1. J. G. Canadell *et al.*, *Proc. Natl. Acad. Sci. U.S.A.* **104**, 18866 (2007).
2. A. C. Manning, R. F. Keeling, *Tellus* **58B**, 95 (2006).
3. J. C. Orr *et al.*, *Nature* **437**, 681 (2005).
4. P. Bousquet *et al.*, *Science* **290**, 1342 (2000).
5. C. Le Quéré *et al.*, *Science* **316**, 1735 (2007).
6. P. K. Patra *et al.*, *Global Biogeochem. Cycles* **19**, GB4013 (2005).
7. C. Le Quéré *et al.*, *Tellus* **55B**, 649 (2003).
8. H. Thomas *et al.*, *Global Biogeochem. Cycles* **22**, GB4027 (2008).
9. U. Schuster *et al.*, *Deep Sea Res. Part II Top. Stud. Oceanogr.* **56**, 620 (2009).
10. U. Schuster, A. J. Watson, *J. Geophys. Res.* **112**, C11006 (2007).
11. H. Lüger, D. W. R. Wallace, A. Körtzinger, Y. Nojiri, *Global Biogeochem. Cycles* **18**, GB3023 (2004).
12. A. Olsen, J. A. Trinanes, R. Wannikhof, *Remote Sens. Environ.* **89**, 309 (2004).
13. A. Corbière, N. Metzl, G. Reverdin, C. Brunet, T. Takahashi, *Tellus* **59B**, 168 (2007).
14. T. Takahashi *et al.*, *Deep Sea Res. Part II Top. Stud. Oceanogr.* **56**, 554 (2009).
15. Materials and methods are available as supporting material on *Science* Online.
16. N. Gruber, *Nature* **458**, 155 (2009).
17. T. Kohonen, *Self-Organizing Maps*. Series in Information Sciences, vol. 30 (Springer, Heidelberg, ed. 2, 1995).
18. S. A. Muller, F. Joos, G. K. Plattner, N. R. Edwards, T. F. Stocker, *Global Biogeochem. Cycles* **22**, GB3011 (2008).
19. C. Sweeney *et al.*, *Global Biogeochem. Cycles* **21**, GB2015 (2007).
20. E. Kalnay *et al.*, *Bull. Am. Met. Soc.* **77**, 437 (1996).
21. P. D. Nightingale *et al.*, *Global Biogeochem. Cycles* **14**, 373 (2000).
22. H. Lüger, R. Wanninkhof, D. W. R. Wallace, A. Körtzinger, *J. Geophys. Res.* **111**, C06024 (2006).
23. T. Takahashi *et al.*, *Deep Sea Res. Part II Top. Stud. Oceanogr.* **49**, 1601 (2002).
24. R. Webster, M. A. Oliver, *Geostatistics for Environmental Scientists* (Wiley, Chichester, UK, 2001).
25. C. Eden, A. Oschlies, *Global Biogeochem. Cycles* **20**, GB2008 (2006).
26. T. Friedrich, A. Oschlies, *J. Geophys. Res.* **114**, C03020 (2009).
27. T. Naegler, P. Ciais, K. Rodgers, I. Levin, *Geophys. Res. Lett.* **33**, L11802 (2006).
28. A. W. King *et al.*, "North American carbon budget and implications for the global carbon cycle"; www.climatescience.gov/Library/sap/sap2-2/final-report/default.htm (NOAA, 2008).
29. W. Peters *et al.*, *Proc. Natl. Acad. Sci. U.S.A.* **104**, 18925 (2007).

30. We thank Seatrade Reefer Chartering, Belgium; Geest Line Ltd, UK; Royal Arctic Line, Denmark; Royal Caribbean International, USA; Atlantic Container Lines Inc., USA; Eimskip Company, Iceland; and Wallenius Lines, Sweden, as well as the captains, officers, and crew of all ships for support of our projects. We acknowledge funding from the European Commission under CarboOcean [project 511176 (GOCE)]; Intercambio de Carbono entre Canarias y Barcelona CTM2005-03893/MAR and CTM2006-27116-E/MAR in Spain; the Natural Environment Research Council's Centre for Observation of Air-Sea Interactions and Fluxes and the National Centre for Earth Observation in the United Kingdom; and Institut National des Sciences de l'Univers and Institut Paul Emile Victor in France.

Supporting Online Material

www.sciencemag.org/cgi/content/full/326/5958/1391/DC1
Materials and Methods
Figs. S1 to S3
Table S1
References

8 June 2009; accepted 7 October 2009
10.1126/science.1177394

Coupling of CO_2 and Ice Sheet Stability Over Major Climate Transitions of the Last 20 Million Years

Aradhna K. Tripati,[1,2]* Christopher D. Roberts,[2] Robert A. Eagle[3]

The carbon dioxide (CO_2) content of the atmosphere has varied cyclically between ~180 and ~280 parts per million by volume over the past 800,000 years, closely coupled with temperature and sea level. For earlier periods in Earth's history, the partial pressure of CO_2 (pCO_2) is much less certain, and the relation between pCO_2 and climate remains poorly constrained. We use boron/calcium ratios in foraminifera to estimate pCO_2 during major climate transitions of the past 20 million years. During the Middle Miocene, when temperatures were ~3° to 6°C warmer and sea level was 25 to 40 meters higher than at present, pCO_2 appears to have been similar to modern levels. Decreases in pCO_2 were apparently synchronous with major episodes of glacial expansion during the Middle Miocene (~14 to 10 million years ago) and Late Pliocene (~3.3 to 2.4 million years ago).

The response of ice sheets and climate to past and future changes in the partial pressure of CO_2 (pCO_2) remains uncertain (*1*). Geologic data can be used to constrain relations between pCO_2 and ice sheet stability, identify climate thresholds, and validate models used for simulating future climate change (*1*). Over the past 20 million years (My), there have been substantial changes in global sea level driven by the growth and decay of continental ice sheets. Among the most pronounced of these fluctuations are the growth of ice on East and West Antarctica, the formation of an Arctic ice cap in the Middle Miocene [~14 to 10 million years ago (Ma)], and the intensification of glaciation in the Northern Hemisphere during the Late Pliocene (~3.4 to 2.4 Ma) (*2*–*4*). The causes of these glacial transitions, however, are the subject of intense debate. Proposed mechanisms include changing ocean circulation due to the closure of the Panamanian Seaway (*5*), upper water-column stratification in the tropics and/or high latitudes (*6*), and orbitally driven variations in the amount or distribution of insolation (*2*). Other authors invoke pCO_2 changes to explain glacial expansion (*7*–*9*).

Although there is speculation about the role of the carbon cycle in driving these well-studied climate changes, there is surprisingly little direct evidence to support a coupling between pCO_2 and climate before the ice core record (i.e., before 0.8 Ma). Estimates of pCO_2 for the past 20 My have been generated with the use of several methods (*10*–*13*), including the difference in the carbon isotopic composition ($\delta^{13}C$) of alkenones and co-occurring foraminifera, $\delta^{13}C$ of bulk carbon and pedogenic carbonates, boron isotope composition ($\delta^{11}B$) of foraminifera, stomatal density on fossil leaves, and carbon-cycle modeling. Most reconstructions support a decoupling between pCO_2 (*10*–*13*) and climate (*14*) during the Miocene and Late Pliocene, although very little pCO_2 data are available, and the few published proxy reconstructions yield conflicting results. In addition, few pCO_2 proxies have replicated the ice core data of the past 0.8 My.

To test the hypothesis that CO_2 and climate were closely coupled across these major transitions, we calculated surface-water pCO_2 (and pH) for three intervals [(i) 20 to 5 Ma, (ii) 3.5 to 2.4 Ma, and (iii) 1.4 Ma to the present] using foraminiferal B/Ca ratios. Yu *et al.* demonstrated that planktic foraminiferal B/Ca ratios can be used to estimate seawater borate/bicarbonate ratios [$B(OH)_4^-/HCO_3^-$] (*15*). Seawater $B(OH)_4^-/HCO_3^-$ will respond to changes in the carbonate system (such as pH, alkalinity, or dissolved inorganic carbon), as well as the total concentration of dissolved boron. To calculate pCO_2 and pH from seawater $B(OH)_4^-/HCO_3^-$, Yu *et al.* assumed alkalinity scaled either with surface-water salinity or whole-ocean salinity and total boron concentrations scaled with salinity. The choice of either of these models had a negligible effect on the reconstruction [<10 parts per million by volume (ppmv)].

We reconstructed surface-water $B(OH)_4^-/HCO_3^-$ at sites 806 and 588 located in the western tropical Pacific Ocean (fig. S1). Surface-water pCO_2 at these sites should reflect atmospheric pCO_2, as today this region is close to equilibrium with the atmosphere (table S2), not strongly affected by upwelling, and characterized by low productivity. Although ocean stratification has probably changed over the past 20 My, the western tropical Pacific probably experienced much smaller fluctuations than other regions (the eastern sides of ocean basins, mid-latitude settings, high-latitude settings) (*6*, *16*, *17*). Surface temperatures in this region are also thought to have been relatively stable over long time scales (*18*, *19*), with fluctuations of <6°C, in contrast to other areas (*16*, *17*). Both sites were drilled in shallow waters (table S1), with well-preserved planktonic foraminifera (*10*, *17*–*20*).

We measured B/Ca ratios, Mg/Ca ratios, and $\delta^{18}O$ values in monospecific samples of the surface-dwelling species *Globigerinoides ruber* and *G. sacculifer* (tables S3 and S4). Average reproducibility for B/Ca ratios of separately cleaned samples was 3.5%. B/Ca ratios were converted to seawater $B(OH)_4^-/HCO_3^-$ ratios with the use of an appropriate value for the apparent partition coefficient (K_D). K_D was calculated for each sample by applying a species-specific calibration between K_D and temperature (table S7) to Mg/Ca-derived estimates of temperature. Calculated $B(OH)_4^-/HCO_3^-$ ratios (and pCO_2 values) for 20 replicates typically differ by less than 4% (table S8), and values calculated using 78 pairs of *G. ruber* and *G. sacculifer* from the same sample agreed to within 3%, on average (table S9) (*21*).

To estimate pH and pCO_2 from $B(OH)_4^-/HCO_3^-$ ratios, a further assumption is required to fully constrain the carbonate system. We use seawater $B(OH)_4^-/HCO_3^-$ ratios and estimates of alkalinity or carbonate ion concentration to determine pH and pCO_2 [section F of supporting online material (SOM)]. We tested the sensitivity of calculated pH and pCO_2 values to the assumption used, including the following assumptions: (i) alkalinity scaled with salinity, (ii) constant carbonate ion concentration, and (iii) variable carbonate ion concentration. Seawater B has an oceanic residence time of ~11 to 17 My (*22*). Although we do not know how seawater B has evolved over the past 20 My, variations in seawater $B(OH)_4^-/HCO_3^-$ ratios on time scales of a few million years should reflect changes in the seawater carbonate system. We assumed total B (fig. S7) may have followed one of five modeled histories (*22*). The equations that we used for our calculations are provided in sections G to I of the SOM.

In total, we used 28 models to calculate pH and pCO_2 from $B(OH)_4^-/HCO_3^-$ ratios (figs. S5 to S8 and table S12). The range of calculated values defines the shaded regions in Figs. 1 and 2. The variable alkalinity model is shown in Figs. 1 and 2 (gray and green circles), because it is typically within 5 ppmv of the average of all 28 models. pCO_2 values calculated using the 28 models agree to within 40 ppmv over the last 800 thousand years (ky), with the difference between minimum and maximum calculated values increasing farther back in time (50 ppmv from 0 to 5 Ma, 60 ppmv from 5 to 10 Ma, and 100 ppmv from 10 to 20 Ma).

The pCO_2 reconstruction accurately reproduces ice core measurements from 0 to 0.8 Ma (Fig. 1). If the variable-alkalinity model is considered (Fig. 1, gray circles), ~30- to 50-ppmv offsets are observed for three (of 41) samples, which may be due to differences in age models [128 and 374 thousand years ago (ka)] or inaccuracies in the reconstruction (at 581 ka). For

[1]Departments of Earth and Space Sciences and Atmospheric and Oceanic Sciences, and Institute of Geophysics and Planetary Physics, University of California, Los Angeles (UCLA), Los Angeles, CA 90095, USA. [2]Department of Earth Sciences, University of Cambridge, Cambridge, CB2 3EQ, UK. [3]Division of Geological and Planetary Sciences, California Institute of Technology, Pasadena, CA 91125, USA.

*To whom correspondence should be addressed. E-mail: ripple@zephyr.ess.ucla.edu

the whole population of pCO_2 estimates from this interval (n = 39 samples), the root mean square error of the residuals (the difference between observed pCO_2 values from ice cores and reconstructed pCO_2 from foraminiferal B/Ca using the variable-alkalinity model) is 13 ppmv (fig. S9). If the other 26 models are considered, then all 41 values lie within error of the ice core record. Although only moderate in resolution, the record shows the change in the amplitude of the 100-ky cycle at 650 ka seen in ice cores (*23*). Our results for the past 1.4 Ma are very similar to those reported in a recently published $\delta^{11}B$ record (*11*).

Results for the Miocene and Late Pliocene support a close coupling between pCO_2 and climate (Fig. 2). Relative to today, surface waters appear to have been more acidic and pCO_2 values higher (Fig. 2, A and B) during the Early and Mid-Miocene (~20 to 15 Ma). This interval was characterized by global warmth, with little evidence for substantial (i.e., similar to modern) ice storage in Antarctica or Greenland (*3*, *14*, *24*). The highest estimates of pCO_2 occur during the Mid-Miocene Climatic Optimum (MMCO), ~16 to 14 Ma, the only interval in our record with levels higher than the 2009 value of 387 ppmv. Climate proxies indicate that the MMCO was associated with reduced ice volume and globally higher sea level (25 to 40 m) (*3*), as well as warmer surface- and deep-water temperatures (*2*, *20*). These results are consistent with foraminiferal $\delta^{11}B$ data that indicate that surface waters were more acidic ~20 Ma (*12*).

After the MMCO in the Mid-Miocene (~14 to 10 Ma), surface-water pH increased and pCO_2 decreased by ~200 ppmv. This pattern mirrors long-term trends in $\delta^{18}O$ records and is correlated with the appearance and growth of ice in both hemispheres, consistent with CO_2 driving this transition. Global cooling appears to have begun at ~14.2 Ma (*2*), and subsequent glacial expansion drove a 0.7 to 1.0 per mil increase in seawater and benthic foraminiferal $\delta^{18}O$ (*25*), as well as a lowering of sea level (~40 ± 15 m) (*3*). In the Northern Hemisphere, this fall in pCO_2 coincides with the onset of perennial Arctic sea ice cover (*26*), the development of substantial ice storage (*14*), and the first Miocene occurrence of ice-rafted debris in the North Atlantic, indicating that glaciers reached sea level (*24*). In the Southern Hemisphere, decreasing pCO_2 is associated with the change from wet- to cold-based alpine glaciers in the McMurdo Dry Valleys (*27*), the transition to cold polar conditions and the growth of ice on West Antarctica (*28*), and the re-initiation of a large ice sheet on East Antarctica (*2*, *29*).

During the Late Miocene (~10 to 7 Ma), seawater pH was relatively high, and pCO_2 was low and stable (~220 ppmv). Small ice sheets on West Antarctica and in the Northern Hemisphere are thought to have expanded while temperatures cooled (*13*). In the latest Miocene (~7 to 5 Ma), pH and pCO_2 exhibit large-amplitude variations, although the trends are poorly defined. This interval has been interpreted as generally being warm, with interglacials representing complete deglaciation of marine-based regions of Antarctica (*30*), consistent with the limited data on our pCO_2 curve.

Our B/Ca record indicates a large increase in pH and a fall in pCO_2 (~150 ppmv) during the Late Pliocene (~3.4 to 2.4 Ma) (Fig. 2, C and D). This evidence for a decline in pCO_2 coincident with the intensification of glaciation is consistent with the hypothesis that pCO_2 was the major driver of ice growth at this time. Model simulations also support the idea that changing pCO_2, and not ocean heat transport, triggered glaciation (*31*). Comparison with other records indicates that decreasing pCO_2 is synchronous with the intensification of continental glaciation in the Northern and Southern Hemispheres, as indicated by increased foraminiferal $\delta^{18}O$ (*32*), the onset of ice rafting in the North Pacific, and increased rates of ice rafting in the North Atlantic (*24*, *33*) and Southern Ocean (*34*). In addition, the interval of low pCO_2 at ~2.5 Ma is associated with the onset of large-amplitude (glacial-interglacial) cycles in deep-sea oxygen isotope records (*32*).

These results show that changes in pCO_2 and climate have been coupled during major glacial transitions of the past 20 My, just as they have

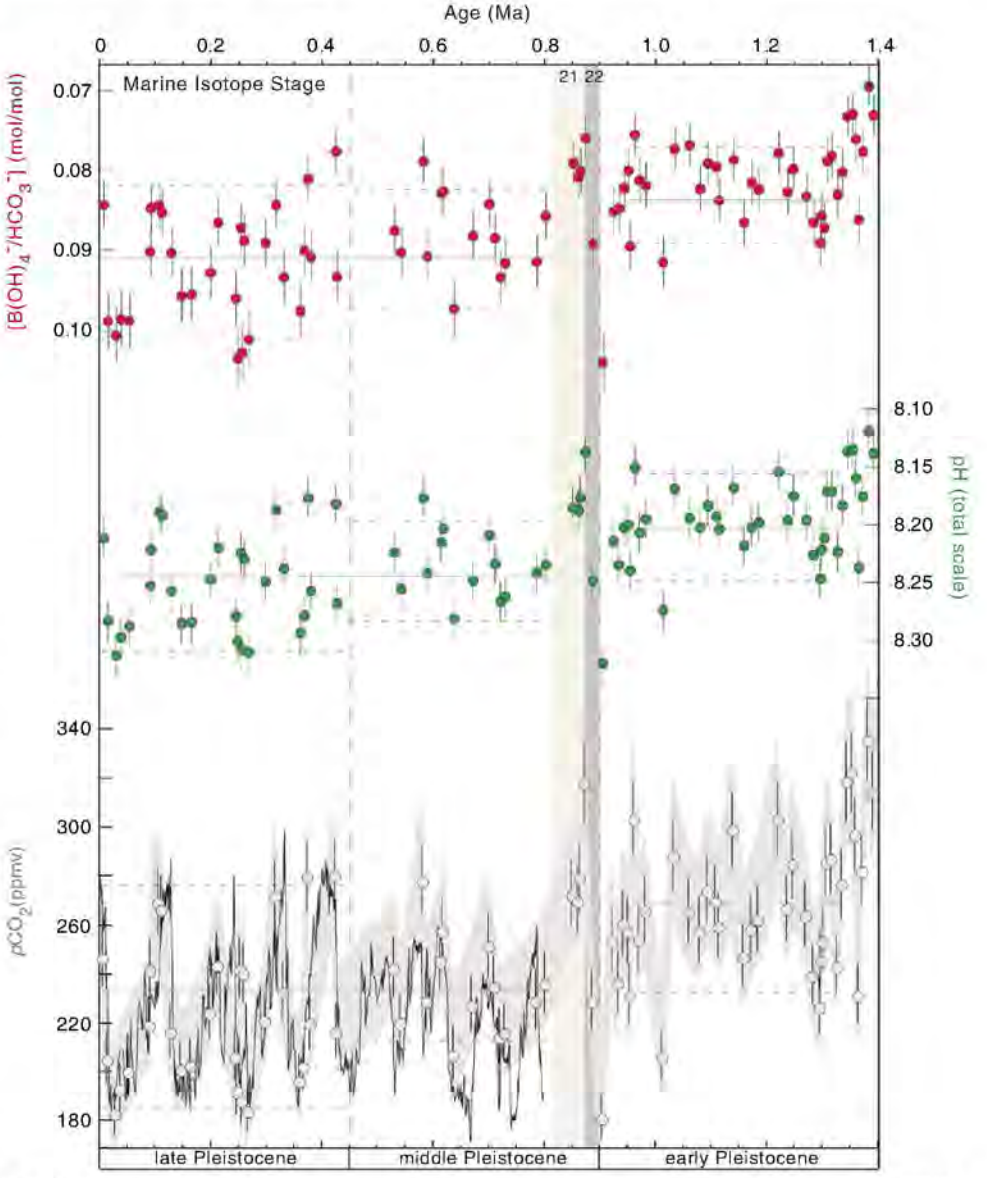

Fig. 1. $B(OH)_4^-/HCO_3^-$ ratios, pH, and pCO_2 from 0 to 1.4 Ma from B/Ca ratios of surface-dwelling foraminifera compared with Antarctic ice core data (solid line) (*23*). Data are mean ± average σ. There is a 3.5% analytical uncertainty in B/Ca ratios (average 1σ), based on analyses of replicate samples (table S8), and a 4% uncertainty in reconstructed seawater $B(OH)_4^-/HCO_3^-$ ratios, based on 78 paired measurements of *G. ruber* and *G. sacculifer* (table S9). This uncertainty in $B(OH)_4^-/HCO_3^-$ equates to a 10- to 20-ppmv uncertainty (1σ) in pCO_2 (~5 to 6%) and a 0.02 uncertainty in pH (~0.2%). The gray shaded region brackets all calculated pCO_2 values. Gray circles are for a model with a value similar to the average of all 28 models. Vertical dashed lines show Early-to-Mid Pleistocene and Mid-to-Late Pleistocene boundaries. Horizontal solid and dashed lines approximately mark shifts in mean and amplitude of values for a model shown in gray. For comparison, $\delta^{11}B$-based pCO_2 estimates indicate pCO_2 of ~220 to 300 ppmv from 0.8 to 1.4 Ma (*11*).

been over the last 0.8 My, supporting the hypothesis that greenhouse gas forcing was an important modulator of climate over this interval via direct and indirect effects. Variations in pCO_2 affect the radiative budget and energy balance of the planet. Such changes will inevitably have consequences for temperature, the hydrologic cycle, heat transport, and the accumulation and ablation of sea ice and glacial ice. The data presented here do not preclude alternative mechanisms for driving climate change over the past 20 Ma. However, they do indicate that changes in pCO_2 were closely tied to the evolution of climate during the Middle and Late Miocene and the Late Pliocene glacial intensification, and therefore, it is logical to deduce that pCO_2 played an important role in driving these transitions. High-resolution records of pCO_2 and other climate parameters should help to resolve whether pCO_2 was a trigger and/or feedback (or both).

These results provide some constraints on pCO_2 thresholds for the advance and retreat of continental ice sheets in the past, which is also relevant in the context of anthropogenic climate change because it is uncertain how continental ice sheets will respond over the coming centuries to increased levels of pCO_2 (*1*). By comparing our reconstruction to the published data sets described above, we are able to estimate past thresholds for the buildup of ice in different regions. When pCO_2 levels were last similar to modern values (that is, greater than 350 to 400 ppmv), there was little glacial ice on land or sea ice in the Arctic, and a marine-based ice mass on Antarctica was not viable. A sea ice cap on the Arctic Ocean and a large permanent ice sheet were maintained on East Antarctica when pCO_2 values fell below this threshold. Lower levels were necessary for the growth of large ice masses on West Antarctica (~250 to 300 ppmv) and Greenland (~220 to 260 ppmv). These values are lower than those indicated by a recent modeling study, which suggested that the threshold on East Antarctica may have been three times greater than in the Northern Hemisphere (*35*).

This work may support a relatively high climate sensitivity to pCO_2. pCO_2 values associated with major climate transitions of the past 20 Ma are similar to modern levels. During the Mid-Miocene, when pCO_2 was apparently grossly similar to modern levels, global surface temperatures were, on average, 3 to 6°C warmer than in the present (*2*, *25*). We suggest that the Mid-Miocene may be a useful interval to study to understand what effect sustained high pCO_2 levels (i.e., a climate in equilibrium with near-modern pCO_2 values) may have on climate.

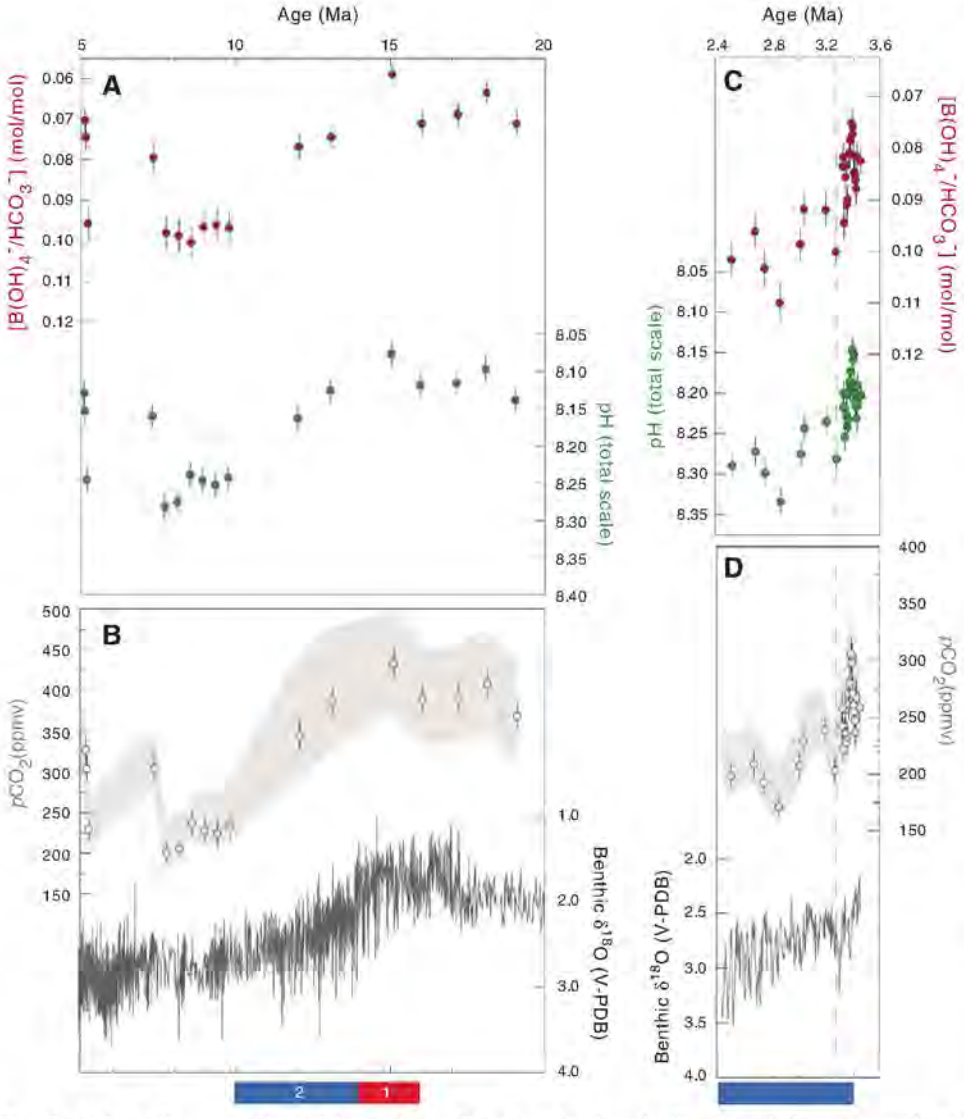

Fig. 2. pCO_2 for Miocene and Late Pliocene from B/Ca ratios of surface-dwelling foraminifera compared with climate records. Error bars are the same as in Fig. 1. The gray shaded region brackets all calculated pCO_2 values. Gray circles are for a model with a value similar to the average of all 28 models. **(A)** $B(OH)_4^-/HCO_3^-$ ratios and pH for 20 to 5 Ma. **(B)** pCO_2 and compilation of benthic foraminiferal $\delta^{18}O$ (*14*) for 20 to 5 Ma. The numbered bars at the bottom of the panel denote the timing of: (1) the MMCO (*2*, *3*, *14*, *20*, *24*) and (2) Mid-Miocene glacial expansion (*2*, *3*, *8*, *14*, *24*–*29*). **(C)** $B(OH)_4^-/HCO_3^-$ ratios and pH for 3.4 to 2.4 Ma. **(D)** pCO_2 and benthic foraminiferal $\delta^{18}O$ (*32*) for 3.4 to 2.4 Ma. The dark blue bar at the bottom of the panel denotes the reported timing of Late Pliocene glacial expansion (*14*, *24*, *32*–*34*). V-PDB, Vienna Pee Dee belemnite.

References and Notes

1. Intergovernmental Panel on Climate Change, *Climate Change 2007: The Physical Science Basis. Contribution of Working Group I to the Fourth Assessment Report of the Intergovernmental Panel on Climate Change*, S. Solomon *et al.*, Ed. (Cambridge Univ. Press, Cambridge, 2007).
2. A. E. Shevenell, J. P. Kennett, D. W. Lea, *Science* **305**, 1766 (2004).
3. K. G. Miller *et al.*, *Science* **310**, 1293 (2005).
4. G. Haug, D. Sigman, R. Tiedemann, T. Pedersen, M. Sarnthein, *Nature* **401**, 779 (1999).
5. G. Haug, R. Tiedemann, *Nature* **393**, 673 (1998).
6. D. M. Sigman, S. L. Jaccard, G. H. Haug, *Nature* **428**, 59 (2004).
7. E. Vincent, W. Berger, in *The Carbon Cycle and Atmospheric CO_2: Natural Variations Archean to Present*, vol. 32, E. Sundquist, W. Broecker, Eds. (Geophys. Monogr. Ser., AGU, Washington, DC, 1985), pp. 455–468.
8. A. Holbourn, W. Kuhnt, M. Schulz, H. Erlenkeuser, *Nature* **438**, 483 (2005).
9. D. Hodell, F. Woodruff, *Paleoceanography* **9**, 405 (1994).
10. M. Pagani, J. C. Zachos, K. H. Freeman, B. Tipple, S. Bohaty, *Science* **309**, 600 (2005); published online 16 June 2005 (10.1126/science.1110063).
11. B. Hönisch, N. G. Hemming, D. Archer, M. Siddall, J. F. McManus, *Science* **324**, 1551 (2009).
12. A. Spivack, C. You, H. Smith, *Nature* **363**, 149 (1993).
13. P. N. Pearson, M. R. Palmer, *Nature* **406**, 695 (2000).
14. J. Zachos, M. Pagani, L. Sloan, E. Thomas, K. Billups, *Science* **292**, 686 (2001).
15. J. Yu, H. Elderfield, B. Hönisch, *Paleoceanography* **22**, PA2202 (2007).
16. A. V. Federov *et al.*, *Science* **312**, 1485 (2006).
17. M. W. Wara, A. C. Ravelo, M. L. Delaney, *Science* **309**, 758 (2005); published online 23 June 2005 (10.1126/science.1112596).
18. S. Nathan, R. Leckie, *Palaeogeogr. Palaeoclimatol. Palaeoecol.* **274**, 140 (2009).
19. M. Medina-Elizalde, D. Lea, *Science* **310**, 1009 (2005); published online 13 October 2005 (10.1126/science.1115933).
20. B. Flower, J. Kennett, *Paleoceanography* **8**, 811 (1993).
21. Materials and methods are available as supporting material on *Science* Online.
22. D. Lemarchand, J. Gaillardet, E. Lewin, C. Allegre, *Chem. Geol.* **190**, 123 (2002).
23. D. Luthi *et al.*, *Nature* **453**, 379 (2008).
24. T. Wolf-Welling, M. Cremer, S. O'Connell, A. Winkler, J. Thiede, in *Proceedings of Ocean Drilling Program, Scientific Results*, vol. 151, J. Thiede, A. Myhre, J. Firth,

G. Johnson, W. Ruddiman, Eds. (Ocean Drilling Program, College Station, TX, 1996), pp. 515–568.
25. K. Billups, D. Schrag, *Earth Planet. Sci. Lett.* **209**, 181 (2003).
26. A. Krylov *et al.*, *Paleoceanography* **23**, PA1506 (2008).
27. A. R. Lewis *et al.*, *Proc. Natl. Acad. Sci. U.S.A.* **105**, 10676 (2008).
28. T. Naish *et al.*, *Nature* **458**, 322 (2009).
29. B. Flower, J. Kennett, *Paleoceanography* **10**, 1095 (1995).
30. T. Naish *et al.*, paper presented at the International Symposium on Antarctic Earth Sciences, Santa Barbara, CA, 26 to 31 August 2007.
31. D. J. Lunt, G. L. Foster, A. M. Haywood, E. J. Stone, *Nature* **454**, 1102 (2008).
32. L. E. Lisiecki, M. E. Raymo, *Paleoceanography* **20**, PA1003 (2005).
33. L. Krissek, in *Proceedings of the Ocean Drilling Program, Scientific Results*, vol. 145, D. Rea, I. Basov, D. Scholl, J. Allan, Eds. (Ocean Drilling Program, College Station, TX, 1995), pp. 179–194.
34. E. Cowan, in *Proceedings of the Ocean Drilling Program, Scientific Results*, vol. 178, P. Barker, A. Camerlenghi, G. Acton, Eds. (Ocean Drilling Program, College Station, TX, 2001), pp. 1–22.
35. R. M. DeConto *et al.*, *Nature* **455**, 652 (2008).
36. We thank K. Caldeira, H. Elderfield, J. Eiler, T. Naish, D. Sigman, anonymous reviewers, and the editor for their comments on this work, which substantially improved the manuscript. We also thank J. Booth, E. Khadun, O. Shorttle, L. Thanalasundaram, and A. Bufe for invaluable assistance with sample preparation; L. Booth, J. Day, and M. Greaves (supported by grant NE/F004966/1) for technical assistance; L. Lisiecki for assistance with the age model; and S. Crowhurst, A. Gagnon, S. John, N. Meckler, B. Passey, N. Thiagarajan, and J. Yu for discussing this work. Support was provided to A.K.T. by UCLA, National Environmental Research Council (NERC) (fellowship NE/D009049/1), and Magdalene College; to C.D.R. by NERC (studentship NER/S/A/2006/14070); and to R.A.E. by a Caltech Chancellors Postdoctoral Scholarship. Samples for this study were obtained from the Godwin Laboratory sample archives and the Ocean Drilling Program.

Supporting Online Material
www.sciencemag.org/cgi/content/full/1178296/DC1
Materials and Methods
Figs. S1 to S9
Tables S1 to S12
References

26 June 2009; accepted 28 September 2009
Published online 8 October 2009;
10.1126/science.1178296
Include this information when citing this paper.

Indirect Emissions from Biofuels: How Important?

Jerry M. Melillo,[1]* John M. Reilly,[2] David W. Kicklighter,[1] Angelo C. Gurgel,[2,3] Timothy W. Cronin,[1,2] Sergey Paltsev,[2] Benjamin S. Felzer,[1,4] Xiaodong Wang,[2,5] Andrei P. Sokolov,[2] C. Adam Schlosser[2]

A global biofuels program will lead to intense pressures on land supply and can increase greenhouse gas emissions from land-use changes. Using linked economic and terrestrial biogeochemistry models, we examined direct and indirect effects of possible land-use changes from an expanded global cellulosic bioenergy program on greenhouse gas emissions over the 21st century. Our model predicts that indirect land use will be responsible for substantially more carbon loss (up to twice as much) than direct land use; however, because of predicted increases in fertilizer use, nitrous oxide emissions will be more important than carbon losses themselves in terms of warming potential. A global greenhouse gas emissions policy that protects forests and encourages best practices for nitrogen fertilizer use can dramatically reduce emissions associated with biofuels production.

Expanded use of bioenergy causes land-use changes and increases in terrestrial carbon emissions (*1*, *2*). The recognition of this has led to efforts to determine the credit toward meeting low carbon fuel standards (LCFS) for different forms of bioenergy with an accounting of direct land-use emissions as well as emissions from land use indirectly related to bioenergy production (*3*, *4*). Indirect emissions occur when biofuels production on agricultural land displaces agricultural production and causes additional land-use change that leads to an increase in net greenhouse gas (GHG) emissions (*2*, *4*). The control of GHGs through a cap-and-trade or tax policy, if extended to include emissions (or credits for uptake) from land-use change combined with monitoring of carbon stored in vegetation and soils and enforcement of such policies, would eliminate the need for such life-cycle accounting (*5*, *6*). There are a variety of concerns (*5*) about the practicality of including land-use change emissions in a system designed to reduce emissions from fossil fuels, and that may explain why there are no concrete proposals in major countries to do so. In this situation, fossil energy control programs (LCFS or carbon taxes) must determine how to treat the direct and indirect GHG emissions associated with the carbon intensity of biofuels.

The methods to estimate indirect emissions remain controversial. Quantitative analyses to date have ignored these emissions (*1*), considered those associated with crop displacement from a limited area (*2*), confounded these emissions with direct or general land-use emissions (*6*–*8*), or developed estimates in a static framework of today's economy (*3*). Missing in these analyses is how to address the full dynamic accounting of biofuel carbon intensity (CI), which is defined for energy as the GHG emissions per megajoule of energy produced (*9*), that is, the simultaneous consideration of the potential of net carbon uptake through enhanced management of poor or degraded lands, nitrous oxide (N_2O) emissions that would accompany increased use of fertilizer, environmental effects on terrestrial carbon storage [such as climate change, enhanced carbon dioxide (CO_2) concentrations, and ozone pollution], and consideration of the economics of land conversion. The estimation of emissions related to global land-use change, both those on land devoted to biofuel crops (direct emissions) and those indirect changes driven by increased demand for land for biofuel crops (indirect emissions), requires an approach to attribute effects to separate land uses.

We applied an existing global modeling system that integrates land-use change as driven by multiple demands for land and that includes dynamic greenhouse gas accounting (*10*, *11*). Our modeling system, which consists of a computable general equilibrium (CGE) model of the world economy (*10*, *12*) combined with a process-based terrestrial biogeochemistry model (*13*, *14*), was used to generate global land-use scenarios and explore some of the environmental consequences of an expanded global cellulosic biofuels program over the 21st century. The biofuels scenarios we focus on are linked to a global climate policy to control GHG emissions from industrial and fossil fuel sources that would, absent feedbacks from land-use change, stabilize the atmosphere's CO_2 concentration at 550 parts per million by volume (ppmv) (*15*). The climate policy makes the use of fossil fuels more expensive, speeds up the introduction of biofuels, and ultimately increases the size of the biofuel industry, with additional effects on land use, land prices, and food and forestry production and prices (*16*).

We considered two cases in order to explore future land-use scenarios: Case 1 allows the conversion of natural areas to meet increased demand for land, as long as the conversion is profitable; case 2 is driven by more intense use of existing managed land. To identify the total effects of biofuels, each of the above cases is compared with a scenario in which expanded biofuel use does not occur (*16*). In the scenarios with increased biofuels production, the direct effects (such as changes in carbon storage and N_2O emissions) are estimated only in areas devoted to biofuels. Indirect effects are defined as the differences between the total effects and the direct effects.

At the beginning of the 21st century, ~31.5% of the total land area (133 million km^2) was in

[1]The Ecosystems Center, Marine Biological Laboratory (MBL), 7 MBL Street, Woods Hole, MA 02543, USA. [2]Joint Program on the Science and Policy of Global Change, Massachusetts Institute of Technology (MIT), 77 Massachusetts Avenue, MIT E19-411, Cambridge, MA 02139-4307, USA. [3]Department of Economics, University of São Paulo, Ribeirão Preto 4EES, Brazil. [4]Department of Earth and Environmental Sciences, Lehigh University, 31 Williams Drive, Bethlehem, PA 18015, USA. [5]School of Public Administration, Zhejiang University, Hangzhou 310000, Zhejiang Province, People's Republic of China (PRC).
*To whom correspondence should be addressed. E-mail: jmelillo@mbl.edu

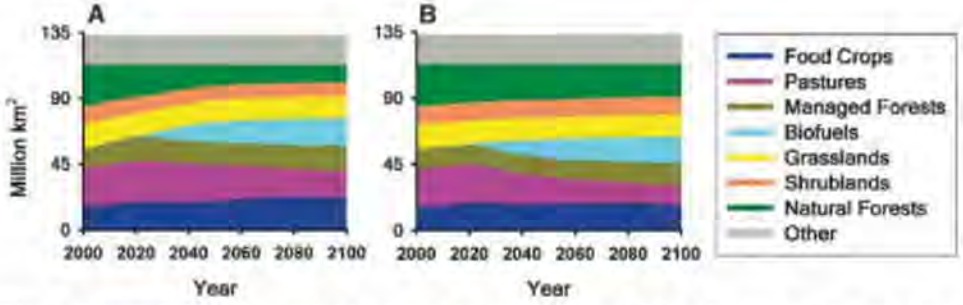

Fig. 1. Projected changes in global land cover for land-use case 1 (**A**) and case 2 (**B**). In either case, biofuels supply most of the world's liquid fuel needs by 2100. In case 1, 365 EJ of biofuel is produced in 2100, using 16.2% (21.6 million km^2) of the total land area; natural forest area declines from 34.4 to 15.1 million km^2 (56%), and pasture area declines from 25.8 to 22.1 million km^2 (14%). In case 2, 323 EJ of biofuels are produced in 2100, using 20.6 million km^2 of land; pasture areas decrease by 10.3 million km^2 (40%), and forest area declines by 8.4 million km^2 (24% of forest area). Simulations show that these major land-use changes will take place in the tropics and subtropics, especially in Africa and the Americas (fig. S2).

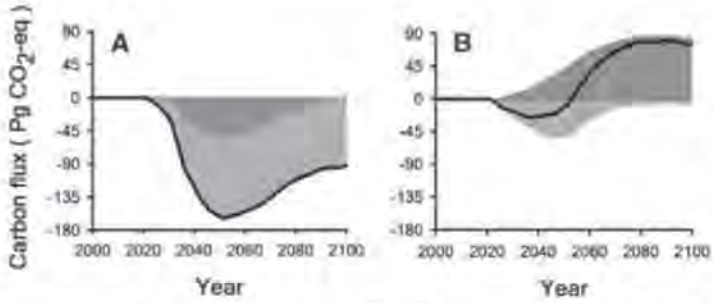

Fig. 2. Partitioning of direct (dark gray) and indirect effects (light gray) on projected cumulative land carbon flux since the year 2000 (black line) from cellulosic biofuel production for land-use case 1 (**A**) and case 2 (**B**). Positive values represent carbon sequestration, whereas negative values represent carbon emissions by land ecosystems. In case 1, the cumulative loss is 92 Pg CO_2eq by 2100, with the maximum loss (164 Pg CO_2eq) occurring in the 2050 to 2055 time frame, indirect losses of 110 Pg CO_2eq, and direct losses of 54 Pg CO_2eq. In the second half of the century, there is net accumulation of 72 Pg CO_2eq mostly in the soil in response to the use of nitrogen fertilizers. In case 2, land areas are projected to have a net accumulation of 75 Pg CO_2eq as a result of biofuel production, with maximum loss of 26 Pg CO_2eq in the 2035 to 2040 time frame, followed by substantial accumulation.

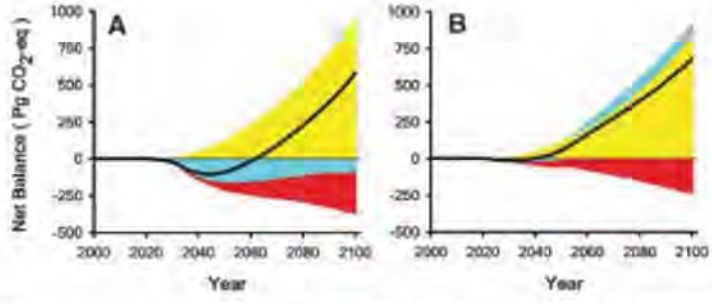

Fig. 3. Partitioning of greenhouse gas balance since the year 2000 (black line) as influenced by cellulosic biofuel production for land-use case 1 (**A**) and case 2 (**B**) among fossil fuel abatement (yellow), net land carbon flux (blue), and fertilizer N_2O emissions (red). Positive values are abatement benefits, and negative values are emissions. Net land carbon flux is the same as in Fig. 2. For case 1, N_2O emissions over the century are 286 Pg CO_2eq; for case 2, N_2O emissions are 238 Pg CO_2eq.

Table 1. Carbon intensity index associated with cellulosic biofuel production for two land-use scenario cases. Units are g CO_2eq MJ^{-1}, with negative values indicating carbon accumulation.

Variable	Case 1			Case 2		
Time period	2000–2030	2000–2050	2000–2100	2000–2030	2000–2050	2000–2100
Direct land C	11	27	0	−52	−24	−7
Indirect land C	190	57	7	181	31	1
Fertilizer N_2O	29	28	20	30	26	19
Total	229	112	26	158	32	13

agriculture: 12.1% (16.1 million km^2) in crops and 19.4% (25.8 million km^2) in pasture (*17*). In both cases of increased biofuels use, land devoted to biofuels becomes greater than all area currently devoted to crops by the end of the 21st century, but in case 2 less forest land is converted (Fig. 1). Changes in net land fluxes are also associated with how land is allocated for biofuels production (Fig. 2). In case 1, there is a larger loss of carbon than in case 2, especially at mid-century. Indirect land use is responsible for substantially greater carbon losses than direct land use in both cases during the first half of the century. In both cases, there is carbon accumulation in the latter part of the century. The estimates include CO_2 from burning and decay of vegetation and slower release of carbon as CO_2 from disturbed soils. The estimates also take into account reduced carbon sequestration capacity of the cleared areas, including that which would have been stimulated by increased ambient CO_2 levels. Smaller losses in the early years in case 2 are due to less deforestation and more use of pasture, shrubland, and savanna, which have lower carbon stocks than forests and, once under more intensive management, accumulate soil carbon. Much of the soil carbon accumulation is projected to occur in sub-Saharan Africa, an attractive area for growing biofuels in our economic analyses because the land is relatively inexpensive (*10*) and simple management interventions such as fertilizer additions can dramatically increase crop productivity (*18*).

Estimates of land devoted to biofuels in our two scenarios (15 to 16%) are well below the estimate of ~50% in a recent analysis (*6*) that does not control land-use emissions. The higher number is based on an analysis that has a lower concentration target (450 ppmv CO_2), does not account for price-induced intensification of land use, and does not explicitly consider concurrent changes in other environmental factors. In analyses that include land-use emissions as part of the policy (*6*–*8*), less area is estimated to be devoted to biofuels (3 to 8%).

The carbon losses associated with the combined direct and indirect biofuel emissions estimated for our case 1 are similar to a previous estimate (*7*), which shows larger losses of carbon per unit area converted to biofuels production. These larger losses per unit area result from a combination of factors, including a greater simulated response of plant productivity to changes in climate and atmospheric CO_2 (*15*) and the lack of any negative effects on plant productivity of elevated tropospheric ozone (*19*, *20*).

We also simulated the emissions of N_2O from additional fertilizer that would be required to grow biofuel crops. Over the century, the N_2O emissions become larger in CO_2 equivalent (CO_2eq) than carbon emissions from land use (Fig. 3). The net GHG effect of biofuels also changes over time; for case 1, the net GHG balance is −90 Pg CO_2eq through 2050 (a negative sign indicates a source; a positive sign indicates a sink), whereas it is +579 through

2100. For case 2, the net GHG balance is +57 Pg CO_2eq through 2050 and +679 through 2100. We estimate that by the year 2100, biofuels production accounts for about 60% of the total annual N_2O emissions from fertilizer application in both cases, where the total for case 1 is 18.6 Tg N yr^{-1} and for case 2 is 16.1 Tg N yr^{-1}. These total annual land-use N_2O emissions are about 2.5 to 3.5 times higher than comparable estimates from an earlier study (*8*). Our larger estimates result from differences in the assumed proportion of nitrogen fertilizer lost as N_2O (*21*) as well as differences in the amount of land devoted to food and biofuel production. Best practices for the use of nitrogen fertilizer, such as synchronizing fertilizer application with plant demand (*22*), can reduce N_2O emissions associated with biofuels production.

The CI of fuel was also calculated across three time periods (Table 1) so as to compare with displaced fossil energy in a LCFS and to identify the GHG allowances that would be required for biofuels in a cap-and-trade program. Previous CI estimates for California gasoline (*3*) suggest that values less than ~96 g CO_2eq MJ^{-1} indicate that blending cellulosic biofuels will help lower the carbon intensity of California fuel and therefore contribute to achieving the LCFS. Entries that are higher than 96 g CO_2eq MJ^{-1} would raise the average California fuel carbon intensity and thus be at odds with the LCFS. Therefore, the CI values for case 1 are only favorable for biofuels if the integration period extends into the second half of the century. For case 2, the CI values turn favorable for biofuels over an integration period somewhere between 2030 and 2050. In both cases, the CO_2 flux has approached zero by the end of the century when little or no further land conversion is occurring and emissions from decomposition are approximately balancing carbon added to the soil from unharvested components of the vegetation (roots). Although the carbon accounting ends up as a nearly net neutral effect, N_2O emissions continue. Annual estimates start high, are variable from year to year because they depend on climate, and generally decline over time.

One of the perplexing issues for policy analysts has been predicting the dynamics of the CI over different integration periods [supporting online material (SOM) text]. If one integrates over a long enough period, biofuels show a substantial greenhouse gas advantage, but over a short period they have a higher CI than fossil fuel (*3*). Drawing on previous analyses (*5*, *23*), we argue that a solution need not be complex and can avoid valuing climate damages by using the immediate (annual) emissions (direct and indirect) for the CI calculation. In other words, CI estimates should not integrate over multiple years but rather simply consider the fuel offset for the policy time period (normally a single year). This becomes evident in case 1. Despite the promise of eventual long-term economic benefits, a substantial penalty—in fact, possibly worse than with gasoline—in the first few decades may render the near-term cost of the carbon debt difficult to overcome in this case.

In case 2, in which there is less willingness to convert land, the economics of biofuels would be favorable sooner. Greater measures to protect forests could make the economics and CI of biofuels even more favorable because improved management on low-quality or degraded land can lead to carbon accumulation in the soil rather than a carbon loss (fig. S3). Our results suggest that tropical regions that are currently suffering substantial amounts of deforestation may also be the most competitive producers of biofuels. Our suggested strategy of not integrating over future fuel offsets increases the near-term CI of biofuels unless forested lands globally are better protected. Success in avoiding deforestation will be reflected in lower estimates of indirect emissions and lower carbon penalties.

References and Notes

1. J. Fargione *et al.*, *Science* **319**, 1235 (2008).
2. T. Searchinger *et al.*, *Science* **319**, 1238 (2008).
3. California Environmental Protection Agency (EPA), "Proposed regulation to implement the low carbon fuel standard," vol. 1 (EPA, Sacramento, CA, 2009); www.arb.ca.gov/fuels/lcfs/030409lcfs_isor_vol1.pdf.
4. E. Gallagher, *The Gallagher Review of the Indirect Effects of Biofuels Production* (Renewable Fuels Agency, East Sussex, UK, 2008).
5. J. Reilly *et al.*, in *Greenhouse Gas Sinks*, D. S. Reay, C. N. Hewitt, K. A. Smith, J. Grace, Eds. (CABI Publishing, Wallingford, UK, 2007), chap 8, pp. 115–142.
6. M. Wise *et al.*, *Science* **324**, 1183 (2009).
7. R. Leemans, A. van Amstel, C. Battjes, E. Kreileman, S. Toet, *Glob. Environ. Change* **6**, 335 (1996).
8. B. Strengers, R. Leemans, B. Eickhout, B. de Vries, L. Bouwman, *GeoJournal* **61**, 381 (2004).
9. M. R. Raupach *et al.*, *Proc. Natl. Acad. Sci. U.S.A.* **104**, 10288 (2007).
10. A. Gurgel, J. M. Reilly, S. Paltsev, *J. Agric. Food Ind. Org.* www.bepress.com/jafio/vol5/iss2/art9.
11. J. Melillo *et al.*, "Unintended environmental consequences of a global biofuels program" [Report 168, MIT Joint Program on the Science and Policy of Global Change (JPSPGC), Cambridge, 2009]; http://globalchange.mit.edu/files/document/MITJPSPGC_Rpt168.pdf.
12. S. Paltsev *et al.*, "The MIT emissions prediction and policy analysis (EPPA) model: version 4" (MIT JPSPGC, Cambridge, 2005); http://globalchange.mit.edu/files/document/MITJPSPGC_Rpt125.pdf.
13. J. Melillo *et al.*, *Nature* **363**, 234 (1993).
14. B. Felzer *et al.*, *Tellus* **56B**, 230 (2004).
15. A. Sokolov *et al.*, *J. Clim.* **21**, 3776 (2008).
16. Materials and methods are available as supporting material on *Science* Online.
17. G. Hurtt *et al.*, *Glob. Change Biol.* **12**, 1208 (2006).
18. P. A. Sanchez, *Science* **295**, 2019 (2002).
19. B. Felzer *et al.*, *Clim. Change* **73**, 345 (2005).
20. X. Wang, thesis, MIT (2008); available at http://globalchange.mit.edu/files/document/Wang_PhD_08.pdf.
21. P. J. Crutzen, A. R. Mosier, K. A. Smith, W. Winiwarter, *Atmos. Chem. Phys.* **8**, 389 (2008).
22. G. P. Robertson, in *Ecology in Agriculture*, L. Jackson, Ed. (Academic Press, New York, 1997), pp. 347–365.
23. H. Herzog *et al.*, *Clim. Change* **59**, 293 (2003).

24. This research was supported in part by the David and Lucile Packard Foundation to the MBL, Department of Energy, Office of Science (BER) grants DE-FG02-94ER61937, DE-FG02-93ER61677, and DE-FG02-08ER64648; EPA grant XA-83240101; NSF grant BCS-0410344; and the industrial and foundation sponsors of the MIT JPSPGC.

Supporting Online Material

www.sciencemag.org/cgi/content/full/1180251/DC1
Materials and Methods
SOM Text
Figs. S1 to S3
Tables S1 to S6
References

6 August 2009; accepted 7 October 2009
Published online 22 October 2009;
10.1126/science.1180251
Include this information when citing this paper.

Elevated CO_2 Reduces Losses of Plant Diversity Caused by Nitrogen Deposition

Peter B. Reich

The interactive effects of rising atmospheric carbon dioxide (CO_2) concentrations and elevated nitrogen (N) deposition on plant diversity are not well understood. This is of concern because both factors are important components of global environmental change and because each might suppress diversity, with their combined effects possibly additive or synergistic. In a long-term open-air experiment, grassland assemblages planted with 16 species were grown under all combinations of ambient and elevated CO_2 and ambient and elevated N. Over 10 years, elevated N reduced species richness by 16% at ambient CO_2 but by just 8% at elevated CO_2. This resulted from multiple effects of CO_2 and N on plant traits and soil resources that altered competitive interactions among species. Elevated CO_2 thus ameliorated the negative effects of N enrichment on species richness.

Two global change factors likely to have widespread influence on plant communities are nitrogen (N) deposition and rising atmospheric carbon dioxide (CO_2) levels (*1*–*7*). Levels of N deposition and CO_2 have risen in recent decades and are expected to increase further (*8*). Because increased CO_2 and N supply often drive plant stoichiometry in opposite directions but productivity in the same direction, and as plant resources are primarily available above-

Department of Forest Resources, University of Minnesota, 1530 Cleveland Avenue North, St. Paul, MN 55108, USA. E-mail: preich@umn.edu

ground versus below ground, there are many possible ways in which competitive or other biotic interactions that influence biodiversity might be affected (*2*–*7*, *9*–*11*). Although increasing N supply frequently results in declining species diversity (*1*, *6*, *7*, *9*), there has been less research about (*4*, *5*, *10*), and no consensus regarding, how rising CO_2 levels will influence species diversity. Even less is known about the influence of rising CO_2 on the effects of N deposition on diversity (*4*, *5*).

Experimental and observational studies in terrestrial ecosystems have typically shown that increases in N availability increase productivity and decrease plant diversity, and this has been explained by a variety of mechanisms (*1*, *6*, *7*, *9*, *12*–*16*). Investigations in different study systems have provided evidence that a decline in diversity under elevated N can result from resource preemption (i.e., from either belowground resource or light competition) and associated competitive exclusion, shifts in competitive intensity aboveground versus belowground, alterations of soil acidity, a switch from one limiting resource to another, and/or a shift in niche dimensionality (*1*, *6*, *7*, *9*, *12*–*16*). Therefore, although the suppression of diversity by increasing N availability is almost ubiquitous, no single mechanism is universally responsible.

In contrast, evidence and theory about CO_2 effects on species richness are less well developed. Much like enriched N, elevated CO_2 could result in decreasing species richness as it also commonly increases productivity (*2*, *17*–*19*), potentially leading to competitive exclusion following resource preemption. Alternatively, as rising CO_2 levels change plant stoichiometry (*17*, *20*), potentially resulting in greater relative limitations by other dominant resources such as N (*18*, *19*, *21*), elevated CO_2 could reduce competitive exclusion and lead to increased species richness. Evidence of CO_2 effects on species richness is scarce (*4*, *5*, *10*, *22*) and shows mixed results, with positive, neutral, and negative responses seen in the few published reports.

Equally important to impacts of multiple global change agents is whether their effects are interactive (*2*–*4*, *18*, *19*), as it will bode poorly for future biodiversity conservation if rising CO_2 exacerbates the considerable negative impacts of N deposition on community-scale species richness (*1*, *6*, *7*, *13*, *14*). However, a plethora of possible mechanisms suggests that synergistic, additive, or antagonistic interactive outcomes of joint CO_2 and N effects are plausible (*23*).

To address the issues raised above, species richness was measured in 48 experimental grassland plots (each 2 m by 2 m) planted in 1997 with 16 perennial species and treated since 1998 with all combinations of ambient and elevated atmospheric CO_2 (ambient and +180 μmol mol^{-1} delivered by means of a free-air CO_2 enrichment technique) and ambient and enriched N (ambient and +4 g N m^{-2} $year^{-1}$ delivered as ammonium nitrate in three equal doses each year) (*11*, *19*, *23*). This experiment, called BioCON, is conducted in an ecosystem co-limited by CO_2 and N (*11*, *19*) and dominated by belowground interactions (*24*, *25*). Although wet and dry N deposition to terrestrial ecosystems is primarily of atmospheric origin, the effects are largely mediated through belowground processes, because uptake by soil microbes and plant roots generally begins the incorporation of this N into the plant biogeochemical cycle. Species richness (the number of species observed in a plot), belowground and aboveground biomass, root C/N ratio, soil solution N concentration, percent soil water content, and percent light transmission were measured in each plot in all years from 1998 to 2007 (*23*) and used to evaluate treatment effects on species richness and the underlying mechanisms (Tables 1 and 2).

From 1998 to 2007, there were significant main effects of N treatment ($P < 0.001$) and year ($P < 0.0001$) on species richness, and a significant interaction between CO_2 and N treatments ($P = 0.02$) (Tables 1 and 3). On average, enriched N supply reduced species richness by 16% under ambient CO_2, but only by 8% under elevated CO_2 (Table 3 and Fig. 1). The N effect was consistently smaller under elevated than under ambient CO_2 from the second to tenth year of the experiment (Fig. 1). From the CO_2 effect perspective, elevated CO_2 had minimal impact (−2%) on observed species richness at ambient N, whereas at enriched N, elevated CO_2 modestly increased species richness by 7% (Table 3). The $CO_2 \times N$ interaction was more pronounced once the experimental plots were well established. For example, during the most recent 7 years, enriched N supply reduced species richness by 15% under ambient CO_2, but only by 5% under elevated CO_2.

What accounts for the more consistently negative effect of added N than of elevated CO_2 on species richness, and what caused the observed $CO_2 \times N$ interaction? To address these questions, it is useful to focus on elements of plot-scale structure or function that might be influenced by CO_2 and N and contribute to effects on species richness, asking (i) which plot-scale attributes were related to species richness, (ii) how did CO_2 and N treatments influence those attributes, and (iii) were such responses consistent with observed treatment effects on species richness? Relevant measures (*6*, *7*, *12*, *13*, *15*, *24*–*26*) include (i) total root biomass, an indication of productivity and potentially of capacity to preempt (competitively obtain) soil resources; (ii) soil solution N, an indication both of resource supply and of resource preemption; (iii) root C/N, which is an indication of species differences in root chemical stoichiometry and hence of both relative physiological limitation by N and of treatment-induced differences in soil N availability; (iv) percent soil water content, an indication both of resource supply and of resource preemption; and (v) percent light transmission, which can indicate variation in the level of asymmetric competition for this aboveground resource.

These five measures were not closely related among plots (*23*) and thus, in theory, each could serve to independently drive species richness. In bivariate relations, species richness was negatively related ($P < 0.001$) to increased soil solution N and root biomass, and positively related to root C/N ratios ($P < 0.001$) and percent soil water content ($P < 0.05$) (Fig. 2, A to D), but unrelated ($P > 0.50$) to percent light transmission. Moreover, all five of these attributes were significant predictors of species richness in multiple regression models (Table 2 and table S1), with residual plots from the full model (Fig. 2, E to H) similar to those for the bivariate relationships for the four belowground attributes (Fig. 2, A to D). This similarity indicates that the associations seen in bivariate relations are also significant (and in the same direction) once the effects on species richness of other important driving variables are accounted for. The question then is whether these attributes responded to CO_2 and N treatments in ways that would "drive" species richness in the observed patterns.

Table 1. Repeated-measures analysis of variance of CO_2 and N effects on species richness. Effects of year, CO_2, and N, and all interactions, on species richness (the number of species observed in a plot during sampling) are shown.

Variable	Whole-plot species richness	
	F value	*P* > *F*
Whole-model R^2	0.70	<0.0001
Effect		
CO_2	0.23	0.655
N	49.43	<0.0001
Year	66.83	<0.0001
$CO_2 \times$ year	0.66	0.741
N × year	2.49	0.0089
$CO_2 \times N$	5.61	0.0228
$CO_2 \times N \times$ year	0.27	0.896

Table 2. Species richness of the plant community as a function of total root biomass, root C/N ratio, soil solution N concentration, percent soil water content, and percent light transmission. Data are mean values for species richness, biomass, C/N ratio, soil solution N concentration, percent soil water content, and percent light transmission for each of 48 plots measured over 10 years (*26*). Model was selected based on Akaike's Information Criteria from a suite of models involving these variables and all possible interactions.

Variable	Whole-plot species richness	
	F value	*P* > *F*
Whole model R^2	0.65	<0.0001
Effect		
Root biomass	9.85	0.0031
Root C/N	6.06	0.0182
Soil solution N	13.91	0.0006
Soil water	3.12	0.0850
Light transmission	6.09	0.0176
Root biomass × soil water	9.11	0.0044

Total root biomass, root C/N, soil solution N, and percent soil water content were influenced by CO_2, N, and their combination in ways that were consistent with CO_2 and N effects on species richness, and with soil and root factor relations with species richness (Tables 1 to 3 and Figs. 1 and 2), whereas percent light transmission was not (*23*). For example, enriched N increased soil solution N concentration and root biomass, and decreased root C/N and percent soil water content (Table 3), all of which are consistent with decreased species richness given relations shown in Figs. 1 and 2. Treatments that made plants N-rich or productive, and soils N-rich or dry, also reduced diversity. Moreover, joint effects of CO_2 and N on biomass, C/N, and soil solution N mirrored their joint effects on species richness (i.e., enriched N effects were smaller at elevated than in ambient CO_2 treatments, significantly so for soil solution N; Table 3). Hence, the main and interactive effects on species richness of CO_2 and N in this experiment were apparently the result of impacts of CO_2 and N on several belowground drivers of species richness, perhaps, most importantly, soil solution N (Figs. 1 and 2 and Table 1), which itself showed a significant $CO_2 \times N$ interaction (Table 3).

The changes in species richness under CO_2 and N can also be viewed through the lens of individual species and functional group responses (*4*, *5*, *10*), given that all plots were initially planted with four species from four functional groups (*11*). The relative abundance of C_3 grasses increased markedly with N enrichment (by 69%) and was associated with a modest increase (+8%) in C_3 grass species richness (Table 3). In contrast, with enriched N, two of the three other functional groups had large decreases in relative abundance, and all three had lower species richness (Table 3), with this suppression more modest at elevated than at ambient CO_2, especially for the C_4 grasses ($P = 0.0006$ for the $CO_2 \times N$ interaction). Additionally, changes in species richness in response to CO_2 and N and their interaction were little influenced by changes in frequency (fraction of plots in which they are present) of either the rarest or most frequent species; instead, a set of species of intermediate frequency and abundance played the major role in this regard (*23*).

These results suggest that changes in ecosystem attributes and in functional group relative abundances together explain the main and interactive effects on CO_2 and N on species richness in this system. The decreasing species richness under enriched N likely resulted from competitive exclusion of other functional groups by increasingly abundant C_3 grasses, and was associated with greater root biomass, lower root C/N, greater soil solution N, and lower percent soil water content under enriched N. At this site, increased C_3 grass biomass under N enrichment can reduce soil water availability, leading to increased mortality of other species (*26*), and the BioCON C_4 grasses show reduced relative abundance in simulated drought treatments (*23*). These enriched N effects were somewhat muted under elevated compared to ambient CO_2, because enriched N-induced increases in root biomass, decreases in root C/N, and especially increases in soil solution N were smaller in the enriched CO_2 treatment (Table 3). Given the relations of species richness to each of these potential drivers (Fig. 2), the smaller responses of these attributes to enriched N (in elevated than in ambient CO_2) likely contributed to the smaller N-induced declines in species richness (Tables 1 to 3 and Figs. 1 and 2) in elevated than in ambient CO_2.

In summary, elevated CO_2 had modest effects on species richness (compared to N enrichment), in part because CO_2 effects on key drivers of species richness were smaller and sometimes offsetting. For instance, CO_2-induced increases (Table 3) in root C/N and percent soil water content, which were linked to increases in species richness, counteract biomass productivity effects

Table 3. Percent response (average, 1998 to 2007) of community and ecosystem variables to elevated CO_2 at both ambient and enriched N, as well as to enriched N under both ambient and elevated CO_2 levels. Variables include species richness, root biomass, root C/N ratio, soil solution N, percent soil water content, percent light transmission (all at plot scale), and species richness and relative abundance of each functional group (defined as the fraction of total aboveground biomass). Also shown is whole-model R^2 and significance levels for analysis of variance for each variable in relation to CO_2, N, and their interaction.

Variable	CO_2 effect (% change)		Significance			N effect (% change)		Whole-model R^2
	Ambient N	Enriched N	CO_2	N	$CO_2 \times N$	Ambient CO_2	Elevated CO_2	
Species richness (plot)	−2.2	+6.9		***	*	−15.9	−8.1	0.64
Root biomass (plot)	+11.0	+19.6	**	***		+33.3	+23.7	0.47
Root C/N (plot)	+4.0	+9.7	†	***		−10.4	−5.4	0.31
Soil solution N (plot)	+37.7	−29.2		***	**	+391.1	+152.5	0.60
Percent soil water content	+10.0	+11.3	**	*		−6.8	−5.6	0.24
Percent light transmission (plot)	−1.2	−2.1		***		+17.1	+16.1	0.31
Species richness, C_4 grass	−11.7	+11.1		***	***	−32.7	−15.4	0.78
Species richness, C_3 grass	−1.7	+1.9		***		+5.7	+9.6	0.40
Species richness, N fixer	−6.2	+0.4		***		−26.4	−21.1	0.66
Species richness, forb	+25.5	+31.1	†	*		−18.4	−14.8	0.39
Relative abundance, C_4 grass	−12.3	−8.4		*		−28.3	−25.2	0.48
Relative abundance, C_3 grass	−3.2	−6.6		***		+72.0	+65.9	0.77
Relative abundance, N fixer	+6.3	+12.4		***		−42.5	−39.2	0.25
Relative abundance, forb	+1.0	+11.0				−1.9	+7.8	0.69

†$P < 0.10$; *$P < 0.05$; **$P < 0.01$; ***$P < 0.001$.

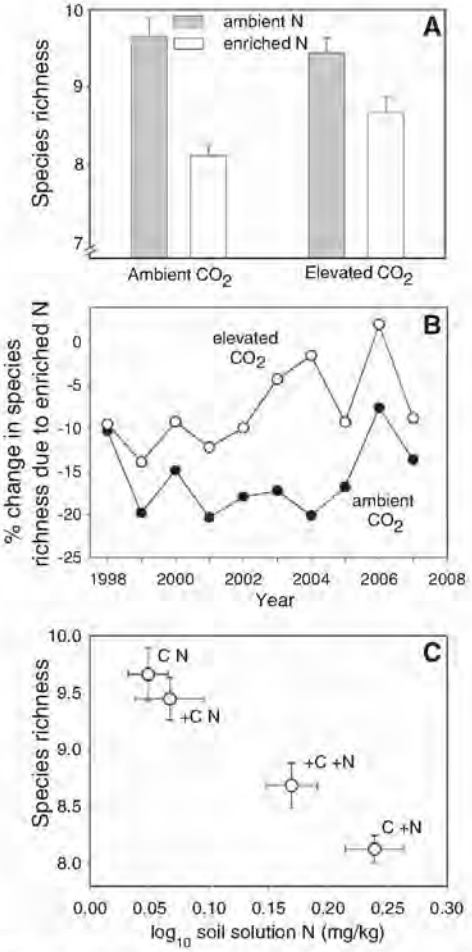

Fig. 1. (**A**) Species richness (±SE among plots) of experimental plots ($n = 48$), under four combinations of CO_2 and N ($n = 12$ plots for each), averaged from 1998 to 2007. (**B**) The percent effect of enriched N treatment on species richness under ambient CO_2 (filled circle) and elevated CO_2 (open circle) conditions from 1998 to 2007. (**C**) Mean species richness (±SE) and soil solution N (mg/kg, 0 to 20 cm depth) (±SE) from 1998 to 2007 for ambient and elevated CO_2-treated plots under ambient and enriched N conditions. Relevant statistics for all panels are shown in Tables 1 to 3 and the text.

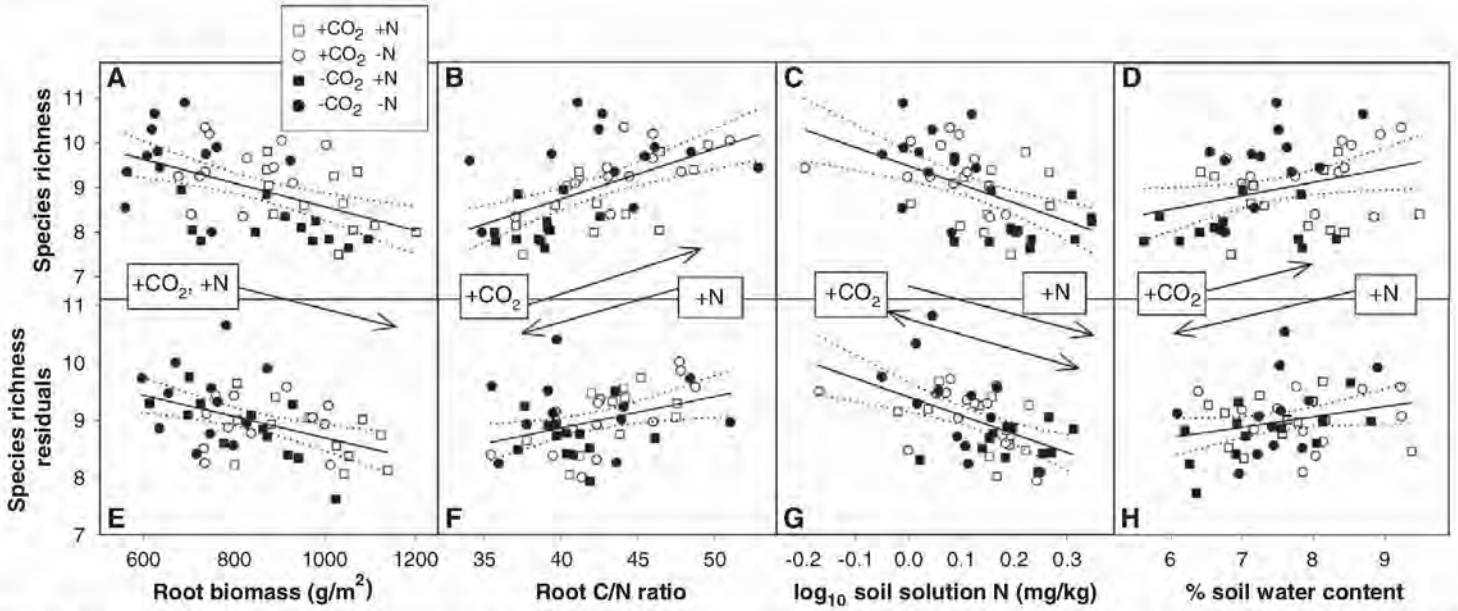

Fig. 2. The relation of mean species richness per plot versus root biomass (0 to 20 cm, g m^{-2}), root C/N ratio, soil solution N (mg/kg, 0 to 20 cm depth), and percent soil water content (0 to 20 cm depth) for all plots (n = 48), each averaged over 10 years [(**A** to **D**), all relations significant $P < 0.05$], as well as the partial residual relationship (**E** to **H**) for each of these from the full multiple regression model. The arrows show directional effects of enriched N (+N) or elevated CO_2 (+CO_2) on both species richness and the ecosystem attribute shown in each panel. Confidence intervals (95%) for the model fit are shown with the dotted lines. Multiple regression model details are provided in Tables 1 and 2.

(which decrease species richness) (Fig. 2). In contrast, enriched N has a consistent negative effect on species richness because its effects on productivity, soil solution N, soil moisture, and root C:N ratio all individually suppress species richness (Fig. 2). Moreover, because the effects of CO_2 and N on the drivers of species richness differ depending on the particular combinations of levels of CO_2 and N, the joint effects of enriched CO_2 and enriched N were nonadditive, i.e., could not be predicted from knowledge of each alone. These results for a temperate perennial grassland contrast with results of a study of multiple global change effects in annual Mediterranean grassland, where such impacts were predictable from knowledge of each alone (*4*). Competition for soil N, for which soil solution N may be a surrogate, and for soil water may be particularly important in BioCON, as (i) there were $CO_2 \times N$ interactions on soil solution N as well as on species richness, (ii) enriched N and CO_2 treatments drove percent soil water content in opposite directions, and (iii) competition for N and water have been shown to influence the outcomes of competition of these species and functional groups at Cedar Creek (*7*, *23*–*25*). Indeed, when averaged over the entire experiment for the four contrasting CO_2 and N levels, the correspondence between species richness and soil solution N was pronounced (Fig. 1)—with treatments diverging along a single species richness and soil solution N axis.

Results of this study have important implications for natural ecosystems under global change, because they demonstrated that within 2 years and persisting for 10, altered CO_2 and N regimes had significant, interactive, impacts on species diversity. From a biodiversity conservation perspective, there was no evidence to support the worst-case scenario in which rising CO_2 and N deposition each suppresses diversity and jointly do so additively or synergistically. Instead, their joint interaction ameliorated the diversity loss due to N enrichment that occurs under ambient CO_2. However, in viewing the possible implications of these results at broad scales and in other ecosystems, it is uncertain whether rising CO_2 and N deposition will generally cause changes in plant biomass, plant or soil stoichiometry, soil chemistry, or soil moisture or other drivers of biotic interactions in ways that lead to the same nonlinear interactive effect on species richness. Regardless, the sensitivity of species richness to factors that themselves were sensitive to CO_2 and N suggests that predicting responses of species richness at local community scales may be challenging, as responses to multiple global change drivers are perhaps not generally predictable from the responses to each alone. Given that humankind is enriching the biosphere in both CO_2 and N (*8*) and that species diversity is a key ecological attribute providing ecosystem services, such uncertainty further contributes to our concern about systemic impacts of global environmental change on Earth's ecological sustainability.

References and Notes

1. C. J. Stevens, N. B. Dise, J. O. Mountford, D. J. Gowing, *Science* **303**, 1876 (2004).
2. R. Oren *et al.*, *Nature* **411**, 469 (2001).
3. M. R. Shaw *et al.*, *Science* **298**, 1987 (2002).
4. E. S. Zavaleta, M. R. Shaw, N. R. Chiariello, H. A. Mooney, C. B. Field, *Proc. Natl. Acad. Sci. U.S.A.* **100**, 7650 (2003).
5. P. A. Niklaus, C. Körner, *Ecol. Monogr.* **74**, 491 (2004).
6. K. N. Suding *et al.*, *Proc. Natl. Acad. Sci. U.S.A.* **102**, 4387 (2005).
7. C. M. Clark, D. Tilman, *Nature* **451**, 712 (2008).
8. IPCC (Intergovernmental Panel on Climate Change), *Climate Change 2007: The Physical Science Basis: Summary for Policymakers* (IPCC Secretariat, February 2007).
9. L. Gough, C. W. Osenberg, K. L. Gross, S. L. Collins, *Oikos* **89**, 428 (2000).
10. C. Potvin, L. Vasseur, *Ecology* **78**, 666 (1997).
11. P. B. Reich *et al.*, *Nature* **410**, 809 (2001).
12. T. K. Rajaniemi, V. J. Allison, D. E. Goldberg, *J. Ecol.* **91**, 407 (2003).
13. M. J. Crawley *et al.*, *Am. Nat.* **165**, 179 (2005).
14. C. J. Stevens, N. B. Dise, D. J. G. Gowing, J. O. Mountford, *Glob. Change Biol.* **12**, 1823 (2006).
15. Y. Hautier, P. A. Niklaus, A. Hector, *Science* **324**, 636 (2009).
16. W. S. Harpole, D. Tilman, *Nature* **446**, 791 (2007).
17. E. A. Ainsworth, S. P. Long, *New Phytol.* **165**, 351 (2005).
18. P. B. Reich, B. A. Hungate, Y. Luo, *Annu. Rev. Ecol. Evol. Syst.* **37**, 611 (2006).
19. P. B. Reich *et al.*, *Nature* **440**, 922 (2006).
20. A. M. Novotny *et al.*, *Oecologia* **151**, 687 (2007).
21. R. W. Sterner, J. J. Elser, Eds., *Ecological Stoichiometry: The Biology of Elements from Molecules to the Biosphere*. (Princeton Univ. Press, Princeton, NJ, 2002).
22. R. T. Belote, J. F. Weltzin, R. J. Norby, *New Phytol.* **161**, 827 (2004).
23. Materials, methods, and supplemental information are available as supporting material on *Science* Online.
24. D. Wedin, D. Tilman, *Ecol. Monogr.* **63**, 199 (1993).
25. R. Dybzinski, D. Tilman, *Am. Nat.* **170**, 305 (2007).
26. M. Davis *et al.*, *Plant Ecol.* **145**, 341 (1999).

27. Funding was provided by the U.S. Department of Energy, National Institute for Climate Change Research; and the NSF, Long Term Ecological Research (LTER), Biocomplexity, and Long Term Research in Environmental Biology (LTREB) programs. Thanks to S. Hobbie, K. Worm, J. Trost, and D. Bahauddin in particular, and to many others for their contributions to the BioCON project; and to R. Dybzinski, K. Suding, I. Woodward, and B. Medlyn for critiquing an earlier version of the manuscript.

Supporting Online Material

www.sciencemag.org/cgi/content/full/326/5958/1399/DC1
Materials and Methods
Table S1
References

8 July 2009; accepted 1 October 2009
10.1126/science.1178820

The Insect Neuropeptide PTTH Activates Receptor Tyrosine Kinase Torso to Initiate Metamorphosis

Kim F. Rewitz,[1] Naoki Yamanaka,[1,2] Lawrence I. Gilbert,[3] Michael B. O'Connor[1,2]*

Holometabolous insects undergo complete metamorphosis to become sexually mature adults. Metamorphosis is initiated by brain-derived prothoracicotropic hormone (PTTH), which stimulates the production of the molting hormone ecdysone via an incompletely defined signaling pathway. Here we demonstrate that Torso, a receptor tyrosine kinase that regulates embryonic terminal cell fate in *Drosophila*, is the PTTH receptor. Trunk, the embryonic Torso ligand, is related to PTTH, and ectopic expression of PTTH in the embryo partially rescues *trunk* mutants. In larvae, *torso* is expressed specifically in the prothoracic gland (PG), and its loss phenocopies the removal of PTTH. The activation of Torso by PTTH stimulates extracellular signal–regulated kinase (ERK) phosphorylation, and the loss of ERK in the PG phenocopies the loss of PTTH and Torso. We conclude that PTTH initiates metamorphosis by activation of the Torso/ERK pathway.

Many organisms undergo distinct temporal transitions in morphology as a part of their normal life process. In humans, for example, passage through puberty is accompanied by changes in body mass and the acquisition of sexual maturity. Likewise, in all holometabolous insects, metamorphosis transforms the immature larva into a completely new body form that is capable of reproductive activity. In both cases, neuropeptide signaling in response to environmental and nutritional cues triggers the transition process (*1*–*5*). In insects, the process is initiated by the neuropeptide known as prothoracicotropic hormone (PTTH) (*3*, *6*, *7*). PTTH signals to the prothoracic gland (PG), the primary insect endocrine organ, which triggers the production and release of ecdysone, the precursor of the active steroid molting hormone 20-hydroxyecdysone (20E) (*8*). The increased level of 20E provides a systemic signal that ends the larval growth period and initiates metamorphosis.

PTTH has been proposed to be structurally similar to certain mammalian growth factors (*9*) that are ligands for receptor tyrosine kinases (RTKs). Previous studies have also indicated that PTTH signaling results in the phosphorylation of cellular signaling molecules that are linked to the mitogen-activated protein kinase (MAPK) pathway in the PG (*10*–*13*). In light of the potential involvement of MAPK pathway components in PTTH signaling, we examined the expression of all *Drosophila* RTKs in the PG to determine whether any showed a tissue-specific expression profile that was consistent with a possible role as a PTTH receptor. We found that after early embryogenesis, the RTK encoded by *torso* is expressed specifically in the PG (Fig. 1, A and B).

The gene *torso* belongs to the so-called terminal group of genes that are required for the correct patterning of anterior and posterior structures during early embryogenesis (*14*–*16*). The presumed ligand for Torso during terminal patterning is Trunk (Trk), which contains a cysteine knot-type motif in the C-terminal region similar to the motif in PTTH (*3*, *15*). Also like PTTH, Trk is thought to be proteolytically processed from a precursor molecule to generate an active C-terminal fragment that is comparable in length to that of PTTH (*17*). Alignment of the protein sequences of Trk and PTTH reveals that they share some conserved structures in the C-terminal region that compose the mature peptide, including all of the six cysteines that are important for intramonomeric bonds of the PTTH homodimeric molecule (*7*) (Fig. 1C). Previously, it was noted that Trk is related to Spatzle (*17*), but a phylogenetic analysis of different insect cysteine knot-type proteins shows that Trk and PTTH form a separate cluster and that PTTH is the closest paralog of Trk (fig. S1). These results raise the possibility that Trk and PTTH share a conserved three-dimensional structure enabling both to activate Torso despite the modest conservation of primary sequence. We did not detect expression of *trk* in the wandering third-instar larval (L3) stage using real-time polymerase chain reaction (PCR) (no product after 30 PCR cycles) or by in situ hybridization to the brain-PG complex (fig. S2), supporting the idea that PTTH, and not Trk, is a ligand for Torso in post-blastoderm stages.

To investigate possible post-embryonic roles of Torso in *Drosophila* development, we used RNA interference (RNAi) to knock down *torso* specifically in the PG. The PG-specific *phantom* (*phm*)-*Gal4* line (*phm*>) was used to drive expression of RNAi constructs under control of upstream activator sequences (UASs) in the PG. As shown in Fig. 2A, this expression of a *torso* RNAi construct produced a phenotype that was almost identical to the one created by the loss of PTTH-expressing neurons (*3*). Reduction of *torso* expression in the PG of *phm>torso-RNAi* larvae delays the onset of pupariation by 5.8 days as compared with the *phm*> + control animals, similar to the 5.4-day delay of pupariation in animals lacking PTTH. As with the loss of the PTTH-producing neurons, *torso* silencing in the PG also leads to excessive growth during the prolonged L3 stage, resulting in increased pupal size (Fig. 2B). To test the specificity of the RNAi, we confirmed that *torso* mRNA levels are reduced in *phm>torso-RNAi* larvae and that the PG cells are morphologically normal, although slightly smaller (fig. S3).

[1]Department of Genetics, Cell Biology, and Development, University of Minnesota, Minneapolis, MN 55455, USA. [2]Howard Hughes Medical Institute, University of Minnesota, Minneapolis, MN 55455, USA. [3]Department of Biology, University of North Carolina, Chapel Hill, NC 27599, USA.

*To whom correspondence should be addressed. E-mail: moconnor@umn.edu

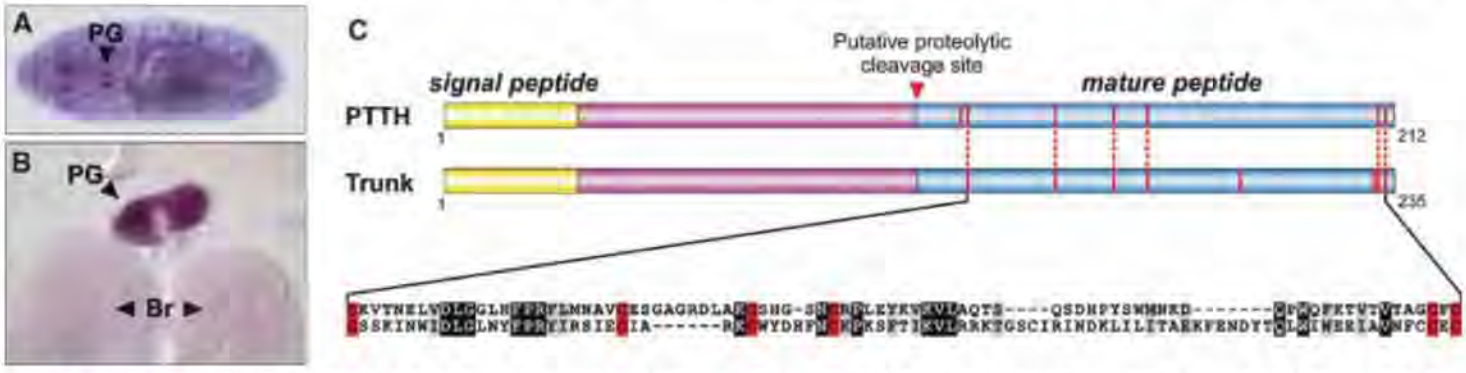

Fig. 1. Torso is expressed in the PG, and its embryonic ligand Trk is structurally related to PTTH. (**A**) RNA in situ hybridization of *torso* in a stage-17 *Drosophila* embryo (dorsal view with anterior to the left). (**B**) RNA in situ hybridization of *torso* in the PG and brain (Br) from a wandering L3 larva of *Drosophila*. (**C**) Sequence similarity between *Drosophila* PTTH and Trk. Processing of the precursors is believed to release the mature C-terminal peptides that form cysteine knot-type structures. Red vertical lines indicate cysteines and numbers refer to amino acid residues.

Because *torso* is a maternal-effect gene, homozygous mutants derived from heterozygous parents are viable. Therefore, we examined the developmental profile and adult size of animals homozygous and transheterozygous for three different *torso* mutations. Larvae with mutations in *torso* exhibited substantial developmental delays, although not as long as those seen by RNAi knockdown, in the time to pupariation as compared with heterozygous controls (fig. S2), and the mutants produced larger adults (table S1). The difference in time delay may result from residual maternally loaded *torso* mRNA. In contrast, *trk* mutants developed on a normal time scale (fig. S2), and adults were similar in size to heterozygous control adults (table S1), demonstrating that the phenotype of *torso* mutants is independent of early embryonic signaling.

In animals lacking PTTH-producing neurons, it is the low level of the active molting hormone 20E that causes the developmental delay and tissue overgrowth (*3*). To investigate whether the *torso* loss-of-function phenotype is also caused by low 20E levels, we fed 20E to *phm>torso-RNAi* larvae. Similar to what was found when the PTTH-producing neurons were removed, feeding these larvae with 20E completely rescued the developmental delay and overgrowth (Fig. 2, A and B). Taken together, these results demonstrate that reducing Torso signaling in the PG alone phenocopies the loss of PTTH, which is consistent with the notion that Torso mediates PTTH signaling in the PG. If this is the case, we expect that the constitutively active $torso^{RL3}$ allele (*14*) might produce precocious pupation, as would overexpression of PTTH. Consistent with this conjecture, we found, using the *daughterless* (*da*)-*Gal4* driver (*da>*), that ubiquitous overexpression of PTTH advances the onset of pupariation by 11.5 hours as compared with (*da>+*) balancer controls ($P < 0.001$) and produces smaller adults, as shown previously (*3*). At 25°C, $torso^{RL3}$ is activated, and heterozygous $torso^{RL3/+}$ animals pupariate 9.2 hours before controls ($P < 0.001$) and form smaller adult males (table S1).

To establish whether PTTH can activate Torso in vivo, we reasoned that if PTTH is a ligand for Torso, then ectopic expression of PTTH in the embryo might elicit partial rescue of *trk* mutants. To examine this, we used the maternal *nanos* (*nos*)-*Gal4* line (*nos>*) to drive ubiquitous early embryonic expression of a UAS-PTTH-hemagglutinin (HA)–tagged transgene in *trk* mutant embryos. In the blastoderm-stage embryo, activation of Torso by Trk induces expression of the downstream target gene *tailless* (*tll*) in the anterior and posterior regions (*15*, *17*). The inability to activate this target gene in *trk* (Fig. 3) or *torso* (*15*) mutants leads to the loss of structures posterior to the seventh abdominal segment. Early embryonic expression of PTTH was observed in 13% ($n = 70$ embryos) of blastoderm-stage embryos derived from trk^1/trk^1; *nos*>PTTH females (Fig. 3). Ectopic expression of PTTH in these embryos was sufficient to activate *tll* in the posterior part of the embryos (11% of embryos showing posterior *tll* expression; $n = 56$). Although PTTH expression did not fully restore wild-type *tll* expression, the partial rescue elicited by PTTH was sufficient to restore posterior structures, such as the Filzkörper, in several *trk* mutant embryos. These results provide genetic evidence that PTTH functions as a ligand for Torso in vivo.

In the embryo, Torso signaling is transduced through the canonical MAPK pathway that includes the *Drosophila* homologs of Ras (Ras85D), Raf (Draf), MAPK kinase (MEK), and extracellular signal–regulated kinase (ERK) (*15*). If Torso is indeed the PTTH receptor, we expect that disrupting MAPK signaling in the PG would result in a phenotype similar to that resulting from loss of the PTTH-producing neurons and Torso signaling. So far, the role of the MAPK pathway in transduction of the PTTH signal has been determined only by in vitro studies of lepidopteran PG (*10*–*13*). In *Drosophila*, the expression of dominant negative forms of Ras and Raf is known to delay development (*18*). To further examine the importance of the MAPK pathway in mediating PTTH/Torso signaling, we used RNAi to reduce the expression of several core components of this pathway, including Ras, Raf, and ERK, in the PG. Loss of either Ras, Raf, or ERK delayed pupariation by 4.3, 2.7, and 6.1 days, respectively (Fig. 2A). ERK silencing in the PG delays pupariation as severely as the reduction of Torso signaling or the complete loss of the PTTH-producing neurons does. The increase in size of *phm>ERK-RNAi* pupae and adults (Fig. 2C and table S1) was also

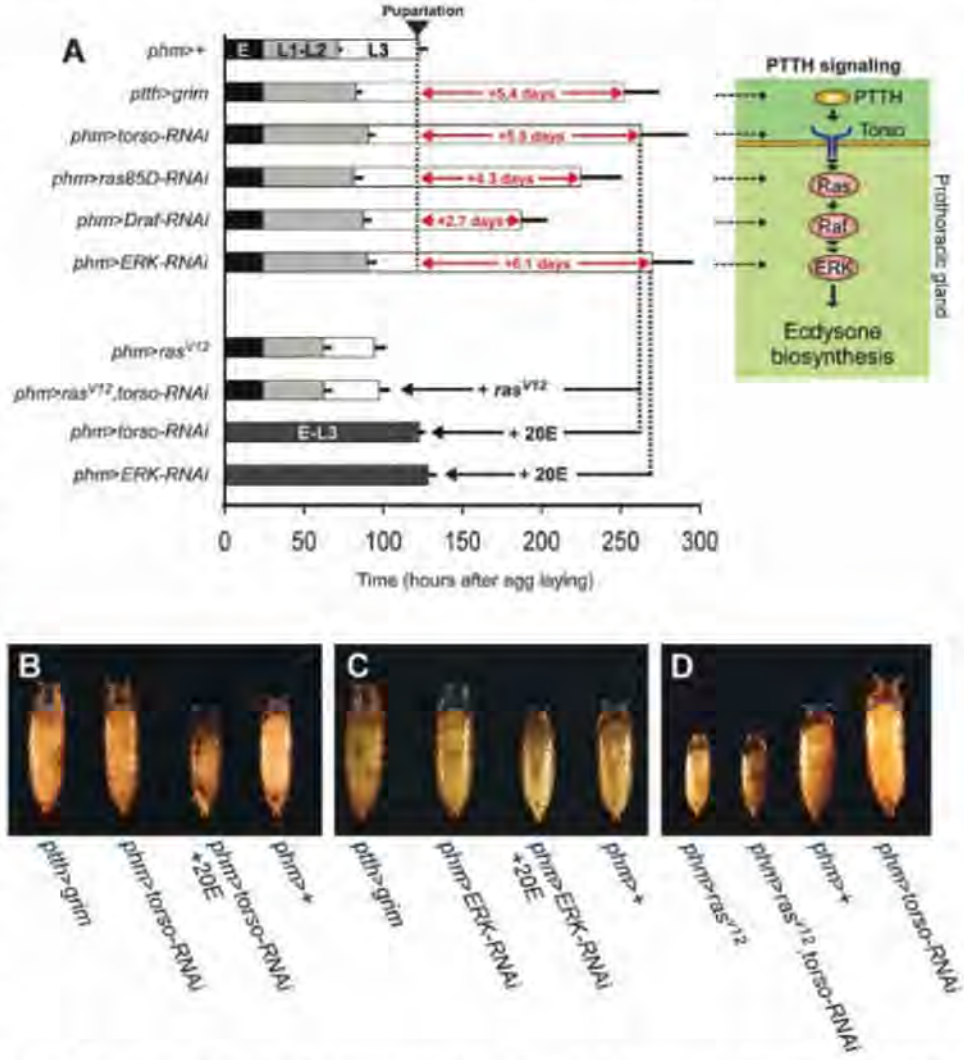

Fig. 2. Disruption of Torso signaling phenocopies loss of PTTH-producing neurons. The *ptth-Gal4* line (*ptth>*) expresses Gal4 specifically in the PTTH-producing neurons (*3*), and the *phm>* expresses Gal4 specifically in the PG (*20*). **(A)** Compared with the control (*phm>+*), reducing Torso (*phm>torso-RNAi*), Ras (*phm>ras85D-RNAi*), Raf (*phm>Draf-RNAi*), and ERK (*phm>ERK-RNAi*) signaling in the PG prolongs the duration of L3, similar to the removal of PTTH [*ptth>grim*: expression of the pro-apoptotic gene *grim* under control of the *ptth* promoter genetically ablates the PTTH-producing neurons (*3*)] in *Drosophila*. Expression of the constitutively active ras^{V12} rescues the developmental delay of *torso* silencing in the PG (*phm>*ras^{V12}, *torso-RNAi*). Feeding with 20E rescues the delay of both *torso* and *ERK* silencing in the PG. Error bars represent SD. A model of PTTH signaling (right) is proposed based on the Torso pathway components in the embryo (*15*). Multiple arrowheads indicate intermediate steps in the pathway. **(B)** Effect on pupal size of *torso* silencing in the PG and 20E feeding. **(C)** Effect on pupal size of *ERK* silencing in the PG and 20E feeding. **(D)** Ras^{V12} expression in the PG rescues the overgrowth phenotype of *torso* silencing. E, embryogenesis; L1, first larval instar; L2, second larval instar.

similar to the increase caused by the loss of PTTH or loss of Torso. The developmental delay, as well as the size increase caused by ERK silencing, were negated by 20E feeding (Fig. 2, A and C). The less-severe phenotypes produced by the loss of Raf and Ras may result from less-efficient knockdown or, in the case of Ras, may reflect partial redundancy with Rap1 (*19*). Consistent with Ras being downstream of *torso*, we also found that expression of constitutively active Ras in the PG completely rescued the *torso-RNAi*–induced delay and overgrowth phenotype (Fig. 2, A and D). Taken together, these results indicate that, as during embryonic terminal patterning, Torso regulation of ecdysone production in the PG is primarily mediated by the MAPK pathway, resulting in the activation of ERK.

To test directly whether stimulation of Torso by PTTH could lead to ERK phosphorylation, we sought to develop a cell culture–based signaling assay. Because we have not been able to produce active *Drosophila* PTTH in tissue culture, we turned to the silkworm *Bombyx mori* (*7*) and cloned a full-length *Bombyx torso* cDNA (fig. S4). As in *Drosophila*, the *Bombyx torso* ortholog is expressed predominantly in the PG of the final (fifth)–instar larvae (figs. S4 and S5). Stimulation of *Drosophila* S2 cells transfected with *Bombyx torso* and *Drosophila ERK* with 10^{-9} M PTTH led to robust phosphorylation of ERK (Fig. 4). PTTH stimulation of ERK phosphorylation was not detected in control S2 cells, either incubated in the absence of PTTH or those stimulated with PTTH but not expressing *Bombyx torso*. *Bombyx* PTTH did not stimulate activation of ERK through *Drosophila* Torso or through the insulin receptor (fig. S6), demonstrating that ERK stimulation by *Bombyx* PTTH is specific to *Bombyx* Torso. These results demonstrate that Torso is a functional PTTH receptor that is able to mediate PTTH signaling through the activation of the ERK pathway.

Our observations define another role for the terminal system, which is the initiation of metamorphosis at the end of larval growth. Therefore, insects apparently use the same core system for two developmentally distinct processes: the establishment of terminal cell fate in the embryo and the termination of larval growth at the correct time to ensure an appropriate final adult body size. Our identification of the PTTH receptor will facilitate further characterization of the system that determines body size in insects. It will be of interest to ascertain just how similar this system is in overall design to the hypothalamus-pituitary-gonadal axis, which controls the timing of puberty in mammals (*5*).

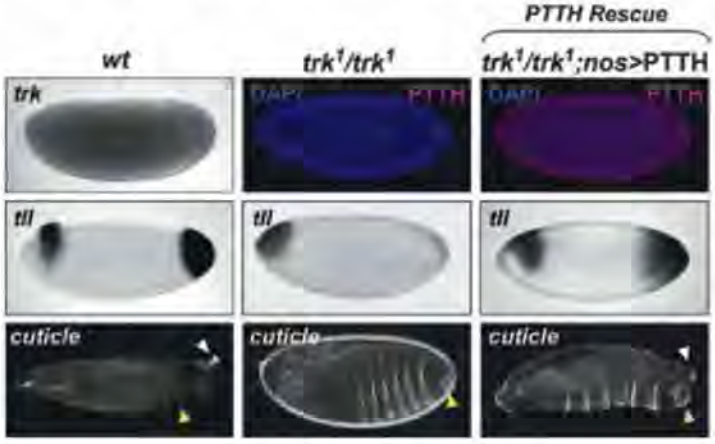

Fig. 3. PTTH is a ligand for Torso in vivo. PTTH partially rescues the terminal phenotype of *Drosophila* trk^1 mutants. RNA in situ hybridization shows that in wild-type (wt) embryos, *trk* is ubiquitously expressed. The *nos>* allows the uniform expression of PTTH in the embryo, which is confirmed by immunolocalization of HA-tagged PTTH in embryos from trk^1/trk^1;*nos*>PTTH females. In trk^1 mutants, *tll* expression is restricted to the anterior domain because of the lack of Trk-dependent activation of Torso. Ectopic expression of PTTH in trk^1/trk^1;*nos*>PTTH embryos partially restores posterior expression of *tll*. Cuticle structures posterior to the seventh abdominal denticle belt are missing in trk^1 mutants, but expression of PTTH in these embryos can rescue the morphology of denticle belt structures (yellow arrowheads) and induce formation of posterior structures such as the Filzkörper (white arrowheads). Shown are lateral views of embryos with anterior to the left. DAPI, 4′,6′-diamidino-2-phenylindole.

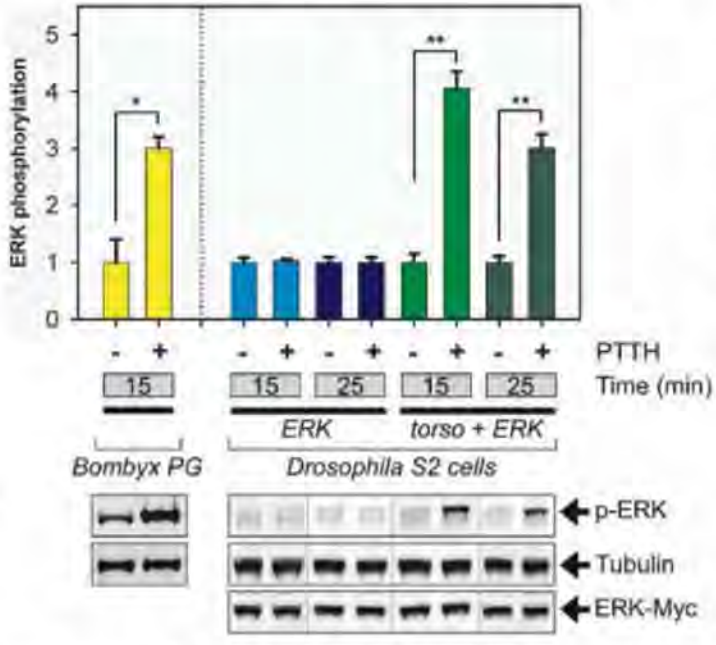

Fig. 4. Characterization of *Bombyx* Torso as a functional PTTH receptor in vitro. Quantified levels of phosphorylated ERK (top) in the *Bombyx* PG and *Drosophila* S2 cell extract determined by immunoblotting (bottom) with an antibody that is specific to the phosphorylated form of ERK (p-ERK) are shown. *Bombyx* PGs from day 4 fifth-instar larvae were incubated for 15 min in medium (control) or medium containing 1 nM *Bombyx* PTTH. *Drosophila* S2 cells overexpressing *ERK-Myc* and *Bombyx torso* were incubated in medium (control) or medium containing 1 nM *Bombyx* PTTH for 15 and 25 min. As a control to show that *Bombyx torso* is responsible for the activation by PTTH that induces ERK phosphorylation, S2 cells transfected with *ERK-Myc*, but not with *torso*, were subjected to the same treatment. Phospho-ERK levels were normalized against total ERK (ERK-Myc). As a loading control, blots were also probed with an antibody to tubulin. Fold changes are relative to control. Error bars represent SD. $^*P < 0.05$, $^{**}P < 0.01$.

References and Notes

1. J. Colombani *et al.*, *Science* **310**, 667 (2005).
2. S. Layalle, N. Arquier, P. Leopold, *Dev. Cell* **15**, 568 (2008).
3. Z. McBrayer *et al.*, *Dev. Cell* **13**, 857 (2007).
4. C. K. Mirth, L. M. Riddiford, *Bioessays* **29**, 344 (2007).
5. S. M. Popa, D. K. Clifton, R. A. Steiner, *Annu. Rev. Physiol.* **70**, 213 (2008).
6. A. Kawakami *et al.*, *Science* **247**, 1333 (1990).
7. R. Rybczynski, in *Comprehensive Molecular Insect Science*, L. I. Gilbert, K. Iatrou, S. Gill, Eds. (Elsevier, Oxford, 2005), vol. 3, pp. 61–123.
8. L. I. Gilbert, R. Rybczynski, J. T. Warren, *Annu. Rev. Entomol.* **47**, 883 (2002).
9. T. Noguti *et al.*, *FEBS Lett.* **376**, 251 (1995).
10. J. L. Lin, S. H. Gu, *J. Insect Physiol.* **53**, 622 (2007).
11. K. F. Rewitz *et al.*, *Insect Biochem. Mol. Biol.* **39**, 475 (2009).
12. R. Rybczynski, S. C. Bell, L. I. Gilbert, *Mol. Cell. Endocrinol.* **184**, 1 (2001).
13. R. Rybczynski, L. I. Gilbert, *Mol. Cell. Endocrinol.* **205**, 159 (2003).
14. J. Casanova, G. Struhl, *Genes Dev.* **3**, 2025 (1989).
15. W. X. Li, *Dev. Dyn.* **232**, 656 (2005).
16. F. Sprenger, L. M. Stevens, C. Nusslein-Volhard, *Nature* **338**, 478 (1989).
17. A. Casali, J. Casanova, *Development* **128**, 1709 (2001).
18. P. E. Caldwell, M. Walkiewicz, M. Stern, *Curr. Biol.* **15**, 1785 (2005).
19. S. Mishra, S. M. Smolik, M. A. Forte, P. J. Stork, *Curr. Biol.* **15**, 366 (2005).
20. H. Ono *et al.*, *Dev. Biol.* **298**, 555 (2006).

21. K.F.R. was supported by a postdoctoral fellowship from the Danish Natural Science Research Council (grant no. 272-07-0340). M.B.O. is an investigator with the Howard Hughes Medical Institute. We are grateful to our collaborators J. T. Warren and R. Rybczynski and to reviewers for helpful comments. We also thank H. Kataoka for *Bombyx* PTTH. The GenBank accession number for *Bombyx* Torso is GQ477743.

Supporting Online Material

www.sciencemag.org/cgi/content/full/326/5958/1403/DC1
Materials and Methods
SOM Text
Figs. S1 to S6
Table S1
References

18 May 2009; accepted 5 October 2009
10.1126/science.1176450

Planarian Hh Signaling Regulates Regeneration Polarity and Links Hh Pathway Evolution to Cilia

Jochen C. Rink,* Kyle A. Gurley,* Sarah A. Elliott, Alejandro Sánchez Alvarado†

The Hedgehog (Hh) signaling pathway plays multiple essential roles during metazoan development, homeostasis, and disease. Although core protein components are highly conserved, the variations in Hh signal transduction mechanisms exhibited by existing model systems (*Drosophila*, fish, and mammals) are difficult to understand. We characterized the Hh pathway in planarians. Hh signaling is essential for establishing the anterior/posterior axis during regeneration by modulating *wnt* expression. Moreover, RNA interference methods to reduce signal transduction proteins Cos2/Kif27/Kif7, Fused, or Iguana do not result in detectable Hh signaling defects; however, these proteins are essential for planarian ciliogenesis. Our study expands the understanding of Hh signaling in the animal kingdom and suggests an ancestral mechanistic link between Hh signaling and the function of cilia.

The Hh signaling pathway plays numerous evolutionarily conserved roles in the regulation of cell growth and patterning during the embryonic and postembryonic development of animals as diverse as fruit flies and humans. The misregulation of this pathway has equally profound consequences, resulting in defects such as cyclopia and tumorigenesis in mammals. Secreted Hh protein alters gene transcription by binding the cell-surface receptor Patched (Ptc), preventing repression of the seven-membrane-spanning receptor Smoothened (Smo) by Ptc. This activates Gli transcription factors and inactivates their inhibitor Suppressor of Fused (SuFu). Despite conservation of these core components and their mode of function (*1*, *2*), Hh signal transduction mechanisms appear to have diversified throughout evolution (*3*). *Drosophila* Hh signaling is cilia-independent and requires the kinesin Costal2 (*4*) (Kif7/27 in vertebrates) and the kinase Fused (*5*). The mouse Hh pathway requires primary cilia (*6*, *7*) and Kif7 (*8*–*10*), but not Fused (*11*, *12*). Zebrafish use cilia, Kif7, Fused, and Iguana/Dzip1 (Igu) (*13*–*19*). *Caenorhabditis elegans* has lost a functional Hh pathway altogether (*20*). Because planarians belong to a group of animals that evolved independently from flies, fish, and mammals (fig. S1), an analysis of planarian Hh signaling could reveal how the mechanistic differences in a highly conserved signaling pathway arose.

Systematic sequence homology searching of the *Schmidtea mediterranea* genome identified single homologs for planarian Hh (*Smed-hh*), Patched (*Smed-ptc*), Smoothened (*Smed-smo*), and Suppressor of Fused (*Smed-sufu*), but three Gli homologs (figs. S2 and S3). Of the Gli homologs, only *Smed-gli-1* exhibited an obvious role in Hh signaling. We cloned (see Supporting Online Material) and analyzed the expression of these planarian Hh components by in situ hybridization (Fig. 1, A to C, and fig. S4). *ptc* expression was reduced by RNA interference (RNAi) of pathway activators (*hh*, *smo*, and *gli-1*) and elevated by RNAi of pathway inhibitors (*ptc* and *sufu*) (Fig. 1B), which suggests that, as in other animals (*21*–*23*), *ptc* is a Hh target in planarians and its expression marks sites of Hh

Department of Neurobiology and Anatomy, Howard Hughes Medical Institute, University of Utah School of Medicine, 401 MREB, 20 North 1900 East, Salt Lake City, UT 84103, USA.

*These authors contributed equally to this work.
†To whom correspondence should be addressed. E-mail: sanchez@neuro.utah.edu

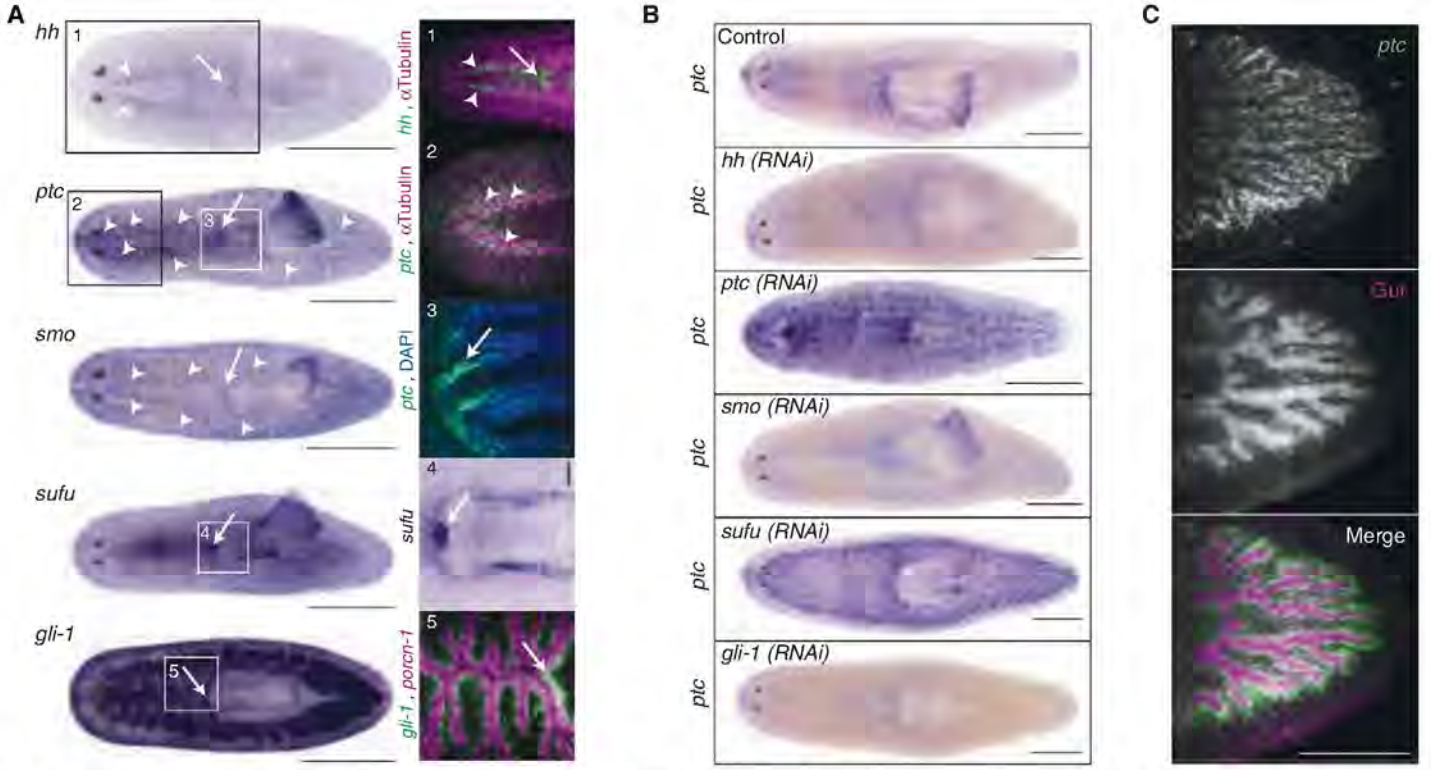

Fig. 1. Planarian Hedgehog signaling. (**A**) Gene expression in intact animals. Boxes magnified on right. 1, Epifluorescence image, *hh* (green), CNS (magenta, α-tubulin antibody). 2, Confocal image, ventral head, *ptc* (green). CNS (magenta, α-tubulin antibody). 3, Root of pharynx, *ptc* (green). Nuclei [blue, 4′,6′-diamidino-2-phenylindole (DAPI)]. 4, *sufu* expression near root of pharynx. 5, *gli-1* (green), gut epithelium (magenta, *Smed-porcn-1* and *Smed-sialin*). Scale bar, 0.5 mm. Arrowheads, ventral nerve cord. Arrow, root of pharynx. (**B**) *ptc* expression in RNAi-treated intact animals. The seemingly paradoxical up-regulation of *ptc* upon *ptc(RNAi)* results from the massive promotion of Hh signaling by *ptc(RNAi)*. Scale bar, 0.5 mm. (**C**) *ptc* expression confocal images in *sufu(RNAi)* intact animals. Scale bar, 0.2 mm.

signaling. Complementary expression of *ptc*, *hh*, and *smo* throughout the central nervous system (CNS), and *hh*, *ptc*, *smo*, *sufu*, and *gli-1* near the root of the pharynx implicates these locations as possible sites of Hh activity (Fig. 1A and fig. S4). *gli-1* expression in cells surrounding the gut enterocytes (Fig. 1A) and particularly strong *ptc* up-regulation upon *sufu(RNAi)* in the same region (Fig. 1C) may indicate a conserved function of Hh in the gastrovascular system (*24*, *25*). Additionally, mitotic activity was increased by *ptc(RNAi)* and *sufu(RNAi)* but decreased by *hh(RNAi)* (figs. S5 and S6), mirroring the mitotic effects of Hh in other organisms (*26*, *27*). Altogether, these initial studies suggest that planarian Hh signaling likely has diverse functions in various adult tissues.

To investigate whether the Hh pathway contributes to the signaling network orchestrating planarian regeneration, we amputated the heads and tails of double-stranded RNA (dsRNA)–fed animals. Targeting the pathway activator *hh* left anterior regeneration unaffected but caused a range of posterior regeneration defects, including reduced or absent tail tissue and concomitant changes in posterior marker expression (Fig. 2, A to B″, and fig. S7). Conversely, RNAi against the pathway inhibitor *ptc* left posterior regeneration unaffected but caused anterior-specific defects, including tail instead of head formation and striking changes in marker expression (Fig. 2, D to F″, fig. S7, and movies S1 and S2). Targeting *gli-1* and *smo* produced identical regeneration phenotypes to *hh(RNAi)*, and *sufu(RNAi)* resembled *ptc(RNAi)* (fig. S8), establishing tail or head regeneration defects as a general consequence of decreased or increased Hh signaling, respectively. Systematic RNAi dosage experiments ranked the range of phenotypes according to severity. Three observations are particularly noteworthy. First, "headless" animals expressed neither head nor tail markers anteriorly (Fig. 2, E′ and E″) but expressed a marker for intermediate anterior cell fate (fig. S9), reminiscent of dose-dependent roles for Hh in other contexts (*28*). Second, "cyclopic" animals resulted from increased Hh signaling. The same phenotype occurs in vertebrates (*29*) but is caused by decreased Hh signaling. This difference, along with lack of expression of *Smed-hh* along the planarian midline, suggests that the midline function of Hh in vertebrates is not conserved in planarians. Third, SuFu has a prominent role in planarians, which is similar to vertebrates but different from *Drosophila* (*30*). RNAi combination of two pathway activators or inhibitors enhanced the respective phenotypes, whereas activator-inhibitor combinations suppressed each other (fig. S10). However, besides the expected and predominant function of Smo as a pathway activator, these experiments also indicated a cryptic inhibitory activity, but the mechanistic basis of this effect is currently unclear. Combined with regeneration time course experiments showing that Hh-related phenotypes originate during early phases of regeneration (fig. S11), our data demonstrate that the different phenotypic classes resulting from altered Hh signaling constitute a series of anterior/posterior (A/P) patterning defects and that early Hh signaling is necessary and sufficient for tail regeneration.

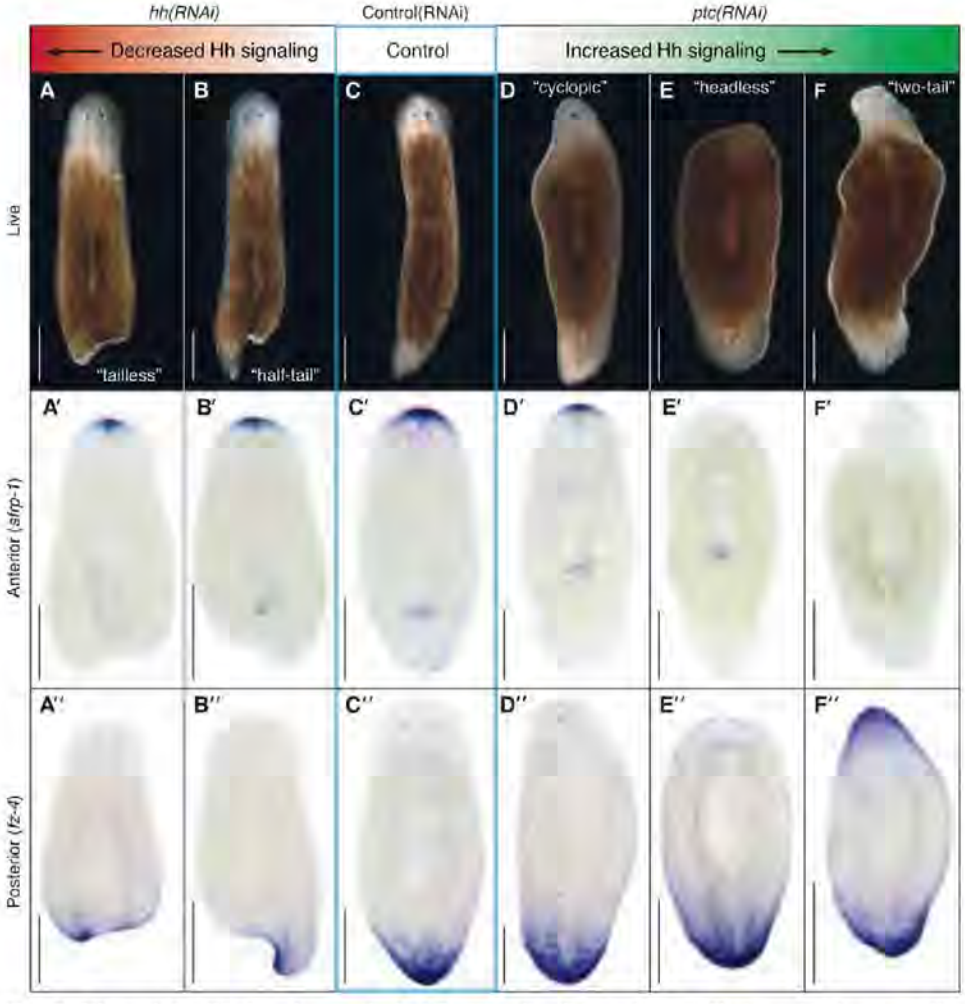

Fig. 2. Misregulated Hh signaling results in A/P patterning defects. (**A** to **F**) Live images of regenerating trunk fragments 14 days after amputation. Decreased Hh signaling achieved by *hh(RNAi)* (A to B″), and increased signaling by *ptc(RNAi)* (D to F″). Phenotypes are arranged according to severity. (A′ to F′) Expression of anterior marker [*Smed-sFRP-1* (*31*, *33*)]. (A″ to F″) Expression of posterior marker [*Smed-fz-4* (*31*)].

The early requirements for elevated Hh signaling in tails and reduced Hh signaling in heads mirrors those for β-catenin signaling (*31*–*33*). In addition, diluted dosages of *APC-1(RNAi)*, which elevate β-catenin activity (*31*), produced a range of phenotypes quite similar to *ptc(RNAi)* (fig. S12). Combining doses of *ptc(RNAi)* and *APC-1(RNAi)* that by themselves elicited only weak defects led to a striking increase in phenotype severity (Fig. 3A). Moreover, a single feeding of β*catenin-1(RNAi)* in *ptc(RNAi)*-fed animals completely suppressed the *ptc(RNAi)* "two-tail" phenotype, causing head formation at both anterior and posterior wounds (Fig. 3B). Thus, the Hh and β-catenin pathways synergize functionally to specify tails, and tail induction by elevated Hh signaling likely depends on β-catenin activity.

Because a Wnt ligand (*Smed-wntP-1*) was recently implicated in activating β-catenin during tail regeneration (*34*, *35*), we examined whether *wnt* expression was regulated by Hh signaling. One day after amputation, *wntP-1* expression was reduced in *hh(RNAi)* animals and strongly increased in *ptc(RNAi)* animals (Fig. 3C, top). In contrast, *wntP-1* expression was not altered in β*catenin-1(RNAi)* or *APC-1(RNAi)* animals (Fig. 3C, bottom), ruling out indirect polarity-associated effects. Expression of an additional *wnt* gene functioning in tail regeneration (*Smed-wnt11-2*) (*34*) showed a dependence on both Hh and β-catenin pathway activity (fig. S13). Unchanged *ptc* expression in β*catenin-1(RNAi)* or *APC-1(RNAi)* animals suggested that β-catenin may not reciprocally control Hh signaling (fig. S14). *wntP-1(RNAi)* suppressed the *ptc(RNAi)* phenotypes at anterior wounds (Fig. 3D) and strongly enhanced the *hh(RNAi)* phenotypes at posterior wounds, synergistically leading to the appearance of a posterior head in 20% of *wntP-1(RNAi);hh(RNAi)* animals (Fig. 3E). These data indicate that Hh-mediated *wntP-1* expression is likely responsible for the posteriorizing effect of *ptc(RNAi)* and that improved *hh(RNAi)* efficiency might be suffi-

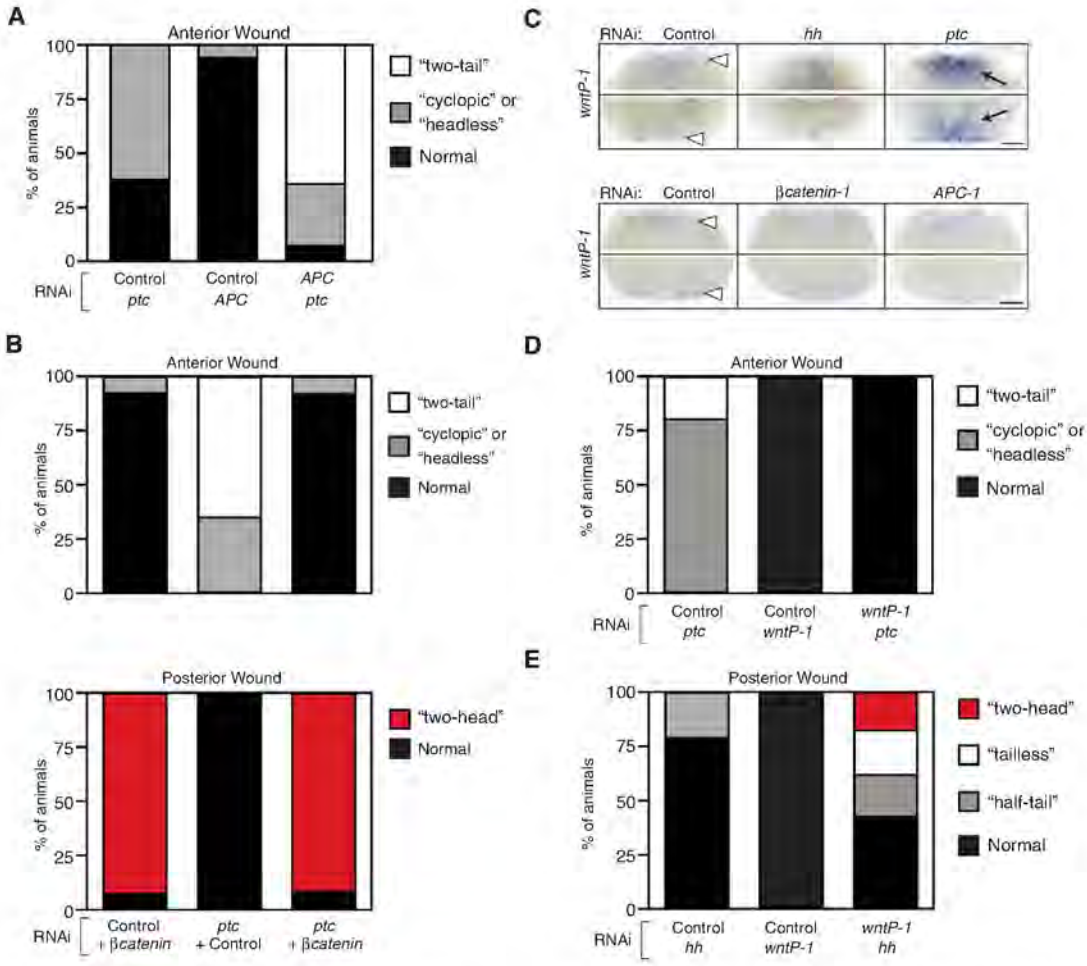

Fig. 3. Hh specifies A/P fate through interaction with Wnt/β-catenin signaling. (**A** and **B**) Quantification of double-RNAi experiments scored for anterior or posterior regeneration defects. Relative frequency of indicated phenotypes in a cohort of trunk fragments scored 14 days after amputation. (A) $N > 15$ animals per condition. (B) $N > 20$ animals per condition. (**C**) *wntP-1* expression at 1 day after amputation. White arrowheads, expression at both anterior (upper panels of each set) and posterior (lower panels of each set) wounds in control animals. Black arrows, up-regulated expression in *ptc(RNAi)*. Scale bars, 0.2 mm. (**D** and **E**) Quantification of double-RNAi experiments scored for (D) anterior and (E) posterior regeneration defects. Relative frequency of indicated phenotypes in trunk fragment cohort scored 14 days after amputation. $N > 21$ animals per condition.

cient for head formation from posterior wounds. In intact animals, *wnt* expression did not respond to alterations of Hh pathway activity (fig. S15), which suggests that Hh control of *wnt* expression is specific to the establishment of A/P polarity during regeneration.

The expression patterns of *hh*, *ptc*, and *wntP-1* did not show a posterior bias, as might be expected from their requirement for tail formation (Fig. 3C and fig. S16). Whereas such bias could be short-lived or difficult to detect, symmetric Hh activity and *wnt* expression would require additional components to specifically inhibit β-catenin activity anteriorly. Nonetheless, our data clearly demonstrate synergies between the Hh and Wnt signaling pathways during regeneration. We conclude that Hh influences A/P fate by controlling *wnt* expression.

The range of Hh-related regeneration defects from subtle to severe (Fig. 2) provided a sensitive readout to assess whether cilia or other signal transduction components play a role in the planarian Hh pathway. We cloned planarian homologs of intraflagellar transport (IFT) proteins (*Smed-IFT52*, *Smed-IFT88*, *Smed*-IFT172, and *Smed-kif3b*) (fig. S17), which are universally required for the assembly of cilia (*36*). Animals fed dsRNA targeting any of the IFT components lost their cilia-dependent gliding ability, advancing more slowly by waves of whole-body contraction and extension (inchworming) instead (Fig. 4A, fig. S18, and movie S3). Consistently, their cilia were severely shortened (Fig. 4B). Additionally, *IFT(RNAi)* animals developed edema (Fig. 4A, inset), likely due to impaired osmoregulation by their heavily ciliated protonephridia. Targeting Hh pathway components did not affect cilia (Fig. 4, A and B). Despite the prominent cilia defects, *IFT(RNAi)*-treated animals showed no evidence of altered Hh signaling during regeneration by morphology and early marker expression (fig. S19), and *ptc* expression was unaffected in the CNS, pharynx, and gut (fig. S20A). Although we cannot entirely exclude subtle, nonregeneration-related, or residual cilia contributions (*17*), our data did not uncover a role for cilia in planarian Hh signaling.

We next cloned the single planarian homologs of *fused* (*Smed-fused*), *cos2/kif27/kif7* (*Smed-kif27*), and *iguana* (*Smed-iguana*) (fig. S17), which were all discovered because of mutations severely affecting Hh signaling in *Drosophila* (*4*, *5*) or zebrafish (*18*, *19*), respectively. Silencing *fused*, *kif27*, or *iguana* neither perturbed *ptc* expression (fig. S20B) nor elicited Hh-related regeneration defects (fig. S21). Hence, these components are unlikely to function in planarian Hh signaling, but the same caveat raised for the IFT genes applies. Intriguingly, as for *iguana(RNAi)* (*37*), *fused(RNAi)* or *kif27(RNAi)*–treated worms instead displayed compromised mobility (Fig. 4C), inchworming, tissue edema (Fig. 4D) and complete loss of cilia (Fig. 4E). Furthermore, the expression patterns of *iguana* and *kif27* closely resembled those of cilia genes (fig. S22). These data demonstrate by multiple functional and morphological criteria that *fused*, *kif27*, and *iguana* are essential for planarian ciliogenesis.

This finding establishes that the ciliogenesis functions of Fused, Kif7, and Iguana are not vertebrate-specific (*15*, *17*) but instead are ancestral. The use of cilia, Fused, Kif7, and Iguana in the zebrafish Hh pathway (*13*–*15*, *18*, *19*), cilia and Kif7 in the mouse Hh pathway (*8*–*10*), and Fused and Cos2 in the *Drosophila* Hh pathway (*3*) further implies that all three model organisms rely on cilia and/or ancient cilia components for Hh signaling. Thus, the association between Hh signaling and cilia is most likely also ancestral (fig. S23). This conclusion is based solely on the ciliogenesis functions of Fused and Cos2/Kif27/Kif7 and is unaffected by whether they also function in planarian Hh signaling. In fact, uncovering evidence to this effect would further strengthen the argument for an ancestral connection.

Our findings suggest that the perplexing diversity in Hh signal transduction mechanisms among flies, fish, and mammals arose from group-specific losses of the ancestral association between cilia and Hh signaling (fig. S23). This raises the question of why core components are highly conserved, yet the contribution of cilia-related proteins to Hh signaling is variable. The dynamic

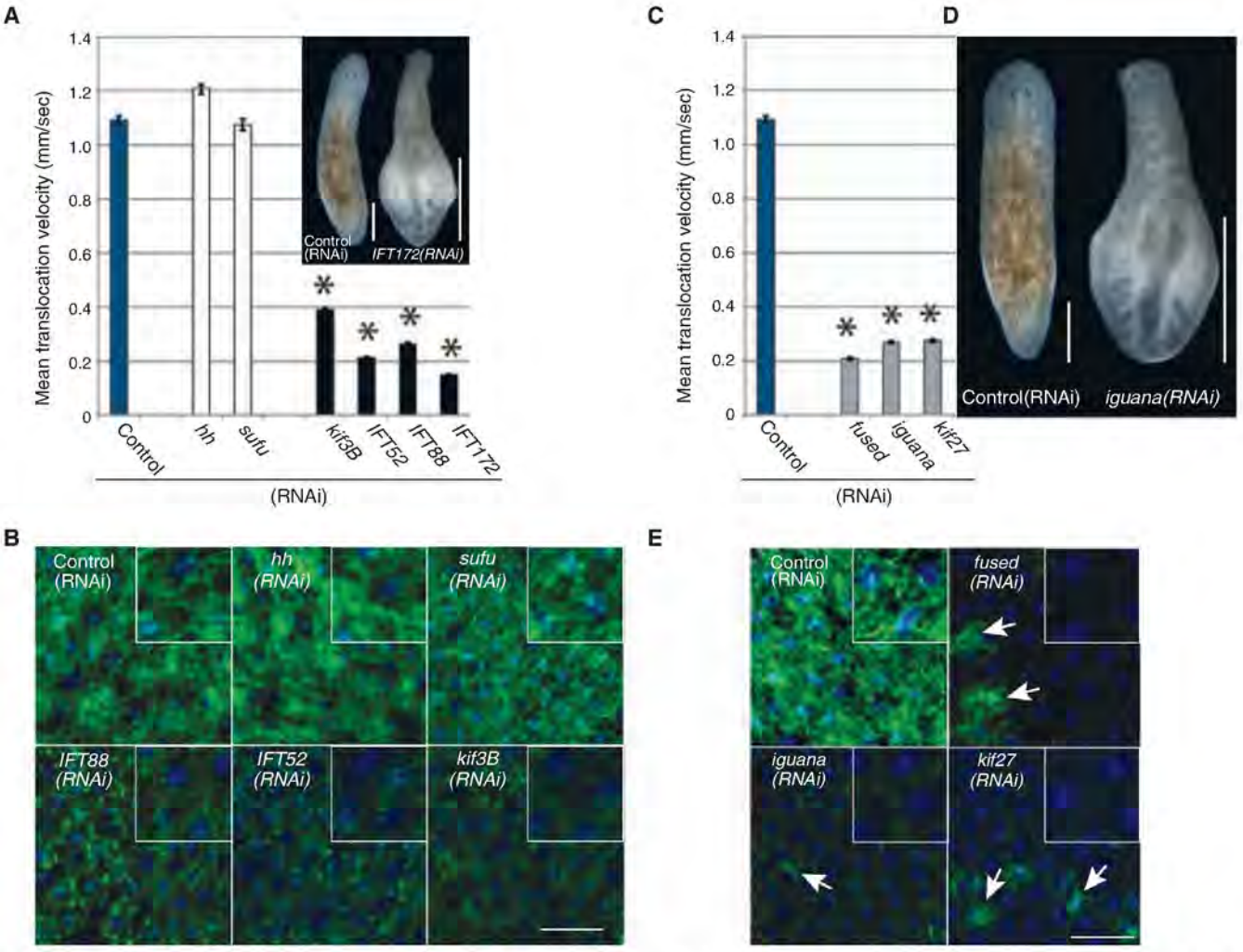

Fig. 4. Hh signaling is cilia-independent, and *kif27*, *fused*, and *iguana* are cilia genes in planarians. (**A**) Mean translocation speed quantified from movies of animals having received the indicated RNAi treatments. Error bars, SEM. *, $P < 0.01$ versus control (one-way analysis of variance). Data is from ≥ 4 movies with $N \geq 5$ animals per movie. (Inset) Example of tissue edema caused by *IFT172(RNAi)*. Scale bars, 0.5 mm. (**B**) Ventral cilia confocal projections (green, acetylated tubulin antibody), overlayed with nuclei (blue, DAPI) to demonstrate epithelial integrity. RNAi treatments as indicated. Insets, zoom. Punctate pattern, remaining cilia stumps. Scale bars, 50 μm. (**C**) Translocation speed calculated as in (A). (**D**) Tissue edema in *iguana(RNAi)* animal 14 days after amputation. Scale bar, 0.5 mm. (**E**) Ventral cilia confocal projections (green, acetylated tubulin antibody) overlayed with nuclei (blue, DAPI) as in (B). Arrows, remaining tufts of cilia on cells not yet affected by RNAi. Residual staining in *fused(RNAi)*, *iguana(RNAi)*, and *kif27(RNAi)* animals due to non–cilia-related staining of subepithelial structures. Scale bar, 50 μm.

shuttling of core components between subcellular compartments in both flies and vertebrates (*9*, *10*, *38*) may have originally been organized by cilia (providing a location) and the associated IFT complexes (providing the motors). The divergence of Hh signaling mechanisms could thus reflect the choice of a new location or motor for organizing the interplay between core components.

References and Notes

1. P. W. Ingham, M. Placzek, *Natl. Rev.* **7**, 841 (2006).
2. L. Lum, P. A. Beachy, *Science* **304**, 1755 (2004).
3. D. Huangfu, K. V. Anderson, *Development* **133**, 3 (2006).
4. J. C. Sisson, K. S. Ho, K. Suyama, M. P. Scott, *Cell* **90**, 235 (1997).
5. T. Preat *et al.*, *Nature* **347**, 87 (1990).
6. D. Huangfu, K. V. Anderson, *Proc. Natl. Acad. Sci. U.S.A.* **102**, 11325 (2005).
7. D. Huangfu *et al.*, *Nature* **426**, 83 (2003).
8. H. O. Cheung *et al.*, *Sci. Signal.* **2**, ra29 (2009).
9. S. Endoh-Yamagami *et al.*, *Curr. Biol.* **19**, 1320 (2009).
10. K. Liem Jr., M. He, P. Ocbina, K. Anderson, *Proc. Natl. Acad. Sci. U.S.A.* **106**, 13377 (2009).
11. M. H. Chen, N. Gao, T. Kawakami, P. T. Chuang, *Mol. Cell. Biol.* **25**, 7042 (2005).
12. M. Merchant *et al.*, *Mol. Cell. Biol.* **25**, 7054 (2005).
13. S. Y. Tay, P. W. Ingham, S. Roy, *Development* **132**, 625 (2005).
14. C. Wolff, S. Roy, P. W. Ingham, *Curr. Biol.* **13**, 1169 (2003).
15. C. W. Wilson *et al.*, *Nature* **459**, 98 (2009).
16. P. Aanstad *et al.*, *Curr. Biol.* **19**, 1034 (2009).
17. P. Huang, A. F. Schier, *Development* **136**, 3089 (2009).
18. K. Sekimizu *et al.*, *Development* **131**, 2521 (2004).
19. C. Wolff *et al.*, *Genes Dev.* **18**, 1565 (2004).
20. T. R. Burglin, P. E. Kuwabara, *WormBook* **2006**, 1 (28 January, 2006); 10.1895/wormbook.1.76.1.
21. L. V. Goodrich, R. L. Johnson, L. Milenkovic, J. A. McMahon, M. P. Scott, *Genes Dev.* **10**, 301 (1996).
22. Y. Chen, G. Struhl, *Cell* **87**, 553 (1996).
23. V. Marigo, M. P. Scott, R. L. Johnson, L. V. Goodrich, C. J. Tabin, *Development* **122**, 1225 (1996).
24. D. Kang *et al.*, *Development* **130**, 1645 (2003).
25. F. Simonnet, J. Deutsch, E. Queinnec, *Dev. Genes Evol.* **214**, 537 (2004).
26. S. Takashima, M. Mkrtchyan, A. Younossi-Hartenstein, J. R. Merriam, V. Hartenstein, *Nature* **454**, 651 (2008).
27. J. J. Trowbridge, M. P. Scott, M. Bhatia, *Proc. Natl. Acad. Sci. U.S.A.* **103**, 14134 (2006).
28. P. W. Ingham, A. P. McMahon, *Genes Dev.* **15**, 3059 (2001).
29. C. Chiang *et al.*, *Nature* **383**, 407 (1996).
30. T. Preat, *Genetics* **132**, 725 (1992).
31. K. A. Gurley, J. C. Rink, A. Sánchez Alvarado, *Science* **319**, 323 (2008).
32. M. Iglesias, J. L. Gomez-Skarmeta, E. Salo, T. Adell, *Development* **135**, 1215 (2008).
33. C. P. Petersen, P. W. Reddien, *Science* **319**, 327 (2008).
34. T. Adell, E. Salo, M. Boutros, K. Bartscherer, *Development* **136**, 905 (2009).
35. C. P. Petersen, P. W. Reddien, *Proc. Natl. Acad. Sci. U.S.A.* **106**, 17061 (2009).
36. L. Pedersen, J. Rosenbaum, *Curr. Top. Dev. Biol.* **85**, 23 (2008).
37. P. W. Reddien, A. L. Bermanage, K. J. Murfitt, J. R. Jennings, A. Sánchez Alvarado, *Dev. Cell* **8**, 635 (2005).
38. S. Y. Wong, J. F. Reiter, *Curr. Top. Dev. Biol.* **85**, 225 (2008).

39. We thank the Sánchez laboratory for helpful comments and C. Adler for sharing data on *iguana*. Work supported by NIH National Institute of General Medical Sciences grants RO-1 GM57260 to A.S.A. and F32GM082016 to K.A.G. J.C.R. was funded by the European Molecular Biology Association. A.S.A. is a Howard Hughes Medical Institute investigator. All sequences associated with this study have been deposited in GenBank and have accession numbers GQ337474 to GQ337490.

Supporting Online Material
www.sciencemag.org/cgi/content/full/1178712/DC1
Materials and Methods
Figs. S1 to S23
Movies S1 to S3
References

6 July 2009; accepted 14 October 2009
Published online 22 October 2009;
10.1126/science.1178712
Include this information when citing this paper.

Promoting Interest and Performance in High School Science Classes

Chris S. Hulleman[1]* and Judith M. Harackiewicz[2]

We tested whether classroom activities that encourage students to connect course materials to their lives will increase student motivation and learning. We hypothesized that this effect will be stronger for students who have low expectations of success. In a randomized field experiment with high school students, we found that a relevance intervention, which encouraged students to make connections between their lives and what they were learning in their science courses, increased interest in science and course grades for students with low success expectations. The results have implications for the development of science curricula and theories of motivation.

Many educators and funding agencies share the belief that making education relevant to students' lives will increase engagement and learning (*1*–*6*). However, little empirical evidence supports the specific role of relevance in promoting optimal educational outcomes, and most evidence that does exist is anecdotal or correlational (*1*–*3*, *5*, *7*, *8*). The purpose of our research is to demonstrate how an intervention specifically designed to enhance the relevance of science to students' lives can enhance interest in science and classroom performance, particularly for students who are most at risk for being disengaged from school.

Numerous curricular reform efforts have emphasized applying science to students' lives, such as providing out-of-school research experiences (*7*, *9*), creating learning modules for specific topics [e.g., "Acids, bases, and cocaine addicts" (*10*, *11*)], developing an undergraduate course [e.g., "The biology and chemistry of everyday life" (*12*, *13*)], and redesigning the academic structure of entire high schools (*14*). For example, the Metro Nashville Public School District redesigned several of its high schools into career academies within which students can choose from thematically focused learning communities (*15*). The intention of these career academies is to enable students to "connect what they learn in school with their career aspirations and goals" (*14*). Although many of these programs have produced positive outcomes, such as improvements in retention in academic programs (*13*) or performance on achievement tests (*7*, *10*–*12*), it is not clear that these effects were due to personal relevance. These educational reforms are multifaceted, and an emphasis on relevance is just one of several components that may have contributed to the programs' outcomes. For example, other potentially effective components are small group instruction (*12*, *16*), repeated exposure to the material (*10*), individual mentoring and teaching (*14*), individualized and/or team-based projects (*7*, *13*, *16*), hands-on activities (*9*), visualization exercises (*11*), increased autonomy (*6*), and increased knowledge development (*17*, *18*).

Programs that emphasize personal relevance may be particularly empowering for students who are disengaged from school because of a lack of confidence. Students can become energized if they believe they are competent in science and can successfully perform classroom tasks. As described by expectancy-value models of motivation (*19*), both an individual's expectancy for success and his or her perception of value for the activity facilitate student motivation. Research on expectancies reveals that expecting to successfully perform a task leads to greater persistence, performance, and interest in academic activities (*19*, *20*). Thus, students who do not believe that they can do well in the classroom are at risk for performing poorly and becoming less interested in academics.

In addition to lacking confidence, students with low success expectancies may not perceive, or may have a harder time perceiving, relevance and value in their schoolwork (*21*). These students may require external support, from teachers or classroom activities, to foster or maintain task engagement (*22*). Interventions that facilitate the perception of relevance in a topic might promote attention and learning for students with low success expectancies (*23*). Instead of withdrawing from the activity, these students may become energized as they discover reasons for exerting effort and becoming more involved in learning (*24*). In contrast, more-confident students may not need this type of motivational boost because their effort and involvement in school are already strong (*22*, *24*).

Reduced interest in academics is particularly problematic for long-term outcomes such as educational and career choices. Research on the development of interest (i.e., experiencing positive affect, value, and knowledge with an activity)

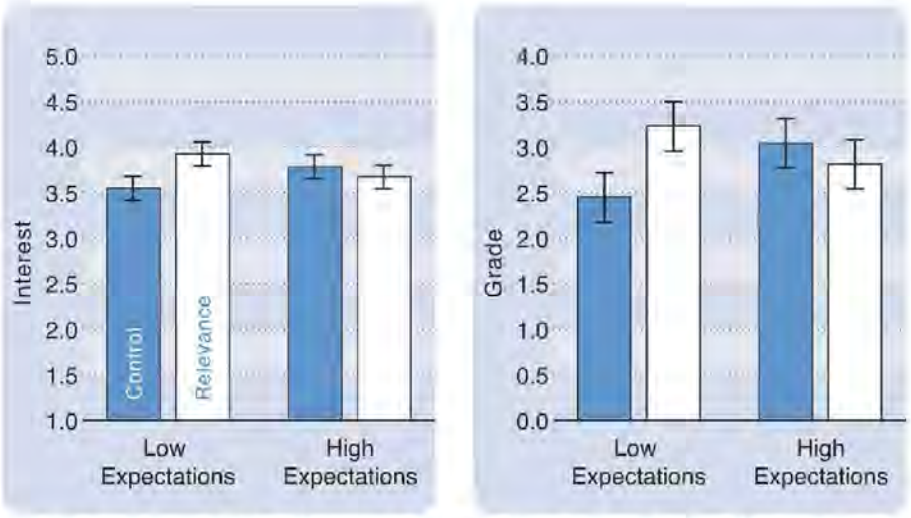

Fig. 1. Science interest (**left**) and course grades (**right**) as predicted by the relevance intervention and performance expectations. Predicted values are computed from the multiple regression equation for the interaction between the relevance intervention and performance expectations (low = −1 SD, high = +1 SD) on final course interest and second-quarter grades. Error bars represent ±2 SEM (0.12 for interest and 0.28 for grades).

[1]Department of Graduate Psychology, James Madison University, Harrisonburg, VA 22807, USA. [2]Department of Psychology, University of Wisconsin–Madison, Madison, WI 53706, USA.

*To whom correspondence should be addressed. E-mail: hullemcs@jmu.edu

demonstrates that interest is a more powerful predictor of future choices than prior achievement or demographic variables (*22*–*25*). For example, Harackiewicz and colleagues (*25*) found that interest in an introductory undergraduate psychology course during freshman year was more predictive of subsequent course taking and majoring in psychology over a 7-year span than were grades from that introductory course. Interest development can begin in situations that promote student engagement with the material [i.e., situational interest (*24*)]. If students repeatedly experience situational interest in relation to a particular topic, they may eventually develop a more enduring interest in the topic (i.e., individual interest). A crucial factor in the progression from situational to individual interest is finding personal meaning and relevance in a topic (*24*). Perceiving a topic to be useful and relevant for other activities or life goals (i.e., utility value) predicts both subsequent interest and performance (*8*).

Making science courses personally relevant and meaningful may engage students in the learning process, enable them to identify with future science careers, foster the development of interest, and promote science-related academic choices (e.g., course enrollment and pursuit of advanced degrees) and career paths. The first step in this process is to investigate whether emphasizing relevance in the classroom promotes interest and performance in science courses. Thus, the goal of our research was to examine the effectiveness of a curricular intervention on interest and performance in high school science classes, particularly for students with low performance expectations.

We conducted a randomized field experiment of a motivational intervention that was designed to help students make connections between their high school science classes and their lives. The intervention was embedded within the entire semester of ninth-grade science courses. We investigated whether this intervention would increase student interest in science, performance in the course, and interest in science-related careers compared with a control condition where students wrote summaries of the material they were studying. Because students wrote about science topics in both conditions, knowledge activation was controlled, and the conditions differed only in terms of personal relevance activation. We predicted that the relevance intervention would promote interest in science and performance in the course, particularly for students with low performance expectations. Subsequently, we expected that increased science interest would lead to more interest in science-related courses and careers.

Participants were 262 high school students taught by seven science teachers (biology, integrated science, and physical science) from two high schools in a small, midwestern city in the United States. Students were 92% ninth-graders (8% tenth-graders), 52% female, 66% Caucasian, 15% African-American, 12% Asian, and 8% Hispanic. The analysis covered one academic semester. Students were randomly assigned within each classroom to either write about the usefulness and utility value of the course material in their own lives (relevance condition, $N = 136$) or write a summary of the material they were studying (control condition, $N = 126$). Teachers were informed that the research concerned the effectiveness of writing assignments but were blind to our hypotheses and students' experimental conditions. To ensure this, the researchers randomly assigned students to conditions at the beginning of the semester by giving students booklets with identical covers but with different instructions inside depending on experimental condition. Students completed their essays in these books, which were collected by the researchers after each assignment, every 3 or 4 weeks starting at the beginning of the semester. Students wrote from 1 to 8 essays [mean (M) = 4.7, SD = 1.4] throughout the semester. The researchers provided teachers with information regarding whether students had completed the essays, but teachers remained blind to condition throughout the semester (*26*).

Students' success expectancies and initial interest in science were measured at the beginning of the semester. Students' interest in science and future plans for science-related courses and careers were measured at the end of the semester [see table S2 for self-report items (*26*)]. Second-quarter grades were obtained from school records for one of the high schools ($N = 100$ students).

The data were analyzed by using multiple regression with dummy codes representing the nesting of students, teachers, and schools (*26*). The focal predictor was the interaction between the dummy code for experimental condition (0 = control, 1 = relevance) and students' performance expectations for the course. We predicted that this interaction term would be negative, such that the intervention effect would be more positive for those with low as opposed to high performance expectations. To examine effects of sex and race and whether the condition effects varied by sex and/or race, the regression models included dummy codes for sex, race, and their interactions with condition (*26*).

As predicted, there was a significant negative interaction between the relevance intervention and students' expectations for success on science interest ($\beta = -0.11$, $P = 0.05$), and the same negative interaction was also significant on second-quarter grades ($\beta = -0.18$, $P = 0.03$). The predicted values from the regression equation indicate that students with low-success expectancies (one standard deviation below the mean) reported more interest in science at the end of the semester (and received higher course grades) in the relevance condition than in the control condition, whereas students with high-success expectancies (one standard deviation above the mean) reported similar amounts of interest (and course grades) regardless of experimental condition (Fig. 1). There were no statistically significant interactions with gender or race, indicating that the intervention did not have differential effects (tables S4 and S5). Lastly, interest in science at the end of the semester was a significant predictor of interest in future science-related courses and careers ($\beta = 0.58$, $P < 0.01$; table S6).

Our results demonstrate that encouraging students to make connections between science course material and their lives promoted both interest and performance for students with low-success expectancies. The effect on performance was particularly striking, because students with low-success expectancies improved nearly two-thirds of a letter grade in the relevance condition compared with the control condition, which is comparable to other social-psychological interventions aimed at reducing the black-white achievement gap (*27*). Differences between conditions for students with high-success expectancies were not statistically significant. These results provide experimental support for expectancy-value models of motivation that hypothesize that perceived value is an important contributor to interest, performance, and future plans (*19*–*21*).

Although our experimental design included randomizing students within classrooms, evaluating the effects of the intervention over time, and assessing change in our dependent variables by including pre- and postmeasures in the analyses, this single study requires replication before generalizations can be made about more diverse settings and students. In addition, although the control condition was designed to activate students' content knowledge, further investigations of the cognitive processes instigated by the intervention are warranted (*28*). Nonetheless, our results show how motivational principles can be used to increase interest and performance in science courses early in high school. Our intervention was effective in raising interest and performance, was easy to implement, and required few external resources. This type of motivational intervention can be easily incorporated into almost any course with little cost to the instructor.

References and Notes

1. M. R. Lepper, J. Henderlong, in *Intrinsic and Extrinsic Motivation: The Search for Optimal Motivation and Performance*, C. Sansone, J. M. Harackiewicz, Eds. (Academic Press, San Diego, CA, 2000), pp. 257–307.
2. National Research Council, *How People Learn: Brain, Mind, Experience, and School* (National Academies Press, Washington, DC, 2000).
3. National Research Council, *Engaging Schools: Fostering High School Students' Motivation to Learn* (National Academies Press, Washington, DC, 2004).
4. P. R. Pintrich, D. H. Schunk, *Motivation in Education: Theory, Research, and Applications* (Prentice Hall, Upper Saddle River, NJ, ed. 2, 2002).
5. T. J. Newby, *J. Educ. Psychol.* **83**, 195 (1991).
6. K. Mitchell *et al.*, *Rigor, Relevance and Results: The Quality of Teacher Assignments and Student Work in New and Conventional High Schools* (American Institutes for Research and SRI International, Washington, DC, 2005).
7. D. I. Hanauer *et al.*, *Science* **314**, 1880 (2006).
8. C. S. Hulleman *et al.*, *J. Educ. Psychol.* **100**, 398 (2008).

9. S. A. Tucker, D. L. Hanuscin, C. J. Bearnes, *Science* **319**, 1621 (2008).
10. N. C. Kwiek, M. J. Halpin, J. P. Reiter, L. A. Hoeffler, R. D. Schwartz-Bloom, *Science* **317**, 1871 (2006).
11. M. C. Linn, H.-S. Lee, R. Tinker, F. Husic, J. L. Chiu, *Science* **313**, 1049 (2006).
12. L. A. Denofrio, B. Russell, D. Lopatto, Y. Lu, *Science* **318**, 1872 (2007).
13. N. L. Fortenberry, J. F. Sullivan, P. N. Jordan, D. W. Knight, *Science* **317**, 1175 (2007).
14. S. H. Russell, M. P. Hancock, J. McCullough, *Science* **316**, 548 (2007).
15. Career Academy (Helping America's Youth, 2008), http://guide.helpingamericasyouth.gov/programdetail.cfm?id=96.
16. Metro Nashville Public School career/thematic centers for 2008-09 (Metro Nashville Public Schools, 2008) www.hillwoodhs.mnps.org/page35350.aspx.
17. F. M. Newmann, H. M. Marks, A. Gamoran, *Am. J. Educ.* **104**, 280 (1996).
18. F. Newmann, A. S. Bryk, J. K. Nagaoka, *Authentic Intellectual Work and Standardized Tests: Conflict or Coexistence?* (Consortium on Chicago School Research, Chicago, 2001).
19. J. Eccles *et al.*, in *Achievement and Achievement Motives: Psychological and Sociological Approaches*, J. T. Spence, Ed. (Freeman, San Francisco, 1983), pp. 75–146.
20. K. A. Updegraff, J. S. Eccles, B. L. Barber, K. M. O'Brien, *Learn. Individ. Differ.* **8**, 239 (1996).
21. J. E. Jacobs, S. Lanza, D. W. Osgood, J. S. Eccles, A. Wigfield, *Child Dev.* **73**, 509 (2002).
22. S. Hidi, J. M. Harackiewicz, *Rev. Educ. Res.* **70**, 151 (2000).
23. S. Hidi, *Rev. Educ. Res.* **60**, 549 (1990).
24. S. Hidi, K. A. Renninger, *Educ. Psychol.* **41**, 111 (2006).
25. J. M. Harackiewicz *et al.*, *J. Educ. Psychol.* **94**, 562 (2002).
26. Materials and methods are available as supporting material on *Science* Online.
27. G. L. Cohen, J. Garcia, N. Apfel, A. Master, *Science* **313**, 1307 (2006).
28. C. S. Hulleman, O. Godes, B. L. Hendricks, J. M. Harackiewicz, *J. Educ. Psychol.*, in press; available online at www.jmu.edu/assessment/research/faculty/hulleman/Enhancing_Interest_revised_JEP_11.18.09.pdf.

29. This article is based on a doctoral dissertation submitted by C.S.H. to the University of Wisconsin-Madison under the supervision of J.M.H. Thanks are extended to M. Alibali, G. Borman, P. Devine, and A. Gamoran for their service on the dissertation committee; to the Madison Metropolitan School District for their assistance with data collection; and to J. Hyde, S. McFadyen-Ketchum, C. Thurber, and T. Hulleman for their comments on earlier versions of this manuscript. This research was supported in part by grants from the Department of Psychology and the Institute for Education Sciences, U.S. Department of Education, through award no. R305C050055 to the University of Wisconsin-Madison and award no. R305B050029 to Vanderbilt University.

Supporting Online Material

www.sciencemag.org/cgi/content/full/326/5958/1410/DC1
Materials and Methods
Tables S1 to S8
Appendix S1
References and Notes

29 May 2009; accepted 5 October 2009
10.1126/science.1177067

Structural Insight into Nascent Polypeptide Chain–Mediated Translational Stalling

Birgit Seidelt,[1]* C. Axel Innis,[2]* Daniel N. Wilson,[1] Marco Gartmann,[1] Jean-Paul Armache,[1] Elizabeth Villa,[3,4]† Leonardo G. Trabuco,[3,4] Thomas Becker,[1] Thorsten Mielke,[5] Klaus Schulten,[3,4,6] Thomas A. Steitz,[2,7]‡ Roland Beckmann[1]‡

Expression of the *Escherichia coli* tryptophanase operon depends on ribosome stalling during translation of the upstream TnaC leader peptide, a process for which interactions between the TnaC nascent chain and the ribosomal exit tunnel are critical. We determined a 5.8 angstrom–resolution cryo–electron microscopy and single-particle reconstruction of a ribosome stalled during translation of the *tnaC* leader gene. The nascent chain was extended within the exit tunnel, making contacts with ribosomal components at distinct sites. Upon stalling, two conserved residues within the peptidyltransferase center adopted conformations that preclude binding of release factors. We propose a model whereby interactions within the tunnel are relayed to the peptidyltransferase center to inhibit translation. Moreover, we show that nascent chains adopt distinct conformations within the ribosomal exit tunnel.

In prokaryotes, proteins are synthesized through translation of mRNA by the 70*S* ribosome, a large ribonucleoprotein complex consisting of a large (50*S*) and a small (30*S*) subunit. Although most polypeptides are thought to passively transit through the exit tunnel of the 50*S* subunit during translation, certain nascent chains appear to specifically interact with or adopt a secondary structure within the exit tunnel (*1*–*3*). This can in turn modulate the rate of translation (*4*) and in some cases induce translational stalling to regulate gene expression (*5*). For instance, stalling during translation of the SecM leader peptide in *Escherichia coli* (*6*–*8*) affects the expression of the downstream *secA* gene (*9*).

In bacteria, translational stalling is also used to regulate the expression of the tryptophan-catabolizing enzymes tryptophanase and tryptophan-specific permease, encoded by the *tnaA* and *tnaB* genes, respectively. In the tryptophanase (*tna*) operon of *E. coli*, the *tnaC* regulatory leader gene is located upstream of these two structural genes (*10*), and the spacer region between the *tnaC* and *tnaA* genes contains several potential Rho-dependent transcription-termination sites. When free tryptophan levels are low in the cell, the TnaC leader peptide is translated and the ribosomes are released from the mRNA, allowing Rho to access and terminate transcription before the RNA polymerase reaches the *tnaA/B* genes. In the presence of free tryptophan, however, the stalled TnaC•70*S* complex masks the Rho-dependent transcription-termination sites, and thus transcription of the downstream *tnaA/B* genes ensues (*10*). Trp^{12}, Asp^{16}, and Pro^{24} of the 24-residue TnaC leader peptide are crucial for stalling (*10*–*12*), and the TnaC•$tRNA^{Pro}$ (Pro^{24}) is located within the peptidyl-tRNA (P) site of the ribosome (*13*), indicating that Asp^{16} and Trp^{12} are retained within the exit tunnel. Moreover, mutations in ribosomal tunnel components alleviate stalling (*11*), which suggests that interactions between the TnaC nascent chain and the ribosomal tunnel are an essential feature of the stalling mechanism.

To gain structural insight into the mechanism by which the TnaC leader peptide induces translational stalling, cryo–electron microscopy (cryo-EM) and single-particle analysis were used to reconstruct an empty *E. coli* 70*S* control ribosome (Fig. 1, A and B), and an *E. coli* 70*S* ribosome stalled during translation of the TnaC leader gene by addition of free tryptophan (TnaC•70*S* complex) (Fig. 1, C and D, and fig. S1) (*14*), at 6.6 Å and 5.8 Å (FSC 0.5 criterion) resolution, respectively (figs. S2 and S3). A comparison with the empty 70*S* ribosome (Fig. 1, A and B) reveals additional density for a peptidyl-tRNA positioned within the P site of the TnaC•70*S* complex and for an mRNA spanning the aminoacyl-tRNA (A), P, and exit-tRNA (E) sites (Fig. 1, C and D, and fig. S4). An atomic model of the complete TnaC•70*S* complex, including the mRNA and $tRNA^{Pro}$ at the P site was generated using molecular dynamics flexible fitting (MDFF) (*15*) (fig. S5). Moreover, additional density within the exit tunnel could be attributed to the TnaC nascent chain (Fig. 1, C and D). At high contour levels, density remained very robust for the C-terminal half of the nascent chain (fig. S6), and

[1]Gene Center and Center for Integrated Protein Science Munich (CIPSM), Department for Chemistry and Biochemistry, University of Munich, Feodor-Lynen-Strasse 25, 81377 Munich, Germany. [2]Department of Molecular Biophysics and Biochemistry, Howard Hughes Medical Institute and Yale University, New Haven, CT 06520, USA. [3]Beckman Institute, University of Illinois at Urbana-Champaign, Urbana, IL 61801, USA. [4]Center for Biophysics and Computational Biology, University of Illinois at Urbana-Champaign, Urbana, IL 61801, USA. [5]UltraStrukturNetzwerk, Max Planck Institute for Molecular Genetics, Ihnestrasse 73, 14195-Berlin, Germany and Institut für Medizinische Physik und Biophysik, Charité, Ziegelstrasse 5-8, 10117 Berlin, Germany. [6]Department of Physics, University of Illinois at Urbana-Champaign, Urbana, IL 61801, USA. [7]Department of Chemistry, Yale University, New Haven, CT 06520, USA.

*These authors contributed equally to this work.
†Present address: Department of Structural Biology, Max Planck Institute of Biochemistry, Am Klopferspitz 18, D-82152 Martinsried, Germany.
‡To whom correspondence should be addressed. E-mail: beckmann@lmb.uni-muenchen.de (R.B.); thomas.steitz@yale.edu (T.A.S.)

continuous density could be seen throughout the entirety of the tunnel at lower contour levels (Fig. 1E). Using density as a restraint, an ensemble of molecular models for residues 4 to 24 of the TnaC peptide was generated using Rapper (*16*) and MDFF (*15*) (Fig. 1F, fig. S7, and movie S1). In agreement with the experimental density, these models featured an extended nascent chain, with root mean square fluctuations (RMSFs) for the Cα atoms smaller than 2 Å (figs. S7 and S8 and movie S1). Because the resolution in our maps is limited to ~6 Å, all subsequent analysis was restricted to the Cα atoms of TnaC.

Inspection of the ribosomal exit tunnel revealed that the density for the TnaC nascent chain fuses with the tunnel wall at a multitude of sites (table S1 and Fig. 2). At the peptidyltransferase center (PTC) of the ribosome, which is the site of peptide bond formation and peptidyl-tRNA hydrolysis (*17*), additional density connects Pro^{24} of TnaC and U2585 of the 23*S* ribosomal RNA (rRNA) (Fig. 2A), whereas the neighboring U2586, together with U1782, form a connection in the region where Asp^{21} is likely to be located (Fig. 2A). Mutations in the U2585 region have been shown to reduce the maximum level of tnaC operon induction (*18*), and the highly conserved Pro^{24} is known to be essential for stalling (*12*). Very strong density links G2061 and A2062 to the region near residues Arg^{23} and Asp^{21}, respectively, of TnaC (Fig. 2B). Although A2062 has not been analyzed for its effects on TnaC stalling, mutations at this position relieve the translational arrest mediated by another leader peptide, ErmCL (*19*). Deeper in the tunnel, two connections are visible linking A2058 and A2059 with the nascent chain in the proximity of Asp^{16} and Lys^{18} (Fig. 2C), which may explain the protection of these nucleotides from sparsomycin-enhanced chemical modification seen during tryptophan-induced TnaC stalling (*20*). Asp^{16} is highly conserved within the TnaC leader peptide, and Asp^{16}Ala mutations abolish the Trp-dependent inactivation of the PTC (*12*). Ribosomes with A2058G mutations are slightly more responsive to Trp-induced stalling in a *rrn* Δ6 strain (*11*), whereas this mutation strongly alleviates secM-mediated translational stalling (*6*). Strong density that extends out from the TnaC nascent chain at the putative location for Lys^{18} fuses with the ribosomal tunnel where U2609 and A752 are located, whereas the adjacent nucleotide A751 appears to contact TnaC in the vicinity of Phe^{13} (Fig. 2C). Consistently, mutations at U2609, as well as an insertion at A751, have been reported to eliminate the induction by tryptophan (*11*). The TnaC nascent chain makes two major contacts with the β-hairpin of ribosomal protein L22 (Fig. 2D): One connects Arg^{95} of L22 with the nascent chain near Thr^{9}, whereas the other is found at the tip of the loop where Lys^{90} and Arg^{92} are located, and fuses with TnaC in the proximity of the highly conserved Trp^{12} residue (Fig. 2D). This latter contact should be important for TnaC stalling because (i) the spacing between Trp^{12} and Pro^{24} is critical for efficient stalling (*10*–*12*) and (ii) mutations of Trp^{12} in TnaC as well as Lys^{90} in L22 also eliminate tryptophan operon induction (*11*). Additional evidence for the close proximity of Trp^{12} to the tip of L22 comes from cross-links between the neighboring Lys^{11} with 23*S* rRNA nucleotides in the vicinity of A751 (*11*), which also makes contact with the tip of the β-hairpin of L22 (Fig. 2D).

Precise positioning of the CCA ends of A- and P-site tRNAs at the PTC is necessary to ensure

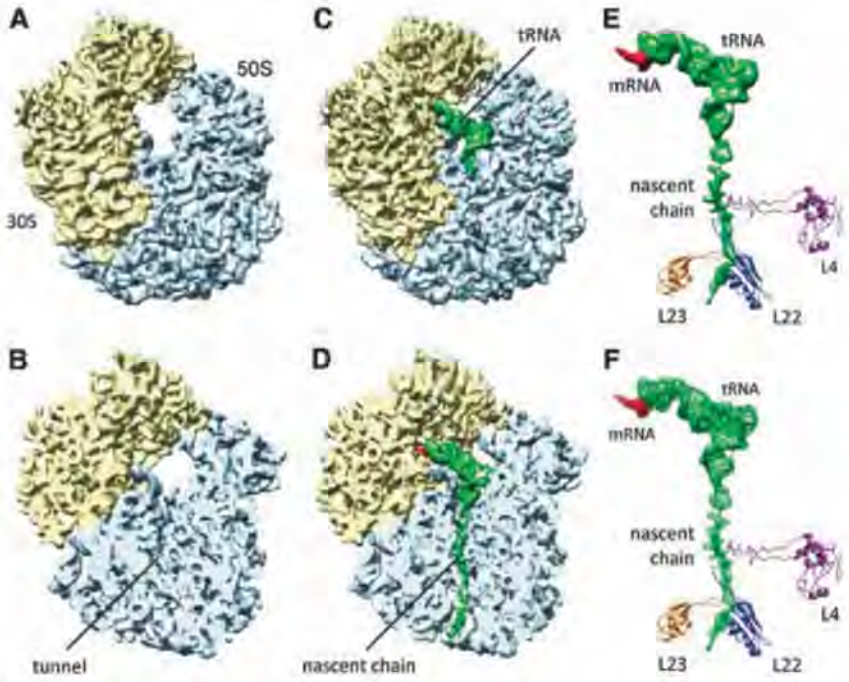

Fig. 1. Cryo-EM reconstruction of the TnaC•70*S* complex. (**A** and **B**) Cryo-EM reconstruction of the control *E. coli* 70*S* ribosome at 6.6 Å resolution, with small and large subunit colored yellow and blue, respectively. (**C** and **D**) The 5.8 Å resolution cryo-EM density of the TnaC•70*S* complex, with density for the TnaC-tRNA shown in green. (**E**) Isolated density for the TnaC-tRNA (green) and mRNA (red) from (C). The relative positions of ribosomal proteins L4 (purple), L22 (blue), and L23 (yellow) are indicated. (**F**) Fitting of molecular models for the TnaC-$tRNA^{Pro}$ into the cryo-EM density from (E).

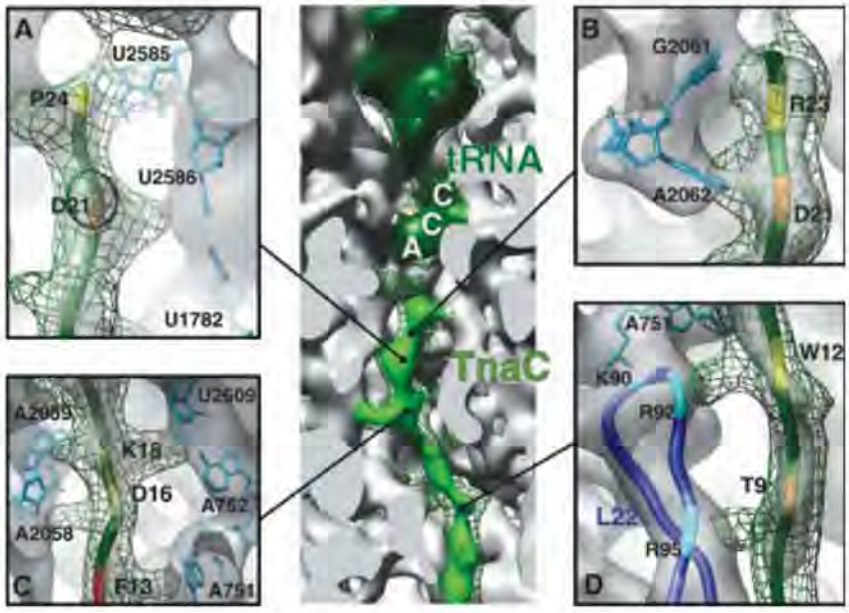

Fig. 2. Interaction between the TnaC nascent chain and the ribosomal tunnel. The central panel shows a section through the large subunit revealing contact points between the TnaC nascent chain (light green) and the ribosome (gray). Density attributed to the P-tRNA is colored dark green and for peptidyl-tRNA at a lower threshold is shown as a green mesh. (**A** to **D**) Different views of connections between the nascent chain (green ribbon) and the 23*S* rRNA (blue sticks) or ribosomal protein L22 (blue ribbon). Density for the TnaC•70*S* complex is shown as a transparent gray surface, whereas the isolated nascent chain at a lower threshold is shown as a green mesh. Important TnaC residues are highlighted yellow, orange, or red.

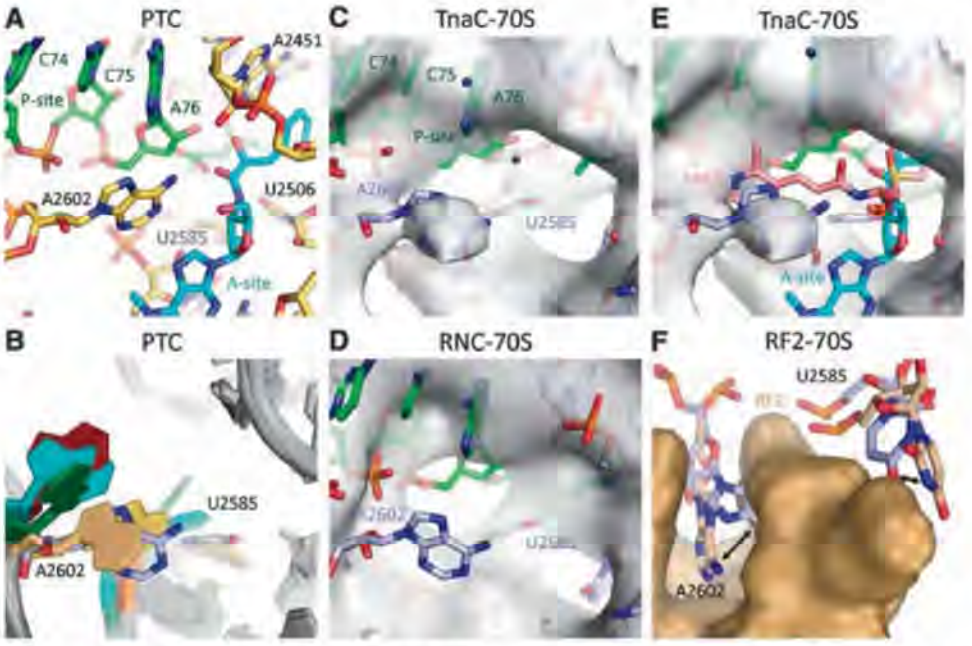

Fig. 3. Silencing of the PTC. (**A**) Conformation of 23*S* rRNA nucleotides at the PTC when tRNA CCA-end mimics are bound to A (cyan) and P sites (green) (PDB1VQN). (**B**) Comparison of A2602 and U2585 conformations in various ribosome crystal structures (red, PDB1VQK; teal, PDB1S72; yellow, PDB2I2T; gold, PDB2JL5/6; blue, PDB1VQ9; green, PDB1VQN). (**C**) View into the PTC of the TnaC-70*S* complex, with the MDFF model of the TnaC-tRNA (green) and nucleotides of the 23*S* rRNA (blue). The cryo-EM density is shown as a transparent gray surface, with an asterisk indicating the connection between P-tRNA and nascent chain. (**D**) View into the PTC of 70*S*-RNC complex, with fitted models as in (A). Note the lack of density (gray) for nucleotide A2602. (**E**) As in (A), but with the antibiotic sparsomycin (SPAR, red; PDB1VQ9) and the terminal A76 and aminoacyl moiety of an A-tRNA (cyan, PDB1VQN) included. (**F**) Comparison of A2602 and U2585 positions (arrowed) between TnaC-70*S* complex (blue) and RF2-70*S* complex (*24*) (gold), with RF2 shown as surface representation (gold).

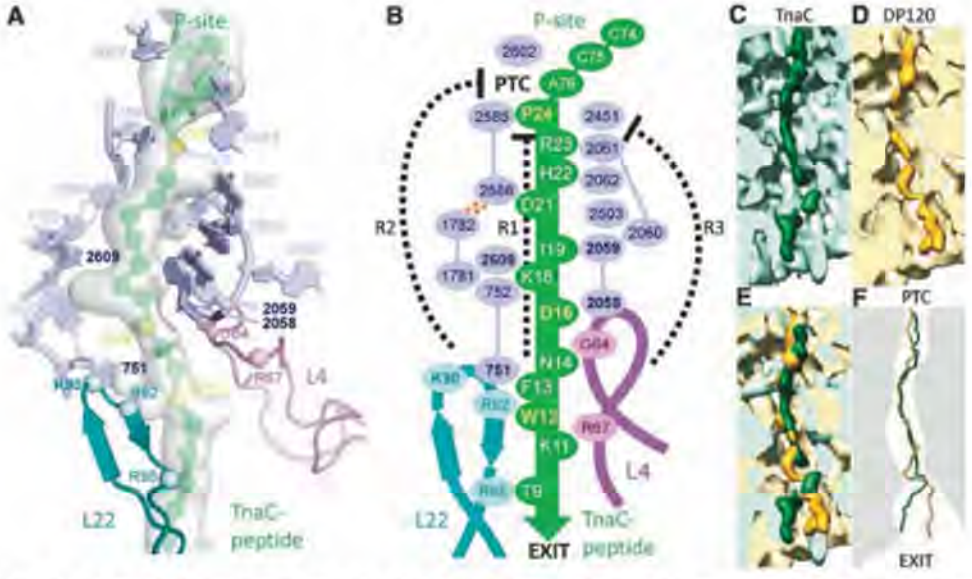

Fig. 4. Relay for PTC silencing and the path of the nascent chain. (**A**) Ribosomal components potentially involved in a relay mechanism to inactivate the PTC, with those implicated in stalling in bold. The TnaC nascent chain is in green, with residues essential for stalling colored yellow. The isolated TnaC-tRNA density is shown as a transparent gray surface. (**B**) Schematic indicating potential relay pathways from Trp^{12} (W12) of TnaC to the PTC, either through the nascent chain itself (**R1**) or through networks of interconnected 23*S* rRNA nucleotides (R2 and R3). (**C** and **D**) Transverse section through the large subunit showing the path of (C) TnaC (dark green) and (D) DP120 (*27*) (orange) nascent chains through the ribosomal tunnel. (**E**) Superposition of (A) and (B). (**F**) Schematic highlighting the similarities and differences between the TnaC and DP120 nascent chain in terms of contacts and passage through the tunnel.

efficient peptide-bond formation (Fig. 3A). Specific conformational changes of highly conserved nucleotides of the 23*S* rRNA within the PTC are associated with binding of different ligands to the PTC. For example, A2602 and U2585 adopt dramatically different conformations in ribosome structures in various functional states (Fig. 3B) (*21*). In the PTC of the 70*S*•TnaC complex, clear density for A2602 indicates that this nucleotide adopts a distinct conformation (Fig. 3C), in contrast to the RNC-70*S* complex, where it appears to be disordered (Fig. 3D). In the 70*S*•TnaC map, visualization of a single nucleotide is also exemplified by A1493 in the decoding center of the 30*S* (fig. S9). The A2602 conformation resembles that of the PTC when the translation inhibitor sparsomycin is bound (Fig. 3E) (*22*). In addition to A2602, continuous density between the nascent chain and the location of U2585 suggests that this flexible base (see Fig. 3B) shifts to interact with Pro^{24} of TnaC (Fig. 3C). Inactivation of the PTC in the 70*S*•TnaC complex requires free tryptophan, whose binding site has been proposed to overlap with that of the antibiotic sparsomycin (*12*, *20*, *23*) and with the amino-acyl moiety of an A-tRNA at the PTC (*10*). Nevertheless, no additional density could be attributed to a free tryptophan molecule (Fig. 3E), despite the purification and cryo-EM analysis in the presence of 2 mM tryptophan (*14*). The conformations of A2602 and U2585 observed in the 70*S*•TnaC complex are incompatible with simultaneous cohabitation of termination release factors (RFs) (Fig. 3F) (*24*). Thus, even if RFs can still bind to the stalled 70*S*•TnaC complexes (*11*), the fixed conformation of A2602 and U2585 would prevent correct positioning of the GGQ motif of the RF within the PTC that is necessary for efficient hydrolysis and release of the nascent chain from the P-tRNA (*24*).

Because residues of the nascent chain that are essential for TnaC-mediated stalling are located far from the PTC, a signal must be propagated from the depths of the tunnel back to the PTC (Fig. 4). Our map allows us to rule out the idea that peptide stalling initiates a cascade of large-scale conformational changes throughout the ribosome, ultimately leading to the inhibition of translation (*25*). Consequently, the "stalling signal" may be relayed back through the nascent chain itself; that is, the interaction between the nascent chain and the tunnel induces a specific conformation in the nascent chain that feedback inhibits the PTC (relay R1 in Fig. 4B) and/or through a series of subtle conformational changes in the network of ribosomal components that comprise the tunnel (R2 and R3 in Fig. 4B).

The surface of the exit tunnel has been described as being "Teflon-like" due to its predominantly hydrophilic nature (*26*). Yet here we have shown that the TnaC-stalled nascent chain makes extensive interactions with the ribosome along the entire length of the exit tunnel (Fig. 4C and fig. S6). This is important to emphasize because density is visible for ~10 of the amino acids preceding

the canonical TnaC sequence, indicating that even residues unrelated to the stalling process can adopt a distinct conformation within the exit tunnel. This notion is supported by a cryo-EM structure of a yeast 80*S* ribosome-nascent chain complex stalled during the translation of a truncated dipeptidyl-aminopeptidase B (DP120) mRNA at 6.1 Å resolution (*27*). Although the DP120 sequence has no stalling capacity, density for this nascent chain is visible, indicating a preferred conformation within the exit tunnel (Fig. 4D). Notably, the DP120 nascent chain follows a different path from that reported here for TnaC (Fig. 4, E and F). Clearly the chemical and electrostatic properties of the tunnel environment play a pivotal role in facilitating this kind of distinct nascent chain behavior (*3*, *4*). The finding that nascent chains with little or no sequence conservation interact with the exit tunnel in a distinct manner and adopt individual conformations may be important not only for initial folding events (*1*–*3*) but also for the variety of nascent chain–mediated regulatory mechanisms (*5*).

References and Notes

1. C. A. Woolhead, P. J. McCormick, A. E. Johnson, *Cell* **116**, 725 (2004).
2. J. Lu, C. Deutsch, *Biochemistry* **44**, 8230 (2005).
3. J. Lu, C. Deutsch, *Nat. Struct. Mol. Biol.* **12**, 1123 (2005).
4. J. Lu, C. Deutsch, *J. Mol. Biol.* **384**, 73 (2008).
5. T. Tenson, M. Ehrenberg, *Cell* **108**, 591 (2002).
6. H. Nakatogawa, K. Ito, *Cell* **108**, 629 (2002).
7. C. A. Woolhead, A. E. Johnson, H. D. Bernstein, *Mol. Cell* **22**, 587 (2006).
8. M. N. Yap, H. D. Bernstein, *Mol. Cell* **34**, 201 (2009).
9. D. Oliver, J. Norman, S. Sarker, *J. Bacteriol.* **180**, 5240 (1998).
10. F. Gong, C. Yanofsky, *Science* **297**, 1864 (2002).
11. L. Cruz-Vera, S. Rajagopal, C. Squires, C. Yanofsky, *Mol. Cell* **19**, 333 (2005).
12. L. R. Cruz-Vera, C. Yanofsky, *J. Bacteriol.* **190**, 4791 (2008).
13. F. Gong, K. Ito, Y. Nakamura, C. Yanofsky, *Proc. Natl. Acad. Sci. U.S.A.* **98**, 8997 (2001).
14. Materials and methods are available as supporting material on *Science* Online.
15. L. G. Trabuco, E. Villa, K. Mitra, J. Frank, K. Schulten, *Structure* **16**, 673 (2008).
16. P. I. de Bakker, N. Furnham, T. L. Blundell, M. A. DePristo, *Curr. Opin. Struct. Biol.* **16**, 160 (2006).
17. M. Simonovic, T. A. Steitz, *Biochim. Biophys. Acta* **1789**, 612 (2009).
18. R. Yang, L. R. Cruz-Vera, C. Yanofsky, *J. Bacteriol.* **191**, 3445 (2009).
19. N. Vazquez-Laslop, C. Thum, A. S. Mankin, *Mol. Cell* **30**, 190 (2008).
20. L. R. Cruz-Vera, A. New, C. Squires, C. Yanofsky, *J. Bacteriol.* **189**, 3140 (2007).
21. T. M. Schmeing, K. S. Huang, S. A. Strobel, T. A. Steitz, *Nature* **438**, 520 (2005).
22. T. M. Schmeing, K. S. Huang, D. E. Kitchen, S. A. Strobel, T. A. Steitz, *Mol. Cell* **20**, 437 (2005).
23. L. R. Cruz-Vera, M. Gong, C. Yanofsky, *Proc. Natl. Acad. Sci. U.S.A.* **103**, 3598 (2006).
24. A. Weixlbaumer *et al.*, *Science* **322**, 953 (2008).
25. K. Mitra *et al.*, *Mol. Cell* **22**, 533 (2006).
26. P. Nissen, J. Hansen, N. Ban, P. B. Moore, T. A. Steitz, *Science* **289**, 920 (2000).
27. T. Becker *et al.*, *Science* **326**, 1369 (2009). Published online 29 October 2009; 10.1126/science.1178535.

28. This research was supported by grants from the Deutsche Forschungsgemeinschaft SFB594 and SFB646 (to R.B.), SFB740 (to T.M.), and WI3285/1-1 (to D.N.W.); by NIH grants GM022778 (to T.A.S.) and P41-RR05969 (to K.S.); by NSF grant PHY0822613 (to K.S.); and by the European Union and Senatsverwaltung für Wissenschaft, Forschung und Kultur Berlin (UltraStructureNetwork, Anwenderzentrum). Computer time for MDFF was provided through an NSF Large Resources Allocation Committee grant MCA93S028. Coordinates of the atomic models of TnaC-70S complex have been deposited in the PDB under accession numbers 2WWL (30S) and 2WWQ (50S). The cryo-EM map has been deposited in the 3D-EM database under accession number EMD-1657.

Supporting Online Material

www.sciencemag.org/cgi/content/full/1177662/DC1
Materials and Methods
Figs. S1 to S9
Table S1
Movie S1
References

12 June 2009; accepted 21 October 2009
Published online 29 October 2009;
10.1126/science.1177662
Include this information when citing this paper.

A Crystal Structure of the Bifunctional Antibiotic Simocyclinone D8, Bound to DNA Gyrase

Marcus J. Edwards,[1] Ruth H. Flatman,[1] Lesley A. Mitchenall,[1] Clare E.M. Stevenson,[1] Tung B.K. Le,[2] Thomas A. Clarke,[3] Adam R. McKay,[4] Hans-Peter Fiedler,[5] Mark J. Buttner,[2] David M. Lawson,[1] Anthony Maxwell[1]*

Simocyclinones are bifunctional antibiotics that inhibit bacterial DNA gyrase by preventing DNA binding to the enzyme. We report the crystal structure of the complex formed between the N-terminal domain of the *Escherichia coli* gyrase A subunit and simocyclinone D8, revealing two binding pockets that separately accommodate the aminocoumarin and polyketide moieties of the antibiotic. These are close to, but distinct from, the quinolone-binding site, consistent with our observations that several mutations in this region confer resistance to both agents. Biochemical studies show that the individual moieties of simocyclinone D8 are comparatively weak inhibitors of gyrase relative to the parent compound, but their combination generates a more potent inhibitor. Our results should facilitate the design of drug molecules that target these unexploited binding pockets.

Bacterial diseases remain a major problem because of the emergence of drug-resistant bacteria combined with the dearth of new antibacterial agents. Despite extensive efforts, there remain relatively few effective drug targets for antibacterials. One of these is the enzyme DNA gyrase, a DNA topoisomerase that controls the topology of DNA (*1*, *2*). Topoisomerases are classified into two types, I and II, depending on whether they catalyze reactions involving the transient breakage of one or both strands of DNA. Gyrase is the only type II DNA topoisomerase that can catalyze DNA supercoiling; this reaction is driven by the free energy of adenosine triphosphate (ATP) hydrolysis (*3*). Gyrase consists of two subunits, GyrA and GyrB (97 kD and 90 kD, respectively, in *Escherichia coli*), which form an A_2B_2 complex in the active enzyme. Because gyrase is essential in bacteria and lacking in humans, it is a valuable drug target (*4*). The complexity of the gyrase supercoiling reaction presents multiple opportunities for intervention. Two well-known groups of gyrase-specific antibacterial agents are quinolones and aminocoumarins. Fluoroquinolones, such as ciprofloxacin, are highly successful drugs (*5*), but their usefulness is diminishing as a consequence of bacterial resistance (*6*). Aminocoumarins, e.g., novobiocin and clorobiocin, are less successful clinically because of toxicity and solubility issues but are very well characterized in terms of their mode of action on gyrase (*7*), including several crystal structures (*8*–*11*). Aminocoumarins act by competitively inhibiting the binding of ATP to the GyrB subunit (*11*). The cloning and sequencing of the biosynthetic pathways for the aminocoumarins novobiocin, clorobiocin, and coumermycin A_1 and the application of bioengineering methodologies (*12*) have enabled the production of a series of modified aminocoumarins with varying potencies against their targets, gyrase and topoisomerase IV (*13*, *14*). This work has raised the possibility of engineering antibacterial agents targeted to gyrase that are based on natural antibiotics.

Simocyclinone D8 (SD8) was isolated from *Streptomyces antibioticus* Tü 6040 (*15*–*18*). The antibiotic consists of a chlorinated aminocoumarin (AC) linked to an angucyclic polyketide (PK) via

[1]Department of Biological Chemistry, John Innes Centre, Colney, Norwich NR4 7UH, UK. [2]Department of Molecular Microbiology, John Innes Centre, Colney, Norwich NR4 7UH, UK. [3]School of Biological Sciences, University of East Anglia, Norwich NR4 7TJ, UK. [4]Department of Chemistry, University College London, 20 Gordon St, London WC1H 0AJ, UK. [5]Mikrobiologisches Institut, Eberhard-Karls-Universität Tübingen, Auf der Morgenstelle 28, D-72076 Tübingen, Germany.

*To whom correspondence should be addressed. E-mail: tony.maxwell@bbsrc.ac.uk

a tetraene linker and a D-olivose sugar (Fig. 1). Because of the presence of the AC moiety, the expectation was that SD8 would target the adenosine triphosphatase (ATPase) domain of GyrB. Although SD8 is a potent inhibitor of *E. coli* gyrase, it does not inhibit the intrinsic GyrB ATPase activity. Instead, SD8 binds to the N-terminal domain of GyrA and prevents DNA binding (*19*). In hindsight, this is not surprising because SD8 lacks the decorated noviose sugar that is attached to the 7-OH of the AC ring and is involved in the majority of the interactions with GyrB in other aminocoumarins (*8*–*11*). In contrast to quinolones and aminocoumarins, which can act on both gyrase and its close relative topoisomerase IV, SD8 is potent against gyrases from *E. coli* and *Staphylococcus aureus* but much less effective against topoisomerase IV from these species (*20*).

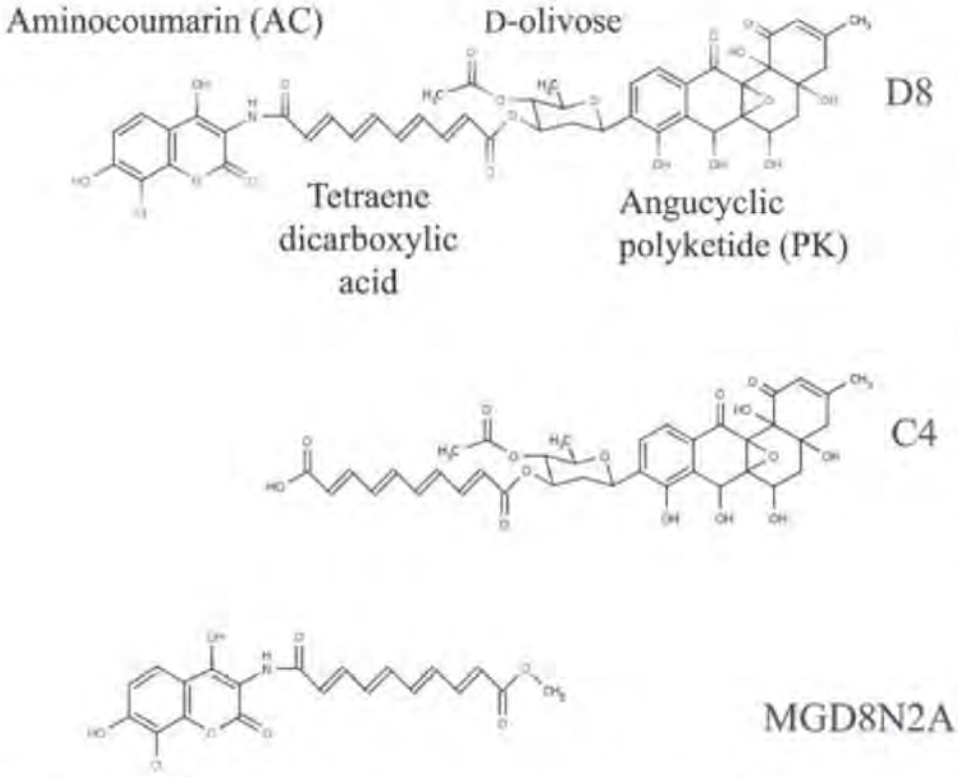

Fig. 1. Structure of simocyclinone D8 and analogs. IC_{50} values for inhibition of supercoiling by gyrase: for D8, 0.6 μM; C4, 70 μM; MGD8N2A, 50 μM.

We have crystallized the N-terminal domain of GyrA (GyrA59) complexed with SD8 and determined the crystal structure at 2.6-Å resolution by molecular replacement from the structure of unliganded GyrA59 that was previously determined (*21*). Our structure reveals a ligand-stabilized homotetramer of GyrA59 subunits consisting of two A59 dimers cross-linked by four molecules of SD8 (Fig. 2). The tetraene linker of SD8 acts as an extended rod, about 10 Å long, that holds the AC and PK moieties apart. Each GyrA subunit has distinct pockets that accept the AC and PK groups, respectively, of two separate SD8 molecules; both pockets lie in the predicted DNA binding saddle. Additional lobes of electron density adjacent to the PK moiety have been modeled as Mg^{2+} ions (Fig. 3A and fig. S1). Although each subunit interacts with two SD8 molecules, because each of these molecules is shared by two subunits from opposing dimers, the stoichiometry remains 1:1, consistent with previous experiments (*19*). In addition to the SD8-mediated dimer-dimer interactions, there is about 1500 $Å^2$ of protein-protein interface. This includes 12 hydrogen bonds, 10 of which involve residues spanning Leu^{17} to Asp^{23}, a region just before α-helix 1 that was not visible in the original GyrA59 structure (*21*). Superposition of the SD8 complex and ligand-free GyrA59 structures gives root mean square deviation values below 1 Å, both for

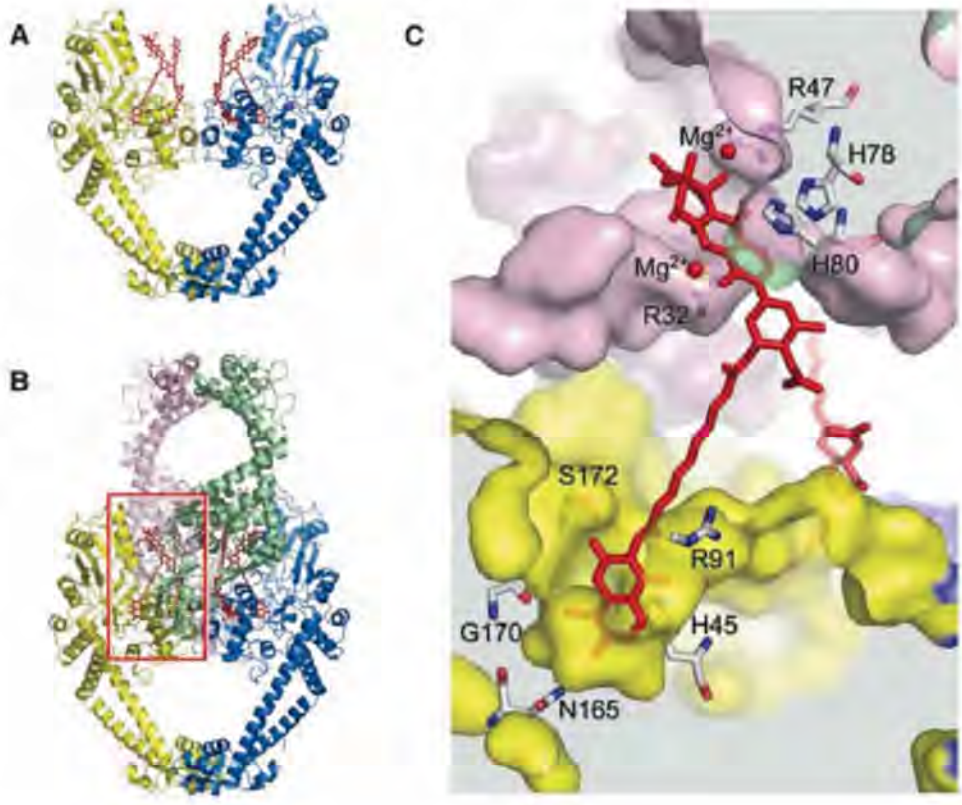

Fig. 2. Crystal structure of the GyrA59-simocyclinone complex. The protein is depicted in cartoon representation, the SD8 molecules are shown as red sticks, and their associated Mg^{2+} ions as small spheres. (**A**) Structure of the GyrA59 dimer and the four SD8 molecules it interacts with. (**B**) Structure of the SD8-mediated tetramer (dimer of dimers). (**C**) Close-up of the red boxed region in (B) showing a section through the complex containing two SD8 molecules. The same color scheme is adopted as for (A) and (B), but the GyrA59 subunits are represented as semi-transparent molecular surfaces. Regions with a white background are either outside the complex or between the subunits; regions with a gray background are within the molecular envelopes. Key residues (*23*) that are close to the SD8 molecule in the foreground are displayed in stick representation.

subunit-subunit and dimer-dimer comparisons, indicating that there are no major conformational changes upon ligand binding (fig. S2). Intriguingly, a single SD8 molecule can be modeled in a "bent" conformation such that it bridges between the AC and PK pockets of the same subunit, while maintaining essentially the same contacts with the protein seen in the crystal structure (fig. S3). This places the tetraene linker close to, and possibly interacting with, α-helix 4.

To investigate the oligomeric state in solution, we performed a series of molecular weight (MW) studies. Analytical ultracentrifugation (table S2) showed that the MW of GyrA59 in the absence of SD8 or at low ligand:protein ratios (<~3:1) was ~120 kD, suggesting a dimer, whereas at high ligand:protein ratios (>~4:1) GyrA59 had a MW of ~250 kD, consistent with a tetramer. By using nanoelectrospray ionization mass spectrometry (nanoESI MS) under conditions where noncovalent interactions are preserved, we assessed the binding of SD8 to GyrA59 and full-length GyrA. In the absence of SD8, both proteins had MWs consistent with dimers (fig. S4). Titration of SD8 into solutions containing the proteins showed dimeric species with either one or two SD8 molecules bound at ligand:protein ratios of <~2:1. With a ligand:protein ratio of 3:1, we began to see formation of a tetrameric species, which increased with increasing SD8 concentrations to become the predominant species at ~7.5:1 (fig. S4). These experiments showed small amounts of three SD8 molecules bound per dimer but no evidence of four, suggesting that a tetramer readily forms once four molecules are bound (fig. S4). We suggest that the dimeric species, observed at limiting ligand concentrations, might represent a single SD8 molecule bound to the AC and PK pockets within the same subunit (fig. S3).

To probe the importance of the two binding pockets, we analyzed the interactions of GyrA59 with simocyclinone analogs lacking either the PK or the AC moiety (Fig. 1). Simocyclinone C4 is a naturally occurring intermediate in the SD8 pathway that lacks the AC moiety; MGD8N2A, which lacks the PK moiety, was generated by chemical hydrolysis of SD8. The parent compound has a minimum inhibitory concentration (IC_{50}) value of 0.6 μM for inhibition of gyrase supercoiling, whereas IC_{50} values of 70 and 50 μM were obtained for analogs lacking either the AC or the PK moiety, respectively (Fig. 1). Although inhibition is greatly reduced, the fact that these SD8 analogs have some activity suggests that cross-linking of the two GyrA dimers is not a prerequisite for inhibition.

One key issue was to establish the in vivo target of simocyclinones; recent transcriptional profiling studies (*20*) suggest but do not prove that gyrase is the target. To address this, we selected spontaneous resistant mutants in *E. coli*. Wild-type *E. coli* and other Gram-negative bacteria are resistant to simocyclinones because the compounds cannot penetrate the outer membrane (*15*); we therefore used an *E. coli* strain (NR698) that is sensitive because it carries an in-frame de-

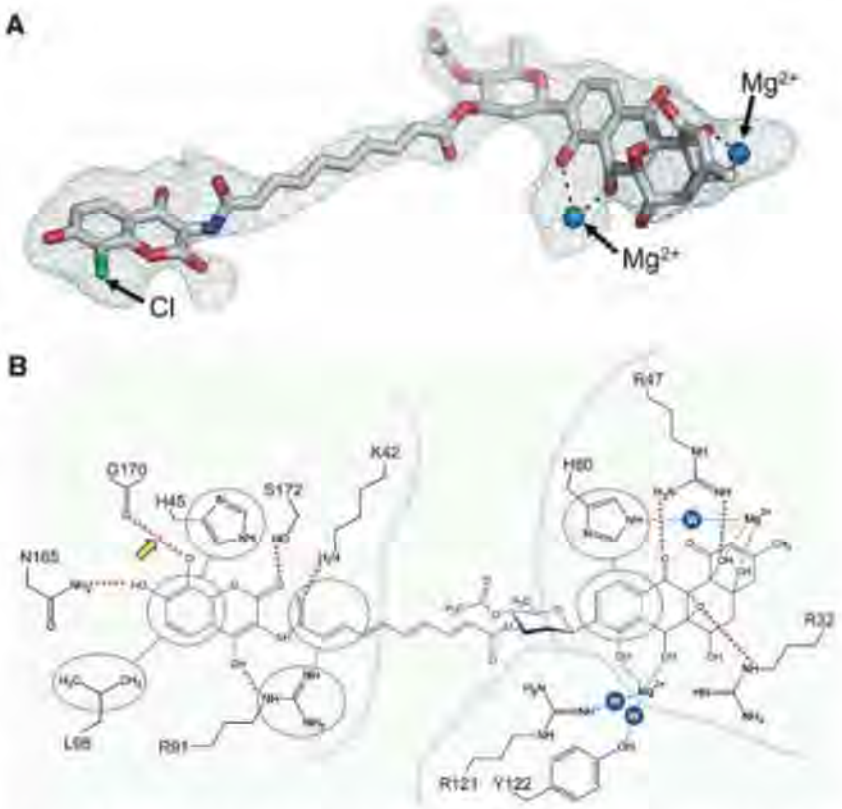

Fig. 3. Binding of SD8 to GyrA. (**A**) Simulated annealing omit electron density map for SD8 contoured at 6 σ and superposed on the final coordinates of the ligand (*27*). (**B**) Schematic figure detailing protein-ligand interactions in the GyrA59-SD8 complex. Red dotted lines represent hydrogen bonds and the single halogen bond (indicated by yellow arrow; see fig. S1). Interactions with the Mg^{2+} ions are shown as pale blue dashed lines. The side chains of Arg^{121} and Tyr^{122} (in the active site) point toward the SD8 molecule across the dimer interface and could interact with it via water molecules (blue shaded circles labeled "W") coordinated to a Mg^{2+} ion. Similarly, His^{80} likely makes a water-mediated interaction with the second Mg^{2+} ion. Nonbonded interactions are represented by the linked green ovals, which encircle the groups involved; subunit boundaries are delineated by gray lines.

Table 1. Properties of simocyclinone- and quinolone-resistant GyrA mutants. NA indicates not applicable. Mutant H78A is not active; K_D for simocyclinone is ~10 times that of wild type. S83W data is from (*19*).

GyrA mutation	Relative IC_{50} (supercoiling)	
	Simocyclinone	Ciprofloxacin
Wild type	1 (0.6 μM)*	1 (0.7 μM)*
Mutations in the simocyclinone-binding site		
Aminocoumarin-binding pocket mutations		
H45A	9.1	2.2
R91A	20	1.1
Polyketide-binding pocket mutations		
H78A	NA	NA
H80A	230	2.8
Mutations in both pockets		
H45A and H80A	>500	2.3
Mutations in the quinolone-resistance–determining region of GyrA		
G81D	40	24
S83W	10	30
A84P	38	28
D87A	7.2	5.2
D87Y	57	30
S83A and D87A	8.3	12

*Actual IC_{50} values are given in parentheses.

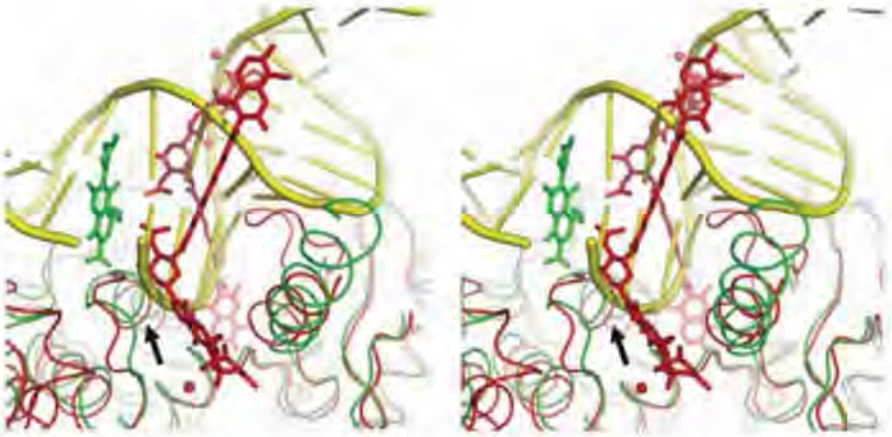

Fig. 4. Stereo view showing a superposition of GyrA59-SD8 and the clinafloxacin-DNA cleavage complex of topo IV [Protein Data Bank (PDB) code 3FOE], focusing on the drug-binding sites in one half of the GyrA/ParC dimers (*28*). The protein backbones are shown as ribbons and the drug molecules in stick representation, with GyrA59-SD8 in red, ParC-clinafloxacin in green, and the DNA from the latter structure in yellow. For clarity, the ParE subunits have been omitted from 3FOE. The SD8 and clinafloxacin binding sites are adjacent but do not overlap. This figure illustrates how SD8 would interfere with DNA binding; this would also be the case if the drug were bound in the "bent-over" conformation proposed in fig. S3. The arrow indicates the position of α-helix 4.

letion in the *imp* (increased membrane permeability) gene (*22*). We isolated 31 spontaneous simocyclinone-resistant mutants and in each case sequenced a ~500–base pair (bp) region of *gyrA*, corresponding to residues Met^{26} to Ser^{172} of the protein. We found *gyrA* mutations in 22 of them, conferring one of the following amino acid changes: $V^{44}\rightarrow G^{44}$ (V44G) (*23*), H45Y, H45Q, G81S, and D87Y (fig. S5). These amino acids are close to the bound SD8 molecule in the crystal structure, consistent with gyrase being the in vivo target. Unlike the 22 *gyrA* mutants, the remaining nine isolates had also acquired resistance to bile salts, suggesting that they could be accounted for by spontaneous second-site mutations that are known to restore outer membrane impermeability to the *imp* mutant (*22*).

On the basis of the spontaneous mutations and the crystal structure information, we made selected site-directed mutations in GyrA to probe its interaction with SD8 in vitro. The mutant proteins, together with wild-type GyrB, were assayed for DNA supercoiling in the presence of SD8 (Table 1). Mutations in either the AC (His^{45} and Arg^{91}) or the PK (His^{80} and Gly^{81}) pocket showed simocyclinone-resistant supercoiling. SD8 binding to an inactive mutant in the PK pocket, H78A (*23*), was investigated by surface-plasmon resonance using the GyrA59 protein. The mutant showed decreased binding affinity for SD8 (K_D values were 1.3 μM for wild type and 10.4 μM for H78A) and had a near-identical far-ultraviolet circular dichroism spectrum to wild-type GyrA, suggesting that it was properly folded.

Quinolone-resistant mutations map to both *gyrA* and *gyrB* in regions known as the quinolone-resistance determining regions [QRDRs (*24*, *25*)]. In the case of *E. coli* GyrA, the QRDR occurs between amino acids 67 and 106 with mutations identified at Ala^{67}, Gly^{81}, Asp^{82}, Ser^{83}, Ala^{84}, Asp^{87}, and Gln^{106} (*26*), mostly occurring either in or just before α-helix 4 (*21*) (fig. S5). From the published structures of quinolone-DNA cleavage complexes of *Streptococcus pneumoniae* topo IV (*27*), we can infer the location of the quinolone-binding site in GyrA, which is adjacent to but not overlapping the SD8 binding sites (Fig. 4). The quinolones do not make substantive contacts with the topo IV ParC protein, being closest to the equivalents of residues Gly^{81} to Ala^{84} and Asp^{87} in GyrA. Therefore, at least some of the mutations in the QRDR of GyrA most likely have indirect effects on quinolone binding. Given the proximity of the quinolone and SD8 binding sites, we investigated whether there was any cross-resistance between the two types of inhibitor. SD8-resistant mutants were tested for their susceptibility to the fluoroquinolone ciprofloxacin, and a range of ciprofloxacin-resistant mutants were tested for their susceptibility to SD8 (Table 1).

Mutations in the simocyclinone-binding pockets (AC and PK) result in near–wild-type amounts of susceptibility to ciprofloxacin (Table 1); QRDR mutations in α-helix 4 of GyrA confer increased resistance to both ciprofloxacin and SD8. None of these amino acids makes direct contacts with bound SD8 (Fig. 3B); given the low resolution of the quinolone-DNA-topo IV complex structures, it is not possible to precisely define any ligand-protein interactions, but it is likely that substitutions at positions 81 to 84 and 87 in GyrA would have an effect on drug binding. The prevalence of mutations at Ser^{83} and Asp^{87} in quinolone-resistant clinical isolates supports this assertion (*26*). In the case of SD8, it is possible that mutations in α-helix 4 of GyrA, which lies between the AC and PK binding pockets, can affect the proposed bridging of the two binding sites by the tetraene linker (fig. S3).

Given the global concerns over drug-resistant bacterial diseases, work on SD8 raises the prospect of developing agents that exploit its bifunctional mode of antibiotic action on a well-validated target. Alternatively, designing monofunctional compounds with enhanced affinity for one or the other of the binding sites may prove fruitful.

References and Notes

1. A. D. Bates, A. Maxwell, *DNA Topology* (Oxford Univ. Press, Oxford, 2005).
2. A. J. Schoeffler, J. M. Berger, *Q. Rev. Biophys.* **41**, 41 (2008).
3. A. D. Bates, A. Maxwell, *Biochemistry* **46**, 7929 (2007).
4. A. Maxwell, *Trends Microbiol.* **5**, 102 (1997).
5. C. M. Oliphant, G. M. Green, *Am. Fam. Physician* **65**, 455 (2002).
6. D. Livermore, *J. Antimicrob. Chemother.* **60** (suppl. 1), i59 (2007).
7. A. Maxwell, D. M. Lawson, *Curr. Top. Med. Chem.* **3**, 283 (2003).
8. V. Lamour, L. Hoermann, J. M. Jeltsch, P. Oudet, D. Moras, *J. Biol. Chem.* **277**, 18947 (2002).
9. F. T. F. Tsai *et al.*, *Proteins* **28**, 41 (1997).
10. G. A. Holdgate *et al.*, *Biochemistry* **36**, 9663 (1997).
11. R. J. Lewis *et al.*, *EMBO J.* **15**, 1412 (1996).
12. S.-M. Li, L. Heide, *Curr. Med. Chem.* **12**, 419 (2005).
13. C. Anderle *et al.*, *Antimicrob. Agents Chemother.* **52**, 1982 (2008).
14. R. H. Flatman, A. Eustaquio, S. M. Li, L. Heide, A. Maxwell, *Antimicrob. Agents Chemother.* **50**, 1136 (2006).
15. J. Schimana *et al.*, *J. Antibiot. (Tokyo)* **53**, 779 (2000).
16. U. Theobald, J. Schimana, H. P. Fiedler, *Antonie Leeuwenhoek* **78**, 307 (2000).
17. U. Galm *et al.*, *Arch. Microbiol.* **178**, 102 (2002).
18. A. Trefzer *et al.*, *Antimicrob. Agents Chemother.* **46**, 1174 (2002).
19. R. H. Flatman, A. J. Howells, L. Heide, H.-P. Fiedler, A. Maxwell, *Antimicrob. Agents Chemother.* **49**, 1093 (2005).
20. L. M. Oppegard *et al.*, *Antimicrob. Agents Chemother.* **53**, 2110 (2009).
21. J. H. Morais Cabral *et al.*, *Nature* **388**, 903 (1997).
22. N. Ruiz, B. Falcone, D. Kahne, T. J. Silhavy, *Cell* **121**, 307 (2005).
23. Single-letter abbreviations for the amino acid residues are as follows: A, Ala; C, Cys; D, Asp; E, Glu; F, Phe; G, Gly; H, His; I, Ile; K, Lys; L, Leu; M, Met; N, Asn; P, Pro; Q, Gln; R, Arg; S, Ser; T, Thr; V, Val; W, Trp; and Y, Tyr.
24. H. Yoshida, M. Bogaki, M. Nakamura, L. M. Yamanaka, S. Nakamura, *Antimicrob. Agents Chemother.* **35**, 1647 (1991).
25. H. Yoshida, M. Bogaki, M. Nakamura, S. Nakamura, *Antimicrob. Agents Chemother.* **34**, 1271 (1990).
26. D. C. Hooper, E. Rubinstein, *Quinolone Antimicrobial Agents* (American Society for Microbiology, Washington, DC, ed. 3, 1993), p. 485.
27. Materials and methods are available as supporting material on *Science* Online.
28. I. Laponogov *et al.*, *Nat. Struct. Mol. Biol.* **16**, 667 (2009).

29. This work was funded by UK Biotechnology and Biological Sciences Research Council (BBSRC) and the European Commission (CombiGyrase LSHB-CT-2004-503466); M.J.E. was supported by a CASE studentship funded by BBSRC and Plant Bioscience Limited, and T.B.K.L. was supported by a John Innes Centre Rotation studentship. We thank A. Zeeck (University of Göttingen) for providing us with a sample of MGD8N2A; P. Johnson for assistance with CD experiments; R. Field, L. Heide, and D. Hopwood for helpful discussions; and N. Ruiz and T. Silhavy for their advice and for the *E. coli imp4213* mutant. Atomic coordinates and structure factors have been deposited in the Protein Data Bank with accession code 2WL2. We dedicate this paper to the memory of Chris Lamb, director of the John Innes Centre from 1999 to 2009.

Supporting Online Material

www.sciencemag.org/cgi/content/full/326/5958/1415/DC1
Materials and Methods
SOM Text
Figs. S1 to S5
Tables S1 and S2

15 July 2009; accepted 8 October 2009
10.1126/science.1179123

GABAergic Hub Neurons Orchestrate Synchrony in Developing Hippocampal Networks

P. Bonifazi,[1]* M. Goldin,[1]* M. A. Picardo,[1] I. Jorquera,[1] A. Cattani,[1] G. Bianconi,[2] A. Represa,[1] Y. Ben-Ari,[1] R. Cossart[1]†

Brain function operates through the coordinated activation of neuronal assemblies. Graph theory predicts that scale-free topologies, which include "hubs" (superconnected nodes), are an effective design to orchestrate synchronization. Whether hubs are present in neuronal assemblies and coordinate network activity remains unknown. Using network dynamics imaging, online reconstruction of functional connectivity, and targeted whole-cell recordings in rats and mice, we found that developing hippocampal networks follow a scale-free topology, and we demonstrated the existence of functional hubs. Perturbation of a single hub influenced the entire network dynamics. Morphophysiological analysis revealed that hub cells are a subpopulation of γ-aminobutyric acid–releasing (GABAergic) interneurons possessing widespread axonal arborizations. These findings establish a central role for GABAergic interneurons in shaping developing networks and help provide a conceptual framework for studying neuronal synchrony.

The coordinated activation of neuronal assemblies features in most physiological brain functions and influences proper network wiring during development (*1*–*3*). In addition to cellular excitability, synaptic efficacy, and the balance of excitation and inhibition, the architecture of network connectivity may be central to the production of synchronous neuronal activity (*4*–*7*). The relationship between network dynamics and topology has been studied using concepts from graph theory and statistical physics (*7*–*9*). Small-world and scale-free organizations are particularly appealing models for brain connectivity because they offer a compromise between computational needs, wiring economy, and robustness (*1*, *10*–*14*). These complex topologies have been found in contexts as diverse as the Internet, social sciences, or biology (*8*, *15*). When applied to neuronal circuits, both models share one common feature: Although most neurons are connected locally, a few "hub" neurons possess long-range connections that link large numbers of cells, thereby bestowing network-wide synchronicity. It has been proposed that neuronal hubs orchestrate behaviorally relevant activity in cortical assemblies, as well as being causal in producing pathological oscillations (*4*–*6*, *16*). However, the existence of neuronal hubs is still speculative, perhaps because of the conceptual and technical difficulties of investigating them, including the rarity of high-connectivity (HC) as compared to low-connectivity (LC) cells. Additionally, definitive functional confirmation that neuronal hubs play a key role in synchroni-

[1]Institut de Neurobiologie de la Méditerranée, INSERM U901, Université de la Méditerranée, Parc Scientifique de Luminy, Boîte Postale 13, 13273 Marseille Cedex 9, France. [2]Department of Physics, Northeastern University, Boston, MA 02115, USA.

*These authors contributed equally to this work.
†To whom correspondence should be addressed. E-mail: cossart@inmed.univ-mrs.fr

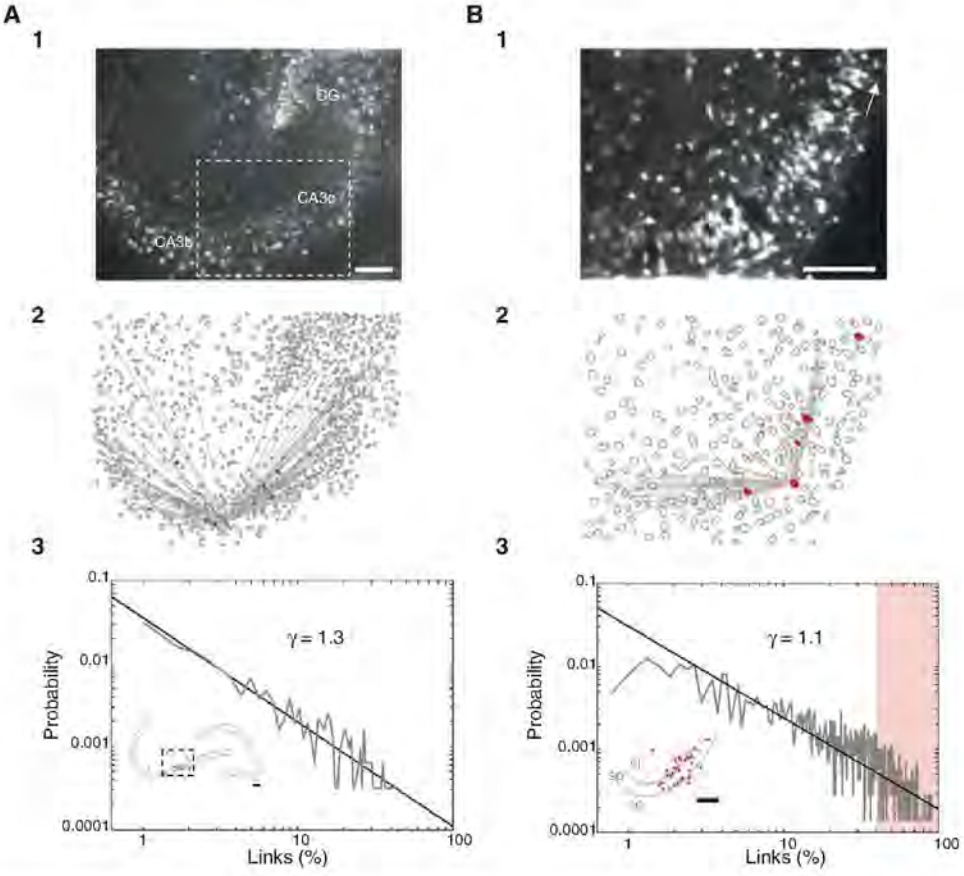

Fig. 1. Analysis of multineuron calcium activity reveals a scale-free topology in the developing hippocampus. (**A**) (1) Two-photon calcium fluorescence image of a rat hippocampal slice loaded with Fura-2AM and visualized with multibeam excitation at ×10 magnification. Scale bar, 100 μm. DG, dentate gyrus. (2) Detected contours of the cells from the fluorescence image shown in (1). Red dots are the 10 highest-connectivity neurons in the represented network based on the analysis of calcium event onsets; gray lines mark the output links of one HC neuron. (3) Probability distribution plot of the fraction of output links over the total population of active neurons imaged with ×10 magnification (gray line, n = 3224 neurons in four slices; SOM). The graph is plotted on a loglog scale, and a power-law distribution with a slope (γ) of 1.3 ± 0.1 (n = 4) is indicated in black (SOM). The inset shows the location of the 30 highest-connectivity neurons (~1% of the population, red dots) on a schematic representation of the hippocampus. The dashed rectangle indicates the size of the area of a x20 movie. Scale bar, 100 μm. (**B**) (1) Same as (A1) but at x20 magnification. The imaged region corresponds to CA3b/c; that is, around the dotted area in (A1). Arrow indicates the direction of the dentate gyrus. Scale bar, 100 μm. (2) Same as (A2) but for the movie taken in B1. (3) Same as (A3) but for a population of 7588 neurons. The probability distribution of output links from smaller CA3 regions also follows a power law with a similar scaling power (γ = 1.1 ± 0.1, n = 45). The probability threshold for HC neurons was fixed to 40% (red-shaded area). The inset indicates the location of HC neurons (red dots) on a schematic representation of the CA3b/c region of the hippocampus. HC neurons represented 5 ± 1% (n = 45) of all functionally connected cells. This value was not significantly different from that calculated in subfields from ×10 data sets of the same size as ×20 images, because HC neurons represented 4 ± 1% of the connected cell population in ×10 movies (n = 4, P > 0.05, Student's t test). sl, stratum lucidum; sp, stratum pyramidale; so, stratum oriens. Scale bar, 100 μm.

zation processes requires testing the causal influence of HC cells on network dynamics, something that cannot be achieved with post hoc data analysis (*13*, *17*, *18*).

To find cells involved in the synchronization of neuronal networks, we designed a method to map functional connectivity (FC) in real time in living brain slices, based on the analysis of multineuron calcium activity. Here we use the term FC to denote the statistical relationship between the activities of neurons (*19*), which should not be confused with the effective connectivity of functional synapses (*20*, *21*). This enabled us to perform targeted electrophysiological recordings and stimulation of neurons with a known degree of FC, while imaging network dynamics. We analyzed the developing hippocampal network because it provides an ideal circuit in which to investigate the existence of hub cells. First, as in most developing brain structures, network activity is concentrated in rhythmic synapse-driven synchronizations, the giant depolarizing potentials (GDPs) (*3*, *22*). Second, the network topology underlying the generation of GDPs is confined to local CA3 circuits in slices (*23*–*25*), which substantially simplifies the experimental approach. Last, understanding the cellular basis of synchronization in developing circuits is important, because several maturation processes rely on early network oscillations (*22*).

Using multibeam two-photon excitation of hippocampal slices from rats and GAD67-green fluorescent protein (GFP) knockin (KI) mice [5 to 7 days old; see the supporting online material (SOM)] loaded with the calcium indicator Fura-2AM (*26*), spontaneous multineuron activity was recorded with a temporal resolution of 50 to 150 ms (Fig. 1 and fig. S1). The FC of the hippocampus was first investigated at a large scale (with a ×10 objective, Fig. 1A). Focusing on the CA3 region, the activity of 806 ± 155 cells (n = 4 slices), distributed across the dentate gyrus to the CA1 region, were simultaneously imaged. Focusing on temporal correlations, a functional connection directed from neuron A to neuron B was established if the activation of A consistently preceded that of B (SOM and fig. S1B). An FC map was thus constructed for all recorded neurons (Fig. 1). In all slices imaged at low magnification, the average distribution of the number of output links per neuron was best fitted by a power-law function with an average scaling power of −1.3 ± 0.1 (n = 4 slices, Fig. 1 and SOM). Power-law distributed connectivity is the signature of a scale-free topology, in which hubs are rare neurons with a high connectivity index (*8*). Neurons with the highest connectivity tended to concentrate more often in the CA3c region (Fig. 1A3, inset). Previous studies have reported that this particular area is a preferential site of initiation for spontaneous GDPs (*25*, *27*).

To increase the chances of finding hub neurons, we next performed experiments in the CA3c area at higher magnification (with a ×20 objective, Fig. 1B). As previously reported (*26*), we were able to combine targeted electrophysiological recordings with calcium imaging. Out of 142 neurons recorded while imaging, only 45 were included in the following analysis because estimation and probing of network topology required very stable experimental conditions (SOM). The connectivity of the networks imaged at x20 was also distributed as a power law with an average scaling factor of −1.1 ± 0.1 (n = 45 slices; Fig. 1 and SOM). HC neurons were preferentially located in the stratum oriens and lucidum at the two borders with the pyramidal cell layer (Fig. 1B3 and fig. S3B3). To test the contribution to network dynamics of neurons with different degrees of connectivity, we targeted cells covering the entire connectivity range (Figs. 2 and 3, n = 20 HC and 25 LC neurons). Neurons were recorded in current-clamp conditions and stimulated while imaging population activity. Two stimulation protocols were applied for each neuron (SOM): (i) a phasic stimulation [short suprathreshold current pulses

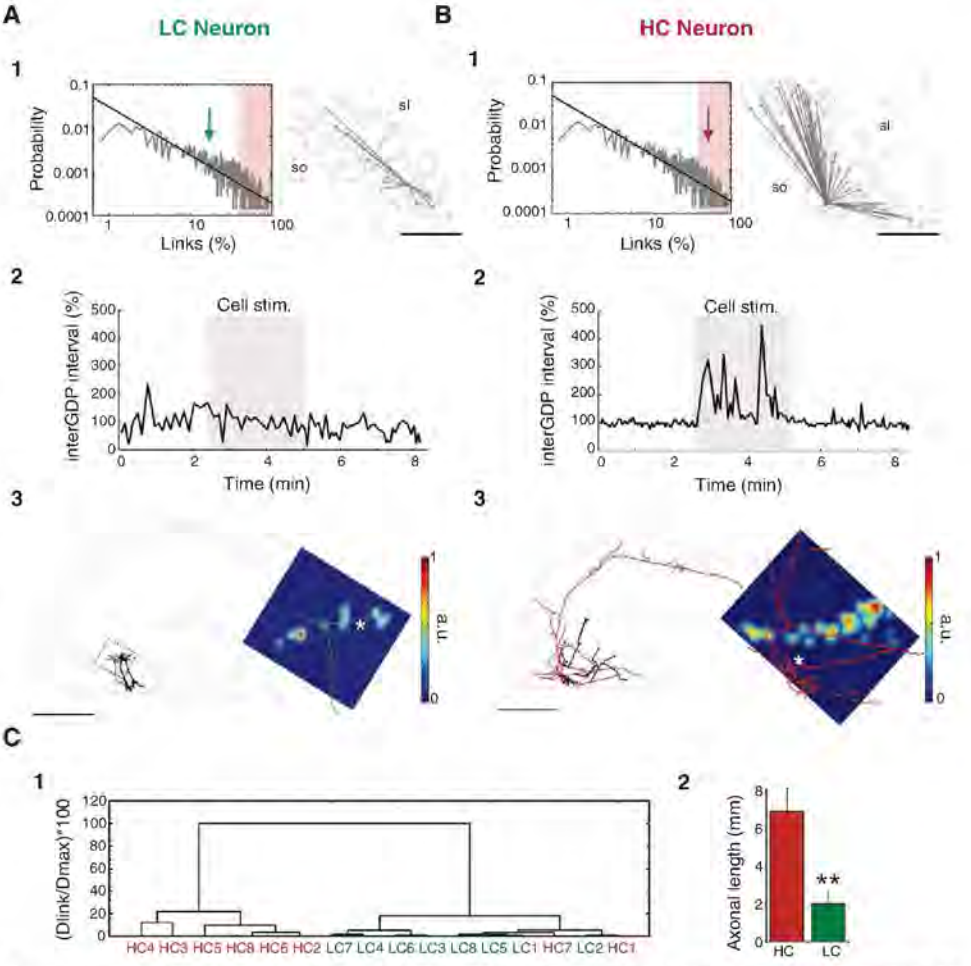

Fig. 2. Stimulation of HC but not LC neurons affects network dynamics. (**A**) Data from a representative LC interneuron. (1) The green arrow indicates the position in the pooled power-law distribution of output links (Fig. 1B) of the recorded neuron. Red-shaded area indicates the HC region, considering a 40% probability threshold. The right contour plot shows the position (solid red dot) and output connections (gray lines) of the illustrated LC interneuron. sl, stratum lucidum; so, stratum oriens. Scale bar, 100 μm. (2) Phasic current-clamp stimulation (200-ms pulses of 75-pA current every 10 s, gray area) of the LC interneuron while being imaged did not affect the occurrence of GDPs (detected from the calcium activity). The interval between GDPs as a function of time is plotted. Values are expressed relative to the average interval between GDPs calculated before the stimulation period. (3) Neurolucida reconstruction of the recorded cell on a schematic representation of the hippocampus reveals an interneuron-like morphology displaying a local axonal arborization (green). Dendritic arborization is black. The black rectangle marks the imaged region. Scale bar, 500 μm. This is a color-coded representation of the functional connectivity map [same as (A1)] (SOM) overlaid with the axonal morphology (green) of the cell. The asterisk indicates the cell body position. Red represents high cell density (a.u., arbitrary units). (**B**) Same as (A) but for a representative HC interneuron. Phasic stimulation of the HC interneuron [same protocol as (A2)] significantly decreased GDP frequency [(2), $P < 0.05$]. The recorded cell displayed a widespread axonal arborization (red) spanning locally toward the cells functionally connected [(3), right panel] and further toward the dentate gyrus and the CA1 region [(3), left panel]. (**C**) (1) Cluster analysis tree of the morphological variables describing the 16 recorded and imaged interneurons (Ward's method, Dlink: Euclidian distances, see SOM). Distances were normalized. Most HC and LC interneurons (based on the analysis of the imaging data) segregated in two different groups. (2) The total axonal lengths of HC and LC interneurons were statistically different ($P < 0.01$).

repeated at 0.1 to 0.2 Hz (the frequency range of GDPs occurrence)]; and (ii) tonic stimulation (continuous positive or negative current injections, bringing the cell to a membrane potential where it fired continuously or was completely silenced, respectively). Cell/network interaction was estimated using three metrics (SOM): (i) the frequency of occurrence of spontaneous network synchronizations (GDPs) during the stimulation relative to the resting condition; (ii) the peristimulus histogram plotting the average fraction of cells activated by the phasic stimulation; and (iii) the phase precession/succession of GDPs relative to a harmonic oscillator mimicking GDPs' rhythm in resting conditions; in this way, the number of observed versus expected GDPs was estimated over time (SOM). A cell was considered as affecting network dynamics significantly if it satisfied any of the above criteria.

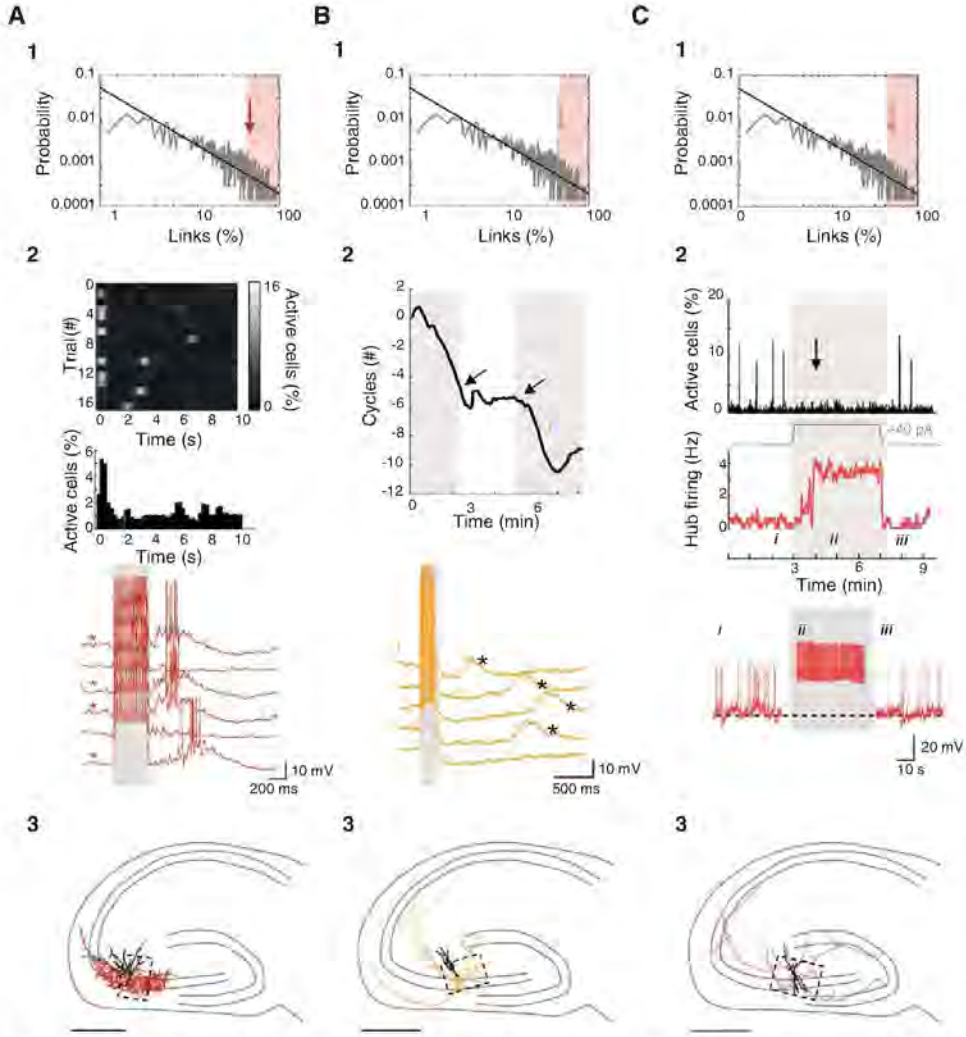

Fig. 3. Perturbations of network dynamics induced by the stimulation of HC interneurons. (**A**) Data obtained from a HC interneuron triggering network synchrony ($P < 0.05$). Frame rate, 10 Hz. (1) The red arrow indicates the position in the pooled power-law distribution of output links (Fig. 1B) of the recorded neuron. (2) Fraction of cells active as a function of time after repetitive phasic stimulation (200-ms pulses of 100-pA current every 10 s) of the HC interneuron (16 consecutive trials). The peristimulus time histogram shows the average across different trials. Red traces are current-clamp recordings from the stimulated HC neuron for six consecutive stimulations (gray). Four out of six trials (indicated by red asterisks in lower panel) triggered GDPs appearing as polysynaptic membrane potential depolarizations. (3) Neurolucida reconstruction of the recorded HC cell on a schematic drawing of the hippocampus. Axonal arborization is in color; dendrites are black. The dashed rectangle indicates the imaged region. Scale bar, 500 μm. (**B**) Same as (A) but for a HC interneuron inducing a phase succession of GDPs when stimulated ($P < 0.05$). Phase succession is illustrated in the top graph of (2) plotting the number of GDP cycles skipped during phasic stimulation (gray) as a function of time. The number of expected GDPs was calculated during resting conditions (white) based on the average interval between GDPs. Arrows indicate transitions between oscillatory regimes. Current-clamp recordings from five consecutive stimulation trials for the period marked by (i) show the progressive delay in the occurrence of a GDP (black asterisks) after stimulation (gray). (**C**) Same as (A) but in a HC interneuron preventing GDPs when stimulated. Graphs in (2) show the fraction of active cells (top histogram), as well as the cell firing frequency (middle), as a function of time. Peaks of synchronous activity (GDPs) disappear when the membrane potential of the cell (bottom) is depolarized by continuous positive current injection (40 pA; SOM). Current-clamp traces show the activity in the HC neuron in resting (i and iii) and stimulated (ii, gray) conditions. The black arrow indicates the time when a significant effect on network dynamics starts ($P < 0.05$).

About a third (8 out of 20 neurons) of the targeted HC cells exhibited a significant cell/network interaction (Figs. 2B and 3). In contrast, no LC neuron but one showed any significant cell/network interaction (24 out of 25 neurons; Fig. 2A and fig. S2A). The effects of neurons significantly affecting network dynamics ($n = 9$) could be summarized as follows (Fig. 3): (i) in four cases, tonic or phasic stimulation induced sustained action potential (AP) firing that significantly decreased the occurrence of GDPs to 48 ± 13% of resting conditions ($P < 0.05$; Figs. 2B and 3C and movie S1); (ii) in three cells, phasic stimulation triggered network synchrony in the form of GDPs in 37 ± 4% of the trials within 1 s after the stimulus ($P < 0.05$; Fig. 3A and fig. S5); (iii) in three cells, phasic stimulations induced a phase succession of GDPs as compared to resting conditions (Fig. 3B, $P < 0.05$). Our evidence suggests that these neurons may act like functional hubs. We will henceforth refer to these as hub neurons.

The developing hippocampal network comprises two major cell types: pyramidal glutamatergic cells and γ-aminobutyric acid–releasing (GABAergic) interneurons. In adult cortical structures, network function is strongly modulated by the action of GABAergic interneurons that represent a minority of the total population but include a variety of subtypes (*28*). Half of the experiments were performed in GAD67-GFP KI mice (*29*) to selectively identify GABAergic neurons. All hub neurons recorded in GAD67-GFP KI mice, based on their HC index, were GFP-positive (fig. S3, $n = 4$). Accordingly, the fraction of GFP-positive cells was four times higher in the HC region than in the total cell population (22% of HC neurons versus 6% of all neurons, $n = 46$ movies in GAD67-GFP KI mice). Therefore, hub neurons are GABAergic, and we next examined whether they represented a specific morphological population. While being recorded, cells were filled with biocytin. All nine hub cells were aspiny neurons and often possessed multipolar dendrites and a cell body located at the border between the pyramidal cell layer and the stratum oriens or lucidum. All HC neurons that were not hubs were morphologically identified as pyramidal cells (fig. S2; 4 cells reconstructed). LC cells not influencing network dynamics exhibited either interneuronal or pyramidal cell morphology (Fig. 2 and fig. S2). All hub neurons had distinctive morphological features, displaying a widespread axonal arborization that most often crossed subfield boundaries, running parallel to principal cell layers toward both the dentate gyrus and CA1 region ($n = 6$ of 9 neurons, Figs. 2 and 3). Three of the hub cells exhibited dense preferential innervation of the CA3 principal cell layer, suggesting a perisomatic, basketlike (*28*) interneuron subtype (Fig. 3A and fig. S3B2). We

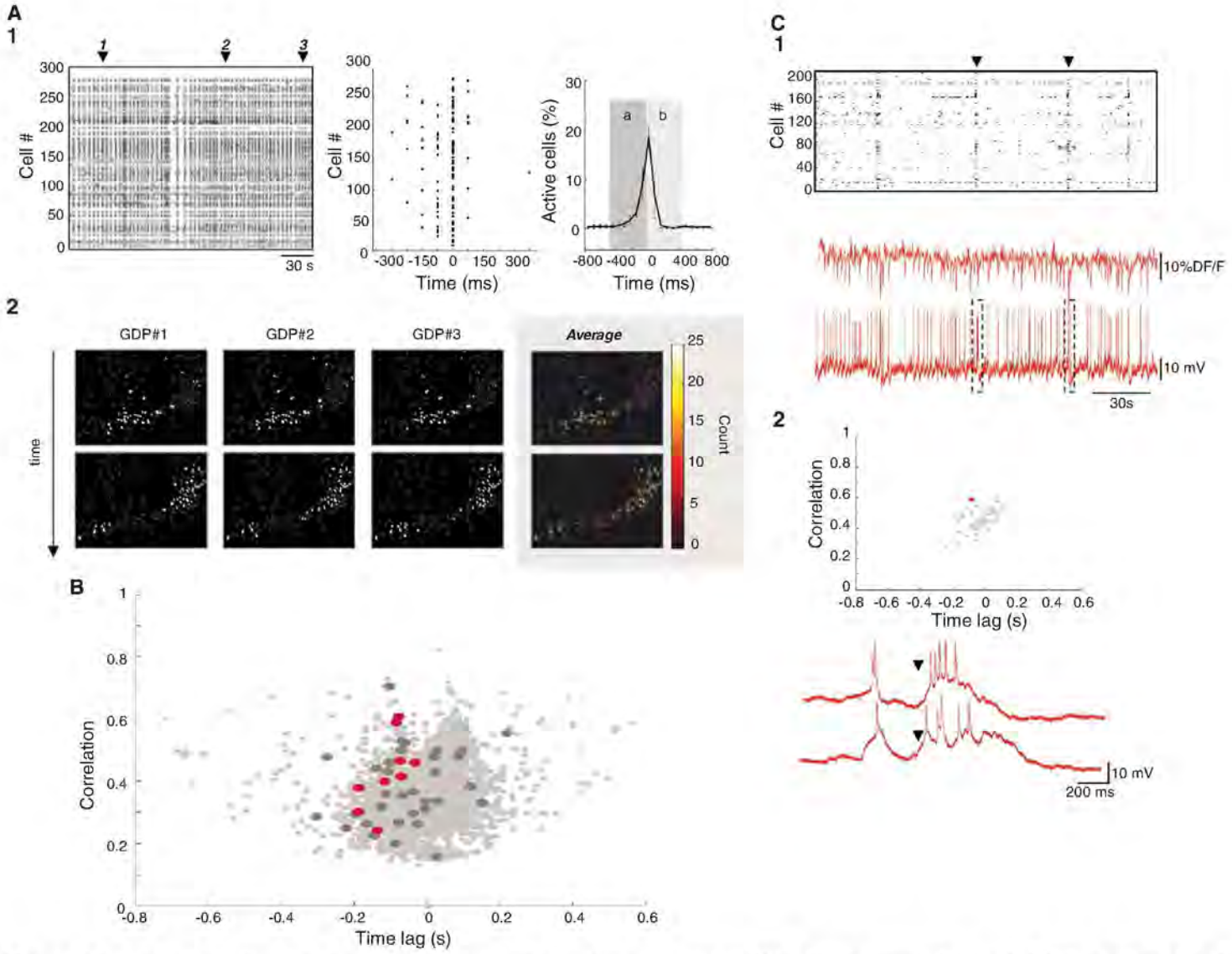

Fig. 4. Hub neurons are activated at the onset of spontaneous network synchronizations. (**A**) (1) Raster plot of the onsets of calcium events in a representative movie (frame rate, 20 Hz). There are many spontaneous GDPs appearing as broken vertical lines in the raster plot. The middle raster plot shows GDP1 on an expanded time scale. The right plot represents the average temporal profile of the fraction of cells sequentially activated in all GDPs recorded in the same network. The peak of cell coactivation was used as zero time reference. Error bars indicate SDs. (2) Contour plots showing cells activated during the buildup [region a in (1)] and at the peak (b) for the three GDPs marked by arrows in the raster plot in (1). Note the similarity between the patterns of cells. Color-coded contour plots on the right quantify how many times a cell is recruited in one of the two temporal windows over 25 representative GDPs. (**B**) Time-correlation graph (SOM), plotting for each imaged neuron (7588 neurons) the average correlation and average time of activation relative to all other cells. Red dots indicate targeted functional hubs and dark gray dots indicate all other recorded neurons. (**C**) (1) Raster plot [calculated as in (A1)] of the network activity (frame rate, 6.67 Hz) while recording an HC hub neuron (red dots) in current-clamp mode (bottom trace). Calcium events (top trace) reflect spiking activity (bottom trace). (2) Same time-correlation graph as in (B) but only for the recorded slice shown in (C1). The red dot marks the HC hub neuron. Red traces show current-clamp recordings of spontaneous activity in the hub neuron at the time of two different GDPs [marked by arrowheads; dashed rectangles in (C1), lower panel]. AP firing occurs in the hub neuron about 200 ms before GDPs.

next performed a multivariate analysis of the morphometric data of eight HC and eight LC interneurons (SOM). Hub interneurons significantly differed from LC interneurons by the length of their axonal tree (6865 ± 1238 μm versus 2150 ± 483 μm, $P < 0.01$, $n = 16$ cells, Fig. 2). Given their extended morphology, it seems probable that hub neurons have a higher probability of being severed in brain slices than other cells and thus probably represent a higher fraction of neurons in vivo [but see (*20*)]. We conclude that functional hubs are GABAergic interneurons with a long axonal arborization. Hub neurons therefore have the features required to activate many postsynaptic targets.

In order to determine the nature of the functional link between hub neurons and other cells, we first asked whether stimulation of hub neurons could directly trigger a calcium response in other neurons, even in the case where the net effect of stimulation was to desynchronize activity. We thus compared functional and effective connectivity maps (SOM and fig. S4). We found that there was a large overlap between the two maps in the case of HC interneurons (53 ± 6% on average, $n = 5$), whereas stimulation of HC pyramids activated only 8 ± 1% of functionally connected neurons ($n = 5$), indicating that these were effectively not connected to follower cells. We next performed targeted paired recordings from HC and follower neurons ($n = 16$ pairs). In the case of HC interneurons, we observed a 37% probability of finding a monosynaptic GABAergic connection between neurons ($n = 8$ pairs, fig. S5). This was significantly different from the case of HC pyramidal cells, because no direct connection could be revealed when recording from them ($n = 8$ pairs, $P < 0.05$, Wilcoxon-Mann-Whitney two-sample rank test). This is in agreement with

Table 1. Comparison of basic electrophysiological properties of hub neurons and LC interneurons. Measurements were obtained from whole-cell recordings in eight hub and eight LC interneurons (see SOM methods). V_{rest}, resting membrane potential (corrected value; SOM); R_{input}, input resistance; $V_{threshold}$, AP threshold (corrected value; SOM); AP width, AP width measured at half-maximal amplitude. Asterisks indicate significant differences. $P < 0.05$ was considered significant. The right column indicates the P value given by Student or Mann-Whitney tests.

Properties	Hub interneurons	LC interneurons	P value
V_{rest} (mV)	−66 ± 5	−64 ± 5	0.33
R_{input} (megohms)	379 ± 85	423 ± 67	0.69
Capacitance (pF)	65 ± 15	54 ± 15	0.64
V_{thresh} (mV)	−53 ± 5*	−39 ± 4	0.04
AP width (ms)	2.05 ± 0.5	1.8 ± 0.5	0.74
AP amplitude (mV)	45 ± 6	39 ± 5	0.43
EPSP frequency (Hz)	4.5 ± 1.5*	1.0 ± 0.4	0.03
EPSP amplitude (mV)	2.1 ± 0.3	2.6 ± 0.5	0.51

the imaging data and comparable to the highest synaptic connectivity rates reported for interneurons in the adult cortex (*21*). It therefore represents a high value given the fact that all the monosynaptically connected neurons were more than 100 μm apart (the average distance between recorded neurons was 130 ± 20 μm, $n = 16$ pairs, fig. S5) and that the connection probability is very likely to increase with age (*30*, *31*). We conclude that the functional connectivity of hub neurons is supported by an effective synaptic connectivity and propose that HC pyramidal neurons are more likely to operate within assemblies (*32*).

Because hub function may depend on differences in cellular excitability or synaptic strength (*33*, *34*), we next examined the basic electrophysiological properties of hub neurons as compared to LC interneurons (Table 1). Of the basic features analyzed (SOM), hub neurons received more spontaneous excitatory postsynaptic potentials (EPSPs) and had a lower threshold for AP generation (Student's t test, $P < 0.05$). A lower AP threshold could indicate a more advanced maturation stage for hub neurons (*35*). Both properties should result in a more efficient activation of hub neurons by synaptic inputs.

Finally, because stimulation of hub neurons significantly affected the occurrence of GDPs, we examined their specific involvement in the spontaneous synchronization process. In agreement with previous estimates (*36*), the dynamic of a single GDP was characterized by a buildup of activity lasting on average 350 ms (Fig. 4, n = 8 slices, SOM). Using cluster analysis (SOM), a stereotypical spatiotemporal synchronization pattern accounted for one-third of the GDPs within the recording period (33 ± 2%, $n = 45$, Fig. 4). For each neuron, we estimated the average correlation and time of activation relative to all other cells in GDPs that clustered together (Fig. 4 and SOM). In almost half of the movies ($n = 20$ out of 45), the time correlation graph presented a bimodal distribution (Fig. 4B), indicating that GDPs repetitively started synchronizing neurons plotted on the left side of the distribution, whereas neurons on the right were activated last. By pooling the data from different slices ($n = 7588$ neurons, 45 movies), we found that the majority of functional hubs clustered on the upper left region of the graph, indicating a more reliable activation at the onset of GDPs (Fig. 4B); this is in agreement with the lower AP threshold and higher synaptic drive described above. Other recorded neurons were evenly distributed across the correlation plot. Cell-attached and whole-cell recordings confirmed that cells activated at the buildup of synchronization indeed fired APs before the occurrence of GDPs ($n = 14$ neurons, fig. S1C). AP firing in hub neurons thus predicts network synchronization in the developing CA3 region.

This study shows that a scale-free topology can underlie synchronous network patterns in living cortical networks. We suggest that hub neurons, composed of a subpopulation of GABAergic interneurons, orchestrate spontaneous network synchronization. Two different morphological types of hub neurons could be distinguished within our sample data set: (i) cells displaying a long axon spanning regions with sparse collaterals, and (ii) basketlike neurons with a dense but more local arborization pattern. Network synchronization could be triggered by phasic stimulation only in basketlike hub neurons (Fig. 3A and fig. S5). In the adult hippocampus, long-range projecting GABAergic hippocampal interneurons have been described (*37*) and their hub function has been suggested but never been probed (*4*). Perhaps the long-axon hub neurons act as connector hubs, whereas basketlike hubs have a local hub function (*19*). Regardless, the present results confirm the crucial role of GABAergic transmission in shaping network patterns at early developmental stages, when GABA exerts a complex excitation/shunting inhibition action (*38*, *39*). The spontaneous activation, before synchrony, of hub neurons with many direct postsynaptic connections is compatible with excitatory actions of GABA. However, hub cell stimulation also often slowed down network oscillations and in some extreme cases completely desynchronized activity. One possible explanation is that the shunting actions of GABA retard or prevent synchronization. However, other possibilities cannot be excluded, including a phase-resetting effect by which a hub cell can either advance or delay bursting in intrinsically oscillating neurons (*39*), depending on their phase at the time of the hub input (*40*).

Single neurons can trigger population synchronization in the disinhibited adult CA3 region (*41*) or elicit a chain of cell activation in the cortex that can translate into behavior or switch the global brain state (*42*–*44*). Therefore, the demonstration that hub neurons functionally operate in the brain helps bridge the gap between single-cell and network activity. This finding should facilitate the investigation of the mechanisms by which many physiological and pathological network oscillations are generated.

References and Notes

1. G. Buzsáki, *Rhythms of the Brain* (Oxford Univ. Press, Oxford, 2006).
2. L. C. Katz, C. J. Shatz, *Science* **274**, 1133 (1996).
3. Y. Ben Ari, *Trends Neurosci.* **24**, 353 (2001).
4. G. Buzsaki, C. Geisler, D. A. Henze, X. J. Wang, *Trends Neurosci.* **27**, 186 (2004).
5. G. Grinstein, R. Linsker, *Proc. Natl. Acad. Sci. U.S.A.* **102**, 9948 (2005).
6. R. J. Morgan, I. Soltesz, *Proc. Natl. Acad. Sci. U.S.A.* **105**, 6179 (2008).
7. D. J. Watts, S. H. Strogatz, *Nature* **393**, 440 (1998).
8. A. L. Barabasi, R. Albert, *Science* **286**, 509 (1999).
9. S. Boccaletti, V. Latora, Y. Moreno, M. Chavez, D.-U. Hwang, *Phys. Rep.* **424**, 175 (2006).
10. L. A. Amaral, A. Scala, M. Barthelemy, H. E. Stanley, *Proc. Natl. Acad. Sci. U.S.A.* **97**, 11149 (2000).
11. R. L. Buckner *et al.*, *J. Neurosci.* **29**, 1860 (2009).
12. V. M. Eguiluz, D. R. Chialvo, G. A. Cecchi, M. Baliki, A. V. Apkarian, *Phys. Rev. Lett.* **94**, 018102 (2005).
13. D. Eytan, S. Marom, *J. Neurosci.* **26**, 8465 (2006).
14. O. Sporns, C. J. Honey, R. Kotter, *PLoS One* **2**, e1049 (2007).
15. D. J. de Solla Price, *Science* **149**, 510 (1965).
16. E. V. Lubenov, A. G. Siapas, *Nature* **459**, 534 (2009).
17. K. V. Srinivas, R. Jain, S. Saurav, S. K. Sikdar, *Eur. J. Neurosci.* **25**, 3276 (2007).
18. S. Yu, D. Huang, W. Singer, D. Nikolic, *Cereb. Cortex* **18**, 2891 (2008).
19. E. Bullmore, O. Sporns, *Nat. Rev. Neurosci.* **10**, 186 (2009).
20. S. Song, P. J. Sjostrom, M. Reigl, S. Nelson, D. B. Chklovskii, *PLoS Biol.* **3**, e68 (2005).
21. A. M. Thomson, C. Lamy, *Front. Neurosci.* **1**, 19 (2007).
22. N. C. Spitzer, *Nature* **444**, 707 (2006).
23. A. A. Cattani, V. D. Bonfardin, A. Represa, Y. Ben-Ari, L. Aniksztejn, *J. Neurophysiol.* **98**, 2324 (2007).
24. M. Canepari, F. Mammano, S. G. Kachalsky, R. Rahamimoff, E. Cherubini, *Cell Calcium* **27**, 25 (2000).
25. L. Menendez de la Prida, S. Bolea, J. V. Sanchez-Andres, *Eur. J. Neurosci.* **10**, 899 (1998).
26. V. Crepel *et al.*, *Neuron* **54**, 105 (2007).
27. S. Bolea, J. V. Sanchez-Andres, X. Huang, J. Y. Wu, *J. Neurophysiol.* **95**, 552 (2006).
28. T. F. Freund, G. Buzsáki, *Hippocampus* **6**, 347 (1996).
29. N. Tamamaki *et al.*, *J. Comp. Neurol.* **467**, 60 (2003).
30. D. Doischer *et al.*, *J. Neurosci.* **28**, 12956 (2008).
31. L. Groc, B. Gustafsson, E. Hanse, *Eur. J. Neurosci.* **17**, 1873 (2003).
32. K. D. Harris, J. Csicsvari, H. Hirase, G. Dragoi, G. Buzsaki, *Nature* **424**, 552 (2003).
33. L. Wittner, R. Miles, *J. Physiol.* **584**, 867 (2007).
34. F. Strata *et al.*, *J. Neurosci.* **17**, 1435 (1997).
35. S. Rheims *et al.*, *J. Neurophysiol.* **100**, 609 (2008).
36. L. M. Prida, J. V. Sanchez-Andres, *J. Neurophysiol.* **82**, 202 (1999).
37. S. Jinno *et al.*, *J. Neurosci.* **27**, 8790 (2007).
38. Y. Ben-Ari, J. L. Gaiarsa, R. Tyzio, R. Khazipov, *Physiol. Rev.* **87**, 1215 (2007).
39. S. T. Sipila, K. Huttu, I. Soltesz, J. Voipio, K. Kaila, *J. Neurosci.* **25**, 5280 (2005).
40. H. Y. Jeong, B. Gutkin, *Neural Comput.* **19**, 706 (2007).
41. L. M. de la Prida, G. Huberfeld, I. Cohen, R. Miles, *Neuron* **49**, 131 (2006).

42. M. Brecht, M. Schneider, B. Sakmann, T. W. Margrie, *Nature* **427**, 704 (2004).
43. G. Molnar *et al.*, *PLoS Biol.* **6**, e222 (2008).
44. C. Y. Li, M. M. Poo, Y. Dan, *Science* **324**, 643 (2009).
45. We thank D. Aronov, M. Colonnese, J. Epsztein, B. Fernandez, G. Fishell, C. Holmgren, B. Gutkin, M. Milh, and R. Khazipov for helpful suggestions and critical comments; C. Allene, K. Bennouar, and F. Michel for help with the experiments; and K. Obata and K. Vogt for kindly providing GAD67-EGFP Ki mice. This work was supported by grants from INSERM, the Ville de Marseille and Region Provence Alpes Côte d'Azur, the Fondation pour la Recherche Médicale, the Agence Nationale pour la Recherche, the Fondation pour la Recherche sur le Cerveau, and the Fondation Bettencourt Schueller. R.C. and A.R. were funded by the CNRS. M. Goldin and P. Bonifazi were funded by Framework Program 6 (FP6) and FP7–Intra-European Fellowships for career development.

Supporting Online Material
www.sciencemag.org/cgi/content/full/326/5958/1419/DC1
Materials and Methods
Figs. S1 to S5
References
Movie S1

27 April 2009; accepted 23 September 2009
10.1126/science.1175509

Deletion of Atoh1 Disrupts Sonic Hedgehog Signaling in the Developing Cerebellum and Prevents Medulloblastoma

Adriano Flora,[1] Tiemo J. Klisch,[1,2] Gabriele Schuster,[1] Huda Y. Zoghbi[1,2,3,4]*

Granule neuron precursors (GNPs) are the most actively proliferating cells in the postnatal nervous system, and mutations in pathways that control the GNP cell cycle can result in medulloblastoma. The transcription factor Atoh1 has been suspected to contribute to GNP proliferation, but its role in normal and neoplastic postnatal cerebellar development remains unexplored. We show that Atoh1 regulates the signal transduction pathway of Sonic Hedgehog, an extracellular factor that is essential for GNP proliferation, and demonstrate that deletion of *Atoh1* prevents cerebellar neoplasia in a mouse model of medulloblastoma. Our data shed light on the function of Atoh1 in postnatal cerebellar development and identify a new mechanism that can be targeted to regulate medulloblastoma formation.

Disruption of the delicate balance between proliferation and differentiation in cerebellar granule neuron precursors (GNPs) underlies medulloblastoma, the most common pediatric tumor of the nervous system (*1*, *2*). A class of particularly aggressive medulloblastomas associated with very poor prognosis show high expression of *Atoh1* (*3*), a transcription factor highly expressed in GNPs also known as *Math1* (*4*), and recent in vitro studies proposed that *Atoh1* might be involved in neoplastic proliferation (*5*, *6*). Given that deletion of *Atoh1* in mice results in perinatal death (*7*), the function of this transcription factor in the developing postnatal cerebellum has remained opaque.

To delete *Atoh1* in the postnatal developing cerebellum, we crossed $Atoh1^{flox/flox}$ mice (*8*) with mice carrying the gene coding for a tamoxifen-inducible Cre recombinase in the *Rosa* locus (R26CreER) (*9*) and a null allele of *Atoh1* (*10*, *11*). After activation of Cre by tamoxifen, $Rosa^{CreER}$;$Atoh1^{+/flox}$ animals (designated here as $Atoh1^{wt}$) maintain one functional allele of *Atoh1*, whereas $Rosa^{CreER}$;$Atoh1^{-/flox}$ mice (designated here as $Atoh1^{\Delta}$) lose *Atoh1* expression. We injected postnatal day 3 (P3) animals and analyzed their cerebella 3 days later. Nissl staining of matching sections of the external granule layer (EGL), the neuroepithelium formed by GNPs, revealed that $Atoh1^{\Delta}$ animals had a much thinner EGL than that of their $Atoh1^{wt}$ littermates (fig. S1). Using phospohistone H3 staining to visualize the *M* phase of the cell cycle and Tuj1 for neural differentiation, we found that the EGL of $Atoh1^{\Delta}$ mice had been depleted of cycling immature precursors (Fig. 1, A and B, and fig. S2). Staining for active caspase 3 did not reveal any apoptosis in the EGL of $Atoh1^{\Delta}$ mice (fig. S1, E and F). We thus investigated whether deletion of *Atoh1* triggers the GNP differentiation to granule neurons or induces these cells to transdifferentiate to other cell types. Shown in fig. S2, cells still populating the surface of $Atoh1^{\Delta}$ cerebellum that had deleted Atoh1 still expressed Zic1, a marker of differentiating postmitotic EGL cells and mature granule neurons, making transdifferentiation unlikely. Proliferating GNPs express *Pax6* at low levels, whereas differentiating postmitotic precursors show high expression of *Pax6* and turn on the neural differentiation marker NeuN. The cells residing on the surface of the cerebellum of $Atoh1^{\Delta}$ expressed high levels of

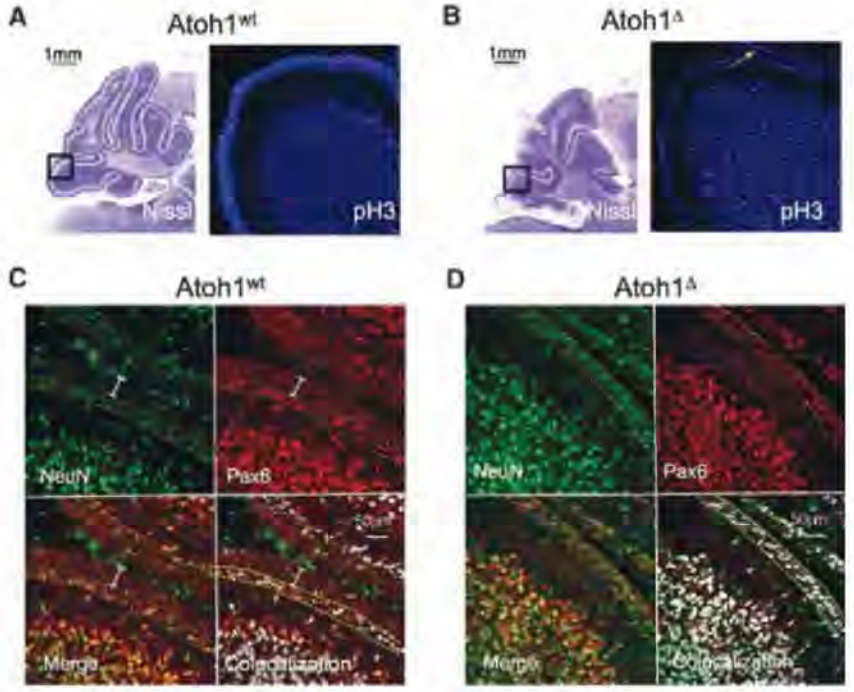

Fig. 1. *Atoh1* deletion disrupts GNP proliferation and induces differentiation. (**A** and **B**) Phosphohistone H3 staining of cerebella of animals injected with tamoxifen. (Left) Nissl staining of cerebella of animals injected with tamoxifen. The boxed regions represent the images to their right, showing the staining for phosphohistone H3. The arrow in (B) indicates a single cycling cell in the $Atoh1^{\Delta}$ EGL. (**C** and **D**) Pax6 and NeuN staining shows the immature GNPs [(C), white bar] not expressing NeuN and the differentiating population [(C) and (D), between the yellow dotted lines] coexpressing both markers. The colocalization pattern is shown on the bottom right.

[1]Department of Molecular and Human Genetics, Baylor College of Medicine, Houston, TX 77030, USA. [2]Howard Hughes Medical Institute, Baylor College of Medicine, Houston, TX 77030, USA. [3]Departments of Neuroscience and Pediatrics, Baylor College of Medicine, Houston, TX 77030, USA. [4]Program in Developmental Biology, Baylor College of Medicine, Houston, TX 77030, USA.

*To whom correspondence should be addressed. E-mail: hzoghbi@bcm.edu

Pax6 and NeuN (Fig. 1, C and D), again suggesting that deletion of *Atoh1* in the postnatal cerebellum activates the differentiation process of cerebellar granule neurons.

To investigate the molecular effects of *Atoh1* deletion, we isolated GNPs from *Atoh1*$^{flox/flox}$ P5 animals and infected them with adenoviruses that express either the green fluorescent protein (GFP) or the Cre recombinase gene. We cultured the transduced cells in the presence of Shh for 3 days (*12*) and evaluated their proliferative status by means of BrdU and phospohistone H3 staining. *Atoh1* deletion led to a sharp decrease in cell proliferation (fig. S3, A and B), suggesting that GNPs are unable to respond to Shh stimulation in the absence of *Atoh1*. We then purified total RNA from the transduced GNPs and performed quantitative reverse transcription polymerase chain reaction (RT-PCR) analysis of the Shh target genes cyclin D2 (*Ccnd2*), *Mycn*, and *Gli1* (Fig. 2A). All of these genes were down-regulated, as was *Gli2*, the main transcriptional effector of Shh signaling in GNPs (*12*–*15*).

To determine whether Gli2 down-regulation was responsible for the failure to proliferate in the absence of *Atoh1*, we infected GNPs with a retroviral vector that expresses Gli2 before deleting *Atoh1*. Cells infected with the Gli2-expressing retrovirus were still able to proliferate in response to Shh (Fig. 2, B and C), showing that down-regulation of *Gli2* after *Atoh1* deletion plays a major role in GNP withdrawal from the cell cycle. Because *Gli2* transcription does not require Shh (*16*), we reasoned that down-regulation of its mRNA is unlikely to be a secondary effect of the blockade of the Shh signal and that *Gli2* might be a direct transcriptional target of Atoh1, which would explain how deletion of *Atoh1* inhibits Shh signaling.

Atoh1 activates its target genes through binding to regions enriched in specific sites called E-boxes (*17*). Computational scanning identified a DNA sequence highly enriched in E-boxes (eight E-boxes) in the second intron of Gli2 (fig. S4A). We designed an oligonucleotide that spans two E-boxes in the cluster that are conserved in mouse and human and used it as a probe for electrophoretic mobility shift assay (EMSA) experiments (fig. S4A, boxed sequence). After incubating the probe with nuclear extracts of Neuro2a cells transfected with an *Atoh1*-Flag expression plasmid, we observed the appearance of a specific complex that was supershifted by an antibody to Flag (fig. S4B, lane 2, arrow, and 3, arrowhead) and completed by the wild-type (wt) unlabeled oligonucleotide but not by an oligonucleotide bearing a point mutation in each of the two E-boxes (fig. S4B, lanes 4 and 5). Next, we cloned the entire sequence that spans the E-box cluster in front of a minimal promoter that drives the expression of the luciferase gene. Cotransfection of Neuro2a cells with the *Gli2* reporter construct and a vector that expresses Atoh1 resulted in strong luciferase expression (Fig. 2D), showing that Atoh1 acts as a positive regulator through binding to this sequence. The control reporter vector containing only the minimal promoter had no effect.

To verify our findings in vivo, we took advantage of a knockin mouse model in which the endogenous Atoh1 protein is tagged with three flag peptides on its C terminus (fig. S5). *Atoh1*$^{flag/flag}$ P5 cerebella were collected and subjected to chromatin immunoprecipitation (ChIP). As a negative control, we took cortex (which does not express *Atoh1*) from the same animals. As shown in Fig. 2E, we obtained a strong amplified band in the cerebellar sample but virtually no signal in the negative control, which implies that Atoh1 binds to this DNA region during cerebellum development. To confirm that this sequence is a transcriptional enhancer, we carried out additional ChIP experiments using an antibody that recognizes the monomethylated form of histone H3 on lysine 4 (me1-H3), a well-defined marker of enhancers (*18*). An antibody that recognizes the trimethylated form of histone H3 on lysine 4 (me3-H3), a marker of promoter sequences (*18*), served as a negative control. As expected, we

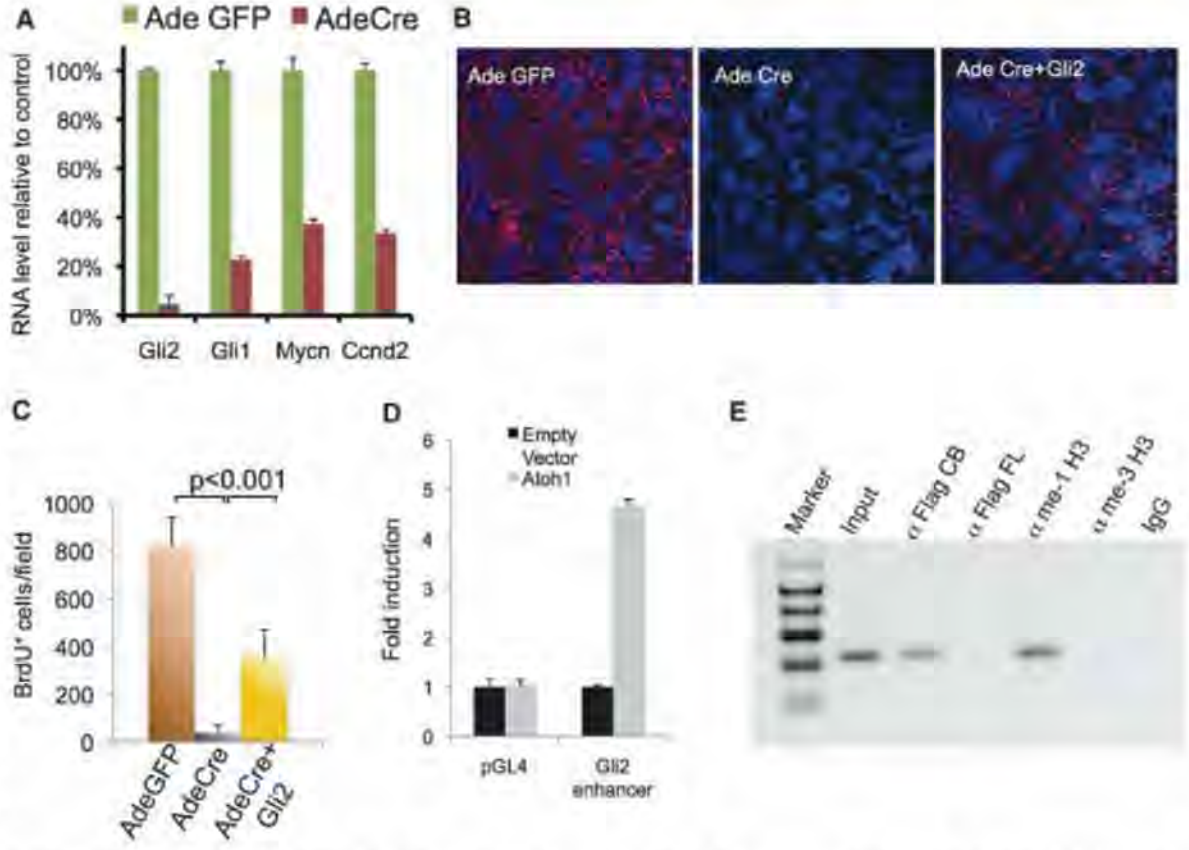

Fig. 2. Atoh1 controls GNP proliferation through regulation of *Gli2* expression. (**A**) Quantitative RT-PCR on RNA extracted from transduced GNPs cultured in the presence of Shh for 3 days. The genes tested are shown below the bar graph. The amount of RNA for each gene was normalized over the glyceraldehyde-3-phosphate dehydrogenase RNA level in each sample and expressed as a percentage over the level of RNA of the GFP-transduced cells. (**B**) Purified GNPs were infected either with a control retrovirus or a GLI2-expressing retrovirus and transduced with an adenovirus expressing GFP or Cre. Cycling cells were labeled with BrdU and visualized through the red fluorescence signal. 4′,6′-diamidino-2-phenylindole counterstaining (blue) reveals the nuclei. (**C**) Quantification of the rescue effect by *Gli2* on proliferation after deletion of *Atoh1* in GNPs (BrdU positive cells per field). Student's *t* test results are shown. (**D**) Luciferase assay showing that Atoh1 can activate transcription when it interacts with the *Gli2* intronic region. Results are expressed as fold induction over the cells transfected with the empty expression vector. The reporter plasmids used in the experiments are shown below the graph. (**E**) ChIP experiment indicating that Atoh1 is bound to the *Gli2* genomic region in the postnatal cerebellum and that this sequence has the epigenetic hallmark of an active transcriptional enhancer. Sample identities are shown above. CB, cerebellum; FL, cortical frontal, lobes.

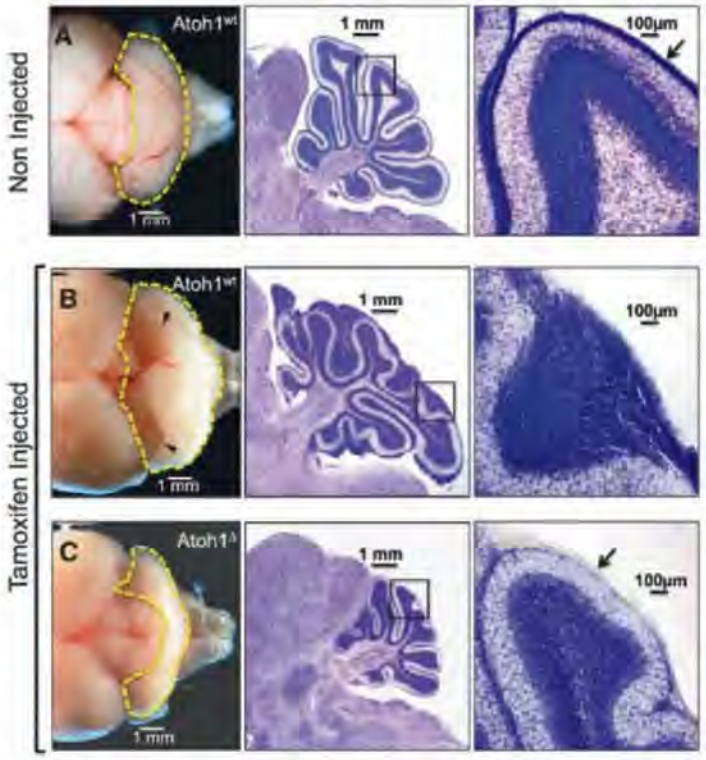

Fig. 3. *Atoh1* deletion prevents tumor formation in a mouse model of Shh-induced medulloblastoma. (**A**) P14 cerebella of a control animal that did not receive tamoxifen and thus doesn't express the activated form of Smoothened. (**B**) A SmoAtoh1^{wt} and (**C**) a SmoAtoh1$^{\Delta}$ animal injected with tamoxifen so as to activate the expression of the constitutively active Smoothened. The treatment is shown on the side of each image series. The cerebellum is outlined with a dotted line; the arrowheads indicate two neoplastic outgrowths. (Middle) Sagittal sections around the midline. Neurons and neuronal precursors are visualized by means of Nissl staining. The boxed regions are shown at high magnification (right); arrows indicate the EGL. The *Atoh1* genotype is shown in the right panels.

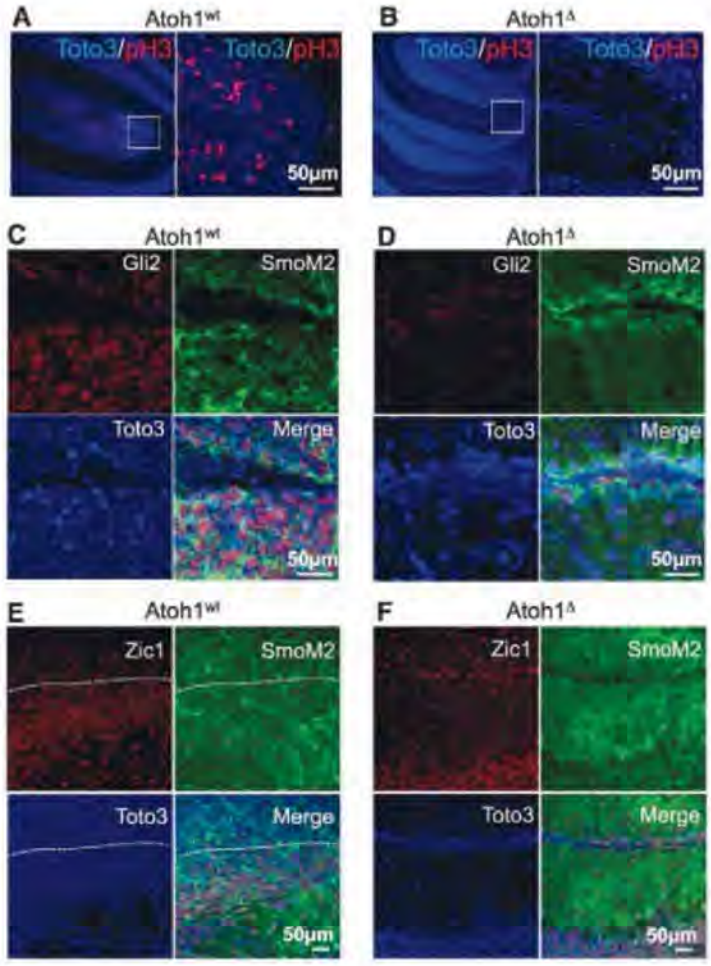

Fig. 4. Disruption of *Atoh1* blocks Shh-induced proliferation and *Gli2* expression in a mouse model of medulloblastoma. (**A** and **B**) The *M* phase of the cell cycle was visualized by means of phosphohistone H3 staining in the cerebellum of Smo*Atoh1*^{wt} (A) or Smo*Atoh1*$^{\Delta}$ (B) animals injected with tamoxifen. The red signal shows actively cycling cells, whereas the blue signal reveals cell nuclei. The boxed portion is magnified (right). (**C**) Gli2 staining of a cerebellar sample from a Smo*Atoh1*^{wt} animal and (**D**) from a Smo*Atoh1*$^{\Delta}$ mouse. (**E**) Zic1 staining of a cerebellar sample from a Smo*Atoh1*^{wt} animal and (**F**) from a Smo*Atoh1*$^{\Delta}$ mouse. The cells above the white line in (E) are the Zic1-negative undifferentiated cells of the neoplastic tissue. The *Atoh1* genotype is shown above each panel.

recovered the DNA sequence corresponding to the *Gli2* intergenic region only when we used antibody to me1-H3, confirming that the region bound by Atoh1 in the *Gli2* gene is an active transcriptional enhancer. We next evaluated whether the two genes are coexpressed in the neural progenitors that give rise to GNPs. Starting at day 14.5 after conception, we observed strong expression of *Gli2* and *Atoh1* in the cells that are populating the surface of the developing cerebellum (fig. S6A). To visualize the Atoh1 protein, we used a mouse model that expresses an Atoh1-GFP fusion protein from the endogenous *Atoh1* locus (*19*). At day 18.5 after conception, a stage of cerebellar development that immediately precedes the postnatal expansion of the GNP population in the EGL, the cells that expressed *Atoh1* in the EGL also expressed *Gli2*. This is consistent with the possibility that *Gli2* is a transcriptional target of Atoh1 (fig. S6B).

If *Atoh1* plays a central role in the regulation of *Gli2*, its expression might be required for the genesis of medulloblastomas induced by constitutive activation of the Shh pathway. To test this hypothesis, we used a mouse model bearing an inducible allele coding for a mutant form of the Smoothened protein, an activator of the Shh pathway, fused with yellow fluorescent protein (YFP) (*Rosa*SmoM2). The expression of the mutant *Smoothened* allele can be activated by means of Cre recombinase, resulting in the formation of medulloblastomas in the developing cerebellum (*20*). We generated *Rosa*$^{SmoM2/CreER}$;*Atoh1*$^{+/flox}$ animals (designated Smo*Atoh1*^{wt}) and *Rosa*$^{SmoM2/CreER}$;*Atoh1*$^{-/flox}$ mice (designated Smo*Atoh1*$^{\Delta}$). Cre-mediated recombination activates the Shh pathway in all of the animals by inducing expression of the *SmoM2* gene, but Smo*Atoh1*^{wt} mice still express *Atoh1* from the functional allele, whereas Smo*Atoh1*$^{\Delta}$ lack *Atoh1* expression. After injecting P4 animals, we harvested the brains 10 days later. Noninjected animals served as controls.

In normal P14 animals, the vast majority of GNPs had already stopped cycling, and the EGL is reduced to a few rows of cells (Fig. 3A), whereas injected Smo*Atoh1*^{wt} mice (15 of 15 animals) showed clearly hypertrophic EGLs (Fig. 3, A and B). All of these animals developed preneoplastic lesions in the external layer of the cerebellum (Fig. 3B, middle and right), in which the EGL lost the typical layered organization (*21*, *22*). None of the injected Smo*Atoh1*$^{\Delta}$ animals showed any evidence of over-proliferation in the EGL (0 of 12 animals) but most had atrophic cerebella (Fig. 3C), strongly suggesting that *Atoh1* deletion blocks the mitogenic activity of Smoothened in GNPs. Moreover, the EGL of Smo*Atoh1*$^{\Delta}$ animals was much thinner than that of control littermates (Fig. 3, A and C, right, arrows). We investigated the proliferative status of the GNPs of Smo*Atoh1*^{wt} and Smo*Atoh1*$^{\Delta}$ animals by means of phosphohistone H3 staining. The ectopic cell masses in Smo*Atoh1*^{wt} mice showed numerous mitotic cells (Fig. 4A), whereas the EGL of Smo*Atoh1*$^{\Delta}$ animals was

negative for the presence of cycling cells (Fig. 4B). Staining for caspase 3 revealed no sign of apoptosis in Smo*Atoh1*$^{\Delta}$ (fig. S7, C and D). As expected, the outgrowths in Smo*Atoh1*^{wt} mice were positive for the YFP staining, which is an indication of SmoM2 expression, and showed high levels of Gli2 (Fig. 4C and fig. S7A, arrow). We also observed strong staining with the antibody to YFP in Smo*Atoh1*$^{\Delta}$ animals (fig. S7B), but Gli2 levels were drastically reduced (Fig. 4D), confirming that *Atoh1* expression is required for *Gli2* expression in the EGL even in the presence of constitutively active Shh signaling. Zic1 staining showed that the cells that underwent recombination in Smo*Atoh1*$^{\Delta}$ activated the granule neuron differentiation program, despite the constitutive activation of the Shh pathway (Fig. 4F). Once again, these data confirmed that *Gli2* expression in GNPs requires *Atoh1* and that its absence abolishes the response to Shh. Moreover, the fact that deletion of *Atoh1*, a gene expressed only in GNPs, is able to prevent medulloblastoma formation strongly suggests that these cells are the cell-of-origin of tumors caused by constitutive activation of Shh signaling in the developing cerebellum.

We provide genetic and molecular evidence that *Atoh1* regulates proliferation of GNPs in the postnatal cerebellum by controlling the activity of the Shh pathway expression through the direct transcriptional regulation of *Gli2*. Consistent with this role, *Atoh1* is also required for the formation of medulloblastomas induced by constitutive activation of the Shh pathway.

A recent report suggests that *Atoh1* acts as a tumor suppressor in colorectal cancer and Merkel cell carcinomas by inducing cell differentiation and apoptosis through the expression of tyrosine kinase receptor type I (Ntrk1), which is the opposite of the function we describe in this paper (*23*). We propose that Atoh1 might activate the transcription of both *Gli2* and *Ntrk1*. The activation of *Gli2* makes the cells competent to transduce the mitogenic signal of Shh, whereas expression of *Ntrk1* allows the cells to respond to differentiative or apoptotic stimuli. If the cells are exposed to Shh, as in the case of GNPs in the EGL, the outcome of *Atoh1* expression is proliferation. On the other hand, if the cells are exposed to a differentiative signal, such as factors that activate tyrosine kinase receptors in the gut, *Atoh1* expression allows the cells to respond by exiting the cell cycle and differentiating.

The central role of *Atoh1* in the regulation of *Gli2* has important implications for the modulation of normal and neoplastic proliferation in the developing cerebellum. The possibility to exploit this developmental mechanism in order to control Shh-induced proliferation makes *Atoh1* a possible target for therapeutic strategies to inhibit medulloblastomas.

References and Notes

1. W. R. Polkinghorn, N. J. Tarbell, *Nat. Clin. Pract. Oncol.* **4**, 295 (2007).
2. R. J. Gilbertson, D. W. Ellison, *Annu. Rev. Pathol.* **3**, 341 (2008).
3. E. Salsano, B. Pollo, M. Eoli, M. T. Giordana, G. Finocchiaro, *Neurosci. Lett.* **370**, 180 (2004).
4. N. Bertrand, D. S. Castro, F. Guillemot, *Nat. Rev. Neurosci.* **3**, 517 (2002).
5. K. J. Briggs *et al.*, *Genes Dev.* **22**, 770 (2008).
6. H. Zhao, O. Ayrault, F. Zindy, J. H. Kim, M. F. Roussel, *Genes Dev.* **22**, 722 (2008).
7. N. Ben-Arie *et al.*, *Nature* **390**, 169 (1997).
8. N. F. Shroyer, D. Wallis, K. J. Venken, H. J. Bellen, H. Y. Zoghbi, *Genes Dev.* **19**, 2412 (2005).
9. T. C. Badea, Y. Wang, J. Nathans, *J. Neurosci.* **23**, 2314 (2003).
10. N. Ben-Arie *et al.*, *Development* **127**, 1039 (2000).
11. Materials and methods are available as supporting material on *Science* Online.
12. R. J. Wechsler-Reya, M. P. Scott, *Neuron* **22**, 103 (1999).
13. S. Blaess, J. D. Corrales, A. L. Joyner, *Development* **133**, 1799 (2006).
14. J. D. Corrales, G. L. Rocco, S. Blaess, Q. Guo, A. L. Joyner, *Development* **131**, 5581 (2004).
15. P. M. Lewis, A. Gritti-Linde, R. Smeyne, A. Kottmann, A. P. McMahon, *Dev. Biol.* **270**, 393 (2004).
16. H. Sasaki, Y. Nishizaki, C. Hui, M. Nakafuku, H. Kondoh, *Development* **126**, 3915 (1999).
17. V. Krizhanovsky, L. Soreq, V. Kliminski, N. Ben-Arie, *J. Mol. Neurosci.* **28**, 211 (2006).
18. A. G. Robertson *et al.*, *Genome Res.* **18**, 1906 (2008).
19. M. F. Rose *et al.*, *Neuron* **64**, 341 (2009).
20. U. Schuller *et al.*, *Cancer Cell* **14**, 123 (2008).
21. T. G. Oliver *et al.*, *Development* **132**, 2425 (2005).
22. J. D. Kessler *et al.*, *Genes Dev.* **23**, 157 (2009).
23. W. Bossuyt *et al.*, *PLoS Biol.* **7**, e39 (2009).

24. We thank H.-T. Chao, X. Liu, and R. Atkinson for experimental support and V. Brandt for helping in editing the manuscript. We thank H. Bellen, G. Dotti, M. B. Bhattacharjee, E. Battaglioli, J. Neul, and members of the Zoghbi lab for critical reading of the manuscript. The confocal microscopy was supported by the Intellectual and Developmental Disabilities Research Center at Baylor College of Medicine (5 P30 HD024064). H.Y.Z. is an investigator and T.J.K. is a postdoctoral research associate with the Howard Hughes Medical Institute.

Supporting Online Material

www.sciencemag.org/cgi/content/full/326/5958/1424/DC1
Materials and Methods
Figs. S1 to S7
References

2 September 2009; accepted 29 September 2009
10.1126/science.1181453

New Products Focus: PCR

Whole Genome Amplification Kit

The PicoPlex Single Cell Whole Genome Amplification kit is a rapid, accurate, and reproducible method for amplifying single genomes. The kit targets the preimplantation genetic diagnostics, cancer research, and stem cell research markets, which require rapid, reproducible amplification to profile patient genotypes, karyotypes, and mutations. PicoPlex enables reference laboratories to begin quantitative polymerase chain reaction less than three hours after collecting patient cells. Researchers can obtain as much genomic information from one cell as they currently do from 10,000 cells. The kit reproducibly amplifies total DNA one million–fold from single cells to produce five micrograms of amplified DNA in less than three hours.

Rubicon Genomics
For information 734-677-6210
www.rubicongenomics.com

PCR Master Mixes

RT Fast SYBR Green quantitative polymerase chain reaction (PCR) master mixes have been optimized with a fast PCR protocol, with enhanced specificity and sensitivity, and detection based on SYBR Green dye. The master mixes contain all the reagents and buffers required for fast real-time PCRs, which include an improved proprietary real-time PCR buffer, a high-performance HotStart DNA Taq polymerase, nucleotides, SYBR Green dye, and, if necessary, reference dyes needed to normalize the instruments' optics.

SABiosciences
For information 888-503-3187
www.sabiosciences.com

Sample Preparation Reagent

The iScript RT-qPCR Sample Preparation Reagent delivers efficient cell lysis, RNA stabilization, and removal of DNA for sensitive quantitative polymerase chain reaction (qPCR) without RNA purification. The buffer accelerates and streamlines reverse transcription-qPCR analysis of cultured cells by eliminating the need for RNA purification and enabling PCR or real-time PCR directly from cell lysates. It removes genomic DNA and stabilizes RNA in as little as five to 10 minutes. This isolated RNA is stable for up to six months when frozen. The reagent enables multiplex real-time detection of up to four targets from as few as 10 cells. The system is suitable for rapid, high throughput gene expression analysis, including validation of small-interfering-RNA–mediated gene knockdown.

Bio-Rad
For information 800-424-6723
www.bio-rad.com/reversetranscription

Thermal Microplate Sealer

The MiniSeal Plus is a budget-priced, semiautomatic thermal microplate sealer. Building on the proven record of the MiniSeal microplate sealer, the new model offers enhanced comfort and safety along with repeatability in sealing plates of many different types and sizes. It is designed for laboratories needing to seal small to medium numbers of plates (10–50) each day, so unlike bigger automated sealers, it does not require a compressed air supply to operate. All operations are electronically controlled through a splash-proof keypad. The compact footprint (310 mm height by 275 mm depth by 181 mm width) means it will fit almost anywhere on a lab bench as well as in a fume hood. It features rapid heat-up, real-time display of sealing head temperature, automatic plate height detection, and precut sealing films.

Porvair Sciences
For information +44-1372-824290
www.porvair-sciences.com

Genotyping Kit

The Type-it HRM (high resolution melting) PCR (polymerase chain reaction) kit enables fast, accurate detection of gene mutations and single nucleotide polymorphisms. It can be used in genotyping research applications including typing of disease or cancer loci, biomarker discovery, and pathogen detection. The kit does not require optimization in the development of new HRM assays, but delivers consistent performance the first time. The kit's unique master mix chemistry and optimized HRM buffer ensure that amplification products and results are consistent, even when analyzing challenging mutations and genomic loci. The kit can be used with the Rotor-Gene Q Real-time PCR and HRM Instrument for outstanding results.

Qiagen
For information 800-362-7737
www.qiagen.com

DNA Contamination Removal

The DNA-ExitusPlus is an effective, noncorrosive, and biodegradable reagent designed to counter DNA contamination. The reagent provides fast, nonenzymatic, nonsequence-specific degradation of DNA and RNA molecules and proteins. It can be used to decontaminate surfaces of equipment, lab furniture, and plastic and glass consumables, and even matrices for the purification and isolation of nucleic acids, such as spin columns. It includes no aggressive mineralic acids or bases that can corrode or damage equipment. All ExitusPlus products are aqueous solutions or powder mixtures, without organic solvents or volatile components that release toxic fumes.

AppliChem
For information 561-750-6120
www.applichem.us

Electronically submit your new product description or product literature information! Go to **www.sciencemag.org/products/newproducts.dtl** for more information.

Newly offered instrumentation, apparatus, and laboratory materials of interest to researchers in all disciplines in academic, industrial, and governmental organizations are featured in this space. Emphasis is given to purpose, chief characteristics, and availabilty of products and materials. Endorsement by *Science* or AAAS of any products or materials mentioned is not implied. Additional information may be obtained from the manufacturer or supplier.

POSITIONS OPEN

ASSISTANT DEAN AND DEPARTMENT CHAIRPERSON
Department of Pharmaceutical Sciences
Feik School of Pharmacy
University of the Incarnate Word

The Feik School of Pharmacy at the University of the Incarnate Word has reopened the search and invites applications and nominations for the position Assistant Dean and Chairperson of the Department of Pharmaceutical Sciences. This is a tenure-track position available at the **ASSOCIATE** or **FULL PROFESSOR** level. The Department of Pharmaceutical Sciences currently has 10 faculty members with plans to grow to 12. The Department also includes a contingent of adjunct lecturers and research collaborators.

The successful candidate will provide leadership and vision for the Department while participating with the Dean in policy making, expansion, and governance of the School. The Chairperson will oversee faculty recruitment and retention, mentor and evaluate faculty, and assume a role in guiding the growth and development of the faculty.

The Chairperson will serve as an advocate for faculty, staff, and students, while helping to maintain an environment that embraces excellence in teaching, scholarship, and community service. The Chairperson is expected to interface with current institutional affiliates, help create new affiliations, and represent the School in local, state, and national organizations. Specific duties of the Chairperson include assigning teaching responsibilities, development of the departmental budget, teaching, engaging in service and scholarly activities, and serving on the School's executive committee.

The preferred candidate will have a terminal degree, at least five years of experience in the academia of pharmacy, a good record of scholarly activity, outstanding communication and interpersonal skills, evidence of management ability, an understanding of changing patterns in pharmacy education, and a commitment to diversity.

Nominations, inquiries, and letters of intent should be addressed to: **Arcelia Johnson-Fannin, Pharm.D, Dean, Feik School of Pharmacy (CPO #99), University of the Incarnate Word, 4301 Broadway, San Antonio, TX 78209.** To be considered for the position an electronic application must be completed at **website: http://jobs.uiw.edu**. The position will remain open until filled. However, review of applicants is expected to begin in early December 2009.

University of the Incarnate Word is an Equal Opportunity Employer.

VERTEBRATE BIOLOGIST

The Department of Biological Sciences at the University of Arkansas solicits applications for a tenure-track **ASSISTANT PROFESSOR** in the field of integrative vertebrate biology. We seek an individual working in broadly defined areas such as physiology, morphology, genetics, or developmental biology. Successful candidates must have a Ph.D. and will be expected to establish an extramurally supported research program, supervise graduate and undergraduate research, and teach at the graduate and undergraduate levels. Review of completed applications will begin January 15, 2010, and will continue until the position is filled. Applications should include curriculum vitae, a statement of current and future research plans, teaching interests, and three letters of recommendation. Application materials should be sent electronically or by surface mail to: **Dr. Jeffrey Silberman, Search Committee Chair, Department of Biological Sciences, 601 SCEN, 1 University of Arkansas, Fayetteville, AR 72701. E-mail: jeff@uark.edu; website: http://biology.uark.edu.** *The University of Arkansas is an Equal Opportunity/Affirmative Action Employer. Applicants must have proof of legal authority to work in the United States at the time of hire. All applicants are subject to public disclosure under the Arkansas Freedom of Information Act.*

POSITIONS OPEN

FACULTY POSITION IN C-H FUNCTIONALIZATION RESEARCH
Department of Chemistry, Emory University

The Department of Chemistry has recently been awarded a National Science Foundation Phase I Center on C-H Functionalization and plans to expand its research capability in this area. Applicants are sought for an **ASSISTANT PROFESSOR** position with research interests that would complement the research activities of the current faculty. Applicants should have research plans related to C-H functionalization, broadly defined, and a proven record of research accomplishments in relevant areas of chemistry such as organic chemistry, (bio)inorganic chemistry, or computational chemistry. The applicant would be expected to establish an active, independent research program and to have a strong commitment to teaching at both the graduate and undergraduate levels. Please submit electronically a cover letter, curriculum vitae, a summary of research interests, specific research plans, and a teaching philosophy statement in a single PDF file to **e-mail: chemistrysearch@emory.edu**. Arrange for three letters of recommendation to be sent to the same address. A Ph.D. is required. Review of applications will begin December 21, 2009.

Emory University is an Affirmative Action/Equal Opportunity Employer and welcomes applications from women and members of minority groups.

FACULTY POSITION
Massachusetts Institute of Technology
Department of Materials Science and Engineering

The Department of Materials Science and Engineering seeks a candidate for a tenure-track faculty position to begin July 2010 or thereafter. Appointment would be at the **ASSISTANT** or untenured **ASSOCIATE PROFESSOR** level. In special cases, a senior faculty appointment may be possible. Faculty duties include teaching at the graduate and undergraduate levels, research, and supervision of student research. We will consider candidates with backgrounds and interests in materials science and engineering or a related field. Candidates should hold a Ph.D. in materials science and engineering or a related field by the beginning of the appointment period. The candidate should have demonstrated excellence in original research.

Interested candidates should submit application materials electronically at **website: https://dmsefacsrch.mit.edu**. Each application should include curriculum vitae, the names and addresses of three or more references, a statement of research interests, and a statement of teaching interests. We request that each candidate arrange for reference letters to be uploaded at **website: https://dmsefacsrch.mit.edu/letters/**.

Questions should be addressed to **e-mail: dmse-search-master@dmsefacsrch.mit.edu**.

Responses received by January 1, 2010, will be given priority.

We especially encourage minorities and women to apply because of MIT's strong commitment to diversity in engineering education, research, and practice.

The Departments of Biological Sciences and Geography, University of Cincinnati, seek a tenure-track **ASSISTANT PROFESSOR** in landscape, ecosystem, or aquatic ecology of watersheds. Preferred research interests are: structure and function of aquatic ecosystems, terrestrial-aquatic interactions, biogeochemistry, or watershed-scale processes, combined with use of geographic information systems, sensor networks, remote sensing, and/or systems modeling. For a complete description of the position, qualifications, and application details, visit **website: https://www.jobsatuc.com (position number 29UC5497).** *The University of Cincinnati is an Affirmative Action/Equal Opportunity Employer. Women, minorities, disabled persons, and Vietnam era and disabled veterans are encouraged to apply.*

National Institute of General Medical Sciences
Center for Bioinformatics and Computational Biology
HEALTH SCIENTIST ADMINISTRATOR

The National Institute of General Medical Sciences (NIGMS), a major research component of the National Institutes of Health (NIH) and the Department of Health and Human Services (DHHS), is seeking applications from exceptional scientists to serve as **Program Officer in the Center for Bioinformatics and Computational Biology (CBCB)**. The Center leads several exciting initiatives, including the National Centers for Systems Biology and the Joint NSF/NIGMS Mathematical Biology Program. CBCB is young and growing, and positioned as a focal point of trans-NIH activities including the Biomedical Informatics Science and Technology Initiative (BISTI) and the NIH Roadmap National Centers for Biomedical Computing (NCBC) program. The Institute is seeking an individual with scientific, administrative, and leadership credentials who can manage individual grant programs in modeling of social dynamics and beha vior. Mathematical and computational modeling, simulation and data dissemination and data mining tools, social dynamics theory and biostatistics fall within this scope. The individual must have expertise in the organization and dynamics of social systems, conceptual and theoretical approaches to studying social dynamics, and integration of components of social behavior. Both human and model organism social systems are of interest. Information about the Center for Bioinformatics and Computational Biology can be found at: http://www.nigms.nih.gov/About/Overview/cbcb.htm

Qualifications: The successful individual will possess a Ph.D., M.D. or equivalent degree in a field relevant to the position, have research experience in the modeling of behavior and social dynamics at the individual, community, population, and/or societal level and a sound knowledge of mathematical and computational methods relevant to social dynamics, as well as leadership and managerial skills, ands strong oral and written communication skills. Applicants must be U.S. citizens.

Salary: The current salary range is **$102,721.00 - 133,543.00 USD per year** depending on experience and accomplishments; a full Civil Service package of benefits (including retirement, health, life and long term care insurance, Thrift Savings Plan participation, etc.) is available. Recruitment or relocation incentive may be awarded and moving expenses will be paid.

How to Apply: Position requirements and detailed application procedures are provided in vacancy announcement **NIGMS-10-360616-CR-DE and MP**, which can be obtained by accessing the NIGMS website at http://jobview.usajobs.gov/GetJob.aspx?JobID=83780262. All applications and supplemental information must be received no later than **December 11, 2009**. For additional Information, contact **Gina Johnson at (301) 594-7593**.

National Heart Lung and Blood Institute

Deputy Scientific Director

The Division of Intramural Research (DIR) of the National Heart, Lung and Blood Institute (NHLBI) is seeking an exceptional candidate for the position of Deputy Scientific Director to provide leadership and support as an active partner with the Scientific Director in leading a large research program. The research program is wide in scope including both basic and clinical scientific research programs in such areas as heart and vascular disease, blood diseases, pulmonary, cardiology, hematology, cell biology, genetics, immunology, biophysics, and biochemistry. The existing faculty is an outstanding group of internationally recognized biomedical researchers covering a wide range of basic and clinical research topics (http://dir.nhlbi.nih.gov/).

This position offers a unique and exciting opportunity for the right individual to share responsibility in providing visionary leadership to an organization dedicated to uncovering new knowledge and technologies, both basic and clinical. A candidate is sought who has a commitment to scientific excellence to help identify emerging areas of opportunity for collaboration and to work with members of the research community to implement strategies for successful research outcomes. The incumbent will serve as the liaison between the DIR and the NHLBI Board of Scientific Counselors (BSC) with full oversight responsibilities for the entire BSC process. He/she will serve as a partner to establish relationships with regional hospitals to expand research opportunities and to impact clinical care. The incumbent will also build trans-NIH scientific and clinical collaborations and participate in trans-NIH initiatives. The candidate is expected to perform the specific duties listed above in addition to co-directing the intramural activities of the DIR with the Scientific Director.

Applicants must have an M.D., Ph.D., or both as well as senior-level research experience or knowledge of research programs in one or more scientific areas, related to the above mentioned DIR areas of interest. The candidate shall have administrative experience running a complex research program or institution. The candidate should be a strong communicator with the ability to work collaboratively to solve problems and to make informed decisions.

The successful candidate will be offered a competitive salary commensurate with experience and qualifications with a full benefits package (retirement, health & life insurance, leave, etc.). Appointees may be US citizens, resident aliens, or non-resident aliens with or eligible to obtain a valid employment authorized visa. Complete applications must be received by December 18, 2009. Review of applications is expected to begin in late December, but applications will be accepted until the position is filled. Please submit a curriculum vitae and three letters of reference in .pdf or Microsoft word format only (no paper applications will be accepted) to: **Robert S. Balaban, Ph.D., Scientific Director, NHLBI, c/o Tara Terndrup, nhlbideputysearch@mail.nih.gov**

WWW.NIH.GOV

Clinical Tenure-Track Position
Division of Intramural Research (DIR)

The National Institute of Allergy & Infectious Diseases (NIAID), Division of Intramural Research (DIR), is seeking an outstanding tenure-track investigator to develop a clinical research program to better understand, treat, and ultimately prevent infectious, immunologic, and/or allergic diseases. The successful candidate will implement and direct an independent clinical research program with an emphasis on clinical studies but which may include translational and basic research. The incumbent can choose the laboratory with which he or she would prefer to be affiliated. Any clinical protocols developed should complement the research goals of the selected laboratory. In addition, the incumbent will be paired with a senior investigator, who will serve as a clinical mentor.

An outstanding postdoctoral record of research accomplishment and an M.D., M.D. /Ph.D., or equivalent degree is required for this position; board eligibility/board certification is also required. The incumbent will be expected to meet the requirements for authorization of patient care privileges by the Credentialing Services of the NIH Clinical Center.

Candidates will be assigned independent resources to include clinical and/or laboratory support personnel, equipment, space, and an allocated annual budget for services, supplies, and salaries sufficient to foster success.

This is a tenure-track appointment under Title 42. Salary is dependent on experience and qualifications.

Interested candidates may contact Dr. Karyl Barron, DIR deputy director at 301-496-3006 or kbarron@nih.gov for additional information about the position.

To apply for the position, e-mail your curriculum vitae, bibliography, and an outline of your proposed research program (no more than two pages), by **January 14, 2010** to Ms. Yushekia Hill at NIAID.DIR.Search@niaid.nih.gov. In addition, send three letters of recommendation to Chair, NIAID DIR Clinical Tenure Track Search Committee, c/o Ms. Yushekia Hill at NIAID.DIR.Search@niaid.nih.gov or 10 Center Drive MSC 1356, Building 10, Room 4A-22, Bethesda, MD 20892-1356. E-mail is preferred. Please note search #027 when sending materials.

NIAID

National Institute of Allergy and Infectious Diseases

Further information about DIR laboratories is available at www.niaid.nih.gov/about/organization/dir and information about working at NIAID is available at www.niaid.nih.gov/careers/sctt.

NYU School of Medicine

The Department of Surgery at NYU Langone Medical Center is seeking to recruit a Basic Scientist, for The Helen and Martin Kimmel Division of Wound Healing & Regenerative Medicine under the direction and leadership of **Harold Brem, MD**.

The Division of Wound Healing is seeking to fill several faculty positions at the rank of Assistant, Associate or Full Professor for scientists that use cellular and/or molecular-genetic approaches to address fundamental aspects of Wound Healing and Regenerative Medicine. The research laboratory is extremely collaborative with numerous resources in place. The program is purely translational and literal bridge to the operating room exists. Candidates with a background in wound healing, angiogenesis, pathology, stem cell biology, and regenerative cardiovascular medicine using mammalian systems or genetic approaches are especially encouraged to apply. Competitive salary, laboratory space and start-up funds are available. Candidates are expected to have a track record from the NIH. A PhD, MD, PhD/MD (or equivalent) is essential.

Website: www.nyuwound.org

Interested individuals should send their resume to the **Helen and Martin Kimmel Program Manager, Tracy Henry** via email to **tracy.henry@nyumc.org**.

NYU School of Medicine

Bioinformatics:
Applications are sought in Bioinformatics for NIH funded researcher to work with **Dr. Harold Brem**, Division Chief of the Helen and Martin Kimmel Wound Center at New York University School of Medicine Department of Surgery- Division of Wound Healing and Regenerative Medicine.

Responsibilities and Duties:
- Data Analysis
- Develop algorithms and software tools in support of project research objectives
- Participating in writing project updates, reports, proposals and scientific articles
- Correlate Wound Electronic Medical Record (WEMR) data to clinical outcomes
- Collaborating with investigators within and outside the program, in furtherance of project objectives

Requirements:
Applicants must hold a MD or PhD degree in Bioinformatics, Biology, Engineering, Physics, Computer Science, Mathematics or a related scientific discipline pertinent to the position. Experience with bioinformatics methods, tools, websites and data resources highly desired. Track record from NIH preferred.

Qualified candidates should send your CV to the **Helen and Martin Kimmel Program Manager Tracy Henry** via email to **tracy.henry@nyumc.org**.

THE HONG KONG UNIVERSITY OF SCIENCE AND TECHNOLOGY

Dean of Science

The Hong Kong University of Science and Technology (HKUST) invites nominations and applications for the position of Dean of Science. The successful candidate is expected to assume office in September 2010 or soon thereafter.

Opened in October 1991, HKUST is a research university dedicated to the advancement of learning and scholarship particularly in science, engineering and business studies, with special emphasis on research and postgraduate education, and a mission to contribute to the economic growth and technological development of Hong Kong and the region. Within a short span of less than two decades, the University has gained international recognition as a leading university in the region. English is the medium of teaching, research and administration.

The School of Science includes five Departments: Biochemistry, Biology, Chemistry, Mathematics, and Physics and offers a whole spectrum of programs in the biological, physical, and mathematical sciences. Current enrollments at the School are around 1,400 undergraduate students and 400 postgraduate students. As the University makes the transition from a three-year to a four-year undergraduate curriculum, there is an anticipated 30 percent expansion of student enrollments beginning in 2012, with a concomitant growth in faculty and staff numbers, underpinned by major campus infrastructural developments.

Committed to its vision on research excellence, the University has identified three high impact scientific areas in the School of Science for special future attention as part of its strategic plan: nanoscience and technology; biological sciences and biotechnology; and environment and sustainable development.

The Dean of Science is an executive as well as a faculty appointment and is a member of the senior administrative team of the University. We seek an individual of outstanding stature who has the vision and capability to lead the School of Science to achieve the next level of excellence.

Concurrent with a professorial appointment, the appointment as Dean will normally be for an initial term of three years which may be renewed for a second term. Salary will be highly competitive with generous benefits.

Applications/nominations together with a curriculum vitae and the names and addresses of three referees should be sent to the Chairman of the Search Committee for Dean of Science, c/o Human Resources Office, HKUST, Clear Water Bay, Kowloon, Hong Kong [email: **searchdsc@ust.hk**, fax no. (852) 2358 0700] **on or before 15 January 2010**. All applications and nominations will be treated in strict confidence. The search will continue until a suitable appointment is made. Additional information about the University and the School is available on the websites www.ust.hk and science.ust.hk respectively.

(Information provided by applicants will be used for recruitment and other employment-related purposes.)

Novartis Institutes for BioMedical Research (NIBR), the global research organization of Novartis, has the following positions open at its Emeryville, CA location (near San Francisco).

Research Investigator II
Translational Sciences/Histopathology, Requisition Number: 3028BR
The individual will be responsible for planning and supervising multiple research projects within an experimental pathology group. Duties will include the conception, implementation and interpretation (including pathological assessment) of immunohistochemistry and histology-based studies that will guide the development of new drugs to treat human cancers. Key areas of research will include investigating and evaluating target expression in normal and cancer tissues and development of assays for biomarkers and patient stratification. Candidates should have a PhD with a strong background in cancer histopathology, as well as experience in translational research.

Senior Research Investigator I
Biological Therapeutics, Requisition Number: 3133BR
Lead cross-functional scientific teams focused on the discovery and pre-clinical development of antibodies and other types of biological drugs for oncology indications. Participate in project reviews, decision-making, and new technology development for the Biological Therapeutics platform at Novartis. Must have a PhD in Immunology, Oncology, or a related field with at least 8 years of postgraduate experience. Biotechnology/pharmaceutical industry experience is required, as is an in-depth knowledge of cancer-associated signaling pathways and/or models of cancer. Experience with transitioning biological therapeutics projects into the clinic preferred; strong background in Immunology a plus.

To apply for the above positions, please visit www.novartis.com, click on the Careers link, pull the menu down to Job Search USA, select the link to Novartis Vaccines and Diagnostics, US (includes NIBR-Emeryville, CA), and enter the Requisition Number in the keyword search field.

Postdoctoral Fellowships
NIBR Postdoctoral Fellowships provide talented scientists with the unique opportunity to conduct innovative, interdisciplinary research. Fellows have a primary mentor at NIBR, may have an academic mentor, and develop their projects in consultation with the mentor(s). In the US, positions are available in Emeryville, CA, (near San Francisco); Cambridge, MA; and East Hanover, NJ; and internationally, in Shanghai, China; Basel, Switzerland; and Horsham, UK.

For more information and to apply, please visit: **http://nibr.com/careers/postdocs.shtml**.

NOVARTIS
INSTITUTES FOR BIOMEDICAL RESEARCH

DO THE WORLD A FAVOUR.

ADVANCE YOUR RESEARCH CAREER IN SWEDEN

Any self-respecting university of technology might claim an interest in the future of the world. But Chalmers has taken the initiative. Building on eight strategically identified areas of advance, we are now seeking ambitious women and men for Assistant Professorships in fields that will further our vision of sustainability. Each researcher will have the chance to design a unique and autonomous programme networking with specialists, students and entrepreneurs across various borders. Additionally, successful candidates will receive a generous support package affording a PhD student, relocation, a leadership programme, mentoring and more.

ASSISTANT PROFESSORS REQUIRED TO THE EIGHT AREAS OF ADVANCE

BUILT ENVIRONMENT
Are you exploring an advanced technology that could be harnessed with social insight to build a better home in the third world – or an engineering breakthrough to improve the supply of drinking water?

ENERGY
Could your research help cast new light on bioenergy, wind turbines, or perhaps carbon capture and storage? Maybe you know how to distribute electricity more efficiently?

INFORMATION AND COMMUNICATION TECHNOLOGY
You might have already heard about what we're doing at Chalmers GigaHertz Centre and the Chase antenna centre, or perhaps you're developing a software system that's safe and reliable?

LIFE SCIENCE
Where does humanity go with the genetic code? How can we harness the productivity of microorganisms in cell factories? What new tools and devices do we need to fight obesity and starvation?

MATERIALS SCIENCE
Are you in soft or hard materials? Are you going lighter, stronger, renewable, recyclable or perhaps even biodegradable? Perhaps you have an alternative to conventional plastics.

NANOSCIENCE AND NANOTECHNOLOGY
Where else could tracking chemical information in biological systems, developing quantum computers and creating artificial life forms be so natural? Here we invite you to turn today's science into tomorrow's technology.

PRODUCTION
Is there any type of production that can't be made more efficient with the help of virtual reality? How could tomorrow's production systems use consumer input to reduce waste?

TRANSPORTATION
Will your research programme help the world to move things or people in a way that is safe, economic and environmentally sustainable?

Chalmers is a highly progressive university situated in Göteborg, Sweden. From this beautiful and dynamic part of the world we have become known locally and globally for education, research and innovation with a wide range of applications. Our strengths are fuelled by numerous intimate relationships with partners in the business world – medicine, communication and the automotive industry to name a few. As we strive to use science and technology to advance sustainability in the world around us, we are reminded of the motto of our founder, William Chalmers. Avancez!

To know how you might qualify for one of these exceptional positions, please visit us at
www.chalmers.se/advance

After all, everybody has to start somewhere.

CHALMERS
UNIVERSITY OF TECHNOLOGY

ASU SCHOOL OF Life Sciences
ARIZONA STATE UNIVERSITY

CYBERTAXONOMIST AND CURATOR OF INSECTS

The International Institute for Species Exploration (IISE) and School of Life Sciences, Arizona State University, invite applications and nominations for the position of Associate Director of the IISE, Cybertaxonomist, and Curator of Insects. The successful candidate will join a trans-disciplinary team of faculty, staff, and students dedicated to modernization and advancement of descriptive taxonomy through innovation in cyberinfrastructure, e-monography, and collaborative taxonomy. Position will be filled at Assistant or Associate Professor rank, salary commensurate with experience. Requirements include an earned doctorate in insect taxonomy and demonstrated commitment to comparative morphology, taxonomic revisions, and collection growth and enhancement. Core research efforts are expected to be collaborative: organizing and leading a 'taxon knowledge community', seeking competitive external funding, leading expeditions, producing online monographs, and working with a team of scholars, scientists and engineers to identify and remove impediments to taxonomy through technology and practices. Candidate will teach a course in area of expertise.

To apply, please submit a letter indicating the level for which you are applying; your curriculum vitae; three publications and/or selected articles; and research and teaching statements. A minimum of three letters of recommendation should be sent electronically; please include the names and e-mail addresses of each letter writer with your application. Your application materials should be sent to **Dr. Quentin Wheeler, Chair, Cybertaxonomist Search Committee, School of Life Sciences, Arizona State University, c/o Ms. Anna Fields, PO Box 874501, Tempe, AZ 85287-4501**. Electronic applications as **pdf** files to **anna.fields@asu.edu** are preferred. The initial closing date of applications is **January 4, 2010**; applications will be reviewed weekly thereafter until the position is filled. A background check is required for employment.

Arizona State University is an Equal Opportunity/Affirmative Action Employer committed to excellence through diversity. Women and minority candidates are encouraged to apply.

For additional information on this position and the School of Life Sciences, please visit **http://sols.asu.edu/jobs**.

ASU SCHOOL OF Life Sciences
ARIZONA STATE UNIVERSITY

Virology Faculty Search

The School of Life Sciences and the Biodesign Institute at Arizona State University invite applications for a tenure-track Assistant Professorship from imaginative, creative individuals with motivation to provide basic understanding of the means by which animal viruses succeed as pathogens and the means by which animal hosts deal with these infections. Candidates must have a doctoral degree at the time of appointment and two or more years of relevant postdoctoral experience. There are no preferences as to the virus(es) selected for study. However, genetic, molecular, structural and/or immunological approaches are favored, and preference will be given to applicants who have interests that complement expertise of existing faculty and who will expand our overall research and instructional capabilities. The successful candidate is expected to develop an innovative, extramurally funded, independent research program, participate in undergraduate and graduate education in the School of Life Sciences, mentor undergraduate, graduate and postdoctoral students, and interact in the multidisciplinary consortium of faculty in the Center for Infectious Diseases and Vaccinology **http://cidv.biodesign.asu.edu** in the Biodesign Institute. A competitive start-up package and a teaching load compatible with high research productivity will be provided.

To apply, submit a cover letter, your curriculum vitae listing your selected references, three representative publications, a separate statement of future research plans and teaching and mentoring philosophy and interests, and arrange for three letters of reference to be sent electronically to **Roy Curtiss, Chair, Microbiology Faculty Search Committee, School of Life Sciences, PO Box 874501, Tempe, AZ 85287-4501**. Electronic applications sent as **pdf** files to **anna.fields@asu.edu** are preferred. The initial closing date for receipt of applications is **January 4, 2010**; applications will be reviewed weekly thereafter until the search is closed. A background check is required for employment.

Arizona State University is an Affirmative Action, Equal Opportunity Employer committed to excellence through diversity. Women and minorities are encouraged to apply.

For additional information on this position and the School of Life Sciences, please visit **http://sols.asu.edu/jobs**.

ASU SCHOOL OF Life Sciences
ARIZONA STATE UNIVERSITY

Immunology Faculty Search

The School of Life Sciences and the Biodesign Institute at Arizona State University invite applications for a tenure-track Assistant Professorship from imaginative, creative individuals with motivation to provide basic understanding of basic immunology and the immunological mechanisms by which animal hosts deal with pathogens. Candidates must have a doctoral degree at the time of appointment and two or more years of relevant postdoctoral experience. There are no preferences as to the aspects (mucosal, systemic or cellular) of the immune system selected for study. However, preference will be given to applicants who have interests that complement expertise of existing faculty and who will expand our overall research and instructional capabilities. The successful candidate is expected to develop an innovative, extramurally funded, independent research program, participate in undergraduate and graduate education in the School of Life Sciences, mentor undergraduate, graduate and postdoctoral students, and interact in the multidisciplinary consortium of faculty in the Center for Infectious Diseases and Vaccinology **http://cidv.biodesign.asu.edu** in the Biodesign Institute. A competitive start-up package and a teaching load compatible with high research productivity will be provided.

To apply, submit a cover letter, your curriculum vitae listing your selected references, three representative publications, separate statements of future research plans and teaching and mentoring philosophy and interests, and arrange for three letters of reference to be sent to **Roy Curtiss, Chair, Microbiology Faculty Search Committee, School of Life Sciences, PO Box 874501, Tempe, AZ 85287-4501**. Electronic applications sent as **pdf** files to **anna.fields@asu.edu** are preferred. The initial closing date for receipt of applications is **January 4, 2010**; applications will be reviewed weekly thereafter until the search is closed. A background check is required for employment.

Arizona State University is an Affirmative Action, Equal Opportunity Employer committed to excellence through diversity. Women and minorities are encouraged to apply.

For additional information on this position and the School of Life Sciences, please visit **http://sols.asu.edu/jobs**.

ASU SCHOOL OF Life Sciences
ARIZONA STATE UNIVERSITY

Biology and Society/Bioscience Ethics

The School of Life Sciences invites applications for a tenure-track position at the Assistant or Associate Professor level beginning Fall, 2010. A Ph.D. is required in an area directly related to our Biology and Society Program, including for example, in areas of Bioscience Ethics, History of Biology or Biomedical Sciences, or Philosophy of Biology or Biomedical Sciences. Candidates must have a primary research interest and record of accomplishments in a relevant area, and a teaching competency in introductory bioscience ethics and at least one related teaching area of competence within Biology and Society at the undergraduate and graduate levels. The successful candidate will be expected to establish (or for more senior applicants to have established) an active research program, including seeking funding as appropriate, and to participate in graduate and undergraduate teaching in the Biology and Society Program (which includes tracks in Bioethics, Policy, and Law; and History and Philosophy of Science). The ideal candidate will work within a School of Life Sciences and must have demonstrated an interest in engaging both life scientists and humanists/social scientists in their research and teaching. To apply, submit a letter indicating the position and level for which you are applying, your curriculum vitae, copies of 2-3 selected articles, a concise statement of research accomplishments and plans; statement of teaching interests, experience, and philosophy; and at least one sample syllabus for an undergraduate course in an area of bioscience ethics. A minimum of three letters of recommendation should be sent electronically; please include the names of each letter writer and email contact information with your application. Application materials should be sent to **Jane Maienschein, Chair of the Biology and Society/Bioscience Ethics Search Committee, School of Life Sciences, Arizona State University, Box 874501, Tempe, AZ 85287-4501**. Or full applications may be sent electronically as **pdf** files to **anna.fields@asu.edu**. The initial closing date is **January 4, 2010**, with applications reviewed weekly thereafter until the search is closed. A background check is required for employment.

Arizona State University is an Equal Opportunity/Affirmative Action Employer committed to excellence through diversity. Women and minorities are encouraged to apply.

For additional information on this position and the School of Life Sciences, please visit **http://sols.asu.edu/jobs**.

ASU SCHOOL OF Life Sciences
ARIZONA STATE UNIVERSITY

Global Change Ecology Positions

The School of Life Sciences at Arizona State University invites applications for tenure track faculty positions from individuals working in **ecology** in the context of **global environmental change**. Three positions are currently open. Arizona State University has made a commitment to growth in this field and anticipates making further hires. Successful candidates will join a growing research emphasis in the School of Life Sciences, the Global Institute of Sustainability, the Central Arizona–Phoenix urban Long-Term Ecological Research program, and a new interdisciplinary graduate program in Environmental Life Science. Arizona State University strongly supports collaborative transdisciplinary research and learning across the spectrum of science and engineering consistent with an institutional commitment to global sustainability. Applications will be accepted to fill the positions at the Assistant or Associate professor levels.

(1) Organismal or physiological ecologist to study responses of organisms (microbes, plants, or animals) to environmental variation in the context of global change. We prefer research that addresses both the mechanisms involved in responses, as well as the functional consequences for individuals, their populations, and their communities.

(2) Community or ecosystem ecologist or an ecologist to ask cutting-edge questions at the interface of these two fields. We prefer research addressing the relationships among species-level traits, community structure and ecosystem function in the context of global change and/or other human–ecosystem interactions.

(3) Global ecosystem ecologist to study the earth's changing biogeochemical cycles at large scales (regional to global) using empirical, theoretical and/or modeling techniques. We prefer research that works across scales with a diversity of system types and their interactions.

Required Qualifications for all positions: a doctoral degree in a related field and evidence of research and teaching excellence, appropriate to rank. Postdoctoral research experience and strong quantitative skills are desirable. Successful candidates are expected to develop innovative, extramurally funded research programs, to teach in undergraduate and graduate programs in the School of Life Sciences, and to mentor undergraduate, graduate, and postdoctoral students and fellows.

To apply, submit an application that includes: a cover letter indicating the position and level for which you are applying and describing your career goals; your curriculum vitae; three reprints; a statement describing research accomplishments and future directions; and a statement detailing teaching and mentoring philosophy, interests and experience. A minimum of three letters of recommendation should be sent electronically; please include the names and e-mail addresses of each letter writer with your application. Your application materials should be sent to **Chair, Global Change Ecology Search Committee, School of Life Sciences, Arizona State University, PO Box 874501, Tempe, AZ 85287-4501**; electronic applications as **pdf** files to **anna.fields@asu.edu** are preferred. Initial closing date for applications is **January 4, 2010**; if not filled, weekly thereafter until search is closed. A background check is required for employment.

Arizona State University is an Equal Opportunity/Affirmative Action Employer committed to excellence through diversity. Women and minorities are encouraged to apply.

For additional information on these positions and the School of Life Sciences, please visit **http://sols.asu.edu/jobs**.

LMU LUDWIG-MAXIMILIANS-UNIVERSITÄT MÜNCHEN
FACULTY OF PHYSICS

The **Faculty of Physics** of the Ludwig-Maximilians-Universität München (LMU) invites applications for a

Full Professorship (W3) for Experimental Physics – Nanomaterials and Energy Conversion –

Possible fields of fundamental research include efficient conversion, storage, saving and utilization of energy with the help of nanomaterials. Preferred focus areas are the development and investigation of novel concepts for the conversion of light energy into electrical or chemical energy, for the electrochemical storage of energy and/or for efficient light emitting materials based on hybrid nanosystems. In addition to the production and characterization of nanomaterials, fundamental research aimed at understanding the microscopic processes is highly desirable.

Participation in the interdisciplinary activities of the cluster of excellence "Nanosystems Initiative Munich" (NIM) and the "Center for NanoScience" (CeNS) as well as in local collaborative research programs is desirable. Active participation in the setup of a "LMUCenter for New Energy" is expected.

Prerequisites for this position are a university degree, a doctoral degree in science, teaching skills at university level and a post-doctoral degree (Habilitation) or equivalent qualification that may have been gained outside the university or may consist in a junior professorship. The candidate should have an outstanding record of internationally recognized research accomplishments.

In general, the age of the candidate should not exceed 52 at the time of appointment. Exceptions thereto may be considered in the case of outstanding candidates.

The LMU is an equal opportunity employer and aims to increase the number of female faculty members. Therefore, applications from female candidates are explicitly encouraged.

Disabled candidates with essentially equal qualifications will be given preference.

The LMU supports dual career couples.

Please submit your application comprising a curriculum vitae, documentation of academic degrees and certificates as well as a list of publications to **Dekan der Fakultät für Physik der Ludwig-Maximilians-Universität München, Schellingstr. 4, 80799 München, Germany**, not later than **31st January 2010**.

Office of the Science and Technology Adviser to the Secretary of State

Jefferson Science Fellowship

The National Academies is pleased to announce a call for nominations and applications for the 2010 Jefferson Science Fellows program. This program establishes a new model for engaging the American academic science, technology and engineering communities in the formulation and implementation of U.S. foreign policy.

Jefferson Science Fellows will spend one year at the U.S. Department of State in Washington, D.C. and may periodically travel to U.S. foreign embassies and/or missions.

Jefferson Science Fellow awards are open to tenured academic scientists, technologists and engineers from U.S. institutions of higher learning. Nominees/applicants must be U.S. citizens and will be required to obtain a security clearance.

Detailed information on the Jefferson Science Fellows program is available on the web:

www.nas.edu/jsf

The deadline for nominations and applications for the 2010 program year is **January 15, 2010**.

The Jefferson Science Fellows program is sponsored by the U.S. Department of State.

THE NATIONAL ACADEMIES
Advisers to the Nation on Science, Engineering, and Medicine

Research Faculty
Computational and Systems Biology

The Computational Biology Program (cbio.mskcc.org) at MSKCC (ski.edu) seeks innovative investigators for tenure-track positions at the Assistant, Associate, or Full Professor level. Pursue basic research, solve biological problems with major emphasis on computational methods, and build active bridges to experimental and clinical research. Actively participate in building out research programs at one of the best clinical-scientific institutions in the world. Work in MSKCC's new Zuckerman Research Center, on Manhattan's Upper East Side, in close proximity to Rockefeller University and the Cornell Weill Medical College. Train graduate students in the Gerstner Sloan-Kettering Graduate School (sloankettering.edu), the Weill Cornell Graduate School of Medical Sciences and in tri-institutional graduate programs.

Areas of special interest include chemical biology, physiology, developmental biology, neurobiology, genetics and cancer biology. Applicants should have a doctoral-level degree and the potential to develop an independent, interdisciplinary research program. MSKCC offers a highly interactive, supportive and dynamic research environment with programs in Computational Biology, Developmental Biology, Molecular Pharmacology & Chemistry, Cancer Biology & Genetics, Structural Biology, Immunology, Cell Biology, Molecular Biology, and Human Oncology and Pathogenesis, as well as unparalleled clinical programs in cancer research, treatment and prevention.

E-mail your application (PDF) to **compbio@mskcc.org** as soon as possible in December 2009 but no later than January 10, 2010. Detailed instructions at **cbio.mskcc.org/faculty-search/**. Need more information? E-mail **Dwana Agosto: agostod@mskcc.org Department Chair: Chris Sander**. MSKCC is an affirmative action, equal opportunity employer.

Memorial Sloan-Kettering Cancer Center
www.mskcc.org

The Department of Critical Care Medicine at the University of Pittsburgh Medical School is recruiting a scientist (MD, or PhD) to fill a newly **endowed chair in basic science of critical illness**. The successful candidate will have a strong track record of independent NIH funding and expertise in basic science and translation research. Expertise in molecular biology is desirable.

The Critical Care Department at the University of Pittsburgh is the first of its kind in the country and includes more than 70 full-time faculty members including 35 NIH-funded investigators, and has an annual extra mural research budget in excess of $15 million. The University of Pittsburgh is ranked 5th in NIH funded support nationally.

The Department oversees the care of more than 8,000 critically ill patients per year. The University of Pittsburgh Multidisciplinary Critical Care training Program trains 25-30 fellows per year and has trained over 700 fellows since its inception 30 years ago.

The successful candidate will work to establish broad collaborations throughout the University and help bridge the basic sciences and clinical research enterprises. Faculty appointment will be commensurate with background, experience and qualifications. Interested applicants should submit a current CV and the names and addresses of three references to:

John A. Kellum, MD
Search Committee Chair
Professor and Vice Chair
Department of Critical Care Medicine
University of Pittsburgh Medical School
604 Scaife Hall
3550 Terrace Street
Pittsburgh, PA 15261
(412) 647-8110 • Fax: (412) 647-8060
kellumja@upmc.edu

The University of Pittsburgh is an Equal Opportunity Employer.

VILLANOVA UNIVERSITY

The Dennis M. Cook Endowed Gregor Mendel Chair in Genetics

We seek a nationally recognized teacher/scholar who will contribute to the Augustinian foundation of Villanova through the development and implementation of an ethical and socially responsible program that includes interaction with and involvement of undergraduate and graduate students in both teaching and research. Research may focus on classical inheritance, functional genomics, gene expression, bioinformatics, evolutionary genetics, or other areas that integrate genes and/or genomic material into the research program. See **http://www.villanova.edu/artsci/biology/jobs/genetics_chair** for more information.

Applicants must apply online at **https://jobs.villanova.edu**. Applications are to include a current and complete curriculum vitae and a cover letter describing a proposed program of teaching, research, and service. Applicants should also provide the names and contact information for four references.

Appointment is expected to be at the Associate Professor or Professor rank, with a starting date of August 2010 or January 2011. Review of applications will begin on **15 January 2010**; the search will remain open until the position is filled. Questions may be addressed to: **Dr. R. Kelman Wieder, Associate Dean for Sciences - Email: Kelman.Wieder @villanova.edu; Ph.: 610-519-4856**.

Villanova is a Catholic university sponsored by the Augustinian order. An AA/EEO Employer, Villanova seeks a diverse faculty committed to scholarship, service, and especially teaching, who understand, respect, and can contribute to the University's mission and values.

Professor and Chair
Department of Biochemistry and Molecular Biosciences
Tulane University School of Medicine

Tulane University invites applications from outstanding biomedical scientists and educators for the position of Professor and Chair of the Department of Biochemistry and Molecular Biosciences at the School of Medicine. Tulane University has a rich collaborative environment and hosts a vibrant biomedical sciences community that includes the School of Medicine, School of Public Health, National Primate Research Center, and several Centers of Excellence for research on Cancer, Gene Therapy, Hypertension and Renal Biology, Infectious Diseases, Aging, Cardiovascular Disease, Lung Biology, and Women's Health. The Biochemistry Chair will oversee and expand a dynamic Department which currently has programs in molecular genetics, cell biology, protein biochemistry and biophysics. The Chair will lead the department in its research and educational missions within the MD, PhD and postdoctoral training programs. Developing successful research programs and effectively mentoring junior faculty in their paths towards independence are essential responsibilities of this position. More information about the department can be found at: **www. tulane.edu/som/departments/biochemistry/ index.cfm**.

The successful candidate will have a proven record of leadership skills, widely acknowledged scientific achievements, excellent administrative, teaching and interpersonal skills and an exciting vision for enhancing the research strengths of an academic department. The emphasis at Tulane on interdisciplinary research and educational initiatives presents exciting opportunities to strengthen interactions both within the department and among departments, research centers of excellence and the National Primate Research Center. An attractive recruitment package is available to further these initiatives. In addition to a curriculum vitae, applications should include a letter describing the candidate's research, teaching, service, mentoring and administrative experience, and vision for building the department and enhancing interdisciplinary programs and resources. Nominations and/or applications should be emailed to **navar@tulane.edu** or mailed to **L. Gabriel Navar, Ph.D., Professor and Chair, Department of Physiology, SL39, Tulane University Health Sciences Center, School of Medicine, 1430 Tulane Avenue, New Orleans, LA 70112**.

Tulane University is an Affirmative Action/Equal Opportunity Employer. We invite women and minorities to apply.

FULL-TIME Post Doctoral Fellow
Windber Research Institute
Windber, PA 15963
United States

The Post Doctoral Fellow in the Integrative Cardiac Health Program at Windber Research Institute will join experienced scientists and researchers to become part of an exciting research environment and growing research team.

Duties/Responsibilities: This position is responsible for studying the molecular biology of cardiovascular disease or breast cancer and will focus on one or more of the following areas: genomics of cardiovascular risk reduction, molecular biology of obesity, molecular characterization of breast cancer progression, or proteomic signatures of metastasis.

Educational Qualifications Required: PhD, MD, or equivalent degree. The successful candidate should have extensive experience with array-based gene expression, SNP typing, or molecular biology. In addition, an established background in cardiovascular or breast cancer biology, and a strong record of research and publication are essential.

Interested applicants should send a letter of interest, resume, and names of three references by mail or email to:

Darrell L. Ellsworth, PhD
Windber Research Institute
620 Seventh Street
Windber PA, 15963, USA
d.ellsworth@wriwindber.org

Only short listed candidates will be contacted for an interview.

Windber Research Institute, an integrated clinical, genomic, and proteomic research facility, curates a tissue repository containing thousands of samples from patients with breast cancer and cardiovascular disease. The primary mission of WRI is to improve patient care and quality of life by rapidly translating molecular and clinical research into effective treatments.

Equal Opportunity/Affirmative Action Employer.

UK UK
UNIVERSITY OF KENTUCKY

The Department of Molecular and Cellular Biochemistry at the University of Kentucky College of Medicine invites applications for a tenure-track faculty position at the Assistant Professor level. Successful candidates must possess a Ph.D., M.D., or equivalent degree. We welcome all qualified applicants, particularly individuals focusing on, but not limited to, the areas of diabetes, neuroscience, cancer, and systems biology.

The successful candidate will benefit from a stimulating and collaborative environment within the department and a strong graduate program, as well as competitive start-up funds, salary, and appropriate space in a state-of-the-art research facility.

Evaluation of applicants will begin January 2010. Applicants should forward a cover letter indicating their area of expertise, curriculum vitae, a description of current and future research plans, and three letters of reference to BCHFacultySearch@uky.edu or use our online application at http://medicine.mc.uky.edu/eforms/form.php?formID=93220042493

see blue.
in everything we do.
UNIVERSITY OF KENTUCKY

For further information about the department, visit: **www.mc.uky.edu/biochemistry**

The University of Kentucky is an equal opportunity employer and encourages applications from minorities and women

IOWA STATE UNIVERSITY
OF SCIENCE AND TECHNOLOGY

Postdoctoral Research Positions in Molecular, Cellular and Computational Biology

Sixteen postdoctoral research positions in molecular biology, cellular biology and computational biology are available immediately at Iowa State University. We seek highly motivated researchers with demonstrated outstanding ability and accomplishment. Opportunities currently are available with the following faculty in the areas described:

- **Gwyn Beattie** – ecology and cell biology of plant pathogenic bacteria; expertise in prokaryotic molecular biology
- **Hui-Hsien Chou** – RNAi applications on model animals or plants
- **Larry Halverson** – thermal tolerance of microalgae
- **Kirk Moloney** – ecological dynamics of invasive species, expertise in simulation modeling using C++ or similar programming language required; position available April 2010
- **Basil J. Nikolau** – metabolomics and functional genomics of metabolism
- **David Oliver** – metabolomics and metabolic flux in plants and microalgae related to amino acids, lipids and nutrition
- **Reuben Peters** – metabolic engineering of bacteria for production of diterpenoid natural products
- **Martin Spalding** – metabolic engineering of microalgae for increased productivity and biofuel production
- **Kan Wang** – gene function/regulation and transformation technology development in maize, soybean and rice
- **Eve Wurtele** – computational biology or computer science required; knowledge of database design, or metabolic/regulatory biology highly desired
- **Olga Zabotina** – expertise in carbohydrate chemistry or biochemistry and knowledge of molecular biology tools are strongly desired

Additional information about the faculty seeking postdocs and their research is available at **www.plantsciences.iastate.edu/postdocs/**. Qualified applicants should send, via e-mail, a complete curriculum vitae and a statement of research interest that identifies the preferred faculty member, and arrange to have three signed reference letters sent to **isupostdoc@iastate.edu** by **January 1, 2010**. Inquiries may be sent to **Dr. Basil J. Nikolau** at **isupostdoc@iastate.edu**.

Iowa State University (ISU) is recognized internationally for research programs in basic sciences, engineering, agriculture and tech transfer initiatives. ISU is an Equal Opportunity/Affirmative Action Employer.

Boston University College of Engineering
Department of Biomedical Engineering

BOSTON UNIVERSITY

Tenured Faculty Position in Synthetic & Systems Biological Engineering

The College of Engineering is seeking an innovative individual to help lead the College's research and educational efforts in Synthetic & Systems Biological Engineering (SSBE). This interdisciplinary position will advance research and education at the intersection of systems and synthetic biology, systems engineering, bioengineering, nanotechnology, and medicine. This person will work closely with leading experimental, modeling, computational, and data generation faculty in the College of Engineering who are advancing engineering to address crucial challenges in synthetic and systems biology. The position will also couple with a University-wide effort in systems biology with faculty from Physics, Biology, Chemistry, Computer Science, and the Medical School, as well as the ability to partner with BU's new National Emerging Infectious Diseases Laboratory, a BSL4 facility at the Medical School.

This position may hold a tenured Associate or Full-Professor appointment in one or more departments based on the individual's research and educational priorities and expertise. The individual should have a strong history of external funding in addition to being internationally recognized for distinguished contributions to synthetic and systems biological engineering.

The College of Engineering is comprised of three departments (Biomedical, Electrical & Computer, and Mechanical) and two graduate divisions (Systems & Materials Science). The College has risen rapidly in distinction, being ranked in the top 40 by *U.S. News & World Report*, and in the top 20 in research dollars per faculty member. Its Biomedical Engineering program is ranked in the top 10 in the nation. The University recently completed a 187,000-square-foot Life Science & Engineering Building. Significant College and University resources will continue in the SSBE area. For more information, please visit the following websites: www.bu.edu/eng; www.bu.edu/eng/bme; www.bu.edu/abl/; www.bu.edu/ece.

Candidates should submit a brief letter of interest and current curriculum vitae to: Jim Collins, Chair, SSBE Faculty Search Committee (ssbesearch@bu.edu)

Applications will be accepted until the position is filled.

Boston University is an affirmative action, equal opportunity employer committed to increasing the cultural and intellectual diversity of its faculty

GRANTS

GRANT FOR POSTDOCTORAL POSITIONS IN SWEDEN

This grant enables researchers with doctorates (PhDs or equivalent) to work at Swedish higher education institutions or research establishments. The programme spans two years. Research areas:

- Natural Sciences
- Engineering Sciences
- Medicine
- Humanities
- Social Sciences
- Educational Sciences.

Call for applications opens early January. Submission deadline is February 25, 2010.

Further information at www.vr.se

Vetenskapsrådet

Roche

Roche Postdoctoral Fellowship in Human Genome Structural Variation (Based in Nutley, New Jersey)

Who we are
At Roche, 80,000 people across 150 countries are pushing back the frontiers of healthcare. Working together, we've become one of the world's leading research-focused healthcare groups. Our success is built on innovation, curiosity and diversity, and on seeing each other's differences as an advantage.

As a cross-divisional unit within Roche Pharma Research, the global Translational Research Sciences (TRS) network provides scientific and technical support to the Disease Biology Areas and to the Lifecycle Teams as a key part of our company's Personalized Health Care strategy. The TRS also interfaces with Roche Diagnostics. Opportunities for close collaboration exist with Roche scientists within the TRS (New Jersey and Switzerland), Roche Molecular Diagnostics (California), 454 Life Sciences (Connecticut) and NimbleGen (Wisconsin and Iceland).

The position
We have an immediate opportunity for a talented scientist to enter the global TRS network through the Roche Postdoctoral Fellowship (RPF) Program. The RPF was established to foster industry-academic collaboration through innovative science and to engage talented scientists by enabling access to cutting edge technology, novel ideas and creative talent.

Within an interdisciplinary team, you will be responsible for conducting research in the area of genome-wide Copy Number Variation (CNVs) using both high-density arrays and paired-end second generation sequencing. Other technologies will be employed in follow-up validation experiments. Projects will focus on drug target and biomarker discovery in oncology, inflammation, virology, CNS or metabolic/vascular disease areas. In collaboration with a team of geneticists, bioinformaticians and statisticians you will contribute to study design, help establish analysis workflows, and support the interpretation and presentation of results. The RPF position is based in Nutley, New Jersey (approx. 20 miles west of New York City) and reports to the head of the global TRS DNA Biomarker laboratory.

Who you are
You have a PhD in genetics, biochemistry or molecular biology with laboratory experience in genome-wide copy number or structural variation research. The ideal candidate has technical experience with multiple platforms for structural variation detection and validation (e.g. qPCR); a broad knowledge of human genetics; and strong informatics skills. You are fluent in English (written and spoken), possess excellent communication and presentation skills, and enjoy team work in a highly matrixed environment.

In addition, you're someone who wants to influence your own development. You're looking for a company where you have the opportunity to pursue your interests across functions and geographies, and where a job title is not considered the final definition of who you are, but the starting point.

Job ID No.: 13403
The next step is yours. To apply online, please visit our career website at **www.rocheusa.com/career** and reference position number 13403.

Roche is an Equal Opportunity Employer fully committed to workplace diversity.

Max-Planck-Institut für Quantenoptik

The Quantum Many-Body Systems Division (Prof. Bloch) at the Max-Planck-Institute of Quantum Optics is seeking applicants for

PhD positions

within the group. The research of the group is focused on the field of ultracold bosonic and fermionic quantum gases with a special interest in strongly correlated quantum systems, quantum information processing and quantum optical applications. We are looking for highly motivated students with a masters/diploma degree in physics, ideally with a background in the field of quantum optics or condensed matter physics, although applications from outside the field will be considered, too. Details about the research projects of the group can be found on the website: www.quantum-munich.de

Interested applicants are asked to send their application including letters of reference to:

Max-Planck-Institut für Quantenoptik
Quantum Many-Body Systems Division
Prof. Immanuel Bloch
Hans-Kopfermann-Str. 1
85748 Garching b. München

Or submit the application via E-Mail to:
immanuel.bloch@mpq.mpg.de

MAX-PLANCK-GESELLSCHAFT

ETH

Eidgenössische Technische Hochschule Zürich
Swiss Federal Institute of Technology Zurich

Professor of Biochemical Engineering

ETH Zurich invites applications for a professorship in Biochemical Engineering at the Institute of Chemical and Bioengineering Sciences. Candidates should demonstrate an exceptional potential to develop an innovative and collaborative research program at the interface between chemical engineering and biochemistry, biology and medicine. The Zurich area offers extraordinary opportunities, including efficient and rapid access to early clinical trials and an impressive local biomedical industry representing some of the global market leaders. The new professor will be expected to teach undergraduate level courses (German or English) and graduate level courses (English) in chemical and biochemical engineering.
Requirements include an internationally recognized research program and excellence in teaching.

Please submit your application together with a curriculum vitae, a list of publications and projects as well as a research plan to the **President of ETH Zurich, Prof. Dr. Ralph Eichler, ETH Zurich, Raemistrasse 101, 8092 Zurich, Switzerland (or via e-mail to faculty-recruiting@sl.ethz.ch), no later than March 31, 2010.** With a view toward increasing the number of female professors, ETH Zurich specifically encourages qualified female candidates to apply.

FELLOWSHIPS FOR POSTDOCTORAL SCHOLARS at Woods Hole Oceanographic Institution

New or recent doctoral recipients with research interests associated with the following are encouraged to submit scholarship applications prior to January 15, 2010.

Departments - Awards related to the following areas are anticipated: Applied Ocean Physics & Engineering; Biology; Geology & Geophysics; Marine Chemistry & Geochemistry; Physical Oceanography.

Institutes - Each of the following Institutes, which foster interdisciplinary research addressing critical issues, will award a scholarship to support related research: Ocean and Climate Change Institute; Coastal Ocean Institute; Deep Ocean Exploration Institute; Ocean Life Institute.

The NOAA-WHOI Cooperative Institute for the North Atlantic Region (CINAR) will award a fellowship in one of five theme areas: Ecosystem Forecasting, Ecosystem Monitoring, Ecosystem Management, Protection and Restoration of Resources, Sustained Ocean Observations and Climate Research.

The National Ocean Sciences Accelerator Mass Spectrometer Facility (NOSAMS) will award a fellowship in the development and implementation of new techniques in radiocarbon studies in Marine Science.

Awards are competitive, with primary emphasis placed on research promise. Scholarships are for 18-months with an annual stipend of $56,000, a modest research budget, and eligibility for group health and dental insurance. Recipients are encouraged to pursue their own research interest in association with resident Scientific and Senior Technical Staff. Communication with potential WHOI advisors prior to submitting an application is encouraged.

Further information and application forms may be obtained at: **http://www.whoi.edu/postdoctoral** or by contacting **(508) 289-2219**, or **postdoc@whoi.edu**

An Equal Opportunity/Affirmative Action Employer.

ECOLOGY FACULTY POSITION FORDHAM UNIVERSITY

The Department of Biological Sciences of Fordham University invites applicants for a tenure track faculty position at the **ASSISTANT or ASSOCIATE PROFESSOR** level for Fall 2010. We seek a population, community or evolutionary ecologist who studies freshwater fish, invertebrates or microbes. The successful applicant will have access to Fordham's biological field station – the Louis Calder Center - and our new Center for Conservation, Evolution and Urban Ecology (CCEUE), as well as the opportunity to work with scientists at the Wildlife Conservation Society, American Museum of Natural History, the New York Botanical Garden, and other scientific institutions in the region. The successful candidate is expected to make use of local and regional resources to develop or continue a rigorous, externally funded research program, and is expected to teach courses and mentor individual research projects at both the undergraduate and graduate levels. Postdoctoral experience is expected. Applicants should email one PDF file containing a cover letter, curriculum vitae, contact information for three references, and a research statement to **thornhill@fordham.edu**. The cover letter should be addressed to **Dr. William Thornhill, Chair, Department of Biological Sciences, Fordham University, 441 E. Fordham Road, Larkin Hall 160, Bronx, NY 10458**. Candidates will be reviewed when their applications are received and we will continue to accept applications until the position is filled.

Fordham University is an independent, Catholic university in the Jesuit tradition that welcomes applications from men and women of all backgrounds. Fordham is an EOE.

The **Beyond Center** at **Arizona State University** seeks applications for a **tenure-track assistant or associate professor**. The Beyond Center is a research unit within the College of Liberal Arts and Sciences that explores fundamental questions in science; led by **Dr. Paul Davies**, Director and **Dr. Lawrence Krauss**, Associate Director. Current prime areas of interest include mathematical biology (the latter with a particular focus on the physical basis of cancer), cosmology, particle theory, foundational questions in quantum mechanics, and astrobiology. The successful candidate will have a tenure home in a relevant academic unit. Candidates should have a PhD and at least two years of postdoctoral research experience in one of the prime areas of interest or a related field, an outstanding record of research accomplishments with a clear potential to establish a vigorous externally funded research program and show a strong commitment to excellence in teaching and public outreach. The successful candidate should be a "big thinker" with a strong interest in foundational scientific questions, and should have good organizational skills. Demonstrated experience in a collaborative, multidisciplinary environment is desired. Complete applications will include a letter of interest, curriculum vitae, a research and teaching plan, and contact information for at least 3 references. Materials should be submitted electronically at **http://physics.asu.edu/employment.php**. Applications will be considered until **January 15, 2010**. The appointment may begin as early as August 16, 2010. Please direct questions to beyondfac@asu.edu. A background check is required for employment.

Arizona State University is an Equal Opportunity/Affirmative Action Employer committed to excellence through diversity. Women and minorities are encouraged to apply.

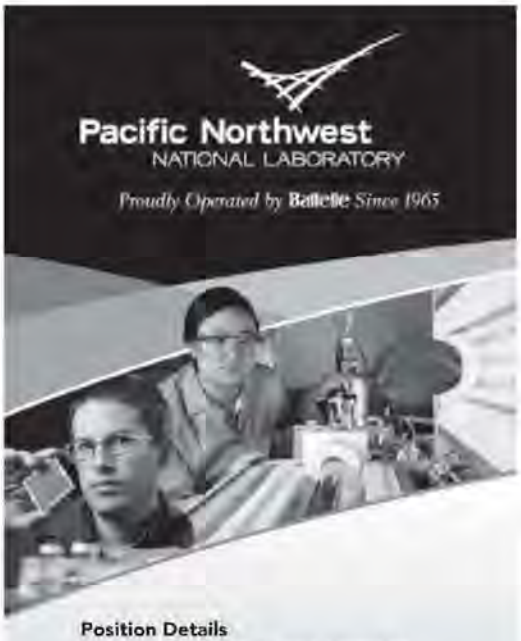

POSITION ANNOUNCEMENT:

Pacific Northwest Distinguished Post-Doctoral Fellowship

Program Overview
For more than four decades, scientists and engineers at Pacific Northwest National Laboratory have advanced the frontiers of science and delivered solutions to our nation's most pressing challenges in energy, environment, and national security. PNNL, known for delivering transformational science and technology and accelerating the rate of innovation, is creating new opportunities for recent PhD graduates to make their own mark on the world.

The Pacific Northwest Distinguished Post-Doctoral Fellowships at PNNL will provide full funding to selected candidates on a major research project of their choice. The position will also include a highly competitive salary, benefits, and relocation, plus the availability of extra funding for travel and conferences. Selected candidates will be hired for a three-year maximum duration to complete their project.

Applicants for 2010
The Pacific Northwest Distinguished Post-Doctoral Fellowship at Pacific Northwest National Laboratory is accepting qualified candidate applications from recent PhD Graduates in Science & Engineering, who wish to conduct research on a project of their choice. Candidates will be required to submit the following items as one **PDF uploaded attachment** when applying to this position:

- Current Resumé or CV (including publication and presentation list)
- Statement of Research Interest — five (5) pages, summarizing thesis and current work, and plans for future work
- Copies of Unofficial Transcripts (all levels)
- A short essay on "Why PNNL is the right place for you" — including which one or two of the **PNNL Core Capabilities** (***www.pnl.gov/research***) are of most interest.

Additional information may be requested from the finalist candidates, including letters of recommendation and official transcripts. Qualified candidates must meet the following minimum requirements:

- Must have completed a PhD in a Science or Engineering field related to the mission areas of PNNL within the last three (3) years, or by the start of the appointment.

For More Information and To Apply
Log on to ***http://www.pnl.gov/research/pnwpostdoc.asp*** for more information about this opportunity and to apply for the position.

Position Details
Duration: Up to three (3) years, depending on performance
Compensation: Competitive
Benefits: Medical, dental, vision, relocation
Location: Richland, WA

Questions?
Please send an e-mail to ***university.recruiter@pnl.gov***. We will send a response to you within two business days.

PNNL is an AA/EEO Employer

---

cnrs

IN 2010
CNRS IS RECRUITING

TENURED RESEARCHERS IN ALL FIELDS OF SCIENCE

- MATHEMATICS • PHYSICS
- NUCLEAR AND HIGH-ENERGY PHYSICS
- CHEMISTRY
- SCIENCE AND TECHNOLOGY OF INFORMATION AND ENGINEERING
- UNIVERSE AND EARTH SCIENCE
- ENVIRONMENT AND SUSTAINABLE DEVELOPMENT
- LIFE SCIENCES • HUMANITIES AND SOCIAL SCIENCES

CNRS encourages junior and senior scientists from around the world to apply for its tenured researcher positions.

CNRS provides an enriching scientific environment:
- numerous large-scale facilities
- highly skilled technical support
- multiple international and interdisciplinary networks
- access to university research and teaching
- lab-to-lab and international mobility

Application forms and further information will be available online at **www.cnrs.fr** in December 2009

KU THE UNIVERSITY OF KANSAS

FACULTY POSITION IN CANCER BIOLOGY

The Department of Molecular Biosciences at the University of Kansas invites applications for a tenure-track/tenured faculty position at the **Assistant/Associate/Full Professor** level. Applications from highly motivated individuals in any area of cancer biology will be considered. Areas of interest include, but are not limited to, cancer progression and metastasis, stem cell biology, cancer cell metabolism, oncogenes or tumor suppressor genes, cancer genetics and/or epigenetics, cancer immunology, and the role of infectious agents in cancer. Our 35 full-time faculty maintain highly visible research programs in multiple areas of the molecular biosciences including computational and structural biology; enzymology; intracellular transport; cell cycle regulation; cell growth and differentiation; cell motility; developmental and cancer biology; viral and microbial pathogenesis; molecular and cellular immunology; neurobiology; and the genetics of complex traits. Our faculty are also diverse in terms of the systems they use, which include bacteria, fungi, Drosophila, nematodes, mice, Xenopus, zebrafish, and human tissue culture cells. The open position is part of an ongoing university-wide initiative to expand cancer research and secure NCI cancer center designation. Applicants at the Assistant Professor level are expected to demonstrate potential for establishing an independent externally funded research program, and those at the senior level are expected to have an ongoing and well-established program, preferably funded through the NCI. We are especially interested in basic cancer researchers who have near-term translational interests, including the development of diagnostic, therapeutic, or similar tools. The department has a robust graduate program of over 70 students and excellent core facilities for NMR; X-ray diffraction; electron, confocal, and light microscopy; gene microarray analysis; proteomics; protein modeling; and high-throughput-screening. The successful candidate will be expected to direct graduate student research and participate in the department undergraduate and/or graduate teaching missions. Review of applications will start January 4, 2010, and will continue until no longer needed. This appointment is expected to begin August 18, 2010, but a later start date may be negotiated. Applicants must have a Ph.D., M.D., or equivalent degree in the biological sciences and at least two years of post-doctoral research experience.

For more information and to apply go to **https://jobs.ku.edu** and search for position number 00001615 where interested applicants can upload a cover letter, curriculum vitae, statement of planned research, statement of teaching interests and philosophy, and a list of references. To ensure full consideration, complete applications should be received by **January 4, 2010**.

EO/AA Employer.

POSITIONS OPEN

Colorado

University of Colorado at Boulder

EDUCATION AND PUBLIC OUTREACH MANAGER

The Laboratory for Atmospheric and Space Physics (LASP) of the University of Colorado at Boulder invites applications for the lead of education and public outreach (EPO). See our **website: http://lasp.colorado.edu** for information on LASP.

The successful candidate should have demonstrated leadership in the development and implementation of science-based education and public outreach activities.

Go to **website: http://www.jobsatcu.com/applicants/Central?quickFind=59477** for full job description and to submit application.

TENURE-TRACK FACULTY POSITIONS
Section of Anatomy

The Section of Anatomy at Southern Illinois University School of Dental Medicine is seeking applicants for two full-time (12-month), tenure-track faculty positions at the **ASSISTANT/ASSOCIATE PROFESSOR** level. Applicants must have a Ph.D. or Ph.D./D.M.D./D.D.S. Postdoctoral training and prior teaching experience in the anatomical sciences are desirable. Teaching duties will include directing a course in histology, neuroanatomy, or oral histology and assisting in teaching gross anatomy. Candidates are expected to be active in dentally related research. Available research equipment is significant and includes instrumentation for confocal microscopy, scanning electron microscopy, RT-PCR, gel electrophoresis, and high performance liquid chromatography. Academic rank and salary are commensurate with experience and qualifications. The school is located on a historic campus, 15 minutes from the campus of Southern Illinois University, Edwardsville and 30 minutes from St. Louis, Missouri. Review of applications will begin immediately and continue until the positions are filled. Applicants should submit a letter of interest with brief statements of teaching experience and preferences and research experience and interests related to dental medicine, curriculum vitae, and three letters of reference to: **Dr. Ann Boyle, Dean, School of Dental Medicine, Southern Illinois University, 2800 College Avenue, Alton, IL 62002-4900. Or by e-mail: aboyle@siue.edu**. *SIU-SDM is an Equal Employment Opportunity/Affirmative Action Employer. Women and minorities are encouraged to apply. SIUE is a state university; benefits under state-sponsored plans will not be available to holders of F-1 or J-1 visas.*

FACULTY POSITION IN PLANT GENETICS

The University of Georgia has long maintained strengths in plant biology. As part of a long-term effort to build on these strengths, the Department of Genetics invites applications for a tenure-track faculty position in any area of plant genetics at the **ASSISTANT PROFESSOR** level. The candidate will be expected to maintain a rigorous, externally funded research program and to contribute to undergraduate and graduate teaching. For information about the breadth of the Department, see **website: http://www.genetics.uga.edu**.

Applications should be sent electronically as a single PDF file (filename format: yourlastname.pdf) that includes a cover letter, curriculum vitae, and brief statements of research and teaching interests to **e-mail: genetics@uga.edu**. Three letters of recommendation should also be sent, either as a PDF to the above e-mail address (filename format: applicantlastname_refereelastname.pdf), or in hard copy, to: **Plant Genetics Search Committee, Department of Genetics, Davison Life Sciences Building, University of Georgia, Athens, GA 30602-7223.** The committee will begin reviewing applications on January 8, 2010, until the position is filled.

The Franklin College of Arts and Sciences, its many units, and the University of Georgia are committed to increasing the diversity of its faculty and students, and sustaining a work and learning environment that is inclusive. Women, minorities, and people with disabilities are encouraged to apply. The University is an Equal Employment Opportunity/Affirmative Action Institution.

POSITIONS OPEN

Yale

The Section of Cardiovascular Medicine seeks exceptional candidates to establish research programs in cardiovascular developmental biology and genetics. Successful individuals will have Ph.D. and/or M.D. degrees and will have a proven record of originality and productivity. The Section is undergoing a major expansion and houses a newly formed Yale Cardiovascular Research Center. Yale University School of Medicine has established a close affiliation with University College London, United Kingdom, that among other benefits provides access to extensive clinical and translational genetics resources at UCL. Although all extraordinary candidates will be considered, we are especially interested in **DEVELOPMENTAL BIOLOGISTS** utilizing zebrafish as their model, who will be able to establish and operate a zebrafish research facility, and in **GENETICISTS** involved in translational genetics research, who will be able to run or participate in a clinical cardiovascular genetics program in addition to basic research efforts.

Please electronically send your curriculum vitae with a list of publications, a summary of research (two pages), and a research plan (three pages) along with the names of three references by December 1, 2009, to **e-mail: michael.simons@yale.edu.**

SENIOR STAFF SCIENTISTS

The Henry M. Jackson Foundation (HJF) is seeking two senior staff **IMMUNOLOGISTS** to support the Enteric Diseases Department, Naval Medical Research Center, Silver Spring, Maryland. Must have expertise in bacterial vaccinology and mucosal immunology. The Department serves as a central research hub for the development of bacterial enteric vaccines within the U.S. Military Infectious Diseases Research Program. Will serve as principal investigators in the discovery and development of innovative vaccines against diarrheagenic *E. coli* (ETEC) or *Campylobacter jejuni* in intramural programs led by **Drs. Stephen Savarino** and **Patricia Guerry.** Will directly supervise research groups to evaluate novel vaccine candidates in small animals, develop assays to assess immune responses and explore protective immunity, and provide immunology support in early clinical phase vaccine trials. Will pursue independent investigations, collaborations, and outside funding opportunities to study basic aspects of immunology of ETEC or *C. jejuni.* Must have a Ph.D. in immunology, microbiology, or related field with three to five years of relevant postdoctoral research experience including assessment of immune responses to mucosal pathogens, a strong animal research background, and successful assay development. Please apply online at **website: http://www.hjf.org/careers.** Click Advanced Search and enter **job number 204937** in the Job Opening ID box. Or transmit your resume to **fax: 240-314-7334.** Please specify title and job number on fax.

POSTDOCTORAL POSITION (100 percent, multiyear) in mouse genetics and neurodegenerative disease available immediately at University of California, Davis to use and generate mouse models to study the genetic, cellular, molecular, and mitochondrial mechanisms of neurodegenerative disease. Expertise in cloning, knockouts, and conditional gene expression as well as molecular and biochemical experience are required. Salary depends upon experience (NIH scale). Send curriculum vitae to **e-mail: gcortopassi@ucdavis.edu. Website: http://cortopassilab.ucdavis.edu/.** *UCD is an Affirmative Action/Equal Opportunity Employer.*

POSITIONS OPEN

Manchester College

ASSISTANT PROFESSOR OF BIOLOGY

The Department of Biology, Manchester College, has a full-time, tenure-track position at the Assistant Professor level beginning September 2010. Details and faculty application are available at **website: http://www.manchester.edu/OHR/facultypositions.htm**. To apply, please send curriculum vitae, faculty application, statements of teaching and research interests, evidence of teaching effectiveness, teaching philosophy, copies of transcripts, and three letters of recommendation to: **Office of Academic Affairs, Manchester College, 604 College Avenue, North Manchester, IN 46962. E-mail: ksmeyer@manchester.edu; fax: 260-982-3211; telephone: 260-982-5051.**

CANCER STEM CELL RESEARCHER

The Wake Forest Institute for Regenerative Medicine (WFIRM) and the Comprehensive Cancer Center of Wake Forest University are soliciting applications to fill a junior or mid-career position in cancer stem cell research and tumor microenvironment. Candidates should hold a Ph.D. or M.D. (or equivalent). Primary appointment with WFIRM, with joint appointment in the Department of Cancer Biology. Electronically submit curriculum vitae and concise statement of research plans to **e-mail: swilder@wfubmc.edu.** *Affirmative Action/Equal Opportunity Employer.*

POSTDOCTORAL POSITIONS

Two Postdoctoral positions available to study differentiation mechanisms of the eye and brain using molecular and genetic approaches. Candidates with experience in molecular biology and a Ph.D. degree are encouraged to send their curriculum vitae, statement of research interests, and the names of three references to: **Dr. Renping Zhou, Laboratory for Cancer Research, School of Pharmacy, Rutgers University, 164 Frelinghuysen Road, Piscataway, NJ 08854. E-mail: bachorik@rci.rutgers.edu.**

MARKETPLACE

The Power of MORE

The Veriti® Thermal Cycler

Applied Biosystems, the most trusted name in PCR instruments, introduces a new line of innovative thermal cyclers.

The Veriti® Thermal Cycler is available in four formats to suit your thermal cycling needs: 96-Well (0.2 or 0.1 mL), 384-Well, and 0.5 mL 60-Well. Each system features a powerful, intuitive touch screen for easy instrument setup and use. Additionally, the Veriti® 96-Well Thermal Cycler features the added control of VeriFlex™ Blocks which gives you six independent temperature blocks for precise control over your PCR optimization. The ability to run fast or standard PCR methods offers you flexibility to shorten your PCR cycling time.

To learn more about the Veriti® Thermal Cycler or to view the product video, visit info.appliedbiosystems.com/veriti

applied biosystems™

Best-in-Class, Real-Time PCR Solutions. Specific for my research.

Only Applied Biosystems delivers the highest-quality, best-in-class workflow solutions for all of your real-time PCR applications. With built-in flexibility, our systems adapt to meet your specific research needs. With 25 years of proven quality, we have the experience you need to bring superior data into your lab. When you want a real-time portfolio that can take your research to the next level, talk to the experts.

As Flexible as You Want to Be.

applied biosystems™

The highest-quality, real-time PCR solutions optimized just for you at www.appliedbiosystems.com/realtimesystems